AD-A122 864 1982 SUMMER STUDY PROGRAM IN GEOPHYSICAL FLUID DYNAMICS 1/4
AT THE WOODS HOLE:.(U) WOODS HOLE OCEANOGRAPHIC
INSTITUTION MA G VERONIS ET AL. NOV 82 WHOI-82-45
UNCLASSIFIED N00014-82-G-0079 F/G 20/4 NL

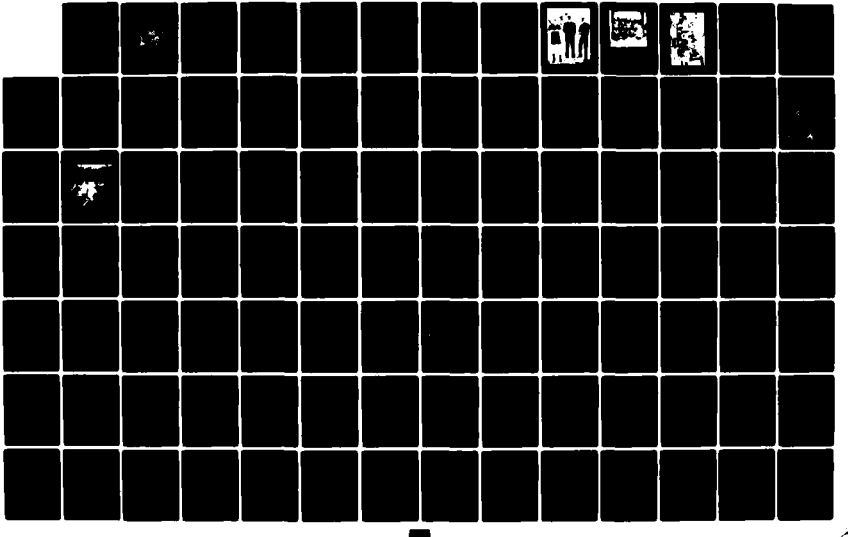

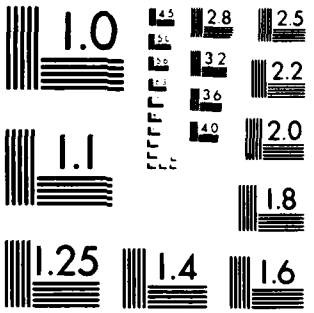

(12)

WHOI-82-45

1982

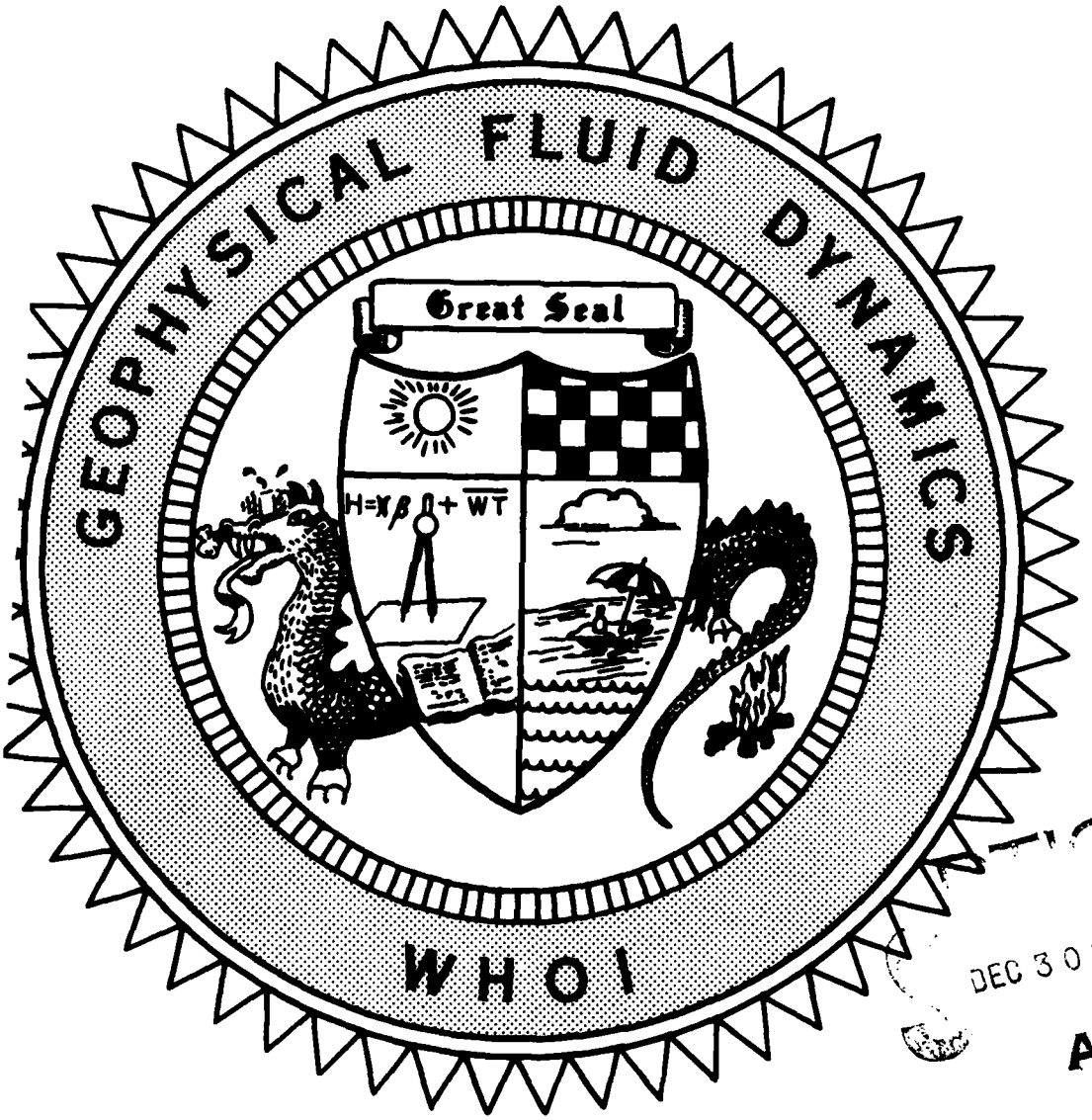

COURSE LECTURES

ABSTRACTS OF SEMINARS

SYMPOSIUM

LECTURES OF THE FELLOWS

SECURITY CLASSIFICATION OF THIS PAGE (When Data Entered)

REPORT DOCUMENTATION PAGE		READ INSTRUCTIONS BEFORE COMPLETING FORM
1. REPORT NUMBER WHOI-82-45	2. GOVT ACCESSION NO.	3. RECIPIENT'S CATALOG NUMBER
4. TITLE (and Subtitle) 1982 SUMMER STUDY PROGRAN IN GEOPHYSICAL FLUID DYNAMICS - THE WOODS HOLE OCEANOGRAPHIC INSTITUTION.		5. TYPE OF REPORT & PERIOD COVERED Technical 6. PERFORMING ORG. REPORT NUMBER
7. AUTHOR(s) George Veronis, Director and Florence K. Mellor, Editor		8. CONTRACT OR GRANT NUMBER(s) N00014-82-G-0079 MCS-82=00450
9. PERFORMING ORGANIZATION NAME AND ADDRESS Woods Hole Oceanographic Institution Woods Hole, Massachusetts 02543		10. PROGRAM ELEMENT, PROJECT, TASK AREA & WORK UNIT NUMBERS
11. CONTROLLING OFFICE NAME AND ADDRESS NORDA/National Space Technology Laboratory Bay St. Louis, MS 39529		12. REPORT DATE November 1982 13. NUMBER OF PAGES 336
14. MONITORING AGENCY NAME & ADDRESS(if different from Controlling Office)		15. SECURITY CLASS. (of this report) Unclassified 15a. DECLASSIFICATION/DOWNGRADING SCHEDULE

16. DISTRIBUTION STATEMENT (of this Report)

Approved for public release; distribution unlimited.

17. DISTRIBUTION STATEMENT (of the abstract entered in Block 20, if different from Report)

18. SUPPLEMENTARY NOTES

This report should be cited as: Woods Hole Oceanog. Inst. Tech. Rept. WHOI-82-45.

19. KEY WORDS (Continue on reverse side if necessary and identify by block number)

1. Geophysical Fluid Dynamics
2. The (Lagrangian) motion of a fluid particle
3. (Eulerian) flow past a fixed point in space

20. ABSTRACT (Continue on reverse side if necessary and identify by block number)

The (Lagrangian) motion of a fluid particle was contrasted with the (Eulerian) flow past a fixed point in space during this twenty-fourth summer program in geophysical fluid dynamics at the Woods Hole Oceanographic Institution.

Seminars on GFD topics are summarized in the abstracts by the staff and visitors. The Fellows' reports reflect the broad range of topics in which they attempted to formulate and solve a tractable problem.

DD FORM 1 JAN 73 1473 EDITION OF 1 NOV 65 IS OBSOLETE
S/N 0102-014-6601 |

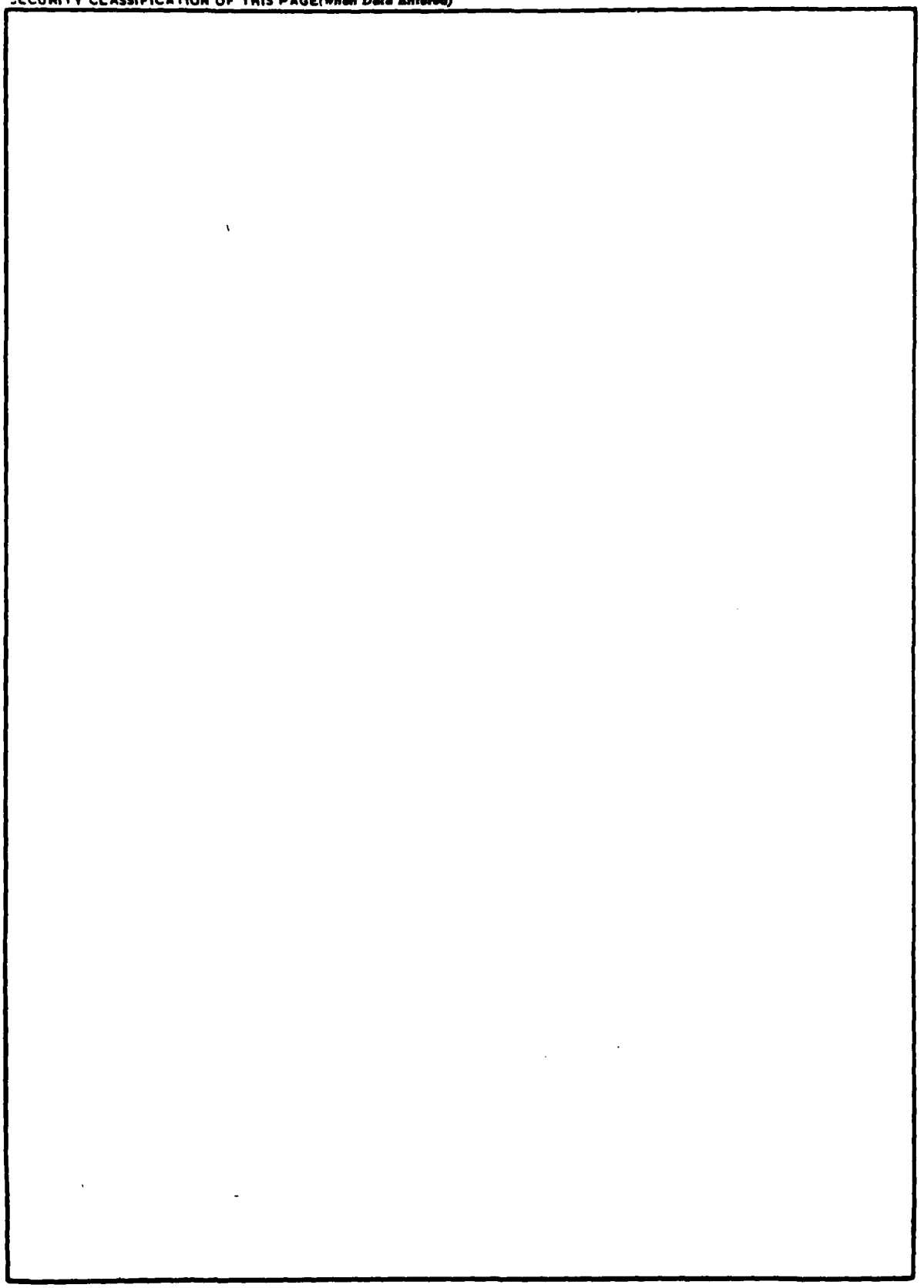

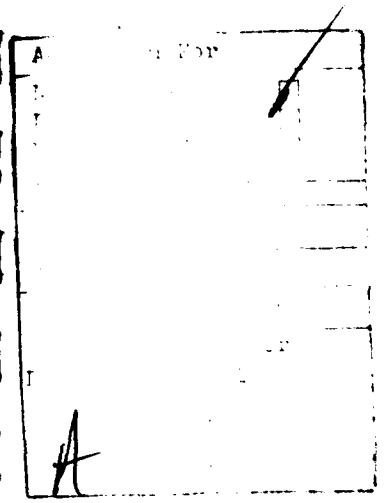

WHOI-82-45

1982 SUMMER STUDY PROGRAM IN GEOPHYSICAL FLUID DYNAMICS THE WOODS HOLE OCEANOGRAPHIC INSTITUTION

PARTICLE MOTIONS IN FLUIDS

by

George Veronis, Director

and

Florence K. Mellor, Editor

WOODS HOLE OCEANOGRAPHIC INSTITUTION
Woods Hole, Massachusetts 02543

November 1982

TECHNICAL REPORT

Prepared for the Office of Naval Research under Contract N00014-82-G-0079 and National Science Foundation Grant MCS-82-00450. Partial support from the Center for Analysis of Marine Systems (CAMS) at Woods Hole Oceanographic Institution. CAMS is supported by The Exxon Foundation, Mobil Foundation, ARCO Foundation, and by an anonymous donor.

Approved for Distribution: Charles Hollister

Charles D. Hollister
Dean of Graduate Studies

1982 SUMMER STUDY PROGRAM

in

GEOPHYSICAL FLUID DYNAMICS

at

THE WOODS HOLE OCEANOGRAPHIC INSTITUTION

PARTICLE MOTIONS IN FLUIDS

GEOPHYSICAL FLUID DYNAMICS PROGRAM

SUMMER - 1982

STAFF

Flierl, Glenn	Massachusetts Institute of Technology
Howard Louis N.	Florida State University
Keller, Joseph B.	Stanford University
Malkus, Willem V.R.	Massachusetts Institute of Technology
Olson, Donald B.	Rosenstiel School of Marine Science/MPO
Rhines, Peter B.	Woods Hole Oceanographic Institution
Salmon, Rick	Scripps Institution of Oceanography
Spiegel, Edward A.	Columbia University
Stern, Melvin E.	University of Rhode Island
Veronis, George	Yale University
Whitehead, John A.	Woods Hole Oceanographic Institution

VISITORS

Andrews, David	University of Oxford
Church, John	CSIRO Marine Laboratories
Davey, Michael	University of Cambridge
Day, Henry	Stanford University
Davis, Russ E.	Scripps Institution of Oceanography
Faller, Alan J.	University of Maryland
Held, Isaac	Princeton University
Herring, Jackson R.	National Center for Atmospheric Research
Hughes, Roger	CSIRO, Melbourne, Australia
Merkine, Lee-Or	Brown University
Rizzoli, Paola M.	Massachusetts Institute of Technology
Tung, K.K.	Massachusetts Institute of Technology
Welander, Pierre	University of Washington
Yamagata, Toshio	Princeton University
Yanase, Shinichiro	Okayama University
Young, William	Scripps Institution of Oceanography

SYMPOSIUM PARTICIPANTS

Aref, Hassan	Brown University
Broecker, Wallace	Lamont-Doherty Geological Observatory
Denman, Kenneth	Institute of Ocean Sciences, Sidney, B.C.
Druffel, Ellen	Woods Hole Oceanographic Institution
Fiadeiro, Manuel E.	Yale University
Hendershott, Myrl C.	Scripps Institution of Oceanography
Holloway, Greg	Institute of Ocean Sciences, Sidney, B.C.
Keffer, Thomas	Woods Hole Oceanographic Institution
Kelly, Kathryn	Scripps Institution of Oceanography
Livingston, Hugh D.	Woods Hole Oceanographic Institution
Price, James F.	Woods Hole Oceanographic Institution
Richardson, Philip	Woods Hole Oceanographic Institution
Riser, Stephen	University of Washington
Rossby, H. Thomas	University of Rhode Island
Rooth, Claes	University of Miami
Sarmiento, Jorge	Princeton University
Smethie, William	Lamont-Doherty Geological Observatory
Steele, John H.	Woods Hole Oceanographic Institution
Wiebe, Peter H.	Woods Hole Oceanographic Institution
Wroblewski, J.S.	Dalhousie University

WOODS HOLE OCEANOGRAPHIC INSTITUTION PARTICIPANTS

Csanady, Gabriel T.
Jenkins, William J.
Pedlosky, Joseph

FELLOWS

Bigg, Grant R.	Adelaide, Australia
Broutman, Dave	University of California at San Diego
Fauve, Stephan	Orsay, France
Haynes, Peter H.	Cambridge, England
Robinson, Walter A.	Columbia University
Shepherd, Theodore G.	Massachusetts Institution of Technology
Swenson, Mark S.	University of California at San Diego
Takahashi, Masaaki	Fukuoka, Japan

PRINCIPAL LECTURERS

Rick Salmon - David Andrews - Peter Rhines - Glenn Flierl

GFD FELLOWS AND STAFF

Back Row: Howard, Rhines, Spiegel, Robinson, Takahashi, Bigg, Flierl.

Middle Row: Veronis, Hughes, Salmon, Keller, Shepherd, Fauve.

1st Row: Olson, Swenson, Haynes, Broutman.

Absentees: Andrews, Aref, Broecker, Church, Csanady, Davey, Day, Davis, Denman, Druffel, Faller, Fiadeiro, Held, Hendershott, Herring, Holloway, Jenkins, Keffer, Kelly, Livingston, Malkus, Merkine, Pedlosky, Price, Richardson, Riser, Rizzoli, Rooth, Rossby, Sarmiento, Smethie, Steele, Stern, Tung, Welander, Whitehead, Wiebe, Wroblewski, Yamagata, Yanase, Young.

GFD SOFTBALL TEAM

1st Row: Veronis, Shepherd, Haynes, Robinson, Malkus

Back Row: Olson, Salmon, Swenson, Bigg, Keller, Broutman, Takahashi, Hughes

Editor's Preface

The (Lagrangian) motion of a fluid particle was contrasted with the (Eulerian) flow past a fixed point in space during this twenty-fourth summer program in geophysical fluid dynamics at the Woods Hole Oceanographic Institution. Peter Rhines opened the lecture series with a discussion of the basic principles for large scale flows in a rotating system and followed that with examples of fluid flows in which particle motions play a particularly significant role. He discussed the distribution of both chemical and physical tracers in oceanographic flows.

Glenn Flierl presented highly idealized, but highly illuminating, examples of flows as seen in the Lagrangian and Eulerian frames of reference and then discussed the observed and calculated transports of properties by Gulf Stream rings.

The application of statistical mechanics to GFD was the focus for the lecture series by Rick Salmon, who showed how to derive a number of important oceanographic results by methods that physicists have used in other contexts for many years.

David Andrews ended the series with the development of a theory of wave-mean flow interactions and the application of those concepts to the observed stratospheric warming in the atmosphere.

Just one week before the beginning of the program, we learned that because of illness, Francis Bretherton would be unable to attend the program as principal invited lecturer. We are especially grateful to Flierl, Salmon and Andrews for coming to the rescue so effectively with the lectures reported in the following pages.

The microsymposium on biological and chemical tracers in the ocean included twenty seminars on different aspects of tracer distributions and the dynamics of mixing and stirring in the ocean.

Seminars on GFD topics are summarized in the abstracts by the staff and visitors. The Fellows' reports reflect the broad range of topics in which they attempted to formulate and solve a tractable problem.

Peter Rhines helped to organize a large part of the activity of the summer. Dave Broutman, Rick Salmon and Mark Swenson, our three Scripps participants, inspired the GFD softball team to its first winning season in 20 years. A photograph of the team is included in the volume to commemorate that achievement.

Florence Mellor tended to our practical needs and kept the program functioning smoothly and was assisted by Betty Hodge. A. L. Peirson and Dorothy Berthel helped with the administrative and financial duties. We are all indebted to them.

Support of the program by the Office of Naval Research, the National Science Foundation and the Woods Hole Oceanographic Institution's Center for Analysis of Marine Systems is gratefully acknowledged.

George Veronis

TABLE OF CONTENTS

PARTICLE MOTIONS IN FLUIDS

Page No

PETER B. RHINES

I. Basic Dynamics of the Large-Scale Geostrophic Circulation. . . 1
II. Potential Vorticity and the Circulation. 5
III. Distortion and Enhanced Diffusion of Passive Scalars by Fluid Strain Fields. 11
IV. More About Dye and Particles 20
V. Return to Dynamics 35

GLENN FLIERL

Particle Motions in Strong Wave Fields 48
Tracers in Rings 66

RICK SALMON

Equilibrium Statistical Mechanics Applied to Geophysical Fluid Dynamics 76

I. Philosophy and Review of the Basics. 76
II. Rotating Flow over Topography 82
III. Stratified Flow and the Equatorial Funneling Effect 89

DAVID ANDREWS

Wave-Mean Flow Interactions - with Applications to the Middle Atmosphere. 99

I. Introduction 99
II. Second Order Mean Flow Induced by Internal Gravity Waves . . 100
III. Quasi-Geostrophic Flow on a β -plane 107
IV. Sudden Stratospheric Warming 111
V. Zonal Mean Models of Transport of Chemical Tracers in the Stratosphere 118
VI. The Generalized Lagrangian Mean. 124

ABSTRACTS OF SEMINARS

Page No.

How Rapid is Prandtl-Batchelor Expulsion?
William R. Young 135

Turbulent Dispersion in Convergent Flow
Alan J. Faller 135

Wave/Shear-Flow Interaction and the Generation of Langmuir Circulations
Alan J. Faller 138

Potential Vorticity Structure in the North Atlantic Subtropical Gyre
Donald B. Olson. 140

Evolution of Strong Vortices
Glenn Flierl 140

Finite Amplitude Long Waves in a Shear Flow
Melvin Stern 141

The Shape of the Main Thermocline
Rick Salmon. 142

Transient Tracers
William J. Jenkins 143

Inverse Methods for Oceanography
George Veronis 144

On the Direction of Eddy Momentum Fluxes in Baroclinic Instabilities
Isaac M. Held 145

Openers and Closures
Willem V.R. Malkus 146

Chaos is Come Again
Edward Spiegel 147

Statistical Mechanics of Fields
Joseph B. Keller 148

The Modified Cumulant Expansion for Divergent Two-Dimensional Isotropic Turbulence
Shinichiro Yanase. 152

Page No.

Thermal Convection: Numerical Experiments near the Onset to Turbulence and Comments on the Application of Closure
Jackson R. Herring 153

Heteroclinic Orbits and Irregular Oscillations
Louis N. Howard. 154

The Response of a Two-Level Ocean to Thermal Forcing
Michael K. Davey 155

On the 2D Transport of Stratospheric Tracers
K. K. Tung 156

The Role of Damped Equatorial Waves in the Oceanic Response to Winds
Toshio Yamagata. 156

Calculating the Reference Level from the Bernoulli Function Conservation
Pierre Welander. 157

A Wave in Anti-Cyclonic Shear
Roger Hughes 160

A Parameterization of Vertical Diffusion
Roger Hughes 160

Property Transport and Lagrangian Particle Statistics
Russ Davis 160

Monopoles over Variable Relief and Boundary Forcing as a Production Mechanism
Paola M. Rizzoli 162

The Coastal Ecosystem of the Northern Adriatic Sea
Paola M. Rizzoli 164

Dispersal by Randomly Varying Currents
Gabriel T. Csanady 166

SYMPOSIUM ON BIOLOGICAL AND CHEMICAL TRACERS IN THE OCEAN

Page No.

Gyres and Tracers
Peter B. Rhines 169

Tracing Transients
William J. Jenkins. 172

The Use of Satellite Derived Surface Properties to Study Ocean Kinematics and Dynamics
Donald B. Olson 174

Global Thermohaline Circulation Modes
Claes G.H. Rooth. 175

The Thermohaline Circulation Seen by Tracers
Manuel Fiadeiro 176

Penetration of Tritium in the North Atlantic Main Thermocline
Jorge L. Sarmiento. 177

Eddy Kinetic Energy from Surface Drifters and Deep Floats
Philip L. Richardson. 177

The Gulf Stream East of Cape Hatteras
T. Rossby 178

Ocean Stirring by Geostrophic Turbulence
Greg Holloway 179

A Comment on Modelling Turbulent Transports in Marine Ecosystems
Greg Holloway 180

The Utility of Multiple Tracer Distributions in Calibrating Ocean Thermocline Models
Wallace S. Broecker 184

Particle Dispersion in the Western North Atlantic
James F. Price. 188

An Idealized Model of Stirring
Hassan Aref 188

The Streakiness of Tracers
Thomas Keffer 190

Page No.

Modeling the Advective and Turbulent Transport of Plankton
J. S. Wroblewski 190

Euphausiid Invasion/Dispersal in Gulf Stream Cold-Core Rings
Peter H. Wiebe 191

Mesoscale Phytoplankton Distributions
Kenneth L. Denman. 192

Advection Modelling of Vertically Migrating Shrimp Larvae
John A. Church 193

Radiocarbon as a Tracer of Ocean Variability
Ellen M. Druffel 193

Western North Atlantic Structure and Variability Inferred from SOFAR Floats
Stephen C. Riser 194

LECTURES OF FELLOWS

Wakes and Mean Flows of Low-Frequency Internal-Wave Packets
Dave Broutman. 195

Second Order Constraints on the Amplitudes of Vertically Propagating Rossby Waves
Walter Robinson. 208

The Temporal Evolution of Taylor Columns Over Topography
Grant R. Bigg. 226

Equatorial Wave Response Due to Oscillating Wind Stress
Masaaki Takahashi. 239

Vertical Convection and Horizontal Advection
Stephan Fauve. 252

Models of Large Scale Flows with Relevance to Southern Ocean Circulation
Peter Haynes 262

Mean Motions induced by Baroclinic Instability in a Jet
Theodore G. Shepherd 287

Isolated 2D Vortices in the Presence of Shear
Mark Swenson 324

I. BASIC DYNAMICS OF THE LARGE-SCALE GEOSTROPHIC CIRCULATION

Peter B. Rhines

INTRODUCTION

Recent evidence indicates that the present circulation of the ocean is best viewed as one of a wide ensemble of possible states. In the broadest sense, the circulation of the ocean involves complex interactions with the land masses (over geological time) and with the atmosphere over a wide range of time scales. The interactions with the atmosphere are profound enough that to model the ocean as isolated from the atmosphere is to severely limit the model's ability to describe important processes, especially over the time scales of climatic change. Some of these processes are shown in cartoon form below.

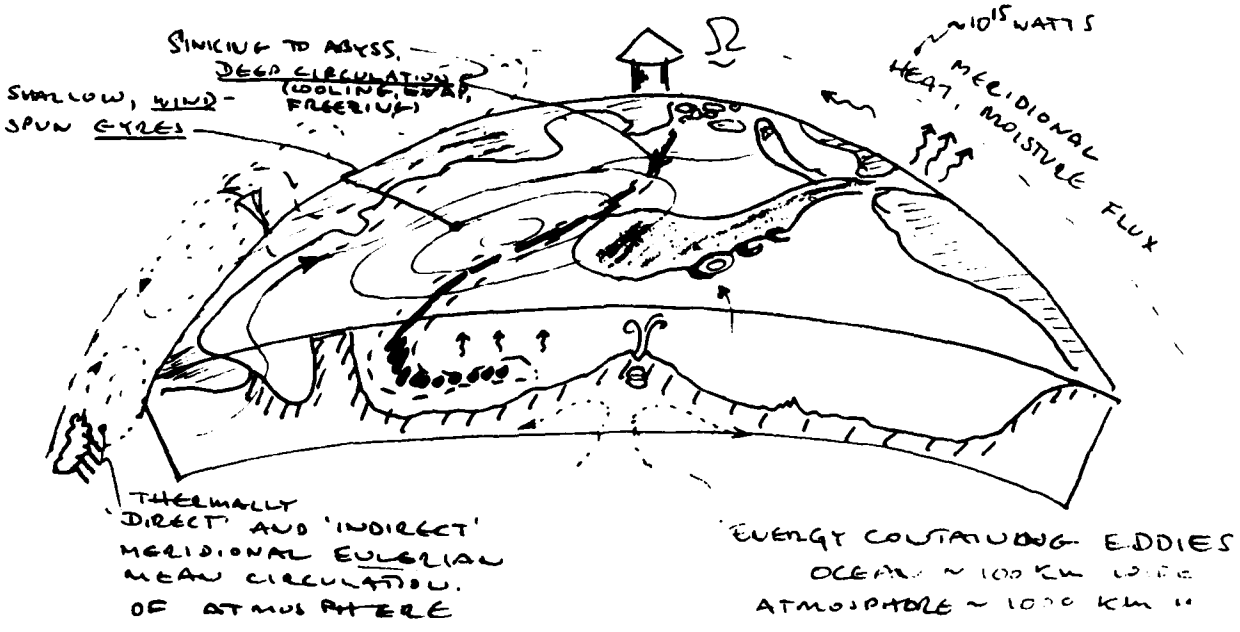

In many respects, the oceans and atmosphere are similar dynamical systems. Still, there are some great differences of which two are particularly striking:

1) There are no lateral boundaries (above the mountain tops) in the atmosphere. Accordingly, the atmosphere exhibits a zonal structure to a greater degree than the oceans.

2) There are significant differences in the forcing of the two

systems. The oceans are primarily forced from above, i.e. wind stress and thermal forcing. (There are exceptions such as tides, boundary mixing, and geothermal heating.) Since the oceans are stably stratified, this makes it very difficult to ventilate the deep oceans. The atmosphere, by contrast, is heated below from infrared radiation and heated internally by condensation in tropical cumulus towers. This leads to a large convective cell (in the average sense) in the tropics, which influences the circulation globally through its efficient transport of heat.

While important features of the oceans' circulation can be explored deterministically (eg. tides, permanent wind-gyre circulation, deep thermocline circulation), the response of the oceans is so rich in scales that much of the structure can be more sensibly studied from a stochastic point of view. From this perspective, one attempts to 'filter' the equations of motion for the general circulation scale, say, and is left to parameterize in some statistical way the influence of other (smaller) scales of motion. Were the interest in a different scale, the parameterization would be different. Nor is the parameterization likely to be faithful to the physics in a wide range of circumstances. Thus the 'filtered' equations of motion for the general circulation scale are not at all obvious.

Of particular interest to oceanographers is the manner in which a passive tracer (marked fluid) evolves in a fluid flow. In this context we would like to explore the mechanism of transport and dilution. Furthermore, the behavior of passive tracers are useful as models of distortion, transport and cascade of dynamical quantities. Especially interesting in this regard is potential vorticity, which is conservative following fluid elements. For a review of some of these ideas, see Moffatt, 1981.

Equations of Motion

For a derivation of the pertinent equations of motion see Pedlosky, 1979.

Mass conservation $$\frac{\partial \rho}{\partial t} + \nabla \cdot \rho \underset{\sim}{u} = 0$$

where ρ = density and u = (u,v,w) = east, north, up velocity, and t = time. x,y and z are east, north and up, and $\hat{\underset{\sim}{x}}, \hat{\underset{\sim}{y}}$ and $\hat{\underset{\sim}{z}}$ are corresponding unit vectors.

Momentum conservation

$$\frac{\partial \underset{\sim}{u}}{\partial t} + \underset{\sim}{u} \cdot \nabla \underset{\sim}{u} + 2 \underset{\sim}{\Omega} \times \underset{\sim}{u} = -\frac{1}{\rho} \nabla p + \nabla \Phi + \nu \Delta \underset{\sim}{u} \quad (1)$$

where $\underset{\sim}{\Omega}$ = rotation rate, p = pressure,
Φ = geopotential, ν kinematic viscosity.

Introduce the scaling $\partial/\partial t \sim T^{-1}$; $\partial/\partial x \sim L^{-1}$; $\partial/\partial z \sim H^{-1}$; $|\underset{\sim}{u}| \sim U$

The horizontal components of (1) then have the size $O(1/\Omega T)$, $O(U/\Omega L)$, $O(1)$ $O(1)$, 0, $O(\nu/\Omega L^2, \nu/\Omega H^2)$ respectively.

At scales where L > 10 km, T > 1 day, $U \sim 10$ cm/s, we have

$$Ro = U/\Omega L \lesssim 10^{-1} \qquad \text{Rossby Number}$$

$$E = \nu/\Omega L^2, \nu/\Omega H^2 \ll 1 \qquad \text{Ekman Number}$$

Only the O(1) terms survive.

This is called geostrophic balance.

Similarly, the vertical momentum equation reduces to $0 = -\rho^{-1} p_z - |g|$ to lowest order. This is the hydrostatic balance.

$\nabla \times$ (1) implies

$$\frac{\partial \underset{\sim}{\omega}}{\partial t} + \underset{\sim}{u} \cdot \nabla (\underset{\sim}{\omega} + 2\underset{\sim}{\Omega}) = (\underset{\sim}{\omega} + 2\underset{\sim}{\Omega}) \cdot \nabla \underset{\sim}{u} + \frac{1}{\rho^2} \nabla \rho \times \nabla p + \nu \Delta \underset{\sim}{\omega} \qquad (2)$$

where $\underset{\sim}{\omega} = \nabla \times \underset{\sim}{u}$. This is the vorticity equation. For a homogeneous, inviscid fluid $\tilde{\nu} = \nabla p \times \nabla \rho = 0$. Notice that this implies that lines of constant $\underset{\sim}{\omega} + 2\underset{\sim}{\Omega}$ coincide with material lines -- a dye arrow initially indicating $\underset{\sim}{\omega} + 2\underset{\sim}{\Omega}$ does so forever.

Consider equation (2) in light of the scaling given above. The twisting term $\rho^{-2} \nabla \rho \times \nabla p$ creates nearly horizontal vorticity since each of $\nabla \rho$, ∇p are nearly vertical. For Ro $\ll 1$, the largest horizontal terms are

$$(2\underset{\sim}{\Omega} \cdot \nabla) \underset{\sim}{u} = -\rho^{-2} \nabla \rho \times \nabla p$$
$$= -\rho^{-2} \left[\rho_y p_z \hat{\underset{\sim}{x}} - \rho_x p_z \hat{\underset{\sim}{y}} \right] + O(f^2 L^2 / gH)$$

Notice that this is consistent with the curl of the geostrophic equation, which can be written

$$f \underset{\sim}{u}_z = -\underset{\sim}{g} \times \frac{1}{\rho} \nabla \rho \qquad (3)$$
$$\underset{\sim}{u} \equiv (u, v), \quad \nabla \equiv (\partial_x, \partial_y), \quad f = 2\underset{\sim}{\Omega} \cdot \hat{\underset{\sim}{z}}$$

Thus, the large-scale geostrophic and hydrostatic balances allow constant density surfaces to lie tilted with respect to equipotential surfaces. In fact, since horizontal pressure gradients and (until recently) velocities are difficult to measure in the ocean, the dominant occupation of oceanographers has been to measure ρ so as to infer $\underset{\sim}{u}(z)$ to within an undetermined constant.

Scaling (3) $f \underset{\sim}{u}_z = O\left(\frac{H^2}{L^2} (\Omega T)^{-2} \right) \frac{\Omega U}{H}$ for rapid rotation and homogeneous fluid.

In either case we have $u_z = 0$ for small aspect ratio. Continuity then implies that $w_{zz} = 0$. This is the Taylor-Proudman approximation and is a reflection of the rigidity imparted to the fluid by the Coriolis force.

Kelvin's Theorem with Rotation

Define $\Gamma \equiv \oint_C \underset{\sim}{u} \cdot d\hat{\underset{\sim}{r}}$ ($\hat{r}$ = unit vector tangent to C). (4)

$$\frac{d\Gamma}{dt} = \oint_C \frac{d\underset{\sim}{u}}{dt} \cdot d\underset{\sim}{r} + \oint \underset{\sim}{u} \cdot \frac{d}{dt}(d\underset{\sim}{r})$$

Take C to be a material surface. Then $\frac{d}{dt}(d\underset{\sim}{r}) = d\underset{\sim}{u}$

Note: $\underset{\sim}{u} \cdot d\underset{\sim}{u} = \frac{1}{2} d|\underset{\sim}{u}|^2$

$$\Rightarrow \frac{d\Gamma}{dt} = \oint_c \frac{d\underset{\sim}{u}}{dt} \cdot d\underset{\sim}{r}$$

Recall:

$$\rho\left(\frac{d\underset{\sim}{u}}{dt} + 2\underset{\sim}{\Omega} \times \underset{\sim}{u}\right) = -\nabla p + \rho \nabla \Phi + \mu \Delta \underset{\sim}{u}$$

Take $\mu = 0$. Substitution

$$\frac{d\Gamma}{dt} = \oint_c -2(\underset{\sim}{\Omega} \times \underset{\sim}{u}) \cdot d\underset{\sim}{r} + \oint_c -\frac{1}{\rho} \nabla p \cdot d\underset{\sim}{r}$$

Using Stokes' Theorem

$$\frac{d\Gamma}{dt} = -2 \oint_c \underset{\sim}{\Omega} \times \underset{\sim}{u} \cdot d\underset{\sim}{r} + \iint_A \frac{\nabla\rho \times \nabla p}{\rho^2} \cdot \hat{\underset{\sim}{n}}\, dA$$

where $\hat{\underset{\sim}{n}}$ = unit vector normal to A.

Take C to lie on a constant density surface $\Rightarrow \nabla\rho \times \nabla p \cdot \hat{\underset{\sim}{n}} = 0$

$$\frac{d\Gamma}{dt} = -2 \oint_c \underset{\sim}{\Omega} \times \underset{\sim}{u} \cdot d\underset{\sim}{r} = -2\Omega \frac{dA}{dt}$$

where A = area enclosed by the projection of C onto a plane perpendicular to $\underset{\sim}{\Omega}$, with the sign convention that A is positive if $\iint \underset{\sim}{\Omega} \cdot \hat{\underset{\sim}{n}}\, dS > 0$ and conversely.

Note: (1) It is not obvious that viscosity is negligible for long. As the contour distorts, gradients become sharp enough for viscosity to become important. Thus, when the contour distorts to such an extent that significant gradients exist on a length scale $(\nu/\Omega)^{1/2}$ viscosity becomes important. See figure below.

(2) Although C is a material circuit, it is not necessarily true that Γ indicates a systematic (Lagrangian) motion of fluid particles or a systematic Eulerian average rotation in a fixed spatial region initially coincident with C. In a later lecture, in fact, we will present an example where the systematic motion of fluid particles is in the opposite direction to the sense of circulation as defined by (4).

(3) Note that when C folds over causing its projection to intersect itself, A may become negative.

REFERENCES

Moffatt, H.K. 1981. J.F.M.. 106.

Pedlosky. J. 1979. Geophy. Fluid Dynam., Springer Verlag, N. Y.

NOTES SUBMITTED BY
MARK SWENSON

II. POTENTIAL VORTICITY AND THE CIRCULATION

Peter B. Rhines

Spherical Shell

Since Γ is the sum of planetary and relative vortex-tube strengths, Kelvin's theorem implies that if north-south motion should occur, large relative vorticity would result. If the time scale of the north-south motion T is fast enough, the 'rigidity' constraint is broken by stretching and bending of columns of fluid. This allows the motion of the fluid to deviate from the zonal free geostrophic contours.

We may rewrite Kelvin's theorem as

$$\frac{d}{dt}\iint \nabla \times \underset{\sim}{u}\cdot\hat{\underset{\sim}{z}}\, dS = -2\,\Omega\,\frac{dA}{dt}$$

where $\hat{\underset{\sim}{z}}$ = vertical unit vector, $\Omega \equiv \frac{\underset{\sim}{\Omega}\cdot\hat{\underset{\sim}{z}}}{|\underset{\sim}{\Omega}\cdot\hat{\underset{\sim}{z}}|}\,|\underset{\sim}{\Omega}|$.

Thus, for a small disk of fluid, we have

$$\frac{d}{dt}\,\underset{\sim}{J}\cdot\hat{\underset{\sim}{z}} = -\frac{2\Omega}{A}\frac{dA}{dt}$$

The thin domain and heavy stratification tend to confine the disk to constant z; thus

$$\frac{dA}{A} \simeq \cos\lambda\, d\lambda$$

$$\Rightarrow \frac{d}{dt}\,\underset{\sim}{J}\cdot\hat{\underset{\sim}{z}} = -\beta v + \text{terms that describe verticle motion}$$

where $\beta = \frac{2|\underset{\sim}{\Omega}|}{a}\cos\lambda$

Note: It only takes slight tilts of the disk to cause the 'other terms' to become significant. Slopes that are observed in the density surfaces of the ocean are of this order.

Potential Vorticity

The natural differential version of Kelvin's theorem replaces A by an equivalent measure of 'height' or 'thickness' changes between marked constant density surfaces (see Pedlosky, 1979).

$$\frac{D}{Dt}\left[\frac{\underset{\sim}{J}+2\underset{\sim}{\Omega}}{\rho}\cdot\nabla\rho\right] = 0 \qquad (1a)$$

For a single homogeneous layer of depth h this becomes

$$\frac{D}{Dt}\left(\frac{\underset{\sim}{J}\cdot\hat{\underset{\sim}{z}}+f}{h}\right) = 0 \quad \text{where } f = 2\Omega\sin\lambda\,. \qquad (1b)$$

A quasi-geostrophic version, Boussinesq, appropriate to meso-scale dynamics is

$$\frac{D}{Dt}\left(\nabla^2\psi + \beta y + \left(f_0^2/N^2\,\psi_z\right)_z\right) = 0 \qquad (1c)$$

where ψ = streamfunction $\&$ pressure and

$$p'_z = -g\rho', \qquad f = f_0 + \beta y, \qquad \rho = \bar{\rho}(z) + \rho'(\underset{\sim}{x}, t)$$

$$N^2 = -\frac{g\bar{\rho}_z}{\bar{\rho}}, \qquad \frac{D}{Dt}\rho' = -w\bar{\rho}_z$$

where we have assumed that the perturbation pressure is hydrostatic and have invoked the β-plane and Boussinesq approximations. This formulation is not appropriate for basin wide flows since the assumptions:

(1) $N^2 = N^2(z)$ only,
(2) f_o = constant,
(3) Cartesian geometry,

are all inaccurate. Neither is it appropriate for flows with length scales less than the first internal Rossby radius of deformation.

Boundary Conditions

(a) Vertical 'coast'. $\underset{\sim}{u}\cdot\hat{\underset{\sim}{n}} = 0 \Rightarrow \nabla\psi \times \hat{\underset{\sim}{n}} = 0$ (free slip) at the boundary.

Note: This says tnat density surfaces must be level at the coast. Therefore it cannot cope with thermal sources at the boundary unless you explicitly include internal Kelvin waves or diffusion layers. Thermal sources thus act as a singular perturbation to the geostrophic equations. In a layer of thickness $\sim NH/f$, Kelvin waves endeavor to level off the coastal density field.

(b) Isothermal lid. $\underset{\sim}{u}\cdot\hat{\underset{\sim}{n}} = 0 \Rightarrow \rho' = -\bar{\rho} f_0 \psi_z / g = 0$ at $z = 0$.

(c) Isothermal bottom.

$\underset{\sim}{u}\cdot\hat{\underset{\sim}{n}} = 0 \Rightarrow w = -\underset{\sim}{u}\cdot\nabla h'$ at $z = H$ (due to a linearization)

where $h = H + h'$ and H = constant.

$$\Rightarrow \frac{f_0}{N^2}\frac{D}{Dt}\psi_z = \frac{\partial(\psi, h)}{\partial(x, y)} \qquad (z = -H)$$

(This is seen by using the density equation in the quasi-geostrophic context,

$$\frac{D}{Dt}\psi_z = -\frac{N^2}{f_0}w.\ )$$

Special Limits of Potential Vorticity, q, where Dq/Dt in (1a,b,c).

(i) $L \gg L_D \equiv NH/f_o$ = Rossby radius of deformation

$\Rightarrow q \simeq f\rho_z/\rho$ for ocean basin scale flows.

(ii) Thin, homogeneous layer, ρ = constant and Ro $\sim \delta h/H$ where $h = H + \delta h$ = ocean depth. In the layer,

$$q \simeq (f_o + \beta y)/h$$

(or, $q \simeq f/\tilde{h}$ for a layered fluid, where $\tilde{h}$ = thickness of constant density layer.) If we imagine the large scale ocean circulation to be steady, these simple large scale limits $\Rightarrow$

$$\underset{\sim}{u} \cdot \nabla (f \rho_z) = 0 , \qquad \underset{\sim}{u} \cdot \nabla \rho = 0$$

away from external mechanical or thermal forcing. This suggests that maps of mean geostrophic contours q = constant on potential density surfaces will be interesting.

More generally, we may consider a potential vorticity balance that is not conservative.

$$\frac{D}{Dt} q = F - \Delta \tag{2a}$$

where F = external forcing and Δ = dissipation. Dividing this equation into eddy and mean quantities we find

$$\frac{\partial q'}{\partial t} + \nabla \cdot \underset{\sim}{u}' q' - \nabla \cdot \overline{\underset{\sim}{u}' q'} = - \underset{\sim}{u}' \cdot \nabla \bar{q} - \bar{\underset{\sim}{u}} \cdot \nabla q' + F' - \Delta' \tag{2b}$$

in the equation for the perturbations and

$$\frac{\partial \bar{q}}{\partial t} + \bar{u} \cdot \nabla \bar{q} = - \nabla \cdot \overline{q' \underset{\sim}{u}'} + \bar{F} - \bar{\Delta} \tag{2c}$$

where $q = \bar{q} + q'$ and $\underset{\sim}{u} = \bar{\underset{\sim}{u}} + \underset{\sim}{u}'$ and $\overline{(\ )}$ defines an appropriate averaging procedure. Notice that, even in the absence of eddies, the mean flow has a fundamentally nonlinear nature since the flow paths depend on the strength of the flow. In energetic flows, where eddy activity can be large, (2c) describes how the mean flow is driven across q contours by the eddy transport of potential vorticity. Equation (2b) describes the eddy field. The terms on the left hand side represent geostrophic turbulence. Furthermore, the q field provides a restoring background field for perturbations in terms on the right hand side which represent Rossby wave restoring effects $q'_t + \underset{\sim}{u}' \cdot \nabla \bar{q} = 0$ or mean flow instabilities $q'_t + \underset{\sim}{u}' \cdot \nabla \bar{q} + \bar{\underset{\sim}{u}} \cdot \nabla q' = 0$

Note: F, Δ represent the effects of boundary forcing on q, ρ which are the result of a complex series of feedbacks between the oceans and atmosphere.

As appropriate to the limits of large scale ocean circulation (see special limits of q), q and ρ are conserved on flow lines in the thermocline equations. These can be written as a single partial differential equation in a variable M such that M_z = pressure (Welander, 1971)

$$\frac{\partial (M_{zz}, M_z)}{\partial (\phi, \lambda)} - \cot \lambda M_\phi M_{zzz} = 0$$

where λ = latitude, ϕ = longitude,

$$u = - (2\Omega a \sin\lambda)^{-1} M_{\lambda z}$$

$$v = (2\Omega a \sin\lambda \cos\lambda)^{-1} M_{\phi z}$$

$$w = (2\Omega a^2 \sin^2\lambda)^{-1} M_\phi$$

$$\rho' = M_{zz}$$

$$M = \int_0^z p\,dz + 2\Omega a^2 \sin^2\lambda \int_0^\phi w_0\,d\phi$$

$$w_0 = w(\phi, \lambda, 0)$$

Note: (1) linear 'density' diffusion adds the term

$$2\Omega a^2 \kappa \sin\lambda \cos\lambda M_{zzzz}$$

where $\underset{\sim}{u}\cdot\nabla\rho' = \kappa\rho'_{zz}$ defines the diffusivity, κ.

(2) A slow time dependence adds the term M_{zzt}.

The density field (or the height field of constant potential vorticity surfaces) is a streamfunction for $\partial_z \underset{\sim}{u}_h$ where $\underset{\sim}{u}_h$ = horizontal velocity. If the deep water were at rest, this would also be a streamfunction for $\underline{u}$ itself.

But, more generally, the importance of w shows that important O(1) deviation of $\underline{u}$ from $\hat{\underset{\sim}{z}}\times\nabla\rho$ occurs in the subtropical gyres. This is the 'downhill' flow in the subtropical gyre, where wind pumping is downward. The horseshoe shapes of the σ_θ surfaces (plotted on constant z) and the constant ψ surfaces (similarly plotted) are displaced in such a fashion that there is a downward component of flow everywhere in the gyre (except the western boundary layer.) Figure 1 shows density, σ_θ and streamfunction at three levels in a theoretical wind-driven gyre of Rhines and Young, 1982. The driving effect, the Ekman layer divergence, is antisymmetric about the mid-line, so only half of each picture is shown. The circulation weakens and shifts poleward with depth.

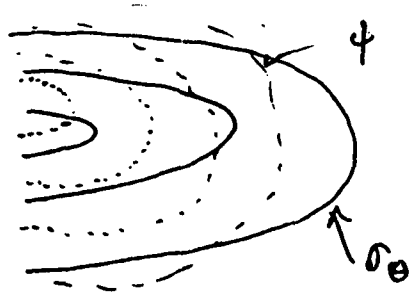

Interpretation of the general circulation of the ocean by considering the intersection of q = const. surfaces and σ_θ = const surfaces yields the following qualitative picture, see fig. 2.

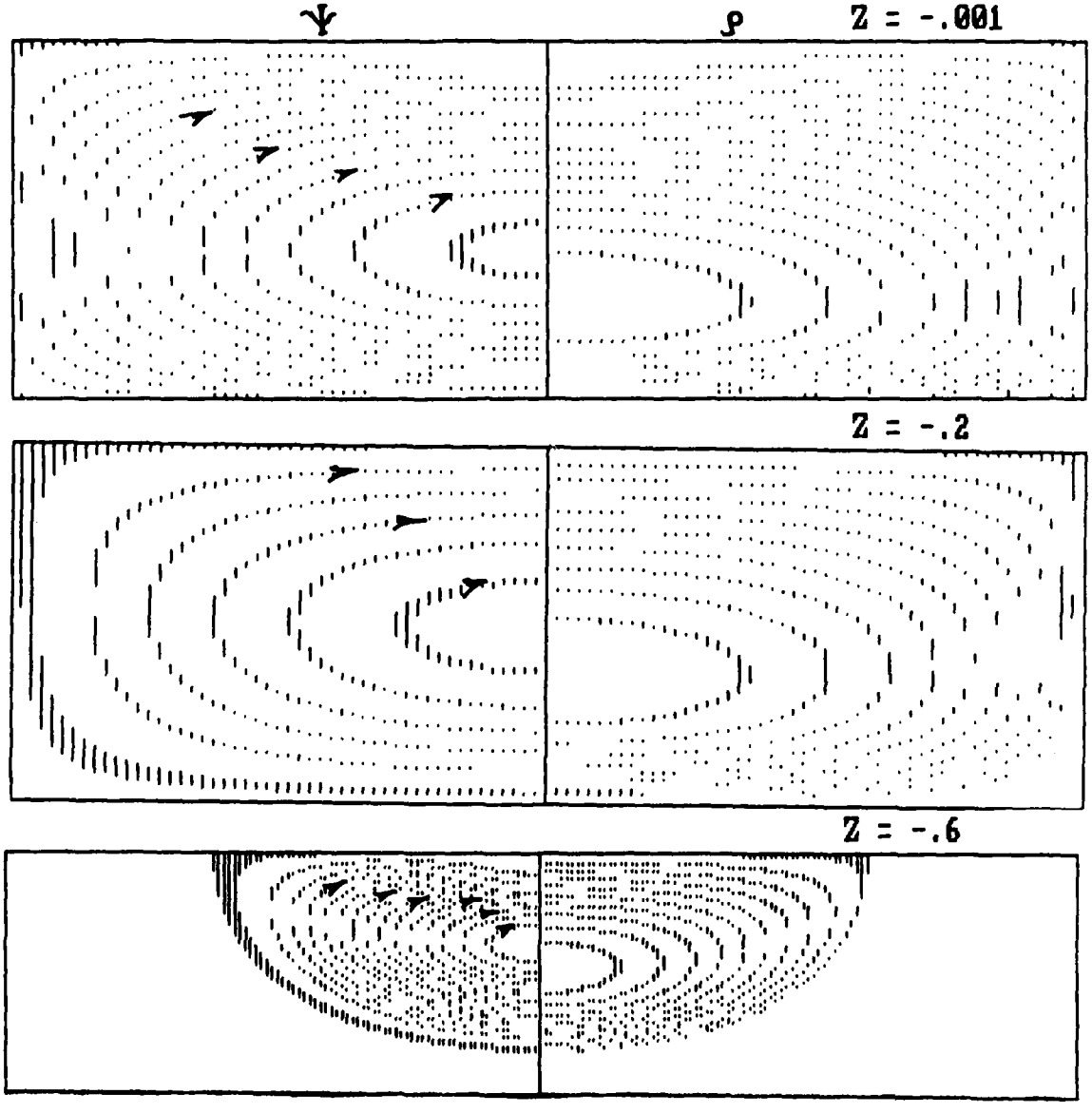

Fig. 1. Streamlines (left panels) and density contours for a theoretical wind-driven gyre (Rhines and Young 1982) at three levels beneath the sea surface. The patterns are symmetric about the mid-line. Note the general similarity between flow lines and density field yet the slight northward displacement of Ψ relative to σ_θ insures that the flow proceeds 'downhill' everywhere in the right half-basin as it must to match the downward Ekman pumping.

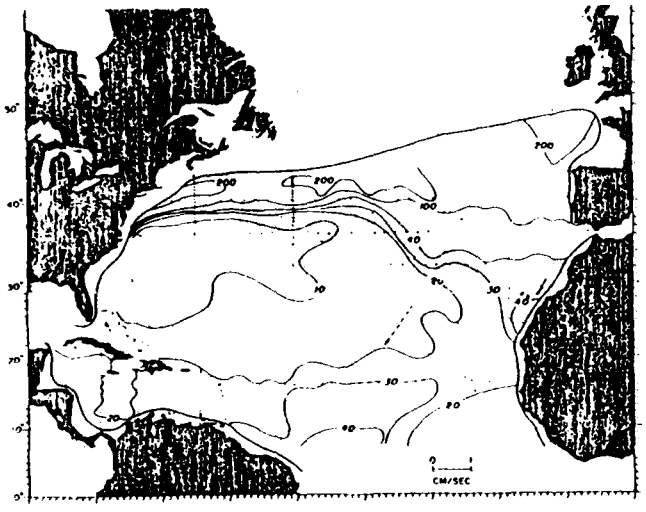

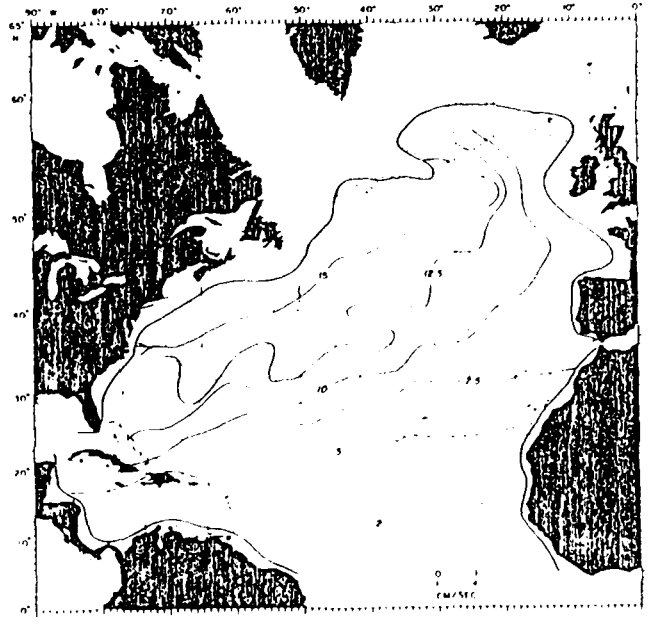

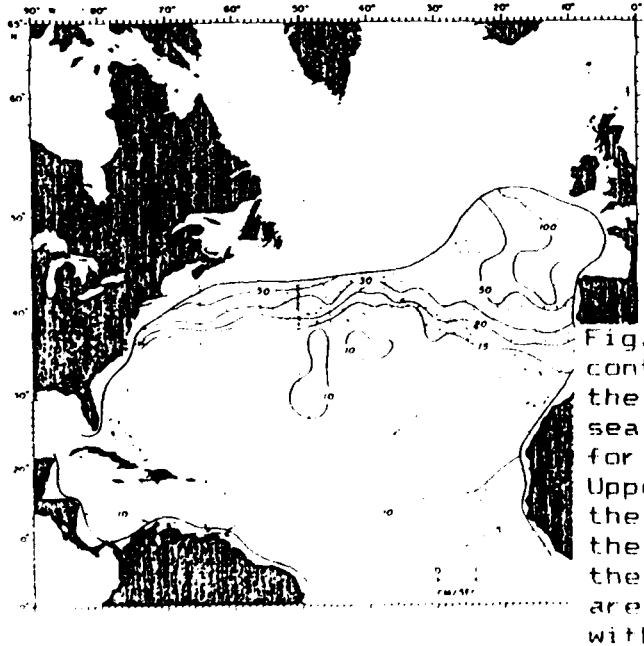

Fig.2 Geostrophic contours (i.e. constant potential vorticity contours on constant potential density ($\sigma\theta$) surfaces) for the North Atlantic. The bowl-shaped $\sigma\theta$ surfaces touch the sea surface in the stippled region which is thus the 'window' for entry of fluid that has been modified by the atmosphere. Upper left: $\sigma\theta$= 26.3-26.5 the q-contours are bent round to the shape of the gyre; lower left: $\sigma\theta$= 26.5-27.0 deeper in the thermocline q forms a plateau where ∇q is excluded from the gyre. Above: $\sigma\theta$=27.3-27.6 still deeper the q contours are 'expressways' connecting the high latitude sea surface with the deep ocean to the south. In quiet regions the pattern is dominated by the 'ramp' q ...

In the deep ocean, the flow is weak and $\bar{q} \simeq \beta_y$. This places a severe restriction on the types of flow possible. The circulation must be closed by quite strong processes such as a western boundary layer. The expressways are indicative of the thermohaline circulation. The flow paths intersect the ocean surface in high latitudes - this is the sea surface 'window' for entry of buoyancy boundary conditions.

The upper layers of the ocean have quite a different character. The upper layer is characterized by wind-driven velocities which allows q-conserving flow about the gyre, including the boundary layer. There is an injection of "new fluid" at the outcrop window. but the volume flux is probably only about 1/3-1/4 of the volume flux in the gyre, indicating a large amount of recirculation. In the intensive inner part of the gyre the relative vorticity becomes the same order as the planetary vorticity. This breaks the Sverdrup restraint on north-south velocity and leads to a "runaway" region. This explains the vastly increased recirculation in that region. Below this region is the plateau, which is a fairly extensive depth interval in which not only is q 'conserved' along flow lines, but also $\partial \bar{q} / \partial \gamma \to 0$. Rhines and Young (1982) explain this in terms of Prandtl-Batchelor expulsion of gradients due to 'shear dispersion' which tends to equalize values of a tracer along streamlines, see following lecture.

REFERENCES

Pedlosky, J. 1979. Geophysical Fluid Dynamics, Springer Verlag, N.Y.

Rhines. P. and W. Young, 1982. Homogenization of potential vorticity in planetary gyres, J.F.M., Sept.

Welander, P., 1971. The Thermocline Problem, Phil. Trans. Roy. Soc. A. Vol. 270, pp. 415-421.

NOTES SUBMITTED BY
MARK SWENSON

III. DISTORTION AND ENHANCED DIFFUSION OF PASSIVE SCALARS BY FLUID STRAIN FIELDS

Peter B. Rhines

To gain intuition about the 'active' tracer, q, we first discuss a passive scalar field advected and diffused with a background shear and strain field. (Fig. 3a). We can write a velocity field as

$$u_i(\underset{\sim}{x} + \delta \underset{\sim}{x}) = u_i(\underset{\sim}{x}) + \frac{\partial u_i}{\partial x_j} \delta x_j \qquad (3.1)$$

where the antisymmetric part of $\partial u_i / \partial x_j$ relates to rotation or vorticity and the symmetric part relates to a pure strain field. Consider a passive tracer $\theta(\underset{\sim}{x}, t)$ which is assumed to obey the following 2-D advection diffusion equation,

$$\frac{D\theta}{Dt} = \kappa \nabla^2 \theta \qquad (3.2)$$

Fig. 3a One of the many fields to which shear-augmented dispersion is relevent. Chlorophyll patterns at the sea-surface just south of Iceland (top left is at 63°15'N 22°50'W). The domain is about 200 km wide. White streaks are cloud. Note preponderance of dipoles. Phytoplankton are to some extent a passive tracer but also can undergo rapid growth or decay at rates that depend on nutrient supply, mixed layer depth and their own concentration.

where K is the molecular diffusivity (further discussion is given by Young, et al., 1982).

STEADY SHEAR

A first example is a uniform shear flow, $\underline{u} = (\alpha y, 0)$

(3.2) becomes

$$\frac{\partial \vartheta}{\partial t} + \alpha y \frac{\partial \vartheta}{\partial x} = \kappa \nabla^2 \vartheta \tag{3.3}$$

Take the tracer distribution to be striped, at t = o:

$$\vartheta(\underline{x}, 0) = 1 + \sin kx \tag{3.4}$$

If there is no diffusion ($\kappa = 0$), ϑ is advected, then we define the advected coordinates,

$$\tilde{x} = x - \alpha y t \tag{3.5}$$

and the solution is

$$\vartheta = 1 + \sin k(x - \alpha y t) \tag{3.6}$$

It is noted that the y-component of wavenumber in the Fourier transform of increases as $k \propto t$.

When there is diffusion ($\kappa \neq 0$), we try a solution of the form

$$\vartheta = \varphi(t) \sin k\tilde{x} + 1 \tag{3.7}$$

This gives

$$\frac{\partial \varphi}{\partial t} + \kappa k^2 (1 + \alpha^2 t^2) \varphi = 0 \tag{3.8}$$

Then the solution is

$$\vartheta = \exp\left(-\kappa k^2 \left(t + \tfrac{1}{3}\alpha^2 t^3\right)\right) \sin k\tilde{x} + 1 \tag{3.9}$$

In order to consider the dissipation of tracer variance $\overline{\vartheta^2}$, multiply eq. (3.2) by ϑ and integrate,

$$\frac{\partial}{\partial t} \tfrac{1}{2} \overline{\vartheta^2} = -\kappa \overline{|\nabla \vartheta|^2} \tag{3.10}$$

where the bar indicates an average over space. Now from eq. (9),

$$\overline{|\nabla \vartheta|^2} = k^2 (1 + \alpha^2 t^2) \exp\left(-\kappa k^2 \left(t + \tfrac{1}{3}\alpha^2 t^3\right)\right) \tag{3.11}$$

$\overline{|\nabla \vartheta|^2}$ increases like $1 + \alpha^2 t^2$ until $t \simeq (Kk^2 \alpha^2)^{-1/3}$ as shown in the figure.

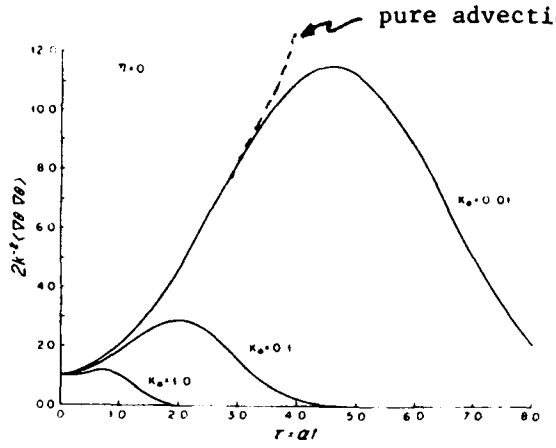

as seen in eq. (3.11), the ordinary diffusion time is $(\kappa k^2)^{-1}$. On the other hand, in the shear flow the increased gradients cause diffusive processes to become important more quickly.

Then the enhanced diffusion time t_* is $(\kappa k^2 \alpha^2)^{-1/3}$, which may be written $t_* = (L^2/\kappa)P^{-2/3} = (L/U)P^{1/3}$ where $\alpha = U/L$, $k = L^{-1}$, and $P = UL/\kappa$, the Peclet number. Thus for typically small κ ($P \gg 1$) shear-augmented diffusion spreads the tracer along streamlines over a time intermediate between the diffusion time L^2/κ and the advection time, L/U. If the streamlines close upon themselves to form a 'gyre' this process acts to replace the initial values $\vartheta_0(x)$ by a distribution $\bar{\vartheta}(\psi)$ which is the (generalized) average of ϑ_0 about streamlines ψ. If $\bar{\vartheta}'(\psi) \neq 0$, a second, slow stage of adjustment occurs as diffusion of the tracer (locked to the ψ - contours by the fast process) occurs, over times $\sim L^2/\kappa$. Under the right boundary conditions the result is the eventual expulsion of gradients of ϑ from the gyre. This is known as Prandtl-Batchelor expulsion (see Dr. Young's lecture this volume, page 135).

Now we suppose $\vartheta(\underset{\sim}{x}, 0)$ is

$$\vartheta(x,0) = \int_0^\infty e^{-a^2k^2} \cos kx \, dk = \frac{\sqrt{\pi}}{2a} e^{-x^2/4a^2} \tag{3.12}$$

Then

$$\vartheta(x,t) = \frac{\sqrt{\pi}}{2\tilde{a}} e^{-\tilde{x}^2/4\tilde{a}^2} \tag{3.13}$$

where $\tilde{a}^2 = a^2 + \kappa\left(t + \frac{1}{3}\alpha^2 t^3\right)$

SHEAR OSCILLATORY IN TIME AND SPACE

We consider the second example of the diffusion problem in the shear flow which oscillates in time and space. Then we suppose that

$$\underline{u} = (u_0 \cos my \cos \omega t, 0) \tag{3.14}$$

Initial condition is as follows;

$$\vartheta(\underline{x}, 0) = \vartheta_0(x) \tag{3.15}$$

where ϑ_0 decreases to zero as $|\underline{x}| \to \infty$.

Define the nth moment by

$$\langle x^n \vartheta \rangle = \int_{-\infty}^{\infty} x^n \vartheta \, dx \tag{3.16}$$

then we have

$$\langle \vartheta \rangle_t = \kappa \langle \vartheta \rangle_{yy} \tag{3.17}$$

$$\langle x\vartheta \rangle_t = \kappa \langle x\vartheta \rangle_{yy} + u \langle \vartheta \rangle \tag{3.18}$$

$$\langle x^2\vartheta \rangle_t = \kappa \langle x^2\vartheta \rangle_{yy} + 2u \langle x\vartheta \rangle + 2\kappa \langle \vartheta \rangle \tag{3.19}$$

and so on.

From eq. (3.17), we get

$$\langle \vartheta \rangle = \text{constant} \tag{3.20}$$

Then (3.18) gives

$$\langle x\vartheta \rangle_t - \kappa \langle x\vartheta \rangle_{yy} = u_0 \langle \vartheta \rangle \cos my \cos \omega t \tag{3.21}$$

The solution is

$$\langle x\vartheta \rangle / \langle \vartheta \rangle = \frac{u_0}{\omega} \frac{1}{(1+\kappa_*^2)} \cos my \, (\kappa_* \cos \omega t + \sin \omega t) \tag{3.22}$$

+ exponentially decaying transient,

where $\kappa_* = \kappa m^2/\omega$ is the ratio of the diffusion time based on the y-scale of the shear to the time of the shear.

The second moment, which expresses the effective diffusion, is determined by (3.19),

$$\langle x^2\vartheta\rangle_t - \kappa\langle x^2\vartheta\rangle_{yy} = 2\langle\vartheta\rangle \frac{u_0^2}{\omega}\frac{1}{1+\kappa_*^2}\cos^2 my\cos\omega t\,[\kappa_*\cos\omega t + \sin\omega t] + 2\kappa\langle\vartheta\rangle \tag{3.23}$$

Now we consider a y and t averaged quantity $\overline{\langle x^2\vartheta\rangle}$, then from (3.23)

$$\frac{\overline{\langle x^2\vartheta\rangle}}{\langle\vartheta\rangle} = \left[\frac{1}{2}\frac{u_0^2}{\omega}\frac{\kappa_*}{1+\kappa_*^2} + 2\kappa\right]t \tag{3.24}$$

Eq. (3.24) shows that the effective diffusivity is

$$\kappa_{eff} = \kappa + \frac{1}{4}\frac{u_0^2}{\omega}\left(\frac{\kappa_*}{1+\kappa_*^2}\right) \tag{3.25}$$

Effective diffusivity is as follows in the special case

$$\kappa_* \ll 1 \qquad \kappa_{eff} = \kappa + \frac{1}{4}\frac{u_0^2}{\omega}\frac{\kappa m^2}{\omega} \tag{3.26a}$$

$$\kappa_* = 1 \qquad \kappa_{eff} = \kappa + \frac{1}{8}\frac{u_0^2}{\omega} \tag{3.26b}$$

$$\kappa_* \gg 1 \qquad \kappa_{eff} = \kappa + \frac{1}{4}\frac{u_0^2}{\kappa m^2} \tag{3.26c}$$

The maximum of κ_{eff} occurs at $\kappa_* = 1$ for a given velocity field. When $\kappa_* = 1$, the effective diffusivity is the product of a particle excursion (U_o/ω) and a particle velocity U_o, which is rather like a mixing length result. If $\kappa_* \gg 1$ we recover the inverse dependence of κ as Taylor (1953).

STEADY STRAIN

As the third example we consider diffusion in a strain field (Batchelor, 1959)

$$(u,v) = (\gamma x, -\gamma y) \tag{3.27}$$

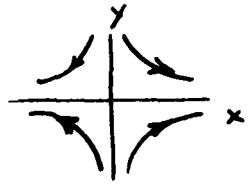

Then the advection-diffusion equation (3.2) becomes

$$\frac{\partial\vartheta}{\partial t} + \gamma x\frac{\partial\vartheta}{\partial x} - \gamma y\frac{\partial\vartheta}{\partial y} = \kappa\nabla^2\vartheta \tag{3.28}$$

A particle initially at (x_0, y_0) moves to $(x_0 e^{\gamma t}, y_0 e^{-\gamma t})$

It is noted that one-particle diffusivity is

$$\frac{d}{dt}\left(\frac{1}{2}\left((x-x_0)^2+(y-y_0)^2\right)\right) = \gamma x_0^2 e^{2\gamma t} \tag{3.29}$$

Take the initial distribution as follows

$$\vartheta(\underset{\sim}{x},0) = \cos kx \cos my \tag{3.30}$$

The advective solution for $\kappa = 0$ is

$$\vartheta = \cos\left(k e^{-\gamma t} x\right)\cos\left(m e^{\gamma t} y\right) \equiv \vartheta_a \tag{3.31}$$

and the full solution, for $\kappa \neq 0$, is

$$\vartheta = \exp\left(\frac{\kappa}{2\gamma}\left\{k^2\left(e^{-2\gamma t}-1\right) - m^2\left(e^{2\gamma t}-1\right)\right\}\right)\vartheta_a \tag{3.32}$$

for long time

$$\vartheta \to \exp\left(-\frac{\kappa m^2}{2\gamma} e^{2\gamma t}\right)\vartheta_a \qquad t\to\infty \tag{3.33}$$

If k = m,

$$\overline{|\nabla\vartheta|^2} = \frac{1}{2}k^2\cosh(2\gamma t)\exp\left(-\frac{2\kappa k^2}{\gamma}\sinh 2\gamma t\right) \tag{3.34}$$

The dissipation time t_* in this case is given by

$$2\gamma t_* = \ln\frac{\gamma}{2\kappa k^2} \tag{3.35}$$

Note the qualitative difference between the behavior in shear and strain fields. A stripe of tracer in a steady shear increases its length like t by shear, and its width like $t^{1/2}$ by diffusion.* Then its area grows like $t^{3/2}$ and hence its peak concentration decays like $t^{-3/2}$. On the other hand, in a strain field, the x-width of a single stripe grows eventually like $e^{\gamma t}$. The y-width approaches a constant $\sim (\kappa/\gamma)^{1/2}$. Then concentration ϑ decreases like $e^{-\gamma t}$.

* Note: the x-width of the stripe $\sim t^{3/2}$ while its y-width $\sim$ const.

MARKOV MODEL OF VELOCITY FIELD

Finally, we consider tracer dispersion by taking patterns of large-scale shear and strain, and adding random time-dependence (Salmon, 1980). Then we introduce the following flow field,

$$\psi = \tfrac{1}{2} J_0(t)(x^2+y^2) + \tfrac{1}{2} S_0(t)(x^2-y^2) + \sigma_0(t)\, xy \tag{3.36}$$

where J_0 is the vorticity and So and σ_0 the strain rates. The model is a reasonable idealization of geostrophic turbulence, which has a very steep wavenumber spectrum and non-local interactions. We consider a white noise process.

$$\langle J_0(t)\, J_0(t') \rangle = 2 D_J \delta(t-t') \tag{3.37}$$

$$\langle S_0(t)\, S_0(t') \rangle = \langle \sigma_0(t)\, \sigma_0(t') \rangle = 2 D_S \delta(t-t') \tag{3.38}$$

If ψ is isotropic then J_0, S_0 and σ_0 are independent and

$$D_J = 2 D_S = \pi \Omega \tag{3.39}$$

where $\Omega = \int_0^\infty k^2 E(k)\, dk$ is the total enstrophy.

Define the initial condition as

$$\theta(\underset{\sim}{x}, 0) = e^{i \underset{\sim}{k} \cdot \underset{\sim}{x}} \tag{3.40}$$

For $\kappa = 0$ distortion equations are

$$\frac{dk_j}{dt} = - k_i A_{ij} \tag{3.41}$$

where $A_{ij} = \partial u_i / \partial x_j$. A line element $\underset{\sim}{r}$ similarly obeys

$$\frac{dr_i}{dt} = A_{ij} r_j \tag{3.42}$$

It is noted that

$$\frac{d}{dt}(\underset{\sim}{r} \cdot \underset{\sim}{k}) = 0 \tag{3.43}$$

From (3.36), (3.41),

$$\frac{dk_1}{dt} = - S_0 k_2 + \sigma_0 k_1 - J_0 k_2$$

$$\frac{dk_2}{dt} = - S_0 k_1 - \sigma_0 k_2 + J_0 k_1$$

This system leads to a Fokker-Plank equation for the joint probability density $f(k_1, k_2, t)$ of the wavevector,

$$\frac{\partial}{\partial t} f(k,\gamma,t) = D_s k^{-1} \frac{\partial}{\partial k}\left(k^3 \frac{\partial f}{\partial k}\right) + (D_s + D_s)\frac{\partial^2 f}{\partial \gamma^2} \qquad (3.44)$$

where k, γ are polar coordinates, $\underset{\sim}{k} = k(\cos\gamma, \sin\gamma)$.

The moments $k_n = \int_0^{2\pi} d\gamma \int_0^{\infty} k\,dk\, k^n f$ are found by forming $\int k^n (3.44)\, dk$:

$$k_0 = 1, \quad k_1 = \exp(3D_s t), \quad k_2 = \exp(8 D_s \tau)$$

Also $\overline{(k-k_1)^2} = k_2^2 - k_1^2 = \exp(16 D_s t) - \exp(6 D_s t)$.

The process is not like diffusion but more like an exponentially rapid cascade to small scale. It is noted that two steady solutions exist

$$f = 1, \quad f \sim k^{-2} \quad (\text{i.e. } F \equiv 2\pi k f = 2\pi k^{-1})$$

corresponding to equipartion of variance, and the "k^{-1}" spectrum of a passive scalar in an inertial range of turbulence, respectively. Yet here the model (large-scale strain) is diametrically opposite the local-in-k presumption of inertial range theory.

This result motivates yet a simpler problem

$$\frac{dx}{dt} = \alpha(t)\, x$$

Let $y = \ln x$, then

$$\frac{dy}{dt} = \alpha(t)$$

The Fokker-Plank equation governing the probability distribution P(y) is

$$\frac{\partial P}{\partial \tau} = D \frac{\partial^2 P}{\partial y^2}$$

where $2D = \int_0^{\tau} \langle \alpha(t')\alpha(t'+\tau)\rangle d\tau$. The solution for the point source is

$$P(y,t) = \frac{1}{\sqrt{2\pi}\sigma} \exp(-|y-y_0|^2/2\sigma^2)$$

where $\sigma^2 = t\int_0^t \langle \alpha(t')\alpha(t'+\tau)\rangle d\tau$. The expression for $P(x,t)$ is log-normal,

$$P(x,t) = \frac{1}{\sqrt{2\pi}\sigma x} e^{-[(\ln x - \ln x_0)^2/2\sigma^2]}$$

REFERENCES

Batchelor, G.K. 1959. Small-scale variation of convected quantities like temperature in turbulent fluid. Part 1. General discussion and the case of small conductivity. J. Fluid Mech., 5, 113-133.

Salmon, R. 1980. Baroclinic instability and geostrophic turbulence. Geophys. Astrophys. Fluid Dynamics, 15, 167-211.

Taylor, G.I. 1953. Dispersion of soluble matter in solvent flowing slowly through a tube. Proc. Royal Soc. London, 219, 186-203.

Young, W., P. Rhines, and C.J.R. Garrett, 1982. Shear-flow dispersion. J. Phys. Oceanog. 12, 515-527.

NOTES SUBMITTED BY
Masaaki Takahashi
Mark Swenson

IV. MORE ABOUT DYE AND PARTICLES

Peter B. Rhines

Wave Crests

Wave crests can behave like stripes of dye.

Consider a wave with intrinsic dispersion relation, $\Omega = \Omega(\underline{k}, \underline{x})$

Add doppler shift of advecting flow $\underline{U}$, $\omega = \Omega + \underline{U} \cdot \underline{k}$

Using geometrical optics, the equations for position and wave-number are:

$$\frac{dx_i}{dt} = \frac{\partial \Omega}{\partial k_i} + U_i$$

$$\frac{\partial k_i}{\partial t} + \left(\frac{\partial \Omega}{\partial k_j} + U_j\right)\frac{\partial k_i}{\partial x_j} = -\frac{\partial \Omega}{\partial x_i} - k_j \frac{\partial U_j}{\partial x_i}$$

Note that for small group velocity $\left(\frac{\partial}{\partial k_j} + U_j\right)$ wave crests behave like a passive scalar in a shear flow.

Exercise

Consider surface gravity waves with dispersion relation

$$\omega = g^{1/2}(k^2 + l^2)^{1/4} + Vl$$

where $V = \alpha y$. There is a weak vertical velocity present, but it can be ignored here. Use the ray-tracing equations (*) above to solve for $\underset{\sim}{k}(t)$ and $\underset{\sim}{X}(t)$ for a wave packet released at $y_o = 0$ ($y = 0$ is a stagnation point of the flow). Show that the wave packet motion reverses from two effects: increasing mean flow as y increases, and reduction of C_g. Show that the packet turns around where the current velocity = 1/2 (initial group velocity).

Effects of Adding 3rd Dimension

In a stably stratified ocean, fluid motion is predominantly along surfaces of constant density. This is the justification for working in only two dimensions. However, even a weak vertical diffusivity, K_z, may be important in the presence of large vertical shears.

Consider, for example, the Okubo-Taylor problem from the second lecture rotated into the x-z plane. Now

$$U = \cos MZ \cos \omega t$$

and because the energy spectrum is dominated by inertial oscillations let $\omega = f$. This velocity structure, combined with nonzero K_z will lead to tracer dispersion, even if $K_x = K_y = 0$.

The presence of vertical shear is also important in interpreting observations. Drifters, for example, have parachute drogues that hang about 100 m beneath the surface. Shear between the surface and 100 m will cause the drogue lines to deviate from the vertical. Lines with different slopes will cause their drifters to sample the flow at different levels, and thus move in different directions. This leads to a sort of "instrumental Stokes drift" for the dispersion of floats.

Shear dispersion will also contribute to the spreading of dye patches, especially in shallow water.

Consider the dispersion of a tracer from an Eulerian viewpoint. Mixing is along isopycnals, but isopycnals undulate, and measurements made at fixed Z will sample different density levels at different times.

Measure $\vartheta(x,t)$ and the Eulerian velocity $u^E(x,t)$. The time averaged flux of tracer is typically written

$$\overline{\vartheta \underset{\sim}{u}}^t = \bar{\vartheta}^t \bar{\underset{\sim}{u}}^t + \overline{\vartheta' \underset{\sim}{u}'}^t$$

This is the "horizontal" flux along a potential density surface only if isopycnal layers are rigid. But mesoscale eddies cause undulations of $\gtrsim$ 100 m amplitude.

To do the bookkeeping correctly at fixed (x,y) it is necessary to keep track of variations in layer thickness. Thus the tracer flux in a layer between two isopycnal surfaces is

$$\overline{h \vartheta \underset{\sim}{u}} = \underset{①}{\bar{h}\,\bar{\vartheta}\,\bar{\underset{\sim}{u}}} + \underset{②}{\bar{\underset{\sim}{u}}\,\overline{h'\vartheta'}} + \underset{③}{\bar{\vartheta}\,\overline{h'\underset{\sim}{u}'}} + \underset{④}{\bar{h}\,\overline{\underset{\sim}{u}'\vartheta'}} + \underset{⑤}{\overline{\underset{\sim}{u}'h'\vartheta'}}$$

where h is the layer thickness and the overbar represents a time average within the thin layer. See figure 3b.

The term $\overline{\theta}\,\overline{h'\underset{\sim}{u}'}$ is a Stokes correction to the mean transport $\overline{h}\,\overline{\theta}\,\overline{\underset{\sim}{u}}$. $\overline{h}\,\overline{\underset{\sim}{u}'\theta'}$ is the standard isopycnal mixing term, representing the eddy flux of tracer variations as seen on an isopycnal sheet of fluid with zero thickness in the vertical. The two remaining terms tend to be smaller if $h' \ll \overline{h}$.

The point is that the standard isopycnal mixing term is only one of five terms in the transport formula. The Stokes correction term could be large if there were systematic motion of boluses of fluid at some level. In this case transport would depend on large vertical gradients of the mean concentration. It would thus behave like an off-diagonal diffusivity, lateral transports resulting from vertical gradients. This 'bookkeeping' is related to the transformed-Eulerian mean equations now being developed in meteorology (see Andrews' lectures, this volume, page 99).

Particle Transport

The Lagrangian displacement vector of a fluid particle is

$$\underset{\sim}{x}^L(t \mid \underset{\sim}{x}^o, t^o)$$

where t is time, and $\underset{\sim}{x}^o$ and t^o are the position and time of particle release.

$\langle \underset{\sim}{x}^L \rangle$ is the average position of an ensemble of particles. In practice this ensemble average is achieved by releasing particles from a point at several times. This gives a valid ensemble average only if the ocean is statistically stationary (or nearly so) and if the release intervals are long compared to the characteristic time-scale of the meso-scale eddies.

The probability density for locating a particle at time t and position X is

$$P(\underset{\sim}{x}, t \mid \underset{\sim}{x}^o, t^o)$$

and

$$\langle \underset{\sim}{x}^L \rangle = \int \underset{\sim}{x}\, P(\underset{\sim}{x}, t \mid \underset{\sim}{x}^o, t^o)\, d\underset{\sim}{x}$$

$$\langle \underset{\sim}{u}^L \rangle = \frac{d}{dt} \langle \underset{\sim}{x}^L \rangle$$

$$= \int \underset{\sim}{x}\, \frac{\partial P(\underset{\sim}{x}, t \mid \underset{\sim}{x}^o, t^o)}{\partial t}\, d\underset{\sim}{x}$$

The Lagrangian mean velocity $\langle \underset{\sim}{u}^L \rangle$ is not adequate measure of tracer motion, because dispersion about the mean is large. In the ocean the kinetic energy of the eddies is generally at least as large as that of the mean flow.

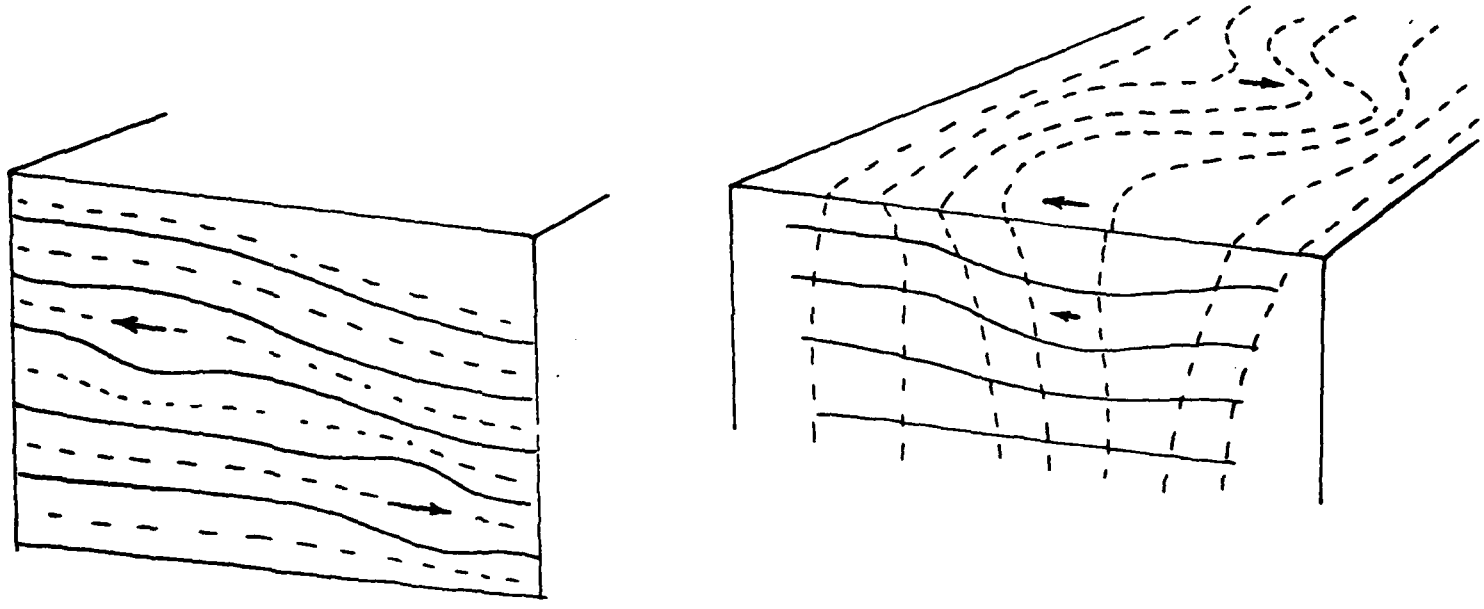

Figure 3b: Two extreme examples of eddy transport of a tracer, S (whose isopleths are dashed). The isopycnal surfaces are solid curves. Left: S is highly correlated with ρ, so that the transport involves term ③ in which thickness and velocity are correlated. Right: S has large horizontal gradients, and is transported by 'isopycnal mixing' involving correlation of S' and horizontal velocity, term ④. Velocity indicated by arrows.

Lagrangian Diffusivity

The Lagrangian diffusivity

$$K_{ij}(t|\underset{\sim}{x}^o,t^o) = \langle u_i^L(t|\ldots)(x_j^L - x_j^{Lo})\rangle$$

where $\underset{\sim}{U}^L$ is the Lagrangian velocity, $\underset{\sim}{X}^L$ the particle displacement, and $\underset{\sim}{X}^o$ the position of the particle at time t = 0.

For simplicity let $\underset{\sim}{X}^o = 0$.

Then $$\frac{d}{dt}\langle x_i^L x_j^L\rangle = K_{ij} + K_{ji}$$

Now $$K_{ij}(t|\underset{\sim}{x}^o) = \int_{t^o}^{t} R_{ji}(\tau)\,d\tau$$

where $R_{ji}(\tau)$ is the covariance of particle velocities separated by time interval τ,

$$R_{ji}(\tau) = \langle u_j^L(t)\, u_i^L(t+\tau)\rangle$$

R_{ji} is assumed to be stationary in time (i.e., it does not depend on t). This implies, however, that the Eulerian fields are spatially homogeneous. Otherwise over time a particle could wander into a region of different kinetic energy, say, which would change $R_{ji}(\tau)$.

In the limit $t - t^o \to 0$ the Lagrangian statistics converge to the Eulerian statistics:

$$\langle \underset{\sim}{u}^L\rangle \to \overline{\underset{\sim}{u}^E(\underset{\sim}{x}^o,t)}^t$$

Velocity correlations will decrease with time. The area under the curve $R_{ij}(\tau)$ can be viewed as the Lagrangian diffusivity.

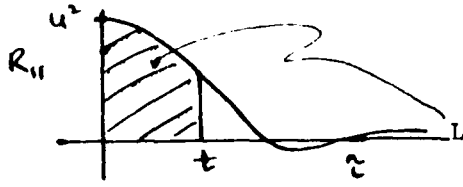

Lagrangian diffusivity

K_{ij} can be split into symmetric and antisymmetric parts.

$$K_{ij} = S_{ij} + A_{ij}$$

where $S_{ij} = 1/2\,(K_{ij} + K_{ji})$ symmetric part
and $A_{ij} = 1/2\,(K_{ij} - K_{ji})$ antisymmetric part.
The trace $S_{ii} = \frac{1}{2}\frac{d}{dt}\langle x_i^L x_i^L\rangle$

The antisymmetric part, A_{ij}, is associated with $\langle u_i^L x_j^L - u_j^L x_i^L\rangle$, the "swirl" of the fluid particles. This is equal to minus the ensemble angular momentum, $\hat{\underset{\sim}{z}} \cdot \underset{\sim}{X}^L \times \underset{\sim}{u}$.

The mean square particle dispersion

$$\langle |\underset{\sim}{x}^L|^2 \rangle = 2 \int_0^\tau \int_0^{\tau'} R_{ii}(\tau)\, d\tau\, dt'$$

$$= 2 \int_0^t (t-t') R_{ii}(t')\, dt'$$

For short times R_{ii} is approximately constant, and

$$\langle |\underset{\sim}{x}|^2 \rangle \simeq t^2 R_{ii}(0) = t^2 \langle |\underset{\sim}{u}|^2 \rangle$$

In other words, for short times decorrelation has not occurred, and ensemble particle dispersion is linear in time.

For long times

$$\langle |\underset{\sim}{x}|^2 \rangle \simeq 2t \int_0^\infty R_{ii}(\tau)\, d\tau \longleftarrow \text{(random walk)}$$

$$- 2 \int_0^\infty t' R_{ii}(t')\, dt'$$

Typically one expects $\int_0^\infty R_{ii}(\tau)\, d\tau \longrightarrow$ a constant. But for a saturated wave field this constant is zero. This is also the case in a closed box, where dispersion is limited.

Typically particle dispersion follows this sequence:

1) Linear dispersion at short time $\langle |\underset{\sim}{x}^L| \rangle \sim t$,
2) Parabolic or random walk dispersion at long times $\langle |\underset{\sim}{x}| \rangle \sim t^{1/2}$, possibly followed by
3) saturation $\langle |\underset{\sim}{x}| \rangle \sim$ constant.

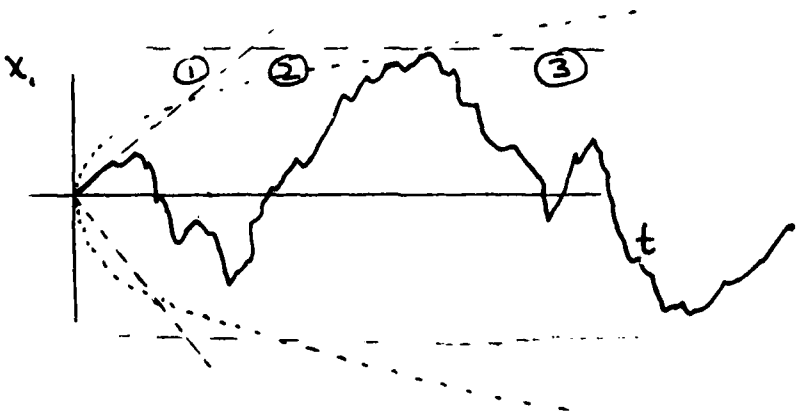

Envelope of Particle Dispersion

Note: In realistic flows there may be several stages of saturation as the ensemble of particles fills out successively larger domains of flow, such as the nested set of gyres one finds in the oceans.

If there is a mean flow, as well as turbulence, the picture will be tilted relative to the axes, and the particle envelope will move linearly away from X^o. Observational examples of this dispersion envelope are shown in Figure 4, from experiments involving neutrally buoyant floats.

The time for the mean flow to emerge from the turbulent dispersion is:

$$t > \Delta t \left(\frac{u'}{\bar{u}^L}\right)^2$$

where

$$\Delta t = \int_0^{\infty} R_{ii}(\tau)\, d\tau \;/\; R_{ii}(0)$$

Note: The interpretation of Taylor's diffusivity is difficult if a curved, sheared mean flow is present. How does one separate eddy- and mean- ? Shear dispersion intermingles the two.

Note that the Lagrangian energy spectrum is defined by

$$\mathcal{E}^L_{ij}(\omega) = \int_0^{\infty} R_{ij}(\tau) \cos\omega\tau \, d\tau$$

In the zero frequency limit,

$$\lim_{\omega \to 0} \mathcal{E}^L_{ij}(\omega) = \int_0^{\infty} R_{ij}(\tau)\, d\tau$$

which is the Lagrangian diffusivity.

Stokes Drift

The Stokes drift may be defined by the difference between the Eularian and Lagrangian mean velocities, $\langle \underset{\sim}{U}^L \rangle - \langle \underset{\sim}{U}^E \rangle$. A Taylor expansion gives

$$\langle \underset{\sim}{u}^L \rangle = \langle \underset{\sim}{u}^E \rangle + \langle \underset{\sim}{x}^L \cdot \nabla \underset{\sim}{u}^E \rangle + \ldots .$$

for displacements small relative to the scale of $\underset{\sim}{U}^E$. In this quasihomogeneous limit $\underset{\sim}{x}^L(t/x_o, to)$ may be approximated as a weak function of $\underset{\sim}{x}$, and a strong function of $\underset{\sim}{x}-\underset{\sim}{x}_o$.

But

$$\langle \underset{\sim}{x}^L \rangle = \langle \int \underset{\sim}{u}^L dt \rangle = \langle \int \underset{\sim}{u}^E dt \rangle + \ldots .$$

so the Stokes correction is

$$\langle \underset{\sim}{x}^L \cdot \nabla \underset{\sim}{u}^E \rangle = \left\langle \frac{\partial}{\partial x_j} (X^L_j u_i) \right\rangle - \left\langle u_i \frac{\partial X^L_j}{\partial x^i_j} \right\rangle$$

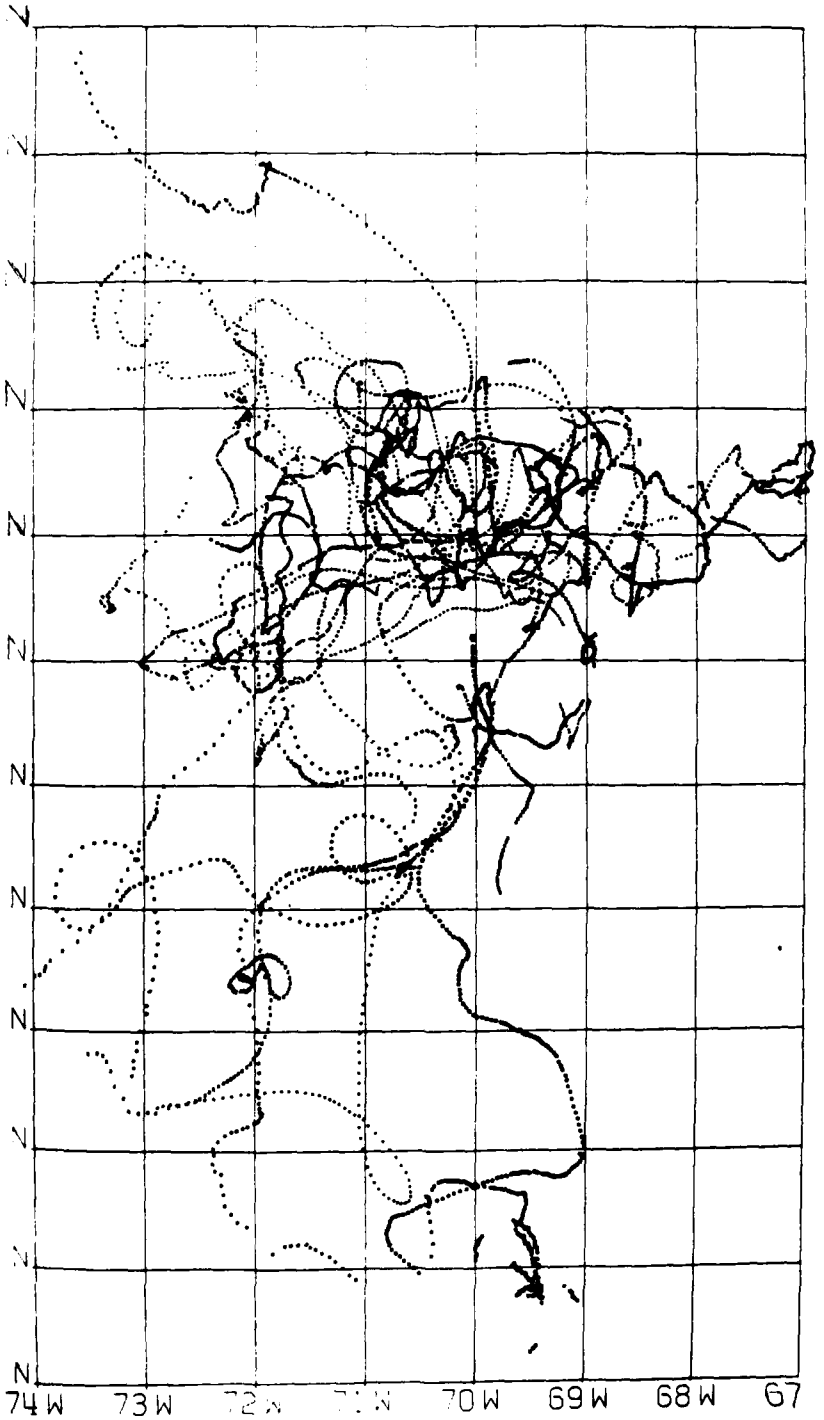

Fig. 4a SOFAR float tracks (daily positions plotted) from the Sargasso Sea in the MODE-73 experiment (from Rossby and Webb). The squares are 1° wide. The floats are nearly Lagrangian particles at depth 1500m.

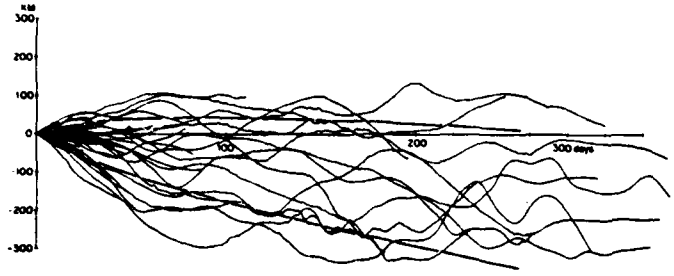

a.

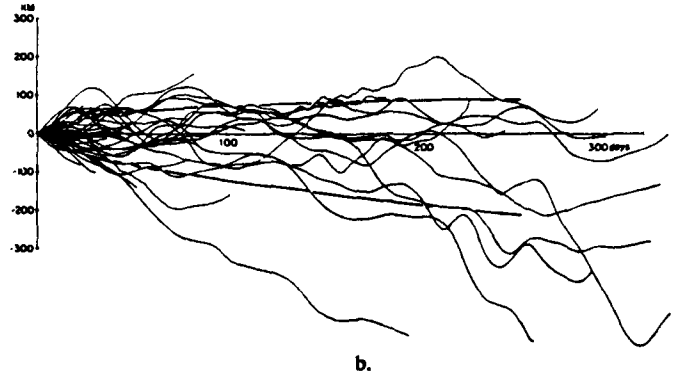

b.

Displacement of floats in E/W and N/S directions, a and b respectively, against time after launch of each float. Bold lines show the expected dispersion (standard deviation about the centre-of-mass) computed by integrating the auto-covariance functions and adding in the mean flow.

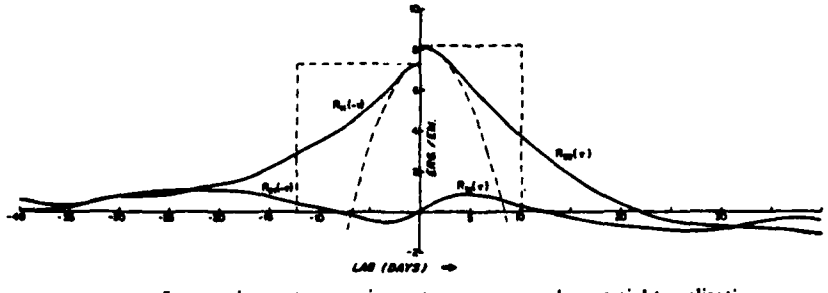

Lagrangian auto-covariance tensor averaged over eight realisations.

Fig 4b x-t and y-t diagrams for these floats and corresponding Lagrangian covariance (as a function of time-lag). From Freeland et al. 1975.

the second term

$$\langle u_i \frac{\partial x_j^L}{\partial x_j} \rangle = \langle u_i \int \frac{\partial u^L}{\partial x_j} d\tau \rangle = \langle u_i \int \frac{\partial u_j^E}{\partial x_j} \rangle + O(a^3)$$

where a is the disturbance amplitude.

For nondivergent flow

$$\frac{\partial u_j^E}{\partial x_j} = 0$$

and so

$$\langle \underset{\sim}{x}^L \cdot \nabla \underset{\sim}{u}^E \rangle = \frac{\partial}{\partial x_j} \langle (X_j^L u_i) \rangle = \frac{\partial \kappa_{ij}}{\partial x_j}$$

to $O(a^3)$

Thus

$$\langle u_i^L \rangle = \langle u_i^E \rangle + \frac{\partial \kappa_{ij}}{\partial x_j} + O(a^3)$$

In a pre-existing mean flow, $\langle \underset{\sim}{U} \rangle$ with curvature there is an additional term of order

$$\frac{\partial^2 \langle U_j \rangle}{\partial x_i \partial x_j}$$

Since $\kappa_{ij} = 0$ at $t = 0$ the Eulerian and Lagrangian velocities are nearly equal for short times.

Example: For surface gravity waves the velocity potential is

$$\phi = a e^{-kz} \cos(kx - \omega t)$$

The principal diffusivity is κ_{XZ}, expressing the orbital angular momentum of the fluid particles.

$$\langle u^L \rangle = \cancel{\langle u^E \rangle}^{0} + \frac{\partial \kappa_{xz}}{\partial z} \qquad = O(a^2)$$

The diffusivity is this large, because for surface gravity waves there is no separatio· between the wave length and the vertical scale over which the intensity varies.

> Note: The validity requires only that the particle displacement be much smaller than the scale of variation of mean quantities. For waves this means small steepness, while for turbulence it requires slight variations in κ_{ij} over an eddy diameter.

In general, the Lagrangian velocity field is divergent:

$$\frac{\partial}{\partial x_i}\left(\frac{\partial K_{ij}}{\partial x_j}\right) \neq 0$$

One simple example is the dispersion of a dye spot in a closed box. After a long time the center of mass of a group of dye particles, $\langle \underset{\sim}{X}^L(t \mid \underset{\sim}{X}^o, \tau^c) \rangle$, will be found near the center of the box. Thus $\langle \underset{\sim}{U}^L \rangle$ will in the mean be towards the center.

Another example is a spot of dye released into an eddy field (say, the planetary boundary layer), near a rigid boundary. If W is the velocity component normal to the boundary,

$$\langle w^E \rangle \equiv 0 \quad \text{but} \quad \langle w^L \rangle > 0$$

i.e., the average vertical velocity of all particles released near the boundary is positive, yet the Eulerian-averaged vertical velocity vanishes.

The correlation between Lagrangian dispersion and eddy activity can be seen by observing ensembles of particle releases in the ocean and in numerical models. For example, Figures 5 through 6 depict particle release patterns from a two-layer eddy-revolving general circulation model of Holland (Holland and Rhines, 1980). The model has three layers, an eastward jet in the center, and two recirculating gyres. Figure 5 illustrates the tendency for particles to remain in their half of the domain. as well as the greater dispersion near the jet than in the recirculating regions. Eventually, the entire lower gyre gets covered. In Figure 6a the Lagrangian velocity is seen to be most clearly defined in the recirculating regions. Figure 6b shows the convergent nature of $\langle \underset{\sim}{U}^L \rangle$ within the gyre.

Figure 7 demonstrates some of the hazards in relying on the Lagrangian mean velocity alone to describe particle dispersion. These are numerical simulations by Russ Davis of particle dispersion in one dimension by turbulence. In the top curve the turbulent energy is spatially homogeneous and the particle distribution is symmetric about the origin. In the lower curve, however, the turbulent kinetic energy increases to the right. Thus particles which initially move to the right experience greater diffusivity than those on the left. generating the long tail on the right side of the distribution.

In the top curve the Lagrangian mean velocity is zero. In the lower curve $\langle U^L \rangle$ is directed to the right since the tail pulls the center of mass of the distribution in that direction. The mode of the distribution, on the other hand, moves to the left. Clearly $\langle U^L \rangle$ alone gives a misleading description of the motion of this particle distribution.

Example: We can tie together some of the ideas of one particle diffusivities, eddy fluxes, and their ambiguity with Lagrangian-mean flow by the following thought problem. Suppose a 2-D incompressible fluid is executing perfect wave motion with particles moving in clockwise circular orbits, $\bar{u}^E = 0$. At t = o a tracer gradient,

$$\theta = \alpha y$$

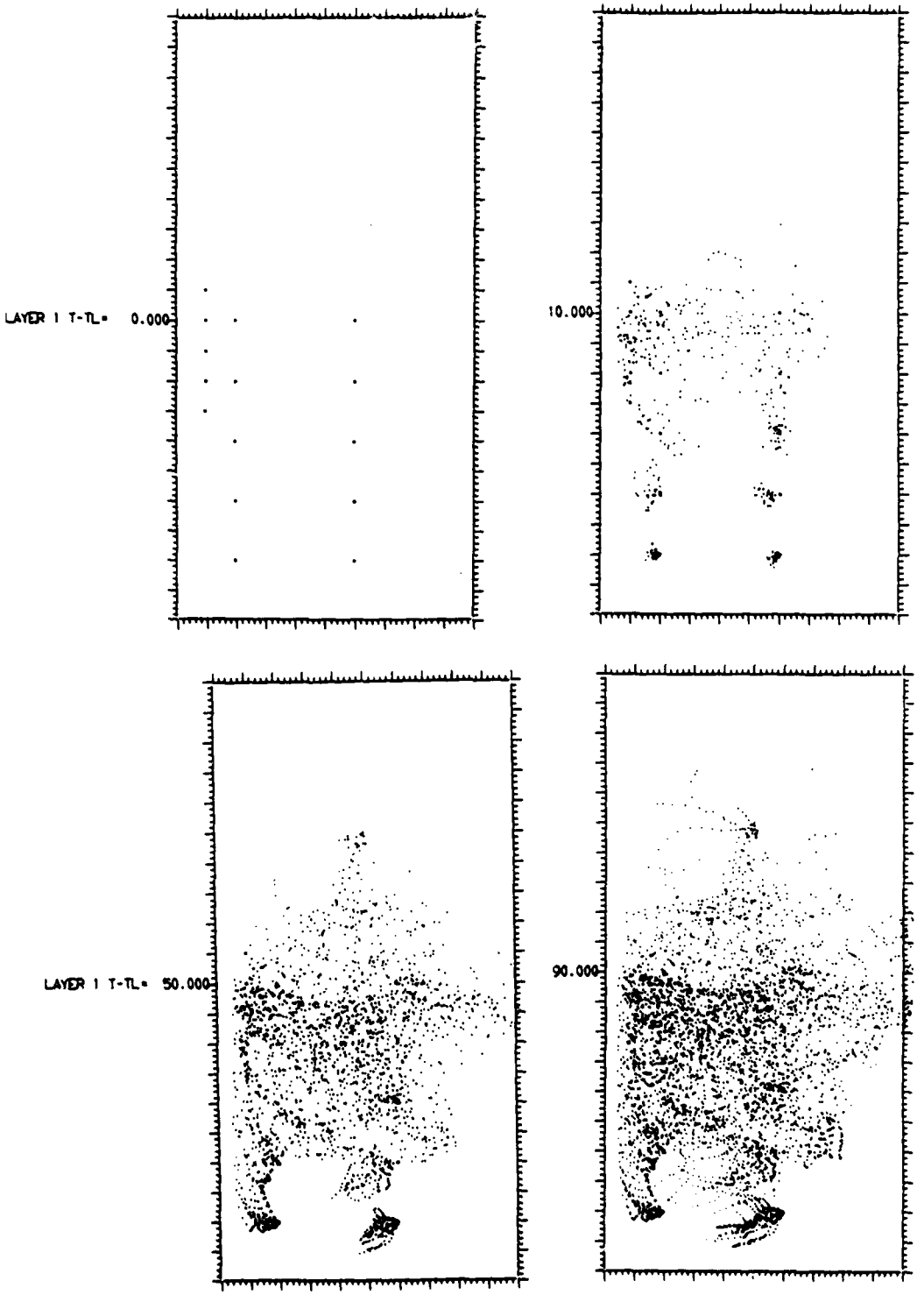

Fig.5 Time-exposure of particle ensembles released in a two-layer wind-driven ocean model of Holland. There are two mean gyres in the upper layer symmetric about the middle latitude. For short times (time in days shown) there is an identifiable mean displacement plus much dispersion. The gyre boundary is evident in the density of occupation of particles. Note that individual realizations of particle clouds can look very different.

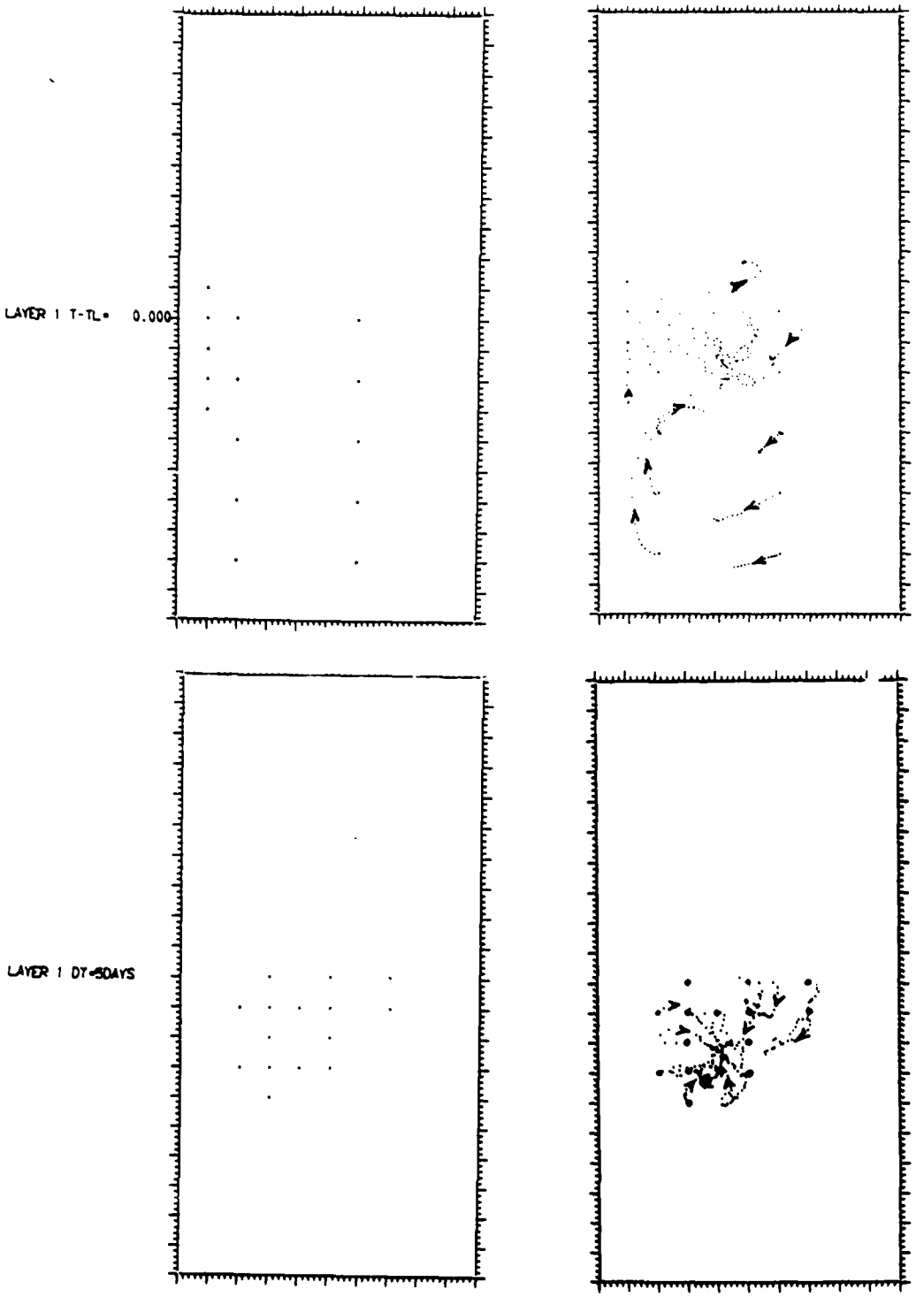

Fig. 6a, 6b

The Lagrangian mean displacement $\langle \underset{\sim}{X}(t;t^{\circ}\ \underset{\sim}{x}^{\circ}) \rangle$ for several release points $\underset{\sim}{x}^{\circ}$. In upper panels the ensemble mean shows the sense of the gyre well but release points in more turbulent regions (lower panels) are dominated by mixing and seek out the centroid of the gyre.

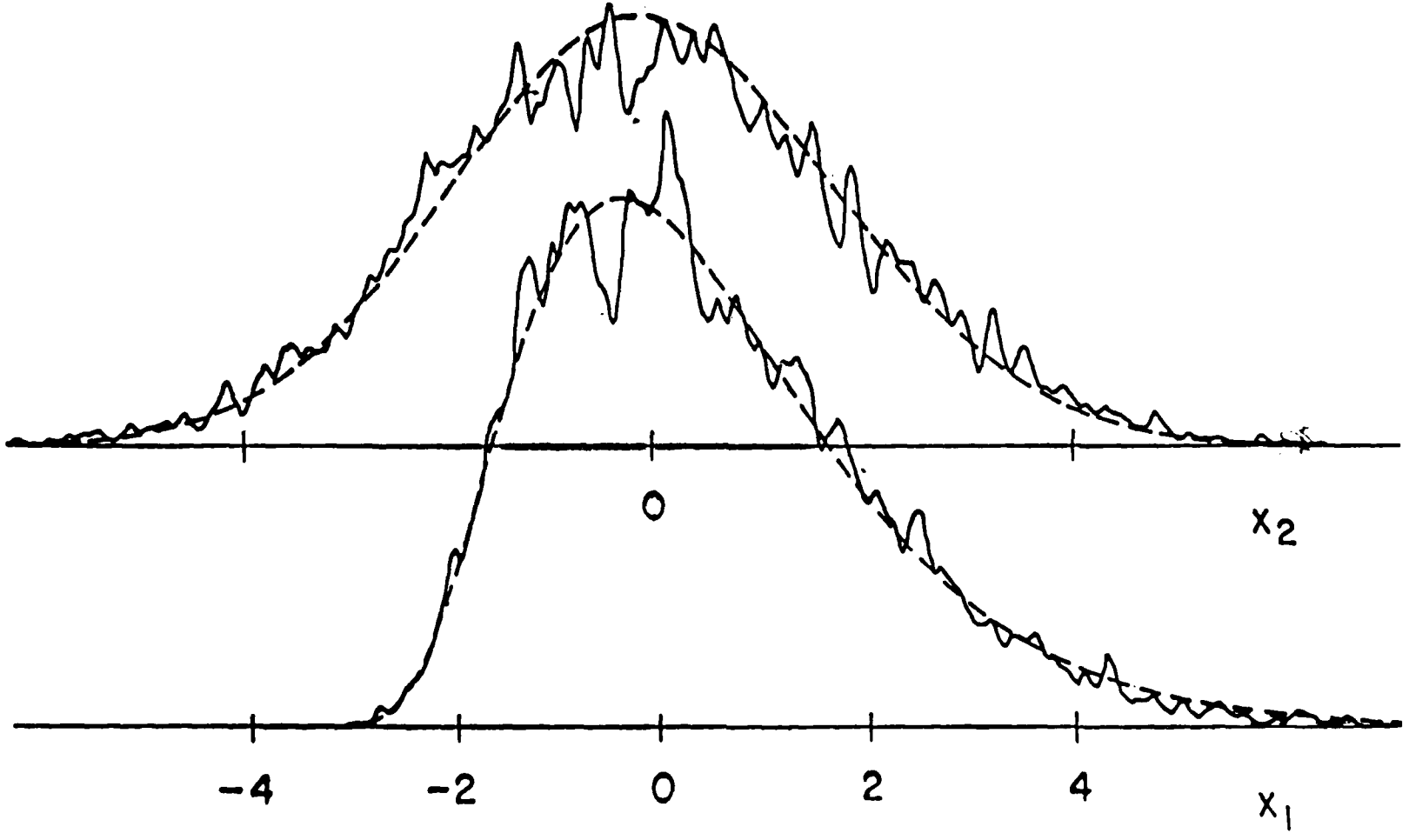

Fig.7 Kinematic simulations of particle dispersal by Dr.R.Davis (Oceanic property transport Lagrangian particle statistics and their prediction. preprint). Upper curve: particle concentration with spatially homogeneous velocity. Lower curve: concentration when the rms velocity increases to the right.

is impressed on the fluid. Notice that a mixing-length calculation would suggest an eddy transport of ϑ in the x-direction:

$$\frac{D\Theta}{Dt} = 0 \; ; \qquad \frac{\partial \bar{\Theta}}{\partial \tau} = - \nabla \cdot \overline{\vartheta' \underline{u}'}$$

where the averaging is, say, with respect to fast time.
Now

$$\vartheta' = -(y'-y_0)\frac{\partial \bar{\vartheta}}{\partial y} \Rightarrow \overline{\vartheta' u'} = -\frac{\partial \bar{\Theta}}{\partial y}\overline{(y'-y_0)u'} = -\alpha K_{xy} < 0$$

near the initial time. Since K_{xy} is just the orbital angular momentum of a particle, the x-transport is nonzero. By drawing a sketch one sees indeed, ϑ' and u' correlated.

Ah, but you say it is a nondivergent flux, hence inconsequential. So, now modify the problem by placing a rigid wall at x = o, where u' vanishes. Let the orbits increase from zero in some manner, to the right of the wall. Now $\overline{\vartheta' u'}$ is divergent, and $\bar{\vartheta}$ changes with time. Yet paradoxically, at lowest order we still seem to have closed orbits and perfect conservation of ϑ following these orbits! To resolve the paradox note the identity

$$\int_0^x \frac{\partial K_{xy}}{\partial x} dx = K_{xy}(x)$$

so that

$$\int_0^x \bar{v}^L dx = K_{xy}(x)$$

using (4.1). Thus the orbits must in fact be slightly open, a Lagrangian drift moves particles toward negative-y, carrying $\bar{\vartheta}$ downgradient via $\partial\bar{\vartheta}/\partial\tau = -\bar{v}^L \partial\bar{\vartheta}/\partial y$. The Eulerian observer instead sees an eddy flux toward negative-x along $\bar{\vartheta}$ contours, and vanishing mean flow, $\partial\bar{\vartheta}/\partial\tau = -\nabla\cdot\overline{\underline{u}'\vartheta'} = \frac{\partial K_{xy}}{\partial x}\frac{\partial\bar{\vartheta}}{\partial y}$
Both agree that

$$\frac{\partial \bar{\vartheta}}{\partial \tau} > 0$$

but the observers differ as to why.

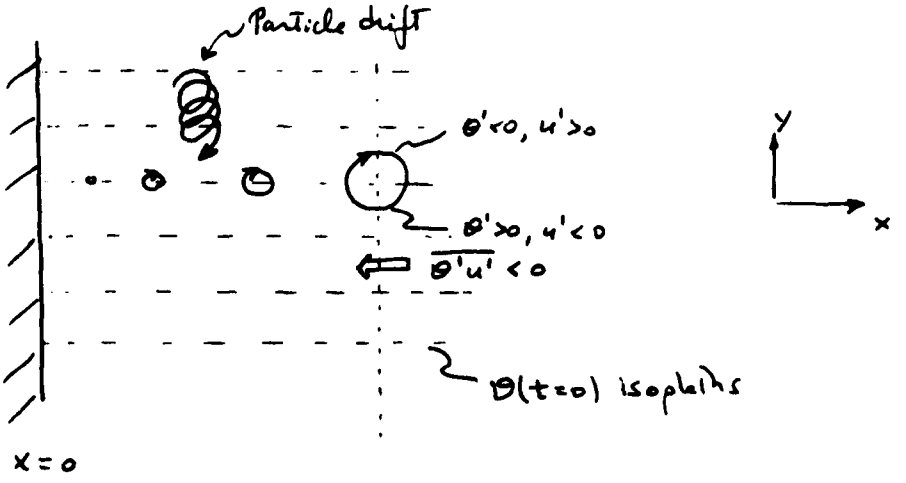

REFERENCES

Holland, W. R. and P. B. Rhines, 1980. An example of eddy-induced circulation. J. Phys. Ocean., 10, 1010-1031.

Taylor, G. I., 1921. Diffusion by continuous movements. Proc. London, Math. Soc., 2, 20, 196-212.

NOTES SUBMITTED BY
Walter Robinson and
Theodore Shepherd

V. RETURN TO DYNAMICS

Peter B. Rhines

Much of the discussion up to this point in the lectures has focused on small-scale structures as turbulence stretches out tracer concentrations, increasing gradients and leading to diffusion (Figure 3). But a significant problem for the oceans concerns large-scale transports and the resulting concentrations of tracers. An example is that of tritium, a by-product of atmospheric nuclear weapons testing that is injected into the ocean at the surface. Following injection, the tritium mixes principally along potential density surfaces below the surface. Depending on the "topography" of these surfaces, the tritium concentrations can take on a variety of forms. Figure 8 shows a set of tritium profiles for different σ_θ surfaces, according to Sarmiento (1982).

QuasiGeostrophic Eddy-Mean Flow Interaction

For an active or passive tracer q, divide into time mean and deviation components $q = \overline{q}^t + q'$. Then the advective-diffusive equation leads to

$$\overline{q'^2}_t + \nabla\cdot\overline{\underline{u}'q'^2} + \overline{\underline{u}'q'}\cdot\nabla\overline{q} = -\overline{\Delta' q'} + \overline{F'q'}$$

where Δ represents dissipation and F forcing. If time mean quantities vary slowly in space, then $\nabla\cdot\overline{u'q'^2}$ is negligible. Then for no external forcing, the principal balance for stationary flow is between down-gradient eddy transport and dissipation:

$$\overline{\underline{u}'q'}\cdot\nabla\overline{q} = -\overline{\Delta' q'}$$

Now introduce a quasigeostrophic, multi-layered fluid. The momentum and potential vorticity equations are, respectively,

$$\frac{\partial}{\partial t}(h_i\underline{u}_i) = -\hat{\underline{z}}\times(h_i q_i \underline{u}_i) - H_i\nabla_H(p + \tfrac{1}{2}|\underline{u}_i|^2) + O(R_o) + \underline{X} - \underline{D}$$

$$\frac{\partial q}{\partial t}_b + \underline{u}_H\cdot\nabla q_b = F - \Delta$$

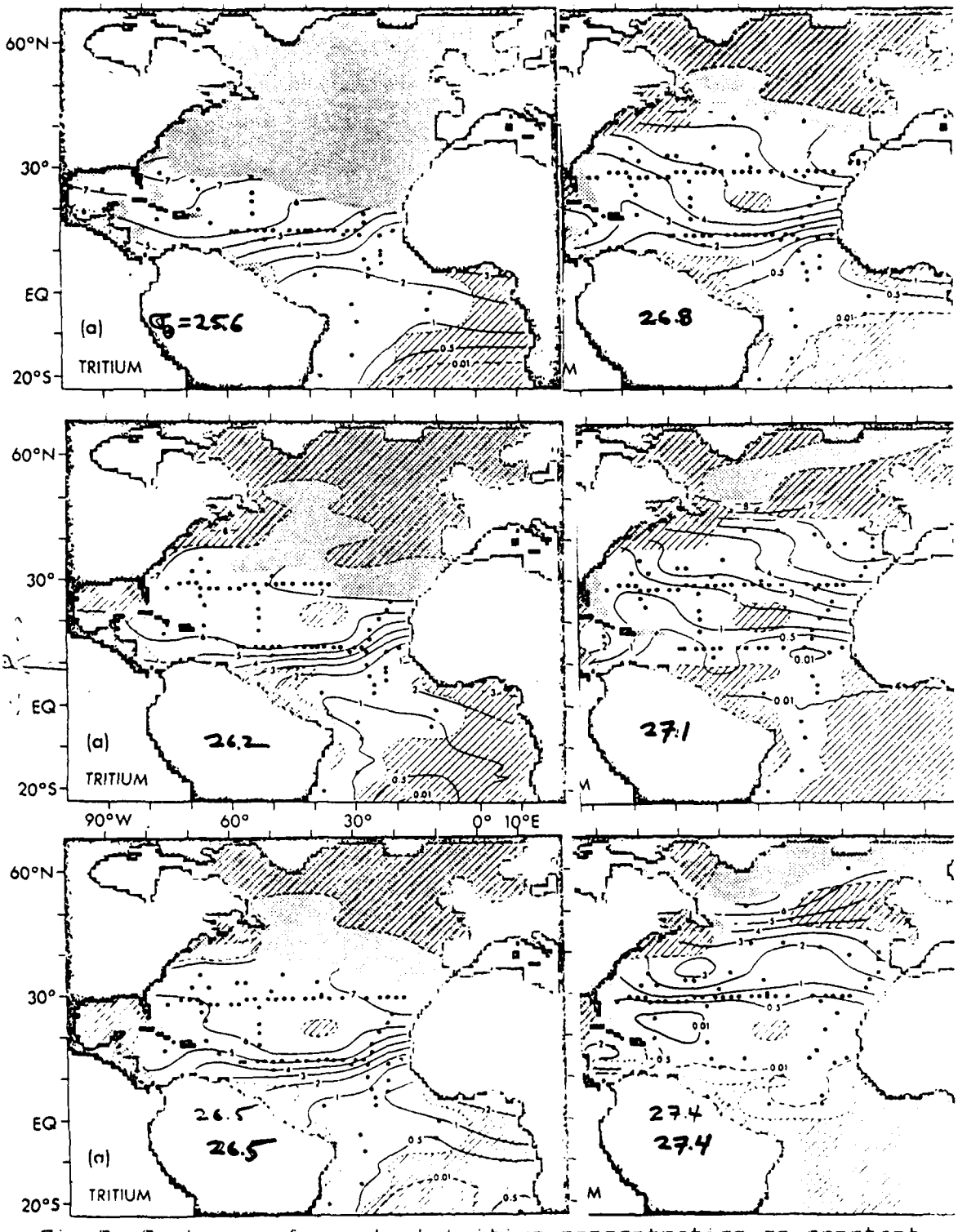

Fig.8 Contours of constant tritium concentration on constant σ_θ surfaces (indicated) according to Sarmiento 1982 based on GEOSECS 1972 data. Concentration is greatest near outcrops (stippled) where the σ_θ surface intersects the sea surface.

where $q = \frac{H_i}{h_i}(J+f)$, $J = \nabla_x \underline{u}|_z$, $h_i = H_i + h_i'$, $\frac{h_i}{H_i} = O(R_o)$. $\hat{\underline{z}}$ is a vertical unit vector, ∇_H the horizontal gradient, and q the potential vorticity in an isopycnal layer of varying thickness, $h_i(x,t)$. $\underline{X}$ and $\underline{F}$ represent external forcing, D and Δ represent dissipation.

After averaging, $\overline{h_i q u}$ is the dominant rotational eddy stress. It can be written as

$$\overline{h_i q \underline{u}} = f\overline{h_i \underline{u}} + H_i \overline{J\underline{u}} - f\overline{h_i' \underline{u}'}$$

where the terms on the right hand side represent, respectively, the net Lagrangian Coriolis force, the lateral Reynolds stress, and wave drag on the level interface. $\underline{u} = (u,v)$ is the horizontal velocity.

Averaging in x leads, in the inviscid, unforced case, to

$$\frac{\partial}{\partial t}\overline{h_i u}^x = \overline{h_i q v}^x$$

while ensemble averaging yields

$$\frac{\partial Q}{\partial t} + \langle \underline{u} \rangle \cdot \nabla Q = -\nabla \cdot \langle q' \underline{u}' \rangle$$

where $q = Q + q'$, $\langle q' \rangle = 0$. The right hand side of the latter equation can be seen as the 3-D, time-dependent response to eddy forcing. Without time dependence (that is, in the statistically steady case), the equation describes what might be called the turbulent 'Sverdrup' balance, with eddies driving fluid across the mean geostrophic contours, Q = constant. Maps of Q are fundamental references, as free flow tends to proceed along Q-contours, forced flow across them.

In order to predict the nature of the eddy stress $\langle q'u' \rangle$ one must consider the following factors:

1) Statistically steady stirring of the mean gradient ∇Q (use mixing-length arguments).
2) Memory loss of q due to the enstrophy cascade.
3) Temporal growth and decay of eddies.
4) Spatially advected growth and decay of eddies.
5) Effect of external forcing, $\underline{F}$.

One can use the Rayleigh damping model, $\frac{Dq}{Dt} = -Rq + F$, to introduce memory loss from dissipation and the enstrophy cascade. If F = 0, then $q \to \overline{q}$. Then

$$\langle q' u_i' \rangle = \frac{\partial Q}{\partial x_k} \int_{-\infty}^{t} \langle u_i(t) u_k^L(t') e^{-R(t-t')} \rangle dt' + \int_{-\infty}^{t} \left\langle \frac{\partial F}{\partial x_j} (\kappa_{ij}(t,-\infty) - \kappa_{ij}(t,t')) e^{-R(t-t')} \right\rangle dt'$$

displacement over one relaxation time.

If F = 0 and $R \ll \underline{L}/u$ = (inertial time scale)$^{-1}$, then $\langle q' u_i' \rangle = -\kappa_{ij} \frac{\partial Q}{\partial x_j}$, where $\kappa_{ij} = \langle u_i(x,t) x_j(t) \rangle$ is the 'arrival' Lagrangian diffusivity and is like Taylor's diffusivity.

Note the difference between ' arrival' and 'departure' statistics. The former considers $x_i^{(o)L}(t^o|\underset{\sim}{x},\tau)$, that is, particles arriving at fixed point x from various origins $x_i^{(o)L}$ while the latter considers $x_i^L(t\,|\,\underset{\sim}{x}^{(o)},t^o)$, that is, particles departing from a fixed release point $\underset{\sim}{x}^{(o)}$. The two Lagrangian velocities can be equal and opposite in the case of motion in a gradient of turbulent energy, for example.

Example:

Mean wake induced by a Rossby-wave packet in a 2-D homogeneous fluid. Expanding in wave steepness with $\nabla Q = (0,\beta)$, gives

$$O(1): \nabla^2\psi_t^{(0)} + \beta\psi_x^{(0)} = 0 \Rightarrow \psi^{(0)} = A(\underset{\sim}{x},\tau)\cos\vartheta \qquad \vartheta = \underset{\sim}{k}\cdot\underset{\sim}{x} - \omega t$$

$$O\left(\frac{\beta L^2}{u}\right): \nabla^2\psi_t^{(1)} + \beta\psi_x^{(1)} = -\nabla\cdot\underset{\sim}{q}^{(o)}\underset{\sim}{u}^{(o)} = -J\left(\psi_1^{(o)}\nabla^2\psi^{(o)}\right)$$

where $\underset{\sim}{u} = \hat{\underset{\sim}{z}}\times\nabla\psi$

The eddy stress is then $\langle\nabla^2\psi^{(o)}\nabla\psi^{(o)}\rangle = \frac{1}{2}\left[\nabla\cdot(\underset{\sim}{k}A^2)\right]\underset{\sim}{k} - \frac{1}{4}|\underset{\sim}{k}|^2\nabla(A^2)$ and this represents the q-transport rotated by $\pi/2$.

For a wave packet, $A^{-1}\nabla A \gg k^{-1}\nabla k$ whence one can write

$$\langle\nabla^2\psi^{(o)}\nabla\psi^{(o)}\rangle = -\nabla\mathcal{E} + \frac{2(\nabla\mathcal{E}\cdot\underset{\sim}{k})\underset{\sim}{k}}{|\underset{\sim}{k}|^2}$$

where $\mathcal{E}$ is the kinetic energy density $\langle\frac{1}{2}|\nabla\psi|^2\rangle$. Note that the eddy stress is the gradient of the kinetic energy density reflected about $\underset{\sim}{k}$.

As the wave packet moves north, fluid is pushed westward as the packet approaches, and pulled to rest as the packet departs. Although the mean flow is ultimately unchanged, low-frequency Rossby waves radiate to the west. Figure 9a gives a schematic picture of the mean flow tendency from the eddy stress; numerical simulation results are shown in Figure 9b, which demonstrate the westward and eastward mean flow induction and the Rossby wave radiation.

An entirely equivalent approach is that using Taylor's diffusivity form,

$$\langle q^{(1)}u_i^{(o)}\rangle = \kappa_{ij}\frac{\partial Q}{\partial x_j} = \kappa_{i2}\beta$$

where the Lagrangian diffusivity of the wave field is

$$\kappa_{ij} = (\omega k)^{-1}\begin{bmatrix} 0 & \partial\mathcal{E}/\partial y' \\ -\frac{\partial\mathcal{E}}{\partial y'} & \frac{k}{\omega}\partial\mathcal{E}/\partial\tau \end{bmatrix}$$

written in 'wave-crest' coordinates (x',y'):

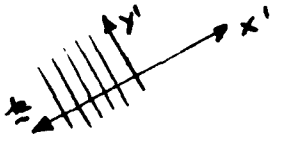

$\kappa_{ij} > 0$ as the wave packet approaches (downgradient mixing) and $\kappa_{ij} < 0$ as the wave packet departs (upgradient mixing). So Lagrangian diffusivities need not represent irreversible mixing. Note that κ_{ij} is traceless, except for

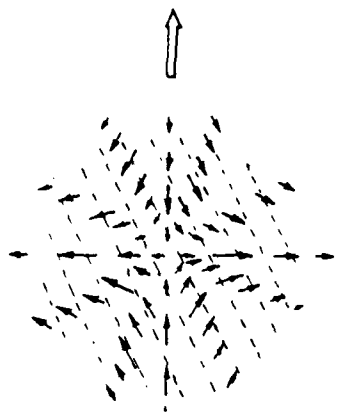

Fig. 9 Above: potential vorticity transport (solid arrows) in a Rossby wave packet traveling north (double arrow is group velocity, wave crests dashed). Below: large-scale flow induced by this transport. The packet is invisibly small on the east side of the induced flow. To the right is shown the zonally averaged zonal flow. The above theory would predict the westward lobe with counterbalancing eastward lobe left behind at the origin of the packet. Here viscosity smears out the wake.

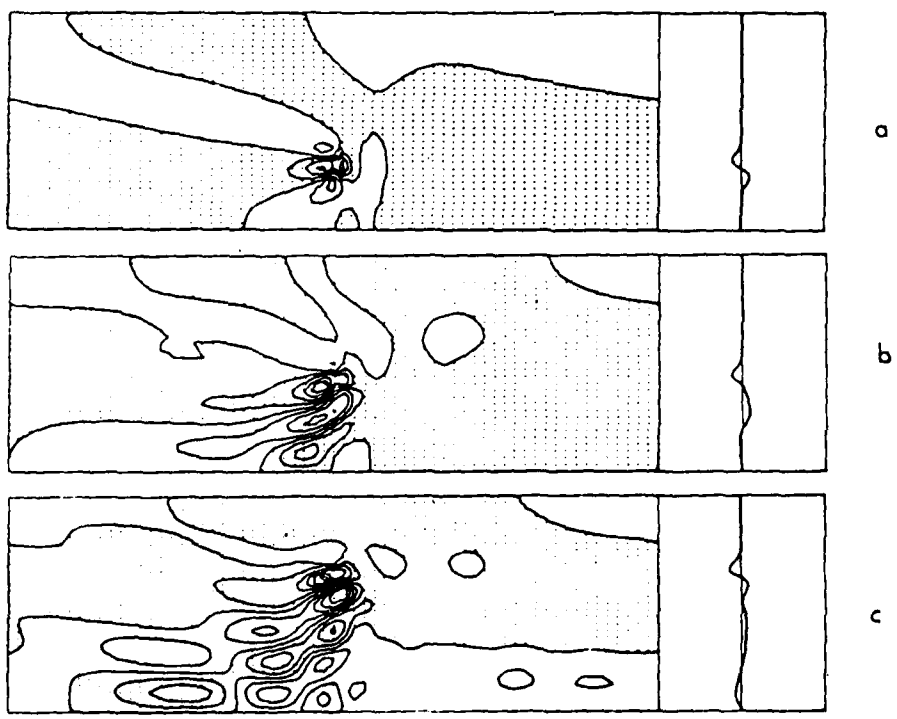

transient situations. The off-diagonal terms describe rotary motion of the particles. Several forms of the induction equation are as follows:

$$\nabla^2\psi_t^{(1)} + \beta\psi_x^{(1)} = -\nabla\cdot(\nabla E\,\vec{\Phi}) = -2\frac{\partial^2 E}{\partial x'\partial y'} = \frac{\partial}{\partial x_i}(\kappa_{ij}\,\partial Q/\partial x_j) = \beta\frac{\partial \kappa_{i2}}{\partial x_i}$$

where $\vec{\Phi}$ indicates rotation through an angle, Φ equal to twice the angle between $\underset{\sim}{k}$ and east, minus $\pi/2$.

Scale analysis shows the principal response to be 'Sverdrup' in the vicinity of the packet, that is

$$\beta\langle v^E\rangle = \beta\frac{\partial \kappa_{i2}}{\partial x_2} \qquad \langle v^E\rangle \equiv \frac{\partial\langle\psi^{(1)}\rangle}{\partial x}$$

In this region, the Stokes drift, given by $\partial\kappa_{ij}/\partial x_j$; just cancels $\langle v^E\rangle$, leaving nearly vanishing cross-contour Lagrangian mean flow:

$$\langle v^L\rangle = \langle v_E\rangle + \frac{\partial \kappa_i}{\partial x_i} = O(L/L_m)^2$$

where L_m is the scale of variation of mean properties; i.e., the packet scale. However, significant Lagrangian drift does occur in the radiated waves, where there is no Stokes drift to cancel $\langle v_E\rangle$. But unless the geometry is re-entrant (that is, 'atmospheric' as opposed to 'oceanic'), the induced flow can only achieve the weak level of $\langle u_E\rangle \sim \frac{K}{L_m}$, while the cross-contour flow is still weaker by the factor $\left(\frac{L}{L_m}\right)^2$.

Example:

Zonal flow induction by a moving corrugated wall.

One-layer, homogeneous-in-x. There are three different 'mean circulations' in this example!

The governing equation is $\nabla^2\psi_t + \beta\psi_x + J(\psi, \nabla^2\psi) = 0$

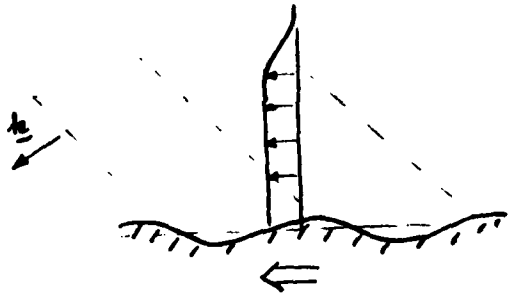

Averaging in x gives

$$\overline{u^E}^x_t = -\beta\overline{\kappa_{y1}}^x = -\beta\tfrac{1}{2}\frac{d}{dt}\overline{(y^L-y_0)^2}^x$$

using Taylor's diffusivity. This gives an Eulerian mean circulation, above the maximum of topography, valid for both turbulence and waves, of $\overline{u^E}^x = -\frac{1}{2}\beta\overline{(y^L-y_0)^2}^x$

As the Rossby wave front progresses northward, the region of westward Eulerian mean flow expands with it.

For waves, the Lagrangian mean flow is then given by

$$\overline{u^L}^x = \overline{u^E}^x + \frac{\partial}{\partial y}\kappa_{xy}$$

With weak damping, or with only a slow increase in the driving amplitude, $\partial \kappa_{xy}/\partial y$ will be small, $O(L/L_M)^2$. The difference between u and u is accounted for by looking at the fluid between topographic peaks, which was ignored in computing u.

But now consider a third 'mean circulation', the Kelvin circulation.

$$\Gamma = \oint_C \underline{u} \cdot d\underline{l}$$

integrating along a contour C moving with the fluid, which originally lay on a latitude circle (C is assumed to be closed, as it would be in a polar stereographic projection). Then one finds Γ according to

$$\frac{d\Gamma}{dt} = \frac{d}{dt} \iint_S \nabla \times \underline{u}|_z \, dx\, dy$$ by circulation theorem where S is the area 'north' of C.

$$= \iint_S \frac{d}{dt} (\nabla \times \underline{u}|_z) \, dx\, dy$$ because C is a material surface.

$$= -\frac{d}{dt} \iint_S \beta y \, dx\, dy$$ from the barotropic potential vorticity equation, since $q = \nabla \times \underline{u}|_z + \beta y$ is conserved at each particle.

Therefore $\Gamma = \frac{1}{2}\beta \int (y^2 - y_o^2)\, dx$ and if L is the length of C, the average Kelvin circulation is given by

$$\frac{\Gamma}{L} = \tfrac{1}{2} \beta \overline{(y^2 - y_o^2)}^x$$

which is equal and opposite to the Eulerian mean circulation.

This emphasizes the importance of defining circulation unambiguously. There is no contradiction, since Γ represents neither the time-average motion of any fluid particle, nor the time-average motion at a fixed point. In fact, this sketch of vorticity induced by north-south particle displacement suggests the senses of both Γ and $\overline{u}^E$.

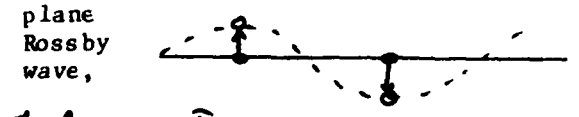

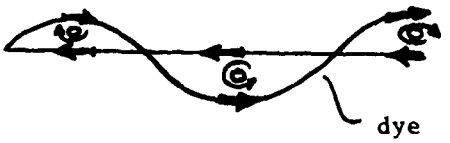

Note that if the wave maker exerts no net force on the fluid, then the total momentum of the flow must be conserved:

$$\int_{-\infty}^{\infty} \bar{u}^{x} dy = 0$$

But at unforced latitudes, $\bar{u}^{x}$ is westward. Thus a sharp eastward jet can be expected to develop at the latitudes of the forcing, increasing in magnitude as the induced westward flow expands. (Figs. 10-12).

In numerical circulation experiments in a box, eddies are generated by the wind-driven eastward jet and by the slower westward reverse circulation near the latitudinal walls. Under quasigeostrophic dynamics, without eddies there could be no mean flow below the surface layer. But with eddies there is the possibility of a vertical transfer of vorticity by means of wave form-drag from the sloping of the interface. A dramatic case is found in Holland's recent simulations using a 3 layer x 4000 km x 4000 km quasigeostrophic model. The gyre circulation in the top layer is wind-driven, but the gyres in the other levels are generated by this vertical vorticity transfer via eddy wave-drag. It is interesting to note that potential vorticity is homogenized over most of the middle layer by this eddy activity; the β y 'ramp' is altered to a plateau bounded by sharp gradients near the walls. Figure 13 shows the contour plot of potential vorticity in the middle layer. Fig. 14 shows an analogous plot for simple two-dimensional turbulence. In either case, the resemblance between q and a passive tracer is striking.

This exclusion of potential vorticity from a large region of closed Eulerian mean streamlines is an effect of mesoscale eddies (via shear dispersion). It is the analog of flux-expulsion in magneto hydrodynamics, and may control the general circulation. It illustrates value of passive scaling to dynamical studies.

REFERENCES

McIntyre, M.E., 1980. An introduction to the generalized Lagrangian-Mean description of wave, mean-flow interaction. Pageoph., 118, 152-176.

Rhines, P.B. and W.R. Holland, 1979. A theoretical discussion of eddy-driven mean flows. Dyn. Atmos. Oceans., 3, 289-325.

Sarmiento, J. 1982. Penetration of tritium in the North Atlantic Main Thermocline. G.F.D. Symposium, Woods Hole, Ma.

Uryu, M., 1979. Lagrangian mean motion induced by a growing baroclinic wave. J. Met. Soc. Jap., 56, 1-20.

NOTES SUBMITTED BY
Walter Robinson
Theodore Shepherd

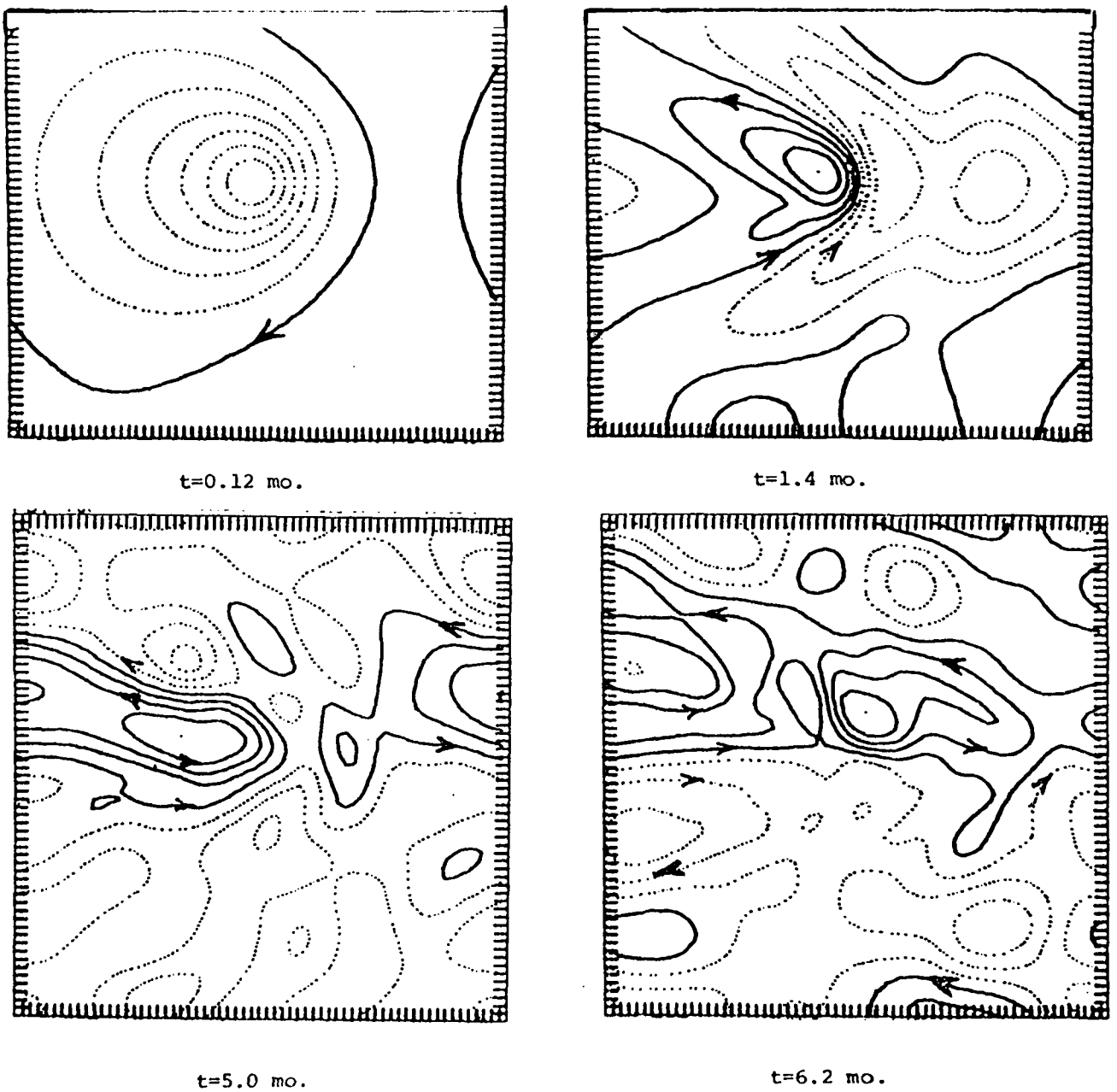

Fig. 10. Time-sequence of streamline patterns showing rectified zonal flow in a computer simulated, homogeneous, beta-plane ocean. The forcing is purely oscillatory, a Gaussian wind-stress curl at the center of the basin. The domain is 2000 km. wide with periodic boundary conditions on velocity. The region of forcing is 250 km. wide. After forcing begins, the wave/eddy field becomes established, principally west of the forcing, and begins to rectify. An eastward jet forms beneath the forcing, westward flow elsewhere, as in the theory. The net east-west transport always vanishes.

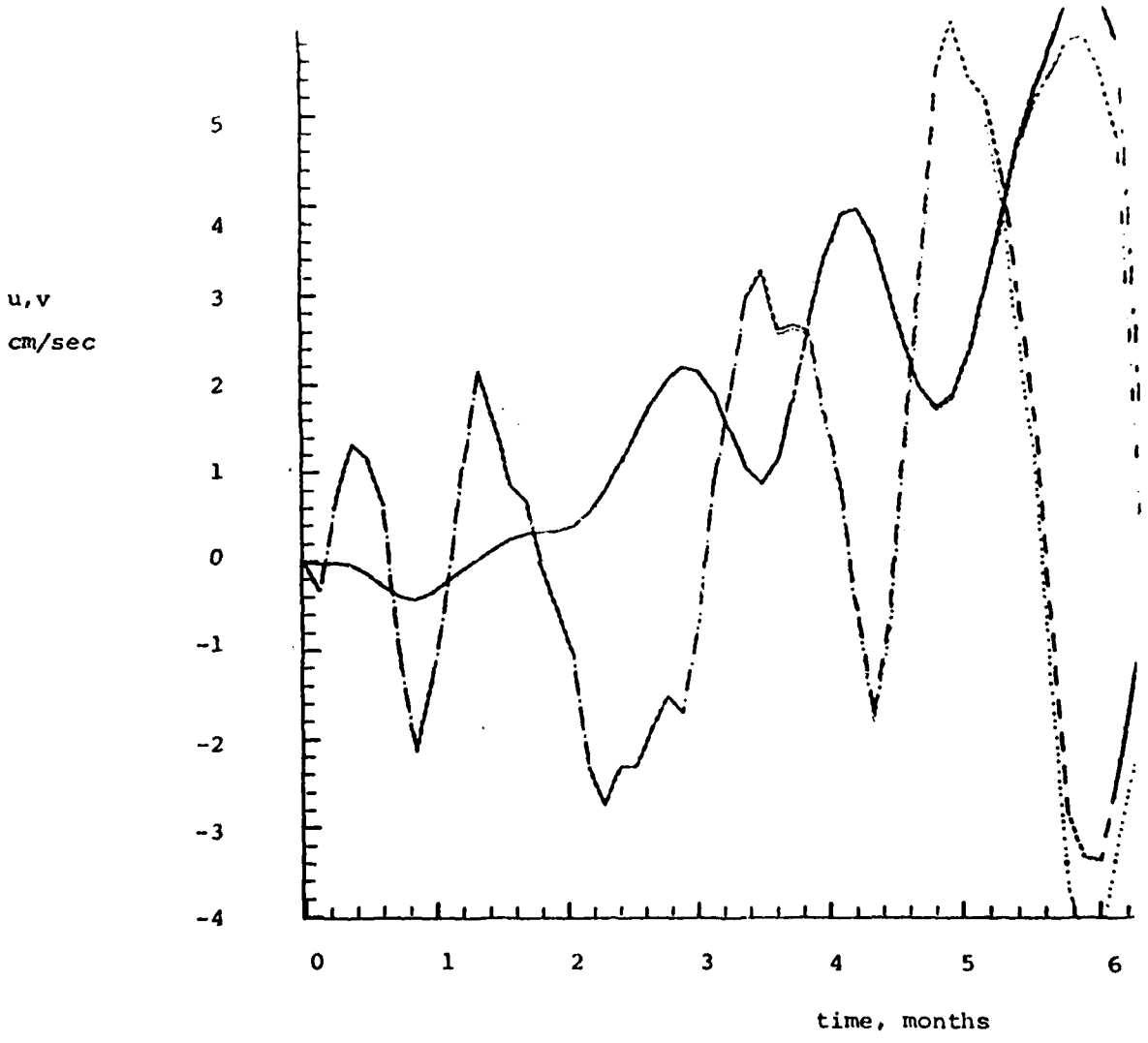

Fig.11 'Current-meter' record to the east of the forcing region in figure 1a. The arrival of waves, and the growing mean eastward flow, are visible. Solid curve, east-west; dashed curve, north south velocity.

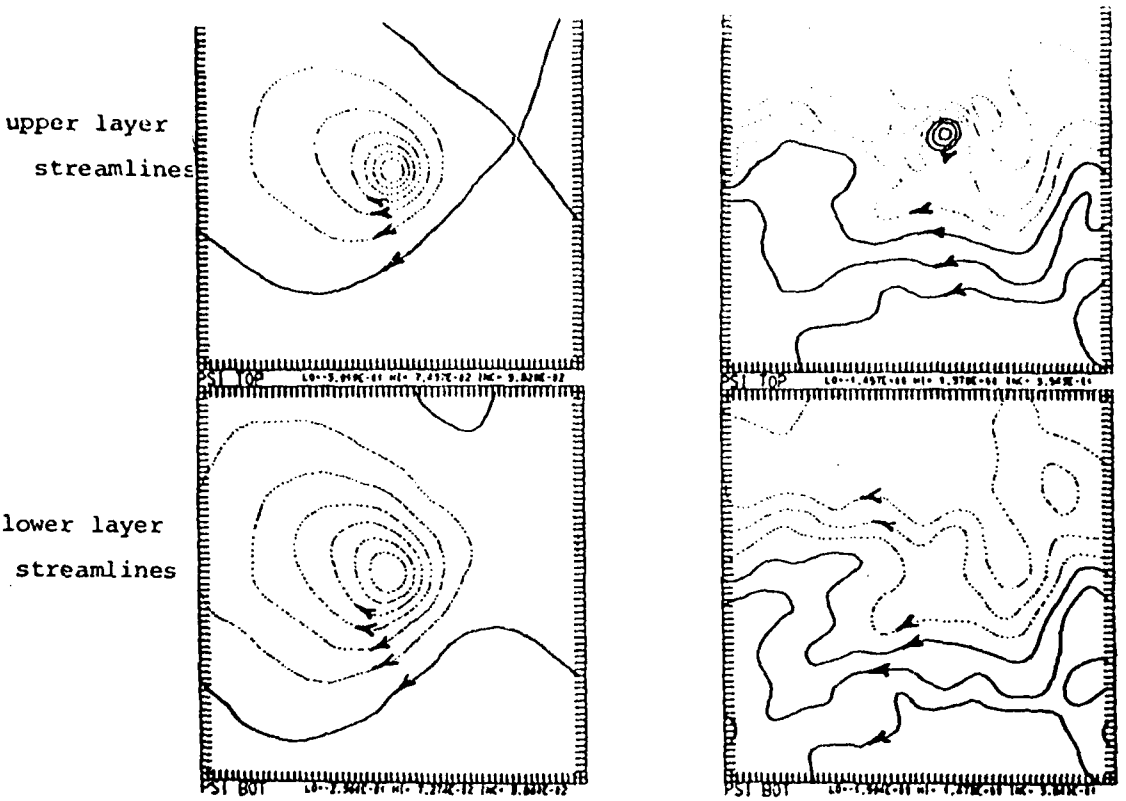

t=0.12 mo.

t=10.6 mo.

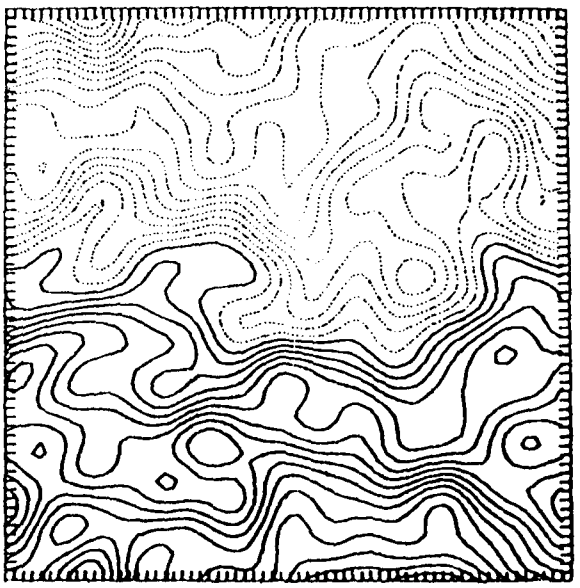

geostrophic
contours

Fig. 12 An experiment just like figure 1, but with realistically rough bottom topography and (2-layer) stratification. The upper panels show upper-level and lower-level streamlines near the beginning, and at 10.6 months. Now the rectified flow is dominantly westward due to the bottom-topographic drag. Note the resemblance of the large-scale flow to the geostrophic contours, f/h = constant.

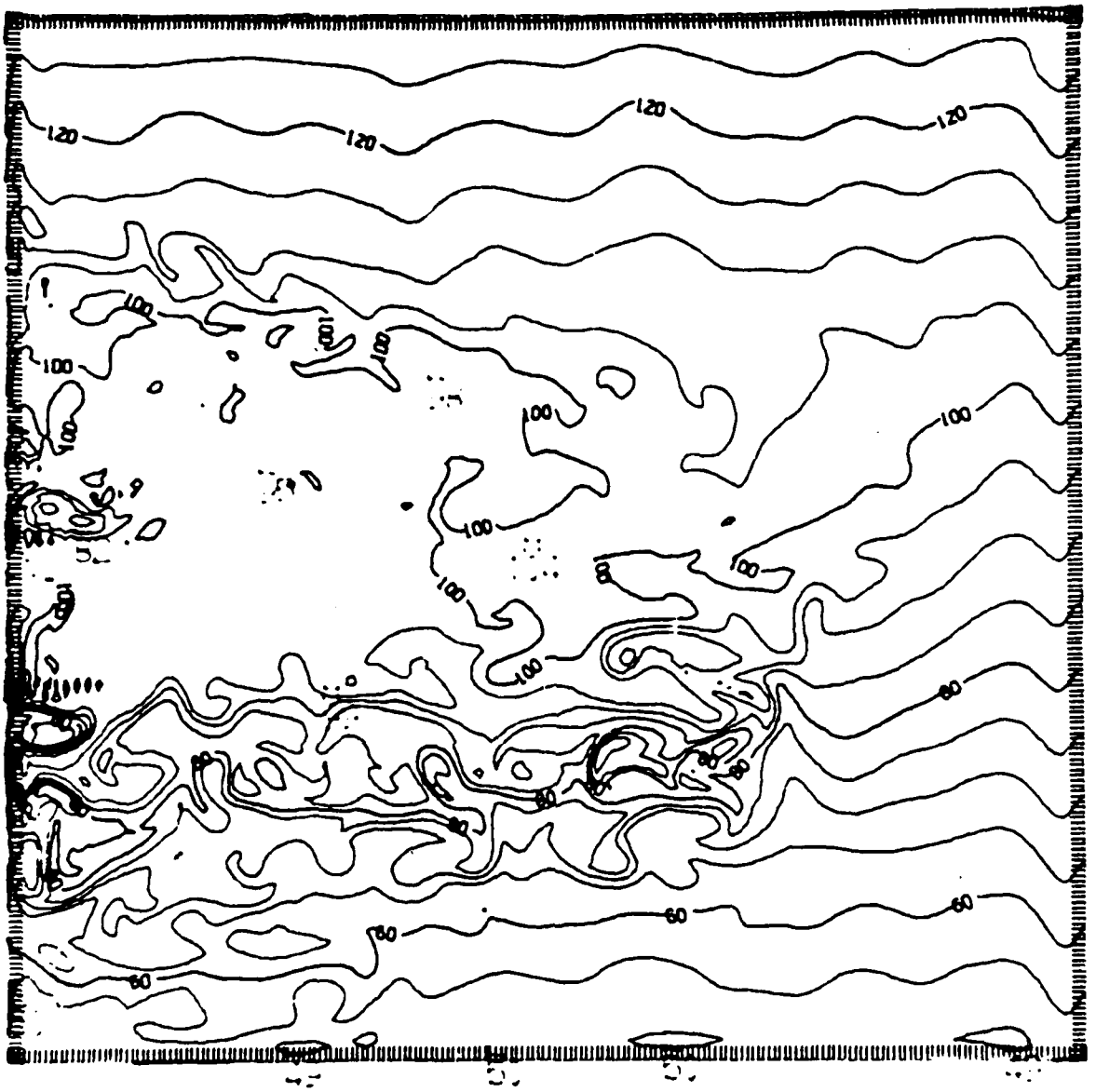

Fig. 13 The potential vorticity in the middle layer of Holland's 3-layer x 4000km x 4000 km wind-driven circulation model. The β-effect is dominant at the edges where the flow is weak but it is distorted by eddies at the edge of the wind-gyre (left-center) and homogenized in the gyre interior. The force corresponding to these eddy transports of q is the inviscid wave-drag of the upper layer on the layers below. which carries the mean circulation downward. Compare with fig. 2

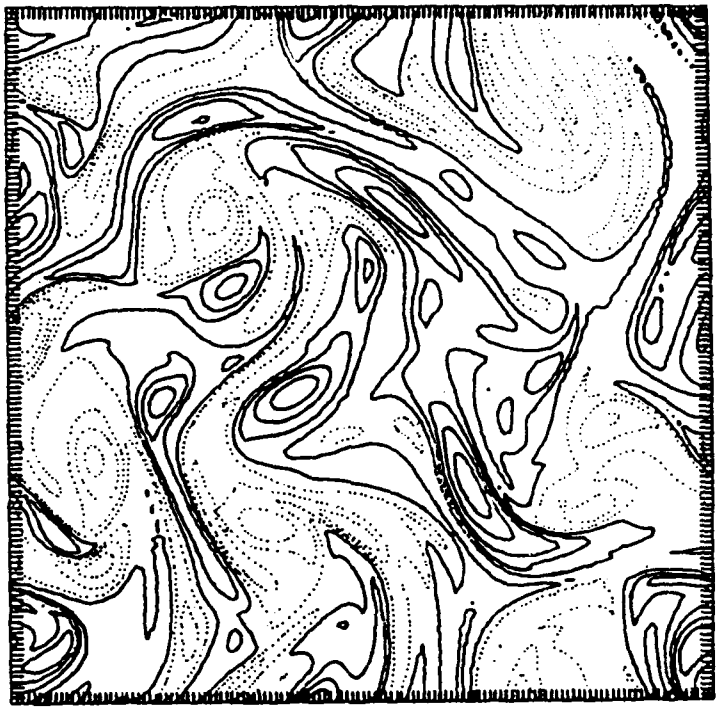

Fig.14 In two-dimensional turbulence the vorticity is an 'active' tracer which cascades to large wavenumber.

PARTICLE MOTIONS IN STRONG WAVE FIELDS

Glenn Flierl

Drifters of various types (Swallow and Sofar floats and surface drifters in oceanography; ghost balloons in meteorology) are used to characterize the mean and mesoscale motion in the ocean and atmosphere. In both of these situations, steep waves are present. For the ocean particle speeds (u) may be 2 ms^{-1} while typical phase speeds (c) may be 0.05 ms^{-1}. For this situation the Stokes' drift may be large. The Stokes' drift for very simple periodic flows and some geophysical situations where $u >> c$ will be considered. Interested readers can find more detail in Flierl (1981).

First Example

These are two simple problems which illustrate wave-induced mean drifts. The first example concerns the case of a longitudinal motion with flow parallel to the direction of the phase propagation. As an abstraction consider a square wave of wavelength λ, velocity amplitude u_o and phase speed c.

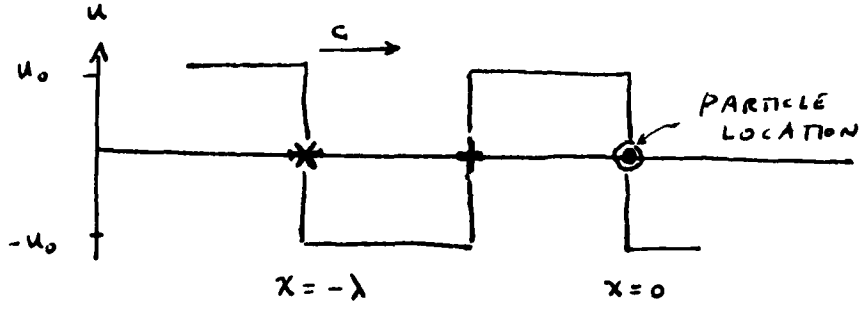

Zonal velocity at t = o as a function of zonal position x

The mean Eulerian velocity $\bar{U}_E$ at any point is zero. The Eulerian wave period $T_E = \lambda/c$.

Consider now the motion of a particle placed at location x = o at time t = o. The position of the particle can be calculated by solving

$$x = u(x-ct)$$

Shortly after t = o the particle is moving eastward at speed u_o while the wave is translating at speed c. The trough of the wave, beginning at point $x = -\lambda/2$ (marked with a + on the figure above), will catch up with the particle at times T_F such that $-\frac{\lambda}{2} + cT_F = u_oT_F$ or

$$T_F = \frac{\lambda}{2(c-u_o)}$$

with the particle being at location

$$x_1 = u_oT_F = \frac{u_o\lambda}{2(c-u_o)}$$

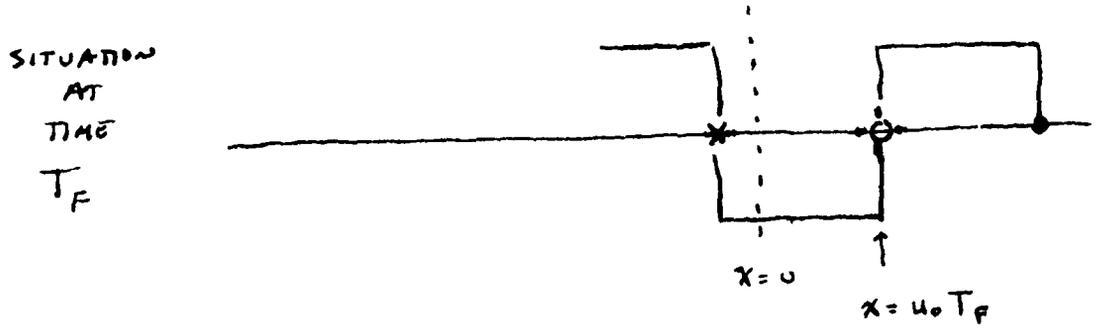

During the next time period, the particle is moving backwards with respect to the wave so that it collides with the face of the next wave (the point *) in time T_B

$$-\lambda + cT_F + cT_B = u_o T_F - u_o T_B$$

or

$$T_B = \frac{\lambda}{2(c+u_o)}$$

and the particle is at location

$$x_2 = \frac{u_o \lambda}{2(c-u_o)} - \frac{u_o \lambda}{2(c+u_o)}$$

Clearly the particle spends more time in the region where it is moving in the prograde direction than it does moving retrograde $T_F > T_B$ so that the net displacement over a Lagrangian period is positive. Therefore, as this process repeats, with succeeding waves, the particle drifts in the prograde direction at a mean speed.

$$\bar{u}_L = \frac{x_2}{T_B + T_F} = \frac{u_o^2}{c} \equiv c\varepsilon^2$$

where ε is the wave steepness u_o/c. The position of the particle as a function of time is sketched below for $u_o = 1/2c$.

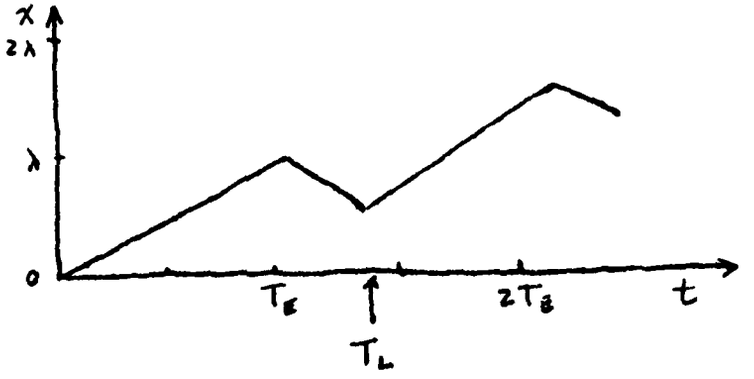

While this discussion illustrates clearly the reason for the Stokes drift -- the particles spend more time in the prograde part of the wave than in the retrograde part -- there is a much simpler procedure for computing the mean Lagrangian velocity, originating with Ursell (1953).

Consider the equation governing the position X of the particle in a reference frame where the wave is stationary ($X = x - ct$)

$$\dot{X} = u(X) - c$$

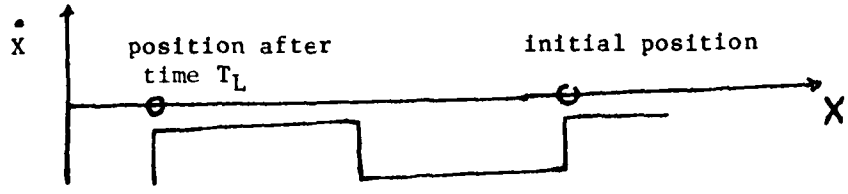

From this equation, the time necessary to move through one cycle of the wave (the Lagrangian period of the motion) can readily be calculated

$$T_L = \int_0^{-\lambda} dX \frac{1}{u(X)-c} = \int_\lambda^0 dX \frac{1}{u(X)-c} = \int_0^\lambda \frac{dX}{c-u(X)}$$

$$= \int_0^{\frac{\lambda}{2}} \frac{dX}{c+u_0} + \int_{\frac{\lambda}{2}}^{\lambda} \frac{dX}{c-u_0} = \frac{\lambda c}{c^2-u_0^2}$$

During this time, the particle moves a distance

$$\Delta x = \Delta X + cT_L = -\lambda + cT_L = c(T_L - T_E)$$

so that the net drift rate is

$$\bar{u}_L = \frac{\Delta x}{T_L} = c(1 - T_E/T_L)$$

(This is a general result which applies to other examples.)

A more realistic but still a simple example is

$$u = u_0 \cos k(x - ct)$$

$$dX = (u_0 \cos kX - c)\, dt$$

so

$$T_L = \int_0^{\lambda} \frac{dX}{c - u_0 \cos kX} = \begin{cases} \dfrac{T_E}{\sqrt{1-(u_0/c)^2}} & u_0 < c \\ \infty & u_0 > c \end{cases}$$

and

$$\bar{u}_L = \frac{-\lambda + cT_L}{T_L} = \begin{cases} c\left(1 - \sqrt{1-(u_0/c)^2}\right) & u_0 < c \\ c & u_0 > c \end{cases}$$

For weak waves, $\bar{u}_L = c\ 1/2\ (u_0/c)^2$ which is roughly Stokes' approximation

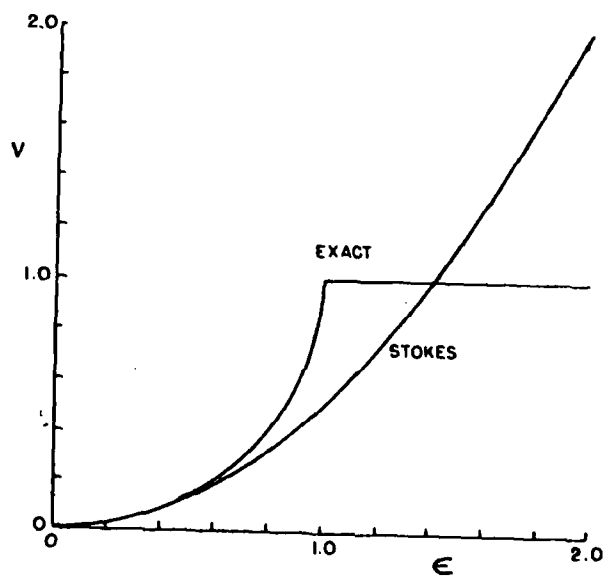

For $u_o > c$, there is a stagnation point in the flow (in the moving frame) through which particles take an infinite time to pass. Thus $u_L \longrightarrow c$.

Two Dimensional Wave Fields

The simple formula above can be applied directly to the case of a two dimensional steadily propagating wave

$$\psi = \psi(x - ct, y)$$

by a simple transformation to coordinates (X,Y) moving with the wave.

$$X = x - ct, \quad Y = y$$

The particle coordinates evolve according to

$$\dot{X} = -\psi_Y(X,Y) - c \equiv -\phi_Y(X,Y)$$

and

$$\dot{Y} = \psi_X(X,Y) \equiv \phi_X(X,Y)$$

where $\phi = \psi + cY$ is the streamfunction in the moving reference frame.

Particles do not leave ϕ = constant lines thus Y = y(X)

$$\psi(X, y(X)) + c\,y(X) = \psi(X_o, Y_o) + c\,Y_o$$

Solving this equation for y(X) and adapting the formula above for T_L gives

$$T_L = \int_0^\lambda \frac{dX}{\phi_y(X, y(X))} \quad \text{and} \quad \bar{u}_L = c\left(1 - \frac{T_E}{T_L}\right)$$

Note that the Stokes drift will be nonzero whenever $T_L \neq T_E$. But now we shall see that it is possible to have $T_L < T_E$ so that U_L is retrograde: this is the second simple case. Consider the u velocity on two streamlines sketched here

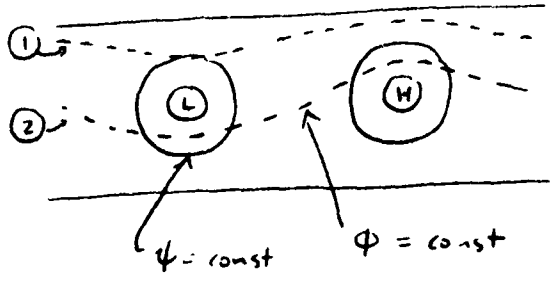

The velocities $-\psi_y(X, y(X))$ are

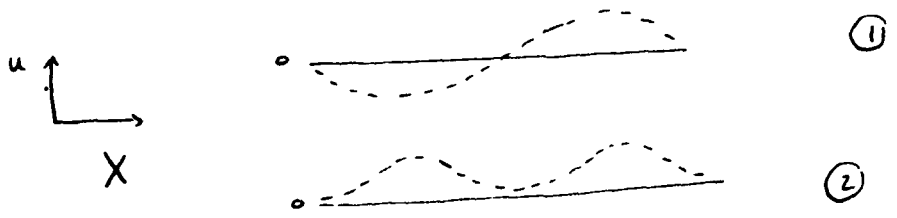

For particles near the wall (e.g. streamline 1) $u(X)/c \sim \varepsilon \cos X$ and $\bar{u}_L/c \sim \frac{1}{2}\varepsilon^2$ i.e., the drift is prograde. For particles near the center of the channel, however, (streamline 2) the velocity is always retrograde (> 0) $u/c \sim \varepsilon^2[\frac{1}{2} - \frac{1}{2}\cos X]$. The particle always sees eastward velocities because the north-south flows push it to the southern side of lows and the northern side of highs. The average Lagrangian drift is $\bar{u}_L/c \simeq 1 - \sqrt{1-\varepsilon^2}$ which is retrograde.

Surface Gravity Wave Problem

For particles at the surface of the fluid $y(x) = \eta(x)$, $\phi_y = c-u$. The kinematic boundary condition at the surface is

$$(u-c)\eta_x = v$$

and Bernoulli's equation gives

$$\frac{(u-c)^2}{2} + \frac{v^2}{2} + g\eta = \frac{c^2}{2}$$

These equations lead to

$$T_L = \int_0^\lambda dX \sqrt{\frac{1+\eta_x^2}{c^2 - 2g\eta}}$$

For weaker waves, use Taylor expansion to get

$$T_L = \frac{1}{c}\int_0^\lambda dX \left(1 + \frac{g\eta}{c^2} + \frac{1}{2}\eta_x^2 + \frac{3}{2}\frac{g^2\eta^2}{c^2}\right)$$

However, $\int_0^\lambda \eta\, dX$ is not zero and it is necessary to first solve the first order problem before proceeding. It is more convenient to use

$$T_L = \int_0^\lambda \frac{dX}{c - u(X,\eta)}$$

$$= \frac{1}{c}\int_0^\lambda dX \left[1 + u_0/c + u_1/c + \frac{1}{2}(u_0/c)^2 + \ldots\right]$$

Then $\bar{u}_L = c\,\frac{k^2\hat{\eta}^2}{2}\left[1 + \frac{1}{\tanh kH}\right]$ (H is depth)

when $\hat{\eta}$ is the wave amplitude.

For irrotational motion we can prove $\bar{u}_L/c \geq 0$. Since $\nabla^2\phi = 0$ (irrotational)

$$\int_0^{S_L} ds\, q = \int_0^{\lambda} c\, dX = c\lambda$$

for $\int_0^{\lambda} u\, dX = 0$

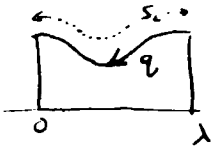

$ds = q\,dt$ where $q = \sqrt{u^2+v^2}$ so

$$\int_0^{T_L} q^2\, dt = \frac{\lambda^2}{T_E}$$

but

$$\int_0^{T_L} q\, dt = S_L$$

Then

$$\frac{1}{T_L}\int_0^{T_L} q^2\, dt \geq \left(\frac{1}{T_L}\int_0^{T_L} q\, dt\right)^2$$

i.e. since

i.e., $\lambda^2/T_L T_E \geq S_L^2/T_L^2 \geq \frac{\lambda^2}{T_L^2}$

$T_L > T_E$

and

$$\bar{u}_L/c = \left(1 - T_E/T_L\right)$$

Return now to the case of periodic Rossby waves in a channel and consider the release of a line of particles at X = 0. Using the methods discussed in the above examples, the positions of the particles as a function of time can be evaluated. In the fixed and moving frames the trajectories as shown in Figs. 1 and 2. For small ϵ , the Lagrangian drift velocity $\bar{u}_L$ is mainly a function of y but as ϵ increases $\bar{u}_L$ becomes a function of the initial longitude as well. For $\epsilon > 1$, there are trapped regions in which the particles move with the wave and $\bar{u}_L = c$ and except for a thin layer near these trapped regions the rest of the fluid moves retrograde in a narrow band at a rapid rate.

The trapped particles drift at speed c because they circulate on closed contours: thus after one Lagrangian period $\Delta X = 0$ so that

$$\Delta x = \Delta X + cT_L = cT_L$$

$$\bar{u}_L = \frac{\Delta x}{T_L} = c$$

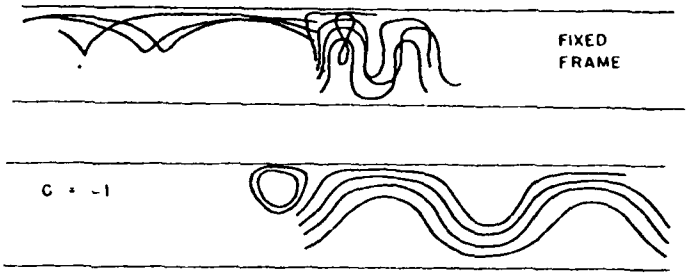

Fig. 1 "Spaghetti" diagrams of particles set in a channel wave along X = 0. The lower figures show the pictures viewed in various moving frames of reference (x(t)-ct,y(t)).

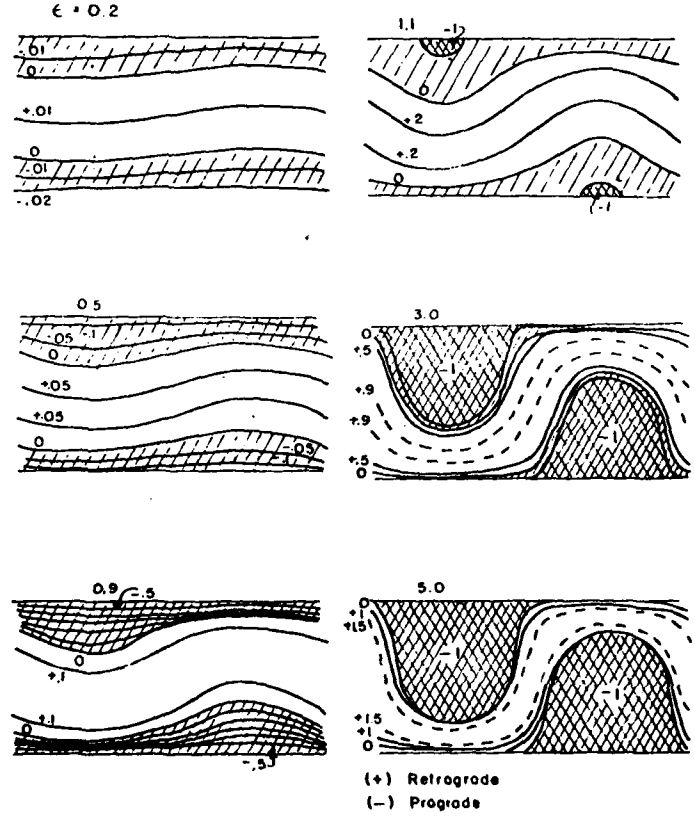

Fig. 2. a) Lagrangian drift rate as a function of initial position (x_o, y_o) for various wave amplitudes ϵ. A segment of the channel from $x = 0, 2\pi$; $y = \pm \pi/2$ is shown. The contours are of v, the labels above each section are ϵ values. (b) A different view. The abscissa is $\phi_o = \psi(x_o, y_o) - y_o$. The shading represents trapped fluid. Positive drifts are retrograde; negative ones prograde.

The next figure shows the simplest measure of the retrograde speed

$$\frac{\bar{u}_L}{c} = v(\epsilon) = 1 - \frac{\pi\sqrt{1+\epsilon^2}}{2K\left(\frac{\epsilon^2}{1+\epsilon^2}\right)}$$

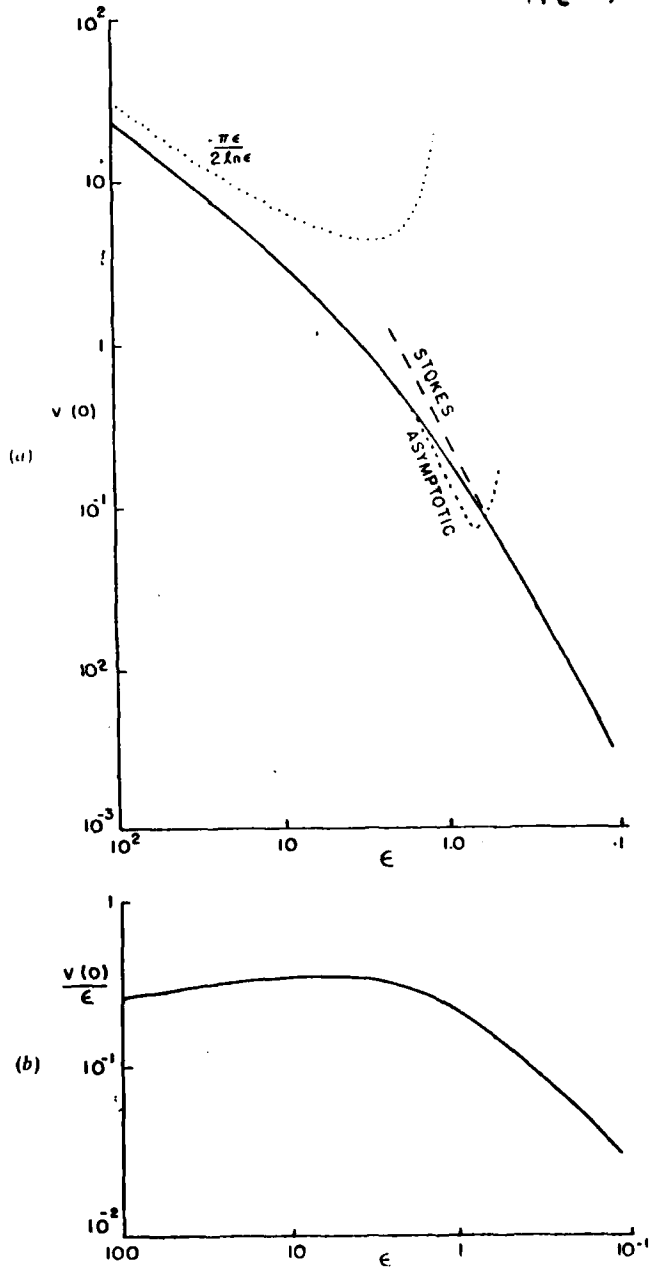

Fig. 3.(a) Drift of the particle initially at (0,0) showing the accuracy of the Stokes' approximation, the largest asymptotic term + $\pi\epsilon/2\ln\epsilon$ and a more complete asymptotic approximation $-1+\pi\epsilon/2\ln(4\epsilon)$. (b) Drift normalized by the maximum fluid speed rather than the phase speed.

as a function of ϵ where K is the first elliptic integral function. Note that the drift becomes essentially a constant fraction of the maximum particle speed -- the particle travels rapidly across the tops of the highs, down between the eddies across the bottom of the lows and then back up. It spends about half its time in the most rapid eastward parts of the flow.

The next figure shows the proportion of the area of the channel that is trapped and moving with the wave.

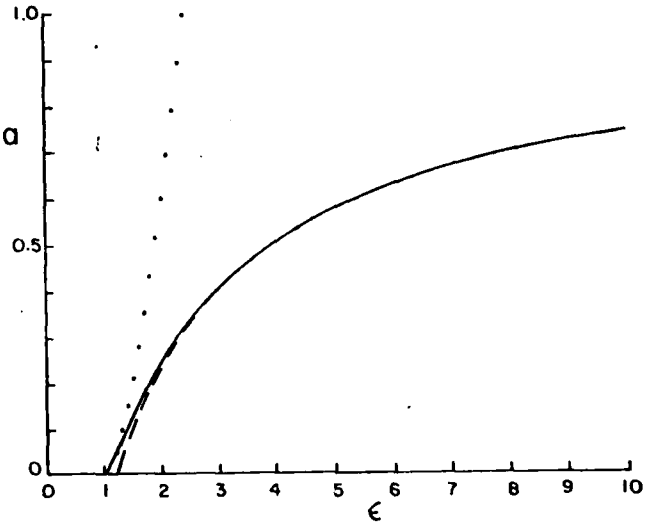

Fig. 4. Trapped area nondimensionalized by total area as a function of wave strength ϵ .

The Lagrangian drift estimates suggest that care must be used in interpreting dispersion experiments. In strong wave fields, particles set even short distances apart may have very different average drifts if the area of the setting overlaps a boundary of the trapped region. Also the inference that might be drawn from the Stokes' approximation that v is independent of x_0 is not correct, so that a zonal line segment of particles will also spread due to difference in drift rates. Thus, spreading of a patch can occur, with the two particle displacements being eventually proportional to t, even in a field without turbulent cascades. In addition, the initial behavior of a statistic such as the r.m.s. two particle distance can be quite complex with the dependence upon t to the first power (in contrast to Taylor's 1921 prediction of $t^{1/2}$ dependence) occurring only after long enough times so that the particles have separated by many wavelengths. The following figure shows the mean square of x-separation for a set of particles in the channel (ϵ =3). The initial transient are large and lead to an initially slower separation rate so that the quadratic nature of the mean square separation does not become apparent for some time.

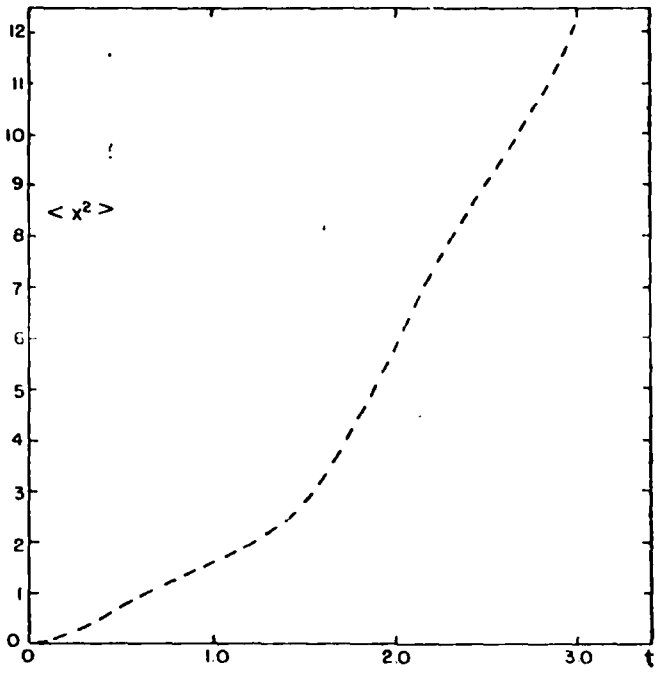

Fig. 5. East-west spread of the initial line of particles in a channel wave. Here $\epsilon = 3$.

Isolated Disturbances

Consider the single disturbance

$$u = u_o \operatorname{sech}^2 kX$$

propagating with velocity c. The time for a particle to move from $+X_o$ to $-X_o$ is

$$\int_{-X_o}^{X_o} \frac{dX}{c - u_o \operatorname{sech}^2 kX} = \int dt = T(X_o)$$

In the stationary reference frame the particle moves a distance

$$\Delta x = -2 X_o + cT(X_o)$$

The total distance the particle moves as the disturbance propagates from $-\infty$ to $+\infty$ is the limit of Δx_o as X_o becomes infinite

$$d_L = c \int_{-\infty}^{\infty} \frac{u(X)}{c - u(X)} \, dX$$

The exact value together with the Stokes' approximation, the progressive vector estimate (= ϵ u) and an asymptotic estimate are shown in the following figure.

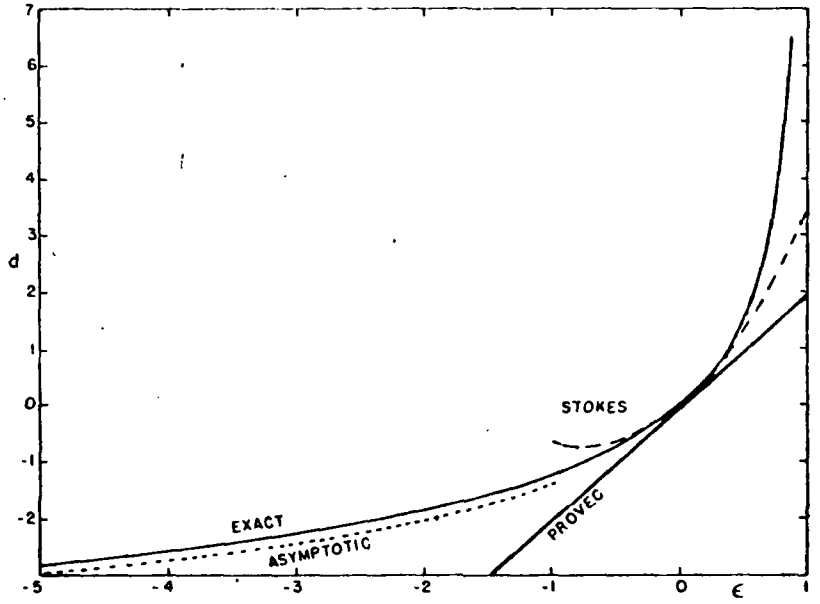

Fig. 6. The displacement in a simple pulse u - sech^2 X for various strengths. The exact results, Stokes' approximation, the progressive vector estimate and an asymptotic estimate for $\epsilon << 0$ are shown.

Some limits are:

i) For $|\epsilon| << 1$ $\quad d_L \rightarrow \int_{-\infty}^{\infty} u(X)\,dX$

ii) as $\epsilon \rightarrow 1$ $\quad d_L \rightarrow \infty$

iii) for $\epsilon \rightarrow -\infty$ $\quad d_L \simeq$ width of pulse

For the case of the single disturbance (moving to the west at speed c, the speeds experienced by particles on various stream lines are shown in the following figure.

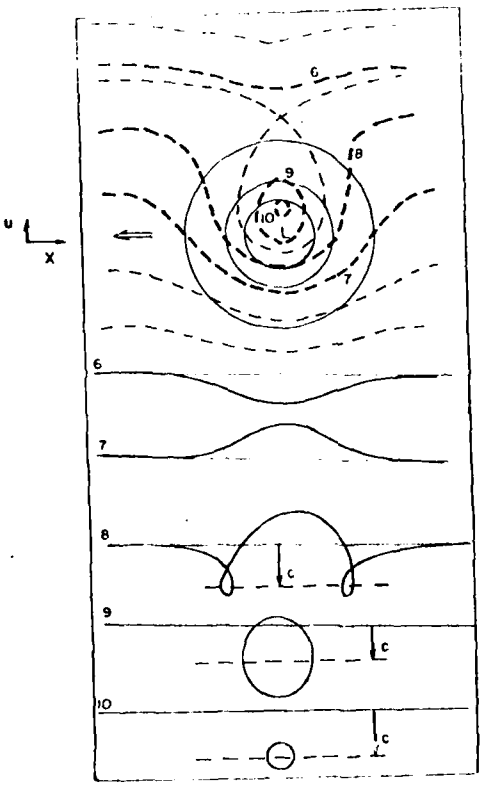

Fig. 7. Reduction of a two-dimensional problem to a one-dimensional case. Solid lines in upper halves represent contours of the instantaneous streamfunction ψ ; dashed contours of the streamfunction in the moving frame ϕ . The lower halves show plots of u (the Eulerian east-west velocity) as a function of X (the co-moving east-west co-ordinate) along the labelled ϕ lines.

The displacements of a line of particles initially at χ = o are shown in the following figure.

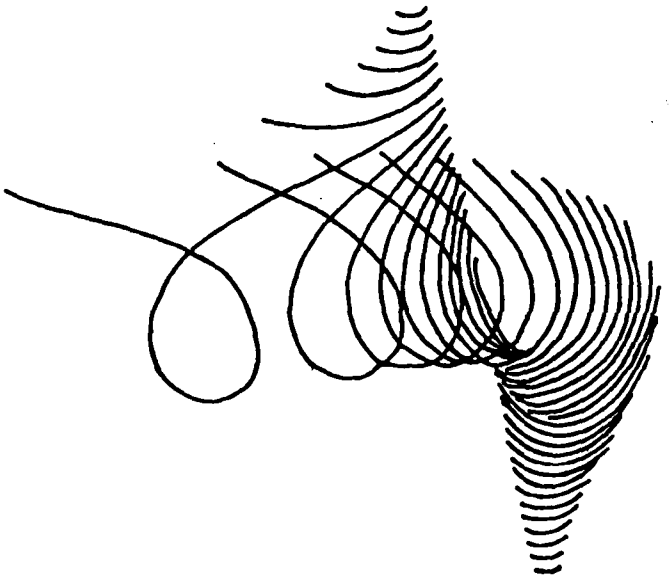

Fig. 8. "Spaghetti" diagram of particles under the passage of an isolated ring.

There is also a trapped region of particles travelling with the eddy.

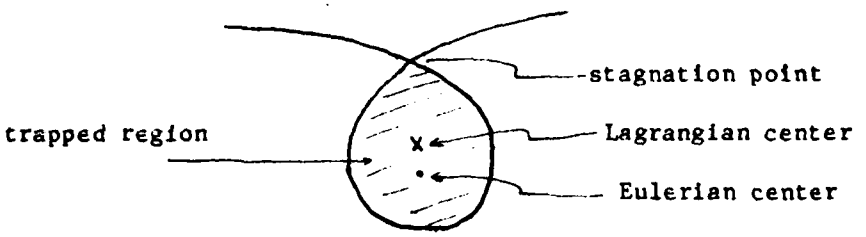

For an oceanic eddy (c.f. Olson, 1980), consider the radially symmetric velocity field

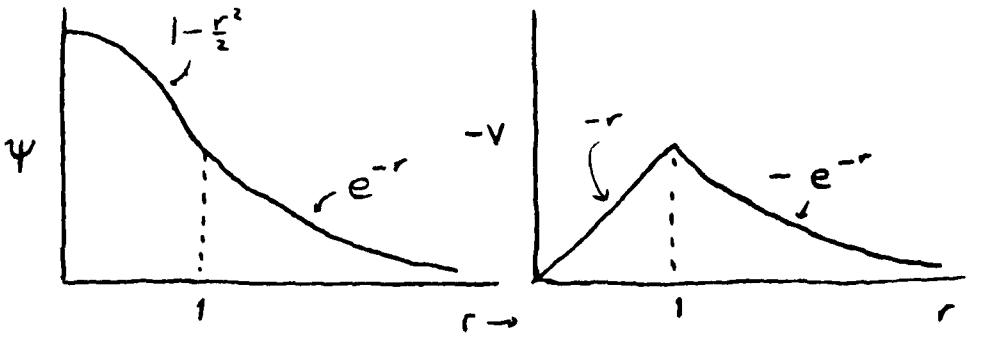

The net eastward displacement as a function of y is

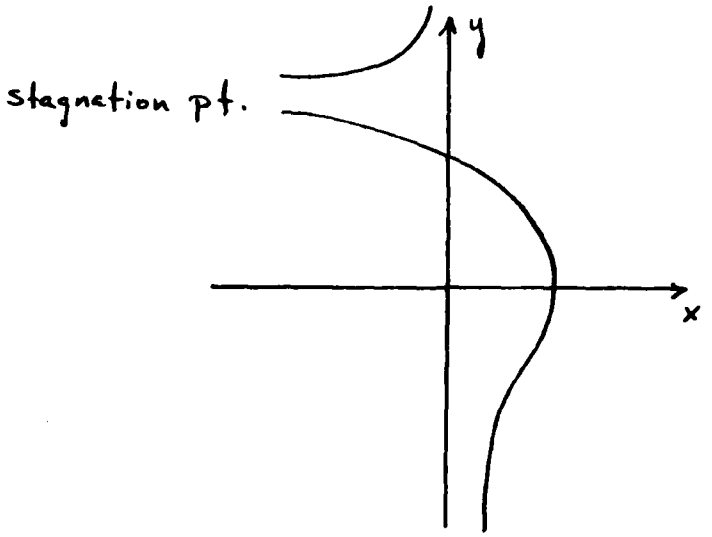

Then in this case, the trapped area as a function of t is: (Note: the area is normalized by the area within the circle of maximum Eulerian velocity).

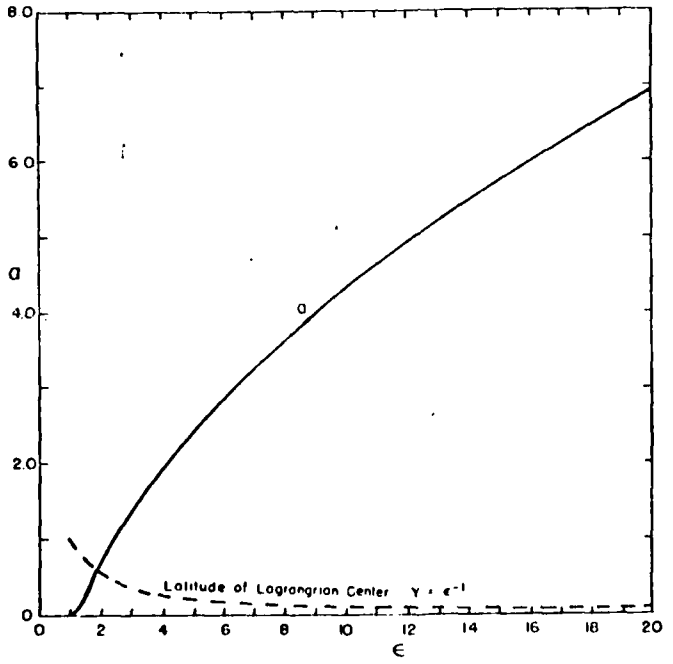

Fig. 9. Trapped area a(ϵ) and also the latitude of the Lagrangian center.

There are two stagnation points in the flow (neither of which are the Eulerian center for nonzero c) and as $\epsilon \to 1$ (from above) these stagnation points approach each other. For warm core rings, $\epsilon \sim 20$ (at the surface) and the area $a \simeq \epsilon$; and ϵ decreases with depth. Two possible vertical structures are possible: 1) the compensated case where $\epsilon \to 0$ as the bottom is approached and 2) a first mode solution for which there can be a second deep trapped volume (not connected to the upper volume). Both trapped regions look like skewed wine glasses.

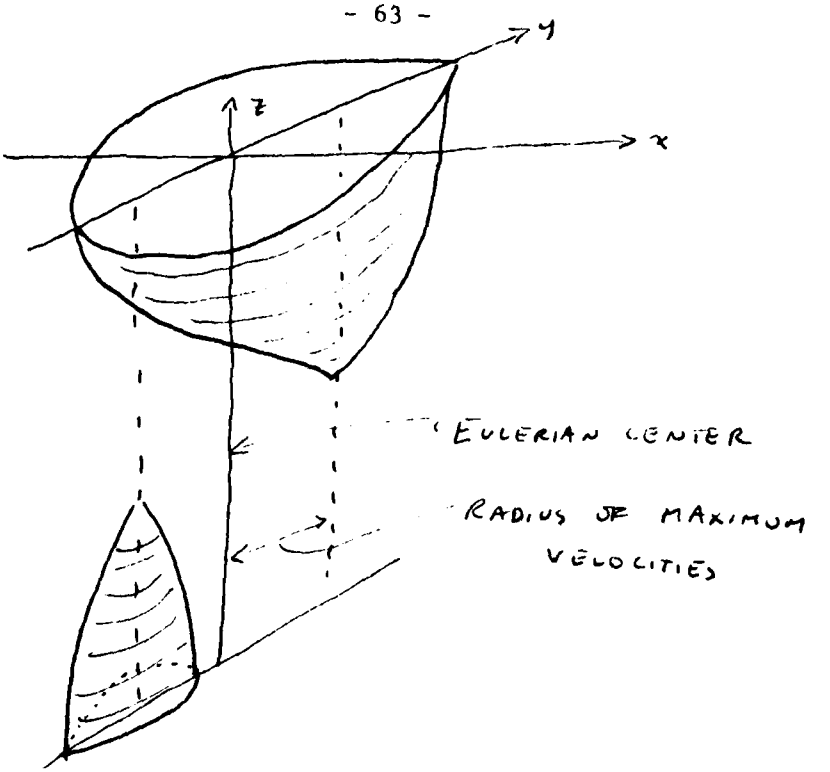

Fig. 10. Trapped regions for baroclinic eddies

The trapped volume for these two cases is

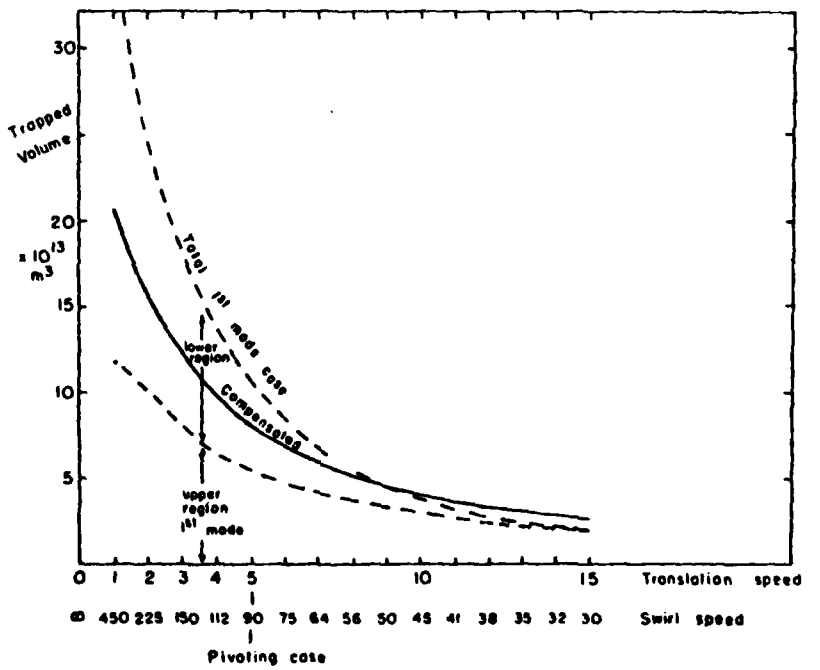

Fig. 11. Trapped volume for Gulf Stream rings as a function of translation speed (swirl speed = 90 cm/sec) or swirl speed (c = 5 cm/sec.).

A more dynamical example is that of a vortex pair (modon).

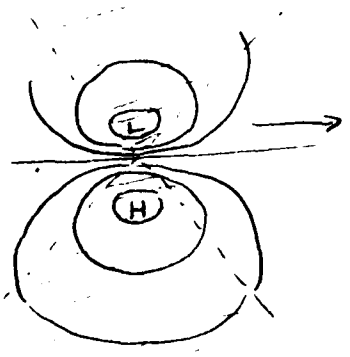

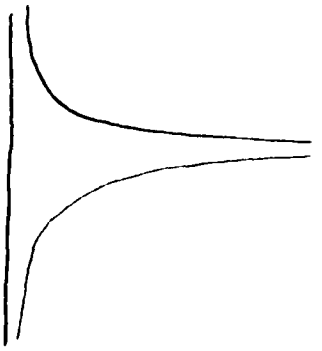

Following similar arguments to those above, we can show that the net displacement of a particle caused by the passage of the modon is prograde.

$$\int_0^{T_L} q\,dt = S_L \qquad \int_0^{S_L} q\,ds = cD = \int_0^{T_L} q^2\,dt$$

and $$\frac{1}{T_L}\int_0^{T_L} q^2\,dt \geq \left(\frac{1}{T_L}\int_0^{T_L} q\,dt\right)^2 \Rightarrow \frac{cD}{T_L} \geq \frac{S_L^2}{T_L^2} \geq \frac{D^2}{T_L^2} \Rightarrow cT_L \geq D$$

$$\Rightarrow \quad d_L = -D + cT_L \geq 0$$

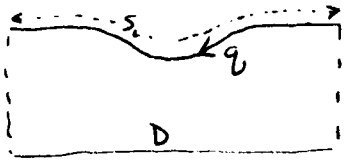

The displacements are sketched in the second figure above. At first sight, the prograde displacement seems puzzling since the streamfunction pattern suggests that there is mainly retrograde flow north and south of the eddy. However, we can show that particles initially in the two hatched areas are moved to the right by the modon by considering the detailed form of the solution. For constant f, $\nabla^2\phi = 0$ outside the eddy

$$\psi = cr_0\left(-\frac{r_0}{r}\right)\sin\theta$$

$$\phi = cr_0\left(\frac{r}{r_0} - \frac{r_0}{r}\right)\sin\theta$$

Inside $\nabla^2\phi = -k^2\phi$

$$\phi = A\,J_1\left(k\frac{r}{r_0}\right)\sin\theta$$

at $r = r_0$ match the two values of ϕ

$$\psi = cr_0\left[2\,J_1\left(k\frac{r}{r_0}\right)/kJ_0(k) - \frac{r}{r_0}\right]\sin\theta$$

and

$$\phi = cr_0\,2\,J_1(kr/r_0)/kJ_0(k)$$

Calculation of $u = -\psi_y$ shows that $u > 0$ in the cross-hatched areas. Thus a particle even initially far north or south of the center of the track feels $u > 0$ for substantial periods of time.

If the modon is on the β-plane, however,

$$\nabla^2\psi + \beta y = F(\psi + cy)$$

and the outside field is now $\psi \sim K_1\left(\frac{r}{r_0}\right)\sin\theta$ (K_1 modified Bessel function) and $u = 0$ when

$$\sin^2\theta = \frac{K_1(r/r_0)}{r/r_0\, K_2(r/r_0)}$$

Thus the regions for which $u \geq 0$ are now more limited and one would find retrograde displacements for particles set to the north or south of the eddy.

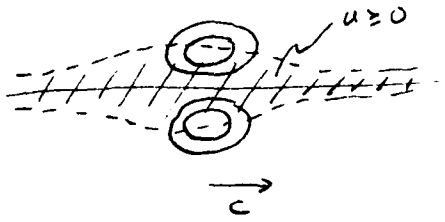

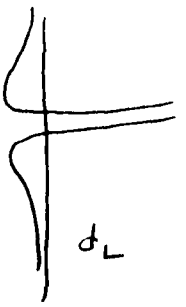

In summary, there is a net drift of particles whenever $T_E = T_L$. For oceanic or atmospheric flows with vorticity, T_L can be larger or smaller than T_E and a general formula is $\bar{u}_L = 1 - T_E/T_L$.

REFERENCES

Flierl, G.R., 1981. Particle motions in large amplitude waste fields. Geophys. Astrophys. Fluid Dynamics, 18, 39-74.

Olson, D.B., 1980. The physical oceanography of two rings observed by the cyclonic ring experiment Part II. Dynamics J. Phys. Oceanogr., 10, 514-528.

Taylor, G.I., 1921. Diffusion by continuous movements. Proc. Lond. Math. Soc. A, 20, 196-211.

Ursell, F., 1953. Mass transport in gravity waves. Proc. Camb. Phil. Soc. 49, 145-150.

NOTES SUBMITTED BY
John Church

TRACERS IN RINGS

Glenn Flierl

Introduction

The problem considered is the distribution of a tracer in the neighborhood of strong, large scale vortices of the type found in the ocean and in planetary atmospheres. The strongest examples of nearly geostrophically balanced vortices in the ocean are rings which are eddy features formed from meanders in western boundary current extensions such as the Gulf Stream or Kuroshio. The intense cut-off highs and lows in the atmosphere are similar to rings in some respects. The features of interest have length scales L $\sim$ 100 km in the ocean and L $\sim$ 1000 km in the atmosphere and have the distinguishing property of remaining coherent for long periods of time ($\sim$6 mos.-1 year, ocean; $\sim$ week or more for the atmosphere). These eddies are of particular relevance to the systems in which they are found, due to their role as both a mixing mechanism and their ability to trap fluid within their cores for long periods of time.

A laboratory example of a strong, nonlinear vortex can be generated by releasing a column of light fluid into an otherwise quiescent denser fluid on a rotating table (Saunders, 1973; Griffiths and Linden, 1981). The result after the geostrophic adjustment phase is a large vortex of upper layer fluid, restrained by Coriolis forces from spreading rapidly into the final state of a thin layer of lighter fluid spread uniformly on the surface of the lower layer. The transition to this final state could occur by frictional breaking of the geostrophic constraint; but it actually takes place much more rapidly. Due to an instability of the vortex (Griffiths and Linden, 1981) the vortex edge breaks into sets of dipoles which carry fluid rapidly outward. This transport, essentially similar to that described for the modons, accomplishes the spin-up on a time scale much shorter than that due to interfacial friction.

Tracers in the Neighborhood of a Ring

The distribution of some tracer or concentration of a cloud of discrete particles, S = S(x,y,t) released at some point x_o, y_o at t = 0 is governed by the advection-diffusion equation

$$\frac{\partial S}{\partial t} + \frac{\partial \phi}{\partial x}\frac{\partial S}{\partial y} - \frac{\partial \phi}{\partial y}\frac{\partial S}{\partial x} = \kappa \nabla^2 S, \qquad (1)$$

where ϕ is the streamfunction for the flow into which the tracer is released. To describe the evolution of the distribution of S it is convenient to introduce the moments of the distribution of S in space. Here the analysis will include the first moment or center of mass

$$\mu \equiv \frac{1}{M_o}\iint x\, S(x,y,t)\, dx\, dy \qquad (2)$$

$$\nu \equiv \frac{1}{M_o}\iint y\, S(x,y,t)\, dx\, dy,$$

and the second central moments

$$\sigma_{ij} \equiv \frac{1}{M_o} \iint (x_i - \mu_i)(x_j - \mu_j) S(x,y,t)\, dx\, dy. \quad (3)$$

In these definitions M_o is the total mass of tracer

$$M_o = \iint S(x,y,t)\, dx\, dy.$$

Then as long as a finite set of moments exist (i.e., S(x,y,t) is bounded) the time derivatives of the first moment are

$$\dot{\mu} = -\frac{1}{M_o} \iint S\, \phi_y\, dx\, dy$$
$$\dot{\nu} = \frac{1}{M_o} \iint S\, \phi_x\, dx\, dy. \quad (4)$$

A simple example in which the evolution of this center of mass of a tracer can be followed is for a constant vorticity flow

$$\phi = a + bx + cy + d\frac{x^2}{2} + exy + f\frac{y^2}{2}.$$

The time rate of change of the first moments for this flow field is

$$\dot{\mu} = -(c + e\mu + f\nu)$$
$$\dot{\nu} = (b + d\mu + e\nu).$$

Therefore the center of mass of an initial patch of tracer behaves just like an advected particle in this flow. In general the situation is more complicated such that it is not possible to express the movement of the center of mass as a function of the streamfunction and first moments alone, i.e.

$$\dot{\mu} \neq F(\phi, \nu, \mu).$$

Another tractable problem involves the behavior of simpler initial distributions of tracer. For example, the distribution of sharply peaked patches of tracer can be described for short periods of time following their release. If the initial distribution is given by a delta function

$$S(x,y,0) = M_o\, \delta(x - x_o)\, \delta(y - y_o) \quad (5)$$

The short time evolution of S can be found for a general flow field, ϕ. For this case the temporal behavior of the center of mass can be expanded in a Taylor series to give

$$\dot{\mu} = -\left\{ \phi_y(\mu,\nu) + \frac{1}{2} \sum_i \sum_j \sigma_{ij} \frac{\partial}{\partial x_i} \frac{\partial}{\partial x_j} \frac{\partial \phi}{\partial y} + \cdots \right\} \quad (6)$$

The evolution of the second central moments which describe the spreading of the patch of tracer can be expanded in a similar way using this result

$$\begin{aligned}
\frac{\partial \sigma_{11}}{\partial t} &= 2\kappa - 2\{\sigma_{11}\phi_{xy} + \sigma_{12}\phi_{yy}\} \\
\frac{\partial \sigma_{12}}{\partial t} &= \frac{\partial \sigma_{21}}{\partial t} = \sigma_{11}\phi_{xx} - \sigma_{22}\phi_{yy} \\
\frac{\partial \sigma_{22}}{\partial t} &= 2\kappa - 2\{\sigma_{12}\phi_{xx} + \sigma_{22}\phi_{xy}\}.
\end{aligned} \tag{7}$$

Then since the second moments of the tracer cloud are small for the period immediately following release, the expression for the time derivative of the center of mass can be approximated by

$$\begin{aligned}
\dot{\mu} &= -\frac{\partial}{\partial y}\{\phi + \nabla^2\phi\, 2\kappa t\} \\
\dot{\nu} &= \frac{\partial}{\partial x}\{\phi + \nabla^2\phi\, 2\kappa t\}.
\end{aligned} \tag{8}$$

Now consider a vortex which exhibits trapped regions as described in the first lecture. Let the streamfunction in the translating coordinate system be

$$\phi = \frac{u_0}{k} K_0(kr) + cy, \tag{9}$$

where K_0 is a modified Bessel function and c is the phase speed for the eddy. Following Eq.(8) it is possible to write an effective streamfunction of the form

$$\phi_{eff} = \frac{u_0}{k} K_0(kr) + cy - u_0 k\, K_0(kr)\, 2\kappa t. \tag{10}$$

The influence of the diffusion introduces an effective opening up of the streamlines in the proximity of the $u_0 = c$ saddle point as shown in sketch below. Fluid will tend to enter the region which is trapped in the absence of diffusion from the lower left quadrant in the figure. Diffusion also allows tracer to leave the trapped region at the lower right edge of the vortex.

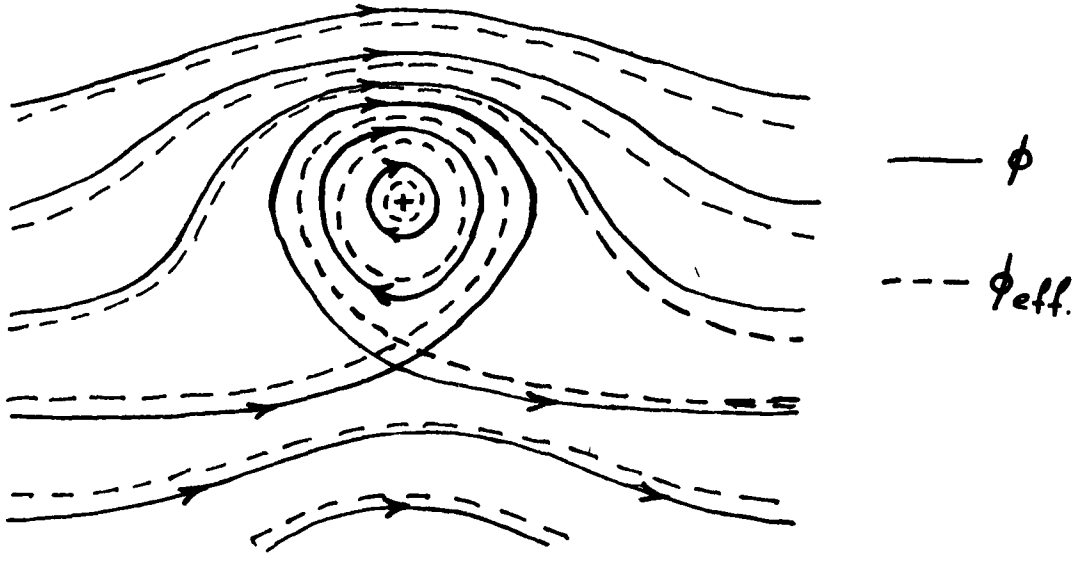

The problem of the dispersion of a tracer in an eddy can also be done numerically. The conservation equation (Eq. 1) is solved in a coordinate system which is translating with the eddy. Sketches of the results for two cases are shown below. In the first case the tracer is originally introduced within the "trapped" region of the eddy. The effect of the diffusion is basically that predicted by the small time expansion above with a plume of tracer proceeding out of the vortex at the lower right. In the alternate case where the tracer is originally distributed outside of the closed streamlines the simulations show tracer diffusing into the ring in the southern portion of the vortex again in agreement with the prediction of Eq.(10).

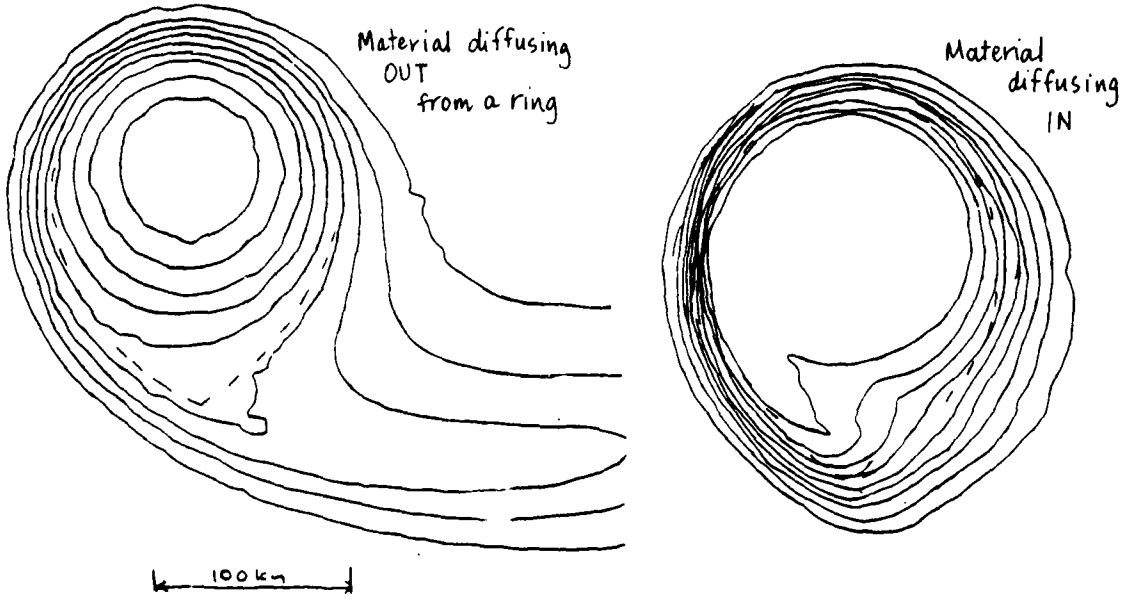

When the Peclét number is very large, the concentration of the tracer becomes homogenized along streamlines (as in the Batchelor-Prandtl theorem)

$$S = S_0(\phi, t),$$

On the streamlines which expand to infinity S is determined by the far field boundary conditions, in this case S = 0. However, the formalism of Young and Rhines cannot be applied directly to this problem because of the stagnation point existing in the flow. One might suspect that the exterior flow will effectively maintain S = 0 at the boundary of the trapped region. A simple analog problem then demonstrates that the tracer will decrease with a time scale L^2/κ but exponentially rather than algebraically. Consider a field with $\phi = \phi(r)$ for all areas with $S \neq 0$ and then two cases to demonstrate the importance of conditions at the edge of the eddy. First consider

$$S = J_0(kr)\, e^{-\kappa k^2 t} \qquad r < r_0$$

$$[J_0(kr_0) = 0]$$

$$S = 0 \qquad r \geq r_0.$$

corresponding to a situation where tracer is swept away to ∞ by a flow outside of a region of closed streamline bound at $r = r_o$. The decay of the concentration at the eddy center is exponential in time. Alternately taking the same initial condition in the case with continuous radially symmetric flow out to infinity so that $S \to 0$ far away, a solution to Eq. 1 is

$$S = \int_0^\infty k\, e^{-\kappa k^2 t}\, g_0(k)\, J_0(kr)\, dk,$$

which leads to a decrease in tracer at the eddy center

$$S(0,t) = \frac{g_0(0)}{2\kappa t}.$$

These two cases behave similarly for small t but there is a much faster long time decay in the first situation where $S = 0$ at $r = r_o$. The difference rises from the nature of the outside ϕ and S fields.

Influence of Rings on Large Scale Property Distributions

In order to study the influence of the passage of strong solitary eddies on the distribution of properties in a region the passage of successive vortices through a channel is considered. The model problem consists of a channel geometry as shown below across which a gradient in S is imposed by fixing S on the boundaries.

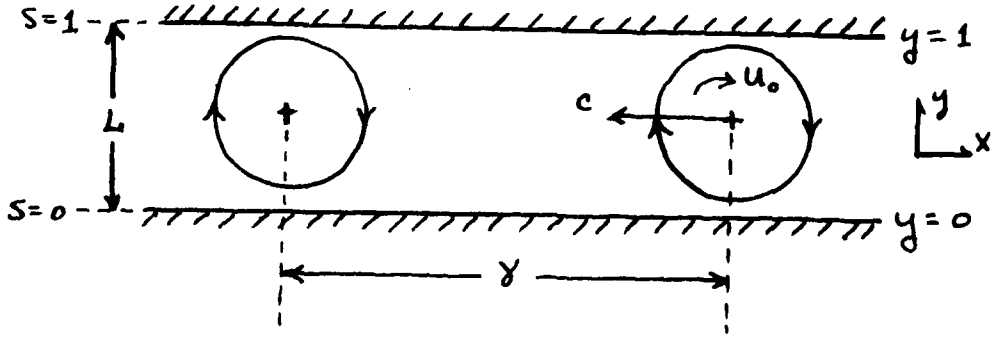

This might be thought of as an analog to the passage of warm core rings through the North American slope water. In the actual situation the lower boundary becomes the Gulf Stream and the upper the continental shelf.

The problem to be solved is again the advection-diffusion equation

$$S_t + \epsilon J(\phi, S) = \delta \nabla^2 S \qquad (11)$$

where the scaling parameters are $\epsilon = u_o/c$ and $\delta = \kappa/cL$. The boundary conditions imposed are

$$S = 0 \text{ at } y = 0$$
$$S = 1 \text{ at } y = 1 \qquad (12)$$

The cross-channel flux per eddy cycle can be found by writing Eq. 11 in flux form and integrating in x to give

$$F_s = \int_0^\gamma \left\{ -\kappa \frac{\partial S}{\partial y} + \frac{\partial \phi}{\partial x} S \right\} dx.$$

From the boundary conditions it can be shown that $F_y = 0$. As long as the flow satisfies the boundary condition $\partial\phi/\partial x = 0$ at $y = 0, 1$, it is possible to write a Nusselt number, Nu, for S as

$$Nu = \frac{1}{\gamma} \int_0^\gamma \left(\frac{\partial S}{\partial y} \right)_{y=0} dx \tag{13}$$

$$= \frac{\text{Actual flux of S}}{\text{Diffusive flux of S}}$$

If an integration is done over a region bound by some streamline, ϕ, and one of the walls, it is easily shown that

$$\int_{\phi_0} \nabla S \cdot \hat{n}\, d\ell = \begin{cases} 0 \text{ if } \phi_0 \text{ is closed} \\ \int_0^\gamma \frac{\partial S}{\partial y} dx = \gamma Nu \text{ for open } \phi_0. \end{cases} \tag{14}$$

For the closed streamlines the Prandtl-Batchelor theorem holds (see Rhines lectures) which follows from

$$\nabla S = \frac{\partial S}{\partial \phi} \nabla \phi,$$

which vanishes in the integral above only if $\partial S/\partial \phi = 0$ inside the region bounded by ϕ_0. On open streamlines the tracer must obey

$$\frac{\partial S}{\partial \phi} = \frac{\gamma Nu}{\int_{\phi_0} |\nabla \phi| d\ell}. \tag{15}$$

From this result integrated from $\phi = 0$ to $\phi = -1$ and the original definition of the Nusselt number we find

$$Nu = \left\{ \int_0^{-1} \left(\frac{\gamma}{\int_{\phi_0} |\nabla \phi| d\ell} \right) d\phi_0 \right\}^{-1} \tag{16}$$

As an application the somewhat artificial case of square eddies is assumed. While the eddy shape is clearly unphysical this makes the problem tractable. Two cases are treated. One involves an eddy whose velocity maximum occurs at the channel walls (y = 0, 1). The second case treats an eddy whose velocity maxima occur within the channel. The problem geometry (page 72) along with the resulting S fields (page 73) is shown in the following diagram.

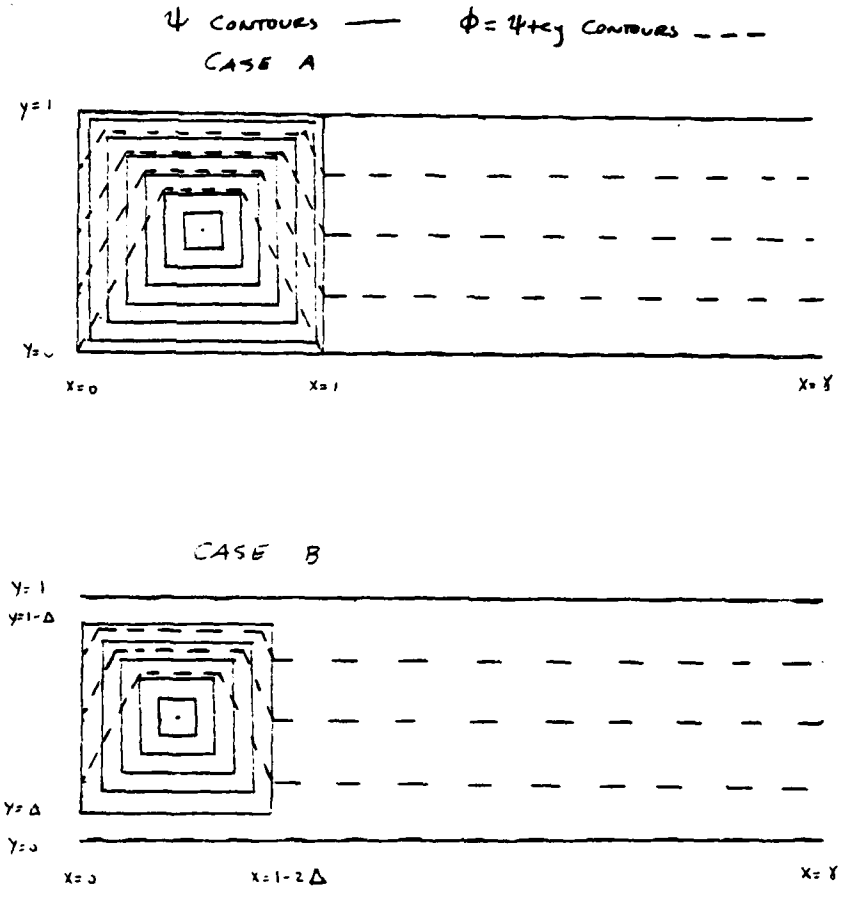

In the situation where the eddy fills the channel the gradient in S outside the eddy is uniform. A very rapid flux of tracer occurs at the walls where the eddy is in contact for this case. In case II the gradients in tracer are concentrated in boundary layers along the walls while the interior of the channel is nearly uniform.

The Nusselt number for the flow field increases in both cases as the eddy steepness, ϵ , increases from small values. In the case where the eddy only occupies a portion of the channel the Nusselt number becomes constant at some value of ϵ and above. This arises due to a diffusive limitation for the flux in the boundary layers. In the situation where the eddy is in contact with the walls there is no such limitation and Nu increases with increased ϵ.

The dependence of Nu on the nonlinearity, ϵ , is shown graphically for the two cases below.

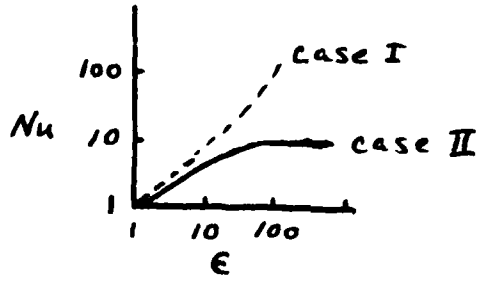

DISTRIBUTION OF S

CASE A

$\epsilon = 1$

CASE B

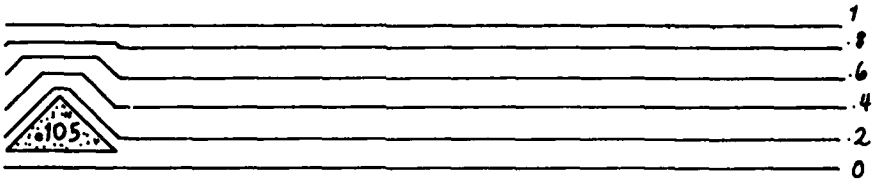

CASE A

$\epsilon = 30$

CASE B

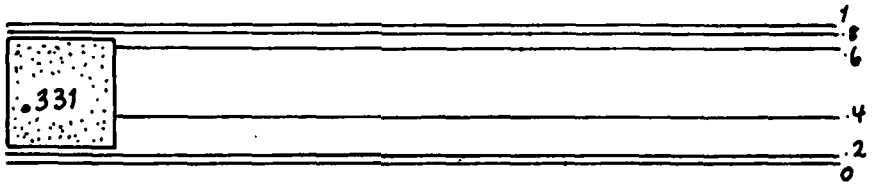

CASE A

$\epsilon = 10^4$

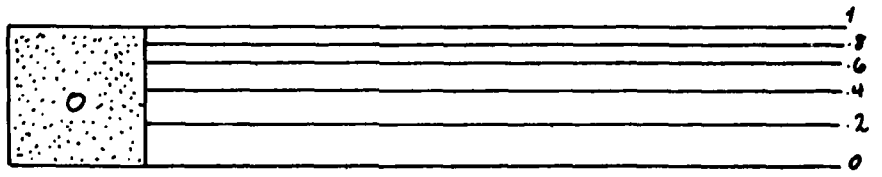

CASE B

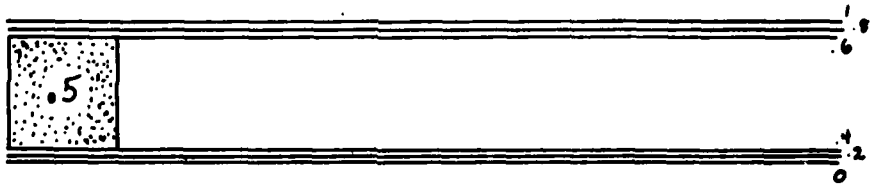

The increased efficiency of the tracer transfer across the channel is given by

$$\kappa_{eff} = \kappa \, Nu(\epsilon)$$

for both cases. For realistic parameter values Nu $\sim$ 4-6 so that very little enhancement to the cross-stream flux actually occurs.

It is also possible to treat the down-channel flux associated with the translation of eddies. Here the boundary condition imposed at the walls would be S = S(x) in general. The simplest case is just

$$S = x \text{ on } y = 0,1.$$

The down-channel flux in the absence of any eddies is then just $-\delta$. The eddy passages can be looked upon as discrete jumps of fluid with the Lagrangian displacement profile discussed in the previous lecture. Schematically the problem appears as follows.

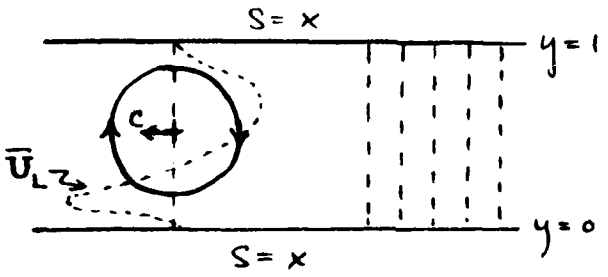

The problem to be solved then becomes

$$\bar{U}_L(y) S_x = \delta \nabla^2 S.$$

Since the concentration minus x, S-x, is periodic a solution can be written

$$S = x + \hat{S}(y).$$

The problem then reduces to an equation for $\hat{S}$ of the form

$$\delta \hat{S}_{yy} = U_L(y)$$

with $\hat{S} = 0$ at y = 0,1. A Nusselt number for the flow can be written as before which gives

$$Nu = 1 + \int_0^1 (\hat{S}_y)^2 dy,$$

in which the last term is proportional to δ^{-2}. The effective diffusivity is then

$$K_{eff} \sim K^{-1}$$

in the down-channel direction. There is then an asymmetry in the effective diffusivity due to the eddies in the two directions with

$$K^{xx}_{eff} >> K^{yy}_{eff}.$$

For small diffusivities the eddies produce a more efficient flux of material in the down-channel direction than in the cross-channel.

REFERENCES

Griffiths, R.W.& P.F. Linden. 1981. The stability of vortices in a rotating, stratified fluid. J. Fluid Mech., 105, 283-316.

Saunders, P.M. 1973. The instability of a baroclinic vortex. J. Phys. Oceanogr., 3, 61-65.

NOTES SUBMITTED BY
Donald Olson

EQUILIBRIUM STATISTICAL MECHANICS APPLIED TO GEOPHYSICAL FLUID DYNAMICS

Rick Salmon

I. PHILOSOPHY AND REVIEW OF THE BASICS

Introduction.

This is an old subject (due mainly to Maxwell, Boltzmann, and Gibbs). The new idea is that equilibrium statistical mechanics gives useful insights into the behavior of realistic, non-equilibrium fluid motion. The pioneering papers on the application of equilibrium statistical mechanics to classical fluids are:

Burgers, Verhandl. Konikl. Akad. Wetenshap, Amsterdam (1929)
Onsager, Suppl. Nuovo Cemento 6, 279 (1949)
Hopf, J. Rational Mechanics 1, 87 (1952)
Lee, Q. Appl. Math., 10, 69 (1952).

These lectures will review the basics of statistical mechanics, emphasizing the differences between the fluid continuum and the conventional molecular gas. Our examples will be drawn from GFD.

Equations of Motion

Consider a system with N (real) degrees of freedom $(y_1, y_2, \ldots, y_n)$ whose evolution in time is governed by N first-order equations,

$$\dot{y}_i = G_i(y_1, \ldots, y_N), \quad i = 1, \ldots, N \tag{1}$$

For example, a two-dimensional inviscid flow within a closed curve C. The stream function ψ obeys the equation,

$$\frac{\partial}{\partial t} \nabla^2 \psi + J(\psi, \nabla^2 \psi) = 0, \quad \psi = 0 \text{ on } C \tag{2}$$

Expand

$$\psi = \sum_i \frac{y_i(t)}{k_i} \varphi_i(x) \tag{3}$$

in the eigenfunctions,

$$\nabla^2 \varphi_i + k_i^2 \varphi_i = 0, \quad \varphi_i = 0 \text{ on } C; \quad \overline{\varphi_i \varphi_j} = \delta_{ij}.$$

(Here the overbar denotes an areal average over the flow). The transform of (2) is

$$\dot{y}_i = \sum_{jk} A_{ijk} y_j y_k \tag{4}$$

where

$$A_{ijk} = (k_j / k_i k_k) \overline{\varphi_i J(\varphi_k, \varphi_j)}$$

The N-dimensional space spanned by $(y_1, \ldots, y_N)$ is called phase space. Each state of the system corresponds to a point in phase space. The evolution of the system is represented by a trajectory in phase space. Let $P(\underset{\sim}{y}, t)$ be the

density of systems in phase space. $P(\underset{\sim}{y}, t)$ has two interpretations: (1) If there is only one system, then P is its probability density. (2) If there are many identical systems evolving at once, then P is their number density in phase space.

For either interpretation, P obeys

$$\frac{\partial P}{\partial t} + \sum_i \frac{\partial}{\partial y_i}\left(P \dot{y}_i\right) = 0 \tag{5}$$

which is the analog of the continuity equation,

$$\frac{\partial \rho}{\partial t} + \nabla \cdot (\rho \underset{\sim}{u}) = 0 \tag{6}$$

for a fluid. Liouville's theorem states that if $\sum_i \partial \dot{y}_i / \partial y_i = 0$, then the phase flow is nondivergent and

$$\frac{\partial P}{\partial t} + \sum_i \dot{y}_i \frac{\partial P}{\partial y_i} = 0. \tag{7}$$

This is the analogue of $D\rho/Dt=0$ for incompressible fluid motion. Equation (7) is equivalent to the statement that in the coordinates y_i, the elements of phase fluid preserve their volume. Canonical coordinates automatically satisfy the Liouville condition, but so too do many noncanonical coordinates. The coordinates introduced above for the two-dimensional fluid are noncanonical, but they satisfy (7) because A_{ijl} vanishes whenever two of its indices are equal.

The evolution of turbulent fluid is highly sensitive to initial conditions. Thus, an initially compact blob of phase fluid (representing a tiny uncertainty in the initial state) evolves so that phase particles which were initially close together become widely separated after finite time. The phase blob "fills" an increasing volume of phase space, even though its own volume is conserved (Fig. 1). This behavior is called "mixing". The phase blob cannot, however, mix through all of phase space since it is constrained by the conservation of energy (enstrophy, etc.) to energy hypersurfaces.

Let $\hat{P}$ be a smoothed or coarse-grained probability density which is constant over the volume of phase space "filled" by P. $\hat{P}$ has a simpler form than P, but can be used instead of P to compute averages

$$\langle F(\underset{\sim}{y}) \rangle \equiv \int \prod_i dy_i \, F(\underset{\sim}{y}) P$$

for any function $F(\underset{\sim}{y})$ that depends smoothly on $\underset{\sim}{y}$. The essence of statistical mechanics (whether equilibrium or nonequilibrium) is to get $\hat{P}$ without first finding P. This obviously requires auxiliary principles or assumptions.

Equilibrium statistical mechanics assumes that $\hat{P}$ is uniform on the intersection of hypersurfaces corresponding to a set of known invariants of the motion. Examples:

3-d turbulence, energy conserved, $\hat{P} \propto \delta(E-E_0)$

2-d turbulence, energy and enstrophy conserved, $\hat{P} \propto \delta(E-E_0)\,\delta(Z-Z_0)$

Where has the Liouville property been used? Observe:

1) Even if P is uniform in one set of phase coordinates, it will not generally be uniform in another arbitrarily selected set.

2) Any two sets having the Liouville property have a constant Jacobian of transformation.

3) The Liouville property guarantees consistency for the same set of coordinates for all time.

Gibbs Viewpoint.

Gibbs was unconcerned with the evolution of a phase space blob and hence did not distinguish between the space-filling exact distribution and its smoothed counterpart. He noticed that if E was a constant of motion, so that $\partial E/\partial t = 0$, then $P = F(E)$ was a steady solution to Liouville's equation. He introduced the

microcanonical ensemble $P \propto \delta(E-E_0)$

and

macrocanonical ensemble $P \propto \exp(-\alpha E)$ as important examples of F.

The connection between the two was clarified by Khinchin, who showed that the probability density for a subset $(y_1, \ldots, y_M)$ of the N coordinates took the form

$$P(y_1, \ldots, y_M) = C \iint \cdots \int \cdots dy_N \, \delta(E-E_0)$$

$$\longrightarrow C' \exp(-\alpha E_M)$$

as $M/N \longrightarrow 0$, where E_m is the energy of the subset. The macrocanonical ensemble is therefore appropriate for a system in contact with an infinite reservoir.

Information Theory Viewpoint

This is an alternate, more flexible approach which emphasizes the guessing nature of the whole subject. Now, $\hat{P}$ represents our state of knowledge about the system, and the entropy $S[\hat{P}]$ measures the uncertainty in precise system state. Example: A random variable has precisely N possible values. Let p_i, i=1,...N be the probability of each value. If

$$(p_1, p_2, \ldots, p_N) = (0, \ldots, 0, 1, 0, \ldots, 0)$$

S should be minimal, but if

$$(p_1, p_2, \ldots, p_N) = \left(\frac{1}{N}, \frac{1}{N}, \ldots, \frac{1}{N}\right)$$

S should be maximal.

There are many choices for the functional S [P] which have these properties (e.g. $S = -\sum_i p_i^2$). However, only the choice

$$S = -\sum_i p_i \ln p_i$$

also has the following desirable property: If A and B are independent random variables, and AB is the composite random variable consisting of a realization of A followed by a realization of B, then

$$S_{AB} = S_A + S_B .$$

(Let p_{ij} = probability that A = a_i and B = b_j. By independence, $p_{ij} = p_i p_j$. Thus

$$S_{AB} = -\sum_{i,j} p_{ij} \ln p_{ij} = -\sum_i p_i \ln p_i - \sum_j p_j \ln p_j = S_A + S_B .)$$

For a random variable y taking continuous values, the entropy generalizes to

$$S = -\sum_i p_i \ln p_i \longrightarrow -\int dy\, p(y) \ln p(y) \cdot M(y)$$

where M(y) is an undetermined measure. If y has the Liouville property, then M(y) must be constant.

The basic strategy is to maximize S subject to constraints which represent the state of knowledge about the system.

Example: Two-dimensional Turbulence

The previously defined $y_i(t)$ satisfy the Liouville condition. Maximize

$$S = -\int\cdots\int \pi_i dy_i\, P(y_1, \ldots, y_N) \ln P(y_1, \ldots, y_N)$$

subject to

known energy $\quad \left\langle \sum_i y_i^2 \right\rangle = E_0$ (8)

known enstrophy $\quad \left\langle \sum_i k_i^2 y_i^2 \right\rangle = Z_0$

normalization $\quad \langle 1 \rangle \equiv \int\cdots\int P \pi_i dy_i = 1$

Using the technique of Lagrange multipliers,

$$P = C \exp\left[-\alpha E - \gamma' Z \right] \qquad (9)$$

where C, α, γ' are determined from (8).

From (9) it follows that

$$\langle E_i \rangle \equiv \langle y_i^2 \rangle = \frac{1}{2} / (\alpha + \gamma' k_i^2) \qquad (10)$$

and, of course

$$\langle Z_i \rangle \equiv \langle k_i^2 y_i^2 \rangle = \frac{1}{2} k_i^2 / (\alpha + \gamma' k_i^2) \qquad (11)$$

and the quantity $\alpha L_i + \beta' \ell_i$ is equipartitioned among the modes in equilibrium. The quantities α and β' play the role of inverse temperatures. Suppose that the wavenumbers k_i are dense enough so that k can be treated as a continuous variable. Then in two dimensions we have the equilibrium wavenumber spectrum,

$$L(k) \propto k/(\alpha + \beta' k^2) \tag{12}$$

Note that $E_0 = \int L(k)\,dk$ diverges logarithmically as $k \to \infty$. The divergence of the total enstrophy $Z_0 \int k^2 L(k)\,dk$ is even worse. These equilibria are therefore attainable only if the system is artifically restricted to a finite number of modes, as if all k except $k_0 < k < k_c$ were excluded from the dynamics.

For such a case, suppose that $Z_0 = k_1^2 E_0$, as if all the energy were initially dumped into wavenumbers near k_1. The equilibrium E(k) is determined by E_0, k_0, k_1, k_c through (12). Let $k_*^2 = \alpha/\beta'$. The following behaviors are found:

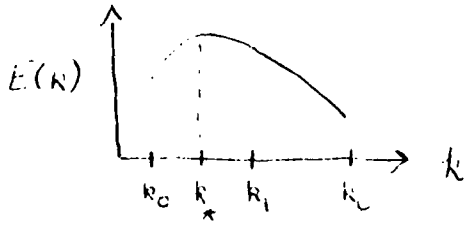

k_1 far from k_0, k_c
($\alpha, \beta' > 0$)

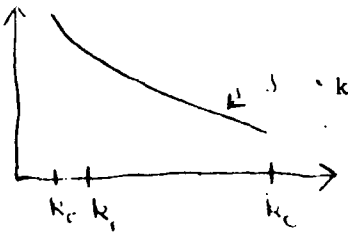

$k_1 \to k_0^+$
($\alpha < 0$, $\beta' > 0$)
enstrophy equipartition

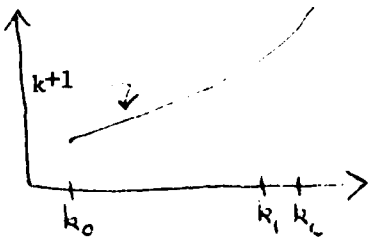

$k_1 \longrightarrow k_c^-$
($\alpha > 0$, $\beta' < 0$)
energy equipartition

To see how these states could anticipate nonequilibrium trends, imagine that k_c is raised by finite increments, with the system allowed to equilibrate between each adjustment. That is, let $k_c \to \infty$ with k_0, E_0, Z_0 (and hence k_1) fixed. Carrying out the algebra gives the results (Kraichnan 1975),

$$\alpha \sim k_c^2/Z_0 \quad , \quad k_*^2 + k_c^2 \sim k_c^2 \exp\left[-k_c^2/k_1^2\right]$$

AD-A122 864 1982 SUMMER STUDY PROGRAM IN GEOPHYSICAL FLUID DYNAMICS AT THE WOODS HOLE..(U) WOODS HOLE OCEANOGRAPHIC INSTITUTION MA G VERONIS ET AL. NOV 82 WHOI-82-45 2/4

UNCLASSIFIED N00014-82-G-0079 F/G 20/4 NL

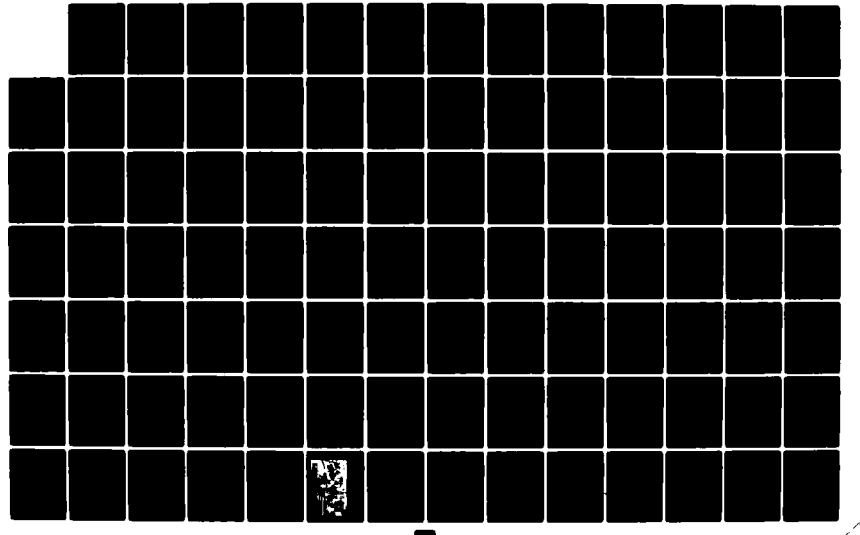

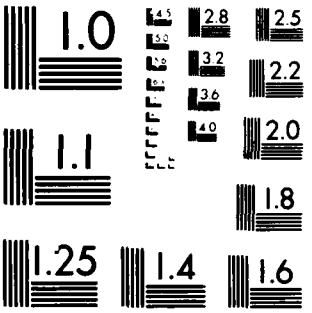

Thus as $k_c \to \infty$ nearly all of the enstrophy is found near k_c, but significant energy remains trapped at k_o. This thought experiment anticipates that enstrophy is transferred to ever-higher wavenumbers (and energy to lower) by the nonlinear terms in the equations of motion. This qualitative behavior could also be predicted by arguments which make no reference to inviscid equilibrium ensembles. Interestingly, however, all of these arguments require some form of statistical average. Without averaging, the time-reversibility of inviscid mechanics provides a counter-example for every example.

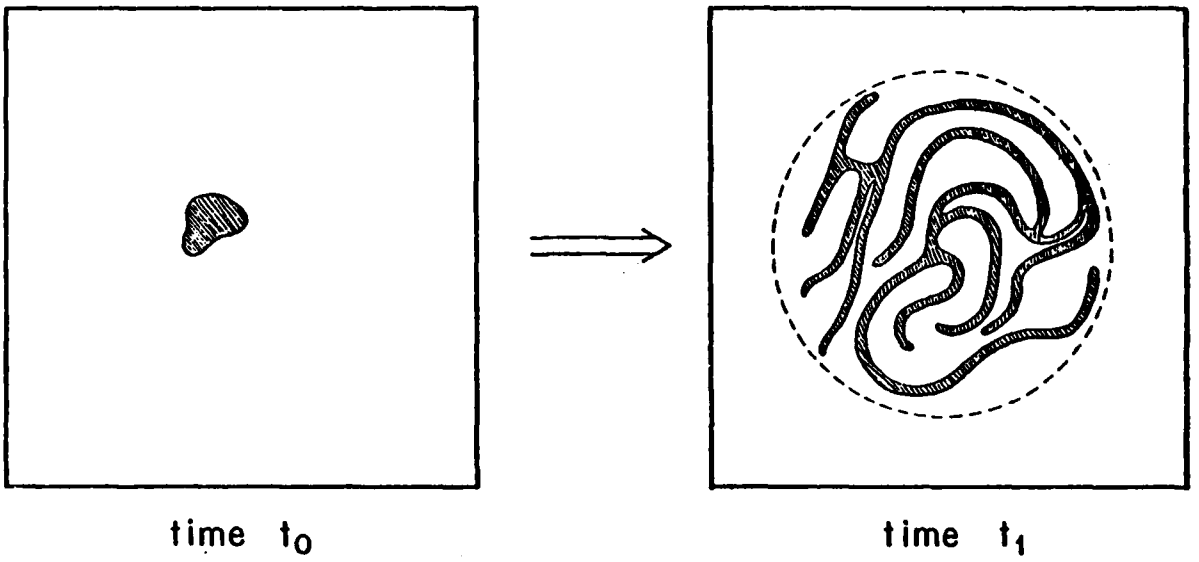

Fig. 1. Mixing in a two-dimensional phase space.

II. ROTATING FLOW OVER TOPOGRAPHY

In absolute equilibrium, only the total energy and enstrophy are known. Suppose instead that at some time t, the energy spectrum is assumed to be known. What is the entropy associated with this (imprecise) state of knowledge? Now we maximize S subject to the many constraints,

$$\langle y_i^2 \rangle = E_i^o, \quad \text{all } i \tag{13}$$

finding that

$$P = C \exp\left[-\sum_i \alpha_i y_i^2\right] \tag{14}$$

with

$$\alpha_i = 1/2E_i^o \tag{15}$$

Substituting (14) into the expression for S, viz

$$S = -\int\int \prod_i dy_i \, P \ln P \tag{16}$$

and performing the integration, we get

$$S = \sum_i \ln E_i^o \tag{17}$$

(to within additive and multiplicative constants.) Thus (17) is the entropy associated with the energy spectrum $\{E_i^o\}$. The equilibrium spectrum can be formed by maximizing (17) subject to total energy and enstrophy conservation.

Carnevale (1982) has studied numerical simulations of inviscid two-dimensional turbulence on a 256 x 256 periodic grid. The experiments (figure 2-5) confirm that the entropy (17) increases monotonically as the equilibrium spectrum is approached. A well-known group of turbulence closure models provides closed evolution equations for the single-time spectrum $\{E_i\}$. Interestingly, and I would say necessarily, these closure equations are consistent with the "H-theorem",

$$dS/dt \geq 0$$

where S is given by (17) (Carnevale et al, 1981).

Why are energy and enstrophy so important when inviscid two-dimensional flow actually conserves an infinite number of integral invariants $(\nabla^2\psi)^n$, where n is any number? One answer is that only the enstrophy (n=2) survives the truncation in modes. A more satisfactory answer is that the contours of the higher (n> 2) invariants are "space-filling" on the energy-enstrophy

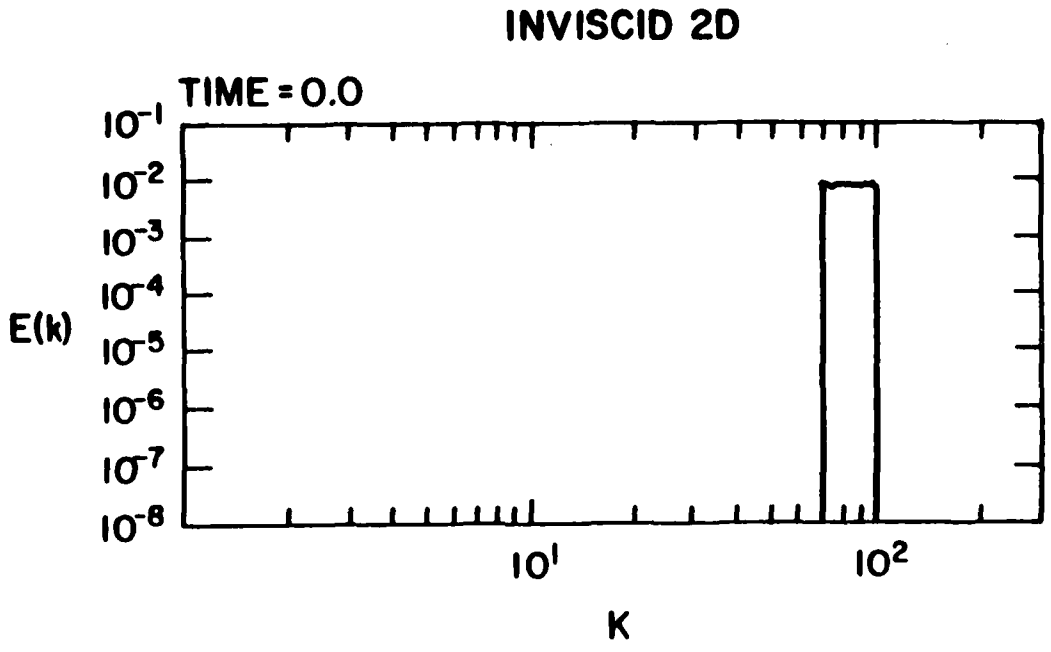

Fig. 2. Randomly generated initial spectrum to test the approach to equilibrium of inviscid numerical simulations of two-dimensional turbulence.

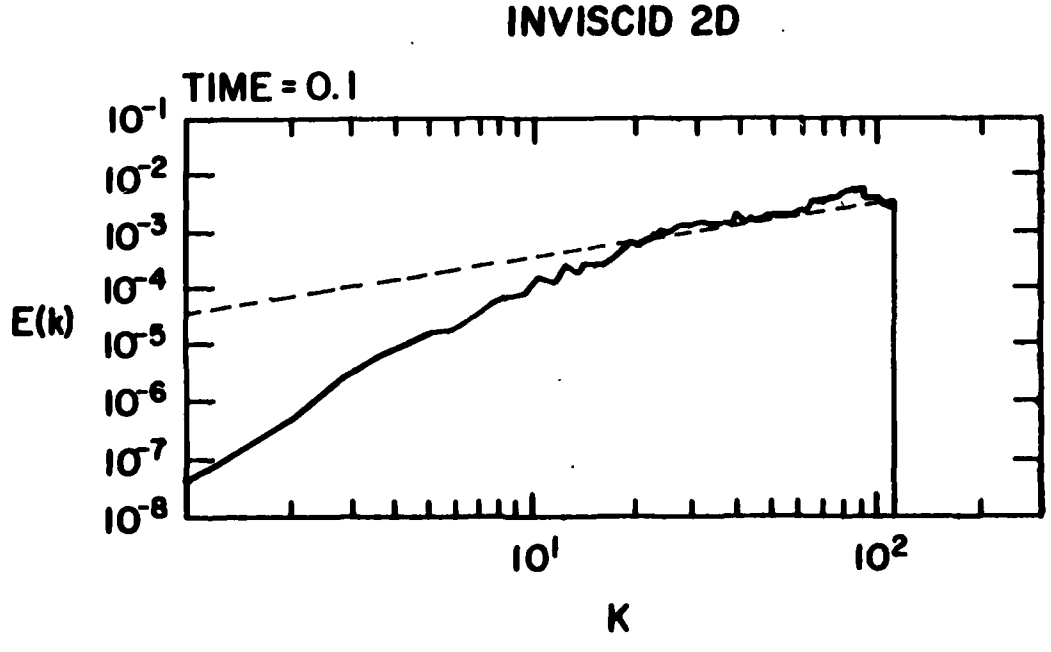

Fig. 3. Energy spectrum after t = .1 turn-overs. The theoretical equilibrium spectrum is dashed.

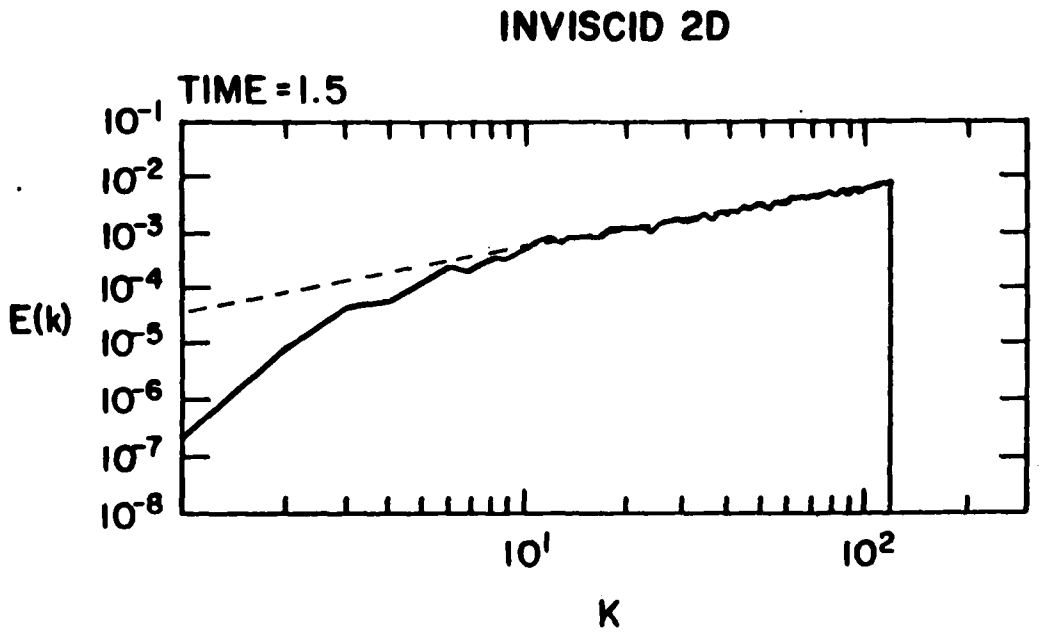

Fig. 4. Energy spectrum at t = 1.5.

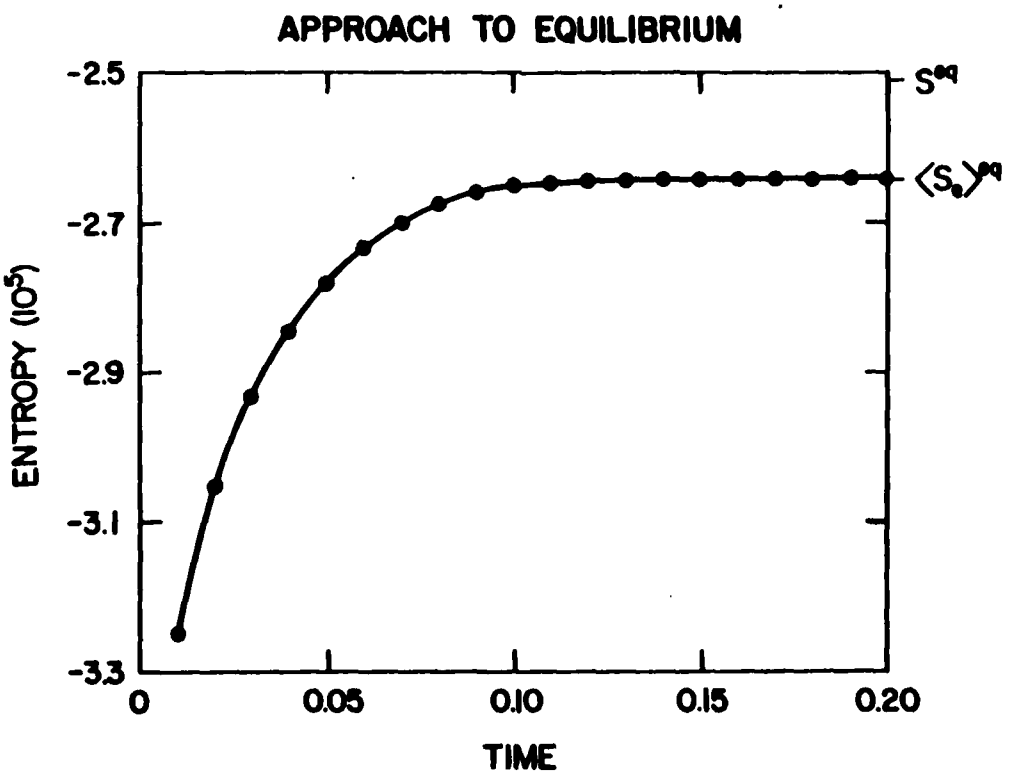

Fig. 5. Entropy evolution in the experiment shown in Figures 2-5. (Courtesy of G. Carnevale.)

hypersurface. Kells and Orszag (1978) have studied the inviscid evolution of low-order systems, in which the existence of these extra invariants (and perhaps others) is most likely to cause nonergodic behavior. They find that the macro-canonical ensemble is correct for as few as N~20 modes.

Now consider the more geophysically relevant case of one-layer quasi-geostrophic flow over topography. Let H be the fluid depth, L the horizontal length scale, and R_o the Rossby number. If either

$$(H/L) \ll 1 \qquad \text{or} \qquad R_o (H/L)^2 \ll 1$$

then the fluid motion is hydrostatic and columnar, and potential vorticity is conserved:

$$\frac{D}{Dt}\left(\frac{\zeta + f}{H}\right) = 0. \tag{18}$$

Here, ζ is the relative vorticity and f the Coriolis parameter. If, moreover,

$$R_o \ll 1, \quad \frac{\Delta H}{\bar{H}} \ll 1, \quad \frac{\Delta f}{f} \ll 1$$

then (18) is well approximated by the quasi-geostrophic equation,

$$\frac{\partial q}{\partial t} + J(\psi, q) = 0, \quad q = \nabla^2 \psi + h, \quad h = f + d, \quad d = \frac{f_0}{\bar{H}}(\bar{H} - H) \tag{19}$$

where ψ is the streamfunction and q the potential vorticity. Expand ψ and h in the previously defined eigenfunctions $\varphi_i(\underset{\sim}{x})$,

$$\psi = \sum_i \frac{y_i(t)}{k_i} \varphi_i(\underset{\sim}{x}), \quad h = \sum_i h_i \varphi_i(\underset{\sim}{x}).$$

The invariants are

energy $E = \sum_i y_i^2$

and

potential enstrophy (less a constant) $Z = \sum_i (k_i^2 y_i^2 - 2 k_i h_i y_i)$

By the same methods as before, we find that

$$\langle y_i \rangle = \frac{\gamma' k_i h_i}{\alpha + \gamma' k_i^2}, \quad \langle y_i^2 \rangle = \langle y_i \rangle^2 + \frac{1}{2(\alpha + \gamma' k_i^2)} \tag{20}$$

where α and β' are the Lagrange multipliers corresponding to energy and potential enstrophy. The mean streamfunction is an energy-weighted version of the topography. In typical cases $\beta'>0$, and we have anticyclonic flow over seamounts. The topography offers the fluid a way to sneak more energy into high wavenumbers: Positive correlation between ψ and h preserves $\mathcal{Z}$ despite the increase in $\Sigma k_i^2 y_i^2$. States with $\beta'<C$ correspond to initial energy sharply concentrated near k_c. For these more artificial states, the spread of energy into other wavenumbers forces a negative correlation between ψ and h to conserve $\mathcal{Z}$.

Holloway (1976) compared numerical solutions to the equations of motion for the following 3 interesting cases:

(i) no topography $\nabla^2\psi_t + J(\psi, \nabla^2\psi) = 0.$
energy and enstrophy conserved
no mean flow

(ii) topography and nonlinearity $\nabla^2\psi_t + J(\psi, \nabla^2\psi + h) = 0$
energy and potential enstrophy conserved
mean flow locked to the topography
topographic enhancement of the wavenumber spectrum

(iii) no nonlinearity $\nabla^2\psi_t + J(\psi, h) = 0$
energy and $\overline{\psi h}$ conserved
no mean flow (if $\overline{\psi h}$ is initially zero)
energy equipartition in equilibrium

The results are show in figure 6.

If the topography has coherent form (as if d=o so that h=f), then the transforms of (20) are useful. These are

$$\nabla^2\langle\psi\rangle + h = \left(\frac{\alpha}{\beta'}\right)\langle\psi\rangle \tag{21}$$

and

$$2\nabla^4(\beta'\nabla^2 - \alpha)\langle\psi'(\underset{\sim}{x})\psi'(\underset{\sim}{x}_o)\rangle = \delta(\underset{\sim}{x} - \underset{\sim}{x}_o) \tag{22}$$

where

$$\psi'(\underset{\sim}{x}) \equiv \psi(\underset{\sim}{x}) - \langle\psi(\underset{\sim}{x})\rangle.$$

To obtain the latter, remember that

$$\sum_i \phi_i(\underset{\sim}{x})\,\phi_i(\underset{\sim}{x}_o) = \delta(\underset{\sim}{x} - \underset{\sim}{x}_o).$$

An interesting special case is beta-plane flow in a rectangular ocean. The mean flow equation,

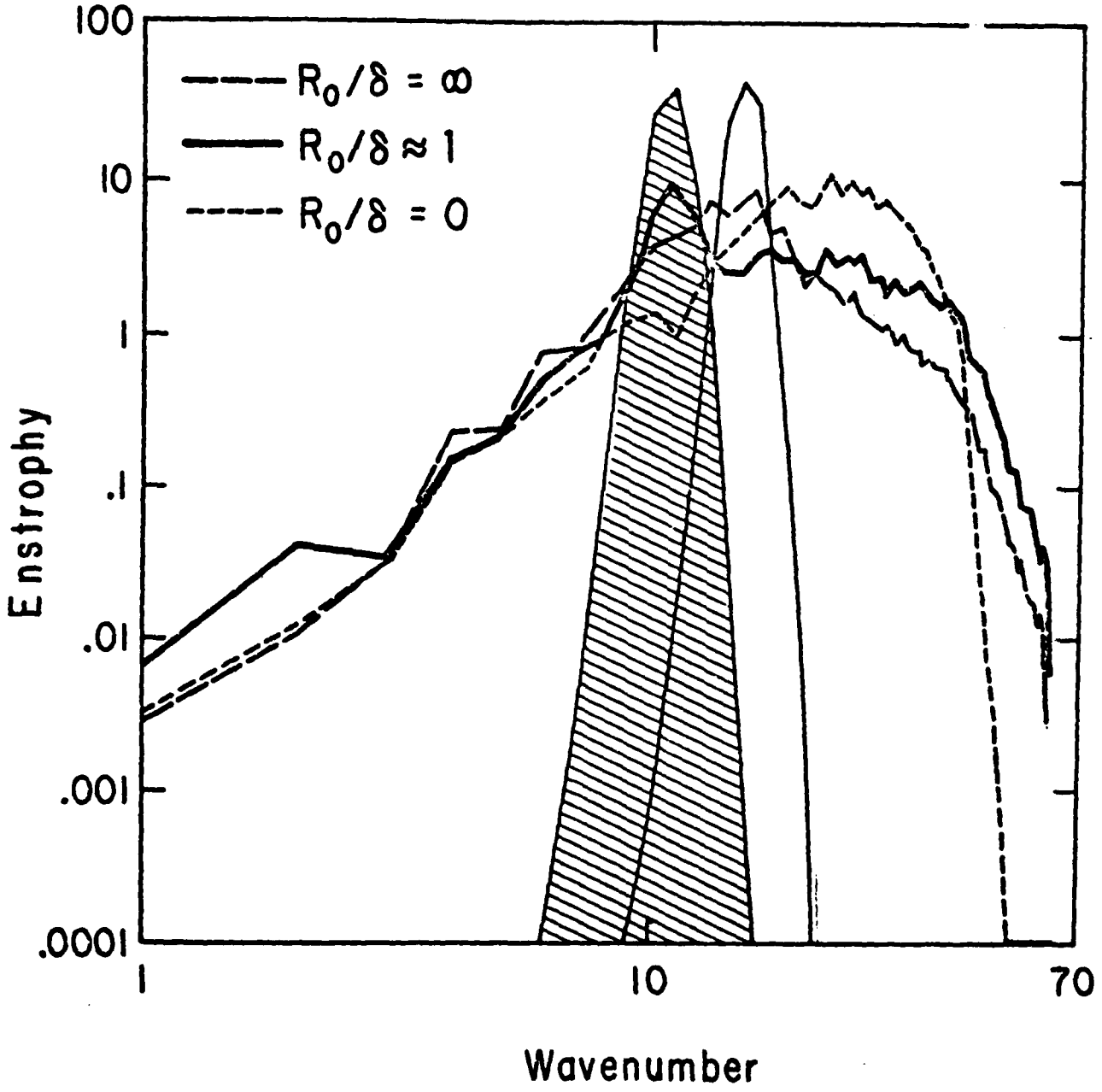

Fig. 6. Enstrophy spectra of two-dimensional turbulence over topography after 2.5 turn-overs beginning from a narrow spectral peak. The three experiments correspond to no topography (long dashes), topography and nonlinearity of equal strength (solid), and no nonlinearity (short dashes). The topography spectrum is hatched. (Courtesy of G. Holloway.)

$$\nabla^2\langle\psi\rangle + \beta(y-y_0) = \frac{\alpha}{\gamma}\langle\psi\rangle \qquad (23)$$

is the same equation considered by Fofonoff (1954). The constant y_0 can be considered the Lagrange multiplier corresponding to a third possible integral invariant, the mean potential vorticity. If the energy constraint is dropped ($\alpha = 0$), then the mean potential vorticity is uniform, but the equilibrium energy is unrealistically large (Rossby number order one). For realistically small initial energy, $\ell = (\gamma/\alpha)^{1/2}$ is much smaller than the ocean basin size, and inertial boundary layers of thickness ℓ close a uniform westward interior flow. These results suggest that energy conservation is a strong constraint on the spatial mixing of potential vorticity.

It is important to realize that the eigenfunction expansions are purely a device for avoiding functional methods. Our development has followed the solid arrows in the diagram below, but the dashed arrow is a possible alternate path.

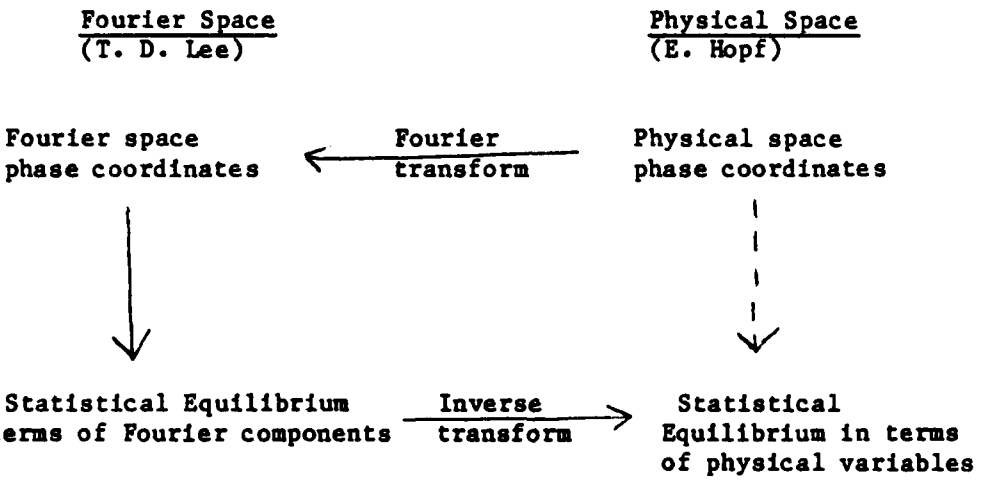

To follow the dashed arrow for the case of two-dimensional turbulence, let the phase coordinates be the values of ψ at horizontal grid-points with spacing Δ. Replace the equations of motion with finite-difference approximations which become exact as $\Delta \to 0$. Verify the Liouville property for the phase coordinates, construct the canonical ensemble, and write the equations for the mean and covariance. As $\Delta \to 0$, these equations become identical to (21) and (22). The details are straightforward.

III. STRATIFIED FLOW AND THE EQUATORIAL FUNNELING EFFECT

Now consider the rotating flow of two immiscible layers of different constant densities between rigid horizontal planes. The quasi-geostrophic equations for potential vorticity conservation take the forms,

$$\frac{\partial q_i}{\partial t} + J(\psi_i, q_i) = 0 \qquad \begin{matrix}(i=1 & \text{top layer} \\ (i=2 & \text{bottom layer}\end{matrix}$$

where
$$q_1 = \nabla^2\psi_1 + F(\psi_2 - \psi_1)$$
$$q_2 = \nabla^2\psi_2 + F(\psi_1 - \psi_2)$$
$$F = f^2/g'H \equiv k_R^2/2.$$

For convenience, the average depth of either layer is assumed to be H. g' is the reduced gravity and k_R^{-1} the internal deformation radius. The quadratic integral invariants of the motion are:

total energy $$\mathcal{E} = \overline{\nabla\psi_1\cdot\nabla\psi_1 + \nabla\psi_2\cdot\nabla\psi_2 + \frac{k_R^2}{2}(\psi_1-\psi_2)^2}$$

consisting of the kinetic energy in the top and bottom layers, and the available potential energy associated with displacements of the interface between layers; and

potential enstrophies $$\mathcal{Z}_1 = \overline{q_1^2}\ ,\ \mathcal{Z}_2 = \overline{q_2^2}$$

It is convenient to adopt the modal variables,

barotropic $$\psi = \tfrac{1}{2}(\psi_1 + \psi_2)$$

baroclinic $$\tau = \tfrac{1}{2}(\psi_1 - \psi_2)$$

Expand ψ and τ in spatial Fourier series. The phase coordinates are the real and imaginary parts of $\psi_{\underset{\sim}{k}}$ and $\tau_{\underset{\sim}{k}}$. Define,

$$U(\underset{\sim}{k}) = k^2|\psi_{\underset{\sim}{k}}|^2 \qquad \text{(barotropic energy in k)}$$

$$E(\underset{\sim}{k}) = (k^2 + k_R^2)|\tau_{\underset{\sim}{k}}|^2 \qquad \text{(total baroclinic energy).}$$

The invariants can now be written,

$$\mathcal{E} = 2 \sum_{\underset{\sim}{k}} \left[U(\underset{\sim}{k}) + E(\underset{\sim}{k}) \right] ,$$

$$(\mathcal{Z}_1 + \mathcal{Z}_2) = 2 \sum_{\underset{\sim}{k}} \left[k^2 U(\underset{\sim}{k}) + (k^2 + k_R^2) E(\underset{\sim}{k}) \right] ,$$

$$(\mathcal{Z}_1 - \mathcal{Z}_2) = 4 \sum_{\underset{\sim}{k}} k^2 (k^2 + k_R^2) \psi_{\underset{\sim}{k}} \tau_{\underset{\sim}{k}}^{*} .$$

Suppose (for simplicity) that the layers are statistically symmetric such that $\langle |\psi_{1\underset{\sim}{k}}|^2 \rangle = \langle |\psi_{2\underset{\sim}{k}}|^2 \rangle$ initially, and thus for all time. It follows that Real ($\psi_{\underset{\sim}{k}} \tau_{\underset{\sim}{k}}^{*}$) = 0 so that $\mathcal{Z}_1 - \mathcal{Z}_2 = 0$. Then the only equilibrium constraints are $\mathcal{E}$ and $\mathcal{Z}_1 + \mathcal{Z}_2$ conserved. The modes enter the expressions for energy and sum-enstrophy precisely as in two-dimensional turbulence, except that the baroclinic mode has effective squared wavenumber ($k^2 + k_R^2$). The inviscid equilibrium states thus turn out to be

$$U(\underset{\sim}{k}) = 1 / (\alpha + \gamma' k^2)$$

and

$$E(\underset{\sim}{k}) = 1 / [\alpha + \gamma' (k^2 + k_R^2)] .$$

In all cases of interest (initial energy not concentrated too near the upper cutoff k_c) U (k) decreases with increasing k for all k. Then $E(k) << U(k)$ for all $k << k_R$ and the equilibrium flow is nearly barotropic on scales larger than the deformation radius. This is the "end state" of baroclinic instability. Figure 7 shows the correlation coefficient between the layers in an inviscid numerical simulation of two-layer flow. The layers were initially uncorrelated. After 500 days the measured coorelation coefficient (solid) closely resembles that predicted by the theory (dashed).

The generalization to an N-layer fluid is straightforward. The energy and sum-enstrophy take the forms

$$E = \sum_{\underset{\sim}{k}} \left\{ E_0(\underset{\sim}{k}) + E_1(\underset{\sim}{k}) + E_2(\underset{\sim}{k}) + \cdots \right\}$$

and

$$\mathcal{Z}_{AVG} = \sum_{\underset{\sim}{k}} \left\{ k^2 E_0(\underset{\sim}{k}) + (k^2 + k_1^2) E_1(\underset{\sim}{k}) + (k^2 + k_2^2) E_2(\underset{\sim}{k}) + \cdots \right\}$$

where $E_n(\underset{\sim}{k})$ is the energy in horizontal wavenumber k and vertical mode n, and k_n^{-1} is the n-th internal deformation radius. Note $k_1 = k_R$. In

uniformly stratified flow, $k_n = n\pi f / \mathcal{N} H$,

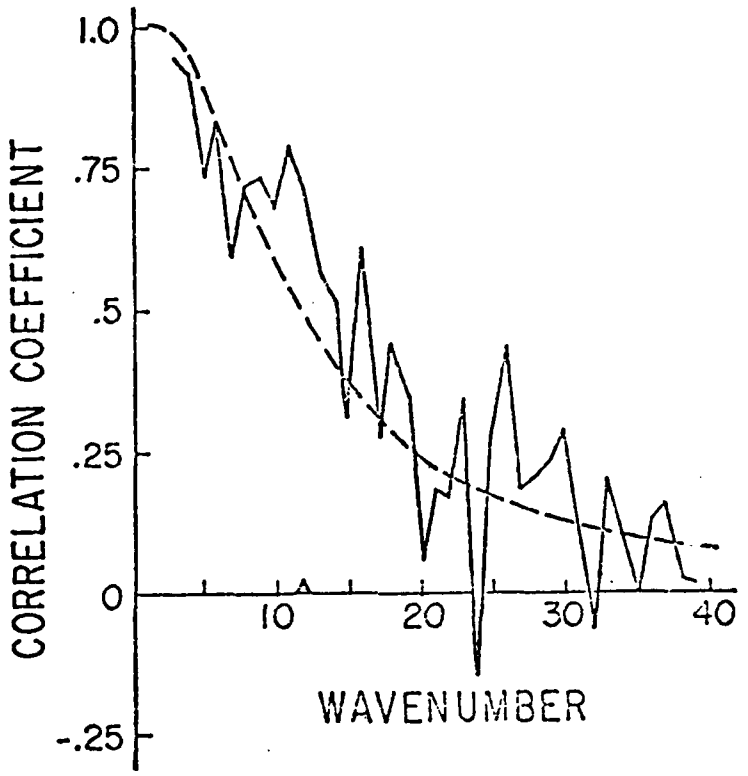

Fig. 7. The correlation coefficient between layers in an inviscid simulation of two layer flow.

where $\mathcal{N}$ is the Vaisala frequency and H the total depth. We expect net energy transfer into modes ($\underset{\sim}{k}$, n) with lower total wavenumbers $k^2 + k_n^2$. But k_n increases with n. This may explain why nonequatorial geostrophic motions show little energy in high vertical modes.

Now consider what happens as k_n varies with latitude through its dependence on f. As the equator is approached, the k_n vanish, removing the inhibition against high vertical mode numbers. Moreover, since the total wavenumber $k^2 + k_n^2$ of each mode (k, n) is smaller than its value at higher latitudes, the total energy should increase toward the equator. Thus a uniformly excited ocean would transfer energy equatorward and into high vertical mode. Observations seem to support this idea (Luyten and Swallow, 1976).

To calculate the inviscid equilibrium states with variable coriolis parameter f(y) and Vaisala frequency $\mathcal{N}(z)$, we adopt the quasi-geostrophic dynamics,

$$\frac{\partial \zeta}{\partial t} + J(\psi, \zeta) = 0$$

$$\zeta = \mathcal{L}[\psi] + f(y) \tag{24}$$

$$\mathcal{L}[\psi] = \nabla^2 \psi + \frac{\partial}{\partial z}\left[\frac{f^2}{\mathcal{N}^2}\frac{\partial \psi}{\partial z}\right],$$

with boundary conditions $\partial\psi/\partial z = 0$ at $z = 0, H$.

The invariants of the motion are the total energy,

$$E = -\iiint dx\,dy\,dz\ \psi\,\mathcal{L}[\psi],$$

and the potential enstrophy at every level,

$$\Omega(z) = \iint dx\,dy\ (\mathcal{L}[\psi] + f)^2, \quad \text{all } z$$

In equilibrium,

$$P \propto \exp\left[-\alpha E - \int \delta'(z)\,\Omega(z)\,dz\right] \tag{25}$$

and integrations of (25) yield the analogs of (21) and (22), viz

$$(\mathcal{L} + f)\langle\psi\rangle = \frac{\alpha}{\delta'}\langle\psi\rangle \tag{26}$$

and

$$2\,\mathcal{L}\left[\delta'\mathcal{L} - \alpha\right] R(\underset{\sim}{x}, \underset{\sim}{x}_0) = \delta(\underset{\sim}{x} - \underset{\sim}{x}_0) \tag{27}$$

where

$$R(\underset{\sim}{x}, \underset{\sim}{x}_0) = \langle \psi'(\underset{\sim}{x})\,\psi'(\underset{\sim}{x}_0)\rangle$$

Equation (27) suggests that the fluctuations will be strongest where the "vertical diffusion coefficient" $f^2/\mathcal{N}^2$ is the smallest.

Now specialize to an equatorial channel $-L < y < +L$ with periodic end conditions on x, $f = \beta y$ and $\mathcal{N}$ = constant. It can be shown that, on account of the channel geometry,

$$\frac{\partial}{\partial t}\left(\iint dx\,dy\ f\,\mathcal{L}\psi\right) = 0. \tag{28}$$

If the integral in (28) is initially zero, then the enstrophy invariant can be reduced to

$$\Omega(z) = \iint dx\,dy\ (\mathcal{L}[\psi])^2, \tag{29}$$

and there is no equilibrium mean flow. Suppose also that $\gamma'(z)$ has no z dependence. These conditions are met if the initial flow is uncorrelated with latitude and if the initial energy density is invariant with depth. The resulting equilibrium displays the "equatorial funneling effect" in its simplest form.

Expand the streamfunction ψ into vertical modes.

$$\psi(x,y,z) = \sum_{s=0}^{\infty} \hat{\psi}_s(x,y) \cos(s\pi z/H) \tag{30}$$

By the foregoing assumptions,

$$\langle \hat{\psi}_s(x,y)\, \hat{\psi}_{s'}(x,y) \rangle = \hat{R}_s(x,y;x_0,y_0)\, \delta_{ss'}, \tag{31}$$

and (27) implies that

$$\hat{\mathcal{L}}_s (\hat{\mathcal{L}}_s - \alpha/\gamma') \hat{R}_s = \frac{1}{2\gamma'} \delta(\underset{\sim}{x} - \underset{\sim}{x}_0) \tag{32}$$

where

$$\hat{\mathcal{L}}_s = \left(\frac{\partial}{\partial x}\right)^2 + \left(\frac{\partial}{\partial y}\right)^2 - k_s^2(y)$$

and

$$k_s^2 = \frac{s^2\pi^2\beta^2 y^2}{N^2H^2} \equiv \frac{1}{r_s^2}\left(\frac{y}{L}\right)^2$$

r_s is the s-th internal deformation radius. For $s=0$ (the barotropic mode), $k_0 = 0$ and

$$\nabla^2(\nabla^2 - \alpha/\gamma')\hat{R}_0 = \frac{1}{2\gamma'}\delta(\underset{\sim}{x} - \underset{\sim}{x}_0)$$

is the same as for two-dimensional turbulence. The equilibrium spectrum for the barotropic mode thus takes the form

$$E_0(\underset{\sim}{k}) \propto k/(\alpha + \gamma' k^2)$$

which is a maximum at $k = (\alpha/\gamma')^{1/2} = O(1/L)$. We therefore anticipate that

$$(\alpha/\gamma')^{1/2} \ll 1/r_s \quad \text{for} \quad s > 0,$$

i.e., that the internal deformation radii are smaller than the basin size. Then for $s>0$ (32) is well approximated by

$$\hat{\mathcal{L}}_s \hat{\mathcal{L}}_s \hat{R}_s = \frac{1}{2\gamma'} \delta(\underset{\sim}{x} - \underset{\sim}{x}_0) \tag{33}$$

Equation (33) has a similarity solution of the form

$$\hat{R}_s = \frac{r_s L}{2\gamma'} \Phi\left(\frac{\underset{\sim}{x}}{(r_s L)^{1/2}}, \frac{\underset{\sim}{x}_0}{(r_s L)^{1/2}}\right) \tag{34}$$

where

$$(\nabla^2 - y^2)^2 \underline{\Psi}(\underset{\sim}{x}, \underset{\sim}{x}_c) = \delta(\underset{\sim}{x} - \underset{\sim}{x}_c) \tag{35}$$

does not involve s. We can therefore deduce the following two important facts without explicitly solving (33).

(1) The latitudinal width of the equatorial energy peak of the s-th vertical mode is $(r_s \; \;)^{1/2}$ = the <u>equatorial</u> deformation radius for mode s.

(2) The average kinetic energy in mode s, at the equator, is

$$\langle \nabla \hat{\psi}_s \cdot \nabla \hat{\psi}_s \rangle|_{y_c} = \Gamma_s \; \Gamma_{x_c} \; \hat{R}_s|_{y_c}$$

By (34) this is independent of s. Thus all vertical modes have the same equilibrium kinetic energy at the equator.

We can make further deductions about the solutions of (33) by WKB reasoning. For $|y| \geq (\; ,\;)^{1/2}$, $\hat{\mathcal{L}}_s$ can be replaced by

$$\hat{\mathcal{L}}_s \rightarrow \left(\frac{\partial}{\partial x}\right)^2 + \left(\frac{\partial}{\partial y}\right)^2 - k_s^2(y_c).$$

Then (33) is identical to the equation of internal modes with <u>constant</u> f. The equilibrium spectra are

$$E_s(k; y_c) = \frac{k}{\mathcal{F}(k^2 + k_s^2(y_c))} \tag{36}$$

Decompose the potential enstrophy invariant (29):

$$\Omega = \sum_s \int \Omega_s(y)\, dy$$

into contributions $\Omega_s(y)$ from mode s and latitude y. Then since

$$\Omega_s(y) = \int (k^2 + k_s^2) E_s(k; y)\, dk,$$

it follows from (36) that $\Omega_s(y)$ is independent of both s and y in equilibrium. The enstrophy invariant is thus equipartitioned among the vertical modes and latitudes.

Figures 8-10 show results from a direct numerical simulation with a 6-layer quasi-geostrophic model in the equatorial channel. The initial conditions are random, with kinetic energy equally divided between the barotropic and first baroclinic modes. All higher modes have infinitesimal initial energy. There is no forcing or viscosity. The internal modes quickly develop equatorial energy peaks of the expected widths (figures 8,9) and the quantity $\Omega_s(y)$ tends toward uniformity in s and y (figure 10).

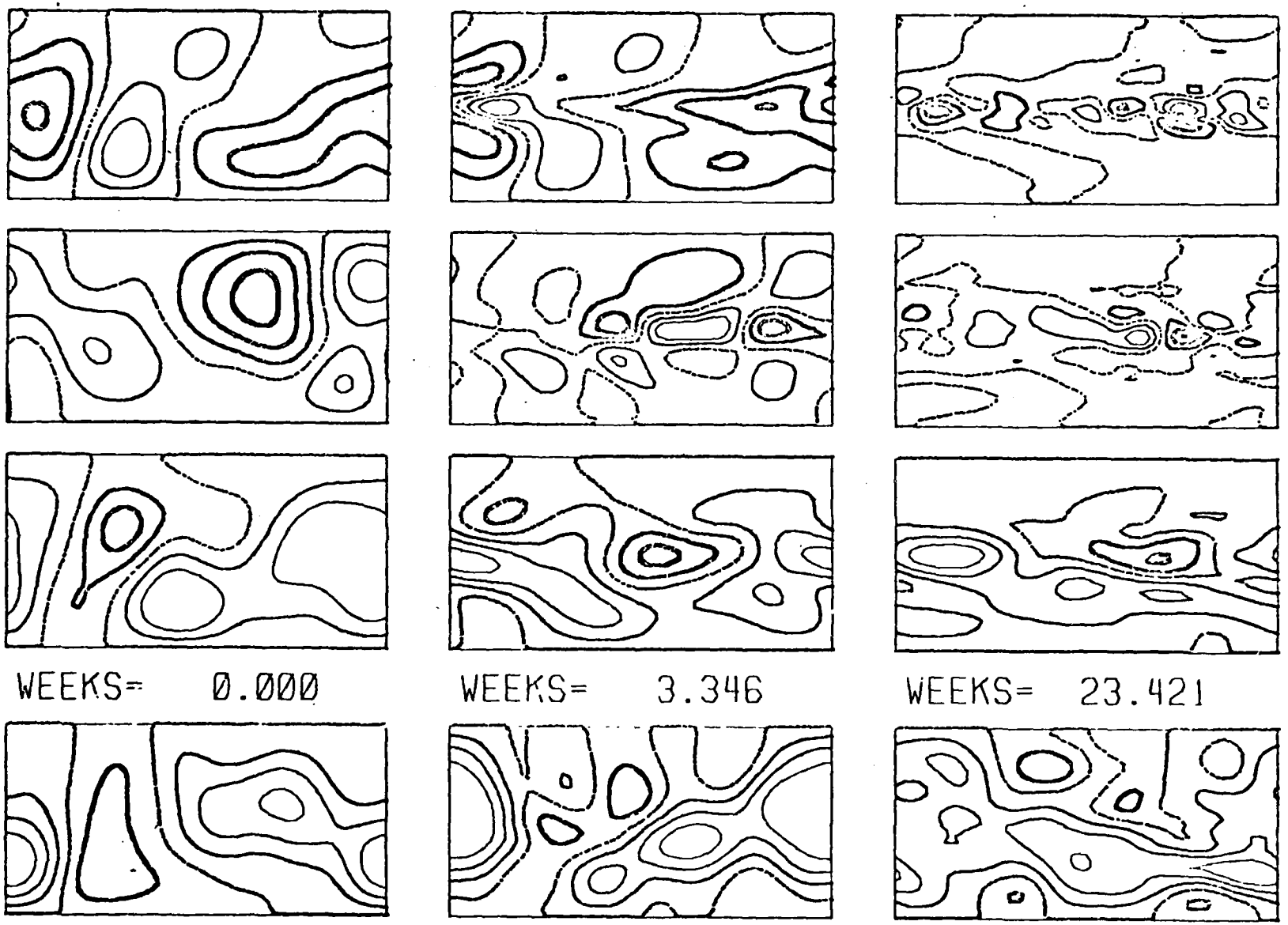

Fig. 8. The vertical-mode streamfunctions $\hat{\psi}_s$ in the equatorial channel for the barotropic mode s = 0 (bottom), s = 1, s = 3, and s = 5 (top). The equator lies along the axis of the channel.

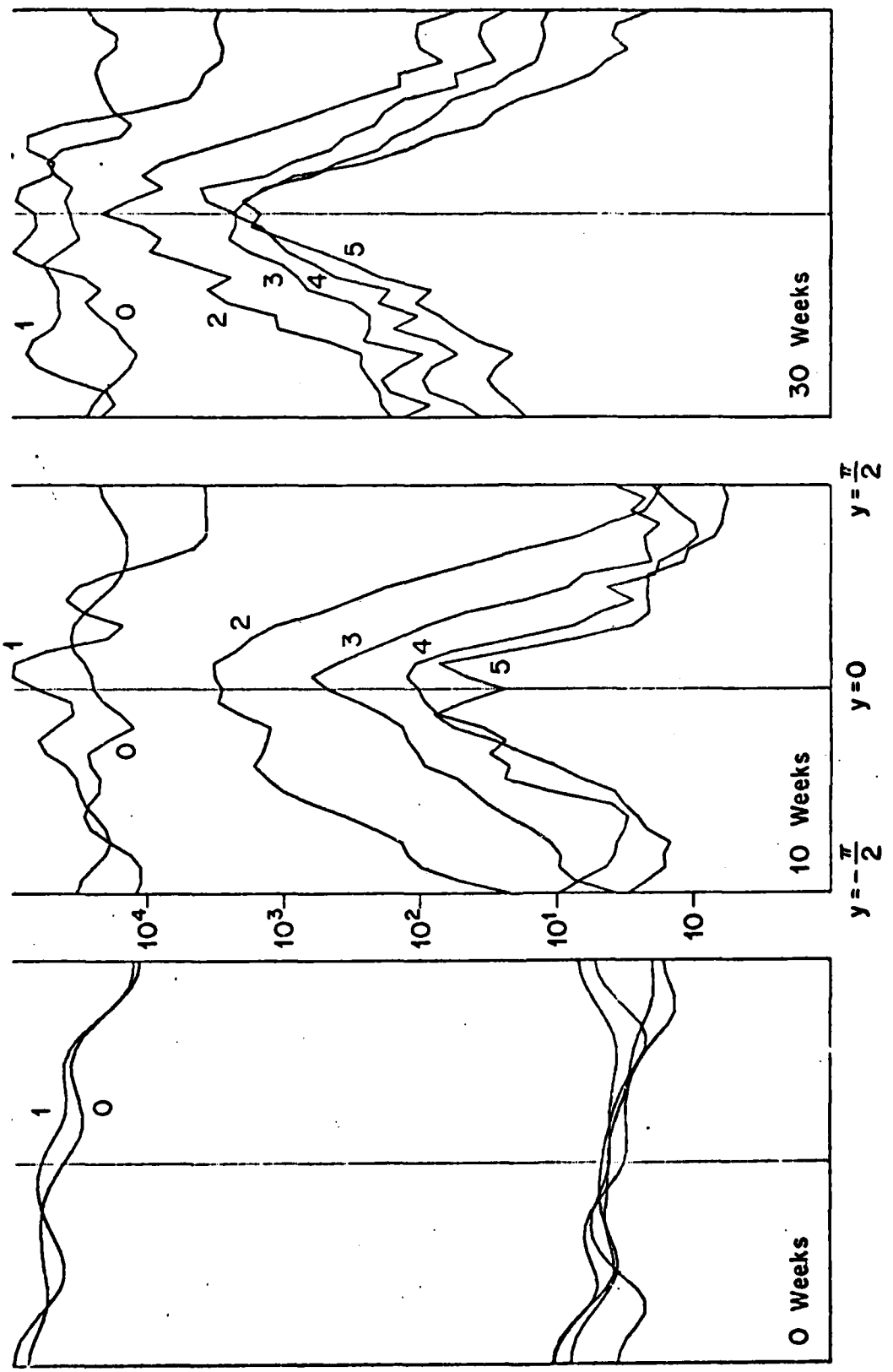

Fig. 9. The kinetic energy averaged over x in the vertical modes s = 0, 1, 2, 3, 4, 5. The equator lies at y = 0.

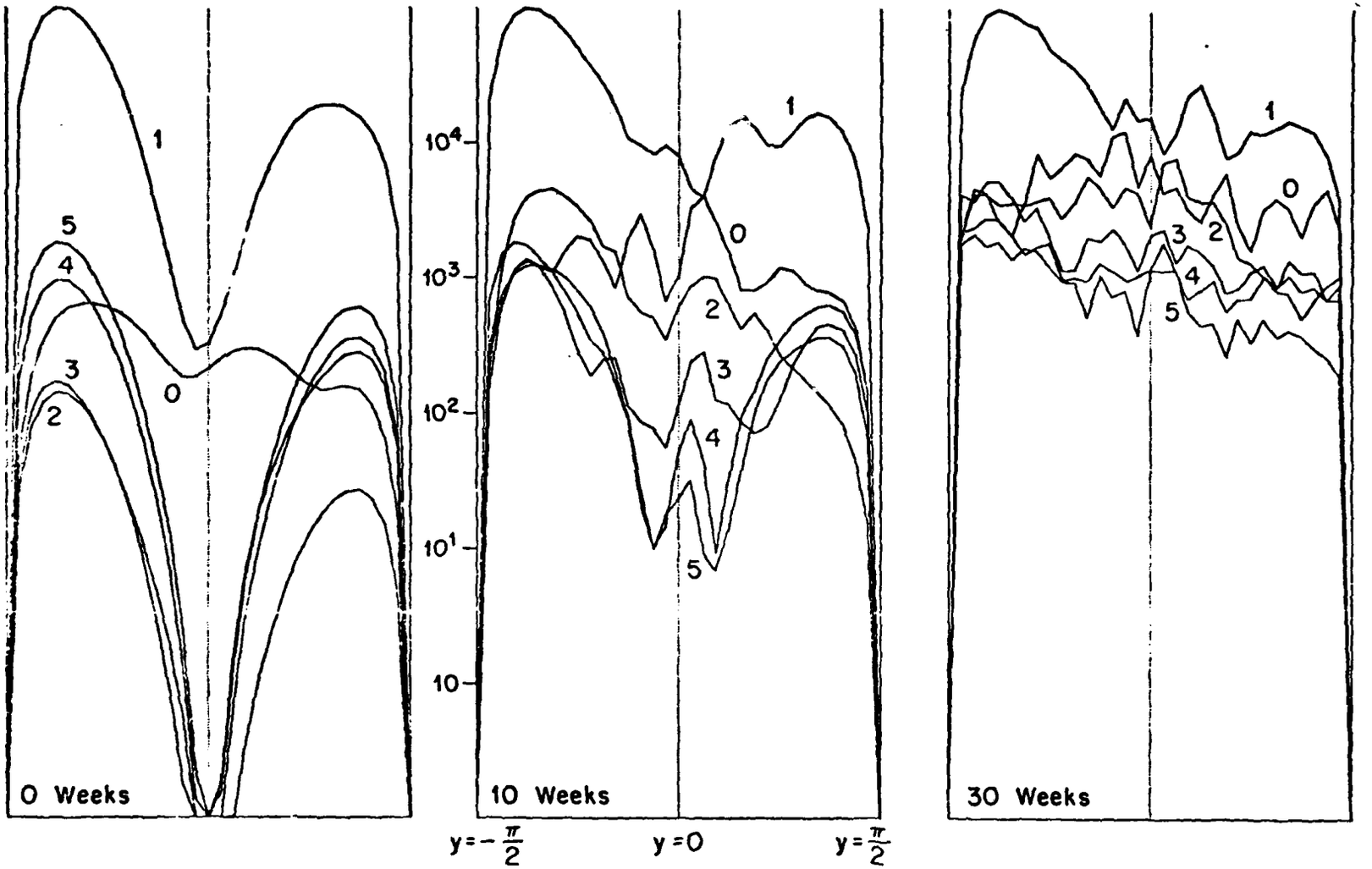

Fig. 10.The quantity $\Omega_s(y)$.

Remarks:

(1) Linear equatorial waves couple the different latitudes and can participate in equilibration. However, waves cannot explain the equipartition between vertical modes, because the latter are decoupled by linearization.

(2) The present theory predicts a spontaneous concentration of energy on the equator. Once there, the energy can be 'wave-like', i.e. it can be concentrated near the linear dispersion curves, but this in no way invalidates the explanations offered here.

(3) Quasi-geostrophic dynamics are invalid near the equator, so my results must be regarded as tentative. However, the solutions for large y should be correct, and they have interesting consequences.

REFERENCES

Primary Reference:

R. Salmon, 1982. Geostrophic turbulence, in Topics in Ocean Physics, Proc. Int. School of Physics Enrico Fermi.

Other references cited in the text:

Carnevale, G. F., 1982. Statistical features of the evolution of two-dimensional turbulence. J. Fluid Mech., 122, 143.

Carnevale, G. F., U. Frisch and R. Salmon, 1981. H-theorems in statistical fluid dynamics. J. Phys. A, 14, 1701.

Fofonoff, N. P., 1954. Steady flow in a frictionless homogeneous ocean. J. Mar. Res., 13, 254.

Holloway, G., 1976. PhD dissertation. U. C., San Diego.

Kells, L. C. and S. A. Orszag, 1978. Randomness of low-order models of two-dimensional inviscid dynamics. Phys. Fl., 21, 162.

Kraichnân, R. H.,1975. Statistical dynamics of two-dimensional flow. J. Fluid Mech. 67, 155.

Luyten, J. R. and J. C. Swallow, 1976. Equatorial undercurrents. Deep Sea Res., 23, 999.

WAVE-MEAN FLOW INTERACTIONS - WITH APPLICATIONS TO THE MIDDLE ATMOSPHERE

David Andrews

I. INTRODUCTION

This subject treats both the influence of the mean flow on wave propagation, and the nonlinear effects by which waves alter the mean flow. Clear examples of these processes occur in the stratosphere and mesosphere.

The first problem is how to define the mean flow and the waves. Meteorologists typically employ a zonal Eulerian average for the mean, but a Lagrangian average may be more appropriate for many problems. In any case, the disturbance or wave is defined as the departure from the mean.

In idealized examples, the waves are of small amplitude. One obtains the linear wave solutions, correct to first order in the amplitude, then examines the second order effects of the waves on the mean flow.

Three different situations will be considered: the interaction of two-dimensional internal gravity waves with a mean flow, U(z); the propagation of Rossby waves in a quasi-geostrophic system with application to stratospheric sudden warmings; and the transport of tracers in the stratosphere. The latter two examples will be treated with the transformed Eulerian-mean equations. This system is similar to the equations of the Lagrangian mean, but is easier to apply to meteorological situations.

Two kinds of theorems are relevant to the solutions of these problems. "Non-acceleration" or "non-interaction" theorems state that small amplitude waves alter the mean flow only in the presence of wave transience, wave forcing or wave dissipation.

Generalized Eliassen-Palm theorems (Eliassen and Palm, 1961) are conservation laws of the form

$$\frac{\partial A}{\partial t} + \nabla \cdot \underset{\sim}{F} = D$$

where A is a wave activity, $\underset{\sim}{F}$ is a flux (the Eliassen-Palm flux) and D represents forcing or dissipation. A, $\underset{\sim}{F}$, and D are averaged quantities, second order in the wave amplitude, which describe the propagation of waves through mean flows. They are useful diagnostics for such phenomena as stratospheric warmings. The wave activity is conservative, if D = 0, unlike wave energy which need not be conserved.

The transformed Eulerian mean formulation may be applied to the transport of tracers. In two-dimensional models of the middle atmosphere it is necessary to parameterize the effects of waves.

All these topics are included in the theory of the generalized Lagrangian mean. A Lagrangian mean is a time average following a particle. In the generalized theory this concept is extended to zonal averages. At least formally the theory is valid for finite amplitude disturbances, but in

practice it can be difficult or impossible to apply. The practical difficulties arise from the fact that definitions of particle displacements about their mean positions are required. The theory does, however, simplify the proofs of the non-acceleration and Eliassen-Palm theorems.

II. SECOND ORDER MEAN FLOW INDUCED BY INTERNAL GRAVITY WAVES

The equations of motion for a two-dimensional, inviscid, adiabatic, Boussinesq fluid in the x-z plane are

$$\frac{Du}{Dt} + p_x = 0 \qquad \frac{Dw}{Dt} + p_z - \theta = 0$$

$$\frac{D\theta}{Dt} + N^2 w = 0 \qquad u_x + w_z = 0$$

where θ is the perturbation buoyancy, and N^2, the Brunt-Väisälä frequency squared, is a specified function of z.

We consider an initial value problem in which the fluid is at rest for $t < 0$. At $t=0$ a moving corrugated lower boundary is turned on, with the height of the lower boundary given by

$$z = h(x,t) = O(a)$$

where a is assumed to be small. The corrugated boundary moves in the positive x direction at a constant speed, c.

We expect that internal waves will propagate away from the boundary, filling the region up to a height

$$z = c_g t$$

where c_g is the vertical group velocity. Above z the fluid will be undisturbed.

We will use a WKB, multiple scale approach to obtain the first order linearized wave solution, and then show how this wave solution affects the mean flow at second order.

The full boundary conditions are,

$$\text{at } z = h \qquad w = \left(\frac{\partial}{\partial t} + u\frac{\partial}{\partial x}\right) h$$

and as $z \to \infty$ the disturbance $\to 0$ for finite t. The domain is assumed to be either infinite or periodic in x, and the averaging operation $\overline{(\ )} = (\ )^*$ is an average over a wavelength. Also, we chose $\bar{h} = 0$.

The Linearized Problem

Expand each variable into its mean and disturbance contributions, i.e.

$$u = \bar{u} + u' \qquad \begin{matrix} u' = O(a) \\ \bar{u} = O(a^2) \end{matrix}$$

Then the linearized equations are

$$\begin{aligned} u'_t + p'_x &= 0 & w'_t + p'_z - \theta' &= 0 \\ \theta'_t + N^2 w' &= 0 & u'_x + w'_z &= 0 \end{aligned} \tag{1}$$

And the linearized boundary conditions are

$$\begin{aligned} &p' \to 0 \text{ as } z \to \infty \quad \text{for finite } t \\ &w' = h_t \text{ at } z = 0 \end{aligned} \tag{2}$$

In order to avoid generating transients, the boundary forcing is turned on slowly. A sinusoidal variation is chosen for the boundary. Thus

$$h' = aG(T)e^{ik(x-ct)} + O(a\mu) \tag{3}$$

where T is a "slow" timescale

$$T = \mu t$$

with $\mu \ll 1$. So G(T) is a slow modulation of the boundary forcing. The $O(a\mu)$ corrections are small and will not be needed explicitly.

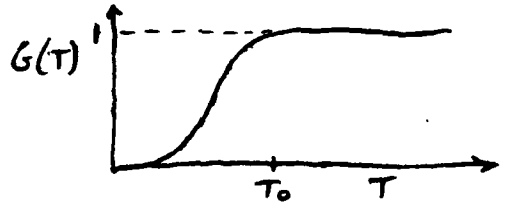

G(T) is chosen to behave as shown. T_o is the value of T at which G(T) reaches 1, where

$$\frac{T_o}{\mu} = O\left(\frac{2\pi}{\mu\omega}\right) \gg \frac{2\pi}{\omega} \quad \text{and} \quad \omega = ck.$$

Thus the operator $\frac{\partial}{\partial t}(\ )' = \left(i\omega + \mu\frac{\partial}{\partial T}\right)(\ )'$

To leading order in μ the lower boundary condition is

$$w' = -i\omega a G e^{ik(x-ct)} + O(\mu a) \quad \text{at} \quad z=0 \tag{4}$$

Now we take N^2 to be constant and look for solutions of the form

$$\{u', w', p', \theta'\} = \{\hat{u}, \hat{w}, \hat{p}, \hat{\theta}\} e^{i(kx+mz-\omega t)}$$

where m is the vertical wavenumber and the hat variables are functions of T and Z, where Z is a "slow" height.

$$Z = \mu z.$$

i.e.,

$$\hat{u} = \hat{u}(T,Z) + O(a)$$

At first order in the wave amplitude we obtain

$$\hat{w} = \frac{-k}{m}\hat{u} \quad , \quad \hat{p} = c\hat{u} \quad , \quad \hat{\theta} = \frac{iN^2k}{m\omega}\hat{u} \tag{5}$$

with the dispersion relation

$$\omega^2 = \frac{N^2k^2}{k^2+m^2} \qquad \text{or} \qquad |m| = \sqrt{\frac{k^2N^2}{\omega^2} - k^2} \tag{6}$$

and the vertical group velocity is given by

$$\frac{\partial \omega}{\partial m} = \frac{-m\omega^3}{N^2k^2} \tag{7}$$

The wave energy density, E, can be used to show that $m < 0$. A wave energy equation can be derived from the linearized equations of motion (1),

$$\frac{\partial E}{\partial t} + \frac{\partial}{\partial z}(\overline{p'w'}) = 0 \tag{8}$$

where the wave energy, E, is given by

$$E = \frac{1}{2}\left[\overline{u'^2} + \overline{w'^2} + \frac{\overline{\theta'^2}}{N^2}\right] \quad \text{to} \quad O(a^2) \tag{9}$$

In a shear flow there would be additional terms on the r.h.s. of equation (8). Using equation (5) the wave energy density may be expressed in terms of $\hat{u}$,

$$E = \frac{N^2k^2}{2m^2\omega^2}|\hat{u}|^2 \tag{10a}$$

and the wave energy flux

$$\begin{aligned} \overline{p'w'} &= \frac{1}{2}\mathrm{Re}(\hat{p}\hat{w}^*) \\ &= \frac{-\omega}{2m}|\hat{u}|^2 \\ &= \frac{-m\omega^3 E}{N^2k^2} \end{aligned} \tag{10b}$$

The wave momentum flux is

$$\overline{u'w'} = \frac{-m\omega^2 E}{N^2 k} \tag{11}$$

and the wave buoyancy flux is

$$\overline{\theta' w'} = O(\mu a^2)$$

Substituting (10) into (8), and using (7) we obtain

$$\frac{\partial E}{\partial t} + \frac{\partial}{\partial z}\left(\frac{\partial \omega}{\partial m} E\right) = 0$$

Since $\frac{\partial \omega}{\partial m}$ is constant, and E is a function of the slow variables only (to $O(a^2)$)

$$\frac{\partial E}{\partial T} + \left(\frac{\partial \omega}{\partial k}\right)\frac{\partial E}{\partial Z} = O(\mu a^2) \tag{12}$$

This has solutions

$$E = E\left(T - \frac{Z}{\left(\frac{\partial \omega}{\partial m}\right)}\right) \tag{13}$$

Using the lower boundary condition (4), and equation (10a) we have

$$E = \tfrac{1}{2} N^2 a^2 \left[G\left(T - \frac{Z}{c_g}\right)\right]^2 \tag{14}$$

where the group velocity, c_g, is now by definition

$$c_g = \frac{\partial \omega}{\partial m}$$

Note that the solution (14) automatically satisfies the condition at $z \to \infty$, provided we choose $m < 0$ so that $c_g > 0$. The vertical distribution of wave energy described by (14) is simply $G(T)^2$ turned on its side

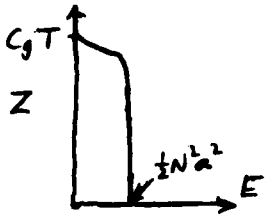

Now consider the induced $O(a^2)$ Eulerian mean flow.
The boundary condition to $O(a^2)$ is

$$\overline{w} + \overline{h w_z'} = \overline{u' h_x} \quad \text{at } z = 0$$

using the Taylor expansion $w(h) = w(0) + h w_z(0) + \ldots$ Recall that to $O(a)$ the boundary condition was evaluated at $z = 0$. But $\overline{u'h_x} = \overline{(u'h)_x} - \overline{hu_x}$ (the first term $\to 0$)

implies that $\bar{w} = -\overline{h(u'_x + w'_z)} = 0$ by continuity.

This is not generally the case, however. For example, in a rotating fluid one needs to allow for a third spatial dimension, in which case the boundary condition becomes

$$\bar{w} = -\overline{hw'_z} + \overline{u'h_x} + \overline{v'h_y} = \overline{v'h_y} \quad \text{at } z=0.$$

But $z = 0$ will lie above the physical boundary in the troughs, and if there were a tendency for the disturbance velocity to be one way along troughs and another along ridges in the boundary, then $\bar{w} \neq 0$; this would be associated with a vertical mass flux into or out of the trough region. However, the Lagrangian-mean $\bar{w}^L = 0$ at $z = 0$, so in this sense the Lagrangian-mean description is simpler than the Eulerian-mean one.

The horizontal momentum equation

$$\frac{Du}{Dt} + p_x = 0$$

$$\Rightarrow \bar{u}_t = -(\overline{u'w'})_z \quad \text{to } O(a^3) \text{ for } z \geq h_{max} \tag{15a}$$

Similarly, the thermal and vertical momentum equations respectively lead to

$$\bar{\theta}_t = -(\overline{\theta'w'})_z \tag{15b}$$

$$\bar{p}_z - \bar{\theta} = -(\overline{w'^2})_z \tag{15c}$$

Equation (7), together with (11) imply that $\overline{u'w'} = \frac{c_g}{c} E(Z,T)$, so one looks for solutions of the form $\bar{u} = \bar{u}(Z,T)$, etc. Then (15a) implies $\bar{u}_T = -\frac{1}{c}(c_g E)_Z$, which with (12) yields $\bar{u}_T = \frac{1}{c} E_T$. This equation can be integrated from an initial condition of rest to

$$\bar{u} = \frac{E}{c} \tag{16}$$

which represents the mean acceleration due to the waves. As the wave front progresses, the fluid accelerates in the frontal region.
Note that $\bar{\theta}_t = \alpha(\mu^2 a^2)$ in this problem, so that net heating is a higher-order effect.

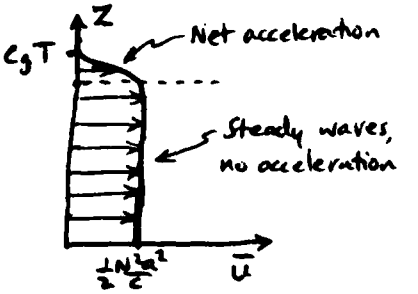

One can check that the force exerted on the fluid by the boundary balances the net acceleration:

$$\mathcal{F} = -\overline{ph_x}\Big|_{z=0} = \frac{\partial}{\partial t}\int_0^\infty \bar{u}\, dz \tag{17}$$

Possible generalizations are the introduction of a non-zero O(1) background flow U(Z), and $N^2 = N^2(Z)$. Then wave energy is no longer conserved, but wave-action A is conserved:

$$A = \frac{E}{\omega - kU(Z)} = \frac{\frac{1}{2}(\overline{u'^2} + \overline{w'^2} + \frac{1}{N^2}\overline{\theta'^2})}{\omega - kU(Z)} \tag{18}$$

satisfies the relation

$$\frac{\partial}{\partial T}A + \frac{\partial}{\partial Z}(c_g A) = O(\mu a^2, a^3) \tag{19}$$

where ω is the intrinsic frequency (Bretherton and Garrett, 1968). $O(\mu)$ dissipation can also be easily introduced into this formalism.

Generalized Eliassen-Palm Theorem for Two Dimensional Internal Gravity Waves

Let us now consider the basic shear flow $\bar{u}$, which is an O(1) quantity, and N^2 to be functions of height so that

$$\underset{\sim}{\bar{u}} = (\bar{u}(z), 0).$$

We will also allow dissipation and forcing to be present. Then the linearized equations for this flow are, if $D_t = \partial_t + \bar{u}\partial_x$,

$$D_t u' + w'\bar{u}_z + P_x' = X' \tag{20}$$

$$D_t w' + P_z' - \theta' = Z' \tag{21}$$

$$D_t \theta' + N^2 w' = Q' \tag{22}$$

$$u_x' + w_z' = 0, \tag{23}$$

where primed quantities are deviations from the zonal averages, X' includes viscosity or externally imposed wave forcing, Z' is a vertical forcing term and Q' is a thermal forcing term. Note that Z' should not be confused with the slowly varying height defined in the previous section. At this point we should also define the y-component of vorticity to be

$$\omega' = u_z - w_x.$$

The disturbance vorticity equation can now be obtained by partially differentiating (20) with respect to z and (21) with respect to x and subtracting to give

$$D_t \omega' + \omega'\bar{u}_{zz} + \theta_x' = X_z' - Z_x' \tag{24}$$

and if we let ζ' be the vertical particle displacement then

$$\omega' = D_t \zeta' + O(a^2), \tag{25}$$

$\bar{\rho}'$ being zero. We will also define q' to be the time integral of Q' following the mean flow $\bar{u}$, that is,

$$Q' = D_t q', \tag{26}$$

Rewriting (22) using (25) and (26) we obtain the equation

$$D_t(\theta' + N^2\rho' - q') = O(a^2)$$

If the initial conditions of our problem specify that the system is at rest at t = 0 then the equation above may be integrated to give

$$\theta' + N^2\rho' - q' = 0. \tag{27}$$

This equation relates particle displacement to buoyancy in the obvious way, that is, a rise in the particle position leads to a decrease in the buoyancy.

If (25) and (27) are incorporated into (24) the disturbance vorticity equation becomes

$$\partial_t(\omega' + \rho'\bar{u}_{zz}) - N^2\rho_x' = X_z' - Z_x' - q_x' \equiv \Delta', \tag{28}$$

where Δ' is the dissipation. Now multiplying (28) by ρ' and taking the zonal average of the resulting equation, noting that

$$\overline{\rho'\rho_x'} = \tfrac{1}{2}(\overline{\rho'^2})_x = 0,$$

we obtain

$$\overline{\rho'\Delta'} = \overline{\rho'\partial_t(\omega' + \rho'\bar{u}_{zz})} = \partial_t(\overline{\rho'\omega'}) - \overline{\omega'w'} + \bar{u}_{zz}\partial_t(\tfrac{1}{2}\overline{\rho'^2}) \tag{28a}$$

However,

$$\overline{\omega w'} = \overline{w'(u_z' - w_x')} = (\overline{w'a'})_z - \overline{u'w_z'} - \overline{w'w_x'},$$

the last two terms of which are zero from the continuity equation (23) and because

$$\overline{w'w_x'} = (\overline{\tfrac{1}{2}w'^2})_x = 0,$$

so that (28a) may be written as

$$\partial_t\{\overline{\rho'\omega'} + \tfrac{1}{2}\bar{u}_{zz}\overline{\rho'^2}\} - (\overline{u'w'})_z = \overline{\rho'\Delta'} + O(a^4). \tag{29}$$

Note that

$$\partial_t(\bar{\ }) = \partial_t(\bar{\ }).$$

Equation (29) is of the form of a conservation law

$$\frac{\partial A}{\partial t} + \frac{\partial B}{\partial z} = \text{Dissipation/forcing} + O(a^4). \tag{29a}$$

This is known as the Generalized Eliassen-Palm theorem for two dimensional internal gravity waves. It is more general than the work of the previous section because it has not employed the two scaling assumptions used there; only O(a) assumptions have been made. It is a generalization of the Eliassen-Palm theorem (Eliassen and Palm, 1961), which considers a linear conservation system with steady waves giving the result

$$(\overline{u'w'})_z = 0.$$

The question we wish to consider, having found the above result, is how do the small amplitude waves influence the mean flow? To examine this problem we will consider the mean momentum equation

$$\bar{u}_t + \bar{w}\bar{u}_z = -(\overline{u'w'})_z + \bar{X}.$$

If we assume that the boundary conditions imply that $\bar{w} = 0$ then (29) may be used to give

$$\bar{u}_t = -\partial_t\{A\} + \overline{\rho'\Delta'} + \bar{X}, \tag{30}$$

where

$$A = \overline{\rho'w'} + \frac{1}{2}\bar{u}_{zz}\overline{\rho'^2}.$$

This equation relates the mean acceleration of the flow to wave transients and dissipation, and forcing terms (plus nonlinear terms in $O(a^4)$). Thus the Generalized Eliassen-Palm Theorem (GEP) gives us an insight into what influences the mean flow. Note also the corollary to (30) for steady conditions in which the whole flow, that is, the linear waves and the mean flow, is conservative, namely

$$\bar{u}_t = 0.$$

This is a nonacceleration theorem which is known as the 'Charney-Drazin' theorem (Charney and Drazin, 1961).

The GEP theorem also gives useful information about 'wave action', namely, that for slowly varying waves the theorem reduces to the conservation equation for wave action

$$\frac{\partial}{\partial t}\left(\frac{\mathcal{E}}{\omega - k\bar{u}}\right) + \frac{\partial}{\partial z}\left(\frac{c_g E}{\omega - k\bar{u}}\right) = \text{dissipation/forcing}, \tag{31}$$

where C_g is the group velocity of the waves of wavenumber k and 'wave action' is the quantity $E/(\omega - ku)$, which is the ratio of the wave energy to its relative frequency. This equation, in the terminology of (29a), suggests that B/A may be regarded as a generalization of group velocity.

III. QUASI-GEOSTROPHIC FLOW ON A β-PLANE

In this section we will derive the GEP theorem for quasi-geostrophic disturbances on a β-plane and examine the implications for the $O(a^2)$ mean flow effects of these waves. In doing this the transformed Eulerian mean equations (TEM) will be derived and discussed.

We will consider our height coordinate in logarithmic pressure terms, that is, define

$$z = -H \ln(p/p_s),$$

where p_s is a standard reference pressure, often taken to be 1000 mb, and H is a standard scale height ($H = RT_o/g$, R being the gas constant and T_o a horizontal average temperature) which is approximately 7 km for the stratosphere.

Let our flow be conservative, then the equations of motion are

$$(\)_t + \underline{u} \cdot \nabla) q = 0 \tag{1}$$

$$\nabla \cdot \underline{u} = 0 \tag{2}$$

$$\underline{u} = (u, v, 0) = (-\psi_y, \psi_x, 0), \tag{3}$$

where q is the potential vorticity defined by

$$q = f_o + \beta y + \psi_{xx} + \psi_{yy} + \rho_o^{-1} (\varepsilon \rho_o \psi_z)_z \tag{4}$$

and

$$\rho_o(z) = \rho_s e^{-z/H}$$

$$\varepsilon(z) = f_o^2 / N^2(z)$$

$$N^2(z) = \frac{R}{H}\left[\frac{dT_o}{dz} + \frac{\kappa T_o}{H}\right],$$

ρ_s being a standard density and $\kappa = R/C_p$, the value of which is approximately 2/7 , C_p being the specific heat of air at constant pressure. For more details see Holton (1979, sect. 11.3).

Now

$$T = \frac{H}{R} f_o \psi_z = \theta e^{-\kappa z/H},$$

θ being the potential temperature, so

$$N^2(z) = \frac{R}{H} \frac{d\theta_o}{dz} e^{-\kappa z/H}$$

and from (4)

$$q = f_o + \beta y + v_x - u_y + \rho_o^{-1} \left(\rho_o f_o \frac{\theta}{\theta_{oz}}\right)_z. \tag{5}$$

This form for the potential vorticity is sometimes more convenient than that expressed in (4).

If we let all our variables be represented as the sum of a zonal mean plus a disturbance, as in the previous section, then

$$\bar{q} = f_o + \beta y + \bar{\psi}_{yy} + \rho_o^{-1} (\rho \varepsilon \bar{\psi}_z)_z \tag{6}$$

$$q' = \psi'_{xx} + \psi'_{yy} + \rho_o^{-1} (\rho_o \varepsilon \psi'_z)_z. \tag{7}$$

The northward eddy flux of potential vorticity is then (Bretherton, 1966)

$$\overline{q'v'} = \overline{q'\psi_x'} = (\overline{\psi_x'\psi_y'})_y + \rho_0^{-1}(\overline{\psi_x'\psi_z'}\rho_0\varepsilon)_z$$

which can be rewritten as

$$\overline{\rho_0 q'v'} = -(\rho_0\overline{u'v'})_y + \left(\rho_0 f_0 \frac{\overline{v'\theta'}}{\theta_z}\right)_z. \tag{8}$$

To obtain the GEP theorem we will use the linearized potential vorticity equation

$$\partial_t q' + v'\bar{q}_y = 0 \tag{9}$$

where

$$\partial_t = \partial_t + \bar{u}\partial_x$$

and, from (6),

$$\bar{q}_y = \beta - \bar{u}_{yy} - \rho_0^{-1}(\rho_0\varepsilon\bar{u}_z)_z.$$

We also define the northward particle displacement η', to O(a), by

$$\partial_t\eta' = v' \tag{10}$$

Combining (9) and (10) gives the equation

$$\partial_t(q' + \eta'\bar{q}_y) = 0,$$

which, if the initial conditions specify that the fluid is at rest at t = o, implies that

$$q' = -\eta'\bar{q}_y. \tag{11}$$

The lefthand side of equation (8) may now be rewritten, using (10) and (11), as

$$\overline{\rho_0 q'v'} = -\rho_0\bar{q}_y\overline{\eta'v'} = -\rho_0\bar{q}_y\overline{\eta'\partial_t\eta'} = -(\tfrac{1}{2}\rho_0\bar{q}_y\overline{\eta'^2})_t + O(a^4)$$

so that (8) becomes

$$\frac{\partial}{\partial t}(\tfrac{1}{2}\rho_0\bar{q}_y\overline{\eta'^2}) + \frac{\partial}{\partial y}(-\rho_0\overline{u'v'}) + \frac{\partial}{\partial z}\left(\rho_0 f_0\frac{\overline{v'\theta'}}{\theta_z}\right) = O(a^4). \tag{12}$$

This is the GEP theorem for conservative quasi-geostrophic disturbances. The quantity

$$A = \tfrac{1}{2}\rho_0\bar{q}_y\overline{\eta'^2}$$

is sometimes called the "density of wave activity" and may be written, using (11), as

$$A = \tfrac{1}{2}\rho_0\overline{q'^2}/\bar{q}_y. \tag{13}$$

The quantity analogous to B in equation (29a) of the last section is

$$\underset{\sim}{F} = \left(0, -\rho_c \overline{u'v'}, \rho_c f_0 \frac{\overline{v'\theta'}}{\theta_z}\right), \tag{14}$$

which is known as the Eliassen-Palm flux vector.

There are several corollaries to (12):

i) For steady conservative linear waves (12) reduces to

$$\nabla \cdot \underset{\sim}{F} = 0, \tag{14a}$$

also $\rho_c \overline{v'v'}$ is identically zero everywhere. This result (14a) was proved by Eliassen and Palm (1961).

ii) As the velocities are geostrophic, $\underset{\sim}{F}$ only involves geostrophic quantities and should be a useful diagnostic. However, as A involves η' $\underset{\sim}{F}$ may not be as useful as it appears when the conservation equation (12) is considered.

iii) When dissipation is included, (12) takes the form

$$A_t + \nabla \cdot \underset{\sim}{F} = 0.$$

iv) Consider the wave action equation II.31 for slowly varying waves and mean flow found in the previous section. A comparison of this equation with (12) suggests that $\underset{\sim}{F}/A$ may be regarded as a generalization of the group velocity c_g of the waves to cases where the waves are not slowly varying.

If we now turn to consideration of the $O(a^2)$ mean flow effect of the waves, first note the appropriate $O(a^2)$ mean flow equations

$$\bar{u}_t - f_0 \bar{v}_a = -(\overline{u'v'})_y \tag{15}$$

$$\bar{\theta}_t + \bar{\theta}_z \bar{w}_a = -(\overline{v'\theta'})_y + \bar{Q}, \tag{16}$$

where $(\bar{v}_a, \bar{w}_a)$ is the mean ageostrophic wind and $\bar{Q}$ is the mean thermal forcing, with the continuity equation

$$\frac{\partial \bar{v}_a}{\partial y} + \bar{\rho}_c^{-1} \frac{\partial}{\partial z}(\rho_c \bar{w}_a) = 0 \tag{17}$$

and the thermal wind equation

$$f_0 \bar{u}_z + \Gamma(z) \bar{\theta}_y = 0, \tag{18}$$

where

$$\Gamma(z) = \frac{R}{H} e^{-\kappa z/H}.$$

Defining the "residual mean meridional circulation" $(\bar{v}^*, \bar{w}^*)$ by

$$\bar{v}^* = \bar{v}_a - \rho_a^{-1}\left(\rho_a \frac{\overline{v'\theta'}}{\bar{\theta}_z}\right)_z \; ; \; \bar{w}^* = \bar{w}_a + \left(\frac{\overline{v'\theta'}}{\bar{\theta}_z}\right)_y \; , \tag{19}$$

we can derive, from (15)-(17), the transformed Eulerian mean eq. (TEM):

$$\bar{u}_t - f_a \bar{v}^* = \frac{1}{\rho_a} \nabla \cdot \underline{F} = \overline{q'v'} \tag{20}$$

$$\bar{\theta}_t + \bar{\theta}_z \bar{w}^* = \bar{Q} \tag{21}$$

$$\bar{v}_y^* + \rho_a^{-1}(\rho_a \bar{w}^*)_z = 0. \tag{22}$$

The TEM equations also include (18).

If the TEM equations are combined then an equation for $\bar{u}_t$ in terms of $\nabla \cdot \underline{F}$ and Q can be found, namely,

$$\left[\left(\;\right)_y^2 + \rho_a^{-1}\left(\rho_a \varepsilon\left(\;\right)_z\right)_z\right]\bar{u}_t = \rho_a^{-1}(\nabla \cdot \underline{F})_{yy} - \rho_a\left(f_a \rho_a \bar{Q}_y / \bar{\theta}_z\right)_z. \tag{23}$$

Thus given boundary conditions for $\bar{u}$, a knowledge of $\nabla \cdot \underline{F}$ in the eddy forcing term and $\bar{Q}$ in the mean diabatic forcing term, equation (23) may be solved for $\bar{u}$. Another point to note about (23) is the nonlocal response of $\bar{u}_t$ to $\nabla \cdot \underline{F}$.

If we are interested in $(\bar{v}^*, \bar{w}^*)$ as well, then by defining

$$\bar{v}^* = -\rho_a^{-1}\bar{\chi}_z^* \quad , \quad \bar{w}^* = \rho_a^{-1}\bar{\chi}_y^* \tag{24}$$

the TEM equations give

$$\left[\left(\;\right)_y^2 + \rho_a \varepsilon\left(\;\right)_z\left(\rho_a^{-1}\left(\;\right)_z\right)\right]\bar{\chi}^* = \frac{\rho_a}{N^2}\left(f_a \frac{\nabla \cdot \underline{F}}{\rho_a}\right)_z + \rho_a \bar{Q}_y / \bar{\theta}_z \tag{25}$$

so that $(\bar{v}^*, \bar{w}^*)$ may be determined through (24) (cf. Eliassen, 1951). Note that one has to be careful about the boundary condition for (25) (Andrews, 1980).

IV. SUDDEN STRATOSPHERIC WARMING

Sudden warmings of the polar stratosphere during winter are perhaps the most spectacular large scale events to occur in this region of the atmosphere. In this section we will apply the theory of the previous lecture to this phenomenon.

These sudden warmings occur about every other year in the winter northern hemisphere stratosphere. They are characterized by the basically westerly polar flow weakening and changing direction and the northward negative temperature gradient reversing so that the pole warms. This sequence of

events occurs very rapidly in January or February with temperature changes of the order of 40°K in five days. The sequence of events can be observed from satellite data (Palmer, 1981a,b); a view of the zonal average wind field for the 1979 warming is shown in Figure 1. It can be seen from the series how dramatically the warming occurs.

Sudden warmings were first observed in 1952 and the currently accepted theory originated with Matsuno (1971) who suggested that planetary Rossby waves of wavenumber m = 1 or 2 propagate from the troposphere into the stratosphere and by nonlinear rectification of these waves the mean flow could be altered. Matsuno invoked transients of the waves to produce the deceleration of the polar jet and used simple analytical and numerical models. An alternative interpretation is that the rapid heating can be ascribed to the descent of air parcels.

A number of numerical models have appeared since Matsuno's work as well as diagnostic studies. Recent discussions, however, have made extensive use of the TEM equations and the EP flux $\underline{F}$. These include Dunkerton et al. (1981) who used Holton's model and Palmer (1981a) who studied satellite data.

Palmer used the "EP" diagnostics $\underline{F}$ and $\nabla \cdot \underline{F}$ in spherical coordinates. In these coordinates the mean momentum equation is

$$\bar{u}_t - f\bar{v}^* = \frac{\rho_s'(z)\nabla \cdot \underline{F}}{a\cos\varphi} \qquad (1)$$

where φ is the latitude and a is the radius of the earth. In terms of angular momentum this equation may be written as

$$\partial_t(\rho_s a\cos\varphi\,\bar{u}) - f\rho_s a\cos\varphi\,\bar{v}^* = \nabla \cdot \underline{F}.$$

As in the β-plane case $\nabla \cdot \underline{F}$ is zero unless there is wave transcience or the fluid is nonconservative or nonlinear. Recall also that F/A measures wave propagation as it is analogous to C_g.

To demonstrate the uses of $\nabla \cdot \underline{F}$ we will consider an idealized situation and then examine Palmer's analysis of the 1979 warming. First, in Figure 2 typical contours of $\nabla \cdot \underline{F}$ are drawn in an "EP cross-section". On this diagram integral curves of $\underline{F}$ are also shown - these can be thought of as rays along which waves propagate, even without slow variation, provided A is positive. The prominent equatorward tilt of these rays is expected from the theory of Rossby waves as wave packets are expected to follow great circle paths. For more details about these diagrams see Edmon et al (1980).

In Figure 3, taken from Palmer (1981a), we see the "EP cross-sections" for the sudden warming of February 1979. On the 17th of February precursor rays from an m = 1 wave are seen coming down from the mesosphere while lower down the field is not unusual. However, by the 19th some of the tropospherically generated waves are tilted toward the pole while a strong convergence zone is developing near the 10 mb level which is possibly causing the deceleration observed in Figure 1. After some rapid changes in the polar convergence picture the "EP cross-section" settles to a strong divergent pattern at 80°N near the 10 mb level with m = 1 waves propagating out of the polar region. For more details of the intricacies of this figure see Palmer (1981a).

Fig. 1. Meridional cross section of zonal mean wind velocity (ms^{-1}). Regions of easterly winds are stippled: (a) 17 February, (b) 19 February, (c) 20 February, (d) 21 February, (e) 23 February, and (f) 27 February. The values of the pressure coordinates used in this and the following figures are related to the scale-height coordinates used in the text by the following: 100 mb-14.7 km; 40 mb-20.5 km; 10 mb-29.4 km; 4 mb-35.2 km; 1 mb-44.1 km.

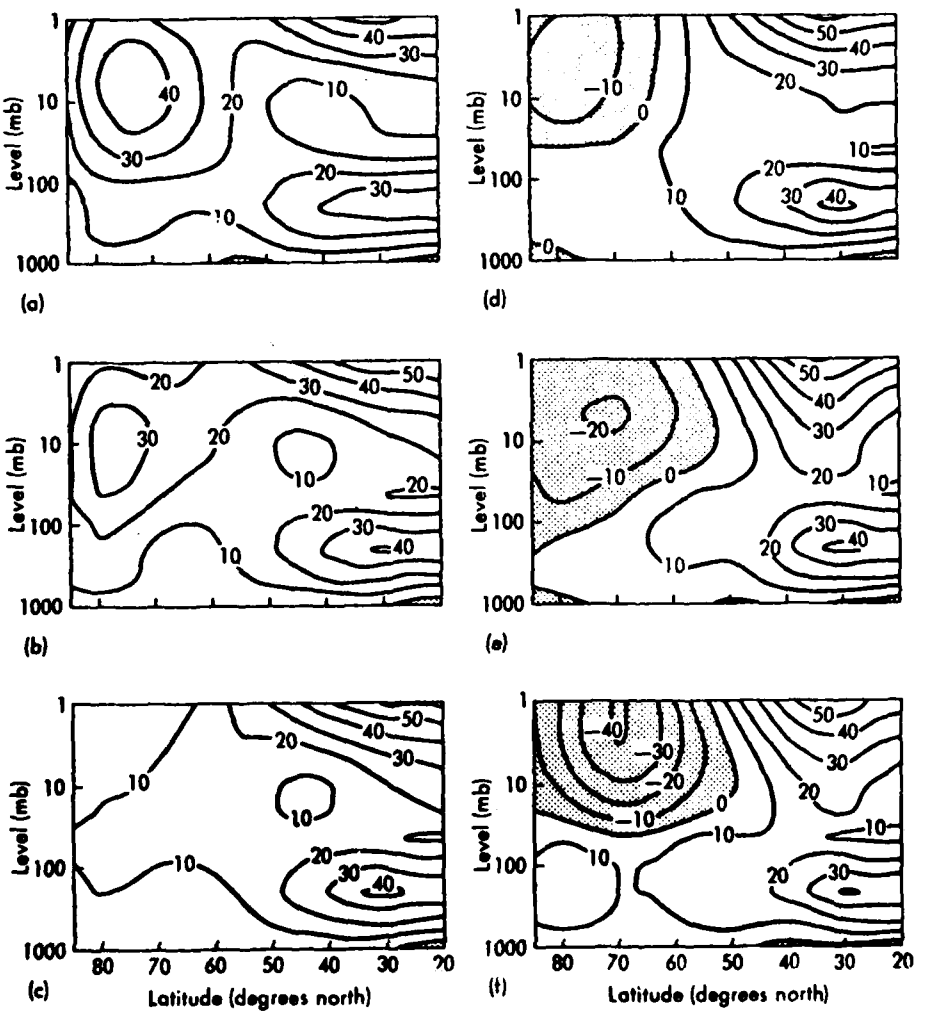

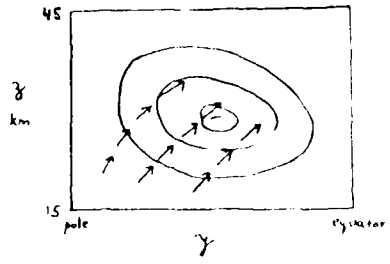

Fig. 2. The continuous curves are contours of $\nabla . \underline{F}$ and the broken lines are curves of E (which are everywhere parallel to the total value of $\underline{F}$). This is an idealized view.

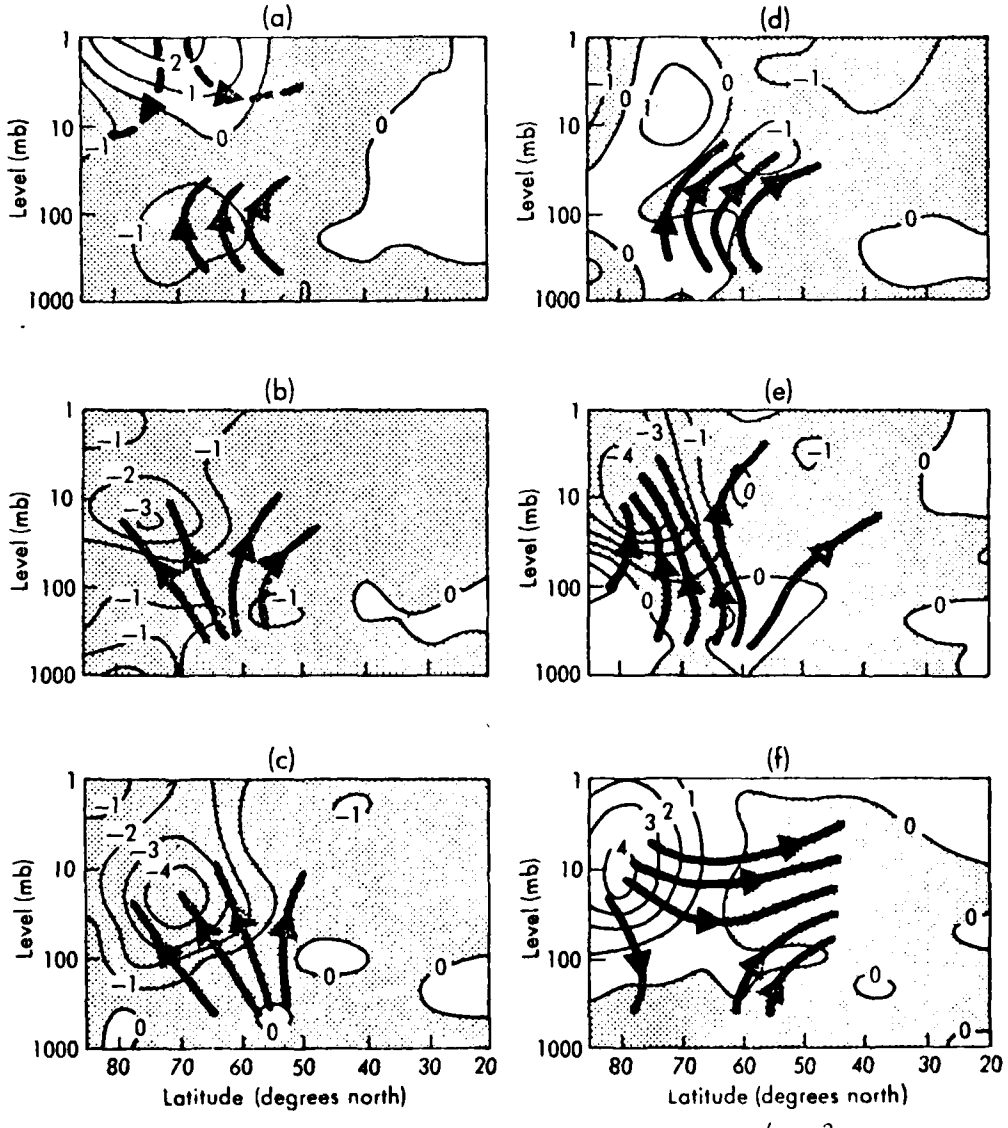

Fig. 3. Contours of $\mathscr{L} \Delta \underline{F}$ labeled in units of $10^{-4} ms^{-2}$, with some integral curves of F. Negative values of $\mathscr{L} \Delta \underline{F}$ are stippled in the figures. (a) 17 February (dashed curves are dominated by wavenumber-1 flux. Full curves are dominated by wavenumber-2 flux), (b) 19 February, (c) 21 February, (d) 23 February, (e) 26 February, and (f) 28 February. For $\mathscr{L}$ see Palmer (1981a)).

Another diagnostic that Palmer uses is found in the terms of (1). In Figure 4 the values of these quantities are plotted for three pressure levels, the fv* term being determined as a residual and the term averaged between 60° and 80°N with cosine of latitude weighting. On the 1 mb plot a strong correlation between $\nabla \cdot \underline{F}$ and $\bar{u}_t$ is seen and the various decelerations observed in Figure 1 are clearly indicated. At lower levels these features are not so obvious and at the 100 mb level, just above the tropopause, there is virtually no correlation.

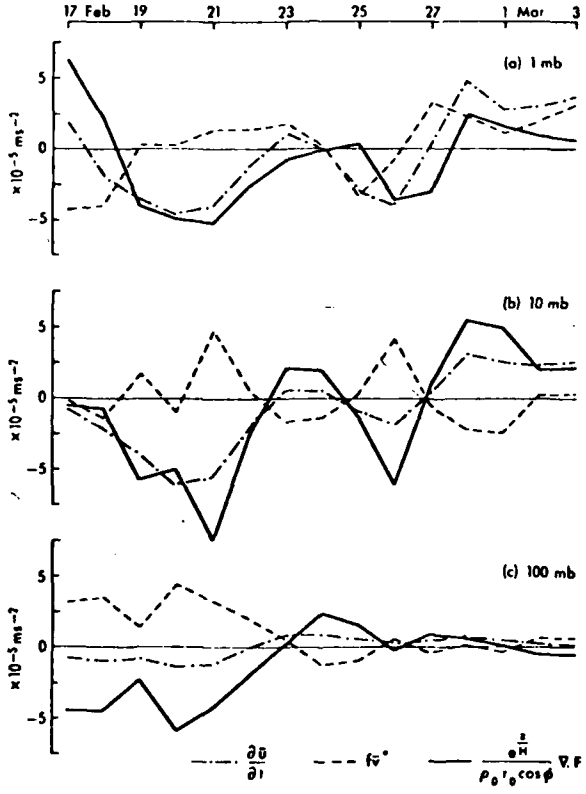

Fig. 4. Momentum budget averaged with cosine of latitude weighting between 60 and 80°N for the period 17 February to 3 March: (a) 1 mb, (b) 10 mb and (c) 100 mb.

In the model of Dunkerton et al. (1981) similar diagrams were produced. They also calculated the residual circulation $\bar{\chi}^*$ which on day 22 of their model looked qualitatively as sketched in Figure 5. Notice the large negative $\bar{w}^*$ near the pole (cf. (24) of the last section) which implies a warming in the polar stratosphere as

$$\bar{\theta}_t = -\bar{w}^* \bar{\theta}_z .$$

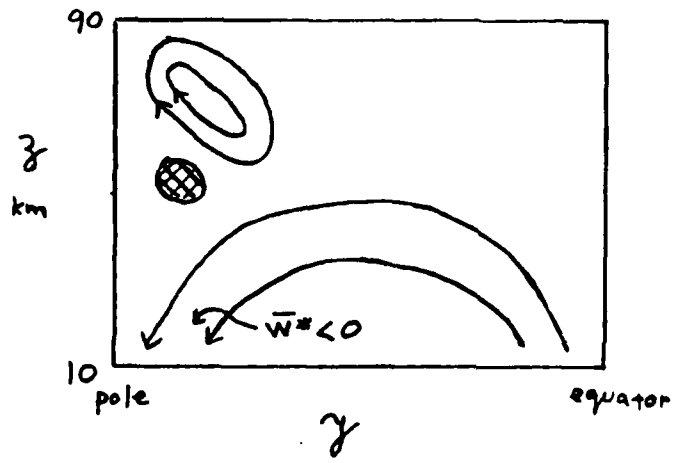

Fig. 5. Plot of $\bar{\chi}^*$ modelled on Dunkerton et al. (1981, fig. 7). Cross-hatched region is where $\nabla . \underline{F} < 0$. Note the cooling in the mesosphere.

The Eulerian equations as opposed to the TEM equations of motion need to include eddy effects to obtain this result as the Eulerian vertical velocity may be opposite in sign to $\bar{w}^*$! This was demonstrated by Mahlman (1969) who found the Eulerian velocity field to indicate positive $\bar{w}$ near the poles while tracer experiments gave the opposite result.

Having examined the use of some diagnostic tools we will now take a short digression in ray theory. If we define a Rossby wave of zonal wavenumber k and phase speed c by

$$\psi' = \hat{\psi}(y,z)\, e^{ik(x-ct)}$$

then the refractive index for these waves is

$$Q_k = \frac{\bar{q}_y}{\bar{u}-c} - k^2 - \frac{\varepsilon}{4H^2},$$

where

$$\varepsilon = \Omega_o^2/N^2.$$

Palmer (1981b) and Karoly and Hoskins (1982) showed that $\underline{F}$ tends to follow "ridges" of Q_K. This is an important point and will be illustrated shortly.

A Qualitative Description of the Dynamics of Sudden Warmings

During a normal winter waves tend to follow paths expected from the curvature of the earth, away from the pole as in Figure 2. However, if the polar night jet is further north than normal a region of low refractive index Q_K may be produced, as shown in Figure 6, which focusses the EP flux towards the pole, that is, $\underline{F}$ follows "ridges" of Q_K. From equation (12) of the last section we can see this convergence near the pole. As the waves are growing in amplitude

$$\nabla \cdot \underline{F} = -\frac{\partial A}{\partial t} = -\frac{\partial}{\partial t}\left(\tfrac{1}{2}\rho_c \bar{q}_y \bar{\eta}^2\right) < 0 \qquad \text{if } \bar{q}_y > 0$$

and from (1), as $(\nabla \cdot \underline{F})/\rho a \cos\theta$ is large and negative near the pole, $\bar{u}_c < 0$.

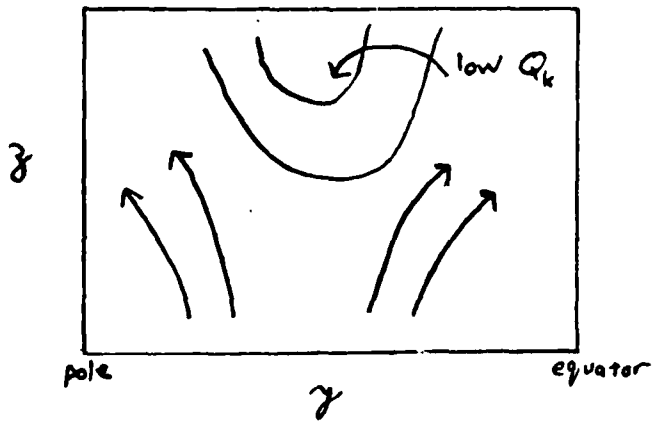

Fig. 6. Integral curves of $\underline{F}$ following "ridges" in Q_k.

Of course the intriguing question that remains about these warmings is what is the mechanism causing the tropospheric waves to get large to begin with? Plumb (1981) has viewed this problem as a resonant self-driving and McIntyre (1982) considers the consequences of nonlinear refractive critical layers but more work needs to be done to clarify this question.

V. ZONAL MEAN MODELS OF TRANSPORT OF CHEMICAL TRACERS IN THE STRATOSPHERE

The main reason for interest in the transport of chemical tracers has to do with the concern that ozone (O_3) may be destroyed by certain pollutants such as halocarbons. This has given rise to much research because O_3 is primarily responsible for the absorption of ultra-violet radiation in the stratosphere and any large increase in the amount of u-v reaching the biosphere could have serious consequences for life forms on the planet. The ozone layer also contributes to the heating of the stratosphere as a result of its interaction with u-v radiation.

In figure 7 the concentration of ozone in the atmosphere is shown (from

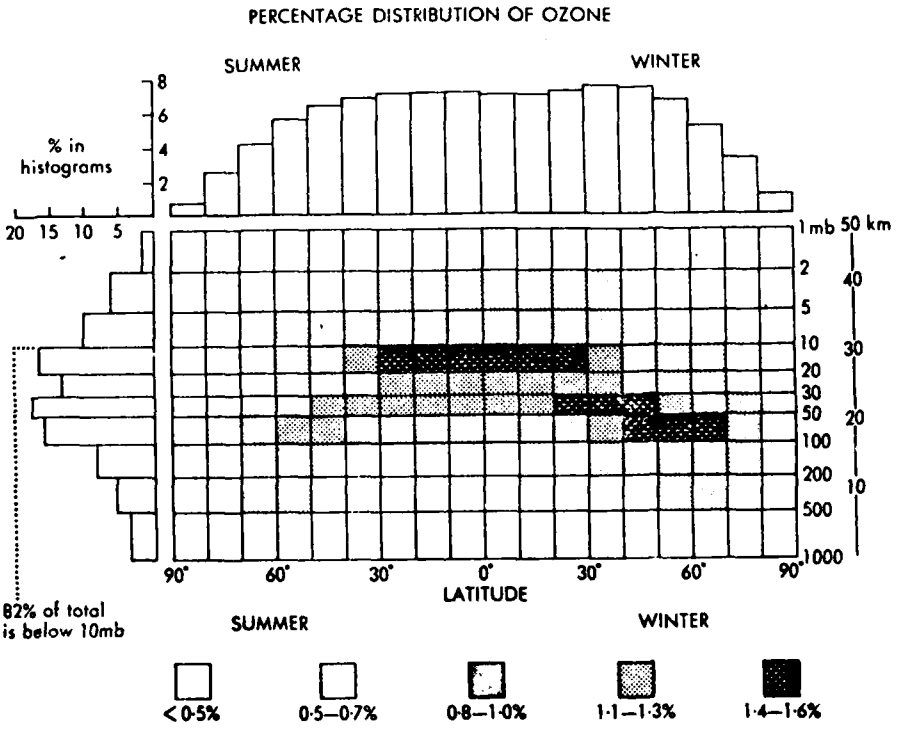

Fig. 7. The mean percentage distributions of integrated ozone amounts. The top histogram shows the mean distribution of total ozone in latitude bands, the left hand histogram shows the mean global distribution of integrated amounts in horizontal layers at different heights and the central diagram the percentage of the total global amounts in annuli round latitude circles in the different latitude bands and height layers.

Murgatroyd, 1982). The two regions of maximum ozone presence are at the equator at about 30 km and in the winter polar regions at a height of around 20 km. However, the ozone is not produced in the latter region so it must be transported there from the equatorial stratosphere. Understanding this distribution involves a knowledge of the chemistry of O_3, a very complex field due to the hundreds of potentially important reactions, a familiarity with radiative transfer problems and a knowledge of the dynamics of the atmosphere. For a discussion of the many aspects of the ozone problem see the review article by Murgatroyd (1982).

All scales of models have been employed to study this aspect of the atmosphere from 3D GCMS, which are highly expensive, though the 1D models often used by chemists to zonal average 2D models. These last can include aspects not treatable by 1D models without the expense of GCMs. Earlier models of this type applied eddy diffusion ideas to mean eddy flux terms but now more models use wave mean-flow theory (Plumb, 1979 and Matsuno, 1980).

Zonal Mean Model of Dynamics of Tracer Transport

We will now consider a model of the dynamics of tracer transport in terms of the primitive equations on a β - plane. A tracer of concentration R will be assumed to be present such that

$$\frac{DR}{Dt} = S, \tag{1}$$

S being a term representing the sources and sinks of the tracer. If we zonally average (1) we obtain

$$\bar{R}_t + \bar{v}\bar{R}_y + \bar{w}\bar{R}_z = \bar{S} - (\overline{v'R'})_y - \rho_c^{-1}(\rho_c \overline{w'R'})_z \tag{2}$$

using the coordinates employed in the quasi-geostrophic flow section.

To simplify our analysis define the residual circulation in a slightly different manner to previously, namely, let

$$\bar{v}^* = \bar{v} - \rho_c^{-1}(\rho_c \bar{\chi})_z$$
$$\bar{w}^* = \bar{w} + \bar{\chi}_y.$$

where $\bar{\chi}_y$ will be defined later in (10). It can then be shown that

$$\bar{R}_t + \bar{v}^*\bar{R}_y + \bar{w}^* R_z = \bar{S} - \rho_c^{-1}\nabla\cdot\underline{G}, \tag{3}$$

where

$$\underline{G} = \rho_c(\overline{v'R'} - \bar{\chi}\bar{R}_z, \overline{w'R'} + \bar{\chi}\bar{R}_y) \tag{4}$$

Also let the O(a) flow be purely zonal, $\underline{\bar{u}} = (\bar{u}(y,z), o, o) + O(a^2)$.

Having set up our system we linearize the tracer equation (2) to give

$$D_t R' + v'\bar{R}_y + w'\bar{R}_z = S' \tag{5}$$

and define particle displacements by $\underline{\xi}' = (\xi', \eta', \zeta')$ with

$$\left.\begin{aligned} D_t\eta' &= v' \\ D_t\zeta' &= w' \end{aligned}\right\}. \tag{6}$$

Also define an integrated source-sink term s' by

$$D_t s' = S' \tag{7}$$

Then, if our initial conditions specify that all quantities are zero at t = o, (5) may be written as

$$R' + \eta' \bar{R}_y + \rho' \bar{R}_z = s' \tag{8}$$

Similarly, if θ' is the potential temperature, then

$$\frac{D\theta'}{Dt} = Q \Rightarrow \theta' + \eta' \bar{\theta}_y + \rho' \bar{\theta}_z = q' \tag{9}$$

where

$$D_t q' = Q.$$

If we follow Andrews and McIntyre (1978) and choose

$$\bar{\chi} = \frac{\overline{v'\theta'}\,\bar{\theta}_z - \overline{w'\theta'}\,\bar{\theta}_y}{|\nabla\bar{\theta}|^2} \tag{10}$$

(recall that $\bar{\chi} = \overline{v'\theta'}/\bar{\theta}_z$ before) then

$$\bar{\rho}' G_{(y)} = \overline{v'R'} - \bar{\chi}\bar{R}_z = \overline{v's'} - \overline{v'\eta'}\bar{R}_y - (\overline{v'\rho'} + \bar{\chi})\bar{R}_z, \tag{11}$$

where $G_{(y)}$ represents the y-component of G. This equation gives us a linear relation between $G_{(y)}$ and the gradients of $\bar{R}$.

Now, from (6),

$$\overline{\eta'v'} = D_t\left(\tfrac{1}{2}\overline{\eta'^2}\right) \tag{12}$$

and

$$\overline{v'\rho'} = (\overline{\eta'\rho'})_t - \overline{\eta'w'} \tag{13}$$

so combining (11) - (13) we obtain

$$\bar{\rho}' G_{(y)} = \overline{v's'} - \tfrac{1}{2}(\overline{\eta'^2})_t \bar{R}_y - \tfrac{1}{2}(\overline{\eta'\rho'})_t \bar{R}_z - B\bar{R}_z \tag{14}$$

$$\bar{\rho}' G_{(z)} = \overline{w's'} - \tfrac{1}{2}(\overline{\eta'\rho'})\bar{R}_z - \tfrac{1}{2}(\overline{\rho'^2})_t \bar{R}_z + B\bar{R}_y \tag{15}$$

where

$$B = \tfrac{1}{2}(\overline{\eta'\rho'})_t + \bar{\chi} - \overline{\eta'w'} = \tfrac{1}{2}(\overline{v'\rho'} - \overline{\eta'w'}) + \bar{\chi}. \tag{16}$$

Therefore, if i,j = 2,3

$$\bar{\rho}' G_i = \overline{w_i's'} - K^{(s)}_{ij}\bar{R}_{,j} - K^{(a)}_{ij}\bar{R}_{,j} \tag{17}$$

where

$$K^{(s)}_{ij} = \tfrac{1}{2}(\overline{\xi_i'\xi_j'})_t = \begin{pmatrix} \frac{1}{2}(\overline{\eta'^2})_t & \frac{1}{2}(\overline{\eta'\rho'})_t \\ \frac{1}{2}(\overline{\eta'\rho'})_t & \frac{1}{2}(\overline{\rho'^2})_t \end{pmatrix}, \tag{18}$$

$$K_{ij}^{(a)} = \begin{pmatrix} 0 & B \\ -B & 0 \end{pmatrix} \tag{19}$$

and (17) should be interpreted in tensor notation.

Employing (3), (4) and (17), the tracer equation may now be rewritten as

$$\bar{R}_t + \bar{v}^* \bar{R}_y + \bar{w}^* \bar{R}_z = \bar{S} - \rho_0^{-1} \nabla\cdot(\rho_0 \underline{\bar{u}'s'}) + \rho_0^{-1}\left\{(\underline{\underline{K}}^{(s)} + \underline{\underline{K}}^{(a)})\cdot\nabla\bar{R}\right\} + O(a^3) \tag{20}$$

where $\underline{\underline{K}}^{(s)}$ and $\underline{\underline{K}}^{(a)}$ represent the matrices given by (18) and (19) respectively.

We can now note the following points:

a) Rewriting the term with (a) in (20) as

$$\rho_0^{-1}\nabla\cdot\left\{\underline{\underline{K}}^{(a)}\cdot\nabla R\right\} = \rho_0^{-1}\nabla\cdot(0, \rho_0 B\bar{R}_z, -\rho_0 B\bar{R}_y)$$

$$= B_y\bar{R}_z - \rho_0^{-1}(\rho_0 B)_z\bar{R}_y$$

$$= -(\tilde{v}\bar{R}_y + \tilde{w}\bar{R}_z)$$

where

$$(\tilde{v}, \tilde{w}) = (\rho_0^{-1}(\rho_0 B)_z, -B_y) \tag{21}$$

shows that $\underline{\underline{K}}^{(a)}$ represents an additional advection term. This suggests considering a new velocity

$$v^+ = \bar{v}^* + \tilde{v}$$
$$= (\bar{v} - \rho_0^{-1}(\rho_0(\bar{\chi} - B))_z, \bar{w} + (\bar{\chi} - B)_y)$$

where from (16)

$$\bar{\chi} - B = \tfrac{1}{2}(\overline{\eta' w'} - \overline{v' s'})$$

which involves Lagrangian quantities η', s', while $\bar{\chi}$ from (10) involves only Eulerian quantities. It may be convenient to use v^+ instead of v^* in model calculations which provide η' and s' easily.

b) As shown in Holton (1981),

$$B = -\tfrac{1}{2}\left\{(\underline{s}'\cdot\underline{n})(\underline{s}'\cdot\underline{\tau})\right\}_t \quad \text{+ nonconservative terms in q' and s'} \tag{22}$$

Here $\underline{n}$ is normal to mean isentropes, i.e.

$$\underline{n} = \frac{\nabla\bar{\theta}}{|\nabla\bar{\theta}|} \tag{23}$$

while τ is tangential; thus if s' = q' = 0 B vanishes when the waves are steady or when particle displacements are either parallel or perpendicular to isentropes.

c) Similarly, the symmetric tensor $\underset{\sim}{K}^{(s)}$ vanishes unless the waves are transient (at least for wave amplitudes of O(a)). $\underset{\sim}{K}^{(s)}$ represents an anisotropic diffusion or 'anti-diffusion' of tracers by the waves. Dispersion occurs as the waves grow (G. I. Taylor, 1915, 1921).

d) The equation for $\bar{\theta}$ is

$$\bar{\theta}_t + \bar{v}^*\bar{\theta}_y + \bar{w}^*\bar{\theta}_z = \left\{ \begin{matrix} \text{diabatic} \\ \text{terms} \\ \text{in} \\ \bar{Q}, Q' \end{matrix} \right\} + \nabla\cdot\left\{ \begin{pmatrix} A & 0 \\ 0 & A \end{pmatrix} \begin{pmatrix} \bar{\theta}_y \\ \bar{\theta}_z \end{pmatrix} \right\} + O(a^3) \tag{24}$$

where $A = 1/2\left\{(\underset{\sim}{\xi}'\cdot\underset{\sim}{n})^2\right\}_L$

The tensor appearing in (24) differs from the tensor appearing in (20) because B contains terms in $\bar{\nabla}\theta$. The asymmetry in the two equations thus goes back to the definition of χ.

A Simple Example

Suppose the waves are linear, steady, inviscid, adiabatic ($Q' = q' = 0$) and chemically inert ($S' = s' = 0$), but that $\bar{Q}$ and $\bar{S}$ are nonzero. Then $\underset{\sim}{K}^{(s)} = \underset{\sim}{K}^{(a)} = 0$ and (20) reduces to

$$R_t + v^*R_y + w^*R_z = S. \tag{25}$$

Using (9) with q' = 0 and the assumption that $(\overline{S'^2})_t = (\overline{\eta' S'})_t = 0$, (10) becomes in this case

$$\bar{\chi} = \frac{\overline{v'\theta'}}{\bar{\theta}_z}$$

as in previous lectures, so for steady, conservative linear waves, $\bar{v}^*$ matches its earlier definition; moreover $\underset{\sim}{\bar{v}}^* = \underset{\sim}{\bar{v}}^L$ (see para. 6) but $\underset{\sim}{\bar{v}}^* \neq \underset{\sim}{\bar{v}}$.

The TEM equations reduce to

$$\bar{u}_t + (\bar{u}_y - f)\bar{v}^* + \bar{u}_z\bar{w}^* = \bar{X} \tag{26}$$

$$(f\bar{u}_z + \Gamma\bar{\theta}_y)_t = 0 \tag{27}$$

$$\bar{v}^*_y + \rho_0^{-1}(\rho_0\bar{w}^*)_z = 0 \tag{28}$$

$$\bar{\theta}_t + \bar{v}^*\bar{\theta}_y + \bar{w}^*\bar{\theta}_z = \bar{Q} \tag{29}$$

$$\bar{R}_t + \bar{v}^*\bar{R}_y + \bar{w}^*\bar{R}_z = \bar{S} \tag{30}$$

Now assume $\bar{Q}$ is independent of $\bar{R}$ (which may not be valid in general, but it greatly simplifies matters) and that $\bar{X} = 0$. Equation (30) then decouples from the others so that (26) - (29) can be solved for the diabatic circulation $\underset{\sim}{\bar{v}}^* = (\bar{v}^*, \bar{w}^*)$ forced by $\bar{Q}$ alone. The solutions for $\bar{v}^*$ can then be used to advect $\bar{R}$ from source ($\bar{S} > 0$) to sink ($\bar{S} < 0$).

A simplified version of this example was studied by Dunkerton (1978) who considered conservative tracers ($\bar{S}$ = o) and neglected $\bar{\theta}_t$ and $\bar{v}\,\bar{\theta}_y$. With these assumptions $\bar{w}^* = Q/\bar{\theta}_z$ and $\bar{v}^*$ can be obtained from (28). The resulting $\bar{v}^*$ is plotted in Fig. 8.

With this simple model, Dunkerton was able to resolve a long-standing paradox. Brewer and Dobson, around 1950, inferred from tracer concentrations a velocity pattern similar to that of Fig. 8, but later measurements of Eulerian mean quantities, showed the existence of an indirect Ferrel cell in the winter hemisphere (Fig. 9). Dunkerton realized that both velocity fields could be correct since the Eulerian and Lagrangian flow fields do not match.

Dunkerton's model has since been extended. Pyle and Rogers (1980) redid Dunkerton's calculation for ozone with a more complicated 2D model. Holton (1981) included transients, dissipation, and considered N_2O, which has a tropospheric source but is fairly inert in the stratosphere, while Tung (1982) reformulated the problem in isentropic coordinates.

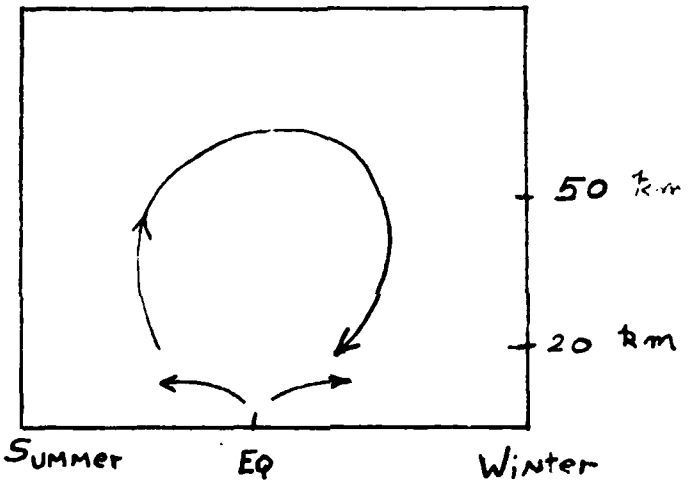

Fig. 8. The residual mean meridional circulation, $\bar{v}^*$, resulting from Dunkerton's model. The flow is consistent with observations of conserved tracers.

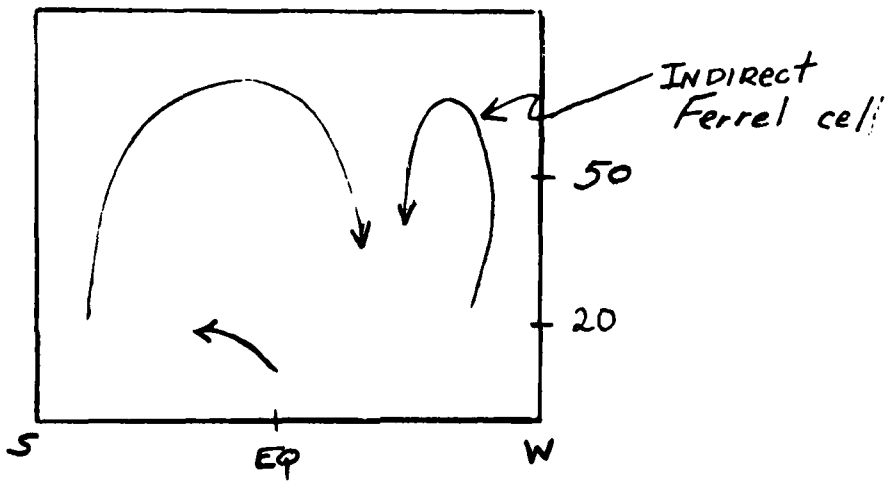

Fig. 9. The velocity field inferred from Eulerian measurements. Wave activity strongly affects the winter hemisphere.

VI. THE GENERALIZED LAGRANGIAN MEAN

David Andrews

Thus far, the discussion has been limited to small amplitude waves. A question which arises is whether these results can be generalized to finite amplitude. The answer turns out to be yes, at least in a formal sense, if instead of using an Eulerian mean or a transformed Eulerian mean, a theory based on Lagrangian means is considered; a Lagrangian description in its classical form, however is inappropriate if particles move very far from their initial positions, as they do when mean flows are present. To overcome this difficulty, an idea originating in the work of Bretherton (1971) makes use of a hydrid theory: It retains the Eulerian coordinates $\underset{\sim}{x}$ and t as independent variables, and Eulerian ideas like "steady mean flow:, but it is Lagrangian because fluid particles are tagged. The hybrid theory is called the"Generalized Lagrangian Mean" (GLM), where the term "generalized" refers to the fact (discussed later) that a number of averaging operators can be defined. Once set up, the GLM leads easily to a nonacceleration theorem and conservation laws for finite amplitude waves (Andrews and McIntyre, 1978a,b; hereafter I and II respectively).

Eulerian Average

We define an Eulerian average $\overline{(\ )}$:

$\phi(x,t) \to \overline{\phi}(x,t)$ with the requirement that it commute with differentiation

$$\partial_\mu \overline{(\ )} = \overline{\partial_\mu (\ )}$$

where μ denotes either a spatial coordinate, x_i, or t. (Other properties of $\overline{(\ )}$ may be found in section 2 of I.) We shall write $\overline{(\ )}^t$ or $\overline{(\ )}^{x_i}$ when the averaging applies specifically to time or space.

Lagrangian Average and Particle Displacement

In the classical theory, $\overline{(\ )}^L$ is defined as a time average following a particle. A particle displacement vector, $\underset{\sim}{\xi}(\underset{\sim}{x},t)$, can then be chosen such that

$$\overline{\xi}^t = 0$$

so that a particle located at $\underset{\sim}{x} + \underset{\sim}{\xi}(\underset{\sim}{x},t)$ oscillates about a mean position $\underset{\sim}{x}$.
When the mean flow is at most O(a) the velocity of the particle is

$$\begin{aligned}\frac{\partial \underset{\sim}{\xi}}{\partial t} &= \underset{\sim}{u}(\underset{\sim}{x} + \underset{\sim}{\xi}(\underset{\sim}{x},t)) \\ &= \underset{\sim}{u}'(\underset{\sim}{x}) + \underset{\sim}{\xi}\cdot\nabla\underset{\sim}{u} \\ &= \underset{\sim}{u}'(\underset{\sim}{x}) + O(a^2)\end{aligned}$$

where the second line follows from a Taylor expansion and where $\underset{\sim}{u} = \bar{\underset{\sim}{u}}^t + \underset{\sim}{u}'$. This can be extended to include an O(1) mean flow by adding an advective term, giving

$$\begin{aligned}\left(\frac{\partial}{\partial t} + \bar{\underset{\sim}{u}}^t\cdot\nabla\right)\underset{\sim}{\xi} &= \underset{\sim}{u}' + \underset{\sim}{\xi}\cdot\nabla\bar{\underset{\sim}{u}}^t + O(a^2) \\ &= u^l + O(a^2)\end{aligned}$$

In either case, the Lagrangian mean of a quantity ϕ is

$$\bar{\phi}^L(\underset{\sim}{x},t) = \overline{\phi(\underset{\sim}{x}+\underset{\sim}{\xi},t)}^t = \bar{\phi}(\underset{\sim}{x}) + \overline{\underset{\sim}{\xi}\cdot\nabla\phi'} + \frac{1}{2}\overline{\xi_i\xi_j}\phi_{,ij} + O(a^3)$$

Here the notation $\phi_{,i} = \frac{\partial}{\partial x_i}\phi$ has been adopted.

In meteorological applications, it is often advantageous to apply spatial averages (e.g. a zonal average) rather than a time average following a particle. We therefore want to generalize the Lagrangian mean to

$$\bar{\phi}^L = \overline{\phi(\underset{\sim}{x}+\underset{\sim}{\xi},t)} \tag{1}$$

where the average on the RHS of (1) is not necessarily over time. Defining

$$\bar{D}^L = (\partial_t + \bar{\underset{\sim}{u}}^L\cdot\nabla)$$

$\underset{\sim}{\xi}$ would then satisfy

$$\bar{D}^L(\underset{\sim}{\xi}) = \underset{\sim}{u}^l(\underset{\sim}{x},t) = \underset{\sim}{u}(\underset{\sim}{x}+\underset{\sim}{\xi},t) - \bar{\underset{\sim}{u}}^L(\underset{\sim}{x},t) \tag{2}$$

with

$$\overline{\underset{\sim}{\xi}} = \overline{u^l} = 0\ ; \tag{3}$$

but can $\bar{(\ )}^L$ and $\underset{\sim}{\xi}$ be found such that they satisfy equations (1), (2) and (3)? To make the notion of a Lagrangian average plausible when $\bar{(\ )}^L = \bar{(\ )}^x$ we consider the following mechanical analogy.

At $t = t_o$, let the wave amplitude be identically zero and consider a line of fluid particles with spacing Δx lying along the x-axis (Fig. 1). A thin massless rod is joined to the particles by elastic bands. As the wave amplitude grows, the particles become displaced from R by an amount equal to the "elastic band vector" $\underset{\sim}{\xi}(\underset{\sim}{x},t)$, where $\underset{\sim}{x}$ is the position along R. Although R is constrained to stay horizontal, it remains in static equilibrium with the particles and thus follows them if they undergo any mean motion. In the limit of $\Delta x \to 0$, equations (2) and (3) show that the particles pull R at velocity $\bar{u}^L = \overline{u(x+\xi,t)}^x$. By requiring that $\xi = 0$ at $t = t_o$, $\bar{u}^L$ can be found in principle by integrating along mean trajectories.

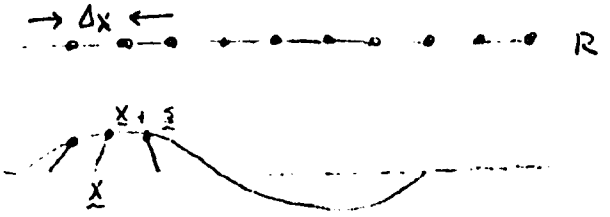

Figure 10.

Given that $(\bar{\ })^L$ can be defined, several interesting properties follow. Defining

$$\phi^3(\underset{\sim}{x}) = \phi(\underset{\sim}{x} + \underset{\sim}{\xi})$$
$$\bar{\phi}^3 = \bar{\phi}^L$$
$$\underset{\sim}{\Xi} = \underset{\sim}{x} + \underset{\sim}{\xi}(\underset{\sim}{x}, t)$$

then (2) implies that

$$\bar{D}^L \underset{\sim}{\Xi} = (\partial_t + \bar{\underset{\sim}{u}}^L \cdot \nabla)\underset{\sim}{\Xi}$$
$$= \underset{\sim}{u}^* + \bar{\underset{\sim}{u}}^L$$
$$= \underset{\sim}{u}^3$$

The point $\underset{\sim}{\Xi} = \underset{\sim}{x} + \underset{\sim}{\xi}$ moves with the actual fluid velocity $\underset{\sim}{u}^3$ when the point $\underset{\sim}{x}$ moves with velocity $\bar{\underset{\sim}{u}}^L$. Use of the chain rule gives (I, equation 2.4a,b).

$$\bar{D}^L \phi^3 = (\partial_t + \bar{\underset{\sim}{u}}^L \cdot \nabla)\phi(\underset{\sim}{x} + \underset{\sim}{\xi}, t)$$
$$= (\phi_{,t})^3 + (\phi_{,j})^3 \Xi_{j,t} + \bar{u}_i^L (\phi_{,j})^3 \Xi_{j,i}$$
$$= (\phi_{,t})^3 + u_j^3 (\phi_{,j})^3$$
$$= \left(\frac{D\phi}{Dt}\right)^3$$

Averaging both sides leaves

$$\bar{D}^L \bar{\phi}^L = \overline{\frac{D\phi}{Dt}}^L$$

Thus the Lagrangian mean of D/Dt acting on ϕ carries through to both D/Dt and ϕ individually without generating eddy contributions. In contrast, the Eulerian average of a total derivative produces an eddy flux term:

$$\overline{\frac{D\phi}{Dt}} = \bar{D}\bar{\phi} + \overline{u' \cdot \nabla \phi'}$$

where $\bar{D} = (\partial_t + \bar{\underset{\sim}{u}} \cdot \nabla)$. For this reason, the Lagrangian mean is especially useful when applied to, for example, the equations for entropy S. It simply transforms

$$\frac{DS}{Dt} + Q = 0$$

into the averaged equation

$$\bar{D}^L \bar{S}^L + \bar{Q}^L = 0$$

Again, eddy terms do not appear.

In general the Lagrangian and Eulerian means of a quantity are not equal. The difference is called the Stokes correction and for small amplitude waves, it can be calculated through a Taylor expansion:

$$\bar{\phi}^S = \bar{\phi}^L - \bar{\phi} = \overline{\xi_j \phi_{,j}} + \tfrac{1}{2} \overline{\xi_j \xi_k} \bar{\phi}_{,jk} + O(a^3)$$

When $\phi = u_1$, $\bar{\phi}^S$ becomes the Stokes drift (Longuet-Higgins, 1969).

Equations for Mean Flow Evolution

Writing the equations of motion as

$$M_j(\underset{\sim}{x},t) = \frac{Du_j}{Dt} + 2(\underset{\sim}{\Omega} \times \underset{\sim}{u})_j + \Phi_{,j} + \rho^{-1} p_{,j} + \chi_j = 0 \qquad (4)$$

where Φ is the gravitational potential
and defining as before

$$\underset{\sim}{\Xi} = \underset{\sim}{x} + \underset{\sim}{\xi}(\underset{\sim}{x},t)$$

we want to evaluate

$$\overline{\Xi_{j,i} M_j(\underset{\sim}{\Xi},t)} = 0 \qquad (5)$$

leaving the averaging operator general for now. The algebra is performed in Appendix B of I resulting in equation (3.8) of the same paper. If the mean quantities are independent of x_1 and $(\bar{\ }) = (\bar{\ })^L$, then the x_1-component of (5) is (equation (3.9) of I)

$$\bar{D}^L(\bar{u}_1^L - p_1) + 2(\Omega \times \bar{u}^L)_1 = -\bar{X}_1^L - \overline{\xi_{j,1} X_j^L} + \overline{p_{,1}^I q} = -\chi_1 \qquad (6)$$

where X_j is the Lagrangian disturbance forcing, q describes diabatic effects, and

$$p_1 = -\overline{\xi_{,1} \cdot \{ \underset{\sim}{u}^L + \underset{\sim}{\Omega} \times \underset{\sim}{\xi} \}} \qquad (7)$$

is the pseudomomentum.

In Eulerian form, the equation governing conservation of mass is

$$\frac{D\rho}{Dt} + \rho \nabla \cdot \underset{\sim}{u} = 0$$

A natural choice for defining a Lagrangian mean density, $\tilde{\rho}$, is that it satisfy

$$\bar{D}^L \tilde{\rho} + \tilde{\rho} \nabla \cdot \bar{u}^L = 0 \tag{8}$$

This definition leads to the relationship (equation (4.3) of I)

$$\begin{aligned} \tilde{\rho} &= \rho^3 J \\ &= \rho^3 \det\{\Xi_{i,j}\} \end{aligned} \tag{9}$$

The equations for the mean state become complete with the equation for entropy (see above)

$$\bar{D}^L \bar{S}^L + \bar{Q}^L = 0$$

and the equation of state

$$\begin{aligned} \tilde{\rho} - F(\bar{S}^L, \bar{p}^L) &\equiv \Delta \\ &= (\tilde{\rho} - \bar{\rho}^L) + F(S^3, p^3) - F(\bar{S}^L, \bar{p}^L) \end{aligned} \tag{10}$$

where $\rho = \underset{\sim}{F}(S,p)$. If the waves are O(a) in amplitude Δ is $O(a^2)$.

Specializing to a longitudinally symmetric mean flow and writing

$$\underset{\sim}{\bar{u}}^L = (\bar{u}^L, \bar{v}^L, \bar{w}^L) \qquad p_1 = p$$

the equations of motion are (equated 5.5 of I):

$$(\bar{u}^L - p)_{,t} + \bar{v}^L(\bar{u}^L_{,2} - p_{,2} - 2\Omega) + \bar{w}^L(\bar{u}^L_{,3} - p_{,3}) = \mathcal{X}_1 \tag{11}$$

y - momentum equation $= -\mathcal{X}_2$ (12)

z - momentum equation $= -\mathcal{X}_3$ (13)

$$\bar{S}^L_{,t} + \bar{v}^L \bar{S}^L_{,2} + \bar{w}^L \bar{S}^L_{,3} = -\bar{Q}^L \tag{14}$$

$$\tilde{\rho}_{,t} + (\rho \bar{v}^L)_{,2} + (\tilde{\rho} \bar{w}^L)_{,3} = 0 \tag{15}$$

$$\tilde{\rho} - F(\bar{S}^L, \bar{p}^L) = 0 \tag{16}$$

We may now ask for the conditions under which steady unidirectional flow is allowed in the presence of waves, i.e., the conditions for which

$$\partial_t \{\bar{u}^L, \bar{p}^L, \tilde{\rho}, \bar{S}^L \cdots\} = 0$$

and

$$\bar{\underset{\sim}{u}}^L = (\bar{u}^L, 0, 0).$$

By inspection it is allowed when

$$\chi_1 = \bar{Q}^L = 0$$

and

$$\partial_t \{ P_1, \chi_2, \chi_3, \Delta \} = 0.$$

The waves must be conservative and steady; if $\chi_1 = 0$ or $\bar{Q}^L \neq 0$, cumulative mean flow changes can be expected.

Wave Action

Suppose that $\bar{(\ )}$ is an ensemble average, and that the quantity α is used to generate the ensemble. We also require $\phi = \phi(x, t; \alpha)$ to be a continuous function of α and that

$$\overline{\phi_{,\alpha}} = (\bar{\phi})_{,\alpha}.$$

Then by taking

$$\overline{\xi_{j,\alpha} \cdot M_j(x, \xi, t)} = 0 \tag{17}$$

the equation

$$\bar{D}^L A + \tilde{\rho}^{-1} \nabla \cdot \underset{\sim}{B} = \mathcal{J} \tag{18}$$

can be derived (Appendix A of II), where

$$A = \overline{\underset{\sim}{\xi}_{,\alpha} \cdot (u^l + \underset{\sim}{\Omega} \times \underset{\sim}{\xi})} \tag{19}$$

$$B_j = \overline{\rho^s \xi_{i,\alpha} K_{ij}} \tag{20}$$

$$\mathcal{J} = \overline{-\xi_{i,\alpha} \chi_i^l} + \overline{(p^l)_{,\alpha} q} \tag{21}$$

$\mathcal{J}$ is zero for conservative motion and K_{ij} is the cofactor of $\Xi_{i,j}$ in $J = \det\{\Xi_{i,j}\}$ (see Appendix A of I). A version of (18) was found by Hayes (1970) without making slow-variation or small amplitude assumptions, although his work was based on a Lagrangian density and therefore could not include dissipation. Using the continuity equation (8), (18) may be rewritten as

$$\partial_t(\tilde{\rho} A) + \nabla \cdot \{ \underset{\sim}{B} + \bar{\underset{\sim}{u}}^L \tilde{\rho} A \} = \tilde{\rho} \mathcal{J} \tag{22}$$

When mean quantities are independent of $\underset{\sim}{x}$ (writing $\underset{\sim}{x} = (x,y,z)$) an ensemble can be generated by translating the disturbance pattern by a horizontal distance α :

$$\phi(\underset{\sim}{x}, t; \alpha) = \phi(x - \alpha, y, z, t)$$

is the x-component of the pseudomomentum. Conservation of p_1, described by (22), arises when mean quantities are independent of x. That only mean quantities and not the whole system need be invariant to translations in x is what distinguishes pseudomomentum conservation from momentum conservation as usually encountered in physics. Similarly, time invariance of the mean state yields conservation of pseudoenergy.

Suppose (II, section 4) the waves are linear and slowly varying, with

$$\zeta \sim e^{i(\underset{\sim}{k}\cdot\underset{\sim}{x} - \omega t - \alpha)}$$

where α is now a phase shift. Taking $(\bar{\ })$ to be an average over phase yields (after some manipulation)

$$\rho A = \frac{E}{\omega - \bar{u}k}$$

$$\underset{\sim}{B} = \underset{\sim}{C}_g \frac{E}{\omega - \bar{u}k}$$

where $\underset{\sim}{C}_g$ is the group velocity. This is the form for action density and flux derived by Bretherton and Garrett (1968)

We also note that in an earlier lecture, a measure of wave activity for quasigeostrophic flow was found to be

$$A_W = \tfrac{1}{2}\rho_0 \bar{q}_y \overline{\eta'^2} + O(a^3)$$

and to satisfy the conservation law

$$\partial_t A_W + \nabla \cdot \underset{\sim}{F}_W = 0 \qquad (22a)$$

Defining A_1 such that

$$\rho_1 = A_W + \bar{V} \cdot \underset{\sim}{A}_1$$

and substituting into 22a gives

$$\partial_t \rho_1 + \nabla \cdot (\underset{\sim}{F}_W - \underset{\sim}{A}_{1,t}) = 0$$

This is not quite the same as conservation or pseudomomentum, but in the case of slowly varying waves, the two agree.

Relationship Between (v*, w*) and vL, wL)

From equation (4.12)

$$\bar{V}^* = \bar{V} - \rho_0^{-1}\left(\frac{\rho_0 \overline{v'\theta'}}{\bar{\theta}_z}\right)_z \qquad (23)$$

and from (5.9)

$$\theta' + \eta' \bar{\theta}_y + \zeta \bar{\theta}_z = q' \tag{24}$$

where q' represents diabatic effects.
If $\underset{\sim}{u} = (u, v, w) + O(a^2)$, the Stokes drift becomes

$$\bar{V}^L - \bar{V} \equiv \bar{V}^S = \underset{\sim}{\xi} \cdot \nabla v' + O(a^3) \tag{25}$$

A linearized version of (2)

$$\bar{D}^L \underset{\sim}{\xi} = u'$$

gives

$$\begin{aligned} \bar{D}_t \xi &= (\partial_t + \bar{u}\partial_x)\xi_x \\ &= u' + \underset{\sim}{\xi} \cdot \nabla \bar{u} \end{aligned} \tag{26}$$

while the linearized density equation in ln p coordinates is

$$\nabla \cdot (\rho_0 \underset{\sim}{u}') = 0 \qquad \rho_0 = \rho_s e^{-z/H} \tag{27}$$

Solving for u' in (26) and substituting into (27) gives

$$\begin{aligned} (\rho_0 u_i')_{,i} &= \{ \bar{D}_t (\rho_0 \xi_i) - \rho_0 \xi_j \bar{u}_{i,j} \}_{,i} \\ &= \bar{D}_t \{ (\rho_0 \xi_i)_{,i} + \bar{u}_{,i} \rho_0 \xi_{i,x} - \rho_0 \xi_{j,i} \bar{u}_{i,j} \} \end{aligned}$$

Thus

$$\bar{D}_t \{ (\rho_0 \xi_i)_{,i} \} = 0$$

and assuming zero wave amplitude initially,

$$\nabla \cdot (\rho_0 \underset{\sim}{\xi}) = 0 \tag{28}$$

From (25), the Stokes drift can be written as

$$\rho_0 \bar{V}^S = \rho_0 \overline{\underset{\sim}{\xi} \cdot \nabla v'} = \nabla \cdot (\rho_0 \overline{\underset{\sim}{\xi} v'}) \tag{29}$$

and from (24)

$$\rho' = \frac{q'}{\bar{\theta}_z} - \eta' \frac{\bar{\theta}_y}{\bar{\theta}_z} - \frac{\theta'}{\bar{\theta}_z}$$

Then

$$\rho_0 \overline{\rho' v'} = -\rho_0 \frac{\overline{v'\theta'}}{\bar{\theta}_z} - \rho_0 \frac{\overline{\rho' q'}}{\bar{\theta}_z} - \rho_0 \frac{\overline{\eta' v'}}{\bar{\theta}_z}$$

and

$$\rho_0 \bar{v}^s = -\rho_0 \left(\frac{\overline{v'\theta'}}{\bar{\theta}_z} \right)_z - \rho_0 \left(\frac{\overline{\rho' q'}}{\bar{\theta}_z} \right)_z$$

$$- \rho_0 \left(\tfrac{1}{2} \overline{\eta'^2} \frac{\bar{\theta}_y}{\bar{\theta}_z} \right)_{tz} + \tfrac{1}{2} \rho_0 \left(\overline{\eta'^2} \right)_{yt}$$

$$= \rho_0 (\bar{v}^* - \bar{v}) \qquad \begin{array}{l} + \text{ nonconservative terms} \\ + \text{ transient terms} \\ + O(a^3) \end{array}$$

Hence $v^* = v^L$ to $O(a^2)$ when the waves are steady and conservative.

Further Thoughts

It would be nice to apply the GLM ideas directly to the atmosphere, but in general difficulties arise (e.g. in obtaining $\underset{\sim}{\xi}$); however it may be possible to calculate $(\ )^L$ and $\underset{\sim}{\xi}$ from simple circulation models. Some progress along these lines has been made by Dunkerton et al (1981) who calculate $(\ )^L$ using a "modified Lagrangian mean". Another possibility utilizes θ or S and Ertel's potential vorticity

$$P = \frac{(\omega + 2\Omega) \cdot \nabla\theta}{\rho}$$

as tracers, since these quantities are conserved in steady nondissipative/non-forced flows. "$P\theta$ tubes" might be useful (averaging around such a tube has some analogy to GLM; cf, McIntyre, 1980). Yet troubles can be expected when the waves reach large amplitude, for $P\theta$ tubes twist up making $\underset{\sim}{\xi}$ ill-behaved.

REFERENCES

Andrews, D. G. and M. E. McIntyre, 1978. An exact theory of non-linear waves on a Lagrangian-mean flow. J. Fluid Mech., 89, 609-646.

Andrews, D. G., 1980. On the mean motion induced by transient inertio-gravity waves. Pure and Appl. Geophys., 118, 177-188.

Bretherton, F. P., 1966. Critical layer instability in baroclinic flows. Quart. J. Roy. Met. Soc., 92, 325-334.

Bretherton, F. P. and C.J.R. Garrett, 1968. The propagation of wave trains in moving media. Proc. Roy. Soc. A, 302, 529.

Bretherton, F.P. 1971 The general linearized theory of wave propagation. Lectures Appl. Math. 13, 61-102.

Charney, J. G. and P. G. Drazin, 1961. Propagation of planetary scale disturbances from the lower into the upper atmosphere. J. Geophys. Res., 66, 83-109.

Dunkerton, T., 1978. On the mean meridional mass motions of the stratosphere and mesosphere. JAS, 35, 2325-2333.

Dunkerton, T., C-P. F. Hsu, and M. E. McIntyre, 1981. Some Eulerian and Lagrangian diagnostics for a model stratospheric warming. J. Atmos. Sci. , 38, 819-843.

Edmon, H. J., B. J. Hoskins and M. E. McIntyre, 1980. Eliassen-Palm cross-sections for the troposphere. J. Atmos. Sci., 37, 2600-2616.

Eliassen, A., 1951. Slow thermally or frictionally controlled meridional circulation in a circular vortex. Astrophys. NorV., 5(2), 19-60.

Eliassen, A. and E. Palm, 1961. On the transfer of energy in stationary mountain waves. Geofys. Publ., 22, 1-23.

Holton, J. R., 1979. An introduction to dynamic meteorology. 2nd ed., Academic Press, New York.

Holton, J.R. 1975 . The Dynamic Meteorology of the Stratosphere and Mesosphere. Amer. Meteorological Society, 216 pp.

Karoly, D, J. and B. J. Hoskins, 1982. Three dimensional propagation of planetary waves. J. Met. Soc. Japan, 60, 109-123.

Mahlman, J. D. 1969. Heat balance and mean meridional circulations in the polar stratosphere during the sudden warming of January 1958. Monthly Weath. Rev., 97, 534-540.

Matsuno, T., 1971. A dynamical model of the stratospheric sudden warming. J. Atmos. Sci., 28, 1479-1494.

Matsuno, T., 1980. Lagrangian motion of air parcels in the stratosphere in the presence of planetary waves. Pageoph. , 118, 189-216.

McIntyre, M. E., 1982. How well do we understand the dynamics of the stratospheric warmings? J. Met. Soc. Japan, 60, 37-65.

Murgatroyd, R. J., 1982. Recent progress in studies of the stratosphere. Q.J. Roy. Met. Soc., 108, 271-312.

Palmer, T. N., 1981a. Diagnostic study of a wavenumber-2 stratospheric sudden warming in a transformed Eulerian-mean formalism. J. Atmos. Sci., 38, 844-855.

Palmer, T.N., 1981b.

Plumb, R. A., 1980. Eddy fluxes of conserved quantities by small-amplitude waves. J. Atmos. Sci., 36, 1699-1704.

Plumb, R. A., 1981. Instability of the distorted polar night vortex: a theory of stratospheric warmings. J. Atmos. Sci., 38, 2514-2531.

Pyle, J.A. and C.F. Rogers, 1980. A modified diabatic circulation model for stratospheric tracer transport. Nature, 287, 711-714.

Taylor, G. I., 1915,1921. TITLE Science Papers II, 1, 172.

Tung, K. K., 1982. On the 2nd transport of stratospheric tracers.

NOTES SUBMITTED BY
THEODORE SHEPHERD
WALTER ROBINSON
GRANT BIGG AND
DAVE BROUTMAN

HOW RAPID IS PRANDTL-BATCHELOR EXPULSION?

William R. Young

The homogenization of a passive tracer in a flow with closed streamlines occurs in two stages: first a rapid process characterized by shear augmented diffusion along streamlines which takes a time of order $P^{1/3}(LU)$, where the Peclet number P is Lu/κ (L, U and κ are length scale, velocity scale and diffusivity).

This rapid process establishes a state where tracer concentration is uniform along streamlines. Substantial variations may exist across streamlines, however. The erosion of these cross-streamline gradients is accomplished by the second stage: a slow diffusive migration of tracer contours across streamlines. This second process takes a full diffusive time L^2/κ.

TURBULENT DISPERSION IN CONVERGENT FLOW

Alan J. Faller

A theory is presented that gives an analytical solution to the kinematic interaction of a convergent (or divergent) mean flow and turbulence for spatially constant convergence and homogeneous turbulence of a specified type. The turbulence is characterized by its mean square velocity, $\overline{v^2}$, and by its Lagrangian autocorrelation function. The problem is formally that of the Langevin equation, and analytical solutions for the time dependence of the ensemble-average variance of many fluid tracers are presented. The solutions are compared with numerical solutions obtained by calculating the Lagrangian motion of a large number of tracers.

This theory is an idealization of convergent flows that arise in Langmuir circulations, longitudinal rolls in the mixed layer of lakes and oceans, where convergent flows cause floating tracers to form lines parallel to the wind (wind rows) and where turbulence tends to disperse the tracers. Similar situations arise with constant density balloons in the upper atmosphere (12-14 km) where the convergent flow caused by the Hadley and Ferrell cells tends to cause the balloons to converge into zonal bands in the vicinity of 30 degrees latitude while planetary waves and "turbulence" disperse the balloons. Still another example might be the subtropical convergences in the oceans where the Ekman transport produces convergence while Rossby waves and turbulent eddies cause dispersion.

Some results of the theory (Faller and Mignerey, 1982) can be summarized in a few equations. For a linearly convergent mean flow, $\tilde{v} = -Ay$, where the y axis is perpendicular to the convergence line and A is the rate of mean flow convergence, and for an autocorrelation of turbulent velocity given by

$$\rho(\tau) \equiv \frac{\overline{v(t)\, v(t-\tau)}}{\overline{v^2}} = e^{-\tau/t}$$

and for the superposition of mean flow and turbulence

$$V_i = \tilde{v} + v_i$$

the mean square position of an infinite ensemble of independent tracers obey the equation

$$\overline{y^2}(t) = \frac{\overline{v^2}T^2}{\alpha(1+\alpha)} - \left[2\left(\frac{\phi_o T}{1-a} - \frac{\overline{v^2}T^2}{1-\alpha^2}\right)\right]\exp(-(1+\alpha)t^*)$$

$$+\left[\overline{y^2}(0) + 2\left(\frac{\phi_o T}{1-\alpha} - \frac{\overline{v^2}T^2}{1-\alpha^2}\right) - \frac{\overline{v^2}T^2}{\alpha(1+\alpha)}\right]\exp(-2\alpha t^*) \qquad (1)$$

where the rotation is

$\overline{v^2}$, the mean square turbulent speed, isotropic and homogeneous,

T , the Lagrangian integral time scale for the turbulence alone,

α = AT, the ratio of the turbulence time scale T to the convergence time scale A^{-1},

ϕ_o , the initial convariance $\overline{v(o)y(o)}$,

$t^* = t/T$.

It is easily shown that (1) is valid for all α by taking the limits as $\alpha \to -1$, 0, and 1.

Note that $\overline{y^2}$ refers to mean square distance of the tracers from the origin (the convergence line), not necessarily the variance of the tracer positions. Thus all tracers can start on one side of the convergence line, and need not be symmetrically distributed. The initial tracer variance is $y^2(0)$.

The steady-state solution is given by the first term of (1) and can also be written

$$\overline{y^2}(\infty) = \frac{\overline{v^2}}{A^2}\frac{\alpha}{1+\alpha}. \qquad (2)$$

If we were to use the advection diffusion equation with the usual diffusion coefficient $K_o = \overline{v^2}\,T$, the steady state tracer variance (i.e., the concentration variance) would be

$$\overline{y_d^2}(\infty) = \frac{\overline{v^2}}{A^2}\alpha \qquad (3)$$

But with a modified diffusion coefficient $K_1 = \overline{v^2} T/(1+\alpha)$ the correct steady-state result, i.e. (2) is obtained. K_1 also follows Spiegel's theorem, namely that:

> When two processes with different time scales interact, the time scale that characterizes the total system is the geometric mean of the time scales of the two processes acting independently.

In the present case the effective time scale would be

$$T^* = \frac{A^{-1} T}{A^{-1} + T} \tag{4}$$

and with a slight algebraic manipulation it is easily seen that

$$K_1 = \overline{v^2} T^* . \tag{5}$$

The steady-state result illustrates an important aspect of Lagrangian statistics. In the steady-state tracer distribution there is no dispersion, so the dispersion coefficient $K_V = V^2 T_V$ based on the total velocity, $V_i = \tilde{v} + v_i$, must satisfy $K_V = 0$. This implies $T_V = 0$, where

$$T_V = \int_0^\infty \rho_V(\tau) d\tau \tag{6}$$

and where ρ_V is the autocorrelation of the total velocity. For the steady state ρ_V is given by

$$\rho_V(\tau) = \frac{\exp(-\tau/T) - \alpha \exp(-A\tau)}{1-\alpha} \tag{7}$$

which does indeed satisfy $T_V = 0$.

Numerical solutions for an ensemble of tracers following Lagrangian trajectories have been obtained using the formula

$$y_{i,m+1} = y_{i,m} + \left(\frac{v_{i,m}}{A} - y_{i,m}\right)\left(1 - \exp(-A\Delta t)\right) \tag{8}$$

where $v_{i,m}$ is a velocity, constant during Δt , for the i^{th} particle at time step m, and $v_{i,m}$ is calculated from

$$v_{i,m} = R\, v_{i,m-1} + (1-R^2)^{1/2} \hat{v}_{i,m} . \tag{9}$$

In (9), R is the one-time-step autocorrelation of $\tilde{v}_i$ and is given by $R = 1 - \Delta t/T$ for small $\Delta t/T$, and $\tilde{v}_{i,m}$ in a randomly selected velocity with variance $\overline{v^2}$. Equation (9) is a first-order Markov process that approximates the exponential autocorrelation used to obtain (1).

Using (8) and (9) for many time steps and many tracers, the steady state solutions for y^2 are in excellent agreement with the analytical model.

Other material discussed in FM includes analytical solutions for an oscillating autocorrelation given by

$$\rho(\tau) = \left(\cos b_i \tau + \frac{b_r}{b_i} \sin b_i \tau\right) \exp(-b_r \tau) \qquad (10)$$

and corresponding transient numerical solutions using a second-order Markov process for $\tilde{v}_{i,m}$, namely

$$\tilde{v}_{i,m} = C_1 \tilde{v}_{i,m-1} + C_2 \tilde{v}_{i,m-2} + \alpha \hat{v}_{i,m}$$

and where C_1 and C_2 are related to b_i and b_r in (10).

The problem of similar numerical calculations when the turbulent intensity is spatially variable was briefly discussed. In particular it was pointed out that with $\overline{v^2} = \overline{v^2}(y)$, one cannot assume symmetrical turbulent velocity distributions as were used with (9). The use of symmetrical velocity distributions violates the equation of continuity for an incompressible fluids. To overcome this difficulty a transition probability model of turbulent dispersion has been invented.

REFERENCE

Faller, A. J. and P. Mignerey, 1982. One dimensional turbulent dispersion in convergent and divergent flows. Physics of Fluids, July.

WAVE/SHEAR-FLOW INTERACTION AND THE GENERATION OF LANGMUIR CIRCULATIONS

Alan J. Faller

Langmuir circulations are helical rolls in the surface layers of lakes and oceans with their axes along the wind direction. (Langmuir, 1938). They give rise to lines of convergence on the ocean surface, and any floating materials that converge into these lines are called wind rows.

Some characteristics of LCs were briefly reviewed. Their spacing on the ocean is from 5 m to 200 m. and they have downdwelling speeds on the order of 1/100 the wind speed. As deduced by E. R. Baylor in 1962 from field observations of LCs (personal communication) small cells tend to agglomerate into larger cells, an energy exchange from higher to lower wave numbers that is now understood to be a ubiquitous characteristic of two-dimensional turbulence. The largest scale in this energy transfer is usually about 2.5 to 3 times the depth of the mixed layer.

Laboratory films of LCs due to the interaction of crossed-wave patterns and wind-driven shear flow (the Craik-Leibovich (1976) theory) were shown, both for the wind blowing with and against the wave propagation direction. The observed circulations were in agreement with specific predictions of the theory (Faller, 1978) and reversed their sense of circulation in response to reversal of the wind direction (Faller and Cartwright, 1982).

The second Craik-Leibovich theory is an instability theory developed from the basic equations:

$$\underset{\sim}{u} + \underset{\sim}{u} \cdot \nabla \underset{\sim}{u} + \nabla(\pi + \underset{\sim}{u} \cdot \underset{\sim}{u}_S) = \underset{\sim}{u}_S \times (\nabla \times \underset{\sim}{u}) + \nu \nabla^2 \underset{\sim}{u} \qquad (1)$$

$$\nabla \cdot \underset{\sim}{u} = 0 \qquad (2)$$

where u_S is the Stokes drift of the wave field. These equations can be derived by the usual expansion in wave amplitude, as in Craik and Leibovich (1976), or by the wave/shear-flow interaction theory of Andrews and McIntyre (1978) as shown in Leibovich (1980).

The instability mechanism has been tested in a series of laboratory experiments by the author and Craig Perini at the University of Maryland. A film was shown illustrating an unstable laboratory flow consisting of small waves (amp. = 0.3 mm, wavelength 30 cm) and shear flow $\frac{\partial u}{\partial z} = O(0.25 s^{-1}.)$ The instability clearly took the form of longitudinal rolls in the surface layer. Again, these experiments give results that appear to be in agreement with the Craik-Leibovich theory.

REFERENCES

Andrews, D. G. and M. E. McIntyre, 1978. An exact theory of non-linear waves on a Lagrangian flow. J. Fluid Mech., 89, 609-646.

Craik, A.D.D. and S. Leibovich, 1976. A rational model for Langmuir circulation. J. Fluid Mech. 73, 401-426.

Faller, A. J., 1978. Experiments with controlled Langmuir circulation. Science, 201, 618-620.

Faller, A. J. and R. W. Cartwright, 1982. Laboratory studies of Langmuir circulation. Tech. Note BN-985, I.P.S.T., Univ. of MD, College Park.

Langmuir, I., 1938. Surface water motion induced by wind. Science, 87, 119-123.

Leibovich, S., 1980. On wave-current interaction theories of Langmuir circulation. J. Fluid Mech., 99, 715-724.

POTENTIAL VORTICITY STRUCTURE IN THE NORTH ATLANTIC SUBTROPICAL GYRE

Donald B. Olson

Following a brief discussion of the Ertel potential vorticity for a stratified fluid on a rotating earth, the distribution and forcing of potential vorticity in a subtropical gyre is considered. If both diabatic forcing, i.e., surface buoyancy fluxes, and the wind stress curl are included the result is an asymmetric gyre which is less intense in the south than in the north. The potential vorticity field which arises due to the Sverdrup balance is asymmetric even in the case of a symmetric wind curl without any diabatic effects. The north-south gradients in potential vorticity are largest in the northern portion of the gyre. There is a tendency to form regions of nearly uniform potential vorticity in the south-central gyre due to the forced response. The well-known production of opposing meridional gradients in potential vorticity between the upper and lower layers in the southern gyre is pointed out. This effect can lead to the breakdown of the flow to the west in the southern gyre due to baroclinic instability.

The simple ideas derived from the consideration of the Sverdrup problem are compared with the observed potential vorticity as approximated from the thickness between isotherms in historical expendable bathythermograph data. The basic asymmetry in the gyre is noted in both the potential vorticity and the baroclinic streamfunction as approximated by the thermocline depth. Portions of the gyre, however, appear to have more in common with a Fofonoff gyre than a Sverdrup circulation. The predicted reversal of the meridional potential vorticity gradient in the southern gyre does appear but takes the form of a set of step-like fronts rather than the smooth gradients expected. These bands of high potential vorticity gradient are associated with eddy potential energy maxima and reversals in baroclinic shear in the surface layers. The possibility that these bands may be related to the final stable state following a large scale instability and turbulent cascade is speculated upon.

EVOLUTION OF STRONG VORTICES

Glenn Flierl

One of the serious flaws in the standard quasi-geostrophic equations, commonly used for understanding the evolution of mesoscale oceanic eddies, is the requirement that the change in thickness between density surfaces must be small compared to the mean thickness. In the case of warm core rings, the thickness of the thermostadt layer may range from 500 m at the center to zero at the edge of the eddy. Yet the prediction of the evolution of such features is vastly simplified by noting that there is a dominant equilibrium balance of forces in the fluid with the beta effect and time derivatives being relatively weak.

I have constructed a non-quasi-geostrophic model for the evolution of a warm core ring using a two layer model in which the upper layer has finite volume so that the interface surfaces on a basically circular boundary. The lowest order flow in the warm pool is much faster than the Rossby wave speeds

βL^2 and is not geostrophic but rather is assumed to be in a state of cyclostrophic balance. The time changes then occur on a time scale set by $(\beta L)^{-1}$ and can be calculated by balancing the net Coriolis forces due to translation of the whole pool with the southward forces caused by the β effect and form drags caused by wave generation in the lower layer. I have assumed that the lower layer is deep compared to the typical upper layer thickness so that the lower layer dynamics is quasi-geostrophic with Rossby waves being generated by the motion of the warm pool.

For very deep lower layers, the generated waves can be calculated explicitly and the form drags can be shown to induce a southward motion of the upper pool and decay of its energy. This wave drag vanishes for very special choices of the size of the upper pool and the lower layer motions are then non-zero only just below the upper layer and have a net counter-clockwise circulation with angular momentum equal and opposite to that of the upper layer.

FINITE AMPLITUDE LONG WAVES IN A SHEAR FLOW

Melvin Stern

The temporal evolution of the cross-stream velocity v in an inviscid and piecewise uniform vorticity boundary layer flow is investigated by means of a large amplitude, long wave, and two dimensional theory. The maximum and minimum v increase up to the time where "shocks" form, whereupon the neglected short wave effects become important. The distribution of the large v ($\pm$) has a universal qualitative character, resembling the distribution in a laminar spike (Kovasznay et al. 1962).

Three dimensional processes are implicit to the extent that they account for an anomalous vorticity layer assumed for the initial state of the two dimensional theory. This predicts other strong nonlinear effects, such as wave breaking and "mode locking".

THE SHAPE OF THE MAIN THERMOCLINE

Rick Salmon

Consider a two-layer ocean in which the lighter fluid has been divided up into M parcels of equal mass. Imagine that the ocean surface is covered by a horizontal network of N square grid-boxes, and let m_i be the number of light-water parcels beneath the i-th grid-box. The depth of the main thermocline at the i-th grid-box is proportional to m_i, which may be zero. A state of the system,

$$\{ m_1, m_2, \ldots, m_N \}, \tag{1}$$

is defined by specifying the number of parcels at each of the N grid-boxes. Each state (1) has an entropy,

$$S = \ln W, \tag{2}$$

where

$$W = \frac{M!}{m_1! \ldots\ldots m_N!} \tag{3}$$

is the number of ways to realize the state. Replacing

$$\ln(m_i!) \sim m_i \ln m_i$$

and then maximizing S subject to the conservation of total mass,

$$\sum_i m_i = M, \tag{4}$$

and potential enstrophy,

$$\sum_i f_i^2/m_i = Z, \tag{5}$$

leads to

$$\ln m_i = a - b\, f_i^2/m_i \quad \text{(where } m_i \neq 0.\text{)} \tag{6}$$

Here a and b are Lagrange multipliers corresponding to (4) and (5). Consistent solutions to (6) exhibit hemispheric regions of uniform potential vorticity f_i/m_i. This argument can be made less heuristic, and can include the contribution of relative vorticity to (5) and the additional constraint of energy conservation. Numerical experiments provide some confirmation.

TRANSIENT TRACERS

William J. Jenkins

Observation of the penetration of man-made substances, in particular nuclear weapons testing fall-out and industrial by-products, are providing us with a unique opportunity to measure mixing and advection in the oceans. The different "boundary conditions", time histories and geochemical behavior of these substances highlight different processes and parts of the ocean and allow us in a crude way to resolve the pathways and transport processes responsible for their redistribution in nature. Due to the sparse sampling inherent in the oft-times difficult measurements, and the uncertainty in some of the boundary conditions, the conclusions drawn on the basis of tracer studies may be by themselves ambiguous, but at least place crude "integral constraints" on the physics operating in the ocean.

There are two extremes in time histories for the transient tracers. At one extreme is the pulse-like injection of bomb produced tracers such as tritium, ^{137}Cs and ^{90}Sr, while the other extreme is characterized by quasi-exponentially increasing concentrations, e.g. ^{85}Kr, fluorocarbons and CO_2. The bomb-produced tracers generally have more northern hemispheric delivery, whereas the "industrial" tracers are more globally uniform.

Carbon-14 produced by the bomb is intermediate between the two classes of tracers since it is largely inventoried in the form of atmospheric $^{14}CO_2$. Its time history is spread out more in time than tritium yet it is now decreasing. $^{14}CO_2$ travels the same pathways as anthropogenic CO_2, but with the important difference that the exchange timescale between the mixed layer and the atmosphere is of the order of 15 years for $^{14}CO_2$, but only a tenth of that for CO_2 alone. Evidence from corals indicates that the pre-anthropogenic ^{14}C age of surface waters was of the order of 300 years - an artifact of the relatively short residence time of water at the surface (a few years) coupled with the larger residence time of the same waters within the thermocline (a few decades).

"Direct" measurement of anthropogenic CO_2 is being attempted, but estimation of the preformed (surface equilibrated) CO_2 contents requires large and perhaps uncertain corrections for <u>in situ</u> production by oxidation of organic materials, and hence is still a somewhat controversial technique. ^{85}Kr (half-life 10.5 years) is a by-product of nuclear fuel reprocessing, has a well documented atmospheric history and being a noble gas has a simple behavior. The difficulty is that measurement of ^{85}Kr requires 200 l of water and specialized shipboard and shore-based equipment. One of the more promising tracers is freon-11 (a Dupont trade name for trichlorofluoromethane) which is also well documented in the atmosphere, apparently inert in the oceans and measurable at sea using small (ca. 100 ml) samples. Preliminary results show major oceanic features in a believable way.

Finally there is tritium (half-life 12.5 y) and its stable, inert daughter ^{3}He. The spike-like entry of tritium into the oceans coupled with the fact that it exists primarily as water (H^3HO) makes it an excellent tracer of decade timescale transport. The daughter, ^{3}He, has the interesting boundary condition in that it is "zeroed" at the ocean surface, and builds up significant excesses in a few months. This extends the sensitivity of tritium to shorter timescales and provides a unique sensitivity to "backfluxing" to the atmosphere.

INVERSE METHODS FOR OCEANOGRAPHY

George Veronis

Determining absolute velocities in the ocean is a long-standing problem that has been attacked mostly via intuitive assertions about a likely level of no motion. Wunsch (1978) formulated the problem in terms of inverse theory which has been used with considerable success in geophysical studies. The basis of the analysis is to assume a level of no motion and then to correct that level so that conservation of mass is satisfied for each of the several conservative layers that can be identified. The resulting system of equations is a strongly underdetermined one and the procedure proposed by Lanczos using singular value decomposition can be applied to find the (unique) solution when contributions from the null space are omitted. This procedure gives a correction that departs minimally from the assumed level of no motion.

One difficulty with the inverse procedure is that large corrections are required if the assumed level of no motion involves large initial imbalances in mass conservation of the layers. These large corrections are often physically unrealistic. Fiadeiro and Veronis (1982) have proposed a means of circumventing the latter difficulty by running an empirical search for a best level of no motion before inverse theory is applied. An important consequence of that search is that it may suffice to give an acceptable level of no motion with no correction. Part of the search procedure is to study the effects of noise to determine how much of an imbalance in mass conservation can be tolerated because it is at or below noise level.

An alternative search procedure that makes use of the common solution of inverse theory leads to results that are close to those obtained with the empirical search. Once that result is obtained one can derive an optimal solution by using a three-way trade-off involving the mean-square residual transports, the magnitude of the correction and the number of eigenvectors for the correction. A great advantage of this procedure is that the imbalances that must be eliminated can be kept small so that for a satisfactory solution the required correction may be so mild that the usual noise amplification accompanying such corrections is avoided.

An alternative attack using all of the eigenvectors to obtain a solution that lies within a prescribed neighborhood of the exact solution to the problem leads to a more flexible and controllable procedure.

For all of the schemes that were adopted it is possible to use conservative layers defined by density, potential vorticity and/or the Bernoulli function to constrain the system. The latter two quantities may require the introduction of higher-order processes. Methods for incorporating these higher-order effects are the subject of an on-going study.

REFERENCES

Fiadeiro, M. E. and George Veronis, 1982. On the determination of absolute velocities in the ocean. J. Mar. Res., (40, supplement) 159-182.

Wunsch, C., 1978. The North Atlantic general circulation west of 50W determined by inverse methods. Rev. Geoph. and Space Phys. 16, 583-620.

ON THE DIRECTION OF EDDY MOMENTUM FLUXES IN BAROCLINIC INSTABILITIES

Isaac M. Held

In the analysis of the instability of atmospheric zonal flows to quasi-geostrophic disturbances, one often encounters unstable modes that are essentially baroclinic, deriving most of their energy from the potential energy of the basic state, but with structures modified somewhat by horizontal shears in the zonal wind. Among these modifications the tilt of constant phase lines with latitude is of particular interest, this tilt being identically zero for normal modes in a purely baroclinic problem. Few general results have been obtained that predict even the sign of this tilt or, equivalently, the direction of the horizontal eddy flux of momentum, given the form of the mean flow.

I argue in this seminar that one can gain some understanding of this problem by examining the very simple special case of an internal jet instability with very small growth rates, growing on a mean flow with small horizontal shears. From the fact that the eddy potential vorticity flux in an unstable mode is everywhere directed down the mean potential vorticity gradient, one can show that the sign of the vertically integrated momentum flux divergence is controlled by the vertical derivative of the mean potential vorticity gradient, divided by the mean vertical shear, and evaluated at the steering level. If this quantity is positive, the momentum fluxes are upgradient if the mean flow has sufficiently large meridional scale, and downgradient if this scale is sufficiently small (even though horizontal curvature of the mean flow may be making a negligible contribution to the potential vorticity gradient). If this quantity is negative, the flux is downgradient irrespective of the meridional scale of the mean flow.

Numerical results show that this same qualitative behavior is also found when growth rates are not small, and for the Eady and 2-layer models. At the most unstable wavenumber, one generally finds a transition from downgradient to upgradient fluxes as the meridional scale of the mean flow increases. The transition occurs at a scale comparable to the relevant radius of deformation or, equivalently, the zonal scale of the mode.

OPENERS AND CLOSURES

Willem V.R. Malkus

The word "closure" is used to describe a method of solution of the infinite sequence of equations which relate moments of (turbulent) flow to other moments, each equation of the sequence requiring a knowledge of unknown higher moments. The usual technique of closure is to hypothesize an additional relation between a higher and lower moment, thus terminating the sequence of equations. Hence the nature of a closure assumption is to restrict the huge number of solutions that could be found to a truncated version of the original moment equations.

In exceptional circumstances a closure can be formally correct. An example is given which leads from the Welander-Keller convection loop to the Lorenz equations.

An "opener" is also a method of solution of moment equations of a flow field. Rather than terminating the sequence of equations by a statistical hypothesis, one explores the entire class of vector fields (among which are the possible fluid motions) compatible with the first, or first few, moment equations. A possible method would be to treat each compatible vector field on the same footing, constructing an average value for any desired quantity. However, the procedure that has been adopted is to seek that solution among the many possibilities which provides a formal upper bound on some important aspect of the flow. For example, upper bounds for heat flux have been found in convection and upper bounds for stress have been found for shear flow. In principal these upper bounds can be brought nearer and nearer to the realized flow by the addition of higher order moments to reduce the class of possible motions. While upper bound theory has produced the only guaranteed quantitative results in turbulence theory, the bounds to date are not particularly close to the observations. The extension of present upper bound results by analytic methods may not be feasible, yet with the greater availability of computing facilities, bound theory provides a unique way to pin down quantitative aspects of turbulence statistics. First steps towards formal bounds on the statistical stability of turbulent shear flow are described. Numerical methods are used to solve ordinary time-dependent, nonlinear equations which determine stable average fields "adjacent to reality ".

CHAOS IS COME AGAIN

Edward A. Spiegel

This is an account of work done with Alain Arneodo and Pierre Coullet on the temporal dynamics of triple convection. We have studied Boussinesq thermohaline convection in a layer rotating about a vertical axis. We adopted Rayleigh boundary conditions, that is conditions that make the solutions of the linear problem trigonometric, and we have assumed bidimensional motion. If you look into last year's notes, you will undoubtedly conclude with us that, in a neighborhood of parameter space of the triple point where the three instabilities are simultaneously marginal, the temporal dynamics may be described by an amplitude equation of the form

$$\dddot{x} + \eta\ddot{x} + \nu\dot{x} + \lambda x = k_6 x\ddot{x}^2 + k_5 x^2\ddot{x} + k_4\dot{x}^3 + k_2 x^2\dot{x} + k_1 x^3 \qquad (1)$$

where x is the amplitude of the normal mode of linear theory that may go unstable. To get this system, we have assumed a finite box so as to make the number of modes that is allowed by linear theory countable. The parameters η, ν and λ are given directly by linear theory. When all three of them vanish, we are at the triple point where linear theory gives three vanishing growth rates. The six k_i are properties of the generalized null vectors that arise in the linear theory at the triple point. There is no need to write down their expression in terms of the various more conventional linear parameters, but we do have those expressions worked out.

The problem in studying (1), if special circumstances do not lead us to a preferred region of parameter space, is that this space is hexadimensional and a complete exploration of it is not possible for us. We have decided to concentrate on the limit of small dissipation, that is, $0 < \eta << 1$. In that limit, if we require that no linear terms are lost, we get the asymptotic normal form for this case, namely

$$\dddot{A} + \ddot{A} + \alpha\dot{A} + \beta A = \pm A^3 \qquad (2)$$

where the amplitude function A and the time have been suitably scaled. There remain two parameters and a sign to be chosen in this version. If you were to go back to the original Boussinesq equations and perform the standard amplitude equations, with the introduction of a slow time, you would get (2) in leading order.

Numerical solutions of (2) reveal the full panoply of modern chaotic dynamical phenomena - period doubly, period halving, strange attractors, hysteresis, intermittent behavior. Among the forms of chaos that we observe is that which occurs near to unstable homoclinic orbits and is suggested by the work of Shil'nikov. The behavior is so rich and complicated that even the amplitude equations are too much to cope with. But just as the Boussinesq equations form a crude model of some features of gfd, and the amplitude equations model the temporal behavior of the Boussinesq solutions, there are mappings that model the temporal behavior in all of the above. We have constructed bidimensional Poincaré maps that provide qualitative models of this behavior, as in a formally related study done with Charles Tresser. These in turn can be reduced to maps in one dimension that leave no doubt that, in triple convection, chaos occurs as close as you want to the triple point of multiple marginality.

STATISTICAL MECHANICS OF FIELDS

Joseph B. Keller

1. INTRODUCTION

Statistical mechanics associates a probability density P(p,q,t) with a mechanical system described by a set of coordinates q and conjugate momenta p. Conservation of probability requires that the temporal evolution of P be governed by the equation

$$\frac{\partial P}{\partial t} - \frac{\partial H}{\partial q}\frac{\partial P}{\partial p} + \frac{\partial H}{\partial p}\frac{\partial P}{\partial q} = 0. \tag{1}$$

Here H(p,q) is the Hamiltonian of the system. In terms of H, the equations of motion of the system are

$$\frac{\partial p}{\partial t} = -\frac{\partial H}{\partial q}, \quad \frac{\partial q}{\partial t} = \frac{\partial H}{\partial p}. \tag{2}$$

2. THE GIBBS DISTRIBUTION

A statistically steady state is one for which P(p,q) is independent of the time t. Of course P must then satisfy (1) with $\partial P/\partial t = 0$. In particular any function of H(p,q), i.e. P[H(p,q)], is a solution of (1) which is independent of t. This follows at once by using (2) in (1).

To find the form of P(H), Gibbs considered two noninteracting systems with Hamiltonians H_1 and H_2. The Hamiltonian of the combined system is H_1+H_2. Then because the systems are independent, their probabilities must be multiplied together to yield that of the combined system. Thus

$$P(H_1+H_2) = P(H_1)\,P(H_2). \tag{3}$$

The continuous solution of (3) is the Gibbs distribution

$$P(H) = e^{-\beta H(p,q)} \Big/ \int e^{-\beta H(p,q)}\,dp\,dq. \tag{4}$$

Here β is a constant which Gibbs chose as $\beta = 1/KT$, where K is Boltzmann's constant and T is the absolute temperature at which the system is assumed to be in equilibrium.

3. THE RAYLEIGH-JEANS LAW

When the Gibbs distribution (4) is applied to a system with a quadratic Hamiltonian, it yields an average energy of KT/2 per degree of

freedom. A scalar field, such as a sound field, in a container of volume V has $(1/8)(4\pi/3)(k/\pi)^3 V$ modes with wavenumbers less than k, for k large. Each mode is a degree of freedom, so the average energy of the field in all modes with wavenumbers less than k is $(KT/2\pi^2)k^3 V$. Thus the average energy density E(k) per unit volume per unit wavenumber is V^{-1} times the derivative of this with respect to k,

$$E(k) = \frac{KT}{4\pi} k^2. \tag{5}$$

This is the Rayleigh-Jeans law for the energy density of black body radiation, except for an extra factor of two on the right side to account for the two states of polarization.

This law leads to an infinite energy density when integrated over k, so it *cannot be correct at* high wavenumbers. The correct law, discovered by Planck, agrees with (5) for small k, but differs from it at high k due to quantum mechanical effects.

4. CORRELATION FUNCTIONS OF FIELDS IN THERMAL EQUILIBRIUM.

The Gibbs distribution (4) can also be used to calculate correlation functions of fields. A convenient way to do this is to write $u(x,t) = [p(x,t), q(x,t)]$ and to introduce the characteristic functional $F[\lambda]$ of the field, defined by

$$F[\lambda] = \int \exp\left[i \int_{-\infty}^{\infty} \int_D \lambda(x,t) u(x,t)\, dx\, dt\right] P[H(u)]\, dp\, dq \tag{6}$$

Here the argument $\lambda(x,t)$ is a vector with the same number of components as u(x,t) and D is the domain of x. From $F[\lambda]$ the moments of u can be found by functional differentiation at $\lambda = 0$:

$$\left.\frac{\delta^n F[\lambda]}{\delta\lambda(x_1,t_1)\cdots\delta\lambda(x_n,t_n)}\right|_{\lambda=0} = i^n \int u(x_1,t_1)\cdots u(x_n,t_n) P[H(u)]\, dp\, dq \equiv i^n \langle u(x_1,t_1)\cdots u(x_n,t_n)\rangle. \tag{7}$$

When the field satisfies a linear equation of motion, the Hamiltonian H is quadratic. Then F can be evaluated explicitly by completing the square, and the result can be written in the form.

$$F[\lambda] = \exp\left(-\frac{1}{2}\int_{-\infty}^{\infty}\int_D\int_{-\infty}^{\infty}\int_D \lambda_i(x,t)\langle u_i(x,t)u_j(x',t')\rangle \lambda_j(x',t')\, dx'\, dt'\, dx\, dt\right). \tag{8}$$

This result (8) shows that the field is Gaussian with mean zero. All moments can be expressed in terms of the two-point two-time moment $\langle u_i(x,t)u_j(x',t')\rangle$. Furthermore, explicit expressions can be obtained for this second moment in terms of certain Green's functions associated with the field's equation of motion.

The derivation of (8) and of the expression for the second moment, as well as various consequences of these results, are given in the author's paper Keller (1970).

5. APPLICATION TO TWO-DIMENSIONAL TURBULENCE

We shall now apply some of the preceding considerations to an incompressible fluid in two dimensional turbulent motion in a domain D. First we introduce the stream function $\Psi(x,y)$, in terms of which the energy E, enstrophy Ω and palenstrophy Φ are given by

$$E=\int_D(\nabla\Psi)^2dxdy\ ,\ \Omega=\int_D(\Delta\Psi)^2dxdy\ ,\ \Phi=\int_D\Delta\Psi(\Delta^2\Psi)dxdy. \tag{9}$$

By analogy with (4), we introduce the distribution.

$$P[E,\Omega,\Phi]=Z^{-1}e^{-\alpha E-\beta\Omega-\delta\Phi}. \tag{10}$$

In (10) α, β and δ are constants, and Z is the normalization coefficient. The distribution (10) without the term in Φ was considered by Salmon (1982).

To use (1) we follow Salmon and introduce as a basis the normalized eigenfunctions φ_i, defined by

$$(\Delta+k_i^2)\varphi_i=0\ \text{in D},\ \varphi_i=0\ \text{on}\ \partial D\ ,\ \int_D\varphi_i^2dxdy=1. \tag{11}$$

Then we write Ψ in terms of the φ_i, with coefficients $k_i^{-1}y_i$, as follows:

$$\Psi(x,y)=\sum_i y_ik_i^{-1}\varphi_i(x,y). \tag{12}$$

By using (12) in (9) we get

$$E=\sum_i y_i^2\ ,\ \Omega=\sum_i k_i^2y_i^2\ ,\ \Phi=\sum_i k_i^4y_i^2. \tag{13}$$

Now (10) becomes

$$P(y_i)=Z^{-1}e^{-\sum_i(\alpha+\beta k_i^2+\delta k_i^4)y_i^2} \tag{14}$$

From (14) we find that

$$\langle y_i^2 \rangle = \frac{1}{2}\left(\alpha + \beta k_i^2 + \delta k_i^4\right)^{-1}. \tag{15}$$

There are asymptotically $(\pi/4)(k/\pi)^2 A$ modes with wavenumbers less than k in a domain of area A, when k is large. Thus the average energy density E (k) of the fluid per unit area per unit wavenumber is

$$A^{-1}\langle y^2 \rangle \frac{d}{dk}\frac{\pi}{4}\left(\frac{k}{\pi}\right)^2 A = k\langle y^2 \rangle / 2\pi. \tag{16}$$

By using (15) for y^2 in (16) we get

$$E(k) = \frac{k}{4\pi}\left(\alpha + \beta k^2 + \delta k^4\right)^{-1}. \tag{17}$$

For large k, this becomes the well-known result

$$E(k) \sim \frac{k^{-3}}{4\pi\delta}. \tag{18}$$

In three dimensions the same analysis yields $E(k) \sim k^{-2}$.

REFERENCES

Keller, Joseph B. 1970. Classical and Quantum Mechanical Correlation Functions of Fields in Thermal Equilibrium. Jour. Math. Phys. 11, 2286-2296.

Salmon, R. 1982. Geostrophic Turbulence. In Topics in Ocean Physics, Soc. Italiana di Fisica, Bologna, Italy.

THE MODIFIED CUMULANT EXPANSION FOR DIVERGENT TWO-DIMENSIONAL ISOTROPIC TURBULENCE

Shinichiro Yanase

We investigate divergent two-dimensional isotropic turbulence of finite Rossby's outer radius of deformation using the modified cumulant expansion. Such flow can be considered as a model of geostrophic turbulence in atmosphere or ocean. β-effect is neglected in order to avoid complexity.

The fluid motion of quasi-geostrophic balance in a uniformly rotating frame is written as

$$\frac{\partial}{\partial t}\left\{(-\Delta+\kappa^2)\psi\right\}+\frac{\partial(\psi,\Delta\psi)}{\partial(x,y)}=-\nu\Delta^2\psi, \tag{1}$$

where ψ is the stream function, ω the vorticity, V the kinematic viscosity, κ the inverse of Rossby's radius of deformation. It can easily be shown that eq. (1) contains two fundamental conserved quantities for $V \equiv 0$.

$$\frac{dE_G}{dt}=-2\nu\Omega, \quad \frac{dQ_G}{dt}=-2\nu P, \tag{2}$$

where

$$\begin{aligned} E_a &= E+\kappa^2 C \quad \text{total energy} \\ Q_a &= Q+\kappa^2 E \quad \text{potential enstrophy,} \end{aligned} \tag{3}$$

and E the kinetic energy. Ω the enstrophy, C the potential energy, P the palinstrophy.

Using the lowest-order approximation of the modified cumulant expansion, we obtain from eq. (1) the equation for $E(k,t)$, the energy spectrum fraction. Numerical integration of the spectrum equation gives the following results:

1) The kinematic energy decays and simultaneously the potential energy increases in times.

2) The motion larger than the radius of deformation is strongly suppresed but the energy spectrum in the corresponding region does not remain constant but changes slowly in time as,

$$E(k,t) \propto t^{-\frac{1}{4}} f(kt^{\frac{1}{4}}),$$

and

$$E(k,t) \propto k^7, \text{ for } k=0.$$

3) In the large wave number region, the similarity law of energy spectrum is identical with nondivergent case and the k^{-3} subrange appears. However, enstrophy cascade is enhanced by the decay of kinetic energy in low-wavenumber region, and the palinstrophy is amplified compared with nondivergent two-dimensional turbulence ($\kappa = 0$).

THERMAL CONVECTION: NUMERICAL EXPERIMENTS NEAR THE ONSET TO TURBULENCE AND COMMENTS ON THE APPLICATION OF CLOSURE

Jackson R. Herring

We have investigated Boussinesq-slip boundary thermal convection, focusing on the nature of the transition from steady convection at low Rayleigh number ($Ra \lesssim 30\ Rc$) to a chaotic regime at $Ra \gtrsim 65\ Rc$, where $Rc = 27\ \pi^4/4$. For most of the calculations reported here, the Prandtl number = 10. The numerical technique is pseudospectral (= Fourier colocation) with an equivalent grid point resolution $\leq$ 32x32x32. Our goals are twofold: (1) to examine the transitional behavior of a dynamical system as the number of modes is increased sufficiently so that the resulting equations are an accurate representation of the underlying physics, and (2) to produce a data base by which to assess closure techniques (DIA, etc.) at turbulent Rayleigh and Reynolds number.

Broadly speaking, what we observe is that the transition from a periodic regime (at $Ra \lesssim 40\ Rc$) through a quasiperiodic regime ($50\ Rc \lesssim Ra \lesssim 60\ Rc$) and into a chaotic regime ($Ra \gtrsim 70\ Rc$) is accompanied by a rapid increase in those turbulence parameters (such as skewness, $S = \langle(\partial u/\partial x)^3\rangle / \langle(\partial u/\partial x)^2\rangle^{3/2}$, isotropization and vertical vorticity) that measure three dimensionality. Moreover, equivalent calculations in two dimensions fail to become turbulent (or chaotic) if the numerics adequately resolve all significant scales of motion. The computed values of the velocity and temperature skewness are shown to be in rough agreement with experiments, such as that of Tavoularis, et al (1978). The value of the Taylor microscale Reynolds number ranged from 2, at $Pr = 10$ to ~ 30 at $Pr = 1$.

An examination of the contour plots of the flow provides an identification of the various frequency components present in the power spectra of the velocity and temperature fields. At low Ra, the periodic regime consists in a single frequency component at the Brunt-Vaisala frequency of the stable core region. At this stage, the flow consists of near two dimensional convection with (three dimensional) imbedded lenticular plumes. As Ra increases, the roll boundaries begin to wave at a somewhat lower frequency, and the system enters a quasiperiodic regime at $Ra \simeq 55Rc$. As Ra increases, further and more complicated time dependence is introduced. This appears associated with a tilting-wagging motion of the thermal plumes, followed by a pinching off of blobs of fluid from the plume outflow anvils. In general, the temperature field appears much more turbulent than the velocity, consistent with the rather large value of the Prandtl number Pr (= 10). At lower Pr (≤ 1) the flow appears much more three dimensional, and at $Ra \simeq 70Rc$ roll boundaries can no longer be identified.

Finally, we consider certain aspects of two-point closures (notably the DIA), inquiring as to what detailed features of the theory need to be preserved unabridged in a comparison of theory and convection experiments (numerical or otherwise). In this connection we present a comparison of closure with the numerical simulation of passive scalar turbulence. We note that the long correlation times at small scales (as suggested by the near laminar nature of

small scales at small Reynolds numbers) is accurately preserved by the DIA, but not by the more abridged Markovian theories such as the eddy damped Markovian or test field model. The research reported here is in collaboration with J.H. Curry, J. Loncharie, and S.A. Orszag.

REFERENCE

Tavoularis, S., J. C. Bennett and S. Corrsin, 1978. Velocity-derivative skewness in nearly isotropic turbulence. J. Fluid Mech. 88, 63-69.

HETEROCLINIC ORBITS AND IRREGULAR OSCILLATIONS

Louis N. Howard

To try to clarify some qualitative aspects of experiments on turbulent convection, R. Krishnamurti and I have studied a 6th order spectral truncation of the equations of 2D convection. This extends the Lorenz model (LM), containing it on an invariant 3D manifold. But it allows also a loss of symmetry corresponding to asymmetric tilted cells which is impossible in LM, and appears not to have been considered in previous extensions of it. At low Rayleigh number (R) the attractors of the 6D model are those of LM, but below the subcritical Hopf bifurcation in LM associated with the chaotic attractor the 'steady cell' Lorenz c.p.'s (critical points) become unstable by a supercritical steady bifurcation out of the Lorenz manifold -- 4 new stable c.p.'s appear. At still higher R these undergo supercritical Hopf bifurcations leading to limit cycles. From here up to over 15 Rc, we have numerically found limit cycle attractors in much of the range, but also a number of chaotic gaps. Approach to these gaps is often, but not always, through a sequence of period doublings. But the chaotic regions seem also to be associated with the occurrence, at special values of R, of heteroclinic orbits joining the unstable Lorenz c.p.'s (which have some stable complex eigenvalues to the 'conduction' saddle point, or to one another; also sometimes homoclinic orbits. These heteroclinic orbits are accompanied by others joining the c.p.'s in the opposite order, so these "heteroclinic pairs" are somewhat like homoclinic orbits. When a certain eigenvalue condition is satisfied, Silnikov's theorem on the existence of a horsehsoe map at a homoclinic orbit can be extended to the doubly heteroclinic case (at least in 3D). This indicates the existence of a chaotic set but not necessarily a chaotic attractor, and our double heteroclinics do sometimes occur at values of R where there are limit cycles. However, these are near the chaotic gaps, and finding these double heteroclinic orbits seems to be a valuable tool in seeking chaotic attractors.

THE RESPONSE OF A TWO-LEVEL OCEAN TO THERMAL FORCING

Michael K. Davey

The N. E. Atlantic is relatively warm (compared to a zonal average), and this warm water has a moderating influence on the climate of W. Europe. Several processes (such as N. Atlantic currents, deep convection in Norwegian/Greenland Sea, eastern boundary currents) probably combine to maintain this state. Various numerical and analytic methods are being used by the ocean modelling group at Cambridge University to investigate several mechanisms -- one is described in this seminar.

The surface heat flow Q depends on the difference between the effective atmospheric temperature T_A and ocean surface temperature T_s, i.e., $Q = Q_g(T_s - T_A)$ (Haney, 1971); $Q_g \approx 30\ Wm^{-2}\ ^oC^{-1}$). This thermal input is spread over some depth, H_M. For this two-level model only cooling ($T_A < T_S$) is considered, so upper level temperature T_1 is the same as T_s, and heat is spread over upper layer depth H_1. This gives a thermal forcing term $F_1 = (T_A - T_1)/\tau$, where $\tau = H_m \rho c_w / Q_g$ is an equilibration time (ρ = reference density, c_w = specific heat of water). For long time scales a similar benthic forcing term $F_2 = (T_B - T_2)/\tau$ is also included to simulate high latitude processes maintaining the basic stratification. T_A and T_B are prescribed, as functions of latitude only.

With no surface wind stress or bottom friction, the flow is purely baroclinic. In the absence of boundaries the meridional temperature gradient (decreasing poleward) establishes a geostrophic zonal flow, on time scale τ, eastward at the upper level, westward below.

When eastern and western boundaries are added, the meridional pressure gradient cannot be geostrophically balanced at the coasts, and Kelvin waves are generated. These rapidly ($\approx$ 200 km/day) pass information along the coasts, creating warm NE and cool SW regions (N. hemisphere), with northward surface currents, near the boundaries.

These anomalies are then spread slowly offshore by Rossby waves, more effectively from the east, at speed $c \approx 1$ km/day. Because the thermal driving depends on the ocean temperature, the eastern Rossby waves decay offshore on scale $c\tau$. In this way a broad warm NE region is generated, almost steady after time τ (there is further slow development by slow, lower-level effects), with an associated weaker northward (upper level) current.

The model is simple enough to be solved analytically in many cases. For the eastern region spin-up by long Rossby waves, analytic solutions can be found with nonlinear advection terms retained in the thermal balance. Steady nonlinear solutions can also be conveniently obtained by solving the problem latitude-by-latitude.

Kelvin waves in this model are very effective at flattening longshore pressure gradients, and perhaps have an unduly strong influence. Further investigation of this is underway. Addition of wind-stress is planned, though numerical methods will probably be needed to obtain solutions.

REFERENCE

Haney, R. L. 1971. Surface thermal boundary conditions for ocean circulation models. J. Phys. Ocean., 1, 241-248.

ON THE 2D TRANSPORT OF STRATOSPHERIC TRACERS

K. K. Tung

A zonally averaged model of stratospheric tracer transport is formulated in isentropic coordinates. There are some conceptual and computational advantages, as well as some disadvantages, in adopting the potential temperature, instead of pressure, as the vertical coordinate. The main disadvantage is the fact that the "density" (mass per unit coordinate volume) in isentropic coordinates is no longer a constant as in the pressure coordinate system under the hydrostatic approximation. However, it can be shown that this density effect is approximately negligible in the calculation of the mean diabatic circulation and the eddy advective transports. What is gained by adopting the new formulation is a conceptually simpler picture of the interplay of diabatic and adiabatic processes in the transport of tracers. Mean diabatic heating (cooling) forces a direct rising (descending) mean mass flow. Along the streamlines of this mean mass circulation tracers are advected in the mean. These surfaces slope downward and poleward in the lower stratosphere. In addition to advection, tracers are also dispersed from their mean path by transient adiabatic processes in a direction parallel to the local isentropic surface. As a result, the lines of mean constant tracer mass mixing ratio slope less steeply than the mean streamlines but more steeply than the isentropic surfaces. The effect of eddy transport on chemically reacting minor constituent gases is also discussed.

THE ROLE OF DAMPED EQUATORIAL WAVES IN THE OCEANIC RESPONSE TO WINDS

Toshio Yamagata

We study the roles of damped equatorial waves in the steady oceanic response to winds by use of both analytical and numerical methods. In particular, the sensitivity of equatorial currents to mixing processes is discussed by using the model which allows the mixing of heat and/or momentum. In the inviscid model the flows set up by winds of zero curl are eliminated by the long Rossby waves emanating from the eastern wall and the Kelvin wave (if excited) emanating from the western wall. The inclusion of mixing processes may lead to the entirely different steady state associated with non-Sverdrupian flows. It is shown that the mixing of heat is essential to maintain these flows. This is because the mixing of heat affects the attenuation of divergent waves far more than does the mixing of momentum. Results from the present study suggest that the mixing processes (especially, of heat) significantly affect the adjustment processes in the equatorial ocean.

CALCULATING THE REFERENCE LEVEL FROM THE BERNOULLI FUNCTION CONSERVATION

Pierre Welander

Assuming ideal, steady and strict-geostrophic flow in the oceans the potential vorticity $P = f\rho_z$ can be estimated from density data along a closed hydrographic section. Since P is conserved along streamlines lying in isopycnal surfaces, an analysis of P(s) along an isopycnal boundary line (s measuring horizontal distance along the section) can serve to determine connecting boundary points for the streamline field in such a surface. The connecting points must have the same P-values, but the analysis may not always lead to a unique connection (some ambiguities may be removed when the density is varied, under a smoothness condition).

The Bernoulli function $B = p + g\rho z$ (no square velocity term in the geostrophic approximation) is also conserved along streamlines, and the connecting streamline points should therefore also have the same B-values. Plotting B(s) against P(s), we get a line which is covered twice as we let s vary from zero to s_o (go once around the section); the same point P,B is met both at the entrance and the exit point of a streamline. We do not know B, but can estimate a baroclinic part of B, say $B^* = -g_o\int^z \rho\, dz + g\rho z$, where z=0 is a level surface. The complete function is $B \equiv B^* + p_o(s)$, where $p_o(s)$ is the pressure along the perimeter at z=0, the same function at all isopycnals. If we plot B*(s) against P(s), the entrance and exit points of a streamline generally falls at different points $P,B^{*'}$ and P,B^* in the P-B*-plane: the line in the P-B-plane has "opened" and is now a curve which encloses a certain area. The function B and therefore $p_o(s)$ can be reconstructed from the curve $B^*(P)$ by collapsing this back to a line which encloses no area. This can be done in many ways for a single curve. However, if we consider many isopycnals this is not the case, since B* must always be adjusted by use of the same function $p_o(s)$. Actually, the problem generally is an overdetermined one.

As an example, an exact analytical solution of the error integral type (Welander, 1971) was used to generate the density field and associated fields of P and B* along a hypothetical rectangular section between 10°N and 20°N, 10°E and 10°W, as shown in Figs. 1a and 1b (the section goes counterclockwise from the NE corner, s runs from zero to 40. The normal velocity is zero at the top (z=0) and the bottom, which has a maximum depth of 800 m. The corresponding curves $B^*(P)$ are drawn for a number of isopycnals in Fig. 2 (full-drawn curves). The lines s = constant are also shown (dashed curves).

The surface $B^*(P,\rho)$ generated in the P-ρ-B*- space must now be collapsed by translating every s-isoline without deformation along the B*-axis, until the volume enclosed by the surface is zero. This can only be done in one way in the present case (a uniform translation of all the isolines can always be added, corresponding to a certain constant pressure change at all points).

It is convenient to minimize the moment $M = \iint (B'-B)^2 dP d\rho$; when this is zero the volume is also zero. If real data are used the zero value cannot generally be reached, but we get the best approximation in a least-square sense. We use discrete values $B_{i,j}$ at density values ρ_i and station coordinates s_j.

Writing $B_{i,j} = B^*_{i,j} + p_j$, the moment is expressed as a quadratic form for the unknown p_j-values; the extremum problem is obviously reduced to solving a system of linear equations for the p_j's. Using only eight stations and three isopycnals the following values for the p_j's (in cm of water) were calculated (p_1 was set = 0, for convenience):

j=2	3	4	5	6	7	8
0.728	-1.4670	-1.034	-0.612	0.119	0.848	0.425
(-0.730)	(-1.459)	(-1.033)	(-0.612)	(0.120)	(0.848)	(0.427)

The exact analytical values are given in the second line. The agreement is thus very good, the example given is, however, a particularly favorable one since the s-isolines are plane curves and the collapsed surface a plane.

Relations of this method to so-called "inverse methods", which deal with the same problem using mass conservation and a different extremum condition, or the "β-spiral methods" which assume mass and vorticity conservation in a local region, remain to be explored.

REFERENCE

Welander, P. 1971. Some exact solutions to the equations describing an ideal fluid thermocline. J. Mar. Res. 29, 60-68.

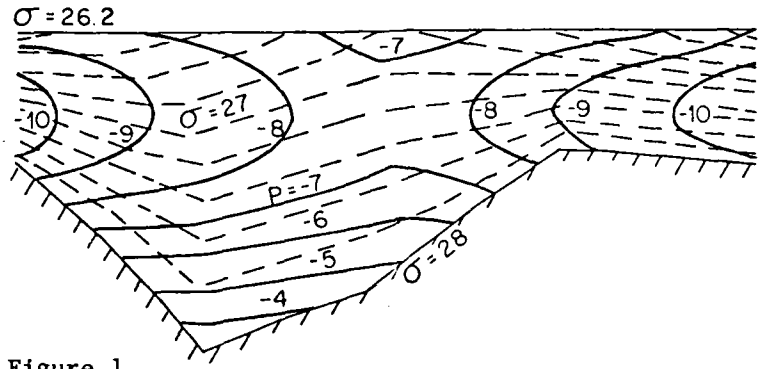

Figure 1
case a).

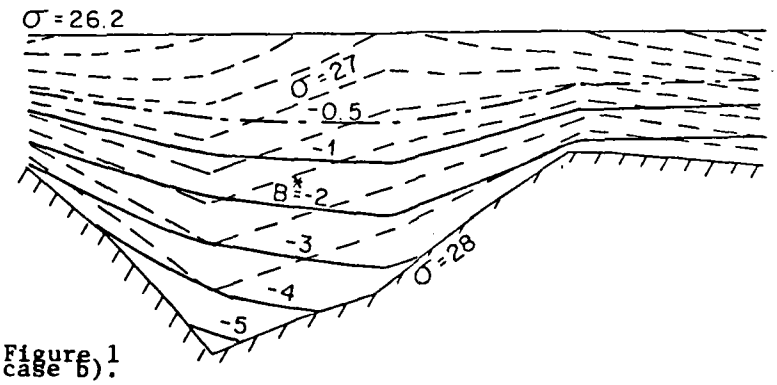

Figure 1
case b).

Fig.1. Isopycnals(dashed), isolines for potential vorticity (full drawn, case a), and isolines for the baroclinic Bernoulli function (full drawn, case b), for the analytical example described in the text.

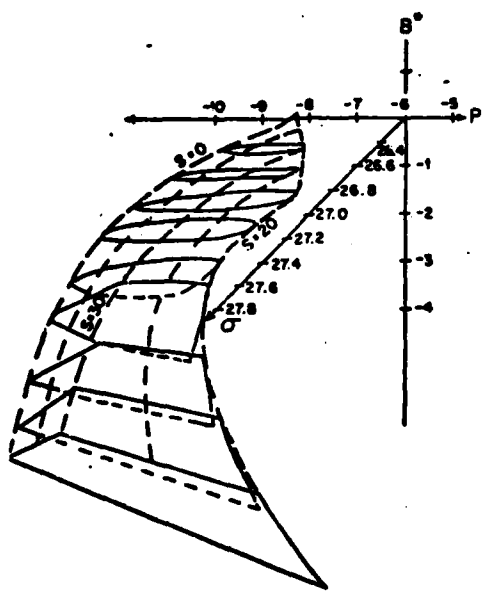

Fig.2. The surface obtained by plotting the baroclinic Bernoulli function against the potential vorticity and density, for the analytical example described in the text.The isolines for s are dashed.

A WAVE IN ANTI-CYCLONIC SHEAR

Roger Hughes

A new type of first baroclinic mode wave which propagates on an anti-cyclonic vorticity field is identified. It is of the vorticity class of waves which contains Rossby waves amongst others. This anti-cyclonic shear wave is produced by pressure variations distorting the vertical stratification in such a manner that the associated vortex stretching generates the velocity variation required for Bernoulli compatability with the initial pressure variation. The wave travels at a speed characteristic of particles within the undisturbed shear flow and is a low frequency and low wavenumber wave.

A PARAMETERIZATION OF VERTICAL DIFFUSION

Roger Hughes

It is supposed that the vertical diffusion within the main thermocline of the ocean is governed by a concentration derivative of unspecified order. Agreement between macro and micro structure determinations of the eddy diffusivity is obtained by an appropriate choice of the order of the derivative. The derivative is found to be fractional and determined according to Liouville. The Green's function for diffusion in an unbounded ocean is determined and used to predict diffusive fronts and plateau development in approximate agreement with observations. The parameterization is used in a model of the annual thermal cycle within the main thermocline. This is used to explain the observed large depth of penetration of the cycle. Work on the above was done with Dr. David Anderson (Oxford).

PROPERTY TRANSPORT AND LAGRANGIAN PARTICLE STATISTICS

Russ Davis

Statistical descriptions of the evolution of the concentration, θ, of a scalar property can be derived from statistics of the motion of Lagrangian particles. The ensemble mean concentration from prescribed initial and source conditions is determined by single-particle statistics, such as the Lagrangian mean velocity $\bar{V}(t,\underline{r}_o) = \frac{\partial}{\partial t}\langle \underline{r}(t,\underline{r}_o)\rangle$ and displacement variance $\langle |\underline{r}^1(t,\underline{r}_o)-\underline{r}_o|^2\rangle$. Here $\underline{r}$ is particle position and $\underline{r}_o$ is position at time t = o. Dispersion of the mean field is the sum of the dispersion of the centroids of the various fields averaged plus a dispersion of each field about its own centroid (relative dispersion). The statistics of relative dispersion are determined by multi-particle statistics. The mean square dimension $\int d\underline{x}\, \langle |\underline{x}-\underline{x}_c|^2\theta\rangle$, where $\underline{x}_c$ is the centroid, is determined by the mean square separation $\langle \underline{s}(t,\underline{s}_o)|^2\rangle = \langle |\underline{r}(t,\underline{r}_o+\underline{s}_o)-\underline{r}(t,\underline{r}_o)|^2\rangle$.

Methods for predicting from low order Eulerian statistics the mean and mean square particle velocity, single particle dispersion, and particle-pair dispersion are discussed and compared with simulations of particles in joint-normally distributed velocity fields. Mean and mean square particle velocity depend on correlation of particle density and the flow in compressible flow or

when particles are deployed on surfaces in which the flow is divergent. These statistics can be estimated using a statistically optimized approximate solution of $\partial_t + \underline{u}.\nabla) \ln \rho = -\nabla.\underline{u}$. When particle velocity statistics are stationary, single particle dispersion depends on the frequency spectrum of particle velocity at zero frequency. This Lagrangian velocity spectrum is predicted by a combination of Corrsin's conjecture (1960) and the assumption of joint-normally distributed particle displacement. Particle migration and dispersion in velocity fields with spatially varying statistics is discussed. Mean-square particle separation can be predicted by an elaboration of the single-particle method. In general the two-particle diffusivity is not a function of the separation or mean square separation alone.

REFERENCE

Corrsin, S., 1960. Progress report on some turbulent diffusion research in Proc. Symp. on Atmospheric Diffusion and Air Pollution. Academic Press.

MONOPOLES OVER VARIABLE RELIEF AND BOUNDARY FORCING AS A PRODUCTION MECHANISM

Paola M. Rizzoli

The word "monopole" recently has been introduced into the literature to designate isolated coherent structures, the main features of which are that i) they are spatially localized; ii) are locally the energetically dominant fluid structure; iii) are persistent; iv) have recirculating flow. For these isolated vortices Gulf Stream rings, both warm- and cold-core, constitute the typical example.

We choose as model the equivalent barotropic, quasi-geostrophic potential vorticity equation on the β-plane over variable topography:

$$\nabla^2\psi_t - \frac{1}{R^2}\psi_t + J\left(\psi, \nabla^2\psi + \beta y + h(y)\right) = 0 \quad (1)$$

where $R = \sqrt{gH}/f_0$ is the deformation radius. Stern (1975) has shown that the necessary condition for the existence of a steady, isolated structure on the β-plane is

$$\iint_{\text{total area}} \psi \, da = 0 \quad (2)$$

from which the dipole nature of every possible solution follows.

Recently, Flierl, Stern and Whitehead (1982) have extended the above theorem to isolated, slowly varying structures in stratified fluids with arbitrary background flow but no net surface or bottom torques. They show that (2) is generalized to:

$$\left(\frac{c}{R^2} + \beta\right) \iint \psi \, da = 0 \quad (3)$$

giving i) $\iint \psi da = 0$ modons as solutions; ii) $c = -\beta R^2$ for slowly varying, propagating monopoles. The latter, however, are not smoothly behaved in the far field. The model equation (1) allows for steadily propagating, monopole solutions with net angular momentum, which are well behaved everywhere. The model equation for them is:

$$\nabla^2\psi + h(y) = h\left(\frac{\psi}{c} + y\right) + \left(\frac{\beta}{c} + \frac{1}{R^2}\right)\psi \quad (4)$$

where $h = F(z)$ is the analytic functional expressing potential vorticity in terms of the stream function in the frame of reference translating with the monopole.

We consider a weakly nonlinear topography, specifically $h(y) = \varepsilon/2\, y^2$ if ε is the small dimensionless parameter of the system. Two parameter ranges are explored.

a) Narrow channel

$L_2 > L_1 > R$ with L_1 = channel width

L_2 = wavelength in along-channel direction

Two dimensionless aspect ratios exist

$$\delta_1^2 = L_1^2/L_2^2 \quad ; \quad \delta^2 = R^2/L_1^2$$

and $\varepsilon = \delta^4$. The Rossby number is $R_o = U/\beta L_1^2 = \delta_1^2 \ll 1$. Steady free solutions are nonlinear radiation, namely nonlinear Rossby solitary waves asymmetric in along-channel direction. These waves are weak and do not possess closed recirculation regions.

b) $L_2 = L_1 > R$

Then the model (4) admits as solutions radially symmetric monopoles, valid in a large channel (away from $y \to \pm\infty$). These monopoles have high intensity and close recirculation regions. Case (b) can be considered as the limit of case (a) when $\delta_1^2 = R_o \to 1$.

We want to pose the problem of boundary forced nonlinear radiation which, as $\delta_1^2 = R_o \to 1$, may approach a structure with closed recirculation regions in a finite domain. The problem of boundary forced linear mesoscale radiation was considered by Flierl et al. (1975) and Pedlosky (1977) into the semi-infinite β -plane; and by Harrison and Robinson (1979) into finite domains. All these models were, however, linear.

Instead, we choose to approach the boundary forced problem posed by model (1) in its fully nonlinear form, precisely in the two above-considered parameter ranges. We choose to approach the problem in its time-dependent form. This means solving the initial-value problem posed by the original model and finding evolution equations which approximate it in the two mentioned parameter ranges both for i) the free wave case, getting the evolution equation for the nonlinear solitary radiation in the zonal channel, ii) the boundary forced case. For the weak amplitude nonlinear radiation, solution of i) leads to a Korteweg-deVries (KdV) evolution equation for the free radiation in the channel; the solution of ii) leads to two KdV evolution equations in the zero and first-order streamfunctions ψ_0 and ψ_1 , coupled through the boundary forcing conditions. These coupled KdV equations are then solved numerically in a set of numerical experiments. For these, the boundary condition is chosen so as to force one single mode of the nonlinear free wave solution allowed by the model. $\delta_1^2 = R_o$ is successively increased to 1 going to the limit of symmetrical, high-amplitude nonlinear waves with closed recirculation regions. These preliminary numerical experiments strongly suggest the possibility of shedding highly nonlinear mesoscale radiation from a northern boundary.

REFERENCES

Flierl, G.R., V. Kamenkovich and A.R. Robinson, 1975. "Gulf Stream meandering and Gulf Stream Rings--Eddy production mechanisms." Report of the MODE-1 Dynamics Group.

Flierl, G.R., M.E. Stern and J. Whitehead, 1982. "On the physical significance of modons." Unpublished manuscript.

Harrison, D.E. and A.R. Robinson, 1979. "Boundary forced planetary waves: a simple model mid-ocean response to strong current variability." J. Phys. Oceanogr., (9, 5, 919-929.

Pedlosky, J., 1977. "On the radiation of mesoscale energy in the mid-ocean." Deep-Sea Res., 24, 591-600.

Stern, M.E., 1975. "Minimal properties of planetary eddies." J. of Mar. Res., 33, 1, 1-13.

THE COASTAL ECOSYSTEM OF THE NORTHERN ADRIATIC SEA

Paola M. Rizzoli

The northern half of the Adriatic Sea is constituted by the continental shelf, which reaches very shallow depths ($\sim$20 m and less) in the northern-most extremity. In particular, the nearcoastal region adjacent to the Italian coastline forms a shallow strip, with isobaths running parallel to the coast and a topography gently increasing towards the interior of the basin. In the region immediately south of the Po River delta--the major source of fresh water input into the Adriatic--important eutrophization phenomena have recently occurred in summertime, with the first emergency of eutrophized "red sea" in the late summer of 1976. The "red sea" is constituted by important algae blooms of dynoflagellata which last for several weeks and affect long strips of water, extending from about 200 m to 3 km from the coast and for several miles in alongshore direction. The controversial question thus arose whether these eutrophization phenomena were caused by anomalous inputs of nutrients, in particular phosphates, injected into the sea by the local industrial waste discharges; or whether instead the nutrient source was due to the Po River waters which, outflowing from the delta mouths, are carried southward along the Italian coastline in the general cyclonic gyre characterizing the Adriatic yearly average circulation. The general question to be answered was therefore: where does the Po River water go? To answer this question the near coastal circulation had to be hydrodynamically studied as part of the general circulation of the Adriatic Sea. This last constitutes on average a cyclonic gyre, with a broad inflow of Ionian and southern Adriatic warm salty water along the Yugoslavian coastline and a narrower, more intense return flow along the Italian one. In the return southward flowing current are embodied the important fresh water inputs of the Adriatic, concentrated in the northwestern side, of which the Po is the dominant one. In wintertime, the interior of the Northern basin is typically vertically well mixed to the bottom; the temperature, salinity, density fields are thus vertically homogeneous. In summertime, on the contrary, a strong stratification is usually present, with shallow pycnoclines varying from 3 to 10 m depth and disappearing only during occasional, short episodes of northeast intense wind. A multilevel hydrodynamic model was

constructed to study the transient Adriatic circulation, which in the near-coastal region south of the Po delta can be approximated by a two-level system. The model numerically integrates the horizontal momentum equation in linearized form, integrated over each level; the continuity equation integrated over the whole depth; advection-diffusion equations for the temperature and salinity; an equation of state relating density to temperature and salinity closes the system. The pressure is hydrostatic and is expressed in terms of a barotropic component, depending upon the surface pressure and sea level, and a baroclinic component, depending upon the interior density field.

The model needs as inputs: i) a realistic bathymetry, ii) the wind stress field at the sea surface, computed from real data, given as surface boundary condition to the horizontal velocity shears evaluated at the sea surface; iii) the air-sea interface evaporation, latent and sensible heat fluxes as well as precipitation when available, given as surface boundary conditions to the temperature and salinity fluxes; iv) the fresh water river inputs at the coast given as horizontal boundary conditions and expressed in terms of daily averages of sea level, v) the sea level distribution at the southern open mouth of the integration basin, evaluated from the harmonic constants of the coastal stations at the same latitude. The model predicts the space-time evolution of i) the sea level; ii) the total horizontal transports integrated over the whole local depth; iii) the horizontal transports in each horizontal layer;iv) the vertical velocity at each level rigid interface; v) the horizontal distribution of temperature, salinity, density in each layer. The model was run in a basic numerical experiment, with real input data, from September 15, 1978, to October 16, 1978, taken as the typical summer test case. The numerical grid had a size of 7.5 km and the resolution was increased to 2.5 km in the near-coastal strip south of the Po delta. Model outputs were recorded every 2 hours and subsequently averaged over 24 hours to filter the tidal signal. The model was sampled at various grid points, from the interior region towards the coastline, at various latitudes south of the Po delta, using salinity as a "tracer" of the fresh Po River water. The general conclusions which can be drawn from the basic numerical experiment are the following. The "signal" of the Po River water, represented by the salinity field, is lost when progressing towards the coastline, even during intense episodes of northeast wind, when significant advective effects are present in the surface layer of 10 m thickness. The nearcoastal strip, of about 10 km width, is almost stagnant. The total transports are essentially zero. Not only is there no sigificant southward transport; in the whole nearcoastal region, of 30-35 km width, the total transport in alongshore direction is most often directed northward, contrary to what occurs in wintertime. This last situation--northward alongshore transport in the nearcoastal region--seems to constitute the average late summer situation, in the absence of a significant wind field and consequent wind-driven currents in the surface layer.

Dynamical considerations (Csanady, 1978; Hendershott & Rizzolli, 1976; Beardsley & Winant, 1979; P. Tung-Shaw, 1981) suggest that the nearcoastal circulation is driven by the bottom torque, which dominates the dynamical balance of forces as soon as an alongshore density gradient is present. This alongshore density gradient determines the direction of the vertically integrated flow in alongshore direction. In wintertime, with a dense water pool concentrated in the interior of the northern basin, density decreases going southward in the nearcoastal strip; the consequent transport is southward flowing. In summer, the density gradient in the nearcoastal region reverses direction, density actually increasing going southward; this produces a recirculation with alongshore current flowing northward. Current-records taken in time-series fashion for 2 years and preliminary experimental results seem to confirm the above dynamical considerations.

REFERENCES

Beardsley, R.C. and C.D. Winant, 1979. "On the mean circulation in the mid-Atlantic Bight." J. Phys. Oceanogr., 9, 3, 612-619.

Csanady, G.T., 1978. "The arrested topographic wave." J. Phys. Oceanogr., 8, 47-62.

Hendershott, M.C. and P. Rizzoli, 1976. "The winter circulation of the Adriatic Sea." Deep-Sea Res., 23, 353-370.

P. Tung-Shaw, 1981. "The dynamics of mean circulation on the continental shelf." WHOI-MIT Ph.D. thesis.

DISPERSAL BY RANDOMLY VARYING CURRENTS

Gabriel T. Csanady

The long-term oceanic dispersal of persistent contaminants may be approached as a problem in turbulent diffusion, with tidal, wind-driven, and other variable currents relegated to turbulence. The mean advection velocity in this problem is typically small compared to the rms fluctuation. Therefore, close to a continuous, concentrated source puffs of contaminant of all "ages" are present and have significant effects. "Old" puffs, i.e. those released a long time previously, give rise to a background concentration field. "Young" puffs affect the local contaminant concentration according to the probability of their presence, quantified by the "visitation frequency".

The behavior of young puffs is governed by variable advection and may be described approximately in terms of probability distributions obtainable from current meter data. The visitation frequency can be calculated from the distribution of escape probability density, a Lagrangian equivalent of flux. A long-term effect of variable advection is the distribution of the contaminant over an "extended" source, which serves as a starting point for the random wall of old puffs. The conventional approach of using the diffusion equation to describe this random walk is therefore valid as a description of the near-source background concentration, provided that the extended source is used in place of the physical source.

SYMPOSIUM ON BIOLOGICAL AND CHEMICAL TRACERS IN THE OCEAN

LAGRANGIAN TRACER MICRO-SYMPOSIUM PERCHED ON QUASI-LAGRANGIAN SOFAR FLOATS

Row 1: Veronis, Broecker, Kolmes, Haynes, Shepherd.

Row 2: Jenkins, Davey, Silcox, Sommer, Wroblewski, Riser, Livingston, Mariano, Smethie, Howard.

Row 3: Martinson, Rossby, [illegible], Penz, Booth, Kelly, Druttel.

Row 4: Day, Ketter, [illegible], [illegible], Olson, Holloway, Fiadeiro.

GYRES AND TRACERS

Peter B. Rhines

Recent theoretical models of the wind-driven circulation point to the very different ways in which tracers entering the sea at its surface can eventually spread throughout the interior. The upper km or so is strongly driven by the divergent mixed/Ekman layer, which creates Sverdrup circulation plus western boundary currents and intense recirculation, particularly in the western regions.

In the subtropical gyres the Ekman fluid is pumped downward and carries with it tracers from the surface. This conjures up a picture of the 'meriodional' (y-z) ocean, with fluid entering and exiting at the boundaries, and flowing up, down, north and south. This picture is deceptive however; unless we integrate the flow field east to west, we must take account of the fluid flowing zonally into or out of the section.

The v-velocity (north-south) that would be required by continuity of mass, alone, in this section is

$$v_E \sim w\ L/D$$

where w is the wind-induced Ekman velocity. L is the north-south scale of the gyre and D is its depth scale. But the Sverdrup relation gives us another estimate of v.

$$v_S \sim w\ f/\beta\ D.$$

The ratio of these two estimates, Rc, is just

$$Rc = f/\beta\ L \sim a/L,$$

a being the Earth's radius. Rc, which may be called the recirculation index, is moderately large, say 2 to 5, for the major subtropical oceans. This means that to this same degree the Eulerian mean circulation involves a large degree of recirculation (fig. 1). The directly injected Ekman fluid squeezes into a narrow current, for it must accelerate in the meridional sense from a velocity vE to a velocity vS. To the level of scale analysis, this band occupies a fraction 1/(1+Rc) of the east-west domain. It is the strong potential vorticity constraint that forces this uneven response, physically analogous to the fast spin of a top due to much smaller down-push on the screw-threaded spindle.

This extensive recirculation manifestly exists, and it forms the core of a theory of the circulation by Rhines and Young (1982), in which lateral eddy flux of potential vorticity, q, creates a gyre structure in which the mean geostrophic contours (q = const. on constant potential density (-) surfaces) bend into closed or nearly closed loops paralleling the mean streamlines. In some fraction of the gyre the fluid is sufficiently isolated from direct mechanical or thermal forcing (on the particular σ_θ- surface in question) that the flow 'spins out' its potential vorticity to the point where it is uniform.

A recent analysis of GEOSECS tritium data, reported elsewhere in this volume by Sarmiento (page 177), is relevant to the competition between directly

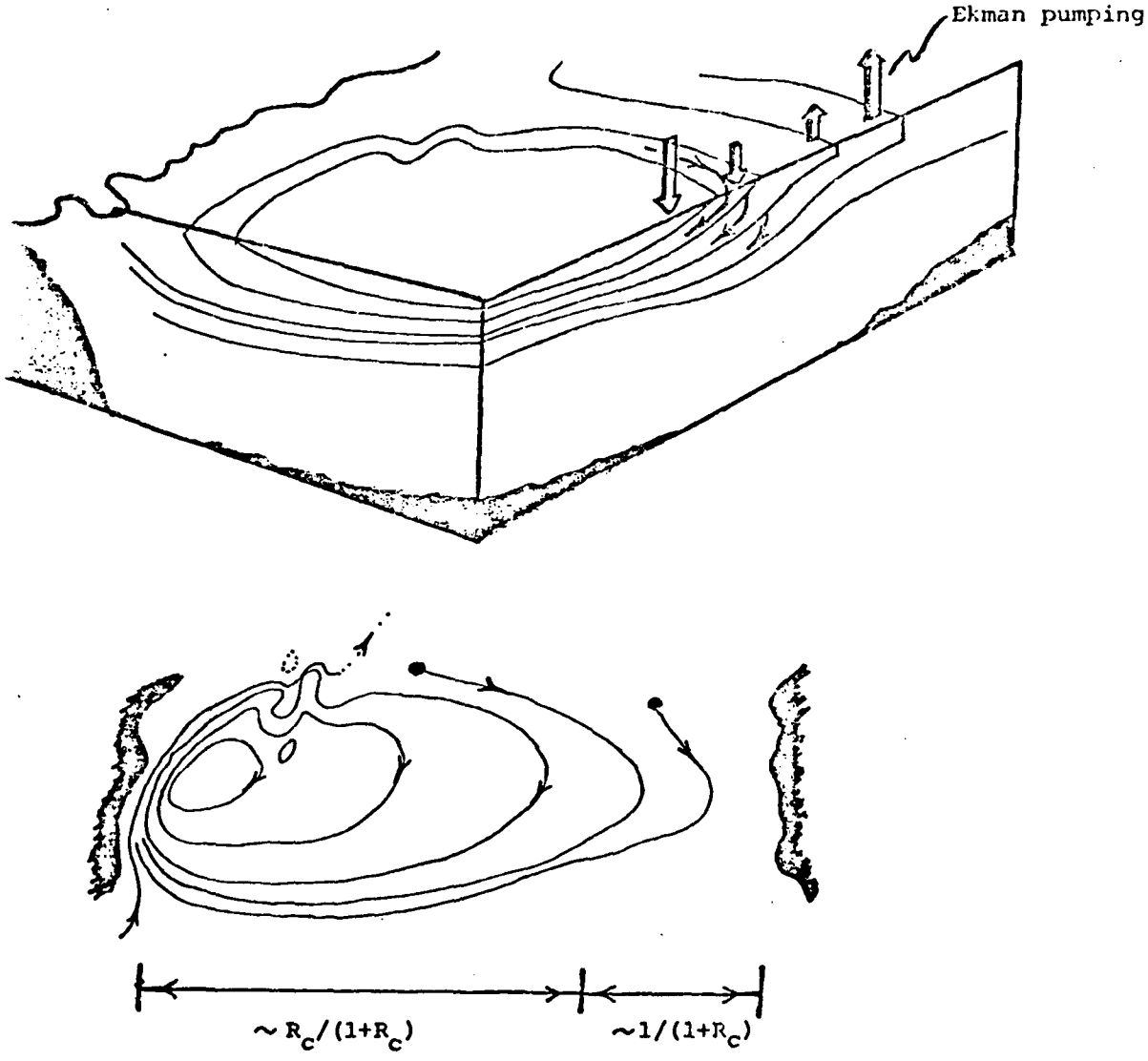

Figure 1: Schematic diagram of the pattern of injection of surface waters downward into the wind gyre. The inflowing water is squeezed into a narrow band (a fraction $\sim(1 + Rc)^{-1}$ of width of ocean). The remainder being occupied by Eulerian recirculation. In the Pacific most isopycnals of the wind-gyre outcrop north of the zero-wind-curl-line, isolating them completely from this simple manner of injection.

injected and recirculating flow. He finds that there is about five times as much tritium in the North Atlantic subtropical gyre (between σ_θ = 26.2 and 27.4) as there would be if it were simply carried down by Ekman pumping. The significance of this overburden of tritium is that it must enter by communication with tritium-rich water to the north: perhaps by cross-isopycnal mixing at the northern edge of the gyre.

The 'recirculation index' of the gyre, which is thus quite large, refers to the Eulerian-mean streamlines while the Lagrangian circulation involves more rapid escape and entry into the gyre via mixing.

These remarks apply to a different degree in different oceans. The down-pumping region in the North Atlantic, which is delineated by the line of vanishing wind-stress curl, extends quite far north to almost 55° N near Britain. Most of the outcrop lines at the sea-surface corresponding to wind-gyre σ_θ surfaces, thus lie in the region of down-pumping. In the North Pacific, however, the zero-curl line runs more east and west near 40° N. (Is this a cause or an effect of the ocean circulation?) This means that most of the wind-gyre σ_θ surfaces reach the sea surface farther north, in the subarctic gyre where the Ekman velocity is upward. Despite the lack of direct exposure to surface properties, the North Pacific succeeds in ventilating to great depth; tritium is seen on σ_θ = 26.0, which outcrops in the subarctic gyre, and even on deeper surfaces which outcrop only in the South Pacific, as Fine, Reid, and Ostland have shown us. The combined advection and mixing by the gyre recirculation is apparently dominant.

The South Pacific provides yet another setting. As Haynes shows elsewhere in this volume (page 262), the Circumpolar Current and the subtropical wind gyre are capable of interacting in a strong fashion; the CPC is deflected by the gyre (as if it were 'topography') and the gyre is deepened by the CPC. This is an example of the way in which two distinct branches of the circulation collaborate to determine the flow paths (the geostrophic contours, $f\,\partial\sigma_\theta/\partial z$ = const. on σ_θ surfaces). Ventilation by the massive vertical scope of the surfaces in this region must be significant.

REFERENCES

Fine, R.A., J.L. Reid and H.G. Ostland, 1981. Circulation of tritium in the Pacific Ocean. Jour. Phys. Oceanogr., 11, 3-14.

Rhines, P.B. and W.R. Young, 1982. Homogenization of potential vorticity in planetary gyres. J. Fluid Mech. Sept.

TRACING TRANSIENTS

William J. Jenkins

The penetration of bomb-produced tritium (half-life 12.5 y) into the oceans has provided us with valuable information about decade timescale transport and mixing. The stable, inert daughter produce ^3He extends this sensitivity down to timescales of the order of a few months and adds a unique boundary condition: sensitivity to "backfluxing" to the atmosphere.

In line with the relative "insensitivity" of the bomb-tritium transient to shorter timescales, data shows the shallow North Atlantic subtropical gyre to be homogeneous in tritium (Fig. 1), due to the rapid recirculation (order few years) relative to the transient timescale (order 1-2 decades). The daughter ^3He, however, shows significant gradients. For example in the eastern subtropical Atlantic, ^3He results from a 1000 km scale triangle show both a component of mesoscale noise and a significant mean gradient which is consistent with geostrophically estimated (Beta Spiral) velocities.

A roughly meridional ^3He section in the Western Atlantic (Fig. 1 taken on the TTO cruise in 1981) between 40°N and 15°N shows the general features of the subtropical ^3He distribuiton: a lense of high ^3He, about 2.5 T.U., is seen at about 500 m (about the σ_θ = 26.85°/oo horizon) with ^3He poor water above and below. The paucity of ^3He in the deep water is a result of low tritium values - the tritium has not yet invaded the deeper gyre, although significant mid-depth incursion is evident to the north The upper waters, due to more effective "communication" with the atmosphere, also are poorer in ^3He. Gradients of ^3He on isopycnals in the shallow waters are consistent with order 1 cm s^{-1} meridional velocities.

An additional contribution of ^3He to our knowledge is its sensitivity to diffusion: i.e., back flux to the atmosphere. A simple pipe model calculation (one dimensional flow with along-stream diffusion) with the upstream end fed by surface water tritium yields a ^3H-^3He pattern which scales as the radiotracer Peclet Number

$$P_e = \frac{u^2}{K\lambda}$$

where u is the velocity, K is the along-stream turbulent diffusivity and λ is the tritium decay constant. All data available for the time frame 1979-1981 fall on a ^3H-^3He curve characterized by $P_e \sim 2$. For velocities of the order of 0.5 cm s^{-1} (geostrophically estimated near the ^3He maximum) this corresponds to a $K \sim 10^8 cm^2 s^{-1}$. However, two dimensional calculations based on tritium invasion of a gyre circulation with a boundary current

$$\psi = \psi_o e^{-\alpha(x+y)} \sin\left(\frac{\pi}{L}x\right) \sin\left(\frac{\pi}{L}y\right)$$

show that shear dispersion in the boundary current can lower the required diffusivity by almost an order of magnitude.

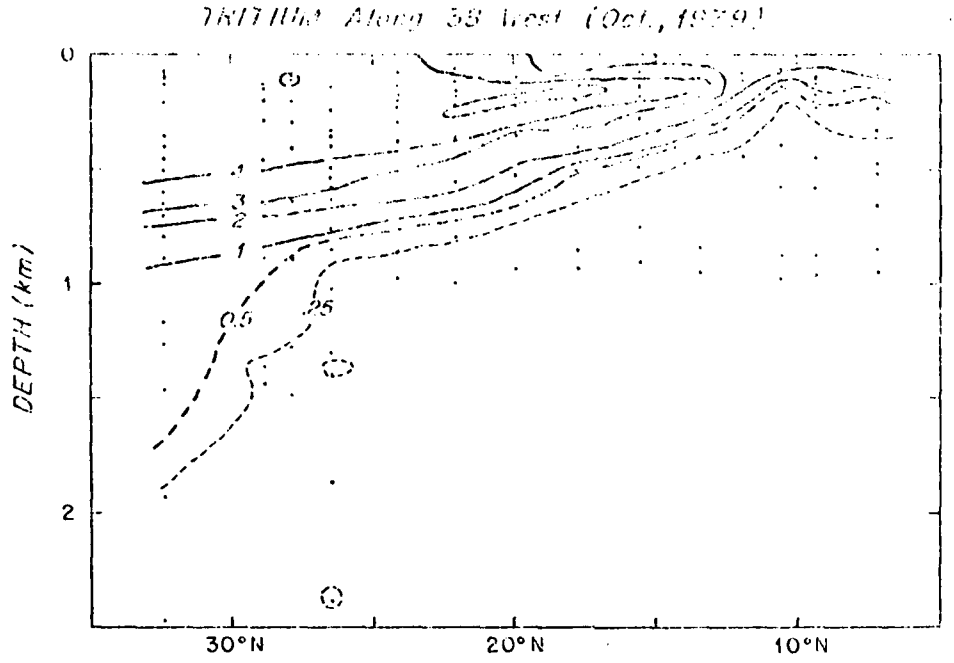

Fig. 1. A tritium section in the Atlantic.

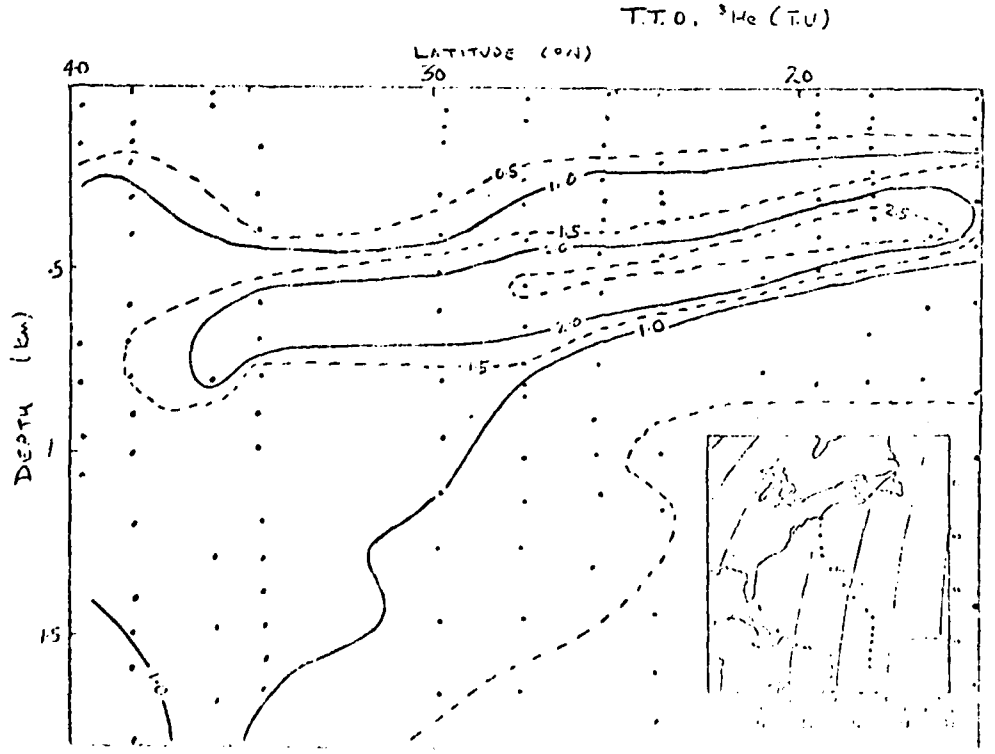

Fig. 2. A ^{3}He section in the Atlantic.

THE USE OF SATELLITE DERIVED SURFACE PROPERTIES TO STUDY OCEAN KINEMATICS AND DYNAMICS

Donald B. Olson

The use of satellite derived ocean properties distributions to follow surface fields is discussed. A consideration of the errors inherent in satellite derived sea surface temperature and chlorophyll suggests that it is extremely difficult to follow isolines in these variables in regions with small horizontal gradients. Even so two-dimensional wavenumber spectra for "clear" imagery from areas as diverse as the Gulf Stream-Slope Water region and the central Sargasso Sea provide similar spectra in terms of wavenumber fall-off to high wavenumbers. These observations suggest that satellites provide a reproducible picture of the spatial structure of the ocean surface which has somewhat universal properties. The possibility of deriving sea surface flow fields from time sequences of satellite images is described. The surface streamfunction field can be derived by inverting the conservation equation for the property as first suggested by Saunders (1973). This technique is tractable with satellite data if it is posed in a natural coordinate system tied to the mean isolines of the property. The problem leaves an undetermined constant of integration for each isoline which must be specified from some other data source. An alternate scheme for obtaining surface velocities involves the tracking of patches of fluid which are identified by anomalous temperature or chlorophyll signals. This Lagrangian method is similar to the cloud-motion technique used to derive winds in the atmosphere. A final approach to the problem of tracing surface features with satellite data involves consideration of the time history of the location of gradient maxima in either temperature or chlorophyll. The governing equation is then a frontogenesis equation rather than a conservation relation for the property. This process of picking out frontal features in images is the most common technique in satellite work. The problem of interpreting the results in some rational framework is only now being explored. An example of following the translation and shape of a Gulf Stream warm core ring from a sequence of satellite derived frontal positions is given.

REFERENCE

Saunders, P. M., 1973. Tracing surface flow with surface isotherms. Mem. Soc. Roy. Sci. de Liege, 6, 99-108.

GLOBAL THERMOHALINE CIRCULATION MODES

Claes G. H. Rooth

Global asymmetries are observed in oceanic heat flux and in salinity distributions. While the subtropical North Atlantic spans only about one-third of the zonal (longitudinal) range of the North Pacific, it appears to contribute at least as much to the global meridional heat flux. About one-half of this flux in the Atlantic is imported from the Southern Hemisphere, and is thought to be associated with a vigorous rate of deep water production in the subpolar regions of the North Atlantic. (A baroclinic circulation of $10^7 m^3/sec$ with a mean temperature differential of 15°C represents a heat flux of 0.6×10^{15} watts (.6 PW or Petawatts)). Coincident with this surprisingly large Atlantic heat flux is a substantial salinity anomaly, the North Pacific being fresh and the North Atlantic salty in its upper layers, relative to mean oceanic conditions.

A causal connection between the high salinity of the North Atlantic and its striking role as a deep water source is likely, as observed quite generally in the oceanographic literature. Salt effects on buoyancy are seen as dominant in view of the small thermal expansion coefficient for sea water at the temperatures in question, and also in consideration of the bound on downward fluctuations of temperature presented by the freezing point. The relative role of processes internal to the oceanic system and of external (atmospheric) interactions in establishing these salinity anomalies is far less clear in spite of a clear preference for the latter in the current literature.

I have recently (Rooth, 1982), referred to as CR hereafter, addressed these questions in the setting of some very crude hydraulic model systems. The main points of this study, which I will review here with some extensions, are the following:

1) An ocean like system, with equatorial symmetry in geometry as well as in forcing, is susceptible to asymmetric circulation instabilities when effects of heat exchange and fresh water transports through the atmosphere are both included as forcing mechanisms.

2) The fact that the oceanic salinity fields are governed by what is effectively a flux B.C. contributes, along with the nonlinear thermal expansion, substantially to the likelihood that this motion mode will occur.

3) If the intensity of the atmospheric fresh water flux is F, then the heat transport and the warming of the downwelling basin is for small F $o(F^{1/2})$ while the thermal effect in the upwelling basin is o(F), in the simple model. This induces significant asymmetries even with quite weak forcing.

The mechanism suggested here for the generation of large scale asymmetries in the global oceanic salinity distributions depends only on meridional water transport within the individual ocean basins and their hydrological catchment areas. If water vapor transport divergences between different catchment areas occur, then we have a forcing mechanism which will fix the circulation topology, while the process presented here and in CR should enhance the response.

Also, the heat advection into the salty basin may enhance evaporation asymmetries by providing a greater heat supply to sustain the associated latent heat flux. Without such extra heat supply, greater insolation would be required (e.g. by differences in mean cloudiness) in the basins with excess evaporation).

REFERENCES

Rooth, C., 1982. Hydrology and ocean circulation. Prog. Oceanog., 11, 131-149.

THE THERMOHALINE CIRCULATION SEEN BY TRACERS

Manuel Fiadeiro

The distribution of conservative and radio-conservative tracers reflects the mean ocean circulation and the processes of diffusion.

Here, it is shown characteristic distributions of salinity and C-14 generated by simple models of the deep ocean circulation in a basin like the Pacific. All the water is fed by the Antarctic Circumpolar Current.

The first model (3DM/I) was described by Fiadeiro and Craig (1978). It corresponds to the classical picture of Stommel and Arons (1960) deep ocean circulation. The upwelling velocity increases linearly from zero at the bottom (4 km) to a maximum value under the thermocline (1 km). The horizontal circulation is cyclonic and fed by western boundary currents.

The second model (3DM/II) was described by Fiadeiro (1982). The upwelling velocity attains a maximum at 3 km and decreases to the base of the thermocline. The idea is to simulate in a crude manner the change in dw/dz produced by the longitudinal gradient of density in the real ocean. The western boundary currents transport denser Antarctic water at the bottom and lighter Intermediate Water at the top. This creates a greater vertical density gradient in the west than in the east. The corresponding horizontal gradients should make dw/dz to increase in the lower layers and decrease in the upper layers.

It is shown that the qualitative features of the tracers are well reproduced with model 3DM/II when the upwelling velocity is 2.6 m/y at 3 km and 1 m/y at 1 km. The convergence of the Deep Water (over the Bottom Water) makes the western boundary current flow south and creates the typical vertical profiles of the southwest Pacific. The minimum values of C-14 occur at a depth of 2.5 km and spread south over the incoming Antarctic Bottom Water. Of the 14.5 Sv of Antarctic Water that flow into the Pacific only 3 Sv cross the thermocline, the rest returns to the Circumpolar. The residence time of the water in the Pacific basin is 700 years.

REFERENCES

Fiadeiro, M. and H. Craig, 1978. Three-dimensional modeling of tracers in the deep Pacific Ocean: I. Salinity and oxygen. J. Mar. Res., 36, 323-355.

AD-A122 864 1982 SUMMER STUDY PROGRAM IN GEOPHYSICAL FLUID DYNAMICS AT THE WOODS HOLE..(U) WOODS HOLE OCEANOGRAPHIC INSTITUTION MA G VERONIS ET AL. NOV 82 WHOI-82-45 3/4

UNCLASSIFIED N000014-82-G-0079 F/G 20/4 NL

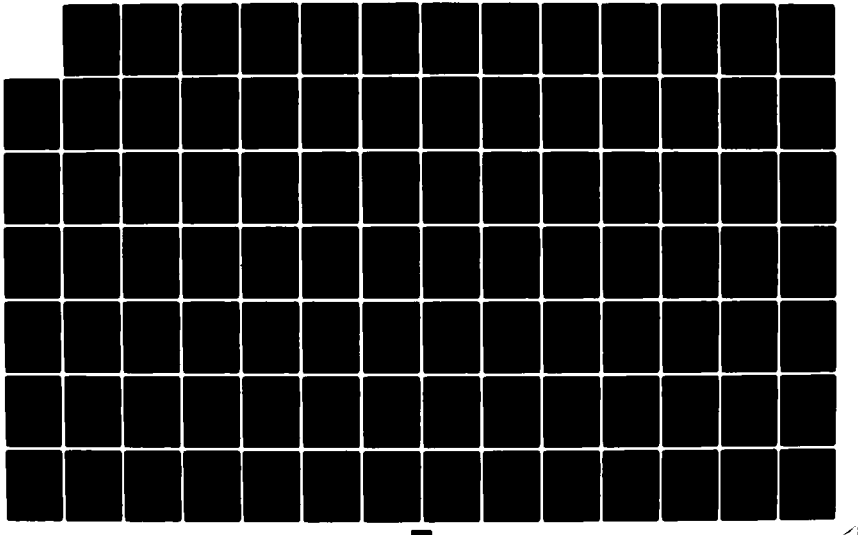

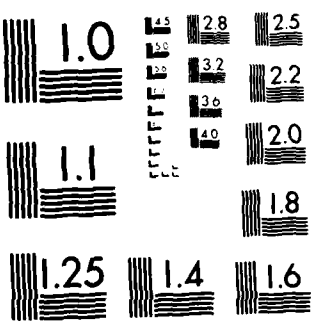

Fiadeiro, M. 1982. Three-dimensional modeling of tracers in the deep Pacific Ocean: II. Radiocarbon and the circulation. J. Mar. Res., 40, 537-550.

Stommel, H. and A. Arons, 1960. On the abyssal circulation of the world. Part I - Stationary planetary flow patterns on a sphere. Deep-Sea Res., 8, 39-64.

PENETRATION OF TRITIUM IN THE NORTH ATLANTIC MAIN THERMOCLINE

Jorge L. Sarmiento

A box model of tritium penetration from the surface mixed layer to the interior along isopycnal surfaces in the North Atlantic requires an equivalent flux of the order of 40 x 10^6 m^3 s^{-1} for the σ_θ range of 25.6 to 27.4 in order to fit 1972 tritium observations. This is far in excess of the ~8 x 10^6 m^3 s^{-1} downward Ekman pumping calculated from yearly mean winds acting on the wintertime outcrops. The implication is that processes other than Ekman pumping, such as wintertime convection and mixing along isopycnal surfaces, are responsible for a majority of the observed tritium simulation using a primitive equation ocean circulation model.

EDDY KINETIC ENERGY FROM SURFACE DRIFTERS AND DEEP FLOATS

Philip L. Richardson

One hundred and ten satellite tracked freely drifting buoys were used to measure velocities and trajectories of the near surface currents in the North Atlantic. Values of mean velocity and the variance about the mean were calculated for different regions. A horizontal map of eddy kinetic energy was prepared on a 2° by 2° grid between latitudes 20-55°N; maximum eddy energy ($\sim$3000 cm^2/sec^2) coincides with the high speed Gulf Stream jet after it leaves the coast and begins large amplitude meanders. A tongue of high eddy energy coincides with Stream's path eastward and around the Grand Banks into the Newfoundland Basin ($\sim$1000 cm^2/sec^2) with a weaker extension eastward across the mid-Atlantic Ridge near 45°N. A second weak extension reaches southeastward from the Stream and crosses the mid-Atlantic Ridge between 30-35°N. North and south of the Stream eddy energy decays rapidly reaching values of 200 cm^2/sec^2 in the mid gyre region and 100 cm^2/sec^2 in the Eastern North Atlantic and North Equatorial Current. Although the gross distribution of eddy energy is similar to that determined from ship drift measurements, there are significant differences. Eddy energy from drifters amounts to approximately twice the value measured by ship drift in the Gulf Stream and one-half the ship drift value in the mid-gyre. It is suggested that the difference in Gulf Stream values is due to the horizontal averaging of mesoscale motion by ship drift measurements and that the difference in the gyre interior is due to errors in velocities determined from the ship drift technique.

THE GULF STREAM EAST OF CAPE HATTERAS

T. Rossby

Since September, 1980, we have maintained a program of bimonthly sampling of the velocity structure of the Gulf Stream. Each section consists of a set of velocity and temperature profiles taken along a 150-200 km long line centered near 36°N, 73°W from the Slope Waters to the Sargasso Sea.

Preliminary analysis of the data (through May, 1982) yields a mean transport of 78 + 11 Sverdrups (based on six complete sections) between the surface and 2000 meters. Numerically this is identical to Worthington's reanalysis of 30 hydrographic sections in this general area, for which he assumed a level of no motion at 2000 meters. Our data, on the other hand, indicate a mean downstream velocity at 2000 meters of 4-5 cm/sec. This would add 10-15 Sverdrups to his estimate. The reasons for this discrepancy are now being examined more closely.

The Pegasus section is located in an area of entrainment from both the Slope Waters and the Sargasso Sea. The rate of entrainment is equivalent to 20 Sverdrups/100 km with about two-thirds of the total being supplied from the Slope Waters.

The variability of the velocity structure from one section to another is striking. Sometimes it is broad, and sometimes it is highly compacted near the north wall (15 C at 200 meters). This is, of course, expected since it is a derivative of the smoother density field. One section revealed a very strong cross stream velocity field (detrainment or subduction?) relative to the density field. We have also, on several occasions, found eddies embedded within and advected by the Stream. We note the qualitative observation that the maximum surface velocity and transport do not seem to be correlated.

The field program is intended to span two complete years. The questions we plan to examine with this data set include 1) mass and heat flux variations (esp. the annual cycle), 2) mean and eddy kinetic energy distribution, 3) the coupling between the baroclinic and barotropic fields, if any, and 4) local dynamics and short term variability.

OCEAN STIRRING BY GEOSTROPHIC TURBULENCE

Greg Holloway

ABSTRACT

Stirring and transport of passive tracer fields by geostrophic turbulence is examined by means of numerical simulation, equilibrium statistical mechanics and turbulence closure theory. A consistent account emerged.

First consider the problem with no mean fields present, i.e. we suppose fields consisting of random fluctuations of vorticity and of tracer. Fluctuations may be given either as initial conditions or by random forcing. The flow evolves as "two-dimensional turbulence". It is seen that tracer variance is transferred efficiently to all scales. A significant result is that the transfer of tracer variance is more efficient than the transfer of vorticity variance. This result, seen both in closure theory and in simulations is due to the role of wavenumber-local interactions which are effective for the transfer of tracer but not of vorticity. A consequence is that tracer variance decays through explicit diffusion more quickly than vorticity variance decays.

A second result, seen from equilibrium statistical mechanics and confirmed by simulations, is that the absolute equilibria spectra (i.e. given no forcing or dissipation) are different for tracer and for vorticity. Because vorticity is not passive (viz. w = curl u), we see again that vorticity does not behave as a passive tracer although each is an advected quantity.

When a mean gradient of tracer concentration is imposed, we may examine average spatial fluxes of tracer. This is done with and without Rossby wave propagation (given by $\beta \neq 0$). With no Rossby waves and for isotropic turbulence, tracer flux may be related to mean gradient through an eddy diffusivity coefficient. Closure theory and direct simulation show that the diffusivity can be reasonably estimated by mixing length $K \propto u'l'$ with u' a characteristic (rms) velocity and l' the scale size of dominant eddies. A further result is to show that the wavenumber decomposition of the tracer flux has dominant contributions on length scales somewhat larger than the most energetic eddy scales.

Rossby wave propagation ($\beta \neq 0$, rigid lid, barotropic) induces an isotropy in an eddy diffusivity tensor. There are both direct and indirect effects. A direct effect is to suppress meridional diffusivity through dephasing of flux components. An indirect effect occurs because β also induces anisotropy in the velocity field, enhancing zonal over meridional motions. The result is further to suppress meridional diffusivity with only slight net suppression of zonal diffusivity. Rossby wave effects also shift the dominant wavenumber contributions to shorter scales for both meridional and zonal fluxes. Turbulence closure theory yields relatively simple estimates for the magnitude and degree of anisotropy of the eddy diffusivity tensor in agreement with simulations.

Intermittancy as measured by ratios of fourth moments to variances is seen to depend upon the wavenumber cascade of variances. In particular, approach to unforced, non-dissipative equilibrium shows a relaxation of intermittancy as moment ratios approach their Gaussian values.

Although an eddy diffusivity concept appears to be appropriate to cases of transports on large scale gradients, the concept is not appropriate for the stirring out from an initial tracer spot which is small compared with eddy sizes. Direct simulations show little evidence of transition toward a pseudo-diffusive regime even after tracer filaments have been drawn out over distances larger than the dominant eddy sizes.

A COMMENT ON MODELLING TURBULENT TRANSPORTS IN MARINE ECOSYSTEMS

Greg Holloway

ABSTRACT

Time dependent velocity fields in the presence of spatially varying productivity potential are shown to induce a mean "virtual velocity" which acts to transport biomass. Effects of such virtual velocity cannot be represented in terms of eddy diffusivity. Inclusion of virtual velocity terms appears to overcome some failures of simpler averaged models of marine ecosystems. In particular, convergence of the virtual velocity provides an effective mechanism for the formation of a phytoplankton maximum at or below the mean compensation depth.

DISCUSSION

The importance of turbulence for the maintenance of primary production in the upper ocean has been appreciated for a long time. Turbulence both enhances production by supplying limiting nutrients and may reduce production by transporting organisms downward to light limiting depths. Efforts to model the role of turbulence usually focus on the specification of eddy diffusion coefficients. In his lecture at the 1982 WHOI-GFD program, Dr. J. S. Wroblewski has demonstrated that time-dependent velocity fields in the presence of spatially varying productivity potential (growth rate) will produce average counter-gradient transports of plankton. (See also Wroblewski and O'Brien, 1981) These transports would seem to imply negative eddy diffusivities in an equation for averaged plankton distribution. However, explicit inclusion of negative diffusivity causes equations for average concentration to become ill-posed. (Solutions become non-unique after arbitrarily short times in absence of higher derivative terms.)

Dr. Wroblewski's results are at once enlightening and discouraging. Especially it would be discouraging if realistic plankton simulation required sophisticated, computer-intensive simulation of the detailed space-and time-dependent velocity field. Such velocity simulation seems barely possible (indeed, doubtful) at modern levels of capability in computational fluid mechanics. In any case, detailed velocity simulation would seem to preclude seasonal or longer duration experiments.

Here I'll try to make two points. First, time-dependent velocity fields in the presence of spatially varying mean production potential give rise to a transport term which is independent of the mean phytoplankton concentration gradient. Therefore, it is inappropriate to represent such transport as a Fickian eddy diffusion. Instead, the transport term appears simply as a virtual velocity carrying the mean concentration. A hope is that inclusion of

virtual velocity effects will re-establish the utility of simpler averaged production models. Second, it appears that strong convergence of the virtual velocity field may provide an efficient means to answer an old problem, namely to explain the formation of chlorophyll maxima at or below the euphotic zone compensation depth.

To provide the clearest derivation of virtual velocity, consider quite a simple phytoplankton model with properties varying only in depth z and time t. Let phytoplankton concentration $p(z,t)$ evolve as

$$\frac{\partial p}{\partial t} + \frac{\partial}{\partial z}\left[(w+w_s)p\right] - \frac{\partial}{\partial z}\left(K\frac{\partial p}{\partial z}\right) = \lambda(z)p \qquad (1)$$

where w is vertical velocity representing actual water motion, w_s is any sinking (Riley, Stommel and Bumpus, 1959; Steele and Yentsch, 1960) and K is explicit diffusion which, in fact, will be negligibly small. The right side of (1) serves only approximately to express biological dynamics where $\lambda(z)$ is a "production potential" determined by light and nutrient availability and expressing (albeit inadequately) herbivore grazing pressure. For more thorough account of the biological dynamics terms see Jamart et al. (1977) or Wroblewski (1977).

Next suppose that p and w may be written in terms of mean and fluctuating parts $p = P + p'$, $w = W + w'$. Averaging is in the sense of an ensemble average although in the present simple case one can think of horizontal averaging. From incompressibility and assumed horizontal uniformity, $\partial w/\partial z = 0$, and hence $W=0$ for our simple case. The goal is to obtain an equation for mean P without reference to fluctuations p' or w'. Averaging (1),

$$\frac{\partial}{\partial t}P + \frac{\partial}{\partial z}(w_s P) + \frac{\partial}{\partial z}\langle w'p'\rangle - \frac{\partial}{\partial z}\left(K\frac{\partial P}{\partial z}\right) = \lambda P \qquad (2)$$

Heuristic arguments and engineering practices have established a tradition of seeking to represent eddy fluxes $\langle w'p'\rangle$ in analogy to Fickian diffusion

$$\langle w'p'\rangle \stackrel{?}{=} -K^*\frac{\partial P}{\partial z} \qquad (3)$$

Guesses such as (3) usually suppose that p is a passive, conserved variable and then depend upon empiricism to estimate eddy diffusivities K^*. In the present case, nonconservation of p according to the right side of (1) yields a counterexample to (3).

Suppose a fluid parcel undergoes an oscillation in the vertical. Parcel displacement might be due to turbulence or might be a manifestation of internal wave activity. Let the vertical displacement ζ be given by

$$\zeta = a\sin\omega t \qquad (4)$$

Suppose the displacement is small compared with the scale height $|\partial \ln\lambda/\partial z|^{-1}$. As the test parcel moves in the varied background, we suppose that production potential as experienced at the parcel varies as $\lambda_0 + \zeta\partial\lambda/\partial z$. Thus

$$\dot{p}' = \left(\lambda_0 + \frac{\partial\lambda}{\partial z}a\sin\omega t\right)(P + p') \qquad (5)$$

where dot (.) denotes time derivative following the parcel. Assume, as we check later, that $p'^2 \ll P^2$. Hence from (5)

$$p' = \lambda_0 P t - \frac{\partial \lambda}{\partial z} \frac{a}{\omega} P \cos \omega t + C \tag{6}$$

Averaged over a period of oscillation,

$$\langle w'p' \rangle = - \frac{a^2}{2} \frac{\partial \lambda}{\partial z} P \tag{7}$$

where $w' = \dot{\zeta} = a\,\omega \cos \omega t$ and $\lambda_0 << \omega$ is assumed. Note that the conditions

$$\left(\frac{\lambda}{\omega}\right)^2 \left(a \frac{\partial \ln \lambda}{\partial z}\right)^2 \ll 1 \tag{8}$$

are just the condition $p'^2 \ll P^2$.

If many wave or turbulence components contribute to the vertical displacement field then those contributions just seem to yield a total displacement variance $\langle \zeta^2 \rangle$, generalizing (7) to $\langle w'p' \rangle = - \langle \zeta^2 \rangle \frac{\partial \lambda}{\partial z} P$. A flux of this form does not represent Fickian diffusion but rather represents advection of mean P by a virtual velocity

$$W^* = - \langle \zeta^2 \rangle \frac{\partial \lambda}{\partial z} \tag{9}$$

Two points are to be stressed. W* is not a transport of water hence does not satisfy any incompressibility constraint. Also, W* is distinct from, and typically much larger than, any sinking w_s. It may be more appropriate to think of W* as a kind of pumping.

The mechanism just described will act in parallel with turbulent exchange processes leading to (3). Thus, the central point of this note is to suggest that (3) be replaced by

$$\langle w'p' \rangle = - K^* \frac{\partial P}{\partial z} + W^* P \tag{10}$$

with W* given by (9). Then (2) is

$$\frac{\partial P}{\partial t} + \frac{\partial}{\partial z}\left[(W^* + w_s) P\right] - \frac{\partial}{\partial z}\left(K^* \frac{\partial P}{\partial z}\right) = \lambda P \tag{11}$$

where K has been included in K*.

Extension of (11) to a model in two or three spatial dimensions is apparent. Thinking of a coastal upwelling environment, let x be the offshore coordinate and U(x,z) the mean offshore velocity. Then

$$\frac{\partial P}{\partial t} + \frac{\partial}{\partial x}\left[(U + U^*) P\right] + \frac{\partial}{\partial z}\left[(W + W^* + w_s) P\right] = \frac{\partial}{\partial x}\left(K_x^* \frac{\partial P}{\partial x}\right) + \frac{\partial}{\partial z}\left(K_z^* \frac{\partial P}{\partial z}\right) + \lambda P \tag{12}$$

with $\partial U/\partial x + \partial W/\partial z = 0$. Analogously to (9) we might suppose $U^* = - \langle \chi^2 \rangle \partial \lambda / \partial x$ where $\langle \chi^2 \rangle$ is a variance of onshore-offshore displacements and K_x^* and K_z^* are horizontal and vertical eddy diffusivities. Further contributions to both W* and U* may arise through any cross terms $\langle \zeta \chi \rangle$.

Some implications of (10) are immediate and, I think, exciting. First, (10) easily allows us to rationalize the results of Wroblewski and O'Brien (1981). A flux which should have been of the form W*P is being misrepresented in terms of $-K^* \partial P/\partial z$, leading to negative and singular values of K*. This problem is most extreme just above the depth of maximum P. Removal of the W*P component should restore a plausible, everywhere positive K* profile of form similar to Jamart et al. (1977). The important result is that we may re-establish the utility of very much simpler, averaged models for primary production by adopting the formulation (10).

The second implication from (10) is to find a highly effective mechanism for the formation and maintenance of a deep maximum of phytoplankton. In many areas where nutrient depletion occurs, a maximum of phytoplankton concentration occurs at depths greater than the compensation depth (depth at which photosynthesis = respiration plus grazing, i.e., $\lambda = 0$ in the present case). As discussed by Steele and Yentsch (1960) and pursued in Jamart et al. (1977), maxima of phytoplankton below compensation depth seem only possible through differential sinking, i.e. $dw_s/dz > 0$. However, to account for observed chlorophyll profiles, one would seem to require $|w_s|$ as large as 1 m/day or more above compensation depth falling to zero somewhat below compensation depth. Possible sinking speeds for phytoplankton of diameters usually less than 10μ and for plausible cell densities are about two orders of magnitude too small to achieve the required effect. (Other facets such as selective grazing (Hobson and Lorenzen, 1972) appear to alter the taxonomic composition at the phytoplankton maximum but not to modify significantly the depth of occurrence relative to compensation depth). Thus a classical mystery of plankton ecology remains. Is W* the explanation?

Consider a plausible (I think) scenario. Suppose $\lambda \approx 1$ day^{-1} at about 20 m with a compensation depth at 30 m, hence $\frac{\partial \lambda}{\partial z} \approx 0.1$ m^{-1} day^{-1}. Vertical displacements due mainly to internal waves may commonly exhibit values of 3 or 4 m at 30 m depth, hence $\langle \zeta^2 \rangle \approx 10$ to 20 m^2 yielding $|W^*|$ of 1 to 2 m day^{-1} above compensation depth. (Displacement by internal tide is not included. Deterministic low frequency processes like tides should be treated explicitly.) Respiration and grazing will cause λ to take small negative values below compensation depth with $\partial \lambda/\partial z \approx 0$. It appears that convergence of W* will achieve just the effect sought by Steele and Yentsch (1960) or Jamart et al. (1977) without appeal to unrealistically large sinking rates. Indeed, sinking could be negligible.

I would like to close by listing some cautions. As remarked previously, the reduction of biological dynamics to a term λp in (1) is not correct. However, inclusion of more realistic biology such as a grazing threshold should not significantly alter my principal result, namely the explanation for a phytoplankton maximum below compensation depth. Of greater concern are the arguments leading to (9). I have posed an extremely simple, heuristic explanation for what is, I feel, the dominant new effect. More careful derivation is possible and may already exist in the literature of chemical or environmental engineering. Especially, my treatment of $\lambda(z)$ is haphazard. I suppose, effectively, that whenever organisms arrive at a level z, net growth or decay is instantaneously equal to the mean $\lambda(z)$. However, the same fluid displacement which carries phytoplankton will also carry grazing zooplankton and dissolved nutrients, inducing perturbations in λ, say λ', which will bear some correlation with p'. Only light availability would appear to behave in the manner that I have assumed. (Note: vertical displacements induced by surface gravity waves do not contribute in $\langle \zeta^2 \rangle$).

Perhaps these considerations, as well as possible biological hysterisis, can be incorporated by replacing $\partial\lambda/\partial z$ in (9) with some $\partial\lambda/\partial z$. Efforts to assign U* in (12) will be less confident than the prescription (9) for W*. However, I hasten to point out that the dynamical basis for K_x^* or K_z^* is even less well established. I would hope that a practical mix of theory and empiricism will lead to refinement of the virtual velocity terms. My point in this note is to demonstrate the existence and apparent importance of these terms. A more careful derivation may be supplied by Prof. J. Keller in these GFD notes.

REFERENCES

Hobson, L.A. and C.J. Lorenzen, 1972. Deep-Sea Res. 19, 297.

Jamart, B.M., D.F. Winter, K. Banse, G.C. Anderson and R.K. Lam, 1977. Deep-Sea Res. 24, 753.

Riley, G.A., H. Stommel and D.F. Bumpus, 1949. Bull. Bingham. Oceanog. Coll. 12 (3), 1-169.

Steele, J.H. and C.S. Yentsch, 1960. J. Mar. Biol. Ass. U.K. 39, 217.

Wroblewski, J.S., 1977. J. Mar. Res. 35, 357.

Wroblewski, J.S. and J.J. O'Brien, 1981. Ecol. Model. 12, 29.

THE UTILITY OF MULTIPLE TRACER DISTRIBUTIONS IN CALIBRATING OCEAN THERMOCLINE MODELS

Wallace S. Broecker

INTRODUCTION

Until valid ocean general circulation models are constructed, the uptake of fossil fuel CO_2 by the sea will have to be determined from reservoir models calibrated through use of the distribution of natural radioisotopes and transient tracers. Two questions arise in connection with this interim strategy. First, how sensitive is the uptake of fossil fuel CO_2 to the basic design of these models? Second, can the design be improved by simultaneously fitting the distributions of several tracers? These questions are explored here comparing the results for a variety of thermocline models. We select the theromocline for this study because it currently holds most of the fossil fuel CO_2 contained by the sea and because we have multiple tracer data for this region of the sea.

The tracers whose distribution we can use as calibrations for our models are ^3H, ^3He, ^{14}C, ^{85}Kr, and the freons. The temporal and geographic input functions of these tracers differ considerably from one another. So also do their geochemistries in the sea. Tritium for example is carried to the sea surface by rain and vapor exchange shortly after it reaches the troposphere. Thus the delivery of this isotope was strongly influenced by the locations of the bomb tests in which major amounts of tritium were produced and by characteristics of the atmospheric dispersal system. Once in the sea the tritium remains there. By contrast the ^{85}Kr and the freons created by man

will perpetually remain mainly in the atmosphere. Thus these gases have become nearly uniformly dispersed throughout the atmosphere and their concentrations in the sea are geographically uniform (except for differences related to the temperature dependence of their solubilities). Because of the large ratio of $HCO_3^- + CO_3^=$ to CO_2 in the sea the ^{14}C produced during bomb tests will ultimately be transferred largely to the sea. However, because of the large concentration of inorganic carbon in the sea the $^{14}C/C$ ratio in surface water has not as yet achieved equilibrium with the atmosphere. For this reason the transfer of $^{14}CO_2$ across the air-sea interface constitutes a major resistance to its ocean uptake. This is not the case for ^{85}Kr and the freons; surface waters are at equilibrium with the atmosphere. ^{3}He is produced by the decay of ^{3}H within the sea and is ultimately irreversibly lost from the sea to the air. Thus its distribution within the sea is quite distinct from those of the other tracers.

CO_2 whose distribution in the sea we wish to calculate differs from the other tracers in two important regards. First its input extends over a much longer period of time . Second its uptake characteristics lie geometrically between those of $^{14}CO_2$ and those of ^{85}Kr and the freons. The equilibration time between surface water and the atmosphere for CO_2 ($\sim$1 year) is longer than that for ^{85}Kr and the freons ($\sim$1 month) and shorter than that for $^{14}CO_2$ ($\sim$10 years). The equilibration time for CO_2 and the isotopic equilibration time for $^{14}CO_2$ differ because chemical equilibration involves the adjustment of the $CO_3^=$ ion content of the water while the isotopic equilibration involves all the carbon in the water. Carbonate ions make up about 10 percent of the carbon dissolved in surface sea water.

The characteristic of the thermocline which makes these differences among tracers potentially important is that ventilation is thought to occur mainly along horizons of constant potential density (i.e., isopycnal surfaces). As these horizons reach the surface during only the peak winter period, the input of the tracers to these outcrop regions will differ from one another. ^{85}Kr and the freons should achieve equilibrium in surface water even during the winter exposure of waters at the isopycnal outcrops. On the other hand, little atmospheric tritium or ^{14}C will enter the outcrop region during this brief exposure. Finally, any tritium derived ^{3}He brought to the surface during the period of outcropping will be lost to the atmosphere. The situation for CO_2 lies between those for ^{14}C and ^{85}Kr.

Thermocline Models

For our sensitivity study we adopt a two dimensional thermocline with outcropping isopycnal horizons. We consider a single hemispheric sector of the ocean (equator to 54°N). We depict this sector through a 15 box model. It consists of three levels of the thermocline (upper, middle and lower). Each is subdivided into three well mixed interior reservoirs and one outcrop reservoir. The latitude boundaries and relative volumes for these 15 reservoirs are shown in Figure 1.

Our strategy then is to see whether the distribution of these tracers in the thermocline places any limits on the flow paths of water among these boxes. We do this by selecting a variety of advective flow paths. For each we select

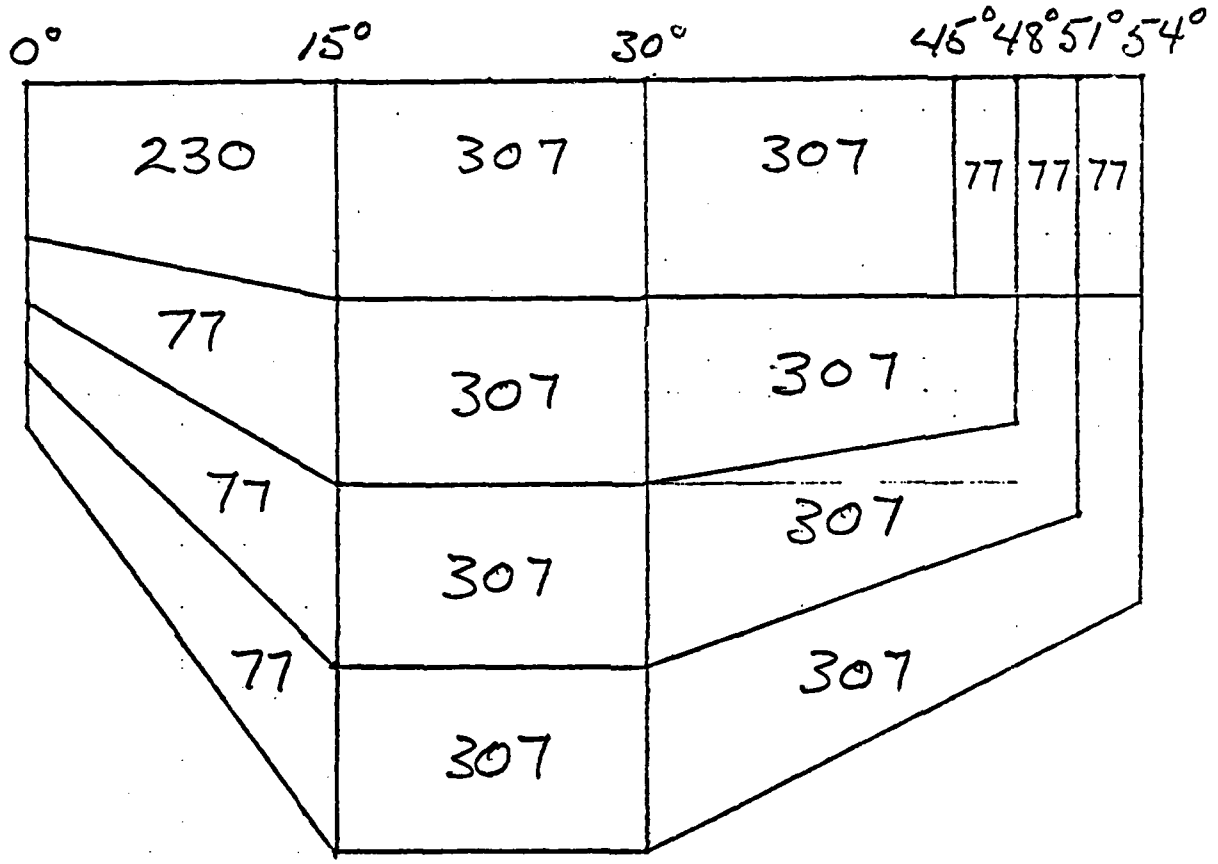

FIG. 1. Volume Unites $10^{14}\mu^3$. Total Volume 15°N to 54°N $2.7 \times 10^{17}\mu^3$

absolute flow rates (and where necessary diffusive mixing rates) which produce the same tritium distribution. This distribution is approximately that observed during the GEOSECS program. We then feed the other tracers into the models and compare the model to model and model to observed distributions generated in this way.

For this preliminary study we select the North Atlantic. The main reason for this choice is that the tracer data base is superior for this region of the ocean. Our comparisons concentrate on the region 15°N to 45°N.

Model #1 is termed the "sidewelling" case. In this model the three levels of the thermocline are ventilated from their respective outcrops. Water passes through the thermocline and exits into the equatorial zone where it upwells to the surface. This upwelled water flows back along the surface and eventually reenters the interior of the thermocline (via the outcrops). The water cycle is closed except for the water flowing along the surface to the north beyond the boundary of the model. An equivalent amount of water is fed into the base of the equatorial thermocline. This upwelling water is assumed to be tracer free. The calculations are made numerically. The tritium is added to the surface of the model in accordance with its input time history.

Model #2 is termed the "upwelling" case. Again each of the layers of the thermocline is ventilated from its respective outcrop. The water is returned to the surface by upwelling in the 15°N to 45°N latitude belt. Upon reaching the surface the water flows back to the outcrop region. Through the proper choice of the advective fluxes (and of the rates of horizontal interchange between adjacent 15°N - 30°N and 30° to 45°N reservoirs) it is possible to achieve a tritium distribution in the 15°N to 45°N region identical to that for model #1. The absolute tritium input rate for model #2 is 1.16 that for model #1.

Model #3 is termed the "backwelling" case. Like the first two models ventilation is entirely from the outcrops of the respective thermocline layers. However, in this case the water also returns to the surface through these outcrops. Hence all cross isopycnal transport occurs at the surface. Advective flow along the surface from the equatorial zone to high latitudes is also included. Again by suitable choice of the magnitudes of these fluxes a tritium distribution identical to that for the first two models can be achieved. In this case the absolute tritium input rate is 0.69 times that for model #1.

Model #4 is termed the "downwelling" case. The thermocline between 15° and 45°N is ventilated from above rather than from the outcrops. Again by suitable choice of absolute fluxes we can achieve a tritium distribution identical to that for the first three models. In this case the absolute tritium flux is 0.94 times that for model #1.

PARTICLE DISPERSION IN THE WESTERN NORTH ATLANTIC

James F. Price

Particle dispersion in the western North Atlantic thermocline is examined using an extensive SOFAR float data set. The float observations were made as part of the 1978 Local Dynamics Experiment (LDE) centered on 31N, 70W, a high eddy energy region near the southern edge of the Gulf Stream recirculation.

Dispersion is partitioned into an advective component, due to the mean transport velocity which was westward at about 0.015 m s^{-1}, and an eddy component (everything else) due mainly to mesoscale motions. For short times after launch, $\lesssim$ 3 days, the root mean square (rms) eddy dispersion has a clearly defined time^{+1} growth proportional to the rms eddy velocity. For long times after launch, $\gtrsim$ 20 days, rms eddy dispersion grows roughly as time$^{+1/2}$. Hence, the long-time eddy dispersion may be described by a diffusivity, $K = \frac{1}{2}\frac{d}{dt}$ dispersion, where (K_{11},K_{22}) are the (zonal meridional) components. In the mid-thermocline, 700 m, $(K_{11},K_{22}) = (8 \pm 2, 5 \pm 2) \times 10^3$ m^2 s^{-1}. In the deep-thermocline, 1300 m, $(K_{11},K_{22}) \cong (1.5 \pm 1, 1.5 \pm 0.5) \times 10^3$ m^2 s^{-1}.

There are two notable qualitative results in this. First, for times of up to several hundred days, K is sufficiently large that the total particle dispersion is dominated by eddy dispersion, rather than advection by the mean velocity. Secondly, these estimates together with those of Freeland et al. (1975), reveal a substantial geographic variation of K. K increases toward the surface and toward the Gulf Stream. Within this very limited sample, it appears that K is proportional to the eddy velocity variance, where the constant of proportionality (integral time scale) is about 8 days.

REFERENCE

Freeland, H.J., P.B. Rhines and H.T. Rossby, 1975. Statistical Observations of the trajectories of neutrally buoyant floats in the North Atlantic. J. Mar. Res., 33, 383-404.

AN IDEALIZED MODEL OF STIRRING

Hassan Aref

The kinematics of an advected particle reduces in the Lagrangian representation to a dynamical system

$$\begin{aligned} \dot{x} &= u(x,y,z,t), \\ \dot{y} &= v(x,y,z,t), \\ \dot{z} &= w(x,y,z,t), \end{aligned} \qquad (1)$$

where u = (u,v,w) is a prescribed velocity field. For turbulent advection u, v and w are given only probabilistically. Hence the results or "laws" one obtains for advection by turbulent flow are statistical. For laminar flows advection in 3D can in principle be chaotic even for steady flow. However, in

most analyses the laminar flow is restricted further to be both steady and two-dimensional (or axisymmetric). This renders the advection problem integrable since path lines and streamlines (or Stokes' streamlines) now coincide. The model proposed here breaks this standard mold by introducing a nonsteady potential flow to produce chaotic advected particle motion. This regime, where a regular flow field produces highly irregular advection, appears to be new. It is proposed to call it the regime of chaotic advection.

The actual model considered is extremely simple: Take a circular tank of radius a containing ideal (incompressible, inviscid) fluid constrained to two-dimensional motion. Place within the tank an agitator modelled as a point vortex of strength Γ. If the flow plane is identified with the complex plane, and the positions of marker particle and agitator are denoted $\zeta(t)$ and $z(t)$, respectively, the equation of motion being considered is

$$\dot{\zeta}^* = \frac{\Gamma}{2\pi i}\left\{(\zeta - z)^{-1} - (\zeta - a^2/z^*)^{-1}\right\}. \qquad (2)$$

Here an asterisk denotes complex conjugation. The first contribution on the RHS of (2) comes from the agitator itself, the second from its image.

Eq. (2) is a Hamiltonian system which is in general nonautonomous since z depends on time (the "stirring protocol"). For the special case

$$z(t) = \begin{cases} +b \text{ when } nT \leq t < (n + 1/2)T \\ -b \text{ when } (n + 1/2)T \leq t < (n+1)T \end{cases}$$

for $n = 0, +1, +2, \ldots$ it turns out that the particle trajectories consist of circular arcs and Eqn. (2) can be explicitly integrated over a time interval T/2. Hence, for this alternating stirrer protocol Eqn. (2) can be reduced to an area preserving map which may then be iterated at high precision.

Numerical experiments with this map for $a = 1$, $\Gamma = 2\pi$ and $b = 1/2$, show that chaos sets in when $T \simeq 0.1$ and apparently persists for larger T. Thus a slow shifting back and forth of the agitator seems to lead to more efficient stirring than a rapid shifting! For T in the quasi-integrable regime ($T \lesssim .05$ for $b = 1/2$) a blob of markers is forever trapped between the KAM tori (streamlines) within which it is found initially. However, for T well into the chaotic regime the blob is spread throughout the tank (within at most ten stirring periods) and very efficient stirring is achieved.

This simple model highlights many issues in the topic of advection. For example, it shows that an advected marker distribution can be extremely complicated even if the flow field is very simple. The marker distribution in the model is statistical in nature (when the stirring is operating in the chaotic regime) but the precise form of this statistics seems elusive.

THE STREAKINESS OF TRACERS

Thomas Keffer

A model to study the spreading behavior of a spot of tracer in an individual realization is developed. The barotropic vorticity equation (with β) is integrated forward in time to steady state using a doubly periodic spectral code to create a turbulent velocity field. A Gaussian spot of tracer is then introduced and the tracer conservation equation is integrated in time using the previously generated velocity field.

The tracer is found to be teased out into "streaks" of width $(\eta/\gamma)1/2$ where η is the sub-gridscale diffusivity and γ is the rms rate of strain. The area inside a contour is found to increase linearly for a short $O(1/\gamma)$ time, then exponentially at a rate less than $\exp(\gamma t)$ until a time t_{free}, then finally, linearly again. The limited spatial and temporal scales of the eddies is found to be important in limiting growth of a contour. A simple model of the growth is offered.

MODELING THE ADVECTIVE AND TURBULENT TRANSPORT OF PLANKTON

J. S. Wroblewski

Plankton models must incorporate time-dependent flow fields to properly resolve the advective and eddy transports which shape the distribution of many biological and chemical variables in the sea. Models which exclusively use coefficients of eddy diffusivity to parameterize mixing processes are unable to achieve the same detail as those models which properly resolve the eddy transport of a passive scalar, P (e.g. dissolved nutrients, phytoplankton, nonmigrating zooplankton, etc.). Time-dependent advection gives rise to an apparent diffusivity K* which is a property of the flow and the gradient of the scalar. K* is not connected with the numerical scheme chosen for the model, i.e., it is not numerical diffusion.

Turbulent fluctuations in the flow and quick local growth of P can result in transport of P against its gradient, sharpening spatial biological features. To obtain the same effect without including advection in the model, one would have to utilize a negative, explicit diffusivity! However, this is not suggested. Rather one should use a realistic flow field when simulating structure in the distribution of P which is primarily governed by advection. Diffusive terms with constant coefficients of eddy diffusivity can then be reserved solely to parameterize subgrid scale mixing of the variable, P.

With the development of "realistic" time-dependent circulation models, biological oceanographers can begin to test hypotheses by simulation modeling. Biological processes in the sea are nonlinear and occur on short time scales (hours). The magnitude of biological rates are often coupled to the time history of vertical transport. For example, phytoplankton growth is often light, limited and governed by vertical mixing. We require understanding of the fluid motion to make progress on many biological problems. In particular, biological modelers require realistic mixed layer models to simulate biological structure in the vertical.

REFERENCES

Wroblewski, J. S. and J. J. O'Brien, 1981. On modeling the turbulent transport of passive biological variables in aquatic ecosystems. Ecological Modeling, 12, 29-44.

Wroblewski, J. S., 1982. Interaction of currents and vertical migration in maintaining Calanus marshallae in the Oregon upwelling zone -- a simulation. Deep-Sea Research, 29, 665-686.

(See comments by Holloway in this volume, page 180).

EUPHAUSIID INVASION/DISPERSAL IN GULF STREAM COLD-CORE RINGS

Peter H. Wiebe

Invasion/dispersal patterns in the distribution and abundance of euphausiid species in four young- to middle-aged Gulf Stream cold-core rings suggest that several different physical exchange mechanisms are operating. The most important of these appear to be horizontal mixing in the mixed layer and exchange due to movement into or out of the trapped region at depth. A zone of minimum exchange is evident between 150 and 400 meters.

In addition to physical transport into or out of a ring, the distribution of a species is a result of its behavioral and physiological response to the new environment, and the biological effects of predation and competition with other species. These aspects of euphasiid biology are less well understood, but changes in vertical distribution and abundance of warm water species invading the ring environs suggest that only a few species such as Stylocheiron carinatum are able to penetrate and take advantage of the changing ring conditions in young- to middle-aged rings (2 to 8 months). Other near surface warm water species penetrate at slower rates regardless of whether they are vertical migrators (Euphausia brevis, E. hemigibba, E. tenera, Thysanopoda aequalis) or non-migrators (S. suhmii, S. abbreviatum). Deeper living species such as S. affine, S. elongatum, Nematoscelis microps, and N. tenella show minimal penetration of ring core waters in these four rings.

Cold-water species expatriated in cold-core rings also show a varied response to ring decay with some species disappearing rapidly -- 3 to 4 months (Thysanoessa longicaudata) -- and others persisting for substantial periods -- 1/2 to 1 year (N. megalops, E. krohnii). Distribution of the latter two species indicate dispersal out beyond the ring core at the surface in the case of E. krohnii and at depths of 400 to 1000 meters in the case of N. megalops.

MESOSCALE PHYTOPLANKTON DISTRIBUTIONS

Kenneth L. Denman

Phytoplankton use the sun's energy to form organic molecules via the photosynthetic process making them the base of the marine food chain. Their distributions in space and time are of importance in determining areas of high potential productivity in the marine food chain. Physically, phytoplankton behave as a passive tracer of the fluid flow, but they are not conservative: they grow, die and are eaten. The time scale for healthy photoplankton to double their weight or biomass by growth is 1-3 days, less than the time scale for enstrophy cascade in oceanic mesoscale eddies ($\sim$ 10 days). Hence, phytoplankton growth should affect their distribution in space, rather than total control by the unsteady ocean currents.

Near surface phytoplankton abundance can now be estimated from the satellite-borne Coastal Zone Color Scanner (CZCS), providing us with a more complete description of their horizontal distributions. Recent investigations have determined a variance spectrum for phytoplankton abundance with a wave number dependence of k^{-3} or steeper over a wave number (actually inverse wave length) range of 1-100 km (Gower, Denman and Holyer, 1980; Austin, 1981). Only in one case has the simultaneous spectrum for temperature been obtained (Olsson, pers. comm.), and the spectra are similar. We have derived structure functions from multiple ship surveys in a coastal region; they imply a spectral power law behavior of k^{-1} for phytoplankton abundance, and k^{-2} for temperature, salinity and dynamic height.

Numerical models of 2-D turbulence give patterns for a conserved passive scalar qualitatively similar to the CZCS phytoplankton images. One example (Holloway, pers. comm.) yields a kinetic energy spectral power law of k^{-5} and a corresponding scalar tracer variance spectrum of k^{-3}. We plan to carry out model experiments with a growing scalar tracer and possibly with two coupled tracers representing phytoplankton and a limited nutrient supply, thereby provided a growth rate variable in both space and time.

REFERENCES

Austin, R., 1981. Annual Report, Scripps Institution of Oceanography, p. 19.

Gower, J. F., K. L. Denman and R. J. Holyer, 1980. Phytoplankton patchiness indicates the fluctuation spectrum of mesoscale oceanic structure. Nature, 288, 157-159.

ADVECTION MODELLING OF VERTICALLY MIGRATING SHRIMP LARVAE

John A. Church

The role of larval advection in determining the complex, large-scale patterns of immigration of penaeid postlarvae in the Gulf of Carpentaria has been found by modelling the interaction between diurnal vertical migration of larvae with wind-forced and tidal currents. Eight vertical migration schemes were modelled which varied both the timing of migration and the position of the larvae in the water column. Both two-dimensional and three-dimensional models of the currents were coupled to the migratory larvae. When the larvae can migrate vertically with a diurnal period, their horizontal advection is enhanced. The largest horizontal advection distances occur when the larvae move diurnally into the bottom boundary layer. Advection distances up to 165 km are possible during the relatively short planktonic larval period. This distance corresponds to, and may determine, the offshore extent of the adult distribution. The onshore advection pattern of larvae varies in both space and time (on a seasonal scale) and is consistent with the observed spatial and temporal recruitment patterns. During the period of highest reproductive activity (March) in the area of the largest fishery, the advection of larvae is offshore and little recruitment of postlarvae to the nursery grounds is accomplished. Six months later, during the next period of reproductive activity (October), when the number of spawning female prawns is much lower, the phase of the tidal currents, relative to the day-night cycle, has progressed 180° and the larvae are moved onshore allowing postlarvae access to their estuarine nursery grounds several months prior to the main fishing season (March).

RADIOCARBON AS A TRACER OF OCEAN VARIABILITY

Ellen M. Druffel

Corals living in the surface layer of the ocean record within their annual density bands a variety of unaltered isotopic records. Among these are past radiocarbon levels reflective of the $^{14}C/^{12}C$ ratio in the sea water, and $^{18}O/^{16}O$ ratios which record temperature at the time of skeletal formation. These records have been obtained for several-hundred year old coral series from temperate and tropical regions of the Pacific and Atlantic Oceans. These results are surveyed and implications of variability of the air-sea gas exchange rate and of ocean circulation are discussed. In particular, isotopic records of corals in the Gulf Stream show that the annual mean water temperature was 1°C cooler around A.D. 1700. Coincident with this was a rise in the $^{14}C/^{12}$ ratio during the Maunder minimum, a period of documented low solar activity. There also appears to be an apparent climatological control on the exchange of $^{14}CO_2$ between air and ocean on decade timescales in the North Atlantic. This correlates with the variation in estimated water mass renewal rates for this area as calculated by Jenkins (1982).

REFERENCE

Jenkins, W.J., 1982. On the climate of a subtropical ocean gyre: decade time scale variations in water mass renewal in the Sargasso Sea. J. Mar. Res., 40, Suppl. 265-290.

WESTERN NORTH ATLANTIC STRUCTURE AND VARIABILITY INFERRED FROM SOFAR FLOATS

Stephen C. Riser

From SOFAR floats set at several depths in the western North Atlantic, it is shown that the Lagrangian motions of trajectors varies markedly over regions as small as a few degrees on a side. Kinetic energy increases to the north and west at both 700 m and 2000 m; at both levels the region in the vicinity of 28°N, 70°W, the MODE region, appears to be a local minimum of kinetic energy. At very low frequencies the trajectories indicate that zonal motions are more energetic than meridional ones on the thermocline and at depth over a flat bottom.

Three regions of the North Atlantic are examined. North of 32°N and west of 60°W, there is evidence of westward recirculation in the thermocline. South of this recirculation regime there is evidence that individual fluid parcels undergo large rms displacements but small net displacements over times of years. South and east of this regime, there is evidence of an eastward mean flow in the thermocline extending possibly as far east as the Mid-Atlantic Ridge.

In deeper water, at 2000 m, trajectories appear to be influenced by bottom topography, though over a flat bottom the tracks are similar to their thermocline counterparts.

LECTURES OF FELLOWS

WAKES AND MEAN FLOWS OF LOW-FREQUENCY INTERNAL-WAVE PACKETS

Dave Broutman

INTRODUCTION

A central theme of Dr. Andrews' lectures is the role of wave-transience in affecting mean flows and mean profiles of temperature and tracers. The examples covered by Dr. Andrews found application in the stratosphere and included the sudden stratospheric warming, where growing planetary waves modify the temperature distribution by as much as 40°C and decelerate upper level winds.

Transience is a marked feature of energetic, near-inertial oscillations in the ocean. Although it is unlikely that they will increase ocean temperatures by 40°C, these oscillations could be very effective at inducing mean flows. If, as for high-frequency, plane, internal gravity waves,

$$\bar{u} \sim \bar{u}^L \sim O\left(\frac{E}{c}\right) \tag{1}$$

where $\bar{u}$ and $\bar{u}^L$ are the Eulerian and Lagrangian horizontal mean velocities, respectively, E is the energy density (see equation (16) and below), and c is horizontal (intrinsic) phase velocity, then for fixed horizontal wavelength, the generation of mean velocities would be heavily dominated by low-frequency waves: in addition to the phase velocity appearing in the denominator in (1), energy spectra typically fall off as the inverse square of the frequency and even faster in the upper ocean and near the inertial and tidal bands. A rough calculation using (1) and the observation that low-frequency waves are marginally stable (i.e. have a minimum Richardson number approaching unity), gives mean-flow magnitudes of nearly half the orbital velocity of the waves.

When Coriolis terms are important, however, mean flows can develop with an entirely different character. Here mean-flow equations are derived for low-frequency internal-wave packets. Of the cases considered, only when rotation is ignored does $\bar{u}$ or $\bar{u}^L$ equal E/c identically, and only when horizontal dependence is ignored does an inertial wave appear in the wake of the packet, as predicted by Hasselmann (1970). These calculations supplement the related work of Andrews (1980), Bretherton (1969), Grimshaw (1975), and Hasselmann (1970).

It is assumed that the Väisälä frequency, N, is constant and that the background (O(1)) mean flow is zero. For the upper thermocline, where low-frequency packets are most energetic and identifiable, these are poor assumptions, but they help to isolate the dependence of mean-flow evolution on wave-frequency. The calculations can probably be extended to include variations in the medium through a WKB analysis without altering the conclusions obtained below. We also ignore ocean boundaries, which is reasonable for the scales to be considered: vertical packet dimensions of a few hundred meters, implying horizontal wavelengths of roughly 5-20 kilometers, depending on frequency. Packets of these scales dominate spectra of vertical shear and show up clearly in upper-ocean data.

The equations to be solved are

$$\underset{\sim}{u}_t + \underset{\sim}{u}\cdot\nabla\underset{\sim}{u} + 2\underset{\sim}{\Omega}\times\underset{\sim}{u} + \frac{1}{\rho}\nabla p + g = 0 \qquad (2a)$$

$$\nabla\cdot\underset{\sim}{u} = 0 \qquad (2b)$$

The fluid is nondissipative, Boussinesq, and incompressible, $2\underset{\sim}{\Omega} = (0,0,f)$, where f is the inertial frequency, assumed constant, and $\underset{\sim}{u} = (u,v,w)$.

MEAN FLOWS

As waves propagate through a fluid, it is well known that they set up stresses that can accelerate mean motions. There are many examples with physical interpretations in the literature. Mathematically, a mean flow arises because a sinusoid is generally not an exact solution to the equations of motion. If sinusoidal motion is assumed, the nonlinear terms try to generate harmonics and mean quantities. Even in the special cases where sinusoidal motion is an exact solution (e.g. plane internal-inertial gravity waves in a uniform, nondissipative, Boussinesq fluid) strictly sinusoidal motion may not be consistent with the condition of no motion initially. For instance, a wave train with a slowly growing leading edge, of the type described in a lecture of Dr. Andrews, induces mean as well as orbital motion. When the wave-train amplitude levels off, the horizontal velocity is $u = \xi\sin(kx-\omega t) + \bar{u}$, where $\bar{u}$ is an $O(\xi^2)$ constant. This is still an exact solution under the assumptions mentioned above provided that ω is the Doppler-shifted frequency.

When rotation (and dissipation) can be ignored, net accelerations produced by the leading edge of a wave packet are cancelled by decelerations in the trailing edge. The mean flow returns to zero after the packet passes, although a net displacement of the fluid occurs if the Lagrangian-mean flow is nonzero.

When rotation is important, the trailing edge may not decelerate the fluid back to zero velocity because the mean motion, now affected by the Coriolis force, changes direction during the passage of the packet. The same forces that set up the motion, therefore, may no longer stop it. Instead, the system is left ringing at inertial

frequency after the packet propagates away. This is illustrated in the following example.

Solutions to (2) are sought of the form

$$(u, v, w, \rho, \theta) = (u'; v'; w'; \rho'; \theta') + (\bar{u}, \bar{v}, \bar{w}, \bar{\rho}, \bar{\theta}) \quad (3)$$

The buoyancy parameter is $\theta = g\rho'/\rho_0$ and a factor of $1/\rho_0$ is included in the pressure variable for simplicity in notation. The primed quantities are $O(\varepsilon)$ and behave like $\exp(\underset{\sim}{K}\cdot\underset{\sim}{x} - \omega t)$, where $\underset{\sim}{K} = (k,0,m)$. The barred quantities are obtained by an Eulerian average over phase and are $O(\varepsilon^2)$.

The $O(\varepsilon)$ equations,

$$u_t' - fv' + p_x' = 0 \quad (4)$$

$$v_t' + fu' + p_y' = 0 \quad (5)$$

$$w_t' + \theta' + p_z' = 0 \quad (6)$$

$$\theta_t' - N^2 w' = 0 \quad (7)$$

$$u_x' + v_y' + w_z' = 0 \quad (8)$$

yield the standard linear-theory results: the dispersion relationship

$$\omega^2 = \frac{k^2N^2 + m^2f^2}{k^2 + m^2} \quad (9)$$

and the relationships

$$(u'; w'; \rho'; \theta') = \left(i\frac{\omega}{f}, -i\frac{\omega k}{fm}, i\frac{(N^2-\omega^2)k}{fm^2}, \frac{N^2k}{fm}\right)v' \quad (10)$$

The $O(\varepsilon^2)$ equations describe the evolution of means and second harmonics. The later component is eliminated by averaging, leaving

$$\mu\bar{u}_T - f\bar{v} + \mu\bar{p}_x = -\mu(\overline{u'^2})_x - \mu(\overline{u'w'})_z \quad (11)$$

$$\mu\bar{v}_T + f\bar{u} + \mu\bar{p}_y = -\mu(\overline{v'^2})_y \quad (12)$$

$$\mu\bar{w}_T + \bar{\theta} + \mu\bar{p}_z = -\mu(\overline{u'w'})_x - \mu(\overline{w'^2})_z \quad (13)$$

$$\mu\bar{\theta}_T - N^2\bar{w} = -\mu(\overline{v'\theta'})_y \quad (14)$$

$$\mu(\bar{u}_x + \bar{v}_y + \bar{w}_z) = 0 \quad (15)$$

These equations are written in terms of the stretched variables $\underset{\sim}{X} = \mu\underset{\sim}{x}$, $T = \mu t$ ($\mu \ll 1$) which vary by an $O(1)$ amount over the scales

of the packet. The boundary condition is that all quantities vanish as $Z \to -\infty$ (envisioning a packet with downward group velocity). The $O(\varepsilon)$ equations have been used to eliminate products of quantities on the right-hand-side of (11)-(15) which are out of phase.

CASE (1) $\partial/\partial X = \partial/\partial Y = 0, \quad f\tau_p \sim O(1)$

By ignoring variations in X and Y, the continuity equation and boundary condition force $\bar{w}$ to be zero everywhere. The buoyancy equation then gives $\bar{\theta} = 0$, leaving the pressure gradient term to balance the Reynolds stresses in the vertical momentum equation.

A high frequency approximation, $\omega/f \gg 1$, reduces the equation for the x-component of the pseudomomentum, $\hat{p}_1$, to

$$\hat{p}_{1,T} = -(\overline{u'^2})_X - (\overline{u'w'})_Z \tag{16}$$

where $\hat{p}_1 \approx E/c$, $E = (\overline{u'^2} + \overline{v'^2} + \overline{w'^2} + \overline{\theta'^2}/N^2)/2$, and $c = \omega/k$. The horizontal momentum equations then become

$$\mu \bar{u}_T - f\bar{v} = \mu \hat{p}_{1,T} \tag{17}$$

$$\mu \bar{v}_T + f\bar{u} = 0 \tag{18}$$

At this stage we assume that the Coriolis term and the acceleration term are the same order, i.e. that $f\tau_p \sim O(1)$, where τ_p is the time scale of the packet. (Since $\tau_p \gg 1/\omega$ for scale separation to hold, this assumption includes the high frequency approximation leading to (16)). The case of strong rotation, $f\tau_p \gg 1$ is considered in the next section.

Defining $\bar{\phi} = \bar{u} + i\bar{v}$, (17) and (18) combine to become

$$\mu \bar{\phi}_T - if\bar{\phi} = \mu \hat{p}_{1,T} \tag{19}$$

which has the solution

$$\bar{\phi} = \frac{E}{c} - if e^{-i(f/\mu)T} \int_{-\infty}^{T} e^{i(f/\mu)T'} \frac{E(T')}{c}\, dT' \tag{20}$$

The second term arises when f is nonzero and represents an inertial wave left in the wake of the packet. Hasselmann (1970) obtains a similar solution for a random field of surface waves or internal waves in shallow water. Related behavior illustrating that Rossby-wave packets leave lower-frequency Rossby waves in their wake is shown in Rhines and Holland (1979).

It therefore appears that transient waves need not induce transient mean flows, even in a nondissipative fluid. This conclusion follows more directly when the equations are rewritten in Lagrangian-mean form:

$$\mu \bar{u}^L_T - f\bar{v}^L + \mu \bar{p}^L_x = -\mu(\overline{\rho' \xi_x})_X - \mu(\overline{\rho' \xi_z})_Y - \mu(\overline{\rho' \eta_x})_Z = \mu \hat{p}_{1T} \tag{21}$$

$$\mu \bar{v}^L_T + f\bar{u}^L + \mu \bar{p}^L_Y = 0 \tag{22}$$

$$\mu \bar{w}^L_T + \bar{\theta}^L + \mu \bar{p}^L_Z = -\mu(\overline{\rho' \xi_z})_X - \mu(\overline{\rho' \xi_z})_Y - \mu(\overline{\rho' \eta_z})_Z = \mu \hat{p}_{3T} \tag{23}$$

$$\mu \bar{\theta}^L_T - N^2 \bar{w}^L = 0 \tag{24}$$

$$\mu(\bar{u}^L_X + \bar{v}^L_Y + \bar{w}^L_Z) = 0 \tag{25}$$

where the Lagrangian mean of a quantity, g,

$$\overline{g(\underset{\sim}{x}, t)}^L = \overline{g(\underset{\sim}{x} + \underset{\sim}{\xi}, t)} \tag{26}$$

is an average taken over all particles whose mean position is x. $\underset{\sim}{\xi}(x,t) = (\xi, \zeta, \eta)$ is the particle displacement, defined such that $\overline{\underset{\sim}{\xi}(x,t)} = 0$ (Andrews & McIntyre (1978)), and the pseudomomentum vector, $\hat{p}$, has components $(\hat{p}_1, 0, \hat{p}_3)$. Dependence on X and Y in (21)-(25) has been included for later reference. Ignoring these dependences for now, the X-momentum equation can be rewritten as

$$\mu(\bar{u}^L - \hat{p}_1)_T - f\bar{v}^L = 0 \tag{27}$$

which in turn can be rewritten as $\bar{D}^L(\bar{u}^L - \hat{p}_1 - fy) = 0$

(Andrews & McIntyre (1978)). $\bar{D}^L$ signifies the rate of change moving with the Lagrangian-mean flow:

$$\bar{D}^L = \frac{\partial}{\partial T} + \underset{\sim}{u} \cdot \frac{\partial}{\partial \underset{\sim}{x}} \tag{28}$$

If the Coriolis force leads to a net change in y during the passage of the packet, $\bar{u}^L$ must remain nonzero after the packet propagates away.

CASE (2) $\partial/\partial X = \partial/\partial Y = 0$; $f\tau_p \gg 1$

The solution given in (20) is derived assuming that the Coriolis terms are small but nonzero. This requires

$$\frac{f\bar{v}^L}{\mu \partial \bar{u}^L/\partial T} = \frac{f^2}{\mu^2} \frac{\bar{v}^L}{\partial^2 \bar{v}^L/\partial T^2} \sim \frac{f^2 T^2}{\mu^2} \sim O(1) \tag{29}$$

where we identify $\tau_p \equiv T/\mu$ with the time scale of the packet. Let $\tau_p = 2\pi n/\omega$ with n measuring the number of wave periods required for the wave packet to reach maximum amplitude at a fixed location. Then $f\tau_p \sim O(1)$ translates to $\omega \sim O(2\pi n f)$. If $n = 4$, say, then ω

must be in the range of 25f for the Coriolis and acceleration terms to be of the same order. Since 25f corresponds to a wave period of less than one hour at midlatitudes, this division not only lies well above f, but also above the frequency of the semidiurnal tide and tidal harmonic at six-hour period. The assumption $f\tau_p \sim O(1)$ therefore excludes what is by far the most energetic parts of the oceanic internal-wave spectrum. The amount that is excluded depends of course on π, but the point is that it is $2\pi\pi f/\omega$ and not f/ω that measures the ratio of the Coriolis to acceleration terms in the mean equations.

The approximate balance to lowest order is now between the Coriolis term and the radiation stresses, so that

$$\bar{v}^L = -\frac{\mu}{f}\hat{p}_{1T} \tag{30}$$

$$\bar{u}^L = \frac{\mu^2}{f^2}\hat{p}_{1TT} \tag{31}$$

Because the mean motion is reduced to an $O(\mu)$ quantity, the Stokes drift appears at the same order

$$\bar{v}^S = \mu(\eta\cdot\overline{v\cdot})_Z \ . \tag{32}$$

More interestingly, $\bar{v}^L$ and $\bar{u}^L$ return to zero after the packet propagates away. If the mean velocities are expanded in powers of μ, inertial motion in the wake still does not appear, for at all higher orders $\bar{v}^L$ and $\bar{u}^L$ can be related to higher-order derivatives of $\hat{p}_1$ with respect to T.

To see what has happened to the inertial motion, we can derive an exact solution for $\bar{\phi}^L = \bar{u}^L + i\bar{v}^L$ analogous to (20) for ϕ except that when written in terms of Lagrangian-mean variables, the solution is valid for all frequencies: no high-frequency approximation is necessary to replace the right hand sides of (21) and (23) with $\hat{p}_{1T}$ and $\hat{p}_{3T}$ respectively. (Psedomomentum is not exactly conserved for localized wave packets since mean quantities depend on position; however, corrections do not appear for this problem until $O(\varepsilon^4)$.) We can thus write

$$\bar{\phi}^L = \int_{-\infty}^{T} e^{i(f/\mu)(T-T')}\,\mu\hat{p}_{1T'}\,dT' \tag{33}$$

Since by assumption $f\tau_p \gg 1$, the phase of the exponential function in the integrand of (33) varies rapidly. An asymptotic expansion can then be found through an integration by parts. Integrating N times leaves

$$\bar{\phi}^L = -i\frac{\mu}{f}\hat{p}_{1T} + \cdots + i^N\mu^N\int_{-\infty}^{T} e^{i(f/\mu)(T-T')}\frac{\partial^N}{\partial T^N}(\hat{p}_1)\,dT' \tag{34}$$

The last integral represents the inertial motion left in the wake of the packet. It does not appear in the asymptotic expansion because it is exponentially small as $\mu \to 0$. (The Riemann-Lesbegue lemma limits the last term in (34) to an $o(\mu^{-N})$ quantity, but using a stationary phase calculation and noticing that the phase function in the integral has no stationary points, the integral can be shown to be exponentially small as μ vanishes (Lighthill, 1978).)

CASE (3) $\partial/\partial x \, , \, \partial/\partial y \sim O(1) \; ; \quad f\tau_p >> 1$

Low-frequency internal-wave packets have horizontal scales that are much greater than their vertical scales; however unlike Hasselmann (1970), we consider horizontal variations because the ratio of the Reynolds stress terms in the x-momentum equation, for example, is

$$\frac{(\overline{u'^2})_x}{(\overline{u'w'})_z} \sim \frac{m}{k}\frac{\Delta Z}{\Delta X} \tag{35}$$

where ΔZ and ΔX are the vertical and horizontal scales of the packet. The ratio thus scales as the number of horizontal wavelengths to the number of vertical wavelengths, not as the ratio of absolute packet dimensions or wavenumbers.

Allowing for the packet to produce mean horizontal pressure gradients and allowing for all the terms in the continuity equation leaves the system of equations given in (21)-(25). We write

$$\bar{V} = V^{(0)} + \mu V^{(1)} + \mu^2 V^{(2)} + \cdots \tag{36}$$

and similarly for all other mean quantities, and attempt an expansion which balances terms geostrophically and hydrostatically at lowest order:

$$-fV^{(0)} + P_X^{(0)} = 0 \tag{37}$$

$$fu^{(0)} + P_Y^{(0)} = 0 \tag{38}$$

$$\theta^{(0)} + P_Z^{(0)} = 0 \tag{39}$$

$$u_X^{(0)} + V_Y^{(0)} = 0 \tag{40}$$

A stream function, $\psi^{(0)}$, can be defined at this order, related to $p^{(0)}$ by

$$f\bar{V}_h^2\psi^{(0)} = \bar{V}_h^2 p^{(0)} \tag{41}$$

where $\bar{V}_h^2 = \partial^2/\partial X^2 + \partial^2/\partial Y^2$, $u^{(0)} = -\mu\psi_Y^{(0)}$, and $v^{(0)} = \mu\psi_X^{(0)}$.

The evolution of the O(1) quantities is obtained from the $O(\mu)$ equations:

$$u_T^{(0)} - fv^{(1)} + p_x^{(1)} = \hat{P}_{1T} \tag{42}$$

$$v_T^{(0)} + fu^{(1)} + p_y^{(1)} = 0 \tag{43}$$

$$w_T^{(0)} + \theta^{(1)} + p_z^{(1)} = \hat{P}_{3T} \tag{44}$$

$$\theta_T^{(0)} - N^2 w^{(1)} = 0 \tag{45}$$

$$u_x^{(1)} + v_y^{(1)} + w_z^{(1)} = 0 \tag{46}$$

These can be manipulated, using (41), to obtain Poisson's equation for $\psi^{(0)}$

$$\nabla_h^2 \psi^{(0)} + \frac{f^2}{N^2} \psi_{zz}^{(0)} = -\hat{P}_{1Y} \tag{47}$$

The formal solution to (47) can be written in terms of a Green's function or derived using a three-dimensional Fourier transform.

Suppose we choose a Gaussian packet envelope:

$$\hat{P}_1 \sim \exp\left\{-\alpha_1^2 (X - C_g^{(x)} T)^2 - \alpha_2^2 Y^2 - \alpha_3^2 (Z - C_g^{(z)} T)^2\right\} \tag{48}$$

where $\underline{C}_g = (C_g^{(x)}, 0, C_g^{(z)})$ is the group velocity. Symmetry considerations lead to

$$\left(\psi_x^{(0)} = p_x^{(0)} = \psi_z^{(0)} = p_z^{(0)}\right)_{Y=0} = 0 \tag{49}$$

so $\vec{v}^L$ is zero along the Y-centerline of the packet, where the wave-amplitude reaches a maximum.

In the far-field, $\psi^{(0)}$ and $p^{(0)}$ decay as $1/r^2$ multiplied by some angular dependence. (An electromagnetic analogy is the potential due to a dipole source.) Consequently, no inertial wake results. Viewed another way, (47) becomes Laplace's equation as $T \to \infty$, $\underline{X}$ fixed, which, because of the boundary conditions, cannot support motion.

As in Case (2) the inertial motion does not appear at higher order. The $O(\mu^2)$ equations give

$$\nabla_h^2 p^{(1)} + \frac{f^2}{N^2} p_{zz}^{(1)} = \hat{P}_{1XT} + \frac{f^2}{N^2} \hat{P}_{3ZT} \tag{50}$$

which also reduces to Laplace's equation after the packet propagates away. Similarly, the $O(\mu^3)$ equations lead to

$$\nabla_h^2 p^{(2)} + \frac{f^2}{N^2} p_{zz}^{(2)} = -w_{zT}^{(1)} \left(1 + \frac{f^2}{N^2}\right) \tag{51}$$

Since the structure of the equation at all higher orders is the same as (51), the expansion yields only decaying motion in the packet

wake.

Again as in Case (2), the inertial motion may result from an expression which is exponentially small as $\mu \to 0$. There is at least one other possibility though: the inertial wake may be limited to packets of infinite horizontal extent, i.e. the limit of $\partial/\partial X$, $\partial/\partial Y$ approaching zero may be a singular one. The idea is that although the horizontal pressure gradients build slowly in a long but finite packet, they can eventually reach an O(1) magnitude. The dynamics change when horizontal pressure gradients are important and inertial oscillations may disappear.

An exact solution to (21)-(25) would reveal whether the limit $\partial/\partial X, \partial/\partial Y \to 0$ is singular. A suggestion made by Glenn Flierl is to try a sinusoidal packet shape

$$\hat{p}_1 \sim \sin\lambda \qquad \lambda = (\underset{\sim}{\alpha} \cdot \underset{\sim}{X} - \sigma T) \tag{52}$$

for $-\pi \leq \lambda \leq \pi$ and $\hat{p}_1 = 0$ otherwise. This allows solutions to be obtained by assuming behavior of the form $A\cos\lambda + B\sin\lambda$ for each of the mean variables. To meet the initial condition, solutions to the homogeneous equations are also needed. The effect of discontinuities in $\hat{p}_{1TT}$ at $\lambda = -\pi, \pi$ requires assessment.

Another possibility is to ignore Z dependence. The equations then reduce to

$$\mu\bar{u}^L_T - f\bar{v}^L + \mu\bar{p}^L_X = \mu\hat{p}_{1T} \tag{53}$$

$$\mu\bar{v}^L_T + f\bar{u}^L + \mu\bar{p}^L_Y = 0 \tag{54}$$

$$\mu(\bar{u}^L_X + \bar{v}^L_Y) = 0 \tag{55}$$

which can be combined to give the "wake-less" equation

$$\mu^2\bar{\nabla}^2\psi = -\mu\hat{p}_{1Y} \; ; \tag{56}$$

however, if X and Y variations are ignored from the outset, so the forcing, $\hat{p}_{1T}$, builds in time everywhere by the same amount, then the governing equation becomes the "wake-full" equation (19). This model, although somewhat contrived, is an example illustrating the singular limit associated with the neglect of horizontal dependences.

NONUNIFORM MEDIA AND CHANGES IN PACKET AMPLITUDE

Grimshaw (1975) derives a general system of mean flow equations that allows for variations in the Vaisala frequency and for background shears. Even in a uniform medium, though, the wave-induced mean flow will be affected by changes in packet amplitude resulting from dispersion, especially since the propagation is three-dimensional and especially when the waves are highly transient or

localized and therefore involve a broad (or at least non-narrow) range of frequencies and wavenumbers. This is often the case in the upper ocean, where packets with as few as three or four crests are observed. A stationary phase calculation describes the attenuation of energy in a uniform medium, but this result can also be obtained from the ray equations. The equation for action density along the ray (in one dimension for now) is

$$\frac{dA}{dt} = -A\left\{\Omega_{kx} + \Omega_{kk}\frac{\partial k}{\partial x}\right\} \tag{57}$$

where $\omega(x,t) = \Omega(k,x,t)$ is the dispersion relation and $d/dt = \partial/\partial t + c_g\,\partial/\partial x$. Since $dk/dt = 0$

$$k_x = \left\{k(x - c_g t)\right\}_x = \frac{(k_x)_{t=0}}{1 + \Omega_{kk}(k_x)_{t=0}\,t} \tag{58}$$

Substituting (58) into (57) and using $\Omega_{kx} = 0$, gives the stationary phase result that the action density decays as $1/t$ as $t \to \infty$.

It may seem surprising that although dispersion results from a spread in frequencies or wavenumbers, bandwidth information does not enter directly into the equation for action density, as it does in the equation for action spectral density, n, in (k,x,t) space:

$$\frac{\partial n}{\partial t} + \frac{\partial n}{\partial k}\frac{dk}{dt} + \frac{\partial n}{\partial x}\frac{dx}{dt} = 0 \tag{59}$$

Here spectral content appears through the term $\partial n/\partial k$; recall, however, that the bandwidth does not enter in the stationary phase calculation either, except at higher order when developed as an asymptotic expansion. Writing

$$\zeta(x,t) = \int_{-\infty}^{\infty} g(k)\, e^{i\psi(k)t}\, dk \tag{60}$$

where $\psi(k) = kx/t - \omega(k)$, we transform variables, using

$$s^2 = i\left(\psi(k_0) - \psi(k)\right) \tag{61}$$

$$G(s) = g(k)\frac{dk}{ds} = g(k)\frac{2is}{\psi'(k)} \tag{62}$$

(Note that using L'Hopital's rule,

$$G(0) = g(k_0)\sqrt{\frac{2i}{\psi''(k_0)}} \tag{63}$$

provided $\psi''(k_0)$ is nonzero.) Equation (60) then becomes

$$\zeta = e^{i\psi(k_0)}\int_{-\infty}^{\infty}\left(G(0) + G'(0)s + G''(0)\frac{s^2}{2} + \cdots\right)e^{-s^2 t}\, ds \tag{64}$$

k_0 is the stationary point, satisfying $\nu'(k_0) = 0$, and a prime in (64) denotes differentiation with respect to s. The bandwidth information in G'(0), G''(0)... appears only as a correction to the lowest-order solution.

The advantage of the ray equation (57) over the method of stationary phase is that it is easily extended to nonuniform media. Complications arise because in general k_x is not known analytically and because in three dimensions, nine equations are required:

$$\frac{d}{dt}\,\bar{\nabla}\underset{\sim}{K} = -\bar{\nabla}\underset{\sim}{K}\cdot\Omega_{\underset{\sim}{K}\underset{\sim}{K}}\cdot\bar{\nabla}\underset{\sim}{K} - \Omega_{\underset{\sim}{x}\underset{\sim}{K}}\cdot\bar{\nabla}\underset{\sim}{K} - \bar{\nabla}\underset{\sim}{K}\cdot\Omega_{\underset{\sim}{K}\underset{\sim}{x}} - \Omega_{\underset{\sim}{x}\underset{\sim}{x}} \qquad (65)$$

Still the system of equations can be integrated numerically. As an approximation, it is probably justified to ignore horizontal variations in the Vaisala frequency and shear, so that the horizontal wavenumbers are conserved, but the point here is that for localized packets, dispersion due to a spread in horizontal wavenumbers should not be dismissed as unimportant. Its affect on packet amplitudes may match that produced by refraction.

CONCLUSION

The character of the mean flow induced by an internal-wave packet is sensitive to the frequency of the waves and the dimensions of the packet.

When horizontal variations are neglected, high frequency waves induce a mean flow given by $\bar{u}^L = E/c$, unless rotation is included. Then $\bar{u}^L$ is given by (20) and an inertial wave oscillates in the wake of the packet. As the wave-frequency decreases toward f, the mean flow adjusts so as to move perpendicular to K at lowest order; moreover, in contrast to the high-frequency case, $\bar{u}^L$ vanishes whenever the packet amplitude levels off (see (29) and (30)).

When horizontal dependences are included, the lowest-order mean-flow equations lead to Poisson's equation for the pressure or stream function regardless of wave frequency. Motions induced by low frequency packets balance hydrostatically and geostrophically. A question suggested by these calculations is whether the limit $\partial/\partial x\,,\partial/\partial y \to 0$ is a singular one, and thus whether it is realistic to expect wakes with inertial oscillations.

Table 1 provides a summary of results.

ACKNOWLEDGEMENTS

I wish to thank Professors Glenn Flierl, Joe Keller and Russ Davis for valuable discussions.

REFERENCES

Andrews, D.G. 1980 On the mean motion induced by transient

inertio-gravity waves. Pageoph 118, 177-188.

Andrews, D.G. and M.E. McIntyre 1978 An exact theory of nonlinear waves on a Lagrangian-mean flow. J. Fluid Mech. 89, 609-646.

Bretherton, F.P. 1969 On the mean motion induced by internal gravity waves. J. Fluid Mech. 37, 785-803.

Grimshaw, R. 1975 Nonlinear internal waves in a rotating fluid. J. Fluid Mech. 71, 497-512.

Hasselmann, K. 1970 Wave-driven inertial oscillations. Geophys. Fluid Dyn. 1, 463-502.

Lighthill, J. 1978 Waves in Fluids. Cambridge University Press, London. 504 pp.

Rhines, P.B. and W.R. Holland 1979 A theoretical discussion of eddy-driven mean flows. Dyn. Atm. Oceans 3, 289-325.

Table 1. Properties of mean flows induced by nondissipative, plane, internal-inertial gravity waves
($\underset{\sim}{U} = 0$, N^2 = constant, $\underset{\sim}{K} = (k,0,m)$)

	Mean-flow Equation	Accuracy	Inertial Wake
$\frac{\partial}{\partial X} = \frac{\partial}{\partial Y} = 0$			
$f = 0$	$\bar{u}^L = E/c$ $\bar{v}^L = 0$	Exact to $O(\varepsilon^2)$	No
$f\tau_p - O(1)$	$\bar{u}^L = E/c - if\int_{-\infty}^{T} e^{-(f/\mu)(T-T')} \frac{E(T')}{c}\, dT'$	Exact to $O(\varepsilon^2)$	Yes
$f\tau_p \gg 1$	$\bar{v}^L = -\frac{\mu}{f}\hat{P}_{1T}$	$O(\mu^2\varepsilon^2)$	Exponentially small as $\mu \to 0$.
	$\bar{u}^L = \frac{k^2}{f^2}\hat{P}_{1TT}$	$O(\mu^2\varepsilon^2)$	
$\frac{\partial}{\partial X}, \frac{\partial}{\partial Y} \sim O(1)$			
$f = 0$ $f\tau_p \sim O(1)$	$\nabla_h^2 \psi^{(0)} = -\hat{P}_{1Y}$	$O(\mu\varepsilon^2)$	(?): Exponentially small or nonexistent
$f\tau_p \gg 1$ *	$\nabla_h^2 \psi^{(0)} + \frac{f^2}{N^2}\psi_{zz}^{(0)} = -\hat{P}_{1Y}$		

* Geostrophic and hydrostatic at $O(\mu^4\varepsilon^2)$.

SECOND ORDER CONSTRAINTS ON THE AMPLITUDES OF VERTICALLY PROPAGATING ROSSBY WAVES

Walter Robinson

I. Introduction

In a compressible atmosphere, in the absence of dissipation, the amplitudes of vertically propagating waves grow roughly exponentially with height. If this growth is unrestricted, the waves will propagate to some level at which breaking occurs, or viscous dissipation becomes important. There they will deposit their energy.

In the atmosphere, significant energy is contained within planetary scale disturbances. Charney and Drazin (1961) point out that this energy can have enormous influence if carried to high altitudes:

> "The kinetic energy density in the lower troposphere is of the order of 10^3 ergs cm^{-3}. If this energy were to travel upward with little attenuation and be converted into heat by friction or some other means at, say, 100 km, where the density is diminished by a factor of 10^{-6}, it would raise the air temperature to about 100,000°K."

How does the atmosphere prevent the unrestricted vertical propagation and growth of Rossby waves? The remainder of the introduction is a brief review of Charney and Drazin's theory that the waves are evanescent in the mean zonal flow. Part II treats the effects of wave, mean-flow interactions, with and without dissipation. Finally, the possibility that instability of the disturbed flow may provide the ultimate constraint on Rossby wave amplitudes is mentioned.

Consider the quasi-geostrophic pseudo potential vorticity equation, linearized on a mid latitude beta-plane (c.f. Holton 1975).

$$\left(\frac{\partial}{\partial t} + \bar{u}\frac{\partial}{\partial x}\right) q' + \frac{\partial \psi'}{\partial x}\frac{\partial \bar{q}}{\partial y} = 0 \qquad (1a)$$

where ψ' is the perturbation geostrophic stream function; q' is the perturbation potential vorticity given by

$$q' = \nabla_h^2 \psi' + \frac{1}{\rho_0}\frac{\partial}{\partial z}\left(\frac{\rho_0 f_0^2}{N^2}\frac{\partial \psi'}{\partial z}\right) \qquad (1b)$$

$\bar{u}$ is the mean flow zonal wind speed; $\partial \bar{q}/\partial y$ is the meridional derivative of the mean flow potential vorticity given by

$$\frac{\partial \bar{q}}{\partial y} = \beta - \frac{\partial^2 \bar{u}}{\partial y^2} - \frac{1}{\rho_0}\frac{\partial}{\partial z}\left(\frac{\rho_0 f_0^2}{N^2}\frac{\partial \bar{u}}{\partial z}\right) \qquad (1c)$$

and Z is a log-pressure coordinate given by

$$Z = H \ln \frac{p_{surface}}{p}$$

In what follows, we take the scale height, H, the Brunt-Väisälä frequency, N, and the zonal wind to be constant with height. The unperturbed density profile is given by

$$\rho_0 = e^{-z/H} \quad \rho_{surface}$$

Because the largest scale disturbances are forced by topography and land-sea thermal contrasts, only stationary disturbances are considered. Thus ψ' has the form

$$\psi' = \phi(z) e^{z/2H} e^{ikx} \sin\frac{\pi y}{L} \tag{1d}$$

and eqn (1) becomes

$$ik\bar{u}\left(-(k^2+\frac{\pi^2}{L^2})\phi + \frac{f_0^2}{N^2}\left(\phi_{zz} - \frac{\phi}{4H^2}\right)\right) + ik\bar{\beta}_y\phi = 0 \tag{2}$$

If lengths are scaled by twice the deformation radius

$$l \sim \frac{2NH}{f_0} = 2L_D$$

times are scaled by the intrinsic frequency of the wave

$$t \sim \frac{1}{\bar{u}k}$$

and heights are scaled by twice the scale height, then the non-dimensional form of (2) is

$$i\left(-K^2\phi + \phi_{zz}\right) + i\hat{\beta}\phi = 0 \tag{3}$$

where

$$\hat{\beta} \equiv \bar{\beta}_y \frac{4L_D^2}{\bar{u}}$$

$$K^2 \equiv 4L_D^2\left(k^2 + \frac{\pi^2}{L^2} + \frac{f_0^2}{N^2}\frac{1}{4H^2}\right)$$

The solution of (3) is

$$\phi = Ae^{inz} + Be^{-inz}$$

where the "index of refraction", n, is given by

$$n^2 = \hat{\beta} - K^2 \tag{4}$$

Thus Rossby waves can propagate vertically only through regions of sufficiently large β . $\bar{u}$ must be positive but less than a critical value $\bar{u}_c$, given (dimensionally) by

$$\bar{u}_c = \frac{\beta}{k^2 + l^2 + \frac{1}{4H^2}}$$

Charney and Drazin find that for an azimuthal wavenumber 2 disturbance u_c is approximately 38 m s^{-1}, a value generally exceeded in the winter upper stratosphere. In the summer, the mean flow is easterly (Figure 1) and the waves are again trapped. A more detailed treatment of the linear problem is

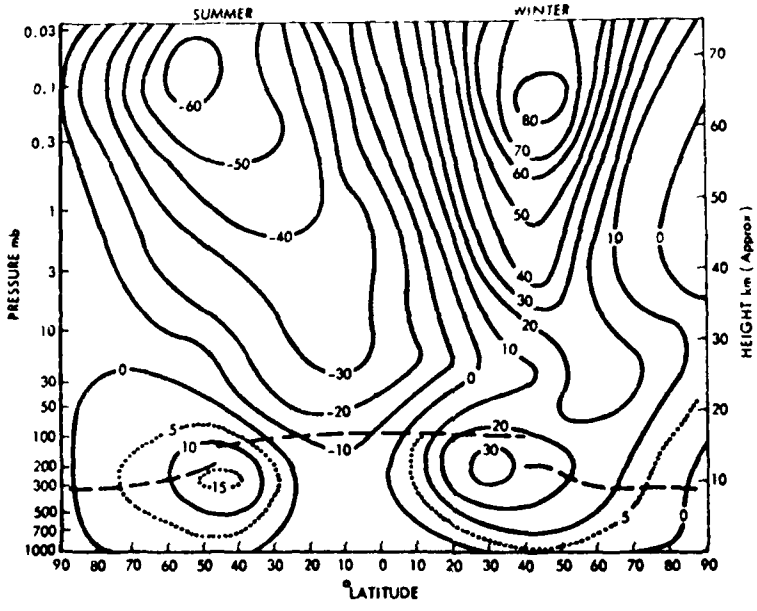

Schematic latitude-height section of the mean zonal wind (m s^{-1}) at the solstices

Figure 1. From Holton (1975).

given by Matsuno (1970). Including the effects of the observed horizontal and vertical shear of the zonal flow in a numerical calculation with spherical geometry, he finds that planetary waves do indeed become vertically evanescent in the winter stratosphere, and are refracted toward the zero wind line in the tropics.

Thus, during winter and summer linear theory provides for the vertical trapping of Rossby waves, and the absence of a terrestrial corona. But near the equinoxes weak westerlies are observed in the stratosphere, which should permit planetary waves to propagate to high levels. Charney and Drazin suggest

> "If large quantities of energy were actually to penetrate into the rarified upper atmosphere, strong non-linear interactions could occur which might modify the upper atmosphere wind and temperature structure in such a way as to insulate it against further energy flux."

The remainder of this report will consider this possibility.

II. Wave Mean-Flow Interactions

A. Mean flow equations

In the presence of wave transcience or dissipation, small amplitude waves can induce $O(a^2)$ modifications in the zonally averaged flow. On a beta-plane the equations for the second order mean flow are (c.f. Takahashi and Uryu, 1981):

$$\frac{\partial \bar{u}}{\partial t} - f_0 \tilde{v} = \frac{\partial M}{\partial y} \qquad \left(M = \overline{\psi'_x \psi'_y}\right) \tag{a}$$

$$\tilde{u} = -\frac{\partial \tilde{\psi}}{\partial y} \qquad \left(B = \overline{\psi'_x \psi'_z}\right) \tag{b}$$

(5)

$$\frac{\partial}{\partial t}\left(\frac{\partial \tilde{\psi}}{\partial z}\right) + \frac{N^2}{f_0}\tilde{w} = -\alpha \frac{\partial \tilde{\psi}}{\partial z} - \frac{\partial E}{\partial y} \tag{c}$$

$$\frac{\partial}{\partial y}(\rho_0 \tilde{v}) + \frac{\partial}{\partial z}(\rho_0 \tilde{w}) = 0 \tag{d}$$

where $\bar{(\ )}$ indicates a zonal average and $\tilde{(\ )}$ denotes second order, zonally averaged quantities α is a Newtonian cooling coefficient (discussed further below).

Only waves with no cross-channel phase variation will be considered, so M, the wave Reynold's stress is identically zero. Thus, all changes in the mean flow result either from dissipation or from the wave heat flux, B. In the absence of dissipation ($\alpha = 0$) equations (5) yield a single equation for the mean flow acceleration in terms of B. As above N^2 and H are assumed constant.

$$\tilde{u}_{tyy} + \frac{f_0^2}{N^2} e^{z/H} \frac{\partial}{\partial z}\left(e^{-z/H} \tilde{u}_{tz}\right) = e^{z/H} \frac{f_0^2}{N^2} \frac{\partial}{\partial z}\left(e^{-z/H} B_{yy}\right) \tag{6}$$

Note that the L.H.S. of (6) is simply $-\tilde{\xi}_{yt}$.

If the waves have the structure described by eqn (1d), B becomes

$$B = -e^{z/H} k\, \mathrm{Im}\left(\phi \phi^*_z\right) \sin^2 \frac{\pi y}{L}$$

and (6) becomes

$$\tilde{u}_{tyy} + \frac{f_0^2}{N^2} e^{z/H} \frac{\partial}{\partial z}\left(e^{-z/H} \tilde{u}_{tz}\right) = -e^{z/H} \frac{f_0^2}{N^2} k\, \mathrm{Im}\left(\phi \phi^*_{zz}\right)\left(\sin^2 \frac{\pi y}{L}\right)_{yy} \tag{7}$$

The lateral boundary conditions for the beta channel are that V must vanish at y = o and y = L. From the first of equations (5), this requires that u_t so vanish at the lateral boundaries. Thus, u_t can be expanded in a series of odd sine modes across the channel. But only the first of these modes will influence the propagation of a wave with $\sin \frac{\pi y}{L}$ meridional structure, and therefore the remaining components may be neglected. This is permissible because only the interaction of a single disturbance mode with the mean flow is being considered. Projecting eqn (7) onto sin and employing the same scaling as in part I yields

$$-\frac{\pi^2}{L^2}\tilde{u}_t + e^{2z}\frac{\partial}{\partial z}\left(e^{-2z}\tilde{u}_{tz}\right) = e^{2z}\frac{2}{3}\frac{\pi^2}{L^2}k\,\mathrm{Im}\left(\phi\phi^*_{tz}\right) = -\tilde{F}_{yt} \tag{8}$$

Here all quantities are non-dimensional and $\tilde{u}$ and $\tilde{F}_y$ now represent the $\sin \frac{\pi y}{L}$ components of those quantities.

In order to determine the response of the mean flow to various configurations of wave forcing, it is useful to consider the Green function for eqn (8).
Let

$$\tilde{u}_t = a e^{z}$$

and

$$\tilde{F}(z) = \frac{2}{3}\frac{\pi^2}{L^2}k\,\mathrm{Im}\left(\phi\phi^*_{zt}\right)$$

Then (8) becomes

$$a_{zz} - \left(1 + \frac{\pi^2}{L^2}\right)a = e^{z}\tilde{F}(z) = -e^{-z}\tilde{F}_{yT} \tag{9}$$

For an infinitely deep atmosphere the boundary conditions for (9) are that a be bounded at $z = \pm\infty$. Inclusion of the correct boundary condition at the ground contributes terms which decay exponentially with height. The simple Green function for a is

$$G(z,z_o) = -\frac{1}{2\nu} \times \begin{cases} e^{\nu(z-z_o)} & z_o > z \\ e^{\nu(z_o-z)} & z > z_o \end{cases}$$

where

$$\nu^2 = 1 + \frac{\pi^2}{L^2}$$

Now $\tilde{u}_t$ can be written

$$\tilde{u}_t = -\frac{e^{z}}{2\nu}\left[\int_{z}^{\infty}\tilde{F}(z_o)e^{z_o}e^{\nu(z-z_o)}\,dz_o + \int_{-\infty}^{z}\tilde{F}(z_o)e^{z_o}e^{\nu(z_o-z)}\,dz_o\right] \tag{10}$$

B. Effects on the index of refraction

Second order changes in the index of refraction (eqn(4)) are given by

$$\tilde{n}_t^2 = \tilde{q}_{yt} - \hat{\beta}\tilde{u}_t \tag{11}$$

It appears plausible that for some range of parameters a wave front could reduce n^2 to zero, resulting in the reflection of the following wave train. However, it turns out that wave fronts generally act to increase n^2, and can decrease n^2 only in thin layers.

Consider a layer between z_t and z_B in which the wave forcing is constant. For the leading edge of a train or packet of vertically propagating Rossby waves, $\tilde{q}_{yt}$ will be positive. Outside of the forced region $\tilde{q}_{yt}$ vanishes and $\tilde{u}_t$ is negative, therefore $\tilde{n}_t^2$ is positive.

Equation (1) gives, for $z_1 > z > z_B$,

$$\tilde{u}_t = -\mathcal{F}_0 e^{2z} \frac{L^2}{\pi^2}\left[1 - \frac{1}{2\nu}\left((\nu+1)e^{(1-\nu)(z_T - z)} - (\nu-1)e^{(1+\nu)(z_B - z)}\right)\right] \tag{12}$$

where $\mathcal{F}_0$ is the constant wave forcing in the layer. If z is in the middle of a thick region of forcing, or if the forcing varies very slowly with height, the last 2 terms become small and

$$\tilde{u}_t \approx -\mathcal{F}_0 e^{2z}\frac{L^2}{\pi^2}$$

Then eqn (11) gives

$$\tilde{n}_t^2 = \mathcal{F}_0 e^{2z}\left(\hat{\beta}\frac{L^2}{\pi^2} - 1\right) \tag{13}$$

In this case the refractive index must increase because for vertically propagating waves, $\hat{\beta}$ is greater than $\frac{\pi^2}{L^2}$.

It is clear from eqn (12) that a decreasing index of refraction is most likely to be found at the top of a deep layer of wave forcing. In this case

$$\tilde{n}_t^2 \approx \mathcal{F}_0 e^{2z}\left[\hat{\beta}\frac{L^2}{\pi^2}\left(1 - \frac{\nu+1}{2\nu}\right) - 1\right]$$

The refractive index will decrease only if

$$\hat{\beta} < \frac{\pi^2}{L^2}\frac{2\nu}{\nu-1}$$

The decrease occurs within a layer with depth of order $1/1-\nu$. Elsewhere, the index of refraction will increase. Even if n^2 does become negative in some region, wave tunneling will permit the propagation of some energy. Thus it seems highly unlikely that a single wave interacting with the mean flow can effectively inhibit its own vertical propagation by creating its own turning point.

C. The stratospheric sudden warming

The general tendency of a vertically Rossby wave front to increase the vertical wavenumber and decrease the mean flow velocity leads to one possible constraint on the amplitudes of vertically propagating waves. If u is reduced to nearly zero, the vertical wavelength will become very short, and dissipation will become important. Critical layer absorption is an essential component of Matsuno's (1971) theory of the sudden warming. The absorption of a wave over a thin layer is accompanied by strong heating in high latitudes and cooling in low latitudes below the critical layer, and deceleration or reversal of the zonal wind above the critical layer.

The sudden warming can be viewed as a backup for the linear trapping of Rossby waves. In mid-winter a disturbance large enough to non-linearly penetrate the zonal jet will grow with height until it destroys the westerly jet, and prevents its own further propagation. Similarly, weak westerlies in late winter permit propagation to high altitudes, and indeed the transition from winter westerlies to summer easterlies in the stratosphere is frequently effected by a "final warming" as opposed to a gradual transition (Holton, 1975).

Second order theory can provide a rough estimate of the disturbance amplitude required to reduce the zonal wind speed to zero. A slowly varying packet of linear waves will propagate vertically with group velocity C_g

$$C_g = \frac{2n}{\beta} \tag{14}$$

For waves varying slowly in the vertical the wave forcing of the mean flow is given by

$$\bar{\mathcal{F}}(Z) = -\frac{2}{3}\frac{\pi^2}{L^2} k n \frac{\partial}{\partial Z}\left(\frac{|\varphi|^2}{2}\right) \tag{15}$$

where Z is a slow vertical variable, and the perturbation streamfunction is given by

$$\psi' = \varphi(Z,T) e^{z} e^{in\tilde{z}} e^{ikx} \sin\frac{\pi y}{L} \tag{16}$$

where T is a slow time. Then the mean flow acceleration is

$$\bar{u}_T = \frac{2}{3} k n \frac{\partial}{\partial Z}(|\varphi|^2) e^{2z}$$

$$= \frac{2}{3} k n \frac{1}{C_g}\frac{\partial}{\partial T}(|\varphi|^2) e^{2z}$$

$$= k\frac{\beta}{3} e^{2z} \frac{\partial}{\partial T}(|\varphi|^2)$$

Therefore, $\tilde{u} = \frac{k\beta}{3} |\psi'|^2$

This is essentially a result obtained by Uryu (1980). Dimensionally this gives

$$h' = \frac{f_0}{\beta} \sqrt{\frac{3\bar{u}}{\bar{q}_y}}$$

for the amplitude (in height) of a disturbance sufficient to reduce a mean zonal wind, $\bar{u}$, to zero. At 60°N, for $\bar{q}_y \approx \beta$,

$$h' = 6.6 \bar{u}^{3/2}$$

in meters.

In Labitzke's (1981) description of the January 1979 sudden warming, the largest zonal winds observed prior to the warming were about 50 m s^{-1}. From the above formula, this would permit maximum wave amplitudes of about 2,300 m, which agrees fairly well with the largest amplitudes observed for planetary wave number 1. This agreement is probably largely fortuitous, as the slowly varying approximation is not even approximately valid during a sudden warming.

D. Dissipation

In the middle atmosphere the principal mechanism for dissipation is radiative damping (Holton, 1975). Solar heating and infrared cooling tend to restore temperatures to their radiative equilibrium values in times that are of the same order as advective time scales. The Newtonian cooling approximation is standard, in which it is assumed that the relaxation rate of a temperature perturbation does not depend on the size of that perturbation. Then

$$\frac{\partial T'}{\partial t} = \alpha (T_0 - T')$$

where T_0 is the temperature in radiative equilibrium, α depends on the concentration of radiatively active molecules (principally CO_2 and O_3), the pressure and the background temperature in a complicated way. Dickinson (1973) gives estimates of α for altitudes between 30 and 70 km based on a detailed radiative transfer calculation. His values correspond to damping times of greater than 15 days at 30 km and 70 km decreasing to less than 5 days at 50 km.

Blake and Lindzen (1973) suggest photochemical effects may increase α substantially. According to their chemical model the equilibrium concentration of ozone is temperature sensitive - ozone concentrations decrease with increasing temperature. The absorption of solar energy by ozone is the principal source of heat in the middle-atmosphere. If the temperature increases, the concentration of ozone decreases, and the absorption of solar energy likewise decreases, and vice versa. Blake and Lindzen find that this photochemical acceleration of radiative damping reduces damping times to about 5 days at 35 km, and to less than 25 days at 50 km. Of course, this effect does not operate in the polar night.

First, we consider the effect of radiative damping on steady linear waves. Using the same scaling as in part I, eqn (3) becomes

$$\epsilon(-K^2\phi + \phi_{zz}) + \epsilon\hat{\beta}\phi + \alpha(\phi_{zz} - \phi) = 0 \tag{17}$$

where α is the radiative damping time now scaled by $\bar{u}k$.

This has solutions the same as those in part I, but now the index of refraction is complex.

$$m^2 = \frac{\hat{\beta} - K^2 + i\alpha}{1 - i\alpha} \tag{18}$$

M has real and imaginary parts

$$m_R = \frac{1}{\sqrt{1+\alpha^2}}\left(n_0^4(1+\alpha^2) + \alpha^4\right)^{\frac{1}{4}} \cos\theta$$

$$m_I = \text{"} \quad \text{"} \quad \text{"} \quad \sin\theta \tag{19}$$

where

$$\theta = \frac{1}{2}\tan^{-1}\left(\frac{\alpha(n_0^2+1)}{n_0^2 - \alpha^2}\right)$$

and

$$n_0^2 = \hat{\beta} - K^2$$

The most striking characteristic of Newtonian cooling is that it damps only the baroclinic portion of the wave potential vorticity, therefore it is sensitive to the vertical wavenumber of the disturbance. Generally an increase in the real vertical wavenumber will lead to an increase in M_I and a decrease in the damping height of the disturbance.

If the amplitude of a wave is increasing with height, i.e., if $M_I < 1$, it is plausible that the action of the wave on the mean flow could increase M_I to a value greater than 1, at which point the wave would cease to grow with height. The remainder of this section explores this possibility.

We now consider the steady state interaction of a slowly varying, vertically propagating wave train with the second order wave induced mean flow. Let

$$\phi = \varphi(Z)\, e^{imz}$$

where

$$\varphi = O(a)$$

and

$$Z = a^2 z$$

If we include second order modifications of the mean flow in the linear vorticity equation, but neglect all interactions with other waves, we obtain the $O(a^3)$ equation

$$\mathcal{C}_z = \frac{\nu \mathcal{C}\left(\tilde{\xi}_y - (K^2+m^2)\tilde{u}\right)}{2m(1-i\alpha)} \tag{20}$$

In order to integrate this equation, it is necessary to find the second order changes in the mean zonal wind and potential vorticity, gradient induced by steady dissipating Rossby waves. With the exception that Ekman damping at the surface is included here and Rayleigh friction is not, this treatment follows closely that of Takahashi and Uryu.

The appropriate boundary condition at the surface for the mean flow equations (eqn (5)) is that

$$\tilde{W} = \frac{\partial}{\partial y}\overline{v'h'} + \tilde{W}_E \quad \text{at} \quad z=0$$

where h' is the topography that forces the disturbance and $\tilde{W}_E$ is the Ekman vertical velocity found at the top of the Ekman layer which is taken to be at z = o. $\tilde{W}_E$ is given by

$$\tilde{W}_E = -\tilde{u}_y D_E$$

where D_E is the depth of the Ekman layer. Combining these two equations with eqn (5c) gives for the bottom boundary condition

$$\frac{f}{N^2}\left(\alpha\frac{\partial\tilde{u}}{\partial z} - B_{yy}\right) = \frac{\partial^2}{\partial y^2}\left(\overline{v'h'}\right) - \tilde{u}_{yy}D_E \quad \text{at } z=0 \tag{21}$$

Non-dimensionalizing as before yields

$$\alpha\tilde{u}_z - B_{yy} = \left(\overline{v'h'}\right)_{yy} - E\tilde{u}_{yy} \tag{22}$$

at z = o

where $h' = h' \frac{2H\bar{u}k}{f}$

and $D_e = 2EH\frac{\bar{u}k}{f}$

Equations (5) may be combined for non-zero α and steady state to yield an equation relating the induced zonal wind to the wave forcing

$$\alpha\left(\tilde{u}_{zz} - \frac{\tilde{u}_z}{H}\right) = B_{yyz} - \frac{B_{yz}}{H}$$

Now

$$B = \overline{\psi_x'\psi_z'} = -ke^{z/H}\,\mathrm{Im}\left(\phi\phi_z^*\right)$$

Therefore

$$\alpha\left(\tilde{u}_{zz} - \frac{\tilde{u}_z}{H}\right) = -ke^{z/H}\,\mathrm{Im}\left(\phi\phi_{zz}^*\right)_{yy}$$

Non-dimensionalizing and considering only the sin $\frac{\pi y}{L}$ component of $\tilde{u}$ yields

$$\alpha(\tilde{u}_{zz} - 2\tilde{u}_z) = \frac{2}{3}\frac{\pi^2}{L^2} k e^{2z} \mathrm{Im}(\phi\phi^*_{zz}) \tag{23}$$

with bottom boundary condition

$$\alpha\tilde{u}_z + E\tilde{u}_{yy} = \overline{(v'h')}_{yy} + \frac{2}{3}\frac{\pi^2}{L^2} k e^{2z} \mathrm{Im}(\phi\phi^*_z) \tag{24}$$

at $z = o$

For a slowly varying, steady, dissipating wave, to leading order

$$\mathrm{Im}(\phi\phi^*_z) = -|\phi|^2 e^{2(1-m_I)z} m_R$$

$$\mathrm{Im}(\phi\phi^*_{zz}) = |\phi|^2 e^{2(1-m_I)z} 2 m_I m_R$$

So eqns (23) and (24) become

$$\tilde{u}_{zz} - 2\tilde{u}_z = \frac{k}{\alpha} m_R m_I \frac{4}{3}\frac{\pi^2}{L^2}|\phi|^2 e^{2(1-m_I)z}$$

and

$$\alpha\tilde{u}_z + \frac{\pi^2}{L^2} E\tilde{u} = \overline{(v'h')}_{yy} - \frac{2}{3}\frac{\pi^2}{L^2} m_R k |\phi|^2 \tag{25}$$

at $z = o$

The boundary condition on the wave solution is required to determine the correlation V'H'. The linearized thermodynamic energy equation gives for W', the perturbation vertical velocity,

$$W' = -\frac{g}{N^2}(\alpha\psi'_z + \bar{u} i k \psi'_z)$$

At the surface

$$W' = ik\bar{u}h' - K_H^2 \psi' 0e$$

where

$$K_H^2 = k^2 + \frac{\pi^2}{L^2}$$

So the non-dimensional surface boundary condition for ψ' is

$$ikh' - K_H^2 E\psi' = -\psi'_z(\alpha + i)$$

and for ϕ,

$$ikh' - K_H^2 E\phi = -\phi(1 + im)(\alpha + i)$$

So at $z = o$

$$\phi = \frac{-ikh'}{(1+im)(\alpha+i) + K_H^2 E}$$

Then $\overline{V'H'}$ is given by

$$\overline{V'H'} = \overline{ik\phi[-i\phi(-(H+m)(\alpha+\lambda)+K_H^2 E)]}$$

$$= Re[ik(-i((1-im_R-m_I)\alpha-\lambda)+K_H^2 E))]|\phi(0)|^2$$

$$= k|\phi(0)|^2((1-m_I)\alpha-m_R+K_H^2 E)$$

And

$$(\overline{V'H'})_{ij} = -\frac{2}{3}\frac{\pi^2}{L^2}k|\phi(0)|^2((1-m_I)\alpha-m_R+K_H^2 E)$$

Then the surface boundary condition for $\tilde{u}$ is

$$\alpha\tilde{u}_z - \frac{\pi^2}{L^2}E\tilde{u} = -\frac{2}{3}\frac{\pi^2}{L^2}k|\phi(0)|^2 \times((1-m_I)\alpha+K_H^2 E) \quad (26)$$

at $z = 0$

If, as before, we write

$$\tilde{u} = Ve^{\tau}$$

the Green function for equations (25) and (26) satisfies

$$G_{\tau\tau} + G = \delta(\tau-\tau_0)$$

at $z = 0$

$$G_\tau + G(1-b) = 0$$

where

$$b = \frac{E}{\alpha}\frac{\pi^2}{L^2}$$

The solution is

$$G(\tau,\tau_0) = \begin{cases} -\frac{e}{2}e^{-\tau_0}(e^{\tau}+\frac{2-b}{b}e^{-\tau}) & \tau<\tau_0 \\ -\frac{e}{2}e^{-\tau}(e^{\tau_0}+\frac{2-b}{b}e^{-\tau_0}) & \tau>\tau_0 \end{cases}$$

Then u is given by

$$\tilde{u} = -\frac{1}{2}\left\{\int_{\tau}^{\infty}(e^{2\tau}+\frac{2-b}{b})e^{-2m_I\tau_0}\mathcal{F}(\tau_0)d\tau_0 + \int_0^{\tau}(e^{2\tau_0}+\frac{(2-b)}{b}e^{-2m_I\tau_0})\mathcal{F}(\tau_0)d\tau_0\right\} + \tilde{u}_B \quad (27)$$

Where

$$\mathcal{F}(\tau) = \frac{k}{\alpha}m_R m_I \frac{4\pi^2}{3L^2}|\phi(\tau)|^2$$

and $\tilde{u}_B$, the mean flow forced from the lower boundary is

$$\tilde{u}_B = \frac{1}{b}\frac{2}{3}\frac{\pi^2}{L^2}k|\phi(0)|^2((1-m_I)\alpha+K_H^2 E)$$

(28)

From eqn (28) it is seen that the response to forcing below the forced region decays exponentially with the distance from the forcing, while, if $M_I \sim 1$, all forcing from below effects the mean flow. This is not surprising. The waves act on the mean flow by transporting heat, and the zonal wind response really arises from the integral of the thermal wind equation from the ground upwards.

If $\tilde{\mathcal{F}}(\zeta)$ is assumed to vary slowly with height, and if M_I is positive and O(1), $\tilde{u}$ can be approximated

$$\tilde{u} = -\frac{1}{2}\left\{ \frac{(e^{2\zeta} + \frac{2-b}{b})}{2m_I} e^{-2m_I\zeta} \tilde{\mathcal{F}}(\zeta) + \int^{\zeta} e^{2(1-m_I)\zeta_0} \tilde{\mathcal{F}}(\zeta_0)\, d\zeta_0 + \frac{1}{2m_I}\frac{2-b}{b}\tilde{\mathcal{F}}(0) \right\} + \tilde{u}_B \quad (29)$$

Given $\tilde{u}$, $\tilde{\phi}_y$ can be obtained,

$$\tilde{\phi}_y = -(\tilde{u}_{yy} + \tilde{u}_{\zeta\zeta} - 2\tilde{u}_\zeta)$$

and for slowly varying $\tilde{\mathcal{F}}(\zeta)$

$$\tilde{\phi}_y \approx \frac{\pi^2}{L^2}\tilde{u} - \tilde{\mathcal{F}}(\zeta) e^{2(1-m_I)\zeta} \quad (30)$$

Once again only those components of the second order quantities which project onto the meridional structure of the disturbance are retained.

Now eqn (20) can be integrated vertically together with eqns (29) and and (30). This is done numerically using a simple leapfrog scheme with a weak 3-point filter to prevent the separation of solutions at neighboring grid points. The integral in eqn (29) is estimated by the trapezoidal rule.

Standard parameter values are

$$\hat{\beta} = 2.2 \quad L = 2.93 \quad k = .179 \quad \alpha = 2.00$$

This corresponds to 60° wide beta channel centered at 60°N with a wave 1 disturbance, a background zonal flow of 27 ms^{-1}, and a radiative damping time of 275 days. This gives a small (.13) growth rate with height for the linear wave, and permits consideration of the transition from a disturbance growing slowly to one decaying slowly with height.

Figure 2 shows the behavior of the disturbance amplitude for these parameters settings and an amplitude of 1 at z = o. This corresponds to a height perturbation of 140 m. The disturbance grows slowly over many scale heights before reaching a maximum amplitude of 480 m. As shown below, the wave can be made to achieve its maximum amplitude at a lower altitude by choosing a smaller damping rate, or a larger initial amplitude, but then the validity of the slowly varying assumption is doubtful. The third order corrections to the disturbance phase are also shown.

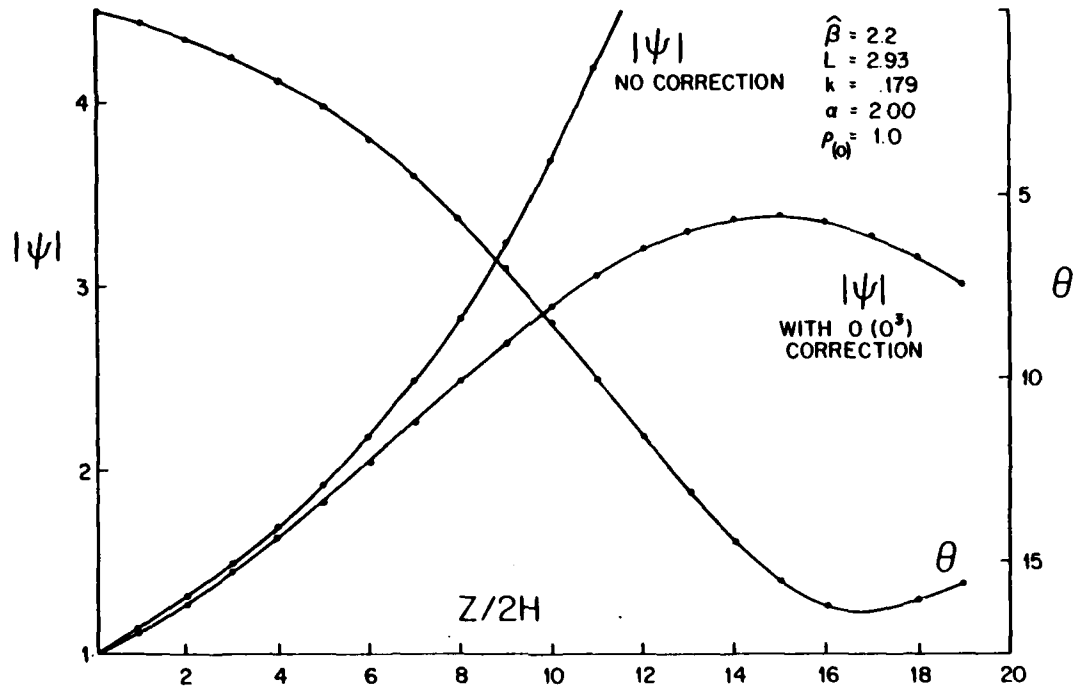

Fig. 2. Third order amplitude and phase corrections for disturbance streamfunction.

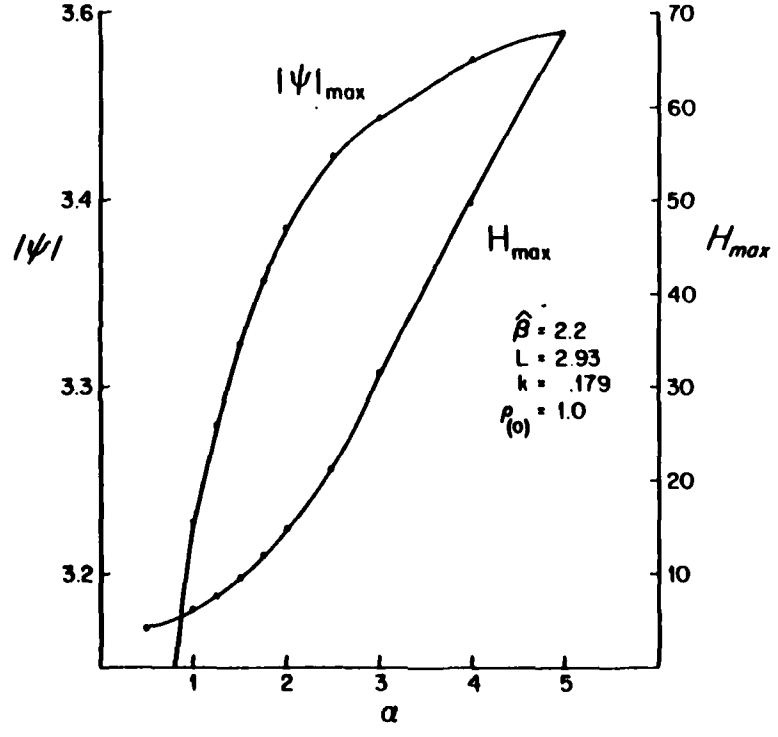

Fig. 3. Dependence of ψ_{max} and H_{max} on

The perturbation temperature is given by,

$$T = \frac{H}{R} \xi \psi'_z$$

where R is the gas constant for air. The maximum amplitude achieved in Figure 2 corresponds to a temperature perturbation of about 10^0K, and a cooling rate of 3.6^0 day^{-1}. This is of the same order as the mean infrared cooling rates calculated by Dickinson, which indicates such large disturbances may lie outside the region in which the Newtonian cooling approximation is valid.

These results and those described below were computed neglecting the forcing of the mean flow due to the lower boundary condition (i.e., neglecting $\tilde{u}_0$ and the $\frac{2-\kappa}{h}$ terms in eqn (29)). It was found that including these terms led to unrealistically low values for both the maximum amplitudes achieved by disturbances and the heights at which the maxima occurred. Neglecting these terms is equivalent to assuming the waves have very small amplitudes at the surface and grow rapidly with height before reaching a region for which the slow growth assumption is valid. Observations of van Loon et al (1973) indicate that this is indeed the case, at least for waves 1 and 2 in mid-winter. The amplitude of wave 1 increases more than an order of magnitude between the surface and 30 km (about 4 scale heights).

The computation was repeated with different parameter settings. Figure 3 shows the dependence of the maximum wave amplitude, $\tilde{\psi}_{max}$, and the height at which that maximum occurs, H_{max}, on α. While $\tilde{\psi}_{max}$ is not especially sensitive to changes in α, H_{max} increases rapidly with increasing α. This is because increasing α both decreases the growth rate of the linear wave, and decreases its effectiveness in modifying the mean flow by reducing m_R.

Figure 4 shows $\tilde{\psi}_{max}$ and H_{max} as functions of the disturbance amplitude at the lower boundary, $\psi'(0)$. For small values of $\psi'(0)$, $\tilde{\psi}_{max}$ varies slowly. Not surprisingly, it takes a greater height to achieve $\tilde{\psi}_{max}$ for smaller values of $\psi'(0)$. As $\psi'(0)$ increases, however, the maximum amplitude occurs closer to the lower boundary, and $\tilde{\psi}_{max}$ is tied more tightly to $\psi'(0)$. Of course, the slowly varying assumption breaks down in this region.

Figure 5 displays the variations of $\tilde{\psi}_{max}$ and H_{max} with L, the meridional wavelength. When L is so small that the wave is nearly evanescent, wave forcing of the mean flow is uneffective. $\tilde{\psi}_{max}$ and H_{max} are both large. As L increases, M_R increases and $\tilde{\psi}_{max}$ and H_{max} decrease. However, for large values of L the wave forcing again becomes uneffective, now because of the L dependence in eqn (25). Thus H_{max} and $\tilde{\psi}_{max}$ increase.

III. Conclusion

The largest amplitudes achieved by vertically propagating, dissipating waves in the calculations described above ($\sim$500m) are in rough agreement with the largest amplitudes observed in the atmosphere. A detailed comparison with observations would require including the effects of sphericity, variations in α and the static stability, and the vertical and horizontal shear of the zonal wind. There is the additional problem that observations of planetary wave amplitudes above 30 km are scarce.

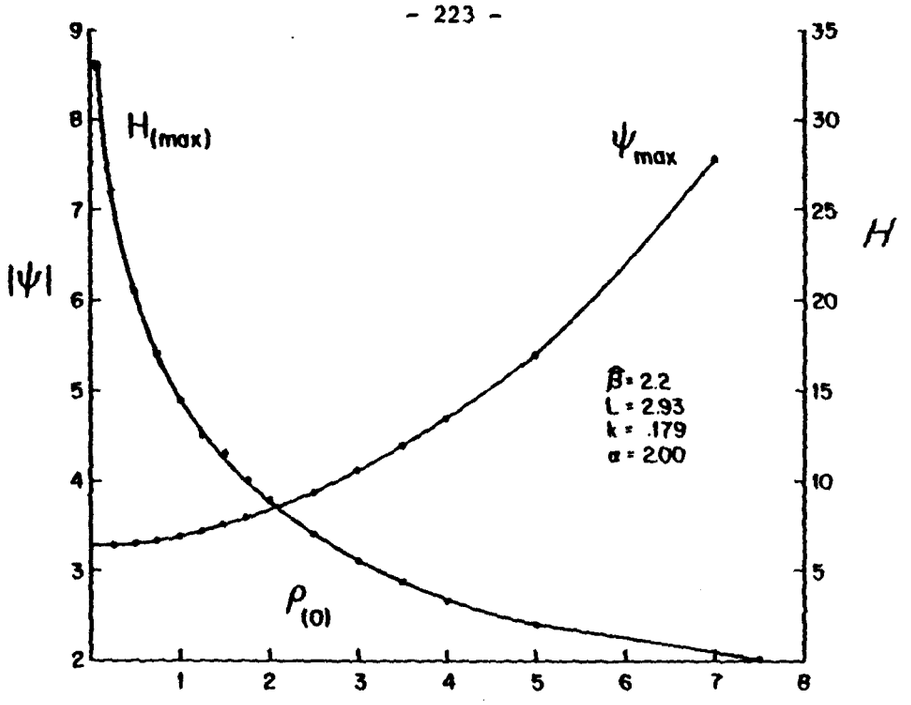

Fig. 4. Dependence of Ψ_{max} and H_{max} on $\mathcal{E}(0)$.

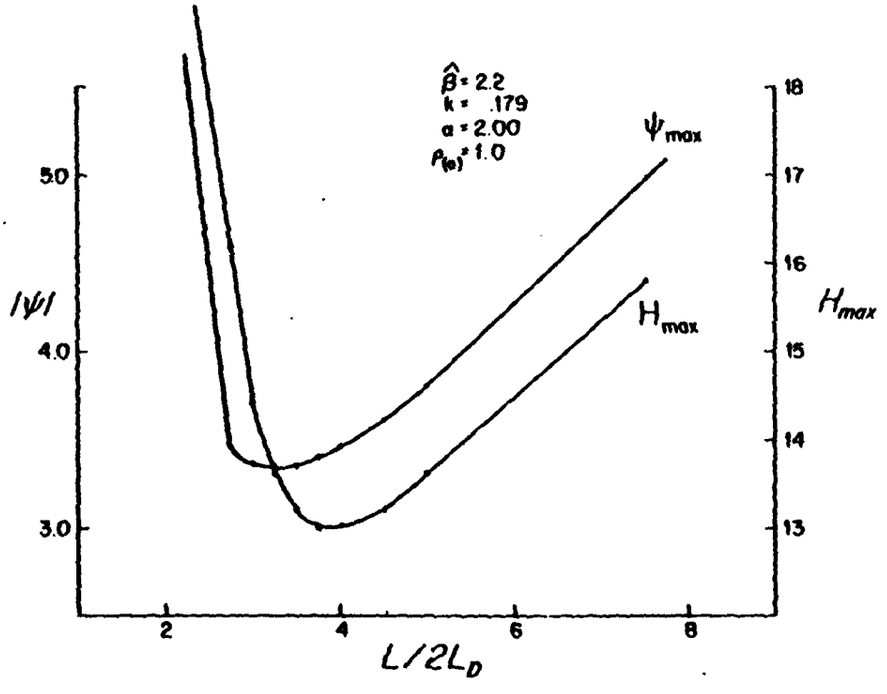

Fig. 5. Dependence of Ψ_{max} and H_{max} on L.

But the greatest drawback to the preceding discussion is the use of small amplitude theory to describe waves that actually have very large amplitudes. Lindzen and Schoeberl (1982) suggest a fully non-linear limit for the amplitudes of Rossby waves. They argue that if a wave becomes so large that the meridional gradient of potential vorticity in the perturbation exceeds the potential vorticity gradient of the mean flow, then instabilities will result which will inhibit further growth of the wave amplitude.

There are two obstacles to pursuing this suggestion. One is the difficulty of the stability analysis for this situation. The other is the absence of any observational evidence for such instability occurring in the stratosphere. However, the reduced static stability of the mesosphere (relative to the stratosphere) make it a favorable locale for the occurrence of baroclinic instability, and observations there are very limited.

It appears that most of the time, in the earth's atmosphere, Rossby wave amplitudes are limited by linear evanescence. During periods of exceptionally strong forcing wave induced critical lines can prevent the unrestricted vertical propagation and growth of waves. Wave, mean-flow interaction coupled with Newtonian damping is also a plausible mechanism for constraining Rossby wave growth. And, finally, the instability of the perturbed flow may be important, both in the mesosphere, and in situations in which dissipation is not strongly dependent on the vertical wavelength.

REFERENCES

Blake, D. and R.S. Lindzen, 1973. The effect of photochemical models on calculated equilibria and cooling rates in the stratosphere. Mon. Wea. Rev., 101, 783-802.

Charney, J.G. and P.G. Drazin, 1961. Propagation of planetary scale disturbances from the lower into the upper atmosphere. J. Geophys. Res., 66, 83-109.

Dickinson, R.E., 1973. Method of parameterization for infrared cooling between altitudes of 30 and 70 kilometers. J. Geophys. Res., 78, 4451-4457.

Holton, J.T., 1975. The dynamic meteorology of the stratosphere and mesosphere. Amer. Met. Soc., 216 pp.

Labitzke, K., 1981. The amplification of height wave 1 in January 1979: a characteristic precondition for the major warming in February. Mon. Wea. Rev., 109, 983-989.

Lindzen, R.S., and M.R. Schoeberl, 1982. A note on the limits of Rossby wave amplitudes. J. Atmos. Sci., 39, 1171-1174.

Matsuno, T., 1970. Vertical propagation of stationary planetary waves in the winter northern hemisphere. J. Atmos. Sci., 27, 871-883.

Matsuno, T., 1971. A dynamical model of the stratospheric sudden warming. J. Atmos. Sci., 28, 1479-1494.

Takahashi, M. and M. Uryu, 1981. The Eolesian-and Lagrangian - mean flows induced by stationary, dissipating planetary waves. J. Meteor. Soc. Japan, 59, 510-533.

Uryu, M., 1980. Acceleration of mean zonal flows by planetary waves. Pageoph., 118, 661-693.

van Loon, H., et al., 1973. Zonal harmonic standing waves. J. Geophys. Res., 78, 4463-4471.

THE TEMPORAL EVOLUTION OF TAYLOR COLUMNS OVER TOPOGRAPHY

Grant R. Bigg

I. INTRODUCTION

The possibility that a region of stagnant fluid may be formed over an object in a uniform rotating flow has been known of since Taylor's classical experiments (1923). Since then a number of workers have studied the mathematical basis for this closed streamline situation for different types of fluid and various parameter ranges. This investigation has recently increased in activity due to speculation by Hide (1961) that the Great Red Spot in Jupiter's atmosphere may be a "Taylor column" and also because of observational evidence from the ocean that such features may appear in the flow regime over seamounts (e.g., Meincke, 1971: Roberts, Hogg, Bishop and Flewellen, 1974; Owens and Hogg, 1980; Gould, Hendry and Huppert, 1981). It has also been suggested that some atmospheric features are created by shedding of vortices in flow over mountain chains.

Most of the work to date examines steady state situations; that is, a uniform flow in a rotating fluid is assumed to have been in existence for all time. The present report investigates the transients that appear when the flow is started from rest because any occurrence of Taylor columns in nature will naturally be accompanied by temporal variation.

The flows to be considered here are such that the free stream speed is smaller than the critical limit required for closed streamline formation. For a discussion of these limits for homogeneous and stratified fluids see Huppert (1975). The special features of the transient flow to be investigated are the way in which closed streamlines first occur after the flow is initiated and the interaction of the vortex formed over the topography with the one swept off as the flow begins.

II. VORTEX FORMATION IN HOMOGENEOUS FLUIDS

Consider the equations of motion for an inviscid, incompressible fluid on an f-plane, viz.

$$\frac{\partial \underline{q}}{\partial t} + (\underline{q}\cdot\nabla)\underline{q} + f(-v, u, 0) = -\frac{1}{\rho}\nabla p - g\underline{k} \qquad (1a)$$

$$\nabla\cdot\underline{q} = 0. \qquad (1b)$$

If it is assumed that a uniform flow of characteristic velocity $U\underline{i}$ is flowing past a topographic feature of characteristic length L and height h in a region of depth $H >> h$ then by nondimensionalizing (1) in a standard way it can be shown that for small Rossby number $\varepsilon = U/fL$ and $h = O(\varepsilon)$ the leading order equation of motion is

$$\frac{\partial \zeta^{(0)}}{\partial t} + (\underline{q}_h^{(0)}\cdot\nabla_h)(\zeta^{(0)} + \frac{h}{\varepsilon}) = 0, \qquad w^{(0)} = 0, \qquad (2)$$

where $\underline{q}_h^{(0)}$ is the zeroth order nondimensional horizontal velocity and $\zeta^{(0)}$ is the vertical component of the zeroth order relative vorticity. Note that L/U is the time constant, HU/L is the parameter associated with vertical velocity and the nondimensional pressure is $[P - \rho gH(1-z)]/\rho UfL$. Equation (2) implies that the problem reduces to two dimensions and, dropping indices,

can be written as

$$\frac{D}{Dt}\left(\zeta + \frac{h}{\varepsilon}\right) = 0. \tag{3}$$

For the details of this procedure see McCartney (1975).

Equation (3) is merely a statement of the principle of conservation of potential vorticity. It is a nonlinear time-dependent equation and as such has not been successfully examined analytically. To simplify the problem this equation was linearized, that is, if the velocity is represented by

$$\underset{\sim}{q} = U(t) + \underset{\sim}{q}',$$

where U(0) = 0 and the $t > o$ $|q'| << |U|$, then, assuming the slope for topography is not large, (3) may be written as

$$\frac{\partial \zeta'}{\partial t} + U\frac{\partial \zeta'}{\partial x} + U\frac{h_x}{\varepsilon} = 0$$

or, as $\zeta' = \nabla^2\psi$,

$$\nabla^2\psi_t + U\nabla^2\psi_x + U\frac{h_x}{\varepsilon} = 0. \tag{4}$$

Note that the total streamfunction for the flow is

$$\Phi = -U(t)y + \psi. \tag{5}$$

The steady solution to (3) is $\nabla^2\psi = -\frac{h}{\varepsilon}$ so to find the vorticity distribution for time-dependent flows let

$$\nabla^2\psi = -\frac{h}{\varepsilon} + F(x,y,t)$$

so that (4) becomes

$$F_t + U(t)F_x = 0. \tag{6}$$

The general solution to (6) is just $F = G(x - \int U(t)dt)$, G being an arbitrary function, so

$$\nabla^2\psi = \frac{1}{\varepsilon}\left[h\left(x - \int U(t)dt, y\right) - h(x,y)\right], \tag{7}$$

as $F(x,y,0) = h/\varepsilon$ due to the flow starting at rest. This equation tells us that the relative vorticity distribution consists of two discrete components -- one located over the topography and another being advected downstream with the flow. Thus the linearization of (3) predicts the presence of anticyclonic vorticity over the topographic intrusion and the generation of a cyclonic vortex downstream; it <u>does not</u> allow trapping of the free vortex. To examine this feature of the initial value problem the nonlinear equations will need to be examined (see Section III); in the remainder of this section the formation of the vortices will be studied.

Returning to our equation (4) for the streamfunction, this may be solved by Laplace transforms if U is a constant or by Fourier transforms for general U(t). The problem reduces in the latter case to inverting a complicated transform:

$$\Phi(x,y,t) = -U(t)y + \frac{1}{4\pi^2}\iint_{-\infty}^{\infty} \frac{H}{k^2+l^2}\left(1 - e^{-ikU_1(t)}\right)e^{i(kx+ly)}\,dk\,dl, \tag{8}$$

where $\hat{H}(k,l)$ is the double Fourier transform of the topography and $U_I(t)$ is the integral of U(t).

As (8) is rather intractable for topographies satisfying the small slope condition, equation (4) was further simplified by assuming that the topography was elongated in the x-direction. This means that in the region of the bump $\partial/\partial x << \partial/\partial y$. Note, however, that this condition breaks down in the far-field and possibly in the vicinity of closed streamlines. Equation (4) now becomes

$$\frac{\partial^2}{\partial y^2}(\Psi_t + U(t)\Psi_x) = -U(t)\frac{h_x}{\varepsilon} \tag{9}$$

This equation can be integrated to give

$$\Psi_t + U(t)\Psi_x = -\frac{U(t)}{\varepsilon}\int_{-\infty}^{y} d\eta \int_{-\infty}^{\eta} h_x(x,\xi)\,d\xi = I(x,y,t), \tag{10}$$

which, upon use of Fourier transforms and an integrating factor, can be reduced to

$$\Phi(x,y,t) = -U(t)y + \frac{1}{2\pi}\int_{-\infty}^{\infty} dk\, e^{ik(x - U_I(t))}\int_0^t d\tau\, \bar{I}(k,y,\tau)\, e^{ikU_I(\tau)}, \tag{11}$$

where $\bar{I}$ is the x-Fourier transform of I. Evaluating the τ integral, (11) may be written as

$$\Phi(x,y,t) = -U(t)y - \frac{i}{2\pi\varepsilon}\int_{-\infty}^{\infty} dk\, e^{ikx}\left[1 - e^{-ikU_I(t)}\right]\int_{-\infty}^{y} d\eta \int_{-\infty}^{\eta} d\xi\, \hat{H}_1(k,\xi), \tag{12}$$

where $\hat{H}_1(k,y)$ is the x-Fourier transform of the topography.

For the particular case of a Gaussian-like topography, $h = h_0 e^{-\alpha x^2 - y^2}$, $\alpha << 1$, (12) may be evaluated to give

$$\Phi(x,y,t) = -U(t)y - \frac{\sqrt{\pi} h_0 e^{-\alpha x^2}}{2\varepsilon}\left\{(y + y\,\mathrm{erf}(y) + \frac{e^{-y^2}}{\sqrt{\pi}})(1 - e^{-\alpha U_I(t)(U_I(t) + 2x)})\right\}. \tag{13}$$

In Figure 1 plots of the streamfunction given by (13) are shown for three different times with $\alpha = .1$, $h_0 = .015$, $\varepsilon = .01$ and $U = -1$. The solution tends to breakdown at the point at which closed streamlines are formed but the plots indicate clearly that the appearance of closed streamlines is a rapid phenomenon, that is, the flow regime is suddenly transformed from a situation in which the streamlines are only moderately distorted to a complicated position. This agrees with the steady state results of McCartney (1975) which suggested that closed streamlines appear from mildly distorted flows due to only small changes in the incident stream. Also, evident in the graphs is the presence of two regions of closed, or almost closed, streamlines. If the assumptions used to derive (9) were not violated in the vicinity of these regions the closed streamlines would be clearer but the trend is there. The streamlines illustrated indicate that the leftmost region is the anticyclonic vortex, while the second vortex is the cyclonic vortex.

The elongation hypothesis has therefore given an indication as to the initial development of Taylor columns in a homogeneous fluid.

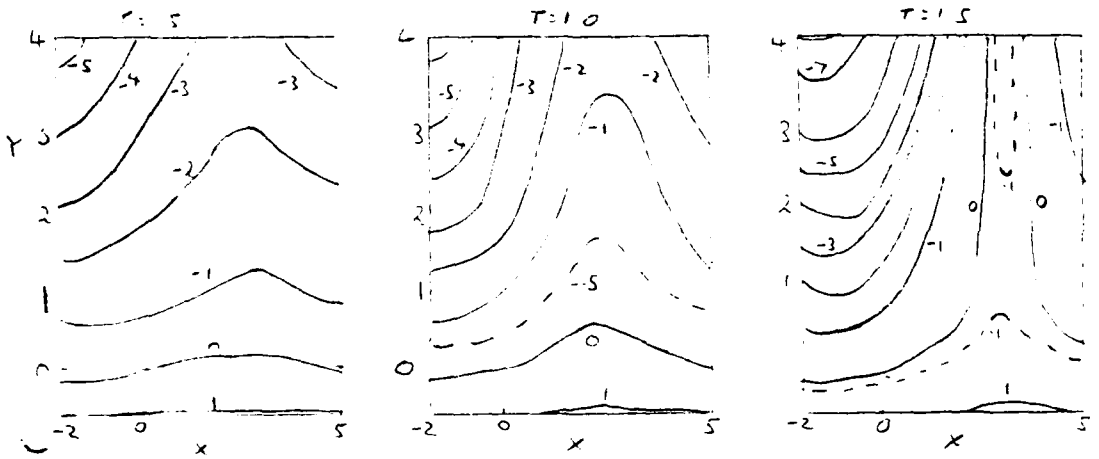

Figure 1. Streamfunction for elongated topography
(α = .1, h_o = .015, ε = .01, U = -1)

III. INTERACTION OF THE FREE AND TOPOGRAPHICALLY-TRAPPED VORTICES

In this section the interaction between the two vortices will be examined assuming that they have already formed and moved apart. The topographically-trapped vortex will be regarded as being fixed at the origin while the "free" vortex, following the implications of (7), will be assumed to be at (1,0) at t = 0. Taking the cyclonic vortex as being at (1,0), rather than an arbitrary position on the x-axis, is done because the time required for closed streamlines to appear is roughly one time unit for unit velocity, which, as t was nondimensionalized by L/U, means that the feature should be one length unit downstream by the elapsing of this time. It should be noted that the vortices are here regarded as point vortices, as a first approximation.

The velocity components of the cyclonic vortex are given by the pair of coupled equations

$$\frac{dx}{dt} = U(t) + \frac{\lambda y}{x^2+y^2} \tag{14a}$$

$$\frac{dy}{dt} = \frac{-\lambda x}{x^2+y^2} \tag{14b}$$

where λ is the strength of the vortex, given by $\iint(h(x,y)/\varepsilon)dxdy$. For $U(t)=U_o$ this system may be solved by dividing (14b) by (14a) and recognizing that the numerator and denominator of the righthand side of the resulting equation are the x and y partial derivatives respectively of

$$\psi = U_o y + \lambda \ln \sqrt{x^2+y^2}. \tag{15}$$

The equation (14b)/(14a) may then be written as

$$\frac{\partial \nu}{\partial y}\frac{dy}{dx} + \frac{\partial \nu}{\partial x} = 0, \tag{16}$$

which has the solution

$$\nu = U_0 y + \lambda \ln\sqrt{x^2+y^2} = \text{constant}. \tag{17}$$

Using the initial condition specified earlier, (17) may be simplified to give

$$x^2+y^2 = e^{-\gamma y}, \quad \gamma = 2U_0/\lambda, \tag{18}$$

which describes the path taken by the "free" point vortex. This equation was also obtained by Huppert and Bryan (1976) as the homogeneous limit of a calculation for stratified flow. They were comparing an analytic model with some numerical results and found that the paths given by (18) were closely followed by the vortices of the numerical model, except that the closed paths indicate that bound vortices should rotate about the origin while numerically there was an area in which the vortices appeared to stabilize. For most of this section the period of the paths of (18) will be investigated and also some reasons for stabilization will be discussed.

However, before this is done the paths given by (18) will be examined. Firstly, if a phase plane analysis is carried out on the system (14) it is found that at $S = (0, -\lambda/U_0)$ there is a center saddlepoint which means that any path approaching the y-axis inside of this point is closed while any path that is outside the critical curve is $2\epsilon^{-1}$. As S is a saddlepoint it is unstable and not even vortices infinitesimally close to S will be trapped there, so this simple model will not allow a free vortex to come to rest. Some typical paths are shown in Figure 2 and the variation of extremal y values with γ, for closed paths, is shown in Figure 3. Note that the negative-y turning point is increasing much faster than the positive-y extremal is decreasing.

The period of a vortex moving along a closed path will now be considered. If it can be shown that the period is large compared to the time scale of the numerical calculations of Huppert and Bryan then the validity of this simple analytic model will be seen to be better than previously suspected. However, as steady state solutions with bound stable vortices have been found (Johnson, 1978a,b) it is clear that the model is not a complete depiction of what is occurring.

The expression for the period of revolution is

$$T = 2\int_{y_{min}}^{y_{max}} \sqrt{\frac{1+(dx/dy)^2}{\left(\frac{dx}{dt}\right)^2+\left(\frac{dy}{dt}\right)^2}}\, dy, \tag{19}$$

where y_{min} and y_{max} are the two roots of the path equation $x = f(y)$. For our path this becomes

$$T = \frac{2\gamma}{U_0}\int_{y_{min}}^{y_{max}} \sqrt{\frac{e^{\gamma y}(1+4y)+3y^2+\gamma^2 e^{2\gamma y}}{(e^{\gamma y}-y^2)(\gamma^2+4e^{\gamma y}(1+\gamma y))}}\, dy. \tag{20}$$

Figure 2. PATHS OF SWEPT OFF VORTEX

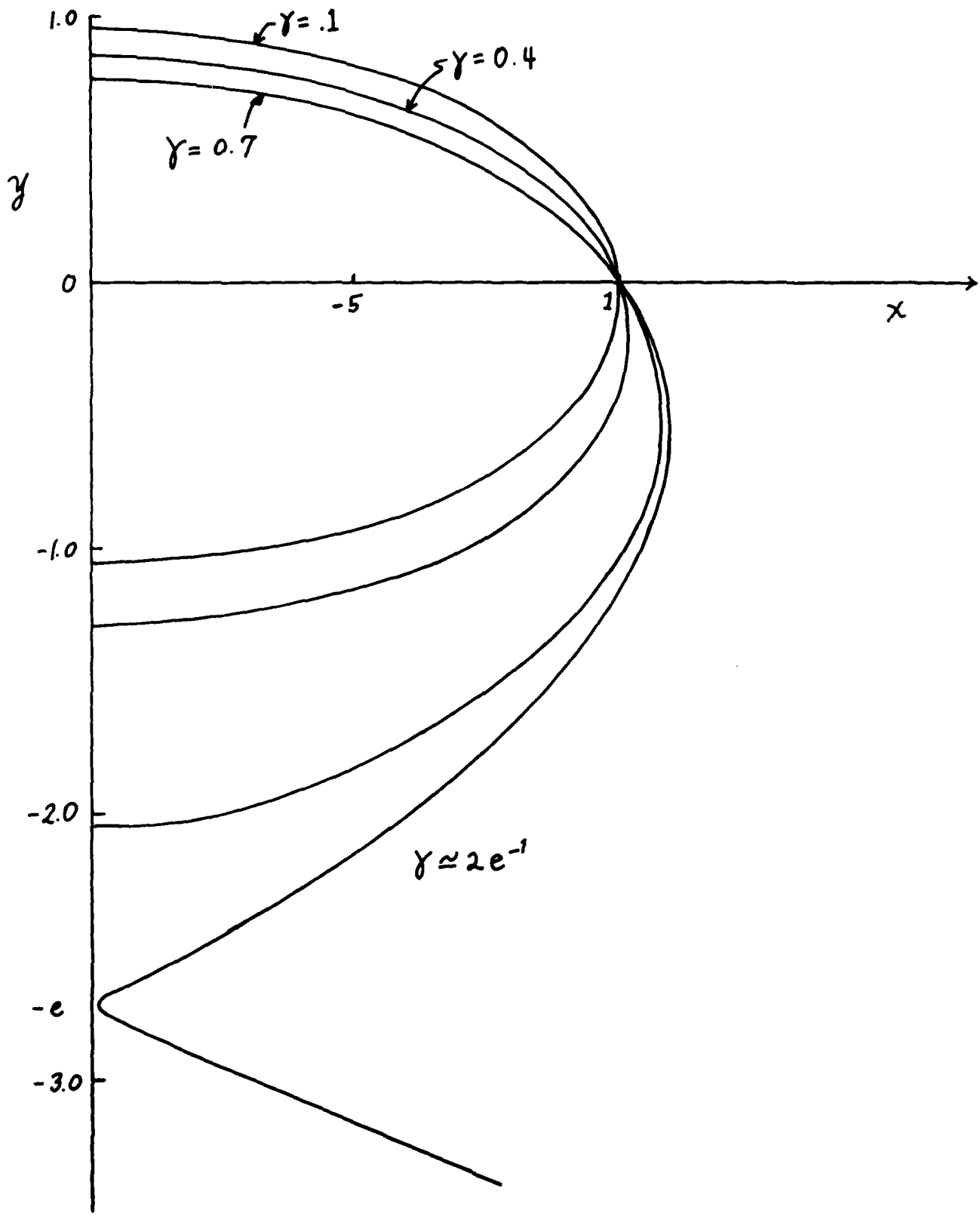

Figure 3. Extremal values for γ

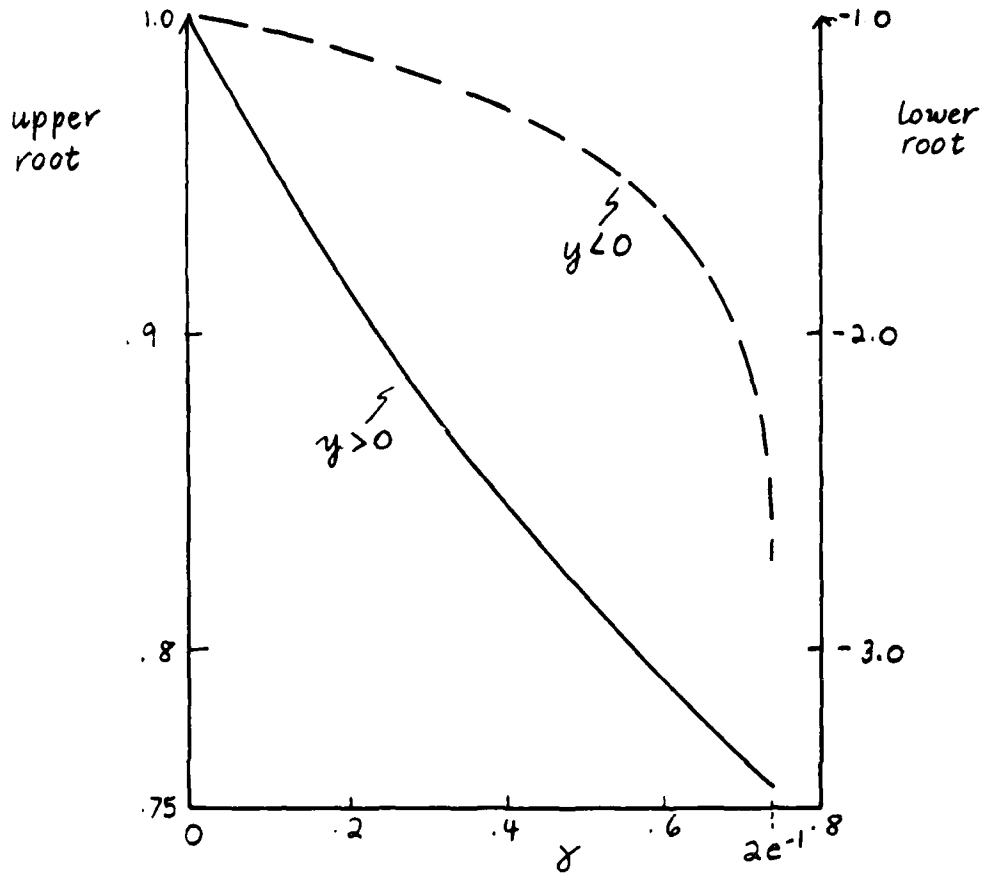

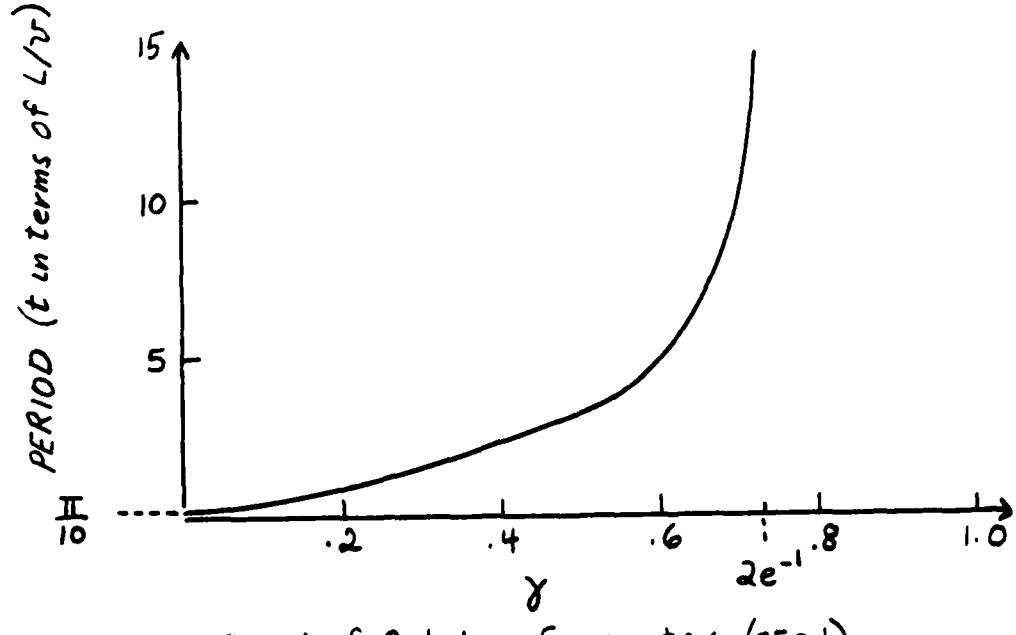

Figure 4. Period of Rotation for vortex ($v = 1$)

It can be shown that this integral has a square-root singularity at both endpoints and a Gaussian-like numerical quadrature may be able to be devised to evaluate (20) with some accuracy, but as a first approximation a truncated Simpson's rule method with several hundred intervals was employed. The results are shown in Figure 4. For the trapped vortex case considered by Huppert and Bryan which, taking stratification into account, has $\zeta \simeq 0.6$ the period predicted here is of the order of 150 days while their calculations only went for 70 days. So the period estimate gives a significantly longer time than was numerically pursued. Another encouraging fact is that the time taken to reach the stable position was about a quarter of the period predicted so at least the initial motion seems to be described by this model.

Two possible reasons for the "free" vortex to be trapped at a particular place will be presented here. From Huppert and Bryan's numerical results there appears to be some movement of the central anticyclonic vortex induced by the cyclonic vortex. It is conceivable that this interaction eventually leads to an equilibrium situation in which the two vortices take up stationary positions.

A second possibility is that as the vortices are actually of nonzero extent perhaps their finiteness can alter the nature of the stability of point S. Certainly this aspect of the problem will play a role in the solution which, considering the closeness of the two vortices, could be of major significance. A model to examine this effect will be described; it is at present incomplete but provides a basis for further work.

Consider the anticyclonic vortex to be as for the earlier discussion, that is, stationary at the origin. Let the cyclonic vortex be a circle of radius a centered at the point (1,0) initially and $(x_f(t),y_f(t))$ in general. Note that $a \ll (x_f + y_f)^{1/2}$. Now if this moving vortex is represented by a collection of point vortices then the motion of one of these vortices located at (x_p,y_p) is given by

$$\frac{dx_p}{dt} = \frac{\lambda y_p}{x_p^2+y_p^2} - \frac{\lambda(y_p-y_f)}{(x_p-x_f)^2+(y_p-y_f)^2} \tag{21a}$$

$$\frac{dy_p}{dt} = \frac{-\lambda x_p}{x_p^2+y_p^2} + \frac{\lambda(x_p-x_f)}{(x_p-x_f)^2+(y_p-y_f)^2}, \tag{21b}$$

The motion of the center of the cyclonic vortex is then given by

$$\frac{dx_f}{dt} = U(t) + \frac{\lambda y_f}{x_f^2+y_f^2} + \frac{1}{\pi a^2}\iint_{R_0} \frac{dx_p}{dt}\,dx_p\,dy_p \tag{22a}$$

$$\frac{dy_f}{dt} = \frac{-\lambda x_f}{x_f^2+y_f^2} + \frac{1}{\pi a^2}\iint_{R_0} \frac{dy_p}{dt}\,dx_p\,dy_p, \tag{22b}$$

where R_o is the circle of radius a around (x_f, y_f). Substituting (21) into (22) and simplifying it is found that

$$\frac{dx_f}{dt} = U(t) + \frac{\lambda y_f}{x_f^2 + y_f^2} + \frac{\lambda}{\pi a^2} \iint_{R_o} \frac{y_p}{x_p^2 + y_p^2} dx_p dy_p \tag{23a}$$

$$\frac{dy_f}{dt} = \frac{-\lambda x_f}{x_f^2 + y_f^2} - \frac{\lambda}{\pi a^2} \iint_{R_o} \frac{x_p}{x_p^2 + y_p^2} dx_p dy_p . \tag{23b}$$

This system of equations has not been fully investigated but should at least be solvable numerically, if not analytically.

So far, the results in this section have assumed that the stream velocity attains its maximum value immediately after the flow begins. The effect of allowing U = U(t) will now be considered.

The system (14) does not appear to have solutions which can be obtained analytically if U is a nonconstant function of time. However, some closed-path conditions can be established by considering (14) rewritten in terms of $R = [x^2 + y^2]^{1/2}$, $\tau = \lambda t$ and x:

$$\frac{dR}{d\tau} = \gamma(\tau) x \tag{24a}$$

$$\frac{dx}{d\tau} = \frac{\gamma(\tau)}{2} \pm \frac{(R - x^2)^{1/2}}{R} . \tag{24b}$$

Note that the variable sign in (24b) is positive when the vortex is in the first and second quadrants and negative elsewhere.

Firstly, consider $0 < \gamma(\tau) < \gamma_c (= 2\epsilon^{-1})$ for all $\tau > 0$ and let the vortex start at (1,0). Then as the vortex moves into the fourth quadrant, equation (24) implies that x is always smaller than the critical path x and thus R is always less than the critical path R, as long as the vortex is in this quadrant, so that the vortex remains in the vicinity of the origin. While the cyclonic vortex is in the third and second quadrants (24a) implies that $dR/d\tau < 0$ so the feature cannot escape in these quadrants. So finally consider the first quadrant. Equation (24b) implies that as the vortex enters the quadrant $dx/d\tau$ is smaller than for the critical path and as $dR/d\tau$ will also be smaller, for a given x, the path of the vortex will move towards the x-axis more sharply than the critical path. This fact, taken in conjunction with the original equations and the entrance of the vortex to the quadrant at a y-value greater than that for the critical path implies boundedness.

If we now let $\gamma(\tau) > \gamma_c$ for all $\tau > 0$ and let the vortex start at (1,0) equation (24) implies that $dR/d\tau$ and $dx/d\tau$ are greater than for the critical case so that the vortex approaches the y-axis at a y greater than the saddlepoint and escape occurs.

As a final note to this section the case of a dip, rather than a bump, on the lower surface of the fluid will be mentioned. For this situation, as $\lambda < 0$, it is found that the sense of rotation of the two vortices is reversed and any advection of the free vortex downstream occurs in the first rather than the fourth quadrants.

IV. VORTEX FORMATION IN STRATIFIED FLUIDS

Consider a flow in a region R as decribed at the beginning of Section II, with the added feature that the fluid is stratified with constant buoyancy frequency N. Then, following Huppert and Bryan (1976), the equations of motion for this system reduce to

$$\nabla_h^2 \underline{\Phi} + \frac{f^2}{N^2} \underline{\Phi}_{zz} = 0 \quad , \text{ in } R \tag{25}$$

$$\underline{\Phi}_{zz} = 0 \quad , \; z = H \tag{26}$$

$$\frac{\partial \underline{\Phi}_z}{\partial t} + \underline{q} \cdot \nabla_h (\underline{\Phi}_z + N^2 h) = 0 \quad , \; z = h \tag{27}$$

$$\nabla_h \underline{\Phi} \to -(0,1) U \qquad x \to -\infty, \tag{28}$$

being the streamfunction for the flow and U a function of time. As Huppert and Bryan found, this problem is very difficult to solve so, to simplify it, the bottom boundary condition (27) was linearized. Therefore, the streamfunction being rewritten as in (5), our equations become

$$\nabla_h^2 \Psi + \frac{f^2}{N^2} \Psi_{zz} = 0 \tag{29}$$

$$\Psi_z = 0 \; , \; z = H \tag{30}$$

$$\frac{\partial \Psi_z}{\partial t} + U \left(\frac{\partial^2 \Psi}{\partial x \partial z} + N^2 h_x \right) = 0 \; , \; z = 0 \tag{31}$$

$$\nabla \Psi \to 0 \; , \; x \to -\infty. \tag{32}$$

Using a Green's function approach to the solution of (29) - (32) it is found that

$$\Psi = \iint_{-\infty}^{\infty} G(x, y, z \; ; x', y', 0) \, \Psi(x', y', t) \, dx' dy', \tag{33}$$

where G satisfies

$$\nabla_h^2 G + \frac{f^2}{N^2} G_{zz} = \delta(r - r') \tag{34}$$

$$G_z = 0 \quad z = 0, H \tag{35}$$

$$\nabla G \to 0 \quad x \to -\infty \tag{36}$$

and Ψ satisfies

$$\Psi_t + U \Psi_x = U h_x \tag{37}$$

(see Duff and Naylor (1966), theorem 7.1.2). It can be shown that

$$G_0(x,y,z;x',y',0) = \frac{1}{2\pi H}\ln(r-r') - \frac{1}{\pi H}\sum_{n=1}^{\infty}(-1)^n K_0\left(\frac{\pi n f}{NH}(r-r')\right)\cos\left(\frac{n\pi z}{H}\right) \tag{38}$$

(see Appendix of Huppert and Bryan (1976) for similar Green's function determination), and (37) may be solved by transform methods to give

$$\psi(x,y,t) = \frac{1}{4\pi^2}\int\int_{-\infty}^{\infty} \hat{h}(k,l)\left(1-e^{-ik U_t(t)}\right) e^{i(kx+ly)}\,dk\,dl, \tag{39}$$

using the notation of Section II.

The solution to (29) - (32) will be examined for Gaussian topography $h = h_0 e^{-x^2-y^2}$, where

$$\hat{h} = \pi h_0 e^{-(l^2+k^2)/4} \tag{40}$$

and, from (39)

$$\psi(x,y,t) = h_0 e^{-y^2}\left(e^{-x^2} - e^{-(x-U_t(t))^2}\right). \tag{41}$$

On $z = 0$ the sum in (38) can be simplified, as

$$\sum_{n=1}^{\infty}(-1)^n K_0(X) = \frac{1}{2}\left(\gamma + \ln(X/4\pi)\right) + \pi\sum_{n=1}^{\infty}\left(\frac{1}{\left[X^2+(2n-1)^2\pi^2\right]^{1/2}} - \frac{1}{2\pi n}\right) \tag{42}$$

(Gradshteyn and Ryzhik (1980, 8.526.2)) where γ is Euler's constant, so the streamfunction on this surface can be found from (33). This integral cannot be evaluated analytically but if $\mu^2 = f^2/(NH)^2$ is small an approximate solution valid near the origin for limited time can be obtained. An indication of the method of solution is given in the Appendix; here plots of the streamfunction at three times are shown in Figure 5.

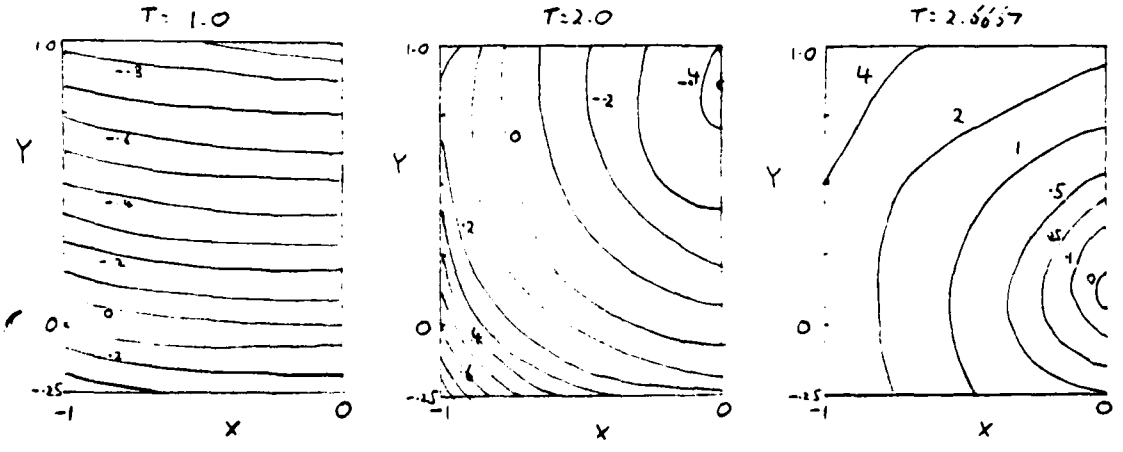

Figure 5. Streamfunction for stratified flow on z = 0 (μ =.5, h_0 = .1, H = 1, U = 1). (Note symmetry about y-axis).

It will be noted that, as for the homogeneous fluid considered in Section II, the transition from a mildly distorted mean flow to closed streamlines is rapid. Also, an asymptotic drift towards the origin is detectable in the motion of the topographically trapped vortex. Note that the smallness of the region of validity of the approximation means that the free vortex cannot be seen; also for $t \gtrsim 4$ the solution breaks down over the entire field. However, even though the approximation is extreme, interesting aspects of the flow are still discernible.

V. FURTHER WORK AND ACKNOWLEDGMENTS

The investigation into the interaction of the two vortices produced by the initiation of flow seems the most promising of the topics considered in this report. The evaluation of the period integral (20) poses some interesting work in numerical analysis and the follow-up of the problem represented by equation (23) could lead to valuable insights into the physics of the trapping of the cyclonic vortex.

I would like to thank the many people involved in this year's program, firstly for selecting me and secondly for assisting me in having an interesting and rewarding summer. In particular I would like to thank Joe Keller and Roger Hughes for some interesting discussions on the material contained in this report, and the GFD Fellows for being such a great bunch. I also wish to acknowledge the financial assistance of the University of Adelaide with travel arrangements.

APPENDIX: STRATIFIED FLOW STREAMFUNCTION

From the various expressions in Section IV the integral we need to evaluate is

$$\psi = -\frac{h_0}{\pi H}\iint_{-\infty}^{\infty} d\xi d\eta\, e^{r'^2}\left(1 - e^{-U_t^2 + 2\xi U_t}\right)\left(\frac{\xi}{2} + \frac{1}{2}\ln\left(\pi\frac{\mu}{4}\right) + \sum_{j=1}^{\infty}\left\{\frac{1}{\left[\mu^2(r-r')^2 + (2j-1)^2\right]^{1/2}} - \frac{1}{2j}\right\}\right)_{,\xi} \quad (A1)$$

where $r'^2 = \xi^2 + \eta^2$ and $r^2 = x^2 + y^2$. Most of the components of this expression may be found fairly easily, at least with integral tables, but the terms involving the inverse square root under the summation are more complex. This factor was simplified by assuming that $\mu^2 = f^2/(NH)^2$ was small and that because of the rapid decay of the integrand away from $r' = 0$ then for small r the approximation

$$\left[a^2 + \mu^2(r-r')^2\right]^{-1/2} \simeq \frac{1}{a}\left[1 - \frac{1}{2}\left(\frac{\mu}{a}\right)^2(r-r')^2 + \ldots\right] \quad (A2)$$

could be made. This substitution enables the integrals in (A1) to be evaluated but effectively destroys the radiation condition, leading to the breakdown of the solution, even in the region of small r, after a short period of time. This is clearly seen in the final expression,

$$\psi \simeq \frac{7h_0\mu^2 S(3)}{16H}\left[-\frac{3}{4} - \frac{U_t}{4} + \frac{3}{4}e^{U_t^2} - \frac{\sinh(U_t^2/2)}{U_t^2} + \frac{1}{2}\cosh(U_t^2/2)\right. \quad (A3)$$

$$\left. - \sqrt{\pi}\left(1 - \left\{(1+U_t^2)I_0(U_t^2/2) + U_t^2 I_1(U_t^2/2)\right\}e^{-U_t^2/2}\right)r\right]$$

where $\zeta(x)$ is the Riemann zeta function, due to the presence of modified Bessel functions of the first kind.

REFERENCES

Duff, G.F.D., and D. Naylor, 1966. Differential equations of applied mathematics. Wiley, New York.

Gould, W. J., R. Hendry and H. E. Huppert, 1981. An abyssal topographic experiment. Deep-Sea Res., 28A, 409-440.

Gradshteyn, I. S. and I. M. Ryzhik, 1980. Table of integrals, series and products. Academic Press, London.

Hide, R., 1961. Origin of Jupiter's Great Red Spot. Nature, 190, 895-896.

Huppert, H. E., 1975. Some remarks on the initiation of inertial Taylor columns. J. Fluid Mech., 67, 397-412.

Huppert, H. E. and K. Bryan, 1976. Topographically generated eddies. Deep-Sea Res., 23, 655-679.

Johnson, E. R., 1978a. Trapped vortices in rotating flow. J. Fluid Mech., 86, 209-224.

Johnson, E. R., 1978b. Topographically bound vortices. Geophys. Astrophys. Fluid Dyn., 11, 61-71.

McCartney, M. S., 1975. Inertial Taylor columns on a beta plane. J. Fluid Mech., 68, 71-95.

Meincke, J., 1971. Observation of an anticyclonic vortex trapped above a seamount. J. Geophys. Res., 76, 7432-7440.

Owens, W. B. and N. G. Hogg, 1980. Oceanic observations of stratified Taylor columns near a bump. Deep-Sea Res., 27A, 1029-1045.

Roberts, D. G., N. G. Hogg, D. G. Bishop and C. G. Flewellen, 1974. Sediment distribution around moated seamounts in the Rockall Trough. Deep-Sea Res., 21, 175-184.

Taylor, G. I., 1923. Experiments on the motion of solid bodies in rotating fluids. Proc. Roy. Soc., Ser. A, 106, 213-218.

EQUATORIAL WAVE RESPONSE DUE TO OSCILLATING WIND STRESS

by

Masaaki Takahashi

ABSTRACT

We discuss equatorial wave response due to oscillating wind stresses whose meridional functional forms are very simple. The model is a single layer model and meridional boundaries are included. The dissipations are included as the forms of Rayleigh friction and Newtonian cooling with same relaxation time.

In the case of symmetric meridional forcing $G = e^{-y^2/4 - i\sigma t}$, if the mixed Rossby-gravity wave is included in the boundary condition, the upwelling at the western boundary does not occur. On the other hand, if the mixed Rossby-gravity wave is not included (Yamagata and Philander, 1982), the upwelling at the western boundary occurs.

In the case of symmetric zonal forcing $F = e^{-y^2/4 - i\sigma t}$, if we include the short Rossby waves at the western boundary, the flow and height fields are quite different from those in the case of long wave approximation.

Finally, in the case of local zonal forcing which exists at the central part of the ocean, the upwelling at the eastern boundary is very weak.

I. INTRODUCTION

The problems of the equatorial wave response due to wind stress have been considered by many authors. Those problems are very interesting because those are relevant to the phenomena of the Somali Current and the El Ninõ. For example, Lighthill (1969) and Anderson and Rowlands (1976) studied the equatorial wave response problem concerning the Somali Current. McCreary (1976) discussed the problem concerning the El Ninõ. Cane and Sarachik (1976, 1977, 1981) studied the linear response problems of the equatorial waves to external forcings in detail.

In the present note, we discuss the equatorial wave response with dissipation due to the oscillating wind stress. In particular, we want to comment on the role of the short waves at the western boundary in the equatorial wave response due to the wind stresses whose meridional functional forms are simple.

In Section II, we introduce the equatorial wave response problem. In Section III, we discuss the equatorial wave response with dissipation due to the simple oscillating wind stress.

II. THE MODEL AND BASIC EQUATIONS

As basic equations for the equatorial wave response problem due to wind stress, we adopt the following shallow water equations on an equatorial β-plane,

$$\frac{\partial u}{\partial t} - \beta y v + g\frac{\partial h}{\partial x} = F e^{-i\sigma t} - \varepsilon u \,, \qquad (1a)$$

$$\frac{\partial v}{\partial t} + \beta y u + g \frac{\partial h}{\partial y} = G e^{-i\sigma t} - \varepsilon^* v \quad , \tag{1b}$$

$$\frac{\partial h}{\partial t} + H\left(\frac{\partial u}{\partial x} + \frac{\partial v}{\partial y}\right) = -\varepsilon^* h \quad , \tag{1c}$$

where $(-\varepsilon^* u, -\varepsilon^* v)$ is Rayleigh friction and $-\varepsilon^* h$ is Newtonian cooling. For simplicity, it is assumed that the Rayleigh friction coefficient is equal to the Newtonian cooling coefficient. $F e^{-i\sigma t}$ and $G e^{-i\sigma t}$ are oscillating zonal and meridional wind forcings. Other symbols have conventional meanings.

We will consider the meridionally bounded problems, then as the boundary condition we impose

$$u = 0 \quad \text{at} \quad x = 0 \quad \text{and} \quad x = X_E \tag{2}$$

First we nondimensionalize (1) by taking $(gH/4\beta^2)^{1/4}$ as a length scale and $(4gH\beta^2)^{-1/4}$ as a time scale. Then eq. (1) is transformed into:

$$\frac{\partial u}{\partial t} - \frac{1}{2} y v + \frac{\partial h}{\partial x} = F e^{-i\sigma t} - \varepsilon u \quad , \tag{3a}$$

$$\frac{\partial v}{\partial t} + \frac{1}{2} y u + \frac{\partial h}{\partial y} = G e^{-i\sigma t} - \varepsilon v \quad , \tag{3b}$$

$$\frac{\partial h}{\partial t} + \frac{\partial u}{\partial x} + \frac{\partial v}{\partial y} = -\varepsilon h \quad , \tag{3c}$$

where $\varepsilon = \varepsilon^* (4gH\beta^2)^{-1/4}$.

In the case of no-external forcing, the eigenfunctions and eigenvalues with no meridional boundary are well known (Matsuno, 1966). We assume wave solutions as follows,

$$(u, v, h) = (u(y), v(y), h(y))\, e^{i(kx - \omega t)} \quad . \tag{4}$$

Then the following equation for v(y) is obtained,

$$\frac{d^2 v}{dy^2} + \left\{ \hat{\omega}^2 - k^2 - \frac{k}{2\hat{\omega}} - \frac{y^2}{4} \right\} v = 0 \quad , \tag{5}$$

where $\hat{\omega} = \omega + i\varepsilon$ is complex wave frequency.

The solutions which tend to zero as $y \to \pm \infty$ are

$$v = \pi^{-1/4} (2^n n!)^{-1/2} e^{-y^2/4} H_n\left(\frac{y}{\sqrt{2}}\right) \quad , \tag{6}$$

where Hn is the Hermite polynomial of the n'th order (Matsuno, 1966). The dispersion relation is given by

$$k^2 + \frac{k}{2\hat{\omega}} + n + \frac{1}{2} - \hat{\omega}^2 = 0 \quad , \tag{7a}$$

or,

$$k_{\pm}^n = -\frac{1}{4\hat{\omega}} \pm \frac{1}{4\hat{\omega}} \sqrt{1 - 8(2n+1)\hat{\omega}^2 + 16\hat{\omega}^4} \quad , \tag{7b}$$

where n=1, 2, ...

In the case of n = o, the dispersion relation is as follows,

$$k = \hat{\omega} - \frac{1}{2\hat{\omega}} \quad , \tag{8}$$

which is the mixed Rossby-gravity wave at the low frequency.

Eq. (3) (F = G = o) has the other wave solution; v ≡ o (Kelvin wave). The solution which tends to zero as $y \to \pm \infty$ is

$$u = \pi^{-1/4} 2^{-1/2} e^{-y^2/4} \tag{9}$$

The dispersion relation is given by

$$k = \hat{\omega} \tag{10}$$

Following Gill (1975), we introduce new dependent variables q and r, which are defined as

$$q = h + u \tag{11a}$$

$$r = h - u \tag{11b}$$

In the present paper, we consider the forced oscillation problem. Then expanding the dependent variables (q, r, v) as series of parabolic cylinder functions $\{D_m(y)\}$,

$$(q, r, v) = \sum_{m=0}^{\infty} (q^m, r^m, v^m) D_m(y) e^{-i\sigma\tau} \quad , \tag{12}$$

and utilizing the orthogonality of the functions, we obtain the following set of equations,

$$(\epsilon - i\sigma) q^0 + \frac{\partial q^0}{\partial x} = F^0 \quad , \tag{13a}$$

$$(\epsilon - i\sigma) q^{m+1} + \frac{\partial q^{m+1}}{\partial x} - v^m = F^{m+1} \quad , \quad m \geq 0 \quad , \tag{13b}$$

$$(\epsilon - i\sigma) r^{m-1} - \frac{\partial r^{m-1}}{\partial x} + m v^m = F^{m-1} \quad , \quad m \geq 1 \quad , \tag{13c}$$

$$2(\epsilon - i\sigma) v^0 + q^1 = 2G^0 \quad , \tag{13d}$$

$$2(\epsilon - i\sigma) v^m + (m+1) q^{m+1} - r^{m-1} = 2G^m \quad , \quad m \geq 1 \quad . \tag{13e}$$

III. THE CASE OF SIMPLIFIED FORCING

a). Meridional forcing

In this subsection, we consider the equatorial wave response due to the following simple meridional forcing,

$$G = G^0 D_0(y) \quad , \tag{14}$$

where G^0 = constant.

From eqs. (13), the equation for q' is

$$\frac{\partial q'}{\partial x} + \left(A + \frac{1}{2A}\right) q' = \frac{G^0}{A} \quad , \tag{15}$$

where $A = \varepsilon - i\sigma$. The solution of q' is

$$q' = C' e^{-\left(A+\frac{1}{2A}\right)x} + \frac{G^0}{A^2+1/2} \quad . \tag{16}$$

It is noted that the first term corresponds to the mixed Rossby-gravity wave reflected at the western boundary.

The equation for r' is, from (13),

$$\frac{d^2r'}{dx^2} + \frac{1}{2A}\frac{dr'}{dx} - \left(A^2 + \frac{5}{2}\right) r' = 0 \quad . \tag{17}$$

The solution is

$$r' = B'_+ e^{\alpha'_+(x-X_E)} + B'_- e^{\alpha'_- x} \tag{18}$$

where

$$\alpha'_\pm = -\frac{1}{4A} \pm \frac{1}{4A}\sqrt{1 + 8\cdot(2\times 2+1)A^2 + 16A^4} \tag{19}$$

In the present note, we adopt 40 cm as the equivalent depth. Then, the time scale and the length scale for nondimensionalization are 1.2 days and 2×10^7 cm, respectively. And we adopt the dissipation time = 20 days, frequency = 2π /1 year. Then, $\varepsilon = 0.56$ and $\sigma = 0.011$.

We consider the slowly oscillating problem. Then it is noted that the first and the second term of eq. (18) corresponds to the n=2 long and short Rossby wave respectively.

For simplicity, following McCreary (1981) it is assumed that the n = 2 short Rossby waves are not excited at the western boundary ($B'_- = 0$). Then we can determine C' and B+' from the boundary condition q' = r' at $x = 0$ and $x = X_E$ as follows:

$$C' = \frac{G^0}{A^2+1/2} \cdot \frac{e^{-\alpha'_+ X_E} - 1}{\left(1 - e^{-(\alpha'_+ + A + 1/2A)X_E}\right)} \quad , \tag{20a}$$

$$B'_+ = \frac{G^0}{A^2+1/2} \cdot \left[\frac{\left(e^{-\alpha'_+ X_E} - 1\right)}{\left(1 - e^{-(\alpha'_+ + A + 1/2A)X_E}\right)} \cdot e^{-\left(A+\frac{1}{2A}\right)X_E} + 1 \right] \quad . \tag{20b}$$

Fig. 1 shows the pressure and velocity fields at t = 0 when we adopt $G^0 = 1$ and $X_E = 23.9$ (actual width = 5000 km).

There is strong meridional flow at the western boundary whose amplitude is 15 on the equator. The meridional flow is very weak at the other regions. Zonal flow becomes 0 suddenly at the western boundary. At the western boundary, the upwelling does not occur. Namely, h = 0 at the western boundary. This result is quite different from the result of Yamagata and Philander (1982). It is because they neglect the term which shows the mixed Rossby-gravity waves, and sufficient energy does not escape from the western boundary. Then, in their case (linear case) the upwelling at the western boundary occurs.

Fig. 1

a

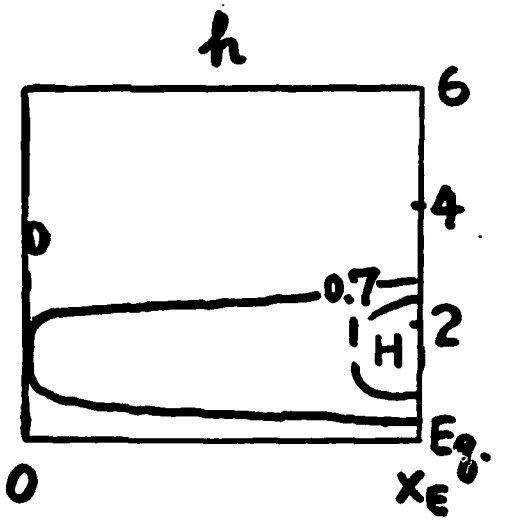

b

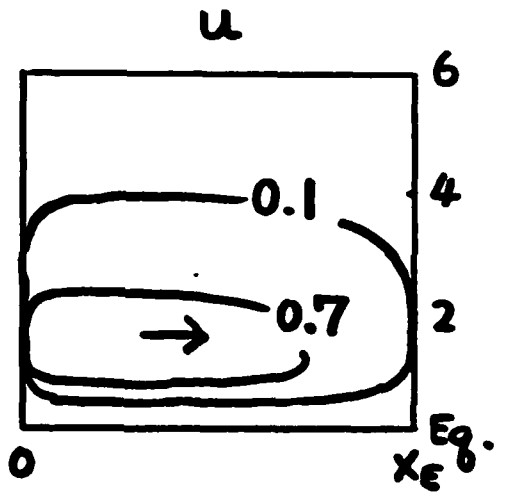

c

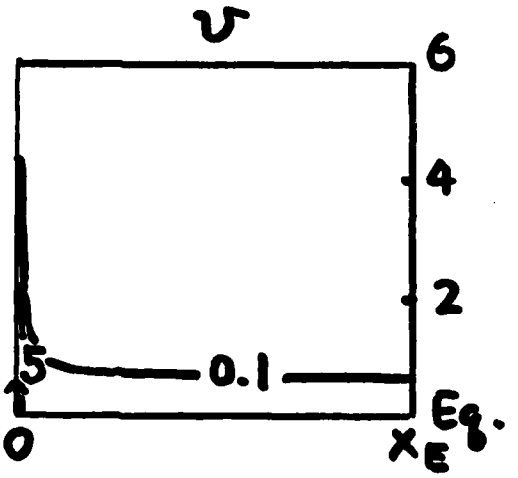

Fig. 1a, b, c: The pressure, zonal flow, meridional flow at t = o due to the meridional wind stress.

When we take into account the n = 2 short Rossby wave and the n = 4 Rossby wave but neglect the n = 4 short Rossby wave, the results of the wave response are not so different from the above results.

b). Zonal forcing

Next we consider the equatorial wave response due to the zonal forcing whose functional form is

$$F = F^0 D_0(y) \quad , \tag{21}$$

where F^0 = constant.

In this case the solution for q^0 is

$$q^0 = C^0 e^{-A\chi} + \frac{F^0}{A} \quad , \tag{22}$$

where C^0 is determined from the boundary condition. It is noted that the first term shows the Kelvin wave.

The equation for r^0 is

$$\frac{d^2 r^0}{d\chi^2} + \frac{1}{2A}\frac{dr^0}{d\chi} - \left[A^2 + \frac{3}{2}\right] r^0 = \frac{1+A^2}{A} F^0 \quad . \tag{23}$$

The solution for r^0 is

$$r^0 = B_+^0 e^{\alpha_+^0 (1-\chi_E)} + B_-^0 e^{\alpha_-^0 \chi} + H^0 \quad , \tag{24}$$

where

$$H^0 = -\frac{1+A^2}{A(A^2+3/2)} F^0 \quad , \tag{25a}$$

and

$$\alpha_\pm^0 = -\frac{1}{4A} \pm \frac{1}{4A}\sqrt{1 + 8\cdot(2\times 1+1)A^2 + 16A^4} \quad , \tag{25b}$$

which correspond to n = 1 long (+ sign) and short Rossby waves.

(i) Case 1:

In this case, we adopt long wave approximation, i.e, $B_-^0 = 0$. Then, we can obtain the following solution from the boundary condition $q^0 = r^0$ at $\chi = 0$ and $\chi = \chi_E$

$$C^0 = \frac{H^0 + \left(\frac{F^0}{A} - H^0\right) e^{-\alpha_+^0 \chi_E} - \frac{F^0}{A}}{1 - e^{-(A+\alpha_+^0)\chi_E}} \quad , \tag{26a}$$

$$B_+^0 = C^0 e^{-A\chi_E} + \frac{F^0}{A} - H^0 \quad . \tag{26b}$$

Fig. 2 shows the pressure and velocity fields at t = 0 when we adopt $F^0 = 1$. Other parameters are the same as those in Case (a). The maximum high pressure exists at the eastern boundary on the equator whose magnitude is 10. The minimum low pressure exists at the western boundary on the equator whose magnitude is -10. The maximum zonal velocity is 6.5 at the middle region on the equator. The meridional velocity is weak whose maximum amplitude is 0.25 at the western boundary.

(ii) Case 2:

In this case, we take into account the n = 1 short Rossby wave and n = 3 long Rossby wave but neglect the n = 3 short Rossby wave. Then we must consider q^2 and r^2. The solution for q^2 is

$$q^2 = \frac{r^0}{2} - A\left[-F^c - Ar^c + \frac{\partial r^c}{\partial \chi}\right] . \tag{27}$$

From (13), the equation for r^2 is

$$\frac{d^2 r^c}{d\chi^2} + \frac{1}{2A}\frac{dr^2}{d\chi} - \left[A^2 + \frac{7}{2}\right] r^2 = 0 \tag{28}$$

The solution for r^2 is

$$r^2 = B_+^2 e^{\alpha_+^2 (\chi - \chi_E)} \tag{29}$$

where

$$\alpha_+^2 = -\frac{1}{4A} + \frac{1}{4A}\sqrt{1 + 8\cdot(2\lambda 3 + 1)A^2 + 16A^4} \tag{30}$$

which corresponds to the n = 3 long Rossby wave. As mentioned above, we drop the term of the n = 3 short Rossby wave in (29).

Using the boundary condition $r^0 = q^0$ at $\chi = 0$ and $\chi = \chi_E$, we can get the following equations for C^0, B_+^0, B_-^0, B_+^2,

$$C^0 + \frac{F^c}{A} = B_-^c + B_+^c e^{-\alpha_+^c \chi_E} + H^0 \tag{31a}$$

$$C^0 e^{-A\chi_E} + \frac{F^c}{A} = B_-^c e^{\alpha_-^c \chi_E} + B_+^0 + H^0 \tag{31b}$$

$$\frac{1}{2}\left[B_+^c e^{-\alpha_+^c \chi_E} + B_-^c + H^c\right] - A\left[-F^c - A\left(B_+^c e^{-\alpha_+^c \chi_E} + B_-^c + H^c\right) + \alpha_+^c B_+^c e^{-\alpha_+^c \chi_E} + \alpha_-^c B_-^c\right] = B_+^2 e^{-\alpha_+^2 \chi_E}$$

$$\frac{1}{2}\left(B_+^0 + B_-^c e^{\alpha_-^0 \chi_E} + H^0\right] - A\left[-F^c - A\left(B_+^0 + B_-^c e^{\alpha_-^c \chi_E} + H^c\right)\right. \tag{31c}$$

$$\left. + \alpha_+^c B_+^0 + \alpha_-^c B_-^c e^{\alpha_-^c \chi_E}\right] = B_+^2 \tag{31d}$$

Fig. 3 shows the pressure and velocity fields at t = o when $F^0 = 1$. In this case, the strong meridional current exists at the western boundary. The maximum amplitude is 26. The maximum zonal velocity is 9.4 at the middle region on the equator. This value is about twice as that in Case 1. Reverse zonal current occurs at the high latitude region. The pressure at the western boundary is weaker than that in Case 1. The magnitude is -5.

Fig. 2

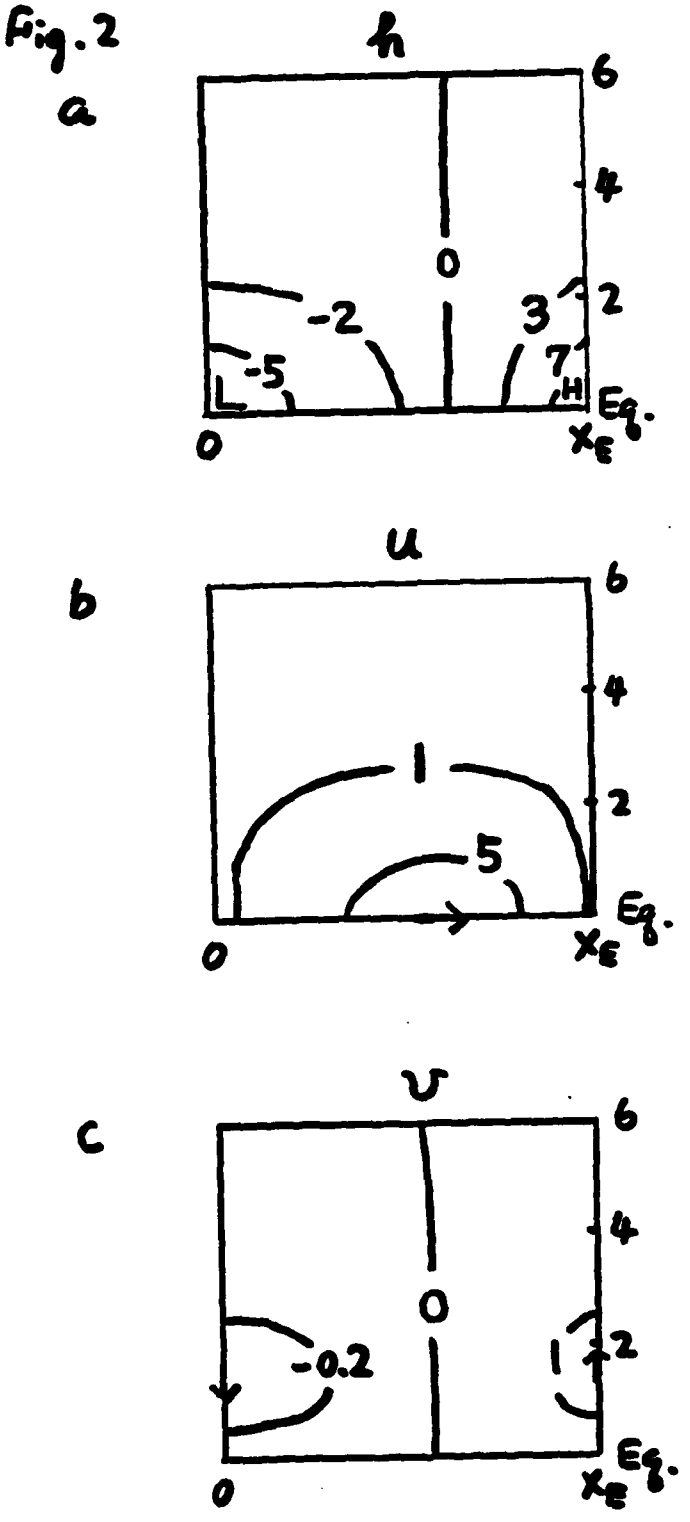

Fig. 2a, b, c: The pressure, zonal flow, meridional flow at t = o due to the zonal wind stress in the long wave approximation.

Fig. 3

a

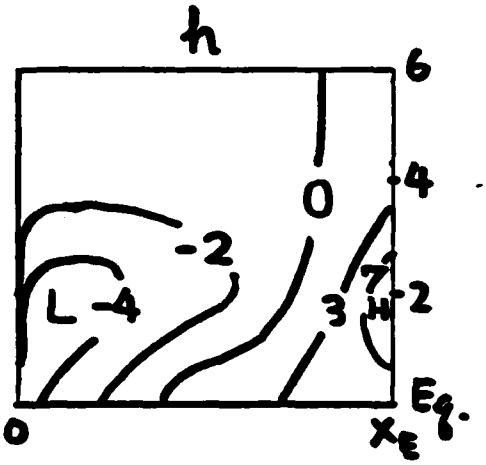

b

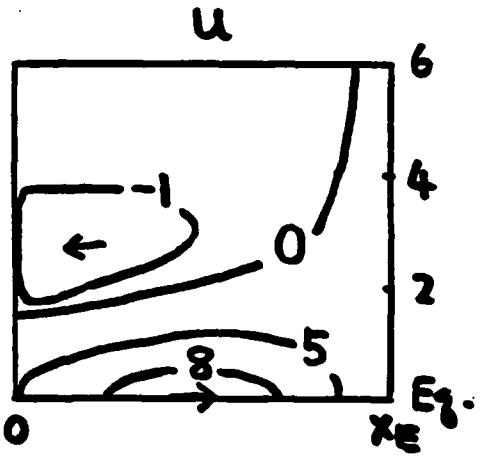

c

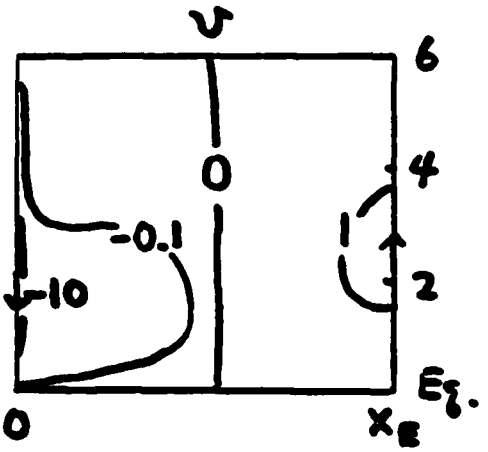

Fig. 3a, b, c: The pressure, zonal flow, meridional flow at t = o due to the zonal wind stress but not for the long wave approximation.

These features are quite different from those in the case of long wave approximation. The role of the short Rossby waves at the western boundary seems to be very important (Cane and Sarachik, 1977).

c). Local zonal forcing

In this subsection, we consider the equatorial wave response due to the local zonal wind stress. We assume the following functional form

$$F = D_0(y)\left(\frac{1}{\pi} - \frac{1}{2}\cos\frac{2\pi x}{X_E} + \frac{2}{3\pi}\cos\frac{4\pi x}{X_E} - \frac{2}{15\pi}\cos\frac{8\pi x}{X_E}\right) \tag{32}$$

$$\equiv D_0(y)\, f(x)$$

In the above expression, zonal dependent part $f(x)$ is nearly

$$f(x) \simeq \begin{cases} 0 & \text{at } 0 < x < \frac{X_E}{4},\ \frac{3\pi X_E}{4} < x < X_E, \\ -\cos\frac{2\pi x}{X_E} & \text{at } \frac{X_E}{4} < x < \frac{3\pi}{4} X_E \end{cases} . \tag{33}$$

The process of obtaining the solution is the same as in Case b (ii) (Appendix).

Fig. 4 shows the pressure and velocity fields at t = o. The position of the minimum low pressure is the place of the maximum gradient of the zonal wind stress. The regions of the low pressure are wider than those in the case of b (ii). Maximum high pressure at the eastern boundary is 2.6 which is smaller than that in Case b (ii). Reverse zonal current is stronger than that in Case b (ii). The meridional current has the reverse current near the western boundary. The maximum meridional current is 21.

IV. CONCLUSIONS AND REMARKS

Assuming the most simple zonal and meridional forcing function, we have discussed the equatorial wave response due to the oscillating wind stress. In the model the meridional boundary exists and the dissipations are included as the form of Rayleigh friction and Newtonian cooling.

In the case of meridional forcing $F = e^{-3/4 - i\sigma t}$, if we contain the mixed Rossby-gravity wave in the model, the upwelling at the western boundary does not occur. On the other hand, if we do not contain the mixed Rossby-gravity wave (Yamagata and Philander, 1982), the upwelling at the western boundary occurs.

In the case of zonal forcing $F = e^{-3/4 - i\sigma t}$, if we adopt the long wave approximation, meridional current at the western boundary is weak and the upwelling at the western boundary is strong. On the other hand, if we contain the short Rossby wave in the model, the meridional current at the western boundary is very strong and the upwelling at the western boundary is relatively weak.

Finally, in the case of local zonal forcing at the middle part of the ocean, the position of the minimum low pressure is the place of the maximum gradient of the zonal wind stress. The upwelling at the eastern boundary is weaker than that in the zonal independent zonal wind stress.

Fig. 4

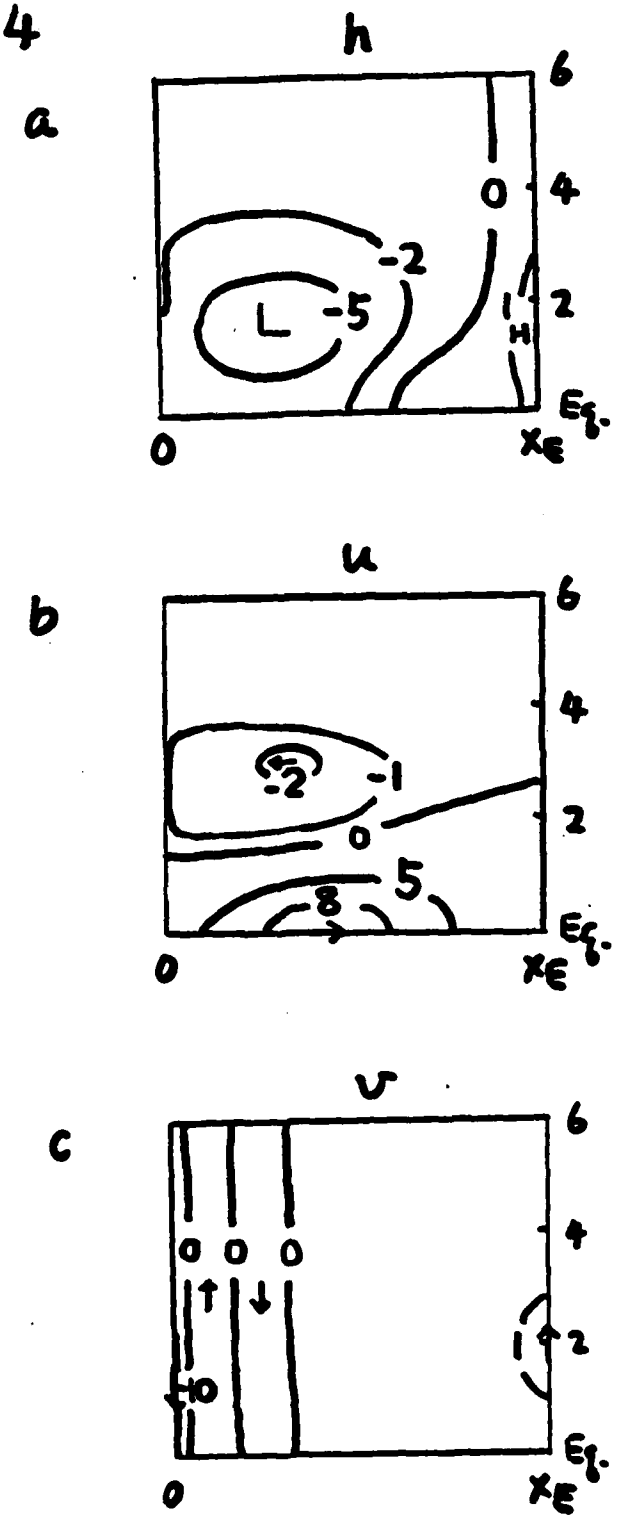

Fig. 4a, b, c: The pressure, zonal flow, meridional flow at t = o due to the zonal wind stress but for local zonal forcing case.

In the present note, we consider the equatorial wave response due to the oscillating wind stress of a very simple functional form. How does the zonally varying meridional wind stress change the equatorial wave response due to the zonal wind stress only? The problem is very interesting. The problem will be considered in the near future.

APPENDIX

The special solution for q^0 is

$$q^0 = \frac{1}{\pi}\frac{1}{A} - \frac{1}{4}\left(\frac{e^{\frac{2\pi i}{X_E}x}}{\left(\frac{2\pi i}{X_E}+A\right)} + \frac{e^{-\frac{2\pi i}{X_E}x}}{\left(-\frac{2\pi i}{X_E}+A\right)}\right) + \frac{1}{3\pi}\left(\frac{e^{\frac{4\pi i}{X_E}x}}{\left(\frac{4\pi i}{X_E}+A\right)} + \frac{e^{-\frac{4\pi i}{X_E}x}}{\left(-\frac{4\pi i}{X_E}+A\right)}\right)$$

$$- \frac{1}{15\pi}\left(\frac{e^{\frac{6\pi i}{X_E}x}}{\left(\frac{6\pi i}{X_E}+A\right)} + \frac{e^{-\frac{6\pi i}{X_E}x}}{\left(-\frac{6\pi i}{X_E}+A\right)}\right). \qquad \text{(A1)}$$

The equation for r^0 is

$$\frac{d^2r^0}{dx^2} + \frac{1}{2A}\frac{dr^0}{dx} - \left[A^2+\frac{3}{2}\right]r^0 = \frac{1+A^2}{A}F^0(x) + \frac{\partial F^0}{\partial x}. \qquad \text{(A2)}$$

Then the special solution for r^0 is

$$r^0 = -\frac{\frac{1+A^2}{A}\frac{1}{\pi}}{\left(A^2+3/2\right)} + a e^{\frac{2\pi i}{X_E}x} + b e^{-\frac{2\pi i}{X_E}x} + c e^{\frac{4\pi i}{X_E}x} + d e^{-\frac{4\pi i}{X_E}x} + g e^{\frac{6\pi i}{X_E}x} + h e^{-\frac{6\pi i}{X_E}x}, \qquad \text{(A3)}$$

where

$$a = \frac{-\frac{1}{4}\frac{1+A^2}{A} - \frac{1}{4}\frac{2\pi i}{X_E}}{\left(-\frac{4\pi^2}{X_E^2} + \frac{1}{2A}\frac{2\pi i}{X_E} - \left(A^2+3/2\right)\right)} \qquad \text{(A4a)}$$

$$b = \frac{-\frac{1}{4}\frac{1+A^2}{A} + \frac{1}{4}\frac{2\pi i}{X_E}}{\left(-\frac{4\pi^2}{X_E^2} - \frac{1}{2A}\frac{2\pi i}{X_E} - \left(A^2+3/2\right)\right)} \qquad \text{(A4b)}$$

$$c = \frac{\frac{1}{3\pi} + \frac{1}{3\pi}\frac{4\pi i}{X_E}}{\left(-\frac{16\pi^2}{X_E^2} + \frac{1}{2A}\frac{4\pi i}{X_E} - \left(A^2+3/2\right)\right)} \qquad \text{(A4c)}$$

$$d = \frac{\frac{1}{3\pi}\cdot\frac{1+A^2}{A} - \frac{1}{3\pi}\frac{4\pi i}{X_E}}{\left(-\frac{16\pi^2}{X_E^2} - \frac{1}{2A}\frac{4\pi i}{X_E} - \left(A^2+3/2\right)\right)} \qquad \text{(A4d)}$$

$$g = \frac{-\frac{1}{15\pi}\frac{1+A^2}{A} - \frac{1}{15\pi}\frac{8\pi i}{X_E}}{\left(-\frac{64R^2}{X_E^2} + \frac{1}{2A}\frac{8\pi i}{X_E} - (A^2 + 3/2)\right)} \qquad \text{(A4e)}$$

$$h = \frac{-\frac{1}{15\pi}\frac{1+A^2}{A} + \frac{1}{15\pi}\frac{8\pi i}{X_E}}{\left(-\frac{64R^2}{X_E^2} - \frac{1}{2A}\frac{8\pi i}{X_E} - (A^2 + 3/2)\right)} \qquad \text{(A4f)}$$

REFERENCES

Anderson, D.L.T. and P.B. Rowlands, 1976. The Somali Current response to the southwest monsoon: the relative importance of local and remote forcing. J. Mar. Res., 34, 395-417.

Cane, M.A. and E.S. Sarachik, 1976. Forced baroclinic ocean motions: I. The linear equatorial unbounded case. J. Mar. Res., 34, 629-665.

_____, 1977. Forced baroclinic ocean motions: II. The linear equatorial bounded case. J. Mar. Res., 35, 395-432.

_____, 1981. The response of a linear baroclinic equatorial ocean to periodic forcing. J. Mar. Res., 39, 651-693.

Gill, A.E., 1975. Models of equatorial currents. Numerical models of ocean circulation. National Academy of Sciences, Washington, D.C., 181-203.

Lighthill, M.J., 1969. Dynamic response of the Indian Ocean to onset of the southwest monsoon. Phil. Trans. R.S. Lond., A265, 45-93.

Matsuno, T., 1966. Quasi-geostrophic motions in the equatorial area. J. Met. Soc. Japan, 44, 25-43.

McCreary, J., 1976. Eastern tropical ocean response to changing wind systems: with application to Nl Nino. J. Phys. Oceanogr., 6, 632-645.

_____, 1981. A linear stratified ocean model of the equatorial undercurrent. Phil. Trans. R.S. Lond., A298, 603-635.

Yamagata, T. and S.G.H. Philander, 1982. The role of damped equatorial waves in the ocean response to winds. To be submitted.

VERTICAL CONVECTION AND HORIZONTAL ADVECTION

Stephan Fauve

ABSTRACT

Internally generated vertical vorticity enters the leading order evolution equation for fixed-flux convection with shear stress-free boundary conditions, and may lead to a time-dependent regime at the convection onset in the case of low Prandtl number fluids.

INTRODUCTION

It is known since the experiments of Benard, that the transition of a fluid layer heated from below to a convective state involves two phases of different characteristic time scales: during the first phase, the layer rapidly resolves itself into cells; the second phase corresponds to a large scale horizontal diffusion of longer characteristic time, which regularize the convective pattern (at least with high Prandtl number fluids).

In the case of fixed temperature boundary conditions (Segel, 1969) and Newell and Whitehead (1969), considering a slow modulation of the convective velocity amplitude, have shown the diffusive character of the spatial nonuniformities propagation. In the case of fixed-flux boundary conditions, (Chapman, 1978), using a shallow water approximation, has derived the nonlinear evolution equation for the leading order temperature disturbance. This equation, which also describes a large scale horizontal diffusion, is connected with the translational and rotational symmetries of the problem (See Section 2.)

The purpose of this work is to show how this diffusion equation is modified, when vertical vorticity modes are taken into account. It is known that these modes, first considered by Ledoux, Schwarzschild and Spiegel (1961), can be coupled to convective modes, linearly in the case of rotating convection (Chandrasekhar, 1961), or nonlinearly by the inertial term $\vec{v}.\vec{\nabla}\vec{v}$ of the Navier-Stokes equation, without rotation (Busse, 1972). In the case of fixed temperature boundary conditions, Siggia and Zippelius (1981, 1982), have shown that the Segel-Newell and Whitehead equation is in error for free-slip boundaries, when the internally generated vertical vorticity is taken into account. The important qualitative effect of vertical vorticity modes, is to add an advective term to the large scale horizontal diffusion. We have obtained the same type of result in the case of fixed-flux convection, (See Section 3), and have begun to look at travelling waves solutions, in the case of a low Prandtl number fluid.

1. Definitions and Governing Equations

We consider an horizontal layer of fluid of depth 2D, heated from below.

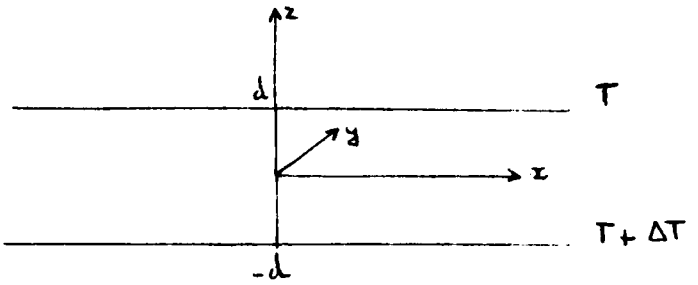

Using d , d^2/K , and ΔT as scales for length, time and temperature, respectively, the dimensionless equations for the velocity $\vec{v}$ and the deviation θ of the temperature from the static distribution, can be written in the Boussinesq approximation:

$$\operatorname{div} \vec{v} = 0$$
$$\frac{1}{\sigma}\left(\vec{v}_t + \vec{v}\cdot\vec{\nabla}\vec{v}\right) = -\vec{\nabla}\pi + \Delta\vec{v} + \theta\,\hat{z}$$
$$\theta_t + \vec{v}\cdot\vec{\nabla}\theta = \vec{v}\cdot\hat{z} + \Delta\theta$$

The physical parameters of the problem are expressed in terms of two dimensionless numbers:

the Rayleigh number $R = \dfrac{g\alpha d^3 \Delta T}{\nu K}$

the Prandtl number $\sigma = \dfrac{\nu}{K}$

g is the acceleration of gravity, α the isobaric thermal expansion coefficient, ΔT the temperature difference across the layer, ν the kinematic viscosity, and K the heat diffusivity. The unit vector $\hat{z}$ is directed opposite to gravity and $\vec{\nabla}\pi$ includes all the terms that can be written in the form of a gradient. The thermal boundary conditions are

$$\theta_z = 0 \quad , \quad z = \pm 1$$

and corresponds to the case when the boundaries are much poorer conductors than the fluid. This problem was first investigated by Jeffreys (1926) and more recently by Sparrow, Goldstein and Jonsson (1964), Hurle, Jakeman and Pike (1967), and Jakeman (1968). These authors have shown that as the ratio of conductivities of fluid to boundary becomes very large, the critical horizontal wavenumber for the onset of convection approaches zero. Childress and Spiegel have exploited this property to develop an expansion scheme in powers of the horizontal wavenumber, which is a method applicable to many types of convection problems (Spiegel, 1981).

Finally, our mechanical boundary conditions are

$$w = 0, \; u_z = v_z = 0; \; z = \pm 1$$

where w is the vertical velocity and $\vec{u}(u,v)$ the horizontal velocity. We have, therefore, for the vertical vorticity $\xi = \vec{\omega}.\hat{z}$, $\xi_z = 0$; $z = \pm 1$.

2. Examples

We consider in this section 2D motions, and write the velocity in terms of a streamfunction $\psi(xzt)$, $v = (-\psi_z, 0, \psi_x)$. We adopt the scalings used by Chapman (1978) for horizontal and vertical length and time

$$\partial_x \to \epsilon \partial_x \quad , \quad \partial_z \to \partial_z \quad , \quad \partial_t \to \epsilon^4 \partial_t$$

but we consider small Prandtl numbers

$$\sigma = O(\epsilon) \text{ (case A)}; \qquad \sigma = O(\epsilon^2) \text{ (case B)}.$$

We must take $\psi = O(\epsilon)$ and $\Theta = O(1)$ in the first case, and $\psi = O(\epsilon^2)$, $\Theta = O(\epsilon)$ in the second, in order to be able to get an evolution equation where nonlinear terms appear at the leading order.

- Case A: $\sigma = O(\epsilon)$.

The Boussinesq equations are in terms of ψ

$$\frac{1}{\sigma}\left(\epsilon^5 \psi_{xzt} + \epsilon^3 \psi_{zzt} + \epsilon^3 J(\psi, \psi_{xz}) + \epsilon J(\psi, \psi_{zz})\right) = \\ = R\Theta_x + \epsilon^4 \psi_{xxxx} + 2\epsilon^2 \psi_{xxzz} + \psi_{zzzz} \qquad (1)$$

$$\epsilon^4 \Theta_t + \epsilon^2 J(\psi, \Theta) = \epsilon^2 \psi_x + \epsilon^2 \Theta_{xx} + \Theta_{zz} \qquad (2)$$

where J is the usual Jacobian.

We expand ψ , Θ and R in powers of ϵ

$$\psi = \psi^{(0)} + \epsilon \psi^{(1)} + \epsilon^2 \psi^{(2)} + \cdots$$
$$\Theta = \Theta^{(0)} + \epsilon \Theta^{(1)} + \epsilon^2 \Theta^{(2)} + \cdots$$
$$R = R^{(0)} + \epsilon R^{(1)} + \epsilon^2 R^{(2)} + \cdots$$

At O(1) equation (2) yields

$$\Theta^{(0)}_{zz} = 0$$

and thus with the boundary conditions

$$\Theta_z = 0, \; z = \pm 1; \; \Theta^{(0)} = f(xt)$$

Equation (1) gives

$$\psi^{(0)} = -R^{(0)} P(z) f_x \qquad \text{where} \qquad P(z) = \frac{1}{24}\left(z^4 - 6z^2 + 5\right)$$

We continue to solve the problem at each order, until we find an equation that determines f(xt). The solvability condition

$$\int_{-1}^{1} \Theta_{zz} \, dz = 0$$

written at $O(\epsilon^2)$ gives the critical Rayleigh number $R(o) = \frac{15}{2}$

(This unusual value is due to the depth 2d of the layer). At $O(\epsilon)$ we have similarly

$$\theta^{(1)} = f_1(x,t)$$

$$\psi^{(1)} = \left(R^{(o)} f_{1x} + R^{(1)} f_x \right) P(z) + \frac{R^{(o)^2}}{\sigma} \pi(z)\, f_x f_{xx}$$

where $\pi^{IV} = PP''' - P'P''$

The solvability condition at $O(\epsilon^3)$ gives

$$R(1) = 0$$

At $O(\epsilon^2)$ we have

$$\theta^{(2)} = Q(z) f_{xx} + R^{(o)} P_1(z) f_x^2 + f_2(x,t)$$

where $Q' = R^{(o)} P - 1$, $P_1'' = P'$

$$\psi^{(2)} = -R^{(o)} R(z) f_{xxx} - \left(R^{(o)} f_{2x} + R^{(2)} f_x \right) P(z) - R^{(o)} P_5(z) f_x^2 +$$

$$+ \frac{R^{(o)^3}}{\sigma^2} \left(S(z) f_x f_{xx}^2 + T(z) f_x (f_x f_{xx})_x \right) +$$

+ terms involving odd z polynomials which do not contribute to the evolution equation.

where $R^{IV} = Q - 2P''$, $P_5^{IV} = P_1$, $S^{IV} = P\pi''' - P''\pi'$, $T^{IV} = P'''\pi - P'\pi''$

The solvability condition at $O(\epsilon^4)$ gives the evolution equation

$$f_t = -r f_{xx} - K f_{xxxx} + \gamma (f_x^3)_x - \frac{\alpha}{\sigma^2} (f_x^3)_{xxx} - \frac{\beta}{\sigma^2} (f_x f_{xx}^2)_x \qquad (3)$$

where $K = 0.8$, $\gamma = 1.2$, $\alpha = 0.01$, $\beta = 0.01$, $r = R^{(2)}/R^{(c)}$
We must require suitable lateral boundary conditions in order to solve this equation.

$$f_x = 0,\ f_{xxx} = 0;\ x = \pm \frac{\pi}{\alpha}$$

which describe shear stress free boundary condition without lateral heat flux.
We expand f and r by a new small parameter

$$f = \varepsilon f^{(1)} + \varepsilon^2 f^{(2)} + \varepsilon^3 f^{(3)} + \cdots$$

$$r = r^{(o)} + \varepsilon r^{(1)} + \varepsilon^2 r^{(2)} + \cdots$$

The leading order yields

$$f^{(1)} = A(\varepsilon^2 t) \cos \alpha x$$

where we have scaled the time like ε^2 . The solvability condition at the third order gives the Landau equation

$$\dot{A} = \alpha^2 r^{(2)} A - \frac{3}{4} \alpha^4 A^3 \left(1 + a \frac{\alpha^2}{\sigma^2} \right) \qquad (4)$$

Since $a > 0$, we have a supercritical bifurcation like in the $\sigma = O(1)$ case. In the steady case the solution to (3) can be reduced to quadratures, but a numerical solution would be a better way of obtaining the form of $f(x)$.

- Case B: $\sigma = O(\epsilon^2)$

A similar procedure gives the evolution equation:

$$f_t - \frac{\lambda}{\sigma} f_{xxt} = -r f_{xx} - \kappa f_{xxxx} - \frac{\alpha}{\sigma^2}(f^3_x)_{xxx} - \frac{\beta}{\sigma^2}(f_x f^2_{xx})_x \qquad (5)$$

It would be interesting to look at the travelling waves solutions of (5) numerically, because of the new time dependent term f_{xxt} on the righthand side. We can notice that the equations obtained for the different scalings of σ, are all of the form

$$f_t = (\quad)_x$$

which is connected with the translational invariance of the problem. All of these equations involve only terms with an even number of x-derivatives, in contrast with the well known KdV equation $f_t = f f_x - f_{xxx}$. The relevant variance is there

$$x \to -x, \quad t \to -t$$

Finally, we can notice that the nonlinear terms of our equations are always cubic in f. This is due to our symmetric boundary conditions. When effects involving asymmetry between the top and bottom layer are introduced, square nonlinear terms are obtained: $(f^2)_{xx}$ when nonBoussinesq effects are taken into account (Depassier, Spiegel, 1981) and $(f_x^2)_{xx}$ with one rigid boundary and the other stress-free (Chapman, Proctor, 1980). (The term $(f^2)_{xx}$ has also been obtained by Childress and Spiegel in bioconvection.)

3. Vertical Vorticity Effect in Fixed-Flux Convection

We now consider the 3D Boussinesq equations, with O(1) Prandtl number and the usual scalings

$$\partial_x \to \epsilon \partial_x \;,\; \partial_y \to \epsilon \partial_y \;,\; \partial_z \to \partial_z \;,\; \partial_t \to \epsilon^4 \partial_t$$

$$u \to \epsilon u \;,\; v \to \epsilon v \;,\; w \to \epsilon^2 w \;,\; \theta \to \theta$$

In this section we adopt the following notations:

$$\vec{\nabla} = (\partial_x, \partial_y, 0) \;; \quad \Delta = \partial^2_{xx} + \partial^2_{yy} \;; \quad \vec{u} = (u, v, 0)$$

The Boussinesq equations are

$$\frac{1}{\sigma}\left(\epsilon^4 \vec{u}_t + \epsilon^2 \vec{v} \cdot \vec{\text{grad}}\, \vec{u}\right) = -\vec{\nabla}\pi + \epsilon^2 \Delta \vec{u} + \vec{u}_{zz} \qquad (1)$$

$$\frac{1}{\sigma}\left(\epsilon^6 w_t + \epsilon^4 \vec{v}\cdot \vec{\text{grad}}\, w\right) = -\pi_z + \epsilon^4 \Delta w + \epsilon^2 w_{zz} + R\theta \qquad (2)$$

$$\epsilon^4 \theta_t + \epsilon^2 \vec{v}\cdot \vec{\text{grad}}\,\theta = \epsilon^2 w^2 + \epsilon^2 \Delta\theta + \theta_{zz} \qquad (3)$$

At O(1) (3) yields

$$\theta^{(0)} = f(xyt)$$

We calculate $\pi^{(0)}$ using (2) and $\vec{u}^{(0)}_{zz}$ using (1). We integrate using the boundary conditions for $\vec{u}_z$
We have therefore

$$\vec{u}^{(0)} = R^{(0)} P'(z)\, \vec{\nabla} f + \vec{U}^{(0)}(xyt)$$

$\vec{U}(o)$ is at this step an arbitrary function of xyt, connected with the vertical vorticity

$$\xi = (\vec{\text{curl}}\ \vec{U}(o))\cdot \hat{z}$$

We now use the continuity equation

$$\vec{\nabla}\cdot\vec{u} + w_z = 0 \qquad (4)$$

and get, using the boundary conditions for w

$$\vec{\nabla}\cdot\vec{U}^{(0)} = 0$$

$$w^{(0)} = -R^{(0)} P(z)\, \Delta f$$

Before following the same procedure at $O(\epsilon^2)$, we should notice a problem which arises when we write the solvability condition for $\theta^{(2)}_z$. We get

$$\frac{1}{2}\int_{-1}^{1}\left(R^{(0)}P(z) - 1\right)dz\ \Delta f = \vec{U}^{(0)}\cdot\vec{\nabla} f$$

The critical Rayleigh number must be independent of $\vec{U}(o)$, so $\vec{U}(o)$ must satisfy the relation $\vec{U}(o)\cdot\vec{\nabla} f = 0$. It is then easy to calculate $\theta^{(2)}$, $\vec{u}^{(2)}$, $\vec{u}^{(2)}$, and $w^{(2)}$, but a same kind of problem arises when we write the solvability condition at $O(\epsilon^4)$:

$$\theta^{(4)}_{zz} + \Delta\theta^{(2)} + w^{(2)} = \vec{v}^{(0)}\cdot\vec{\text{grad}}\,\theta^{(2)} + \vec{u}^{(2)}\cdot\vec{\nabla} f + f_t$$

The evolution equation for f involves the term $\vec{U}^{(0)}\cdot\vec{\nabla} f_z$. In order to eliminate it, we consider a solution $(\vec{v}, \theta)$ of the Boussinesq equations, and make the transformation

$$\vec{v} \to \vec{v} + \vec{V}(xyt)\ ,\quad \theta \to \theta + \Theta(xyzt)$$

If $\vec{V}$ is constant, and $\Theta = 0$, we have a new solution if $\vec{V}\cdot\vec{\nabla}\theta = 0$. If $\vec{V}$ is slowly varying in x and y, we write the equations for $\vec{V}$ and Θ

$$\frac{1}{\sigma}\left\{\epsilon^4\vec{V}_t + \epsilon^2\left(\vec{V}\cdot\vec{\nabla}\vec{V} + \vec{V}\cdot\vec{\nabla}\vec{v} + \vec{v}\cdot\vec{\nabla}\vec{V}\right)\right\} = -\vec{\nabla}P + \epsilon^2\Delta\vec{V} \qquad (1')$$

$$\frac{1}{\sigma}\epsilon^4\vec{V}\cdot\vec{\nabla} w = -P_z + R\Theta \qquad (2')$$

$$\epsilon^4 \Theta_t + \epsilon^2 \left(\vec{V}.\vec{\nabla}\theta + \vec{v}.\vec{\text{grad}}\,\Theta + \vec{V}.\vec{\nabla}\Theta \right) = \epsilon^2 \Delta\Theta + \Theta_{zz} \qquad (3')$$

At the leading order (3') yields

$$\Theta^{(0)} = F(xyt)$$

Using (2') and (1') we get

$$\vec{\nabla} F = 0$$

Therefore (3') at $0(\epsilon^2)$ yields

$$\vec{V}^{(0)}.\vec{\nabla}\theta^{(0)} = 0$$

Generalizing this result, we adopt the following condition

$$\int_{-1}^{1} dz\, \vec{V}.\vec{\nabla}\theta = 0$$

where $\vec{V}$ is the nondivergent part of $\vec{U}$. Consequently we can eliminate the term $\vec{U}^{(0)}.\vec{\nabla} f_z$ from the evolution equation, and we get

$$f_t + \frac{\lambda}{\sigma}(\hat{z}\times\vec{\nabla}h).\vec{\nabla} f = -r\nabla^2 f - \kappa\nabla^4 f + \gamma\,\vec{\nabla}.\left[(\vec{\nabla}f)^2\vec{\nabla}f\right]$$

where

$$\lambda = \frac{R^{(0)}}{2}\int_{-1}^{1} P'^2\, dz$$

and

$$h(xyt) = \xi^{(0)}(xyt)$$

The equation for the vertical vorticity

$$\frac{1}{\sigma}\left\{\epsilon^4 \xi_t + \epsilon^2\left[(\vec{v}.\vec{\text{grad}}\,v)_x - (\vec{v}.\vec{\text{grad}}\,u)_y\right]\right\} = \epsilon^2\Delta\xi + \xi_{zz} \qquad (5)$$

gives the equation for h(xyt) at $0(\epsilon^2)$

$$\vec{U}^{(0)}.\vec{\nabla}h - \lambda R^{(0)} J(f, \nabla^2 f) = \sigma\nabla^2 h$$

The leading order vertical vorticity h effect is therefore to add an advective term $(\hat{z}\times\vec{\nabla}h).\vec{\nabla}f$ to the evolution equation for f. The equation for h describes the generation of vertical vorticity due to the convective motion. These two equations can be written

$$f_t + \vec{\nabla}.\left\{(\hat{z}\times\vec{\nabla}h) f + r\vec{\nabla}f + \kappa\vec{\nabla}(\nabla^2 f) - \gamma(\vec{\nabla}f)^2\vec{\nabla}f\right\} = 0$$

$$\vec{\nabla}.\left\{\sigma\vec{\nabla}(\nabla^2\phi) - h\vec{U}^{(0)} + \lambda R^{(0)}\nabla^2 f\;\hat{z}\times\vec{\nabla}f\right\} = 0$$

or using a stream function for $\vec{U}^{(0)}$, $\vec{U}^{(0)} = \vec{\text{curl}}(\phi\hat{z}) = \vec{\nabla}\phi\times\hat{z}$

$$f_t + \frac{\lambda}{\sigma} J(f, \nabla^2\phi) = -r\nabla^2 f - \kappa\nabla^4 f + \gamma\,\vec{\nabla}.\left[(\vec{\nabla}f)^2\vec{\nabla}f\right]$$

$$\sigma\nabla^4\phi + J(\phi, \nabla^2\phi) = \lambda R^{(0)} J(f, \nabla^2 f)$$

To see at which order the vertical vorticity is generated, we expand f, ϕ, and r in powers of a new small parameter ϵ (Malkus and Veronis, 1958).

$$f = \epsilon f^{(1)} + \epsilon^2 f^{(2)} + \epsilon^3 f^{(3)} + \dots$$

$$\phi = \epsilon \phi^{(1)} + \epsilon^2 \phi^{(2)} + \epsilon^3 \phi^{(3)} + \dots$$

$$r = r^{(0)} + \epsilon r^{(1)} + \epsilon^2 r^{(2)} + \dots$$

At the leading order we have

$$-r^{(0)} \nabla^2 f^{(1)} - \kappa \nabla^4 f^{(1)} = 0$$

We choose a square planform

$$f(1) = \cos x \cos y$$

The solvability condition gives

$r^{(1)} = 0$ at the second order

$r^{(2)} = \frac{5\gamma}{2}$ at the third order

and we obtain

$$f^{(3)} = \frac{\gamma}{64\kappa} \left(\frac{1}{6} \cos 3x \cos 3y + \frac{1}{5} \cos 3x \cos y + \frac{1}{5} \cos x \cos 3y \right)$$

The vertical vorticity is generated at the fourth order

$$\sigma \nabla^2 \phi^{(4)} = \frac{\lambda R^{(0)} \gamma}{2\epsilon \kappa} \left(\sin 2x \sin 4y - \sin 4x \sin 2y \right)$$

Consequently we have at the leading order for $\vec{U}(0)$

$$\vec{U}^{(1)} \propto \begin{vmatrix} 2 \sin^2 x \cos 4y - \sin 4x \cos 2y \\ \cos 2x \sin 4y - 2 \cos 4x \sin^2 y \end{vmatrix}$$

Finally, we can notice that the advective term due to the vertical vorticity do not affect the Liapounov functional introduced by Childress (Chapman, 1978)

$$V(f) = \int dx\, dy \left[\gamma (\vec{\nabla} f)^4 + \kappa (\nabla^2 f)^2 - r (\vec{\nabla} f)^2 \right]$$

since

$$\int dx\, dy\, f\, J(f, \nabla^2 \phi) = 0$$

with the boundary conditions

$$f_x = f_y = 0 \quad , \quad x = y = \pm\pi$$

Extensions of the present work

With the Prandtl number scaled with ϵ^2, we have obtained

$$\sigma(f_t + \vec{U}^{(0)} \cdot \vec{\nabla} f) - \lambda \nabla^2 f_t = -r\nabla^2 f - \kappa \nabla^4 f$$

$$h_t + \vec{U}^{(0)} \cdot \vec{\nabla} h = \lambda R^{(0)} J(f, \nabla^2 f) + \nabla^2 h$$

These equations have no nonlinear terms except coupling nonlinear terms between f and h, and we must get them using the reconstitution method (Spiegel lectures in 1981). We have begun to look at the travelling waves solutions of the equations, which may exhibit an interesting spatial behavior. We have also looked at rotating convection. When the rotation order of magnitude is ϵ, the effect of rotation is simply to inhibit convection. The case of O(1) rotation, recently considered by Riahi (1982) in the case of infinite Prandtl number, may involve interesting instabilities in the case of finite Prandtl number. In particular the question of the existence of overstability should be studied.

ACKNOWLEDGMENTS

I would like to thank Prof. E. Spiegel for proposing this problem and for his constant advice and supervision, Profs. L. Howard, J. Keller and W. Malkus for many helpful discussions and F. Mellor for having typed my manuscript. I also thank Prof. G. Veronis and the Woods Hole Oceanographic Institution for offering me a GFD fellowship.

REFERENCES

Benard, H., 1901. Rev. Gen. Sci. Pures Appl. 11, 1261. See also for a discussion of Benard's experiments, Lord Rayleigh (1916), Phil. Mag. 32, 529.

Busse, F. H., 1972. J. Fluid Mech. 52, 97.

Busse, F. H. and N. Riahi, 1980. J. Fluid Mech. 96, 243.

Chandrasekhar, S., 1961. Hydrodynamic and Hydromagnetic Stability, Oxford.

Chapman, C. J., 1978. Woods Hole Oceanogrphic Institution Tech. Rpt. WHOI-78-67.

Chapman, C. J., M.R.E. Proctor, 1980. J. Fluid Mech., 101, 753.

Childress, S., and E. A. Spiegel, 1981. Pattern formation in a suspension of swimming micro-organisms: nonlinear aspects.

Despassier, M. C. and E. A. Spiegel, 1981. Astron. J., 86, 496.

Hurle, D.T.J., E. Jakeman and E. R. Pike, 1967. Proc. Roy. Soc., A296, 469.

Jakeman, E., 1968. Phys. Fluids, 11, 10.

Jeffreys, H., 1926. Phil. Mag. 2, 833.

Ledoux, P., M. Schwarzschild and E. A. Spiegel, 1961. Ap. J., 133, 184.

Malkus, W.V.R., and G. Veronis, 1969. J. Fluid Mech., 4, 225.

Newell, A. C. and J. A. Whitehead, 1969. J. Fluid Mech., 38, 279.

Proctor, M.R.E., 1980. J. Fluid Mech. 101, 759.

Riahi, N., 1982. ZAMP, 33(1), 81

Segel, L. A., 1969. J. Fluid Mech., 38, 203.

Siggia, E. D. and A. Zippelius, 1981. Phys. Rev. Letters, 47(12), 835.

Sparrow, E. M., R. J. Goldstein and V. H. Jonsson, 1964. J. Fluid Mech., 18, 513.

Spiegel, E. A., 1981. Woods Hole Oceanographic Institution Technical Report WHOI-81-102.

Zippelius, A. and E. D. Siggia, 1982. Preprint.

MODELS OF LARGE SCALE FLOWS WITH RELEVANCE TO SOUTHERN OCEAN CIRCULATION

Peter Haynes

1. INTRODUCTION AND MOTIVATION

Recent theories (Rhines and Holland, 1979) of the large scale wind-driven circulation of the ocean have exploited the idea that in subsurface layers remote from direct wind forcing flow takes place along contours of constant potential vorticity, simply because the steady flow is governed by the equation.

$$(\underset{\sim}{u}.\nabla)q = 0 \tag{1.1}$$

where $\underset{\sim}{u}$ is the velocity and q is the potential vorticity. For large scale flows, that is on length scales greater than the Rossby radius of deformation, we expect relative vorticity to be unimportant so that q is equal to $\underset{\sim}{f}.\nabla(\ln\rho)$ where $\underset{\sim}{f}$ is the Coriolis parameter and ρ is the density. In weak flows contours are roughly zonal, so in an ocean with meridional boundaries the flow is blocked, and there can be no velocity in the subsurface layers. However, motion can occur, firstly if the forcing sufficiently deforms the q contours so that they no longer intersect the boundaries, essentially if they become closed, and secondly, if the zonally oriented q contours have an uninterrupted path and reach no boundaries. The first case is the basis of the theory presented by Rhines and Young (1982a), and they then use the result that, under certain assumptions, concerning the eddy flux of potential vorticity the potential vorticity will be homogenized in regions of closed streamlines (Rhines and Young, 1982b) to determine the vertical structure of the wind driven circulation. The second case is only true in the Southern Ocean, where the unblocked contours around the Antarctic allow a strong current to flow. The wind stress during this current cannot be balanced by pressure gradients, neither does the Sverdrup constraint control the transport of water, since here the flow is along rather than across q contours, so that the dynamical balance must come from horizontal momentum transport, bottom friction (Gill, 1968) or topographic drag.

The problem which will be considered is that of the wind driven circulation of the South Pacific. The dynamics contains both the ingredients remarked above, the subtropical gyre is bounded meridionally, and the transport is presumably largely controlled by the Sverdrup constraint; poleward, however, the gyre is bounded by the Antarctic Circumpolar Current, and it seems likely that this will affect the structure of the circulation in the gyre.

Observations show that the wind driven gyre in the South Pacific penetrates much deeper than that in the North Pacific or North Atlantic although we would still expect the depth to be constrained by (20). Figure 1 is taken from the atlas produced by Levitus (1982). We see the wind driven flow between 500 m and 1000 m dominated by the subtropical gyres in each of the world oceans, and the Anatarctic Circumpolar Current. Deeper, however, in Figure 2, there is little evidence of organized wind-driven flow in the North Pacific or North Atlantic, but in the Southern Oceans, and in particular, in the South Pacific, an appreciable wind gyre can still be seen. There is also consider-

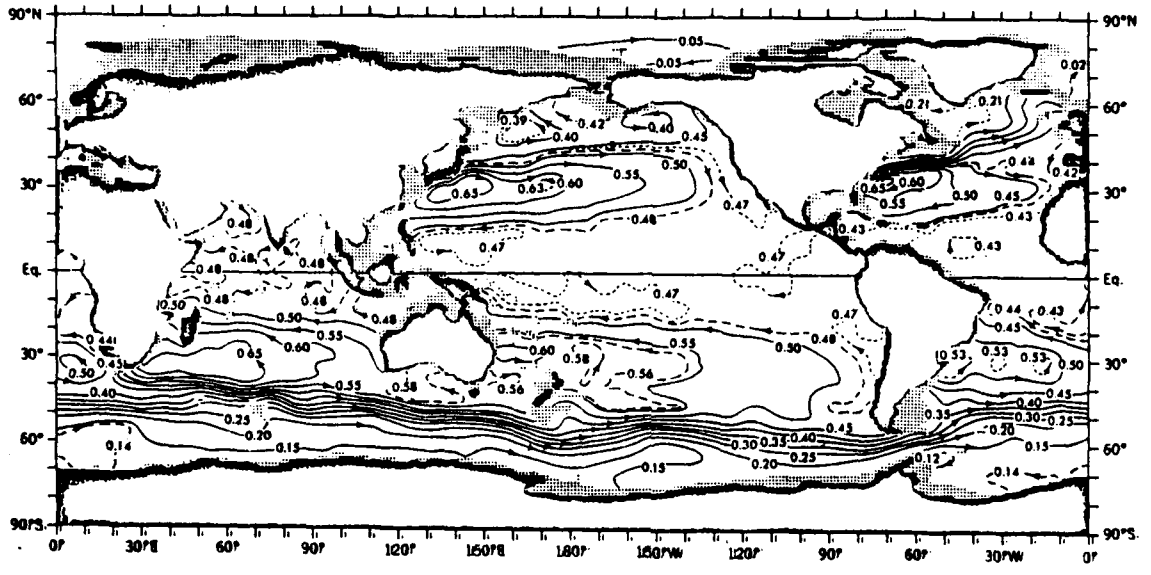

Fig. 1. Annual mean geopotential thickness (geop. m) of the 500-1000 m layer. (From Levitus, 1982)

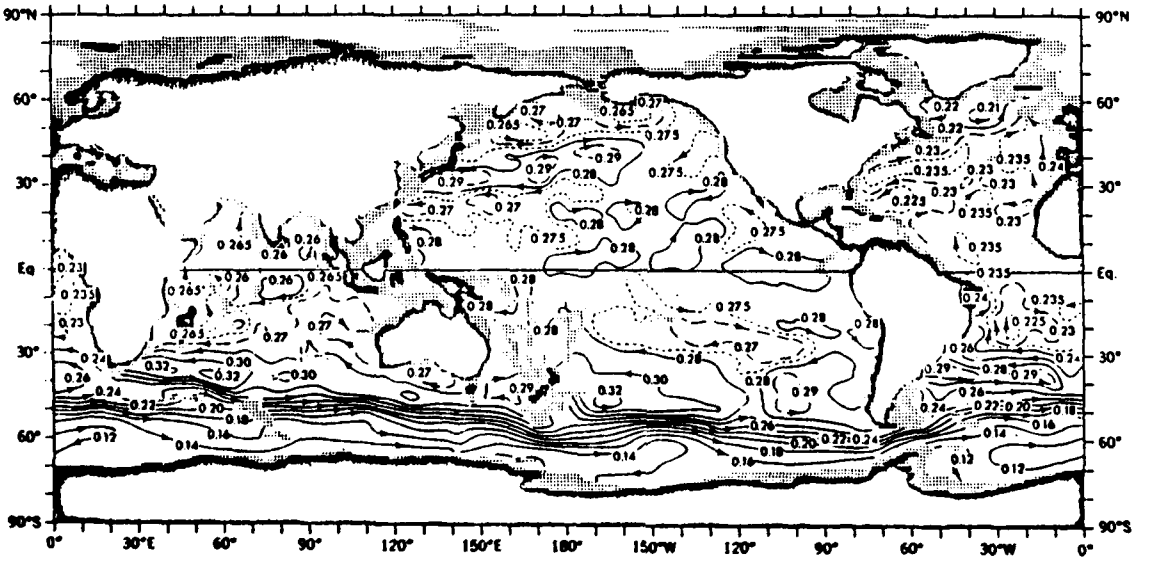

Fig. 2. Annual mean geopotential thickness (geop. m) of the 1500-2000 m layer. (From Levitus, 1982)

able evidence of topographic interaction with this circulation (at 120°W) where the East Pacific Rise reaches about 2700 m depth. The structure of the isopycnals in Figure 3 shows them plunging in the region of strong vertical shear in the circumpolar current and then rising again to form the bowl of the wind gyre, even below 2000 m.

It is natural to speculate that this deep circulation results from the proximity of the subtropical gyre and the strong eastward current.

2. TOWARDS A PLAUSIBLE MODEL OF THE SOUTH PACIFIC CIRCULATION

As has been noted, the wind-gyre and circumpolar curent system cannot be controlled by a single dynamic balance and a solution of the full dynamical problem would of necessity be extremely complicated. Here, attention will be focused on the structure of the wind gyre. The zonal current, and its depth structure, will be imposed and no attempt made to understand its dynamics. In the real oceans the subtropical gyres are driven by wind stress curl of one sign only, and the return flow occurs in a western boundary current. To avoid the complications involved if such currents exist, a wind stress curl distribution will be applied which has regions of positive and negative values, and so drives a closed 'mid ocean' gyre (Rhines and Young, 1982a).

It will be assumed that quasi-geostrophic dynamics may be applied, and further, that the motion is large scale so that relative vorticity may be ignored. These simplifications are necessary for an analytically tractable problem since, as remarked earlier, the forcing must be strong enough to deform the q-contours, and indeed close them, and the dynamics are essentially nonlinear.

Before attempting to solve a problem which is in any sense realistic, a pair of simple problems will be investigated, for the purpose of highlighting the important physical mechanisms involved. The response of a two layer model to wind forcing will be determined; firstly, if the fluid is at rest without the forcing, and secondly, if there is a uniform zonal current.

The equations of motion are

$$J(\psi_1, q_1) = w_0 \tag{2.1}$$

$$J(\psi_2, q_2) = 0 \tag{2.2}$$

where ψ_1 and ψ_2 are the upper and lower layer streamfunctions, q_1 and q_2 are the upper and lower layer potential vorticities, and w_0 is the wind stress curl, which imposes a vertical velocity in the upper layer.

The potential vorticity may be written in terms of the streamfunction thus,

$$q_1 = \beta y + F(\psi_2 - \psi_1) \tag{2.3}$$

$$q_2 = \beta y + F(\psi_1 - \psi_2) \tag{2.4}$$

where x, y denote zonal and meridional Cartesian coordinates respectively,

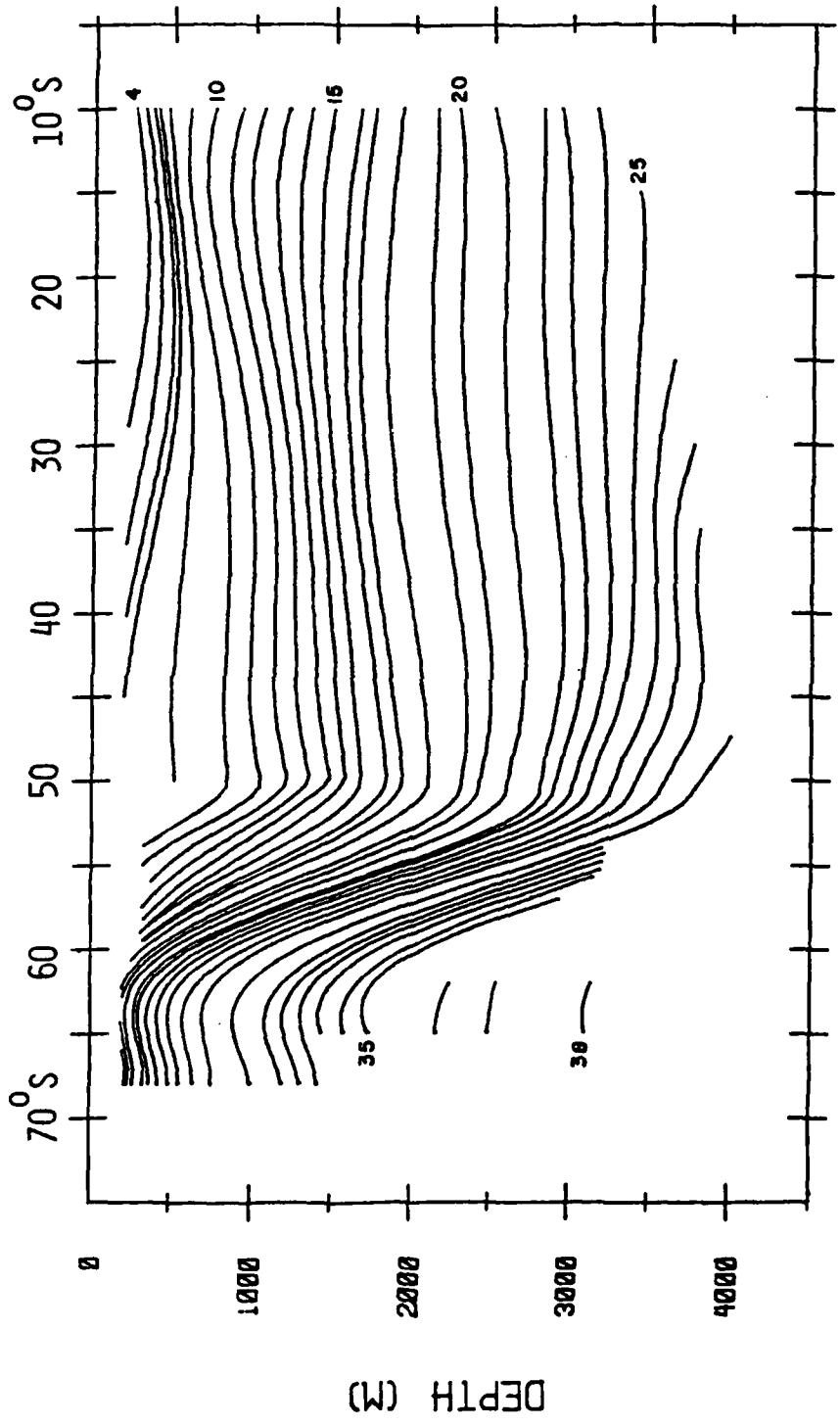

Fig. 3. Vertical section of smoothed isopycnals along 40°W. (From Coats, 1982)

β is the gradient of the Coriolis parameter, and F is equal to the inverse square of the Rossby radius of deformation.

A convenient form for the wind forcing, exactly as used in Rhines and Young (1982a) is

$$w_0 = \alpha x \qquad |\underline{x}| < r_c$$
$$= 0 \qquad |\underline{x}| > r_c \tag{2.5}$$

This forcing satisfies the condition $\int_{-\infty}^{\infty} w_0 \, dx = 0$ necessary for a closed mid ocean gyre.

If there is no zonal flow this problem has been solved by Rhines and Young (1982a). Adding (2.1) and (2.2) gives the equation

$$J(\psi_1+\psi_2 \, , \, \beta y \quad) = w_0 \tag{2.6}$$

and may be solved for $\psi_1+\psi_2$ by integrating westward from $x = +\infty$.

Equation (2.2) may now be written as

$$J(\psi_2 \, , \, F(\psi_1+\psi_2)+\beta y) = 0 \tag{2.7}$$

so that ψ_2 is constant along lines of constant $F(\psi_1 + \psi_2 \quad) + \beta y$. Since ψ_2 is zero at large distances from the forcing region, it must be everywhere zero, unless the lines of constant $F(\psi_1 + \psi_2) + \beta y$ close, when ψ_2 is allowed to be nonzero in this closed region, although the functional dependence of ψ_2 on $F(\psi_1+\psi_2) + \beta y$ cannot be determined from the equations as they stand.

From (2.6)

$$\psi_1 + \psi_2 = \frac{\alpha}{2\beta}(x^2 + y^2 - r_c^2) \qquad |\underline{x}| < r_c$$
$$= 0 \qquad |\underline{x}| > r_c \tag{2.8}$$

and the lines $F(\psi_1 + \psi_2) + \beta y$ are circles with center at $y = -\beta^2/\alpha F$, in $|\underline{x}| < r_c$. These lines close, and ψ_2 can be nonzero, if

$$\beta^2/\alpha F < r_c$$

that is, if the forcing is sufficiently strong.

Contrast this result with the solutions if there is a zonal flow. Then (2.8) becomes

$$\psi_1 + \psi_2 = \alpha/2\beta\,(x^2+y^2-r_0^2) - 2Uy \qquad |\underline{x}| < r_c$$
$$= -2Uy \qquad |\underline{x}| > r_c \tag{2.9}$$

Then (2.7) and the conditions on ψ_2 outside the forcing region give the solution to the problem as

$$\left.\begin{aligned}\psi_1 &= -Uy + \frac{\alpha}{2\beta}\frac{(\beta/UF-1)}{(\beta/UF-2)}(x^2+y^2-r_0^2)\\ \psi_2 &= -Uy - \frac{\alpha}{2\beta}\frac{}{(\beta/UF-2)}(x^2+y^2-r_0^2)\end{aligned}\right\}\ \text{in } |\underline{x}|<r_0$$
$$\psi_1 = \psi_2 = -Uy \quad \text{in } |\underline{x}|>r_0 \tag{2.10}$$

These solutions are valid everywhere providing the $F(\psi_1+\psi_2)+\beta y$ lines do not become closed. We see that these solutions have a different character from those obtained with no zonal flow. Firstly, there is always a response to the wind forcing in the bottom layer. If $0<\beta/UF<2$, the size of this response will be greater than that in the upper layer. There is a sharp resonance structure when β/UF is equal to 2, which is when the zonal flow brings the freely propagating Rossby waves to rest, so that these are trapped in the forcing region.

If we turn the problem upside down (2.10) is simply the response of the two layer system to the topography, h, defined by

$$h = \frac{H\alpha}{2FU}(x^2+y^2-r_0^2) \quad \text{in } |\underline{x}|<r_0$$
$$0 \quad \text{in } |\underline{x}|>r_0 \tag{2.11}$$

Of course the wind stress imposes a vertical velocity, upward in $x<0$ and downward in $x>0$ which corresponds to 'negative topography' at the surface. The response in the lower layer is larger than in the upper for because the interface tends to conform to this wind imposed topography, so that the response in the upper layer is small.

Similar calculations to that presented above have been done for three and four layer models, with each layer being the same depth and containing fluid traveling at the same uniform velocity, U in it without the forcing. In a three layer model the resonant conditions are $\beta/UF=1$ and $\beta/UF=3$ and the response is largest in the lowest layer if $0<\beta/UF<1$. With four layers resonance occurs if $\beta/UF = 2-\sqrt{2}$ or 2 or $2+\sqrt{2}$ and if $0<\beta/UF<2-\sqrt{2}$ the largest response is in the lowest layer.

Finally, a continuously stratified model is considered. The vertical coordinate is denoted by z, the sea surface being at $z=0$ and the bottom at $z=-H$. The governing equation, the large scale quasi-geostrophic potential vorticity equation, is

$$J(\psi, q) = 0 \tag{2.12}$$

where $q = \beta y + (f^2\psi_z/N^2)_z$, N^2 being the buoyancy frequency, assumed constant, and f the Coriolis parameter. If the streamlines do not close we deduce that

$$\frac{f^2}{N^2}\psi_{zz} + \beta y = -\beta'\psi/U \tag{2.13}$$

by going along ψ = constant lines until out of the forcing region. The boundary conditions are

$$J(\psi, \psi_z) = w_0 \quad \text{at} \quad z = 0 \tag{2.14}$$

$$J(\psi, \psi_z) = 0 \quad \text{at} \quad z = -H \tag{2.15}$$

If the streamlines do not close on $z = -H$ we may deduce that $\psi_z = 0$ on $z = -H$. Integrating (2.12) between $z = -H$ and $z = 0$ gives a condition on the barotropic streamfunction ψ_B, defined by

$$\psi_B = \int_{-H}^{0} \psi \, dz \tag{2.16}$$

which is just

$$J(\psi_B, \beta y) = w_0 \tag{2.17}$$

The solution for ψ is

$$\psi = -Uy + \frac{\alpha}{2\beta}(\beta/U)^{1/2}\frac{N}{f}(x^2+y^2-r_0^2)\frac{\cos N/f(\beta/U)^{1/2}(z+H)}{\sin N/f(\beta/U)^{1/2}H} \tag{2.18}$$

obtained by solving (2.13) with the boundary condition (2.15) and the constraint (2.16), given ψ_B from (2.17). Here the largest response is at $z = -H$, that is at the bottom, and it appears that the results from the layer models are most relevant to the continuous model if the westward flow speed is greater than the propagation speed of all the free modes., i.e., the system is superresonant.

A wind stress imposed on a constant zonal current is not a satisfactory model for the South Pacific circulation, but the intuition gained from these simple examples will be used later to explain the results for more complicated systems. The simplest modification that can be made to the constant current is to confine it to being south of same latitude -- this provides a model which is worth more detailed study.

3. TWO LAYER MODEL

We solve the two layer quasigeostrophic equations

$$J(\psi_1, q_1) = w_c + R\nabla^2(\psi_2 - \psi_1) \tag{3.1}$$

$$J(\psi_2, q_2) = 0 + R\nabla^2(\psi_1 - \psi_2) - D\nabla^2\psi_2 \tag{3.2}$$

where q_1 and q_2 are given in terms of ψ_1 and ψ_2 by (2.3) and (2.4). The extra terms on the righthand sides represent weak eddy effects producing vertical transfer of momentum, and bottom drag. We neglect these terms to leading order, but expect that they will be necessary to determine the

circulation in the region of closed streamlines. The forcing w_0 will be of almost the same form as before apart from a shift of origin so that

$$w_e = \alpha x \qquad |\underline{x} - (0,\ell)| < r_0$$
$$= 0 \qquad |\underline{x} - (0,\ell)| > r_0$$

We seek solutions with

$$\psi_1 = \psi_2 = 0 \quad \text{in} \quad y > 0$$
$$\psi_1 = \psi_2 = -Uy \quad \text{in} \quad y < 0$$

outside the forcing region. It is difficult to pose these as upstream or downstream conditions since, depending on the velocities of the fluid, information may propagate either eastward or westward. It would be possible therefore, that there is no solution to this ill posed problem; fortunately this turns out not to be the case. The geometry of the system is shown in Figure 4.

Adding (3.1) and (3.2) and integrating we obtain

$$\psi_B = \psi_1 + \psi_2 = \frac{\alpha}{2\beta}\left(x^2 + (y-\ell)^2 - r_0^2\right) - 2Uy \quad \text{in} \quad y < 0$$
$$= \frac{\alpha}{2\beta}\left(x^2 + (y-\ell)^2 - r_0^2\right) \quad \text{in} \quad y > 0$$

In the forcing region, and for $y > 0$ the $F\psi_B + \beta y$ contours, on which ψ_2 is constant, are circles with centers at $y = 1 - \beta^2/F\alpha$, while in $y < 0$, they are circles with centers at $y = 1 + 2\beta U/\alpha - \beta^2/\alpha F$. Contours made up of these lines must close, so that there must be a response in the bottom layer, however weak the forcing is. This consists of a circulation in the closed streamline region, plus a "topographic" response when the zonal current is deflected by the wind stress induced topography. If $2\beta U/\alpha - \beta^2/\alpha F$ is less than zero some of the current flows to the north of the closed streamline region, this seemingly bizarre result will be discussed later, if the flow is superresonant then this can be avoided. It has been noted that the layer models behave most like a continuously stratified model when the flow is superresonant.

Where the $F\psi_B + \beta y$ contours are not closed ψ_2 may be found by tracing these contours until they leave the forcing region. Thus in $y > 0$ it is found that

$$\psi_2 = 0$$

$$\psi_2 = -Uy - \frac{\alpha\left(x^2 + (y-\ell)^2 - r_0^2\right)}{2\beta\left(\beta/UF - 2\right)} \qquad \text{in } y < 0 \text{ (inside forcing region)}$$
$$= -Uy \qquad \text{in } y < 0 \text{ (outside forcing region)}$$

However, where the contours close it is necessary to follow Rhines and Young (1982a) and use the weak diffusive terms to solve for the functional dependence of ψ_2 on $F\psi_B + \beta y$. (3.2) implies that

$$F\psi_B + \beta y = A(\psi_2) + O(R, D) \tag{3.3}$$

Model of South Pacific Circulation (Mark I)

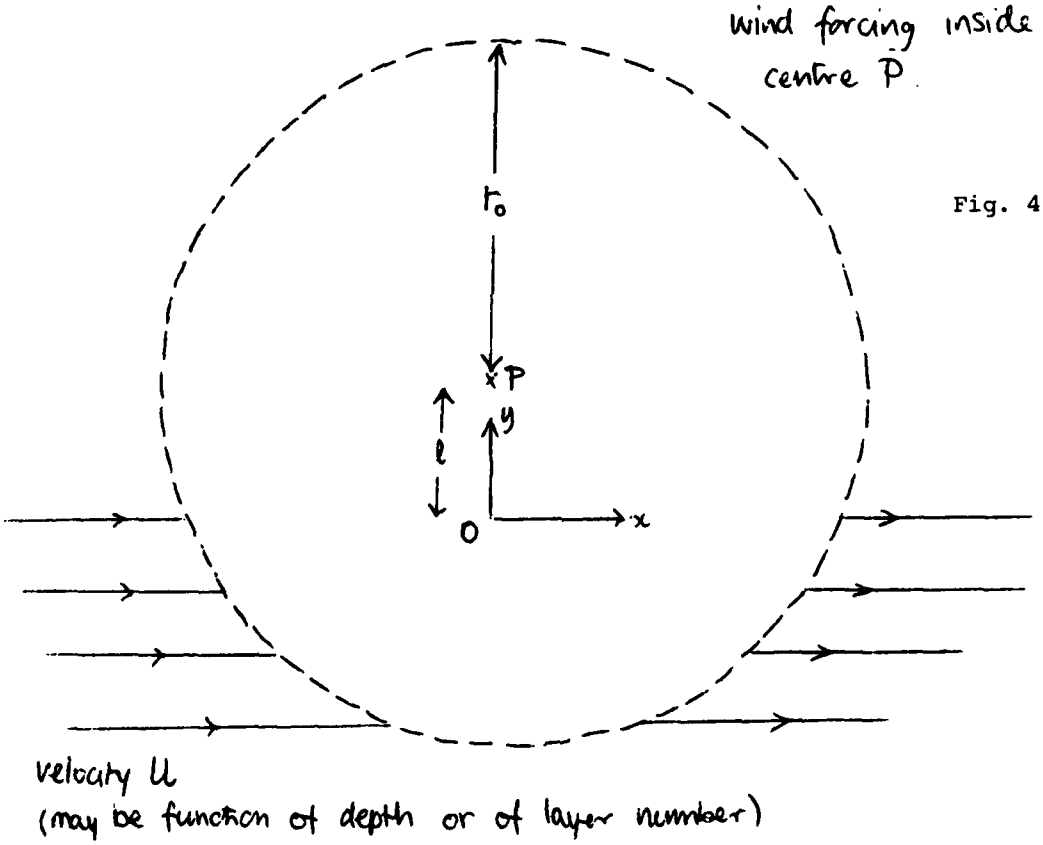

Fig. 4.

then integrating inside a closed ψ_2 contour gives

$$0 = \int R\nabla^2(\psi_1-\psi_2) - D\nabla^2\psi_2 \, dA \tag{3.4}$$

Substituting in (3.4) from (3.3) it is found that

$$(2R+D) \oint \nabla\psi_2 \cdot \underline{n} \, ds = R \frac{dA}{d\psi_2} \oint \nabla\psi_2 \cdot \underline{n} \, ds \tag{3.5}$$

where the $dA/d\psi_2$ can be taken outside the integral because it is a function of ψ_2 and therefore a constant on the contour of integration. It is deduced that, providing the circulation is nonzero

$$F\psi_B + \beta y = \frac{2R+D}{R} \psi_2 + \text{constant}$$

where the constant is determined at the edge of the closed streamline region, and for superresonant flow is found to be zero.

Thus

$$\psi_2 = \frac{R}{2R+D}\left(\frac{\beta y}{F} + \frac{\alpha}{2\beta}\left(x^2+(y-l)^2-r_0^2\right) - 2Uy\right) \qquad \text{in } y < 0$$

$$= \frac{R}{2R+D}\left(\frac{\beta y}{F} + \frac{\alpha}{2\beta}\left(x^2+(y-l)^2-r_0^2\right)\right) \qquad \text{in } y > 0$$

inside the region of closed streamlines.

Figure 5 shows the streamline patterns in the top and bottom layers, for superresonant flow and cases of strong and weak forcing. In the latter case, if there were no zonal current, there would have been no flow in the lower layer. It is concluded tentatively that the presence of the current does indeed allow the wind-driven circulation to penetrate deeper. The interface height shows the bowl shape expected in a gyre except near the poleward edge where the response is "topographic". As remarked before, in superresonant flow the interface adjusts to a similar form to the wind induced topography, which here is increasing the upper layer thickness, so the interface rises. This feature is not seen in Figure 3, but as will be seen, if there is strong enough vertical shear in the current the interface slope due to the shear dominates the "topographic" response.

The obvious next step is to go to a three layer model to see if the current-enhanced gyre survives, and how it is modified.

4. THREE LAYER MODEL

It is assumed for simplicity that the layers are all of the same thickness, but the zonal currents in each layer will be allowed to be different, and will be of strength U_1, U_2, and U_3 in layers 1, 2 and 3. The quasigeostrophic potential vorticity equations in each layer are

$$J(\psi_1, \beta y + F(\psi_2-\psi_1)) = W_0 + R\nabla^2(\psi_2-\psi_1) \tag{4.1}$$

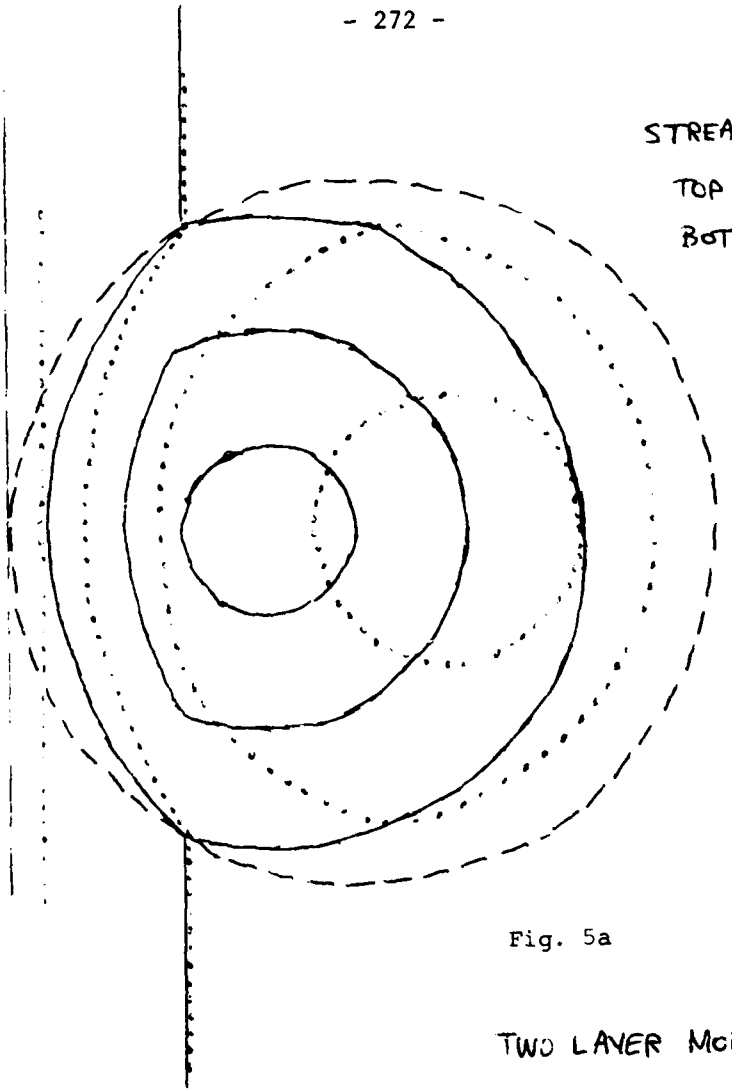

Fig. 5a

TWO LAYER MODEL $\beta/U_F = 1$ I O

STRONG FORCING $\frac{\beta^2}{F\alpha} = 1/4 r_0$

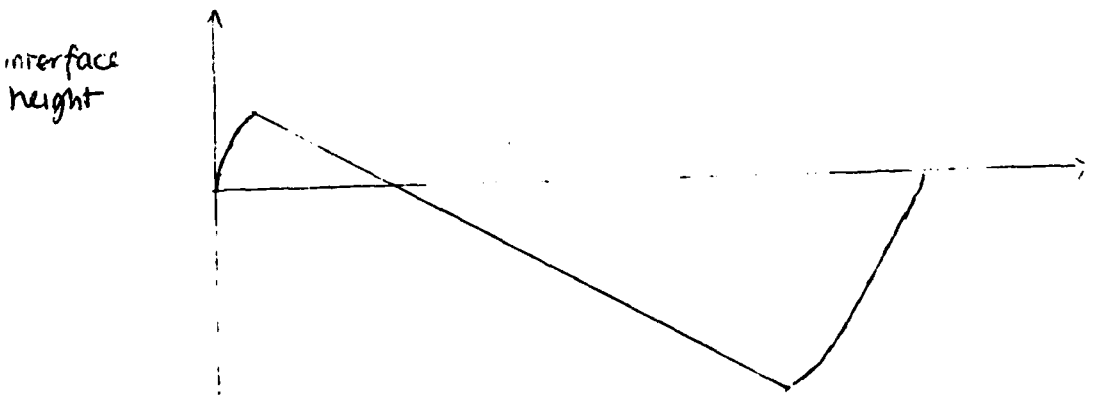

AD-A122 864 1982 SUMMER STUDY PROGRAM IN GEOPHYSICAL FLUID DYNAMICS AT THE WOODS HOLE..(U) WOODS HOLE OCEANOGRAPHIC INSTITUTION MA G VERONIS ET AL. NOV 82 WHOI-82-45

UNCLASSIFIED N00014-82-G-0079 F/G 20/4 NL

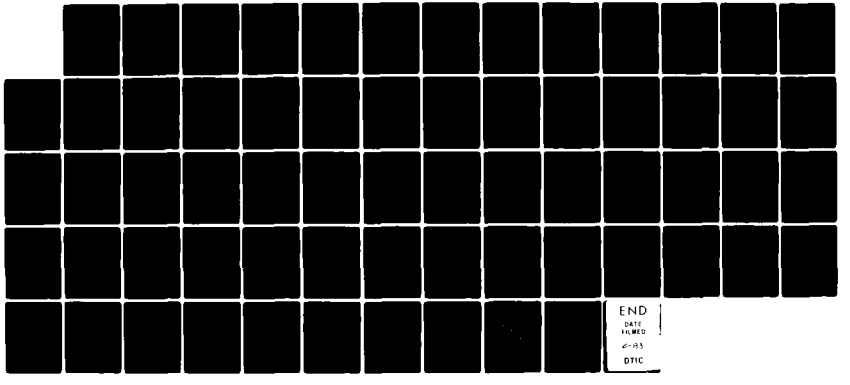

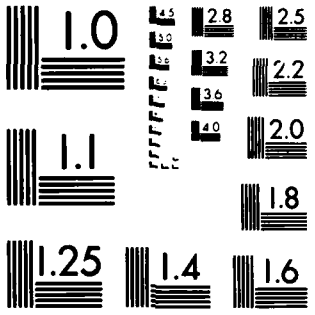

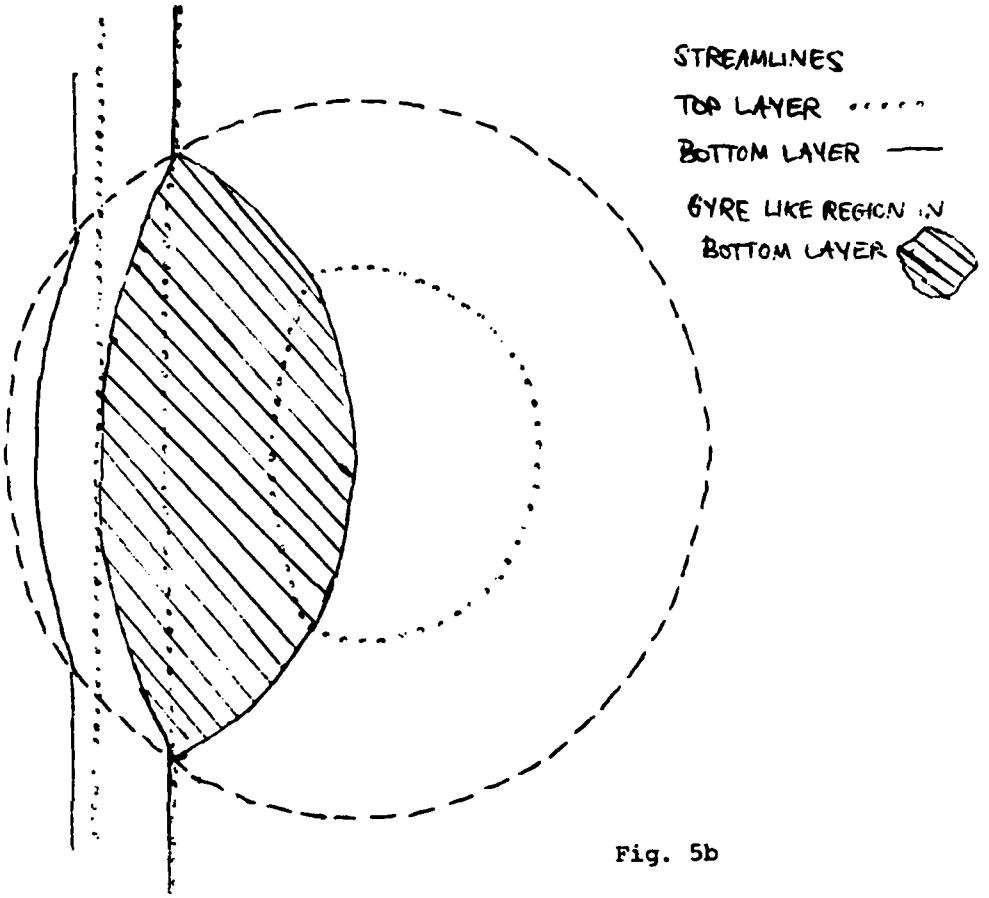

Fig. 5b

TWO LAYER MODEL $(\beta/_{UF} = 1)$

WEAK FORCING $\beta^2/_{Fd} = r_0$ $D = 0$

$$J(\psi_2, \beta y + F(\psi_1 + \psi_3 - 2\psi_2)) = 0 + R\nabla^2(\psi_1 + \psi_3 - 2\psi_2) \qquad (4.2)$$

$$J(\psi_3, \beta y + F(\psi_2 - \psi_3)) = 0 + R\nabla^2(\psi_2 - \psi_3) - D\nabla^2\psi_3 \qquad (4.3)$$

where again R and D are small parameters.

These can be solved in a manner exactly analogous to that used in the two layer model. Adding the equations gives

$$J(\psi_1 + \psi_2 + \psi_3, \beta y) = w_0 \qquad (4.4)$$

which can be solved for the barotropic streamfunction

Then (4.2) and (4.3) imply that

$$\psi_2 = Q_1(F\psi_B + \beta y) \qquad (4.5)$$

$$\psi_3 = Q_2(F\psi_2 + \beta y) \qquad (4.6)$$

where Q_1 and Q_2 must be determined from the upstream conditions or, in regions of closed streamlines, using the weak diffusive terms. A gyre like response is found in all layers, however small the forcing, providing that $\beta/U_2F - 1 < 0$ and $\beta/(U_1 + U_2 + U_3)F - 1 < 0$. Figure 6 shows schematically the regions into which the flow divides, as far as what determines the flow in these regions. In region (a) there is no flow in the bottom two layers and all the transport, determined by (4.4) is on the top layer. In region (b) there is no flow in the bottom layer, the flow in the middle layer is determined by the weak diffusion and the residual transport is in the top layer. In regions (c) and (d) there is flow in all three layers and weak diffusion determines the flow in the bottom two layers. In region (e) the flow in the second layer communicates with the region away from the forcing but in the third layer the flow is still determined by the weak diffusion. In region (f) the bottom two layers communicate with the unforced region and the response is "topographic".
Explicitly the situations are, in the regions

$$\psi_2 = \alpha/6\beta\,(x^2 + (y-\ell)^2 - r_0^2) + \beta y/3F \qquad \text{in regions (b), (c)}$$

$$\psi_3 = \frac{R}{3F(R+D)}\left(\frac{F\alpha}{2\beta}(x^2 + (y-\ell)^2 - r_0^2) + 4\beta y\right) \qquad \text{in region (c)}$$

$$\psi_2 = \alpha/6\beta\,(x^2 + (y-\ell)^2 - r_0^2) + \beta y/F - \frac{(U_1+U_2+U_3)}{3}y \qquad \text{in region (d)}$$

$$\psi_3 = \frac{R}{3F(R+D)}\left(\frac{F\alpha}{2\beta}(x^2 + (y-\ell)^2 - r_0^2) + 4\beta y - (U_1+U_2+U_3)y\right) \qquad \text{in region (d)}$$

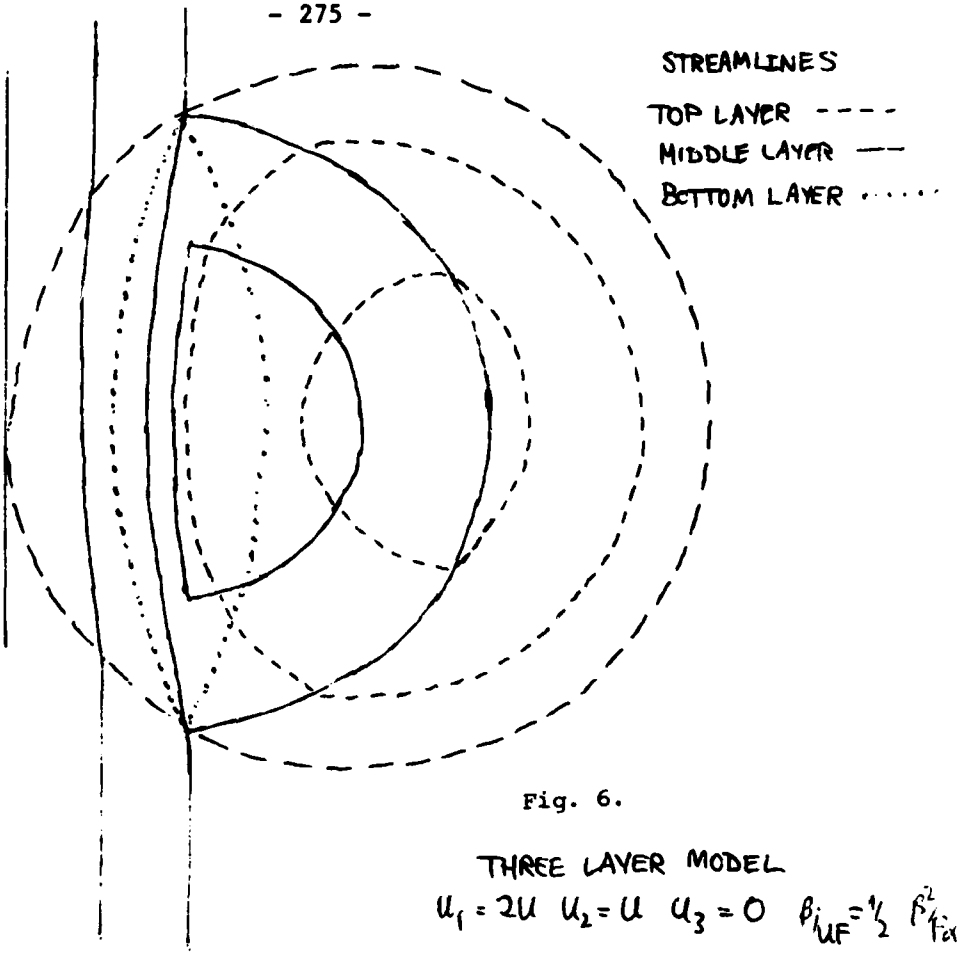

Fig. 6.

THREE LAYER MODEL

$u_1 = 2u \quad u_2 = u \quad u_3 = 0 \quad \beta_{i_{UF}} = \frac{1}{2} \quad \beta^2_{f_{ix}} = \frac{1}{2} r_c$

$R = D$

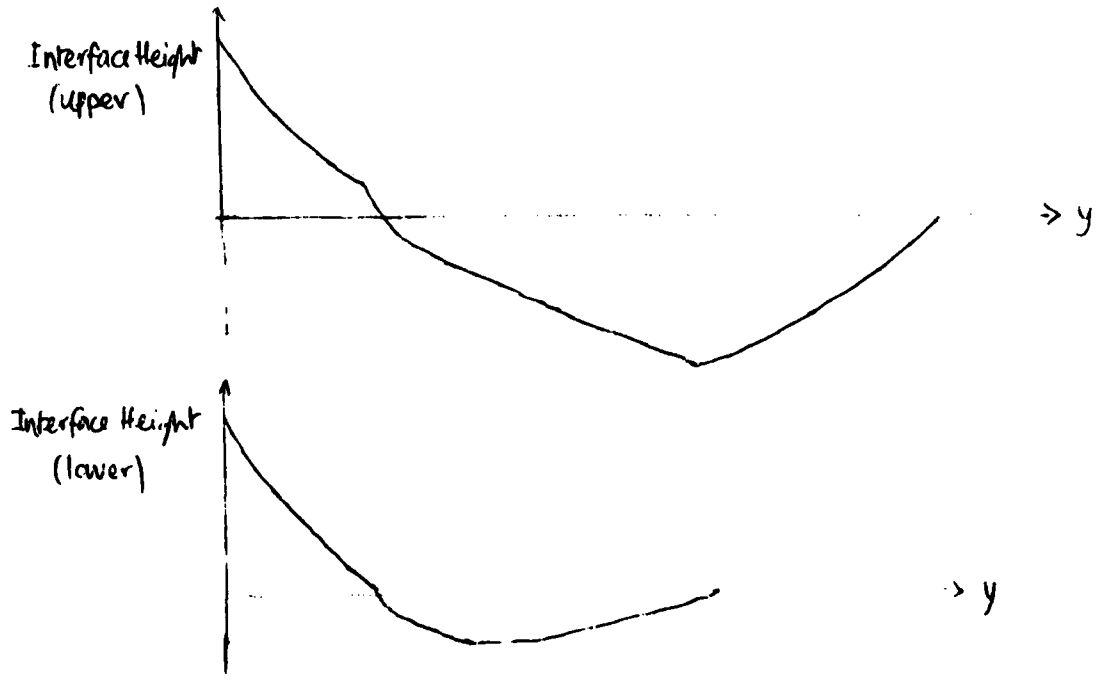

$$\psi_2 = -U_2 y - \frac{F\alpha U_2 (x^2+(y-\ell)^2-r_0^2)}{2\beta(\beta-FU_1-FU_2-FU_3)} \qquad \text{in regions (e), (f)}$$

$$\psi_3 = \frac{R}{\ell+D}\left((\beta/F-U_2)y - \frac{\alpha U_2 F (x^2+(y-\ell)^2-r_0^2)}{2(\beta-F(U_1+U_2+U_3)} \right) \qquad \text{in region (e)}$$

$$\psi_3 = -U_3 y + \frac{\alpha U_2 U_3 F^2 (x^2+(y-\ell)^2-r_0^2)}{2(\beta-F(U_1+U_2+U_3))(\beta-FU_2)\beta} \qquad \text{in region (f)}$$

while the barotropic transport

$$\psi_B = -(U_1+U_2+U_3)y + \frac{\alpha}{2\beta}(x^2+(y-\ell)^2-r_0^2) \qquad \text{in } y > 0$$

$$= \alpha/2\beta\,(x^2+(y-\ell)^2-r_0^2) \qquad \text{in } y < 0$$

The streamfunction in the upper layer ψ_1 is given by $\psi_B - \psi_2 - \psi_3$. Figures 6 and 7 show the streamline patterns and interface heights for two cases, one with equal velocity in each layer $U_1 = U_2 = U_3 = U$ and the other with vertical shear $U_1 = 2U$, $U_2 = U$, $U_3 = 0$. In the first case there is a closed gyre in the third layer, which would not have resulted for these parameter values if there had been no zonal current. In the second case, where there is actually no current in the third layer, there is still a gyre in this layer. With vertical shear the wind-driven circulation can penetrate even to below levels where there is no current! A feature which is common to both models is that the boundary of the region of closed streamlines moves poleward as the layers go from top to bottom. This feature was noted by Rhines and Young (1982a) in their model which is identical to the one on its equatorward side, but the poleward boundary of their gyre is vertical. Because of the neighboring current in this model the poleward boundary slopes upward and equatorward.

In the model without vertical shear the interfaces rise in the poleward part of the gyre, the "topographic" response, but the vertical shear causes strong interface slope to be superimposed on this, and the interfaces look much more like the isopycnals in Figure 3.

5. CONTINUOUSLY STRATIFIED MODEL

These layer models, with superresonant current velocities, can give intuition about the continuously stratified case, as shown in Section 2.

Rhines and Young (1982b) have shown that under appropriate assumptions concerning eddy fluxes, potential vorticity will homogenize on isopycnal surfaces in regions of closed streamlines in planetary scale flows. It is therefore appropriate to expect that when solving the continuously stratified version of the problem considered in Sections 3 and 4, the potential vorticity inside regions of closed streamlines may be written

$$q = Q(z) \qquad (5.1)$$

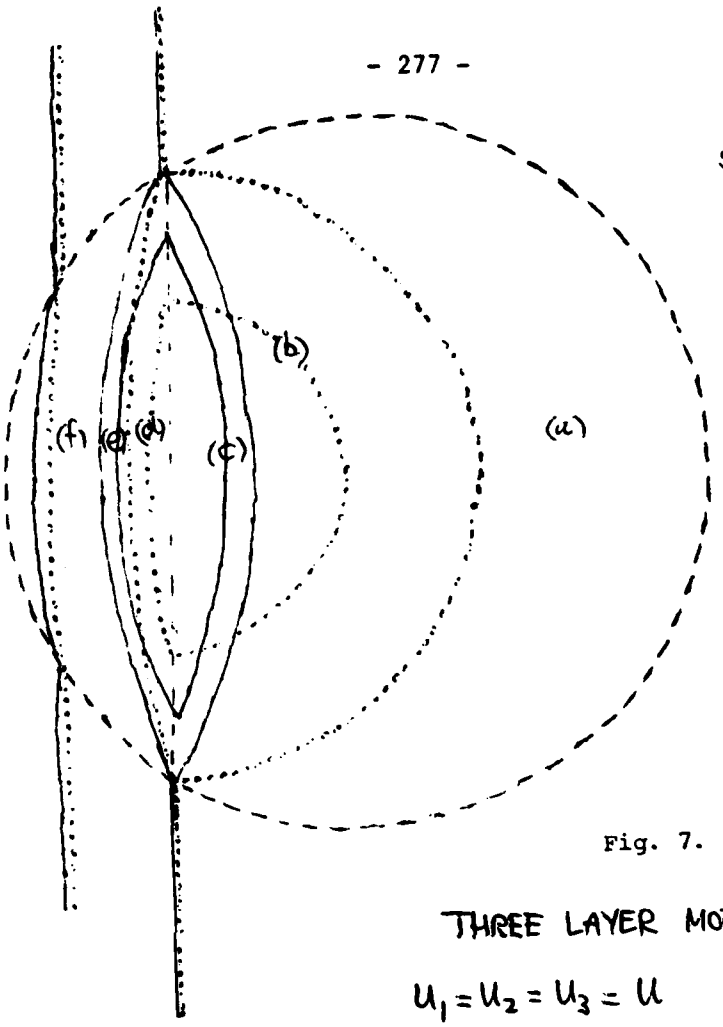

Fig. 7.

THREE LAYER MODEL

$U_1 = U_2 = U_3 = U$ $\quad \beta/UF = 1/2 \quad \beta^2/Fx = 1/2 r_c$

$R = D$

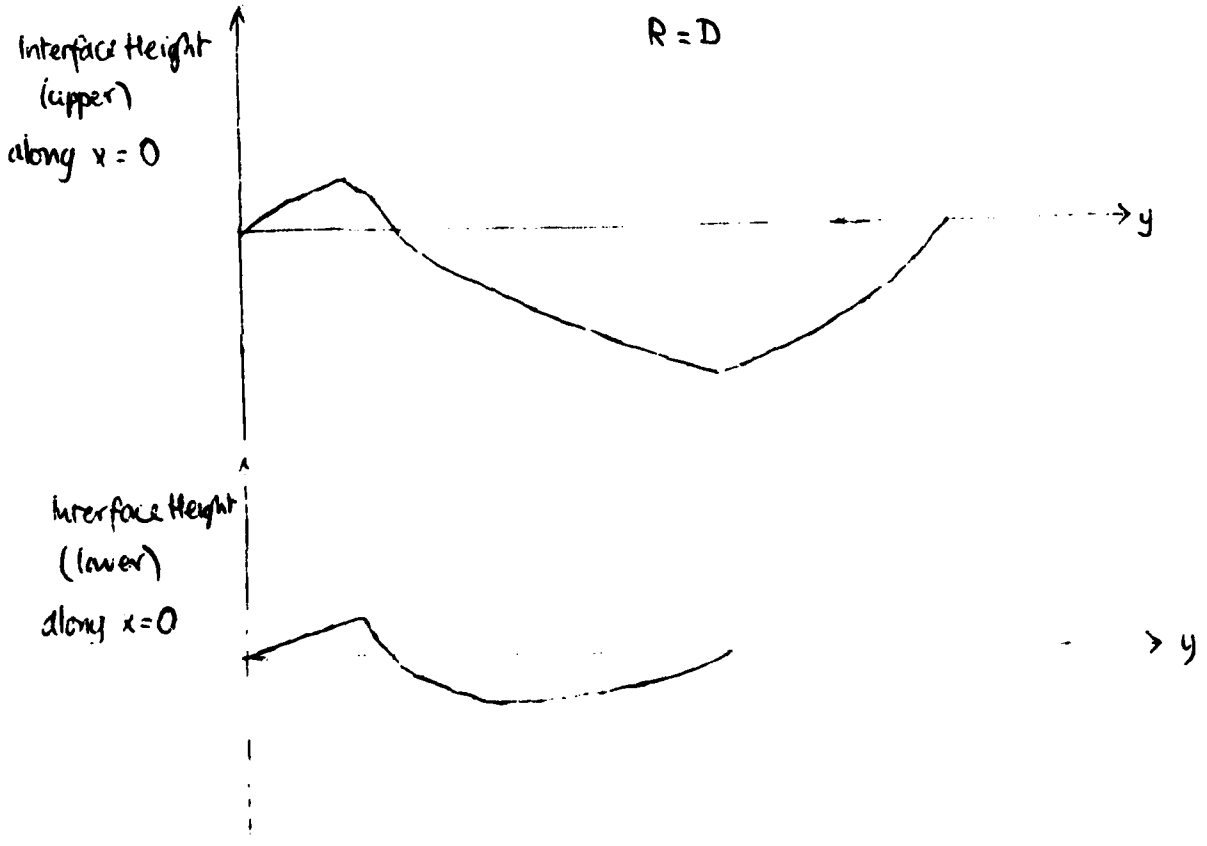

For completeness it is noted again the equation of motion is

$$J(\psi, q) = 0 \tag{5.2}$$

where $q = \beta y + \frac{f^2}{N^2}\psi_{zz}$

and the boundary conditions are

$$J(\psi, \psi_z) = w_0 \qquad \text{on } z = 0 \tag{5.3}$$

$$J(\psi, \psi_z) = 0 + D\nabla^2\psi \qquad \text{on } z = -H \tag{5.4}$$

when the $D\nabla^2\psi$ denotes weak Ekman friction, which will be used to determine the bottom boundary condition uniquely when the streamlines at the bottom become closed. The geometry of the problem, and the forcing will be exactly the same as in the layered models in Sections 3 and 4, but only the case of current velocity (equal to U) independent of depth will be considered.

The flow divides into three regions, one at rest, one where the streamlines are closed and the potential vorticity is determined by (5.1), and one where the streamlines connect to regions of no forcing and the potential vorticity is determined by

$$q = \frac{f^2}{N^2}\psi_{zz} + \beta y = -\beta\psi/U \tag{5.5}$$

Unfortunately the function Q(z) is not determined by the problem as specified (as noted in Rhines and Young (1982)). In the 3 layer model it was found that, if the current was superresonant, the weak diffusion resulted in q = 0, in the second layer, which was remote from forcing and bottom drag. The continuously stratified problem is therefore solved after assuming that Q(z) = 0, so that in regions of closed streamlines

$$\frac{f^2}{N^2}\psi_{zz} + \beta y = 0 \tag{5.6}$$

Integrating (5.2) with respect to z, it is found that the barotropic streamfunction ψ_B, defined by

$$\psi_B = \int_{-H}^{0} \psi \, dz \tag{5.7}$$

obeys the equation

$$J(\psi_B, \beta y) = w_0 \tag{5.8}$$

and is therefore given by

$$\psi_B = \alpha/2\beta\,(x^2 + (y-\ell)^2 - r_0^2) \qquad \text{in } y > 0 \text{ (inside forcing region)}$$

$$= 0 \qquad \text{in } y > 0 \text{ (outside forcing region)}$$

$$= \alpha/2\beta\,(x^2 + (y-\ell)^2 - r_0^2) - UHy \qquad y < 0 \text{ (inside forcing region)}$$

$$= -UHy \qquad y < 0 \text{ (outside forcing region)}$$

The constraint (5.7) will be imposed, rather than applying a boundary condition at $z = 0$.

By analogy with the three layer model it is expected that the flow will be divided into five regions; at the equatorward side of the gyre the wind driven flow will be limited to an upper region of the water column (Region 1). Going poleward this flow will penetrate to the bottom and there will be closed streamlines throughout the vertical extent of the fluid. (Region 2 in $y > 0$, Region 3 in $y < 0$). On the surface the most poleward closed streamline marks the edge of Region 4, in which above a certain depth the response is "topographic", and below it there are still closed streamlines. Finally, in the poleward part of the gyre the response is purely "topographic" throughout the whole depth of the fluid, the zonal current is diverted to the south as it flows past the gyre. The flow in each of these regions is now solved in detail.

Region 1

The circulation is assumed to penetrate to a depth $D(x,y)$, so that (5.6) holds in $0 > z > -D(x,y)$. The boundary conditions $\psi = \psi_z = 0$ are applied at the base of the gyre, and with the constraint (5.7) these are sufficient to uniquely determine the streamfunction ψ, which is given by

$$\psi = -\frac{\beta y N^2}{2f^2}(z+D)^2 \qquad \text{(in the forcing region)} \qquad (5.9)$$

and the depth of penetration of the circulation

$$D = \left(-\frac{6f^2}{\beta y N^2}\psi_B\right)^{1/3} \qquad (5.10)$$

The circulation penetrates to the bottom on the curve defined by $D(x,y) = H$ which in this case is a circle centered at $\ell = \beta^2 N^2 H^3/6\alpha f^2$

Regions 2 and 3

Here (5.6) holds in $0 > z > -H$. The boundary condition (5.4) implies that to leading order in R, $\psi = F(\psi_z)$ on $z = -H$, but at this order the function F cannot be determined. However, integrating (5.6) over the region enclosed by a closed ψ_z contour, it is found that

$$C \cdot \int J(\psi,\psi_z)\,dA = R\int \nabla^2\psi\,dA - \frac{dF}{d\psi_z}\oint \nabla\psi_z\cdot\underline{n}\,ds \qquad (5.11)$$

and it is deduced that ψ = constant on $z = 0$ in this region.
When $D = H$, $\psi = 0$ on $z = -H$ so

$$\psi = 0 \text{ on } z = 0 \text{ (when streamlines on the bottom are closed)} \qquad (5.12)$$

This boundary condition and the constraint (5.7) are sufficient to solve for ψ,

$$\psi = -\frac{\beta y N^2}{2f^2}(z+H)^2 + \frac{2}{H^2}\left(\psi_B + \frac{\beta y N^2 H^3}{6f^2}\right)(z+H) \qquad (5.13)$$

The streamline $\psi = 0$ (which bounds the closed streamline region) is most equatorward on $z = 0$, and in $y < 0$ consists of a circle centered at $\ell + \frac{\rho u H}{\alpha} + \frac{\beta^2 N^2 H^3}{12 f^2 \alpha}$, which is the boundary of Region 4.

Region 4

In $0 > z > -D(x,y)$ the streamlines are open and (5.5) holds, while in $-D(x,y) > z > -H$, the streamlines are closed and (5.6) holds. On $z = -D$ ψ and ψ_z are continuous, (5.13) and (5.7) give two more conditions, leaving one more needed to solve for ψ and determine the unknown D. This last condition comes from the fact that the surface $z = -D$ is composed of streamlines and so $\psi = 0$ on $z = -D$. Defining nondimensional $\mathcal{D}$ and $\mathcal{H}$ by $\mathcal{D} = \frac{N}{f}\left(\frac{\beta}{u}\right)^{1/2} D$, $\mathcal{H} = \frac{N}{f}\left(\frac{\beta}{u}\right)^{1/2} H$, the equation for $\mathcal{D}$ is found to be

$$\mathcal{D} + (\mathcal{H}-\mathcal{D})(1-\cos\mathcal{D})/2 - \sin\mathcal{D} - (\mathcal{H}-\mathcal{D})^2/12 = \left(\frac{\beta}{u}\right)^{1/2} \frac{N\psi_B}{(-u_y f')} \tag{5.14}$$

With the forcing chosen here lines $\mathcal{D}$ = constant are circles so that the surface $z = D(x,y)$ is made up of circles with centers a function of z. In $0 > z > -D$

$$\psi = -uy + A\cos\frac{N}{f}\left(\frac{\beta}{u}\right)^{1/2} z + B\sin\frac{N}{f}\left(\frac{\beta}{u}\right)^{1/2} z \tag{5.15}$$

where

$$A = -Uy\left(\tfrac{1}{2}(\mathcal{H}-\mathcal{D})\sin\mathcal{D} - \cos\mathcal{D}\right)$$
$$B = -Uy\left(\tfrac{1}{2}(\mathcal{H}-\mathcal{D})\cos\mathcal{D} + \sin\mathcal{D}\right)$$

In $-D > z > -H$,

$$\psi = -\frac{N^2}{2f^2}\beta y(z+H)^2 + \frac{N^2}{2f^2}\beta y(z+H)(H-D) \tag{5.16}$$

When $D = H$ there are no closed streamlines in the whole water column.

Region 5

There the potential vorticity is determined by the upstream conditions so that (5.5) holds everywhere. (5.6) implies that $\psi_z = 0$ on the bottom, since it is zero outside the forcing region. With the constraint on the total transport (5.7) the problem is closed and

$$\psi = -uy + \left(\frac{\beta}{u}\right)^{1/2} \frac{N}{f} \frac{\alpha}{2\beta}\left(x^2 + (y-\ell)^2 - r_0^2\right) \frac{\cos\frac{N}{f}\left(\frac{\beta}{u}\right)^{1/2}(z+H)}{\sin\frac{N}{f}\left(\frac{\beta}{u}\right)^{1/2} H} \tag{5.17}$$

just the topographic response discussed in Section 2. Outside the forcing region ψ just corresponds to uniform flow south of $y = 0$ and rest north of $y = 0$.

Figure 8 shows a meridional section of the gyre along $x = 0$, with the various regions considered. Figure 9 shows the horizontal structure of the surface and bottom streamlines, and the barotropic streamlines.

The problem of the continuously stratified gyre has thus been completely solved. The following features are worth noting. The wind-driven circulation inevitably penetrates all the way to the bottom -- this should be compared to the case with no zonal current solved by Rhines and Young (1982a) where the wind-driven is limited in depth. Consequently, provided their gyre does not penetrate to the bottom (they considered fluid of unbounded depth) that is if

$$H^3\beta^2 N^2/6\alpha r_0 f^2 > 1$$

for the forcing considered here, then the gyre with neighboring current penetrates deeper than the gyre without the current. The gyre has potential vorticity which is continuous across its poleward boundary but discontinuous across its equatorward boundary. Contrasting with the no current case, however, the poleward boundary of the gyre is not vertical but slopes upward and equatorward. This effect might be modified however, if there were vertical shear in the current, which would be an obvious (and simple) sophistication to consider.

It may be noted that the methods used to solve this problem could also be applied to large scale flow over topography in a continuously stratified fluid where the streamlines become closed. Homogenization of potential vorticity could be used to resolve the functional dependence of ψ on q in these regions.

6. MODEL WITH CONTINUOUS VELOCITY PROFILE

One immediate objection to the physical realism of the models presented so far might be that they have all involved discontinuous velocity profiles. The upstream profile used before was therefore replaced by one in which the upstream profile was made up of a region of no motion, a region of uniform shear, and then a constant velocity profile, as shown in Figure 10. For simplicity a two layer model was used (equations 2.1 -2.4). As before the motion in the second layer is along contours of $F\psi_B + \beta y$, given by

$$\begin{aligned} F\psi_B + \beta y &= \beta y + \frac{\alpha F}{2\beta}\left(x^2 + (y-\ell)^2 - r_c^2\right) && \text{in } y > 0 \\ &= \beta y + \frac{\alpha F}{2\beta}\left(x^2 + (y-\ell)^2 - r_c^2\right) + \Lambda y^2 F && \text{in } 0 > y > -Y_0 \\ &= \beta y + \frac{\alpha F}{2\beta}\left(x^2 + (y-\ell)^2 - r_c^2\right) - 2\Lambda Y_0 (y + Y_0/2) && \text{in } y < -Y_0 \end{aligned}$$

In $y > 0$ the contours are circles centered at $\ell - \beta\gamma/\alpha F$, in $0 > y > -Y_0$, ellipses centered at $(\ell - \beta^2/\alpha F)(1 + 2\Lambda\beta/\alpha)$, and with ratio of semi-major axis to semi-minor axis $(1 + 2\Lambda\beta/\alpha)^{1/2}$, and in $y < -Y_0$ circles centered at $\ell + 2\beta\Lambda Y_0/\alpha - \beta\gamma/\alpha F$

It can be shown that at the point $((r_c^2 - \ell^2)^{1/2}, 0)$ the ellipse which passes through this point has gradient $(r_c^2 - \ell^2)^{1/2}/\ell - \beta\gamma/\alpha F$, while the circle bounding the forcing region has gradient $(r_0^2 - 1^2)/1$. It is deduced that the $F\psi_B + \beta y$ contours must look qualitatively like those in Figure 10, so that some of the water entering the forcing region must travel to the north of the gyre.

Fig. 8.

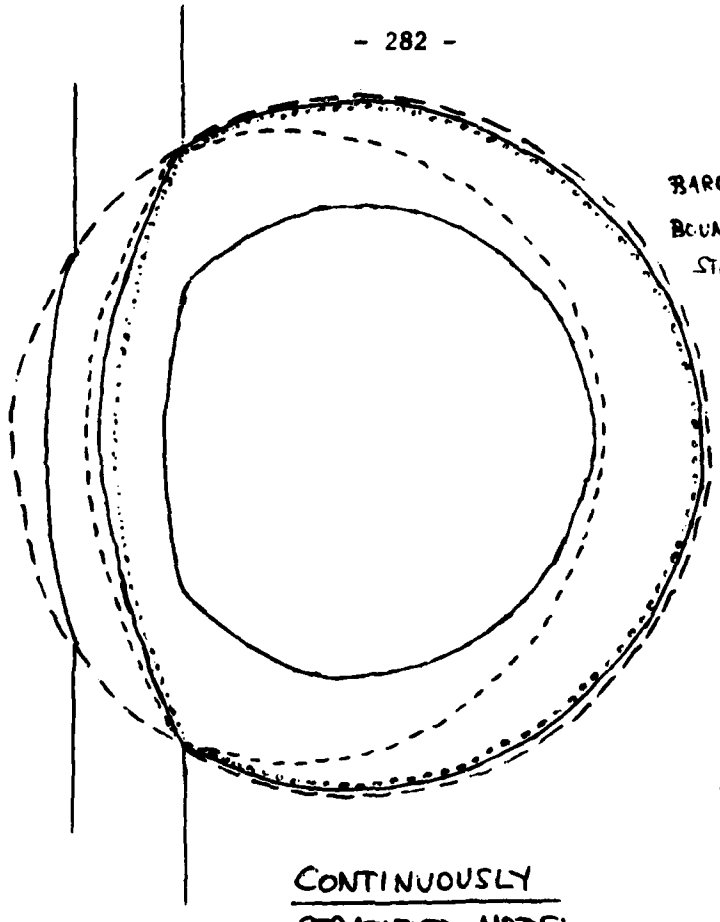

$$\frac{\beta U f}{r_0 \alpha N}\left(\frac{U}{\beta}\right)^{1/2} = \frac{2}{\pi}$$

$$\frac{Hf}{N}\left(\frac{\beta}{U}\right)^{1/2} = \frac{\pi}{2}$$

CONTINUOUSLY STRATIFIED MODEL

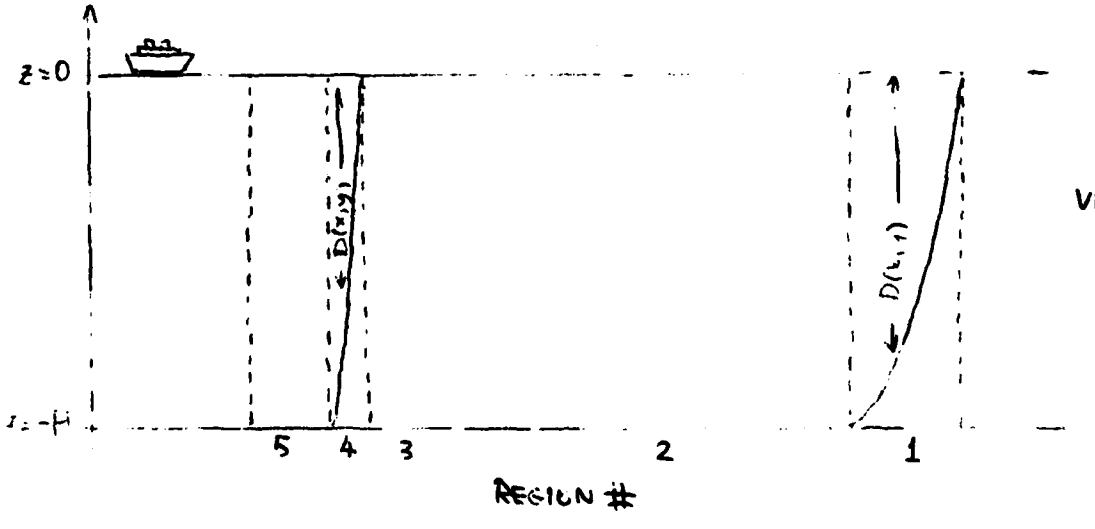

VERTICAL STRUCTURE ON x = 0

Fig. 9. MERIDIONAL CROSS SECTION ALONG x = 0

Fig. 10.

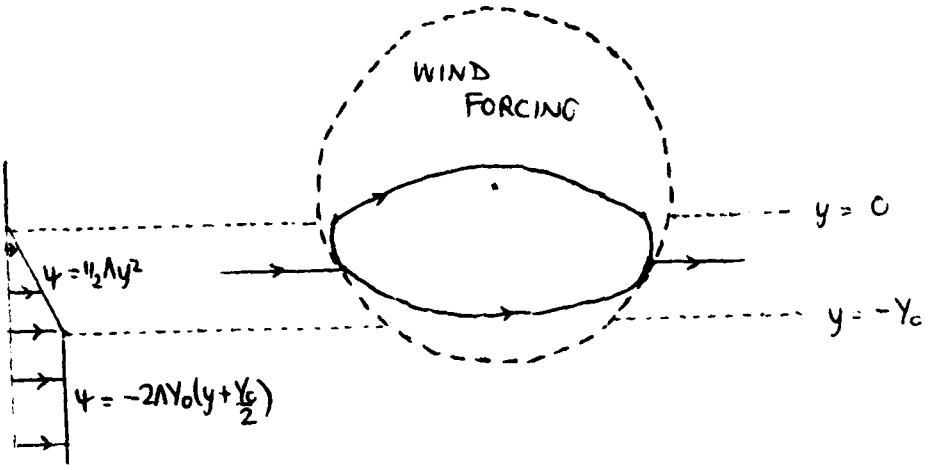

GEOMETRY OF GYRE WITH UPSTREAM FLOW WITH HORIZONTAL SHEAR

Fig. 11a

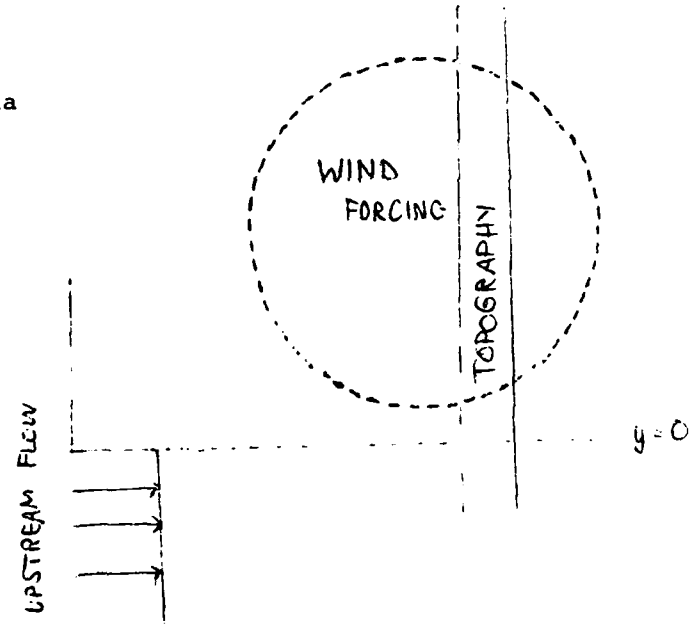

Fig. 11b

UPPER LAYER STREAMLINES .....

LOWER LAYER STREAMLINES ——

NORTHERN BOUNDARY OF REGION WITH MOTION IN BOTTOM LAYER.

Physically this is reasonable, the flow follows f/h contours in each layer, the wind stress means that some of these are closed and others pass to either side of the closed region, just as when fluid flows past an obstacle some passes to each side. However, there is no evidence that such a flow occurs in the South Pacific. It should be noted that to do this fluid would have to move equatorward in the western boundary currents, which are not included in the model gyre considered here. It is to be expected that if western boundaries were included, plus perhaps a dynamically balanced Antarctic Circumpolar Current, the equatorward excursion of water might be inhibited. However, this effect means that not much value has been gained from the extra sophistication in the model gyre.

7. SOME REMARKS ON THE EFFECT OF TOPOGRAPHY

It was noted in the Introduction that there is evidence for considerable interaction between the wind-driven circulation and the bottom topography in the South Pacific -- not surprisingly if the wind driven flow does, indeed, penetrate to great depths.

In one layer large scale quasigeostrophic flow the (barotropic) streamfunction satisfies the equation

$$J\left(\psi_B,\ \beta y + \frac{fh}{H}\right) = W_c \tag{7.1}$$

where f is the Coriolis parameter, h is the height of the bottom topography and H is the layer depth. The wind stress just drives the flow across potential vorticity contours, which are now controlled by topography as well as the gradient of planetary vorticity, and (7.1) can be regarded as a modified Sverdrup balance equation. The corresponding two layer flow obeys the equations

$$J\left(\psi_1,\ \beta y + F(\psi_2-\psi_1)\right) = W_c + R\nabla^2(\psi_2-\psi_1) \tag{7.2}$$

$$J\left(\psi_2,\ \beta y + F(\psi_1-\psi_2) + \frac{fh}{H}\right) = 0 + R\nabla^2(\psi_1-\psi_2) - D\nabla^2\psi_2 \tag{7.3}$$

which are just equations (3.1) and (3.2) with a topographic term. However, due to the extra internal degree of freedom no simple equation can be derived for the barotropic streamfunction; in fact it is found that

$$J(\psi_B, \beta y) = W_c - J(\psi_2, fh/H) \tag{7.4}$$

and so no simple modified Sverdrup balance applies. It is suggested that under certain conditions, because of the extra freedom afforded by the stratification, the net transport may be much greater (or less) than that suggested by a simple barotropic model with topography.

There are additional complications, consider response to a forcing W_o which is localized (exactly as in previous sections). It is known that the response will be confined to the upper layer unless the potential vorticity contours close in the lower layer. If there is no response in the lower layer, then ψ_B is known, and $\psi_1 = \psi_B$ unless contours of $F\psi_B + \beta y + fh/H$ close. (Note the topographic influence). Inside these closed contours, to leading

order in R and D

$$fh_{/H} + \beta y + F\psi_1 = A(\psi_2) \tag{7.5}$$

and integrating (7.3) over the region bounded by a closed streamline in the lower layer implies that

$$R \oint \nabla\psi_1 \cdot \underline{n}\, ds = (R+D) \int \nabla\psi_2 \cdot \underline{n}\, ds$$

and hence from (7.5) that

$$\frac{R}{F}\frac{dA}{d\psi_2} = \frac{R}{FH}\frac{\oint \nabla h \cdot \underline{n}\, ds}{\oint \nabla\psi_2 \cdot \underline{n}\, ds} + R+D \tag{7.6}$$

This equation for $A(\psi_2)$ is awkward to solve due to the topographic term; indeed a closed solution may not be written down. One way of approaching the problem might be to solve iteratively, perhaps assuming weak topography, such a solution is needed to solve the problem and perhaps highlight the effect of topography on the transport.

There is evidence that the Antarctic Circumpolar Current is deflected to the north when it crosses the East Pacific Rise, thus perhaps bringing a zonal current into a region of strong wind stress curl. This motivated investigation of the problem with the geometry shown in Figure 11a, with a current to the south of a wind-forcing region, but with topograhy to divert the current into the forcing region.

This is an example of a problem which is not well posed. In the 2 layer model, if $0 < \beta/uF < 1$, then the response to topography is such that in each layer the disturbance is of the same sign, but the magnitude of that in the upper layer is larger. As shown in Figure 11b this results in the streamlines in the top layer leaving the region of nonzero velocity in the lower layer. When they enter a region of zero velocity in the lower layer they must follow y = constant lines, and so a streamline may be followed from $x = -\infty$, turn northwards, and then go back to $x = -\infty$, meaning that the velocity profile assumed may not be posed. However, a solution to the large scale quasi-geostrophic equation is

$$\psi_1 = \frac{\beta y}{F(1-\beta/uF)}, \quad \psi_2 = 0 \quad \text{in} \quad \frac{hf(1-\beta/uF)}{H\beta(\beta/uF-2)} < y < \frac{\max(h)(1-\beta/uF)}{H\beta(\beta/uF-2)}$$

$$\psi_1 = -Uy + \frac{fUh}{H\beta(\beta/uF-2)} \quad \text{in} \quad y < \frac{hf}{H\beta}\frac{(1-\beta/uF)}{(\beta/uF-2)}$$

$$\psi_2 = -Uy + \frac{fUh(1-\beta/uF)}{H\beta(\beta/uF-2)}$$

and $\psi_1 = \psi_2 = 0$ in $y > \max(h)(1-\beta/\mu F)/H\beta(\beta/\mu F - 2)$

where h = h(x) 0 (and so represents a ridge) and h(x) 0 as x . As shown in Figure 11b, this flow field consists of eastward flow over the topography in both layers, with some fluid in the top layer returning westward over a quiescent second layer. Of course this is without wind forcing and seems to be an example of eastward flow being blocked by topography. It is interesting to speculate whether such a flow could be set up (e.g., in the laboratory) but this example still serves to show that the deceptively simple large scale flow equations have solutions with a rich and complicated structure.

CONCLUSIONS

In summary, the Rhines and Young (1982a) theory of the wind-driven circulation has been used to show that the presence of a zonal current poleward of a region of nonzero wind stress curl will increase the depth of the resulting gyre, and in particular the presence of the Antarctic Circumpolar Current is believed to be the reason for the deep wind gyre in the South Pacific. Such deep flows are certain to be strongly influenced by topography and it would be well worth investigating this effect in detail.

ACKNOWLEDGMENTS

I would like to thank Peter Rhines, who suggested that this problem would be worth studying, for many stimulating discussions throughout the summer. Additionally, I would like to thank all those involved in the GFD program for giving me such a rewarding and enjoyable time at Woods Hole.

REFERENCES

Coats, D. A., 1982. The Absolute Flow Field in the Pacific Ocean. Univ. of California. PhD. Thesis.

Gill, A. E., 1968. A linear Model of the Antarctic Circumpolar Current. J. Fluid. Mech., 32, 465-488.

Levitus, S., 1982. Climatological Atlas of the World Ocean (GFDL Princeton).

Rhines, P. B. and W. R. Holland, 1979. A Theoretical Discussion of Eddy induced Circulation. Dynamical Atmospheric Oceans, 3, 289-325.

Rhines, P. B. and W. R. Young, 1982a. A Theory of Wind-Driven Circulation. I. Mid Ocean Gyres. J. Mar. Res., 40 (Suppl.).

Rhines, P. B. and W. R. Young, 1982b. Potential Vorticity Homogenization in Planetary Gyres. J. Fluid Mech. (In press)

MEAN MOTIONS INDUCED BY BAROCLINIC INSTABILITY IN A JET

Theodore G. Shepherd

1. INTRODUCTION

In the development of the theory of wave, mean-flow interaction, 'non-acceleration' theorems (Charney and Drazin, 1961; Eliassen and Palm, 1961) have provided useful results concerning the extent to which waves can alter a mean flow. In particular, such theorems highlight the fact that in many cases of interest, waves can induce a weak mean flow which exactly cancels the effects of eddy transports, leaving no net effect on the initial mean flow. In such instances, usually involving a steady, conservative wave field, a description of the situation in terms of eddy fluxes of heat and momentum and weak zonal mean flows would seem to be an unnecessarily cumbersome way of saying that 'nothing is happening'.

Even when the cancellation between eddy and induced mean flow effects is not zero, however, it may still be desirable to take account of the cancellation in the interests of a more succinct description of the dynamics. In the context of the atmospheric circulation, this desire has led to the 'Transformed Eulerian-Mean' (Andrews and McIntyre, 1976) and the 'Generalized Lagrangian-Mean' (Andrews and McIntyre, 1978).

A particular example of a situation in which the non-acceleration theorems do not hold, and one of crucial importance to the atmospheric circulation, is that of a growing baroclinic wave - in this case, it is wave transience which provides the irreversibility. Following the initial studies of Charney (1947) and Eady (1949) the subject of baroclinic instability has certainly received a great deal of attention, much of it related to the way in which growing baroclinic waves affect Eulerian-mean profiles of wind and temperature, and to their role in the atmospheric general circulation. However, the studies have generally been confined to the domain of Eulerian-mean statistics, and have thus suffered to some extent from the implications of the non-acceleration theorems mentioned above.

Recently, Uryu (1979) has examined the Lagrangian-mean motion induced by a growing Eady mode, and has found it to be strikingly different in both character and magnitude from the corresponding Eulerian-mean motion. In this paper, Uryu's work will be extended to baroclinic waves resulting from a basic flow with both meridional and vertical shear, as such a situation is more applicable to the atmosphere and can allow for a variety of different effects. In addition, the Transformed Eulerian-mean circulation will be examined. However, Uryu also computes the Lagrangian-mean motion due to the ageostrophic part of the wave. That is not necessary for these calculations, and so will not be done here.

Since the phenomena under consideration are mid-latitude synoptic-scale baroclinic disturbances, the mid-latitude quasi-geostrophic beta-plane channel will be employed. In general, the instability problem for an arbitrary baroclinic parallel flow $U = U(y,z)$ is non-separable, and is thus difficult to solve. The earliest studies of Charney (1947), Eady (1949), and Phillips (1954), of course, allowed only $U = U(z)$. Progress for $U = U(y,z)$ can be made in a variety of ways. One method is to use a perturbation expansion

assuming weak meridional shear (e.g. McIntyre, 1970). Alternatively, one may use a discretized representation in the vertical coordinate, the most celebrated of these being Phillips's two-layer model (1954). For reasons of both generality and simplicity, the latter route will be taken in this work.

2. THE ALGORITHM

(a) Solution of the instability problem

Using standard quasi-geostrophic scaling (Pedlosky, 1979), the governing equations for the inviscid two-layer model are those of conservation of quasi-geostrophic potential vorticity in each layer:

$$\frac{\partial Q_1}{\partial t} + J(\psi_1, Q_1) = 0 \tag{1a}$$

$$\frac{\partial Q_2}{\partial t} + J(\psi_2, Q_2) = 0 \tag{1b}$$

where $Q_1 = \nabla^2\psi_1 + \beta y + F(\psi_2 - \psi_1)$ and $Q_2 = \nabla^2\psi_2 + \beta y + F(\psi_1 - \psi_2)$. Here F is the Froude number L^2/L_R^2, L_R is the internal deformation radius, the layers are taken to have equal depths $\Delta Z = 1/2$, and $\psi_i (i = 1, 2)$ is the geostrophic streamfunction for each layer. The vertical velocity $w_{\frac{1}{2}}$ is defined at the interface, and satisfies

$$w_{\frac{1}{2}} = \varepsilon F \frac{d}{dt}(\psi_2 - \psi_1) \tag{1c}$$

where ε is the Rossby number and $\frac{d}{dt} \equiv \left[\frac{\partial}{\partial t} + J(\psi, \right]$. Boundary conditions are as follows:

(i) $w = 0$ at $z = 0, 1$;
(ii) periodicity in x ; (1d)
(iii) $v = 0$ at the channel walls $y = \pi, -\pi$.

To investigate the linear instability problem, consider a basic state zonal jet $U_1 = U_1(y)$, $U_2 = U_2(y)$. Then if $\bar{\psi}_i(y) = -\int^y U_i(y)$ is the basic state streamfunction, $\psi_i = \bar{\psi}_i + \varphi_i$ where the perturbation streamfunction φ_i satisfies the linearized perturbation equations

$$\frac{\partial q_1}{\partial t} + J(\bar{\psi}_1, q_1) + J(\varphi_1, \bar{Q}_1) = 0 \tag{2a}$$

$$\frac{\partial q_2}{\partial t} + J(\bar{\psi}_2, q_2) + J(\varphi_2, \bar{Q}_2) = 0 \tag{2b}$$

where

$$\bar{Q}_1 = -\frac{dU_1}{dy} + \beta y + F(\bar{\psi}_2 - \bar{\psi}_1)$$

$$\bar{Q}_2 = -\frac{dU_2}{dy} + \beta y + F(\bar{\psi}_1 - \bar{\psi}_2)$$

$$q_1 = \nabla^2\varphi_1 + F(\varphi_2 - \varphi_1)$$

$$q_2 = \nabla^2\varphi_2 + F(\varphi_1 - \varphi_2)$$

and $Q_i = \bar{Q}_i + q_i$ $(i = 1,2)$.

Introducing normal-mode trial solutions of the form

$$\psi_i(x,y,t) = Re\left\{\phi_i(y)e^{ik(x-ct)}\right\}$$

where $k \in \mathbb{R}$, equations (2a, b) may be cast in the form

$$(U_1(y)-c)\left[\frac{d^2\phi_1}{dy^2} - k^2\phi_1 + F(\phi_2-\phi_1)\right] + \phi_1\frac{\partial\bar{Q}_1}{\partial y} = 0 \qquad (3a)$$

$$(U_2(y)-c)\left[\frac{d^2\phi_2}{dy^2} - k^2\phi_2 + F(\phi_1-\phi_2)\right] + \phi_2\frac{\partial\bar{Q}_2}{\partial y} = 0 \qquad (3b)$$

subject to the boundary condition

$$\phi_1 = \phi_2 = 0 \quad \text{at} \quad y = \pi, -\pi \qquad (3c)$$

The perturbation velocities are evaluated geostrophically as

$$u_i = Re\left\{\phi_i'(y)e^{ik(x-ct)}\right\} \quad ; \quad v_i = Re\left\{ik\phi_i(y)e^{ik(x-ct)}\right\}$$

Now, equations (3a, b,c) provide an eigenvalue problem for the complex phase speed c: if $Im(c) \equiv c_i > 0$, then the eigenmode is unstable. In general, the problem is still not solvable analytically. Two possible analytical approaches are those of a perturbation expansion in terms of some small parameter such as the meridional shear (e.g. Stone, 1969; Simmons, 1974), or a severely truncated set of meridional modes (e.g. Yamagata, 1976; Kim, 1978). However, a numerical solution of the eigenvalue problem is easy, and does not suffer from the restrictive assumptions of the analytical methods. Consequently, numerical methods will be employed in the present work.

First, assume that there is no meridional shear in the lower-layer jet; this will simplify the algebra without compromising the dynamics unduly. Then without loss of generality, one may set $U_2(y) \equiv 0$. Second, consider the specific case $U_1 = \tilde{U} + 2\hat{U}\cos^2\left(\frac{y}{2}\right)$. Note that when $\tilde{U} = 0$, the jet is zero at the channel walls; for positive $\tilde{U}$ and $\hat{U}$, it is everywhere westerly.

For a cosine jet, it seems natural to choose a spectral representation of the eigenmode $\phi_i(y)$; this also has the advantage of maintaining a simple relationship between the vorticity and the streamfunction. In order to satisfy the boundary condition (3c), consider the truncated spectral expansion

$$\phi_i(y) = \sum_{m=1}^{N} A_i^m \sin(my) + \sum_{m=1}^{N} B_i \cos\left[(m-\tfrac{1}{2})y\right] \qquad [i=1,2] \qquad (4)$$

Note that for the symmetric jet considered here, the problems for the symmetric modes ($A_1 \equiv 0$) and for the antisymmetric modes ($B_1 \equiv 0$) can be treated separately. Details of the solution procedure are given in the Appendix.

(b) Eulerian-mean (EM) circulation

Assuming that an unstable mode has been obtained from the eigenvalue problem, the Eulerian-mean circulation induced by this growing wave can be calculated. In general, there will be more than one unstable mode for a given k, and one would tend to examine only the most unstable of them.

If the unstable modes are assumed to have amplitude a, then the zonal-mean flow change will be $o(a^2)$, and will be given by taking the zonal average of equation (1) to obtain

$$\frac{\partial}{\partial t}\left(\bar{\psi}_{1yy} + F(\bar{\psi}_2 - \bar{\psi}_1)\right) = -\overline{J(\psi_1, q_1)} \tag{5a}$$

$$\frac{\partial}{\partial t}\left(\bar{\psi}_{2yy} + F(\bar{\psi}_1 - \bar{\psi}_2)\right) = -\overline{J(\psi_2, q_2)} \tag{5b}$$

where the overbar denotes a zonal average. Boundary conditions are

$$\frac{\partial \bar{u}_i}{\partial t} \equiv -\frac{\partial^2 \bar{\psi}_i}{\partial y \partial t} = 0 \qquad \text{at} \quad y = \pi, -\pi \tag{5c}$$

from the momentum balance. To evaluate the right-hand side forcing correlations of (5a, b), the rule

$$\overline{\mathrm{Re}\{Ae^{ikx}\}\,\mathrm{Re}\{Be^{ikx}\}} = \tfrac{1}{2}\mathrm{Re}\{AB^*\}$$

is used. Since the time dependence of such correlations will be e^{2ikct}, introducing the solution form

$$\bar{\psi}_i(y,t) = \Psi_i(y)e^{2ikct}$$

enables (5a,b) to be written

$$2ikc\left[\Psi_{1yy} + F(\Psi_2 - \Psi_1)\right] = -\tfrac{k}{2}\mathrm{Im}\left\{\psi_1^*\psi_{1yyy} - \psi_{1y}^*\psi_{1yy} + F(\psi_1^*\psi_{1y} - \psi_{1y}^*\psi_1)\right\} \tag{6a}$$

$$2ikc\left[\Psi_{2yy} + F(\Psi_1 - \Psi_2)\right] = -\tfrac{k}{2}\mathrm{Im}\left\{\psi_2^*\psi_{2yyy} - \psi_{2y}^*\psi_{2yy} + F(\psi_2^*\psi_{2y} - \psi_{2y}^*\psi_2)\right\} \tag{6b}$$

subject to $$\frac{d\Psi_i}{dy} = 0 \qquad \text{at} \quad y = \pi, -\pi \quad [i = 1, 2] \tag{6c}$$

Now, for both symmetric and antisymmeteric modes, the right-hand side of (6a, b) will consist of series of terms sin ( ) x cos ( ) and can thus be expressed as a single series of the form $\sum_{m=1}^{2M}$ ( ) sin my. Note that to preserve accuracy, the truncation wavenumber must be doubled. Then equations (6a,b) take the form

$$\Psi_{1yy} + F(\Psi_2 - \Psi_1) = \sum_{m=1}^{2M} E_1^m \sin(my) \tag{7a}$$

$$\Psi_{2yy} + F(\Psi_1 - \Psi_2) = \sum_{m=1}^{2M} E_2^m \sin(my) \tag{7b}$$

where, for example, in the case of an unstable mode $\phi_i = \sum_{m=1}^{N} A_i^m \sin(my)$

$$E_i^m = \frac{-1}{8c_i}(1-\delta_m^1)\sum_{n=1}^{m-1}\left\{(m-n)\left[(m-n)^2-n^2\right]\mathrm{Im}\{A_1^{(m-n)*}A_1^n\} + F(m-n)\left[\mathrm{Im}\{A_1^{(m-n)*}A_2^n\} - \mathrm{Im}\{A_2^{(m-n)*}A_1^n\}\right]\right\}$$

$$- \frac{1}{8c_i}(1-\delta_m^N)\sum_{n=m+1}^{N}\left\{(n-m)\left[(n-m)^2-n^2\right]\mathrm{Im}\{A_1^{(n-m)*}A_1^n\} + F(n-m)\left[\mathrm{Im}\{A_1^{(n-m)*}A_2^n\} - \mathrm{Im}\{A_2^{(n-m)*}A_1^n\}\right]\right\}$$

$$+ \frac{1}{8c_i}(1-\delta_m^N)\sum_{n=1}^{N-m}\left\{(n+m)\left[(n+m)^2-n^2\right]\mathrm{Im}\{A_1^{(n+m)*}A_1^n\} + F(n+m)\left[\mathrm{Im}\{A_1^{(n+m)*}A_2^n\} - \mathrm{Im}\{A_2^{(n+m)*}A_1^n\}\right]\right\}$$

if $m \le N$; and if $N < m \le 2N$ then

$$E_1^m = \frac{-1}{8c_i}\sum_{n=m-N}^{N}\left\{(m-n)\left[(m-n)^2-n^2\right]\mathrm{Im}\{A_1^{(m-n)*}A_1^n\} + F(m-n)\left[\mathrm{Im}\{A_1^{(m-n)*}A_2^n\} - \mathrm{Im}\{A_2^{(m-n)*}A_1^n\}\right]\right\}$$

In the interests of brevity, this will be the only formula of this type presented. The others are similar.

Now, the particular solution of (7a, b) is

$$\Phi_i^{(p)}(y) = \sum_{m=1}^{2N} G_i^m \sin(my) \tag{8a}$$

where $$G_1^m = \frac{-\left(FE_2^m - (m^2+F)E_1^m\right)}{m^2(m^2+2F)} \quad ; \quad G_2^m = \frac{-\left(FE_1^m - (m^2+F)E_2^m\right)}{m^2(m^2+2F)} \tag{8b}$$

To this must be added a solution of the homogeneous version of (7a, b) in order to satisfy the boundary condition (6c). The full solution is

$$\Phi_i(y) = \Phi_i^{(p)}(y) + (-1)^i\left(\sum_{m=1}^{2N}(-1)^m m G_i^m\right)\frac{\sinh(\sqrt{2F}\,y)}{\sqrt{2F}\cosh(\sqrt{2F}\,\pi)} \tag{8c}$$

In the upper layer (i = 1), that $\frac{d\Phi_1}{dy} = 0$ at $y = \pm\pi$ is self-evident from (8c) and (8a). On the other hand,

$$\left.\frac{d\Phi_2}{dy}\right|_{y=\pm\pi} = \sum_{m=1}^{2N}(-1)^m m\left(G_1^m + G_2^m\right) \tag{9}$$

and this is not exactly zero. Analytically, however, $\frac{d\Phi_2}{dy}$ ought to vanish at $y = \pi, -\pi$ if $\frac{d\Phi_1}{dy}$ does. To see this, adding equations (5a) and (5b) together eliminates the baroclinic terms, leaving only

$$\frac{\partial}{\partial t}\left(\overline{\psi}_{1yy} + \overline{\psi}_{2yy}\right) = -\frac{\partial}{\partial y}\left(\overline{u_1 v_1}\right) - \frac{\partial}{\partial y}\left(\overline{u_2 v_2}\right)$$

Integrating once in y, and recognizing that $v_1 = 0$ at $y = \pm\pi$, yields

$$2kc_i e^{2kc_i t}\left(\Phi_{1y} + \Phi_{2y}\right) = -\left(\overline{u_1 v_1} + \overline{u_2 v_2}\right)$$

and thus

$$\Phi_{1y} = -\Phi_{2y} \quad \text{at} \quad y = \pm\pi.$$

It is seen that the extent to which the right-hand side of (9) does not vanish, is a measure of the error involved in making a finite spectral truncation. Define

$$(\text{Error})_1 = \frac{\sum_{m=1}^{2N} (-1)^m m (G_1^m + G_2^m)}{\sum_{m=1}^{2N} (-1)^m m G_1^m}$$

From (8c), the Eulerian-mean zonal acceleration is given by

$$\frac{\partial \overline{u_i}}{\partial t} = -2kc_i e^{2kc_i t} \left\{ \sum_{m=1}^{2N} m G_i^m \cos(my) + (-1)^i \left(\sum_{m=1}^{2N} (-1)^m m G_1^m \right) \frac{\cosh(\sqrt{2F}\, y)}{\cosh(\sqrt{2F}\, \pi)} \right\} \tag{10}$$

Now, the Reynolds stresses can be found in a similar way. For appropriately defined coefficients D_i^m,

$$\overline{u_i v_i} = \frac{k}{2} e^{2kc_i t} \operatorname{Im}\{\phi_i'^* \phi_i\} = \frac{k}{4} e^{2kc_i t} \sum_{m=1}^{2N} D_i^m \sin(my) \tag{11a}$$

and

$$-\frac{\partial}{\partial y}(\overline{u_i v_i}) = -\frac{k}{4} e^{2kc_i t} \sum_{m=1}^{2N} m D_i^m \cos(my) \tag{11b}$$

Analytically, both $\overline{u_1 v_1}$ and $\frac{\partial}{\partial y}(\overline{u_1 v_1})$ ought to vanish at $y = \pm\pi$ for these geostrophic velocities. The form of (11a, b) implies that the former will be satisfied exactly, but that the latter will be only approximately true. Consequently, introduce another error measure

$$(\text{Error})_2^{(i)} = \frac{\sum_{m=1}^{2N} (-1)^m m D_i^m}{\sum_{m=1}^{2N} m |D_i^m|}$$

The mean zonal-momentum balance for this system is

$$\frac{\partial \overline{u_i}}{\partial t} - \frac{1}{\varepsilon} \overline{v_i} = -\frac{\partial}{\partial y}(\overline{u_i v_i}) \tag{12}$$

and thus by using (10) and (11b), the EM meridional velocity $\overline{v_i}$ can be obtained. This is, of course, an ageostrophic velocity, as $\overline{v_i} \equiv 0$ geostrophically. Within the accuracy of the computation, $\overline{v_1} = -\overline{v_2}$.

Finally, $\overline{w_{\frac{1}{2}}}$ can be obtained by using the continuity equation evaluated at this order. Assuming layer depths of $\Delta z = \frac{1}{2}$, and using the fact that $\overline{w} = 0$ at $z = 0, 1$,

$$\frac{\partial \overline{w_i}}{\partial z} \equiv -2\overline{w_{\frac{1}{2}}} \quad \text{and} \quad \frac{\partial \overline{w_i}}{\partial z} = -\frac{\partial \overline{v_i}}{\partial y}$$

together imply that

$$\overline{w_{\frac{1}{2}}} = \frac{1}{2} \frac{\partial \overline{v_i}}{\partial y} \tag{13}$$

It can be seen from the form of the expressions that $\frac{\partial \overline{u_i}}{\partial t}$, $\frac{\partial}{\partial y}(\overline{u_i v_i})$, and $\overline{v_i}$ are represented as a series of cosines and will thus be symmetric in y, while $\overline{w_{\frac{1}{2}}}$ and $\overline{u_i v_i}$ will be antisymmetric.

(c) Transformed Eulerian-mean (TEM) circulation

As described in the Introduction, in many situations of interest the picture of wave, mean-flow interaction can be unnecessarily complicated when cast in terms of conventional Eulerian zonal-mean statistics. The transformed Eulerian-mean formulation introduces a 'residual circulation' defined, in pressure coordinates, by

$$\bar{v}^* = \bar{v} - \varepsilon \frac{\partial}{\partial p}\left(\frac{\overline{v'\theta'}}{\bar{\theta}_p}\right) \tag{14a}$$

$$\bar{\omega}^* = \bar{\omega} + \frac{\partial}{\partial y}\left(\frac{\overline{v'\theta'}}{\bar{\theta}_p}\right) \tag{14b}$$

where θ equals potential temperature, in terms of which the inviscid zonal-mean momentum equation takes the form

$$\frac{\partial \bar{u}}{\partial t} - \frac{1}{\varepsilon}\bar{v}^* = \nabla \cdot \underset{\sim}{F} \tag{14c}$$

where $\underset{\sim}{F}$, called the 'Eliassen-Palm flux', is given in the quasi-geostrophic approximation by $\underset{\sim}{F} = \{F_{(y)}, F_{(p)}\}$ with

$$F_{(y)} = -\overline{v'u'} \quad , \quad F_{(p)} = \left(\frac{\overline{v'\theta'}}{\bar{\theta}_p}\right) \tag{14d}$$

(see Edmon et al, 1980). In terms of the two-layer model, the equivalent expressions are

$$\bar{v}_i^* = \bar{v}_i + (-1)^i \varepsilon F \overline{v_i(\psi_2 - \psi_1)} \tag{15a}$$

and

$$\frac{\partial \bar{u}_i}{\partial t} - \frac{1}{\varepsilon}\bar{v}_i^* = (\nabla \cdot \underset{\sim}{F})_i = -\frac{\partial}{\partial y}(\overline{u_i v_i}) + (-1)^i F \overline{v_i(\psi_1 - \psi_2)} \tag{15b}$$

while $\bar{\omega}^*_{\frac{1}{2}}$ is obtained from continuity, since $(\bar{v}^*, \bar{\omega}^*)$ is nondivergent:

$$\bar{\omega}^*_{\frac{1}{2}} = \frac{1}{2}\frac{\partial \bar{v}_i^*}{\partial y} \tag{15c}$$

The correlations on the right hand sides of (15a, b) are computed in the same fashion as described in section (b) above.

Now, the advantages of the TEM formulation are described in some detail in Edmon et al. (1980), but a few points are especially worthy of note. The first is that when the nonacceleration theorems are valid, $\nabla \cdot \underset{\sim}{F} = 0$ and $\bar{v}^*$, $\bar{w}^*$, and $\frac{\partial \bar{u}}{\partial t}$ may all vanish; this justifies the use of the term 'residual circulation' in describing $(\bar{v}^*, \bar{w}^*)$, as it is that part of the mean meridional circulation which is not cancelled by steady, conservative wave effects. Similarly, $\nabla \cdot \underset{\sim}{F}$ can be seen as representing the 'true' forcing of the mean state by the eddies, and as corresponding to transient and irreversible eddy processes.

A second feature is that under the quasi-geostrophic assumption, $\nabla \cdot \underset{\sim}{F}$ is equal to the northward eddy transport of potential vorticity,

$$(\nabla \cdot \underset{\sim}{F})_i = \overline{v_i q_i} \tag{16}$$

This is particularly useful because the sign of $\overline{v_1 q_1}$ can often be anticipated from physical arguments. For example, for growing disturbances one expects $\overline{v_1 q_1}$ to be downgradient (Rhines and Holland, 1979). In the present study, the cases to be considered will generally have $\bar{Q}_{1y} > 0$ and $\bar{u}_{1y} < 0$, whence one would expect the E-P flux to be divergent in the lower layer and convergent in the upper layer.

The TEM heat equation is far simpler than its EM counterpart, and has the advantage of being eddy-free. The two are given in pressure coordinates as

$$\frac{\partial \bar{\theta}}{\partial t} + \bar{\theta}_p \bar{\omega}^* = Q \tag{17a}$$

$$\frac{\partial \bar{\theta}}{\partial t} + \bar{\theta}_p \bar{\omega} = Q - \frac{\partial}{\partial y}(\overline{v'\theta'}) \tag{17b}$$

where Q is diabatic heating. When $Q = 0$, heating (or cooling) of the mean state is reflected solely in the adiabatic heating (or cooling) associated with sinking (or rising) TEM motion. For the case of baroclinic instability, the unstable motions obtain their energy by means of a northward transport of heat which reduces the available potential energy of the mean flow. Viewed in terms of the TEM circulation, this can only be accomplished by heating in the north through negative $\bar{w}^*$, and cooling in the south through positive $\bar{w}^*$, that is to say a thermally direct TEM meridional cell. The EM circulation has no such 'a priori' constraint.

Finally, the TEM meridional velocities may be thought of as being in some sense 'mass-flux' velocities. This can be seen by considering a multi-layer fluid with layer depths $h_i = H_i + h_i'$, where under the quasi-geostrophic assumption $h_i'/H_i \sim o(\epsilon)$. The mean layer depths H_i are constant. Following Rhines and Holland (1979), the mean momentum equation in each layer may be expressed either as

$$H_i \frac{\partial \bar{u}_i}{\partial t} - \frac{1}{\epsilon}\overline{h_i v_i} = H_i \overline{q_i v_i} \tag{18a}$$

or alternatively as

$$H_i \frac{\partial \bar{u}_i}{\partial t} - \frac{1}{\epsilon} H_i \bar{v}_i = -H_i \frac{\partial}{\partial y}(\overline{u_i v_i}) \tag{18b}$$

Judging from the right hand sides of equations (18a, b), the first corresponds to the TEM momentum equation while the second corresponds to the EM equation. Consequently, $\bar{v}_i^*$ may be identified with $\frac{1}{H_i}\overline{h_i v_i}$, a mass-weighted velocity. In some sense $\overline{h_i v_i}$ is a quasi-Lagrangian quantity, because the layer interfaces move freely in the vertical.

(d) Generalized Lagrangian-mean (GLM) circulation

A more radical approach to eddy, mean-flow interaction than the TEM formulation, is provided by the concept of a Lagrangian mean. Strictly speaking, a Lagrangian mean is a mean following a particle trajectory, on the basis of which it enjoys the conceptual advantage of being eddy-free. However, one would generally like to have mean quantities defined as functions of spatial and temporal Eulerian coordinates, yet which embody some characteristics of the Lagrangian mean. It was to this end that the Generalized Lagrangian-mean was proposed by Andrews and McIntyre (1978).

In its most general form for finite-amplitude disturbances, the GLM formulation is unfortunately quite difficult to apply. But for disturbances of small amplitude a, the Lagrangian displacement of fluid particles $\boldsymbol{\xi}(\xi, \eta, \zeta)$ is given in terms of the Eulerian fields as

$$\left(\frac{\partial}{\partial t} + \bar{\mathbf{u}} \cdot \nabla\right)\boldsymbol{\xi} = \mathbf{u}' + (\boldsymbol{\xi} \cdot \nabla)\bar{\mathbf{u}} + o(a^2) \tag{19}$$

where $\underset{\sim}{u}'$ is the perturbation velocity. From these particle displacements, the generalized Lagrangian-mean is defined as

$$\bar{\phi}^L(\underset{\sim}{x},t) \equiv \overline{\phi(\underset{\sim}{x},t)}^L \equiv \overline{\phi(\underset{\sim}{x}+\underset{\sim}{\xi}(\underset{\sim}{x},t),t)} \tag{20}$$

and represents a mean along a line of fluid particles distorted by the waves. A Taylor expansion of (20) with respect to $\underset{\sim}{\xi}$ leads to the small-amplitude approximation for the Stokes correction $\bar{\phi}^S$,

$$\bar{\phi}^S \equiv \bar{\phi}^L - \bar{\phi} = \overline{\underset{\sim}{\xi}\cdot\nabla\phi'} + \tfrac{1}{2}\overline{\underset{\sim}{\xi}\cdot(\underset{\sim}{\xi}\cdot\nabla)\nabla\bar{\phi}} + O(a^3) \tag{21}$$

Equations (19) to (21) were provided in Andrews and McIntyre (1978, Section 2).

For the present investigation, the quantities of interest are $\bar{v}_i^L$, $\bar{w}_{\frac{1}{2}}^L$, and $\frac{\partial \bar{u}_i^L}{\partial t}$. The Stokes corrections for these terms, assuming a basic state mean flow $U_1 = U(y)$, $U_2 = 0$, are as follows, to leading order in wave amplitude and Rossby number:

$$\frac{\partial \bar{u}_1^S}{\partial t} = \frac{\partial}{\partial t}\left\{\frac{\partial}{\partial y}(\overline{\eta_1 u_1}) + \tfrac{1}{2}\overline{\eta_1^2}\frac{d^2U(y)}{dy^2}\right\} \tag{22a}$$

$$\frac{\partial \bar{u}_2^S}{\partial t} = \frac{\partial}{\partial t}\frac{\partial}{\partial y}(\overline{\eta_2 u_2}) \tag{22b}$$

$$\bar{v}_1^S = \frac{\partial}{\partial y}(\overline{\eta_1 v_1}) \tag{22c}$$

$$\bar{v}_2^S = \frac{\partial}{\partial y}(\overline{\eta_2 v_2}) \tag{22d}$$

$$\bar{w}_{\frac{1}{2}}^S = \frac{\partial}{\partial y}(\overline{\eta_2 w_{\frac{1}{2}}}) \tag{22e}$$

The terms involving vertical displacements ζ are of a higher order in ε for this quasi-geostrophic system, and have consequently been neglected. The 'flux form' of the displacement-velocity correlations is obtained by considering that

$$\overline{\underset{\sim}{\xi}\cdot\nabla\phi} = \overline{\frac{\partial}{\partial x}(\xi\phi)} + \frac{\partial}{\partial y}(\overline{\eta\phi}) - \overline{\phi\nabla\cdot\underset{\sim}{\xi}}$$

but $\nabla\cdot\underset{\sim}{\xi} = 0$ (Andrews and McIntyre, 1978, section 9). The expression for $\bar{w}_{\frac{1}{2}}^S$ could equally well have been in terms of the upper-layer displacement η_1, but that would have involved a more elaborate computation.

It is seen from (22 a-e) that the only particle displacement fields needed are those of η_1 and η_2; they are obtained from (19), namely

$$ik(U(y)-c)\,\eta_1 = v_1 = ik\varphi_1 \tag{23a}$$

$$-ikc\,\eta_2 = v_2 = ik\varphi_2 \tag{23b}$$

It then follows that

$$\overline{\eta_1 u_1} = e^{2kc_i t}\tfrac{1}{2}\mathrm{Re}\left\{\left[\frac{\phi_1}{|U-c|^2}(U-c_r+ic_i)\right][-\phi_1'^*]\right\}$$

$$= \frac{e^{2kc_i t}}{|U-c|^2}\tfrac{1}{2}\left\{(c_r-U)\,\mathrm{Re}\{\phi_1\phi_1'^*\} + c_i\,\mathrm{Im}\{\phi_1\phi_1'^*\}\right\} \tag{24a}$$

$$\overline{\eta_2 u_2} = \frac{e^{2kc_i t}}{|c|^2}\,\frac{1}{2}\left\{c_r \mathrm{Re}\{\phi_2\phi_2'^*\} + c_i\,\mathrm{Im}\{\phi_2\phi_2'^*\}\right\} \tag{24b}$$

$$\overline{\eta_1 v_1} = e^{2kc_i t}\,\frac{1}{2}\,\mathrm{Re}\left\{\left[\frac{\phi_1}{|U-c|^2}(U-c_r+ic_i)\right][-ik\phi_1^*]\right\}$$

$$= \frac{e^{2kc_i t}}{|U-c|^2}\,\frac{1}{2}\,kc_i\,\mathrm{Re}\{\phi_1\phi_1^*\} \tag{24c}$$

$$\overline{\eta_2 v_2} = \frac{e^{2kc_i t}}{|c|^2}\,\frac{1}{2}\,kc_i\,\mathrm{Re}\{\phi_2\phi_2^*\} \tag{24d}$$

$$\overline{\eta_2 w_{\frac{1}{2}}} = \varepsilon F\,\overline{\eta_2(u_2-u_1)}_t = \varepsilon F e^{2kc_i t}\,\frac{1}{2}\,\mathrm{Re}\left\{\left[\frac{\phi_2}{|c|^2}(-c_r+ic_i)\right][ik(c_r+ic_i)(\phi_2^*-\phi_1^*)]\right\}$$

$$= \varepsilon F\,\frac{e^{2kc_i t}}{|c|^2}\,\frac{k}{2}\left\{(c_r^2-c_i^2)\,\mathrm{Im}\{\phi_2^*\phi_1\} + 2c_r c_i\left[\mathrm{Re}\{\phi_2^*\phi_1\} - \mathrm{Re}\{\phi_2^*\phi_2\}\right]\right\} \tag{24e}$$

$$\overline{\eta_1^2} = \frac{e^{2kc_i t}}{|U-c|^2}\,\frac{1}{2}\,\mathrm{Re}\{\phi_1^*\phi_1\} \tag{24f}$$

The right hand sides of equations (24 a-f) are computed using the procedure described in section (b) above. Products such as $\{\phi_1^*\phi_1\}$ will be represented as cosine series and will thus be symmetric in y, while products like $\{\phi_1'^*\phi_1\}$ will be antisymmetric in y. When applying (22a) and (22c), differentiation of (24a) and (24c) must include differentiation of U(y), but it still turns out that all Stokes quantities are either symmetric or antisymmetric due to the symmetry of U(y).

It should be mentioned that while $\frac{\partial\overline{u_1}}{\partial t}$ and $\frac{\partial\overline{u_1}^L}{\partial t}$, and $\overline{w}_{\frac{1}{2}}$ and $\overline{w}_{\frac{1}{2}}^L$, are formally of the same order in amplitude and Rossby number, in general $\overline{v}^L$ is one order larger in Rossby number than $\overline{v}_1$. Thus, the Lagrangian-mean $\overline{v}_1^L$ is only formally correct to leading order in Rossby number; to include $\overline{v}_1$ while neglecting terms involving either the vertical particle displacement or ageostrophic corrections to the stability problem would be inconsistent.

Finally, a remark ought to be made concerning the relationship between the TEM circulation (v*,w*) and the GLM circulation ($\overline{v}^L, \overline{w}^L$). For steady, conservative waves, the two circulations are identical and, indeed, are often zero. Because of the 'eddy-free' (although forced) form of the TEM equations (e.g. as given in Edmon et al. 1980), one is tempted to view the TEM as having at least some of the characteristics of the GLM. But they are really quite different concepts; not the least striking is the fact that while the TEM circulation is nondivergent, the GLM circulation can be (and usually is) divergent or convergent (Andrews and McIntyre, 1978, section 9).

3. APPLICATIONS TO THREE CASES

Case A will be simply the Phillips model, namely $\tilde{u} = 1$, $\hat{u} = 0$, with 'atmospheric' values of $\beta = 1$, $F = 4$. This can be solved analytically, and the Lagrangian-mean results can be compared directly with those of Uryu (1979); even though Uryu's study uses the Eady model, the Eulerian-mean circulations associated with the two models are very similar indeed, and so one might expect the Lagrangian-mean circulations to compare as well.

Because of the observational fact that mid-latitude baroclinic storms tend to be baroclinically growing and barotropically damped, one set of experimental parameters will be chosen to ensure baroclinic instability and barotropic stability. This can be done if the northward mean potential-vorticity gradient $\overline{Q}_{iy}$ is of one sign within each layer, but of opposite signs in the two layers. For $u_1(y) = \tilde{u} + 2\hat{u}\cos^2(\frac{y}{2})$, $u_2(y) = 0$,

$$\overline{Q}_{1y} = \beta + F(\tilde{u}+\hat{u}) + \hat{u}(F+1)\cos y \tag{25a}$$

$$\overline{Q}_{2y} = \beta - F(\tilde{u}+\hat{u}) - \hat{u}F\cos y \tag{25b}$$

For positive settings of the parameters, it is evident that one needs

$$\text{(i) } \overline{Q}_{1y} > 0 \ \forall y \iff \beta + F(\tilde{u}+\hat{u}) - \hat{u}(F+1) > 0 \iff \beta + F\tilde{u} > \hat{u}$$
$$\text{(ii) } \overline{Q}_{1y} < 0 \ \forall y \iff \beta - F(\tilde{u}+\hat{u}) + \hat{u}F < 0 \iff \beta < F\tilde{u} \tag{25c}$$

Consequently, case B will have $\tilde{U} = 1$, $\hat{U} = 1$, as well as $\beta = 1$, $F = 4$, which easily satisfies (25c).

Finally, a case in which (25c) is not quite satisfied, although $\overline{Q}_{1y} > 0$ and $\overline{Q}_{2y} < 0$ over most of the domain, is that of $\tilde{U} = 0$, $\hat{U} = 0.5$, $\beta = 1$, $F = 15$. This case, C, has a jet which vanishes at the channel walls and is very similar in shape to one of the cases studied in a numerical instability calculation of Simmons (1974). Cases B and C differ principally in the deformation radius (a factor of two), and in the fact that $\overline{Q}_{1y}$ changes sign within each layer (though only barely) in case C.

The jets for cases B and C are shown in figures 1a, b. For easy reference, the cases are summarized in table form below:

CASE	β	F	$\tilde{U}$	$\hat{U}$	U(y)	Most unstable Mode at k =	Cr	Ci
A	1.0	4.0	1.0	0	1	2.0	.34	.27
B	1.0	4.0	1.0	1.0	$1 + 2\cos^2(\frac{y}{2})$	2.0	1.08	.54
C	1.0	15.0	0	0.5	$\cos^2(\frac{y}{2})$	3.5	.39	.23

In all calculations, the Rossby number ϵ is taken to be 0.1.

(a) The Phillips model: Case A

The instability problem for this parameter setting was solved long ago by Phillips (1954), who also computed the Eulerian-mean circulation associated with the growing wave.

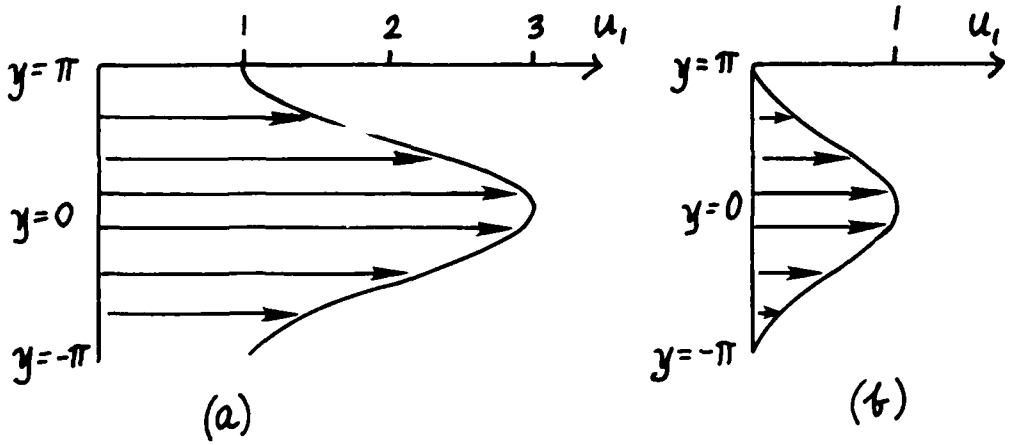

Figure 1: Upper layer basic state zonal jet: (a) case B (b) case C

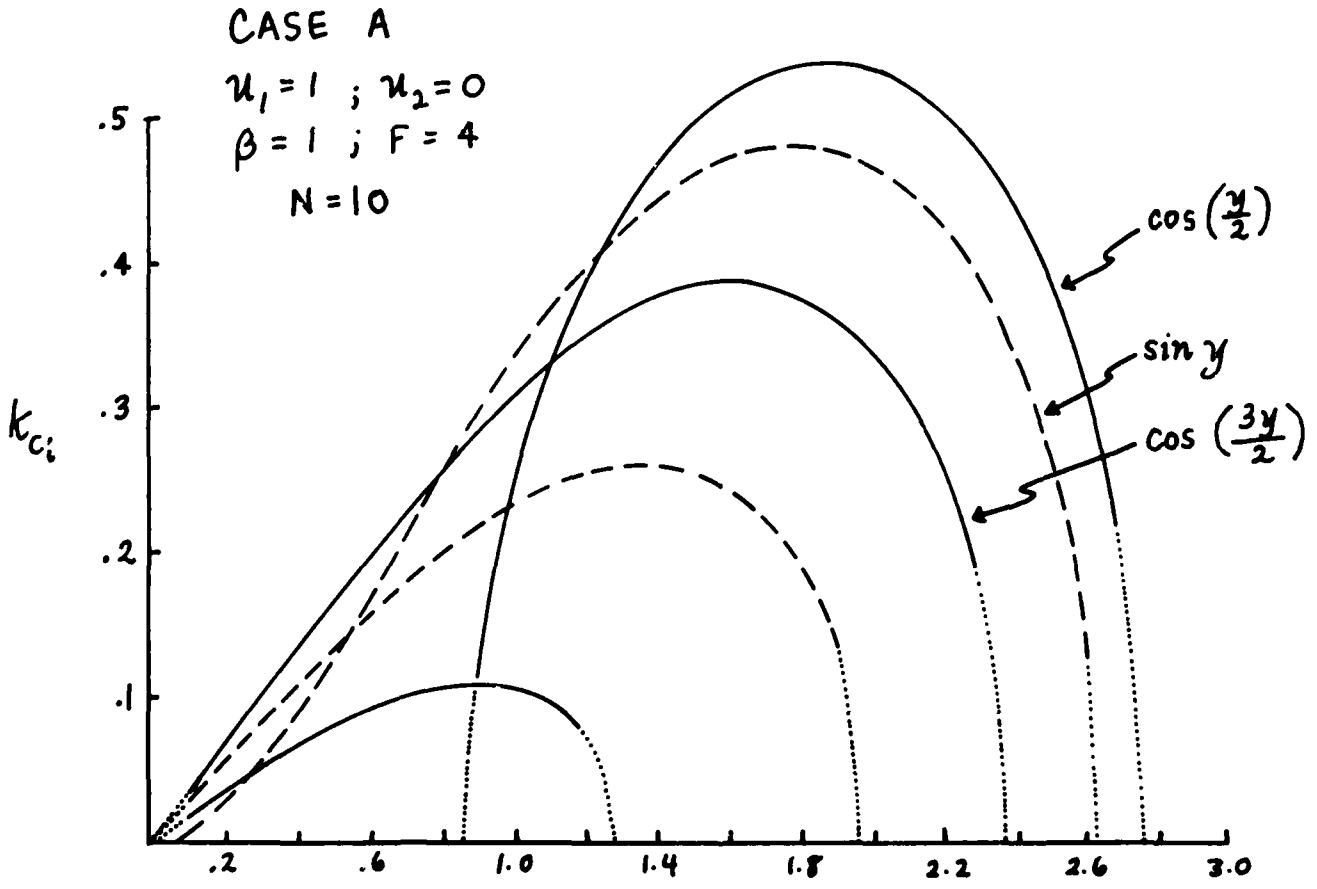

Figure 2: Growth rate vs. zonal wave number k for case A. (——) symmetric modes; (– –) anti-symmetric modes.

Growth rates, determined numerically, are plotted as a function of zonal wavenumber k in figure 2; it is seen that the most unstable mode is found to have meridional structure $\Phi(y) \propto \cos\left(\frac{y}{2}\right)$ (i.e. the gravest mode of the system) at approximately k = 2.0, and is handled exactly by the spectral representation. Higher modes have growth rates which are comparable, and it is impossible to predict from a linear calculation the ultimate 'winner' in any competition between growing modes; however, the mean circulations associated with the higher modes are simply multiple copies of those from the gravest mode, and hence, since the mean flow is independent of y, there is no need to consider the higher modes.

Analytically, the Phillips model allows unstable modes of a single meridional wavenumber, the most unstable for k = 2.0 being given by

$$\psi_i = Re\left\{B_i \cos\left(\frac{y}{2}\right) e^{ik(x-ct)}\right\} \qquad [i=1,2] \tag{26a}$$

(Expressions for the B_i's to within a constant, and for c, are given in Phillips (1954)). The geostrophic velocities are then

$$u_i = Re\left\{\tfrac{1}{2} B_i \sin\left(\tfrac{y}{2}\right) e^{ik(x-ct)}\right\} \tag{26b}$$

$$v_i = Re\left\{ik B_i \cos\left(\tfrac{y}{2}\right) e^{ik(x-ct)}\right\} \tag{26c}$$

For such single mode solutions the Reynolds stress vanishes exactly, and the spectral coefficients E_i^m and G_i^m of equations (7) and (8) turn out to be antisymmetric in $(z-\frac{1}{2})$. In fact, most of the algebra of section 2(b) turns out to be unnecessary, and one finds that

$$\tfrac{1}{2}\overline{v}_i = \frac{\partial \overline{\psi}_i}{\partial y} = (-1)^i \varepsilon e^{2kc_i t}\left(\frac{A}{1+2F}\right)\left\{\cos y + \frac{\cosh\left(\sqrt{2F}\, y\right)}{\cosh\left(\sqrt{2F}\,\pi\right)}\right\} \tag{26d}$$

$$\overline{w}_{\frac{3}{2}} = \tfrac{1}{2}\frac{\partial \overline{v}_i}{\partial y} = \frac{\varepsilon}{2} e^{2kc_i t}\left(\frac{A}{1+2F}\right)\left\{\sin y - \sqrt{2F}\,\frac{\sinh\left(\sqrt{2F}\, y\right)}{\cosh\left(\sqrt{2F}\,\pi\right)}\right\} \tag{26e}$$

where $A \equiv \frac{kF}{4} Im\{B_1 B_2^*\}$.

Since A is positive for a growing wave, equations (26d,e) represent a thermally indirect meridional circulation about the center of the channel with narrow thermally direct cells at the walls; this situation is shown in figures 3 and 4, and is understood to be responsible for the Ferrel cell in the observed atmospheric mean meridional circulation. The zonal acceleration $\frac{\partial \overline{u}_i}{\partial t}$ is due solely to the Coriolis torque, and over the central part of the channel (where the disturbance amplitude is concentrated) it is positive in the lower layer and negative in the upper layer. This, of course, leads to a weakening of the vertical mean wind shear in the center of the channel.

Applying equations (15a-c) in this case to obtain the TEM circulation, it turns out that

$$\tfrac{1}{\varepsilon}\left(\overline{v}_i^* - \overline{v}_i\right) = -\left(\nabla \cdot \underline{F}\right)_i = (-1)^{i+1} 2A e^{2kc_i t} \cos\left(\tfrac{y}{2}\right) \tag{27a}$$

$$\left(\overline{w}_{\frac{1}{2}}^* - \overline{w}_{\frac{3}{2}}\right) = \tfrac{1}{2}\left(\frac{\partial \overline{v}_1^*}{\partial y} - \frac{\partial \overline{v}_1}{\partial y}\right) = -A\varepsilon e^{2kc_i t} \sin y \tag{27b}$$

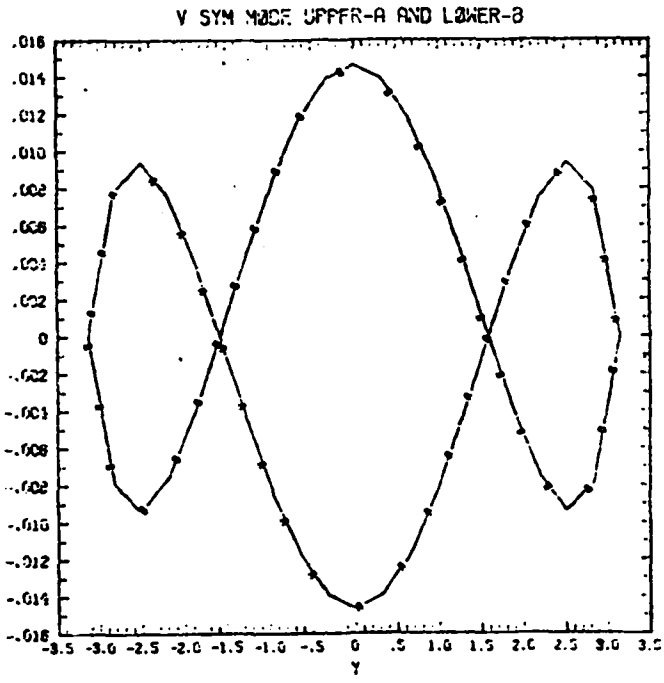

Figure 3: EM $\bar{v}_i$ for the symmetric mode of case A. A → upper layer $\bar{v}_1$, B → lower layer $\bar{v}_2$.

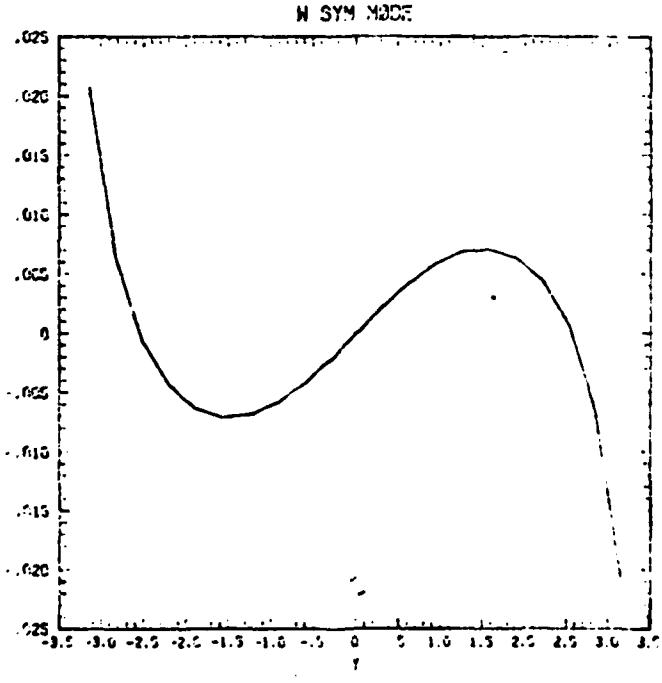

Figure 4: As in figure 3, but $\bar{w}_{\frac{1}{2}}$.

It is evident that the ratio $\frac{(\bar{v}_i^* - \bar{v}_i)}{\bar{v}_i} \approx 2(1+2F) = 18$ for F = 4, so the TEM circulation dominates the EM circulation; moreover, it is of the opposite sign in the center of the channel. Figures 5 and 6 show the TEM meridional circulation to be a single thermally direct cell, which agrees with the direct cell over mid-latitudes found in the TEM observational analysis of Edmon et al. (1980). Equation (27a) also implies that the E-P flux vector will point directly upward, and will have its greatest magnitude at the center of the channel. That F has no horizontal component is simply a reflection of the fact that in the Phillips model of baroclinic instability, there is no momentum flux. Note that since $(\nabla\cdot\underline{F})_i/\bar{q}_{i,y} < 0$ for i = 1,2, the potential vorticity flux is everywhere downgradient.

As for the GLM circulation, equations (22a-e) apply but with the simplification that $U(y) \equiv 1$. The meridional particle displacements are

$$\eta_1 = \frac{v_1}{ik(1-c)} = \frac{B_1 \cos(\frac{y}{2}) e^{ik(x-ct)}}{|1-c|^2}(1-c_r+ic_i) \tag{28a}$$

$$\eta_2 = \frac{v_2}{ik(-c)} = \frac{B_2 \cos(\frac{y}{2}) e^{ik(x-ct)}}{|c|^2}(-c_r+ic_i) \tag{28b}$$

from which the Stokes corrections are simply

$$\frac{\partial \bar{u}_1^S}{\partial t} = e^{2kc_i t}\frac{kc_i}{4}\frac{(1-c_r)}{|1-c|^2}|B_1|^2\cos y \tag{28c}$$

$$\frac{\partial \bar{u}_2^S}{\partial t} = e^{2kc_i t}\frac{kc_i}{4}\frac{(-c_r)}{|c|^2}|B_2|^2\cos y \tag{28d}$$

$$\bar{v}_1^S = -e^{2kc_i t}\frac{kc_i}{4}\frac{|B_1|^2}{|1-c|^2}\sin y \tag{28e}$$

$$\bar{v}_2^S = -e^{2kc_i t}\frac{kc_i}{4}\frac{|B_2|^2}{|c|^2}\sin y \tag{28f}$$

$$\bar{\omega}_i^S = e^{2kc_i t}\frac{k\varepsilon}{4|c|^2}\left[2c_r c_i\left(|B_2|^2 - \mathrm{Re}\{B_2^* B_1\}\right) - (c_r^2 - c_i^2)\,\mathrm{Im}\{B_2^* B_1\}\right]\sin y \tag{28g}$$

An interesting result that is immediately evident from equations (28e,f) is that $\bar{v}_i^S$ is convergent towards the center of the channel in each layer. This was also found by Uryu (1979) for the Eady mode, and is indicative of horizontal particle mixing.

The GLM meridional circulation, obtained by adding the Stokes corrections to the Eulerian-mean quantities, is shown in figures 7 and 8. The vertical particle motion is upward in the south and downward in the north, as would be expected in order to release the available potential energy of the mean flow, and tilt the potential temperature isotherms back to horizontal. Mean particle motion is thus upward and northward in the south, and downward and southward in the north, demonstrating motion in the 'wedge of instability'.

It should be noted that $\frac{1}{\varepsilon}\bar{v}_i^L$ is one order larger in ε than $\frac{\partial \bar{u}_i^S}{\partial t}$, so the Coriolis torque associated with $\bar{v}_i^L$ cannot be causing the zonal acceleration. In fact, in the Lagrangian-mean momentum equation $\frac{1}{\varepsilon}\bar{v}_i^L$ is balanced geostrophically to leading order in ε by the divergence of radiation stress,

$$\frac{1}{\varepsilon}\bar{v}_i^L = \frac{1}{\varepsilon}\frac{\partial}{\partial y}(\overline{\eta_i v_i}) = -\frac{1}{\varepsilon}\frac{\partial}{\partial y}\left(\overline{\psi_i \frac{\partial \eta_i}{\partial x}}\right)$$

as pointed out by Uryu (1979).

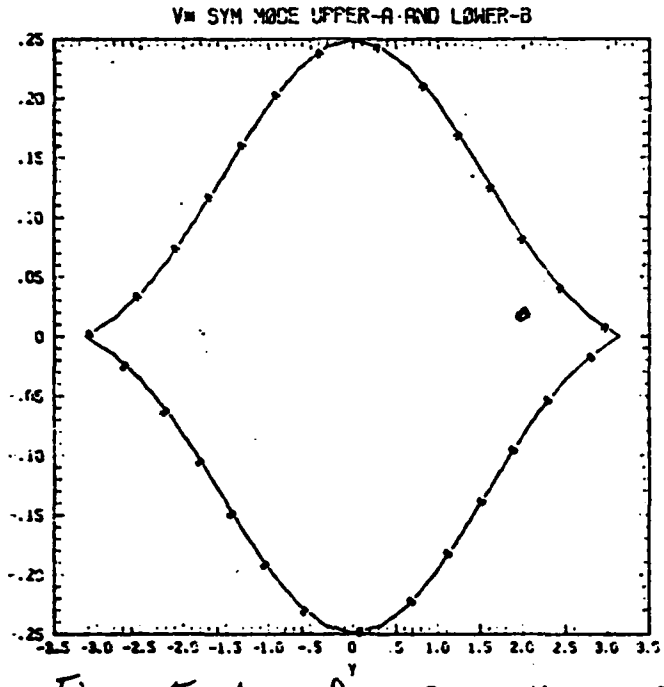

Figure 5: As in figure 3, but the TEM $\bar{V}_i^*$.

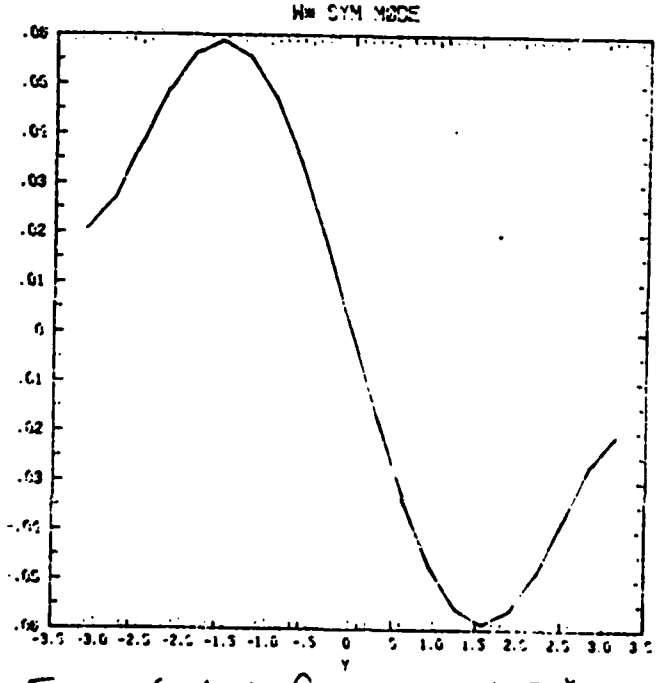

Figure 6: As in figure 3, but $\bar{w}^*_{\frac{3}{2}}$.

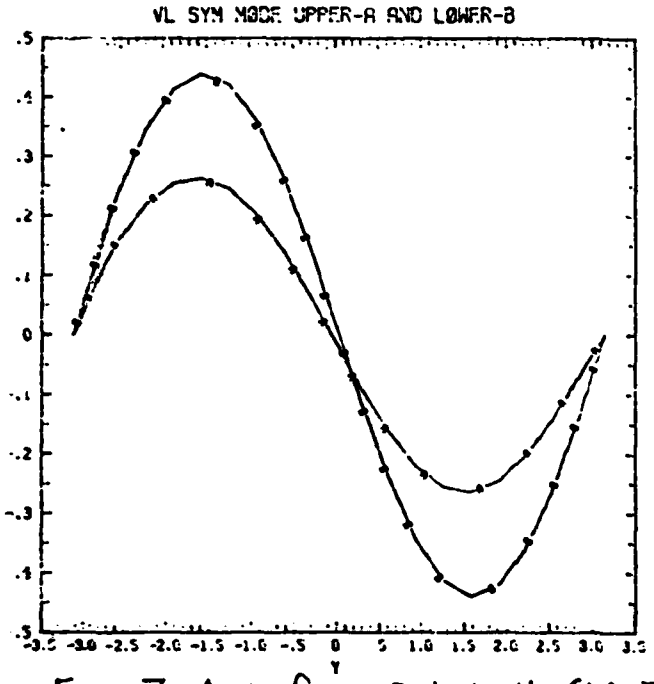

Figure 7: As in figure 3, but the GLM $\bar{v}_i^L$

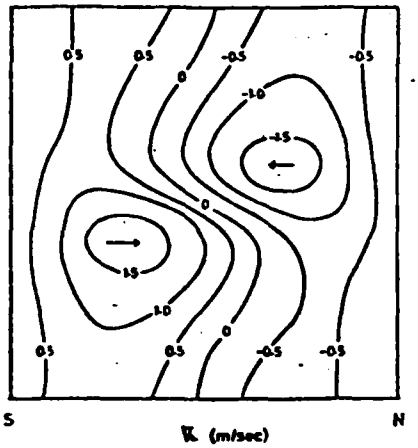

Figure 9a: Distribution of Lagrangian mean meridional velocity, $\bar{V}_L$.

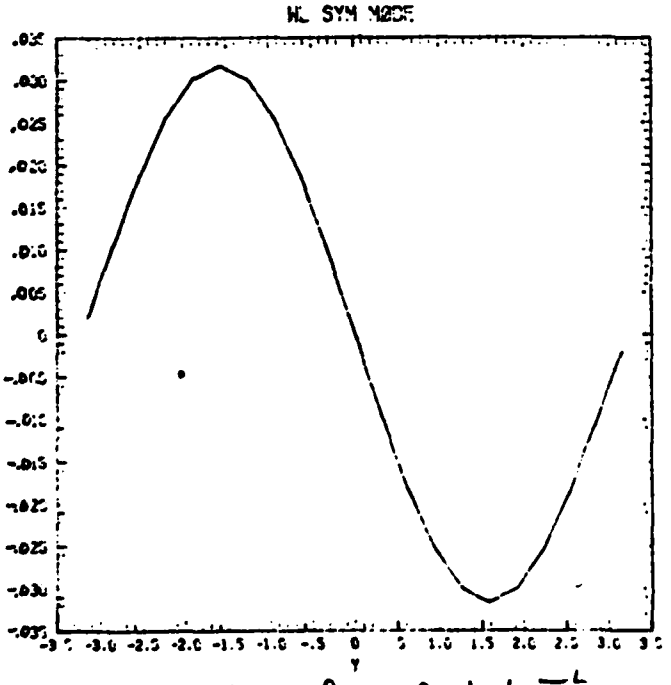

Figure 8: As in figure 3, but $\bar{w}_{\frac{3}{2}}^L$.

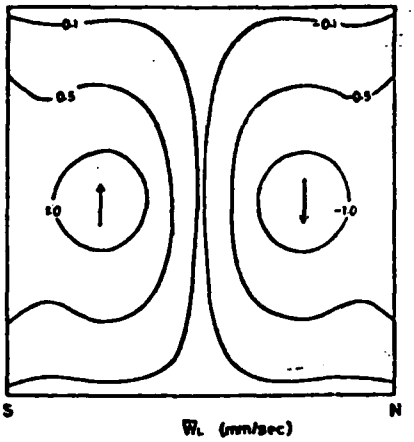

Figure 9b: Distribution of Lagrangian mean vertical velocity, $\bar{W}_L$.

(From Uryu (1979), based on an Eady mode)

The GLM meridional circulation from the Eady model, as calculated by Uryu, is shown in figures 9a and 9b. $\bar{w}^L(z)$ at $z = \frac{1}{2}$ is identical to $\bar{w}^L_{\frac{1}{2}}$ in the Phillips model, but $\bar{v}^L(z)$ in the Eady model is affected significantly by higher-order terms which are symmetric in y.

A particularly striking result of Uryu's calculation is the fact that $\frac{\partial \bar{u}^L_1}{\partial t}$ and $\frac{\partial \bar{u}^L_3}{\partial t}$ tend to be of the same magnitude but of opposite sign, leaving a weak $\frac{\partial \bar{u}^L_2}{\partial t}$ which, in the center of the channel, is positive in the upper part and negative in the lower part of the flow. The results of the two-layer model calculation are very similar to those of the Eady model; figures 10 and 11 show the three quantities $\frac{\partial \bar{u}^L_1}{\partial t}$, $\frac{\partial \bar{u}^L_2}{\partial t}$, and $\frac{\partial \bar{u}^L_3}{\partial t}$ in the upper and lower layers, while figure 12 reproduces Uryu's corresponding results. Note that although $\frac{\partial \bar{u}^L_2}{\partial t}$ must vanish at the channel walls, $\frac{\partial \bar{u}^L_1}{\partial t}$ need not. The smallness of $\frac{\partial \bar{u}^L_2}{\partial t}$ in the central lower layer is particularly remarkable.

It is interesting that although $\bar{w}^*_{\frac{1}{2}}$ seems to be a good substitute for $\bar{w}^L_{\frac{1}{2}}$, $\bar{v}^*_1$ and $\bar{v}^L_1$ are really quite different; thus one must be cautious when trying to infer the GLM from the TEM.

(b). A zonal jet: Cases B and C

With an upper jet which varies in y, no single meridional mode is an eigenfunction for the instability problem. A truncation wavenumber N_0 will be considered adequate if (i) increasing N beyond N_0 does not alter the important spectral amplitudes by more than 1%; and (ii) the relative error measures defined in section 2(b) are less than 10^{-3}.

A plot of growth rates against zonal wavenumber k is given in figure 13 for case C; case B is similar in character. It is seen that with meridional shear in the mean jet, the most unstable symmetric and antisymmetric modes are very close to each other in growth rate, and are substantially more unstable than the next ones down. Consequently, both modes ought to be considered, especially since in the atmosphere one does see baroclinic storms of both a symmetric (e.g. an isolated cyclone) and an antisymmetric (e.g. a cyclone, anticyclone dipole) character.

For case B, the most unstable modes occur near k = 2.0, and the criteria mentioned above are satisfied for a truncation of N = 5. The amplitude and phase of the symmetric mode are shown in figures 14 and 15 (note that the phase is only defined within mod (π), and are rather similar to those found in a similar computation by Simmons (1974). The westward tilt of phase with height is evident, as is the distortion of phase lines by the jet in the 'obvious' (i.e. advective) sense; this latter effect was also found by McIntyre (1970) for the perturbed Eady problem.

The antisymmetric mode amplitude for case B is shown in figure 16, and is seen to be concentrated in the central part of the channel, though not, of course, right at the center. The phase is very similar to figure 15. Finally, the symmetric mode amplitude for case C is given in figure 17; the smaller deformation radius in this case confines the instability amplitude very strongly to the center of the channel. The scale of the wave amplitude is intermediate between that of the jet, 2π, and the deformation radius, π/L in this case, in agreement with Simmons (1974). Similarly, the phase variation occurs over the same scale. For case C, a truncation of N = 15 is required to satisfy the convergence criteria for the most unstable modes at k = 3.5.

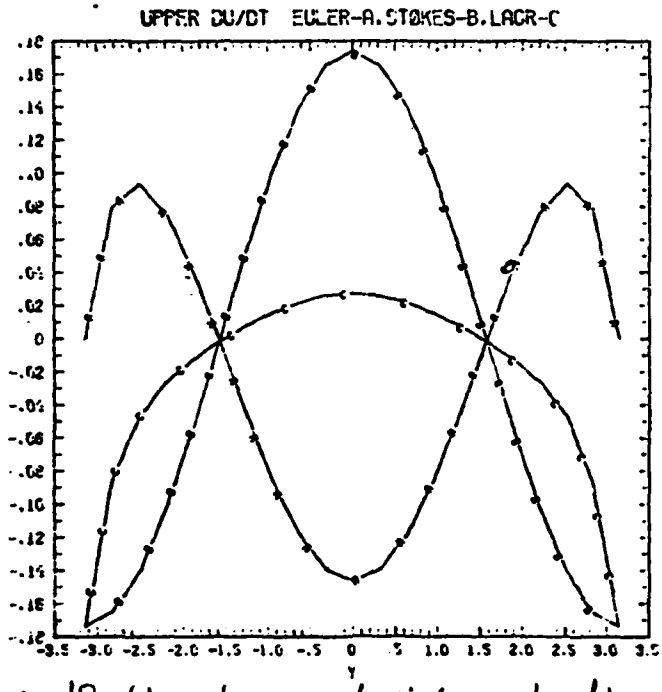

Figure 10: Upper layer zonal wind accelerations for the symmetric mode of case A. A → $\frac{\partial \bar{u}}{\partial t}_1$, B → $\frac{\partial \bar{u}}{\partial t}^S_1$, C → $\frac{\partial \bar{u}}{\partial t}^L_2$.

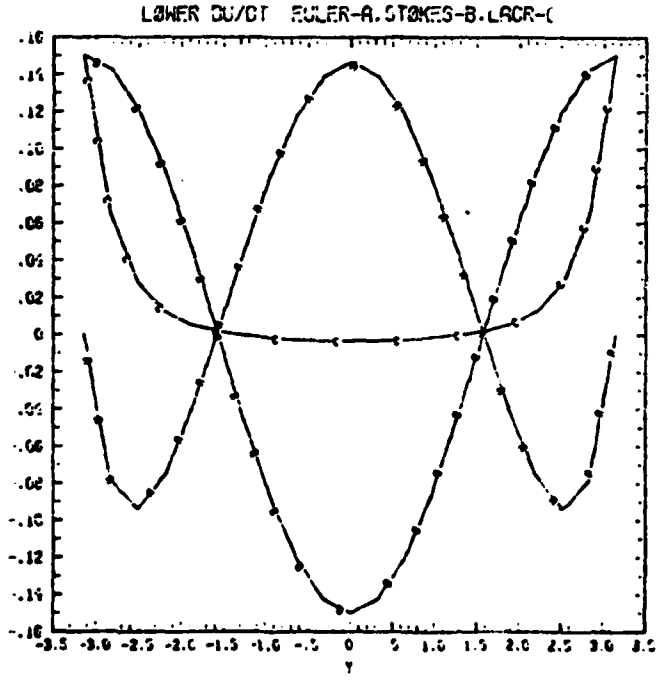

Figure 11: As in figure 10, but for the lower layer.

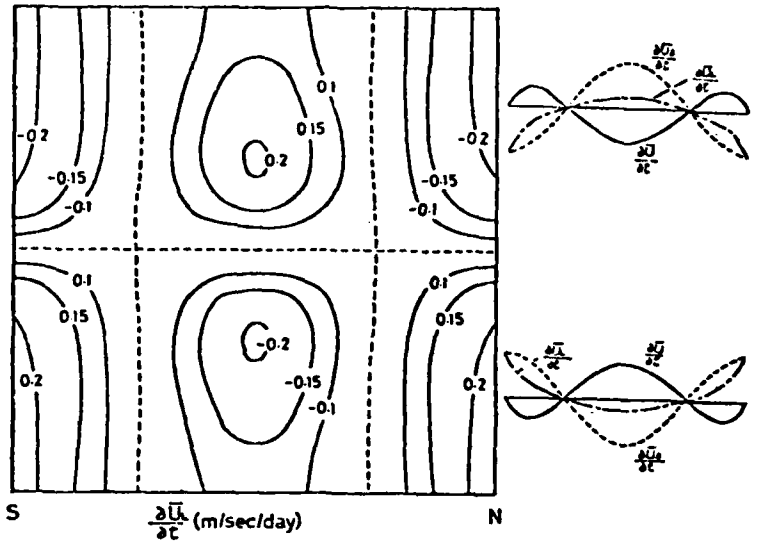

Figure 12: Distribution of the acceleration of Lagrangian mean zonal flow, $\partial \bar{U}_L / \partial t$. In the right part, the latitudinal distributions of $\partial \bar{U}_L / \partial t$, $\partial \bar{U}_S / \partial t$ and $\partial \bar{U} / \partial t$ at two representative levels are shown. (From Uryu (1979))

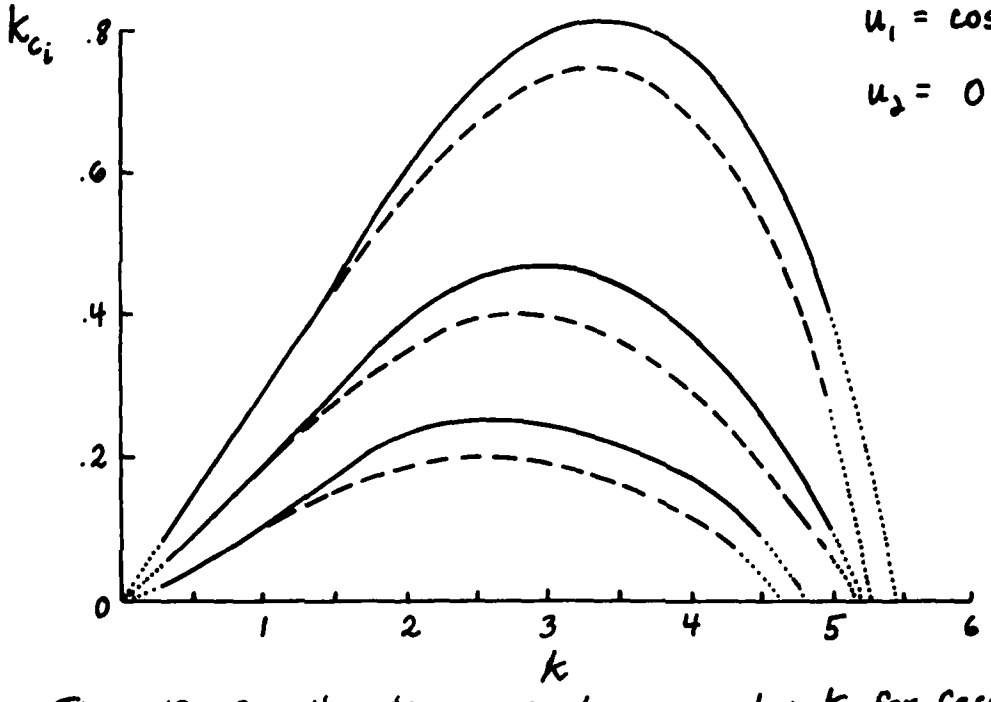

Figure 13: Growth rate vs. zonal wavenumber k for Case C. 20-wave spectral resolution.

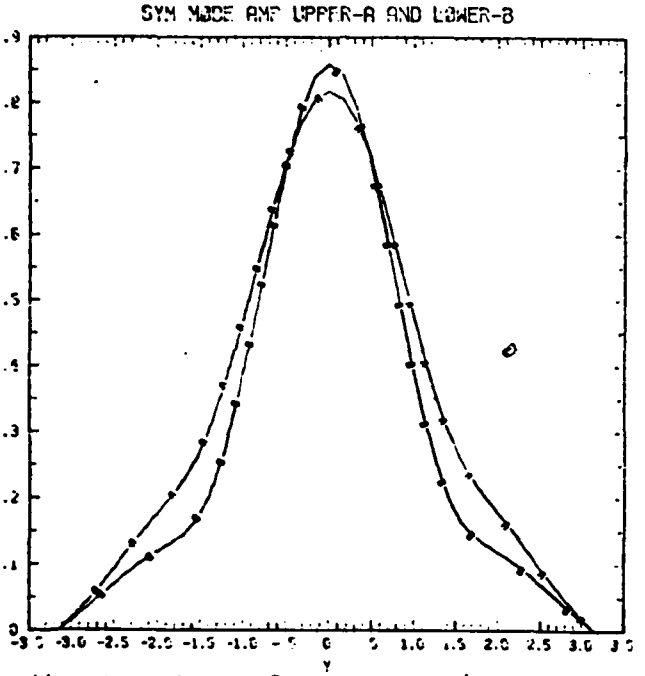

Figure 14: Amplitude of the symmetric unstable mode, case B. A→ upper layer, B→ lower layer.

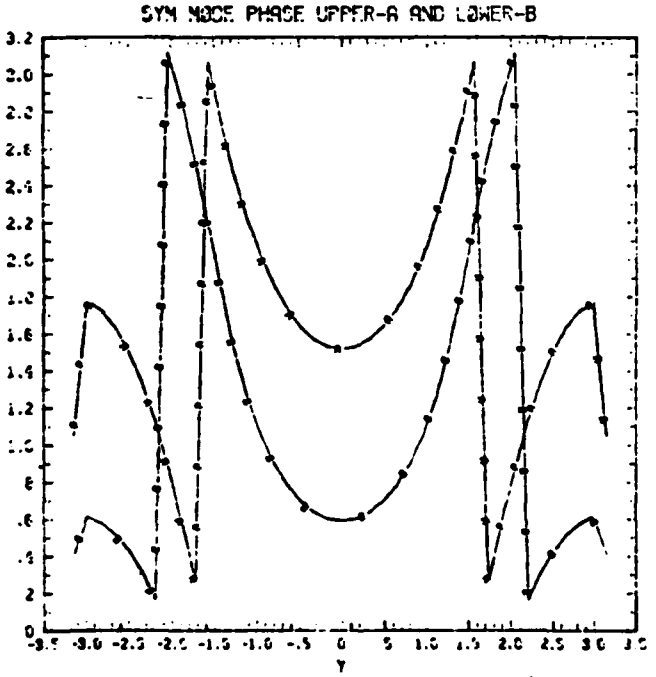

Figure 15: As in figure 14, except for the phase.

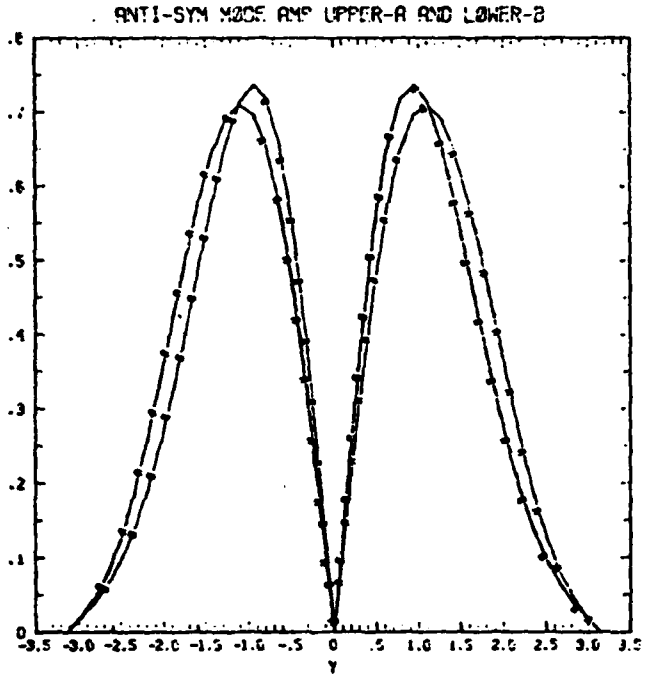

Figure 16: Amplitude of the anti-symmetric unstable mode, Case B. A → upper layer, B → lower layer.

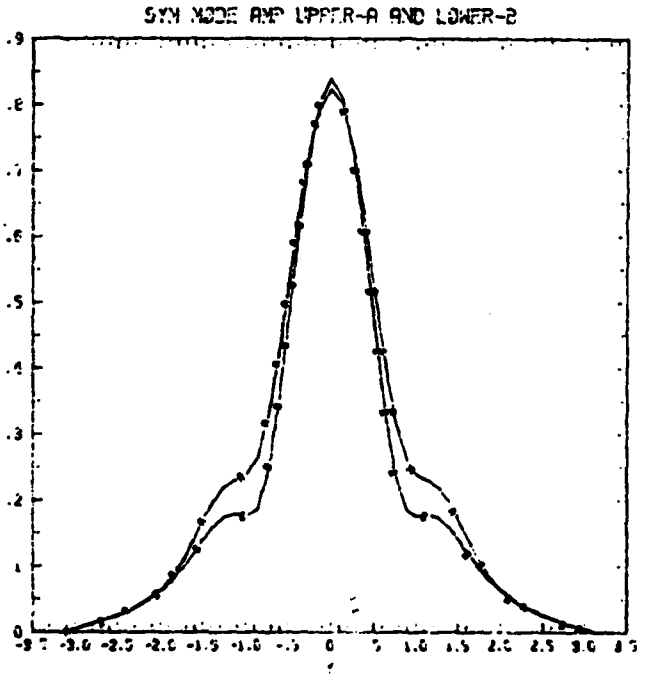

Figure 17: Amplitude of the symmetric unstable mode, Case C. A → upper layer, B → lower layer

Generally, the various mean circulations of case C are very similar to those of case B, except for being concentrated more strongly in the center of the channel. The only exception is with $\bar{v}_1^L$, which will be remarked on later. Otherwise, the circulations for case C will not be shown.

The induced Eulerian-mean circulation is found via equations (10) through (13). $\frac{\partial \bar{u}_i}{\partial t}$ and $\overline{u_i v_i}$ for the two layers are shown for the symmetric mode of case B in figures 18 and 19, respectively. Unlike the Phillips model, here the Reynolds stress does not vanish, and the zonal accelerations in the two layers are not equal and opposite. The upper layer Reynolds stress exceeds that of the lower, but the net acceleration is greatest in the lower layer because of the effect of the meridional circulation - which is shown in figures 20 and 21. These results all agree with those of Simmons (1974). As in case A, the EM circulation is a strong central thermally indirect cell bounded by two thermally direct cells, although here the activity tends to be kept away from the channel walls.

The antisymmetric mode of case B gives an EM meridional circulation which is almost exactly the reverse of that from the symmetric mode: a strong central direct cell bounded by weaker indirect cells, indicated by $\bar{w}_2$ in figure 22. The Reynolds stresses are similar for the two modes, though they have their maxima further away from the channel center for the antisymmetric mode. As for the zonal accelerations $\frac{\partial \bar{u}_i}{\partial t}$, shown in figure 23, they are quite different. In figure 18, $\frac{\partial \bar{u}_1}{\partial t}$ and $\frac{\partial \bar{u}_2}{\partial t}$ seem to be of similar form; but in figure 23 they are strikingly different in character, and are of opposite sign in the center of the channel.

The TEM circulation, computed using equations (15a-c), is shown for the symmetric mode of case B via $\bar{v}_i^*$ and $\bar{w}_2^*$ in figures 24 and 25. As with case A, it represents a single large thermally direct meridional cell, though once again the activity is confined more to the center of the channel. In addition, although formally $\bar{v}_i^*$ and $\bar{v}_i$, and $\bar{w}_2^*$ and $\bar{w}_2$, are of the same order in ε, in fact the TEM exceeds the EM by about an order of magnitude. The TEM circulations associated with the antisymmetric mode are simply two symmetric mode circulations side by side, and so are not shown. The divergence of E-P flux, shown in figure 26, is negative in the upper layer and positive in the lower, as in case A. But here the flux vectors point both upwards and outwards from the center of the channel, reflecting the importance of momentum fluxes in this problem. Spreading out of the E-P flux vectors with height has been observed in the atmosphere by Edmon et al. (1980), although they ascribe it to nonlinearity rather than to meridional shear in the mean flow.

The GLM vertical velocity $\bar{w}_2^L$ for the symmetric mode of case B is shown in figure 27; once again it seems to agree very closely with $\bar{w}_2^*$ in both magnitude and shape, and exhibits the available potential energy-releasing particle motions associated with baroclinic instability.

As for the meridional velocity $\bar{v}_i^L$, although it is always convergent towards the center of instability activity, its nature varies considerably from case to case. Figures 28 and 29 show $\bar{v}_i^L$ from the symmetric mode of cases B and C, while figures 30 and 31 show the same thing for the antisymmetric mode. The lower layer $\bar{v}_2^L$ has a simple convergent character and is limited in extent to where the instability amplitude is concentrated, vanishing well away from the channel walls. But the upper layer $\bar{v}_1^L$ has contribu-

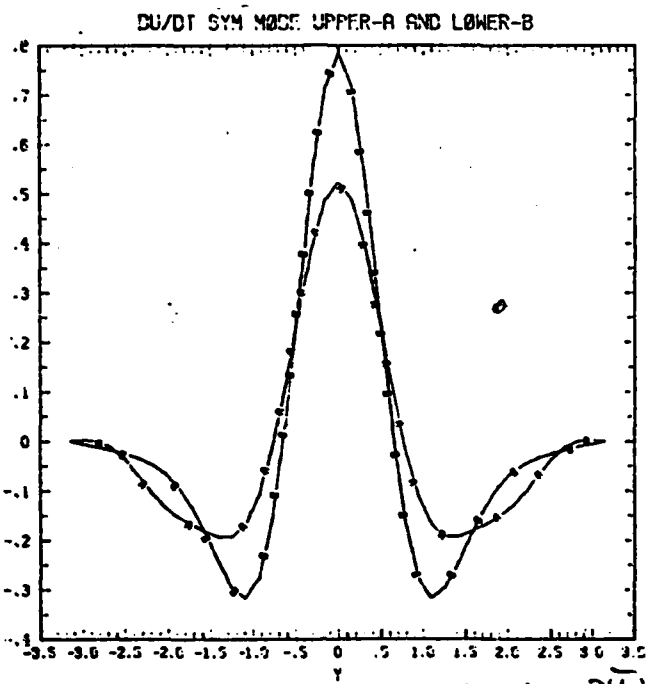

Figure 18: EM zonal wind acceleration $\frac{\partial \overline{u_i}}{\partial t}$ for the symmetric mode of Case B. A → upper layer, B → lower layer.

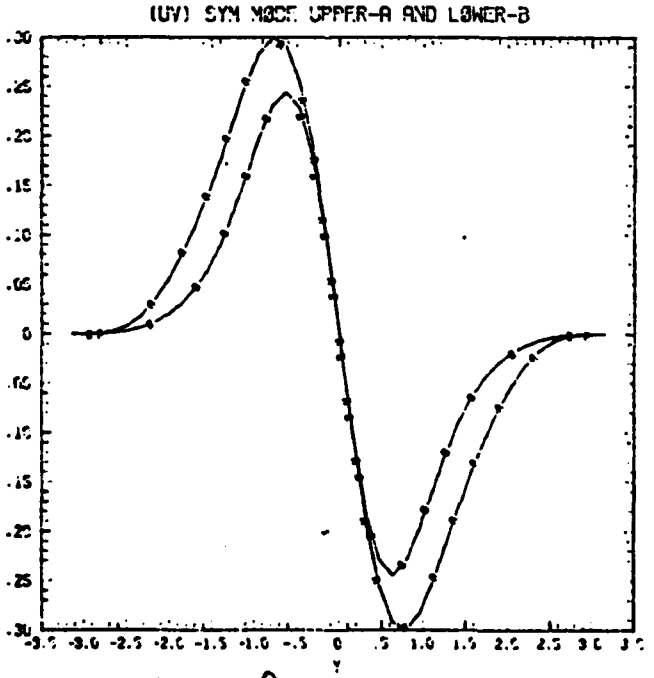

Figure 19: As in figure 18, but $\overline{u_i v_i}$.

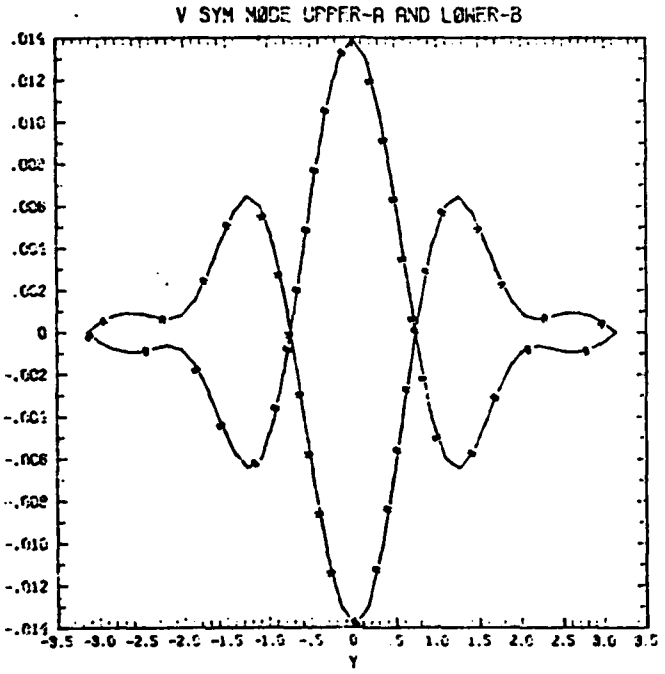

Figure 20: As in figure 18, but $\bar{v}_i$.

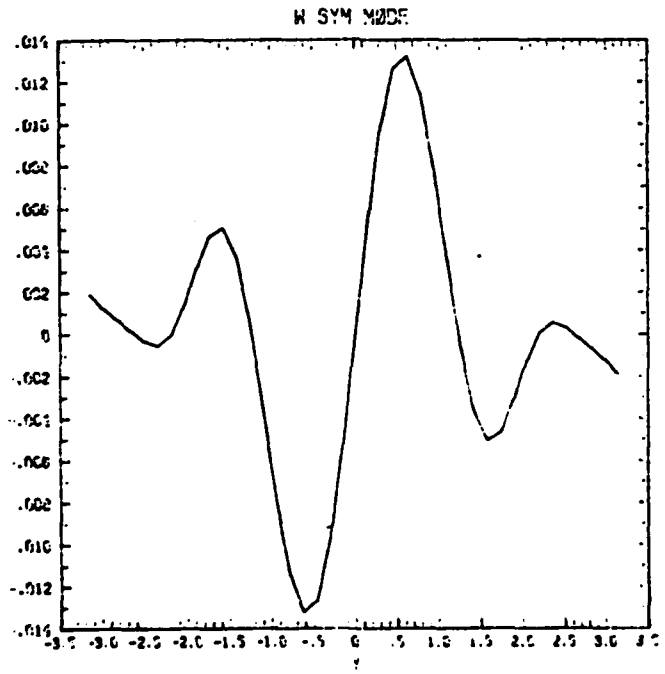

Figure 21: As in figure 18, but $\bar{w}_{\frac{1}{2}}$.

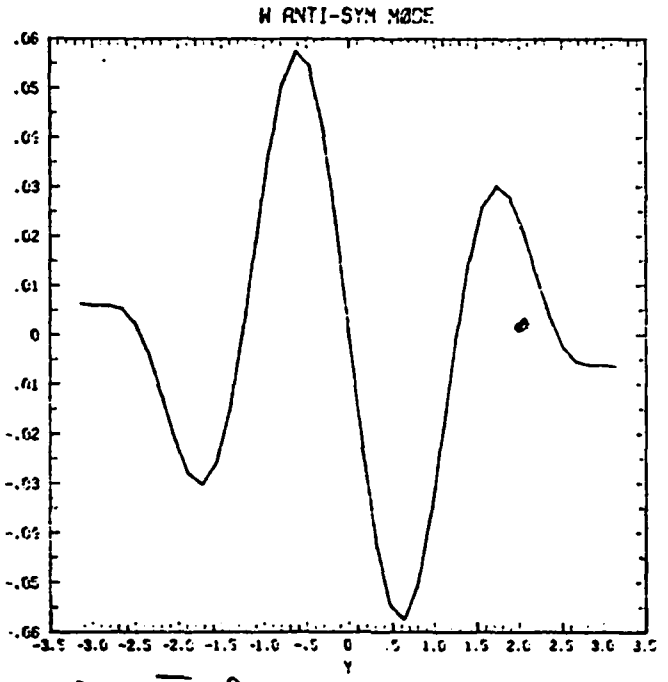

Figure 22: $\overline{w_3}$ for the anti-symmetric mode of case B.

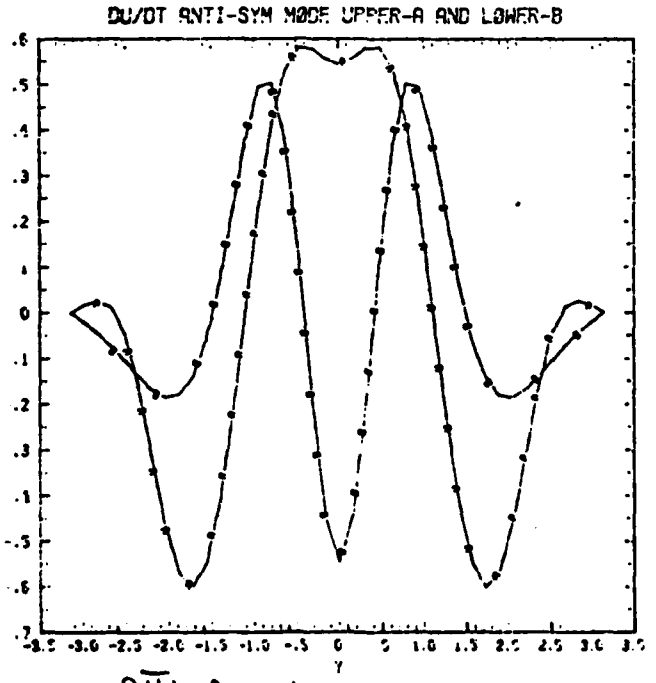

Figure 23: $\frac{\partial \overline{u_i}}{\partial t}$ for the anti-symmetric mode of case B.

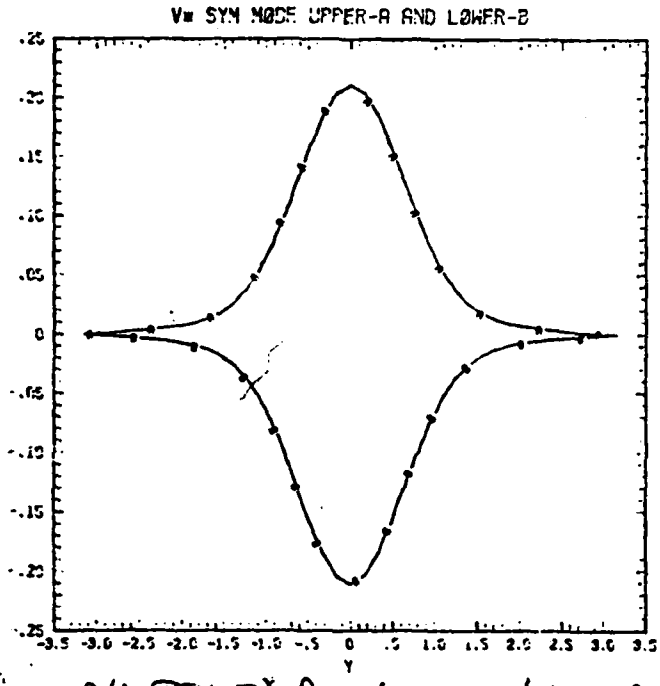

Figure 24: TEM $\bar{V}_i^*$ for the symmetric mode of case B.

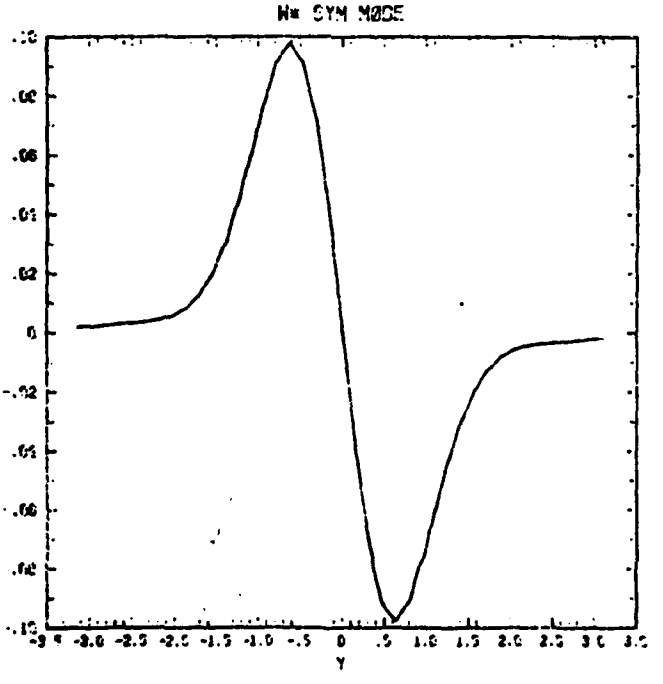

Figure 25: As in figure 24, but $\bar{W}_{\frac{1}{2}}^*$.

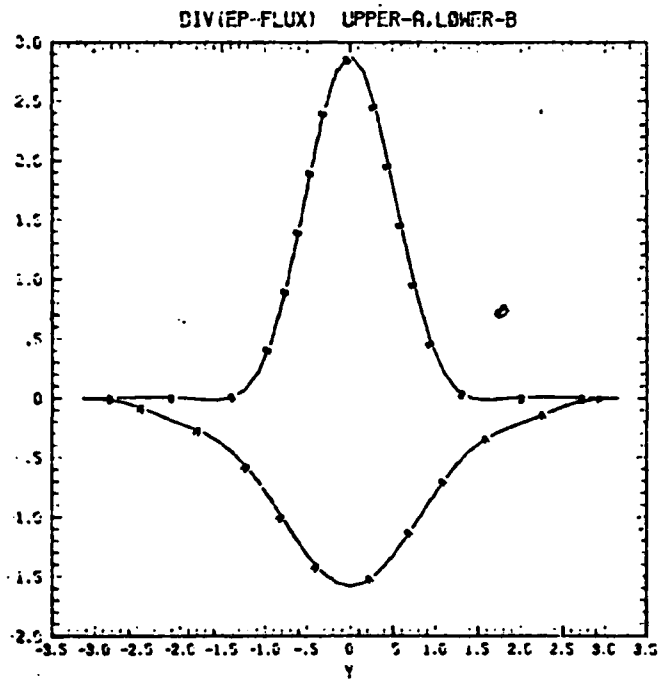

Figure 26: As in figure 24, but $(\nabla \cdot \underset{\sim}{F})_i$.

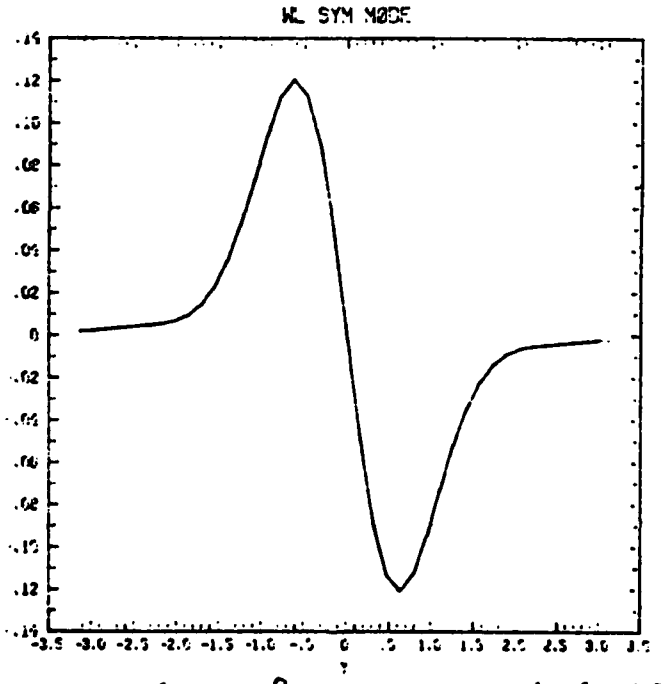

Figure 27: As in figure 24, but the GLM $\overline{w}^L_{\frac{1}{2}}$.

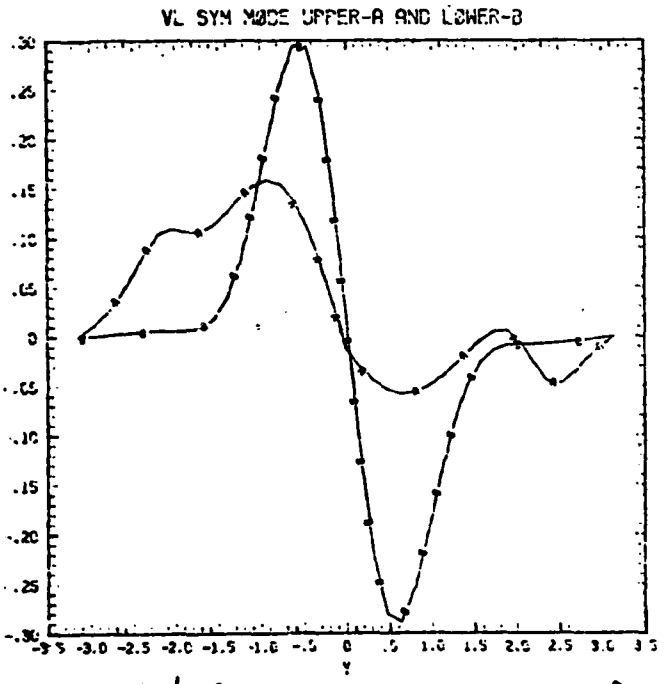

Figure 28: $\bar{V}_i^L$ for the symmetric mode of case B.

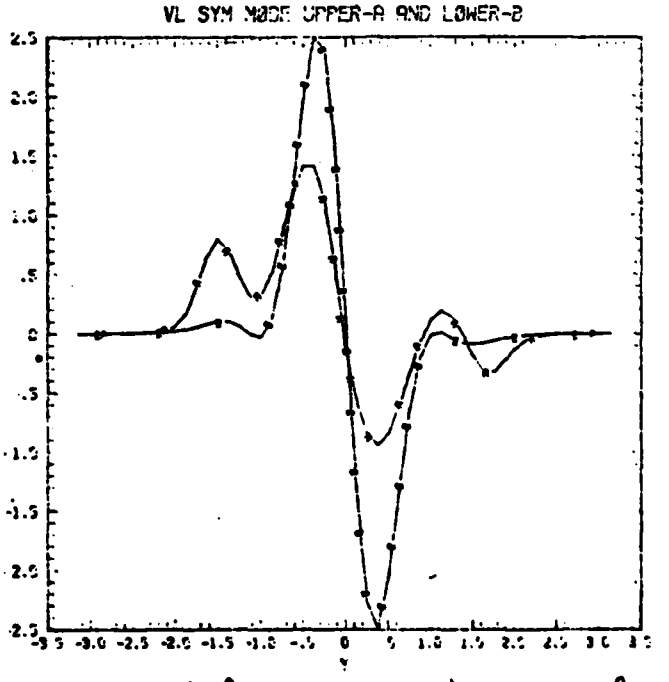

Figure 29: $\bar{V}_i^L$ for the symmetric mode of case C.

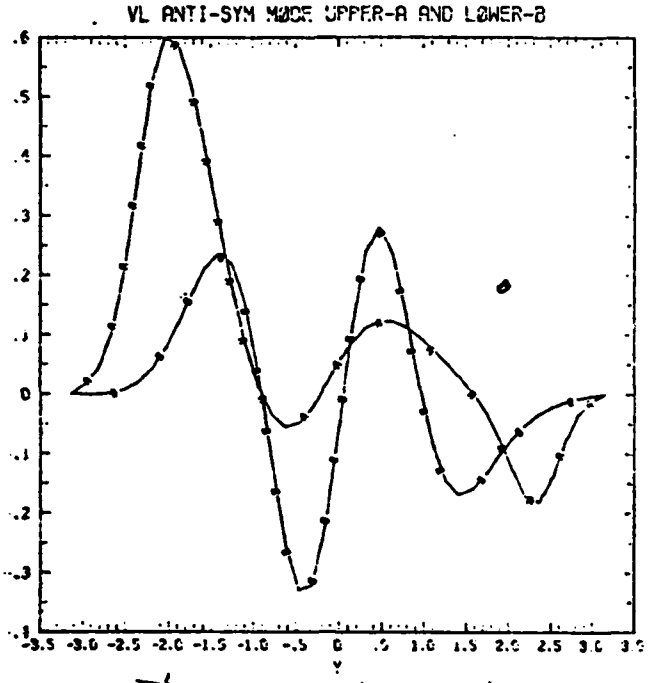

Figure 30: $\bar{V}_i^L$ for the anti-symmetric mode of case B.

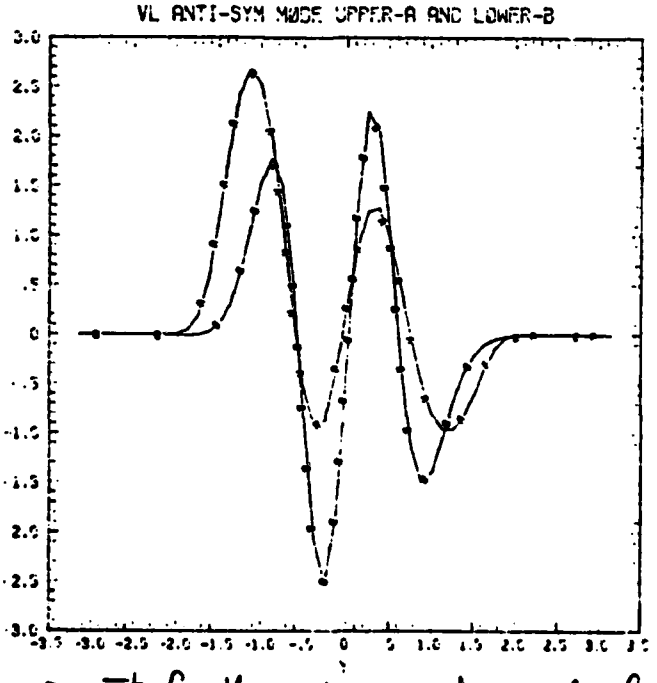

Figure 31: $\bar{V}_i^L$ for the anti-symmetric mode of case C.

tions arising from the meridional variation of the upper layer jet, and it thus exhibits a variety of behaviors. For the symmetric mode (figures 28 and 29), the maximum strength of $\overline{V}_i^L$ is much less than that of $\overline{V}_i^L$, ranging from 15% of $\overline{V}_i^L$ for case B to 40% with case C. In addition, there is a secondary maximum of convergence or divergence between the instability activity and the channel walls; in case B this equals the primary maximum in strength and is close to the walls.

Similar results hold for the anti-symmetric mode (figures 30 and 31) except that there are two centers of instability activity instead of one. However, the velocities in the two layers are closer in strength than with the symmetric mode, and unlike the symmetric mode, the maxima may not be aligned - figure 30 is a particularly clear example of this. It would seem rather difficult to make any general conclusions about the GLM $\overline{V}_i^L$, save for its convergent character already noted.

Recall that in case A, the Stokes correction $\frac{\partial \overline{v}_i}{\partial t}$ tended to oppose the Eulerian acceleration $\frac{\partial \overline{v}_i}{\partial t}$, leaving only a small residual $\frac{\partial \overline{v}_i^L}{\partial t}$ of opposite sign to $\frac{\partial \overline{v}_i}{\partial t}$. This was possible in part because $\frac{\partial \overline{v}_i}{\partial t}$ was antisymmetric about $(z - \frac{1}{2})$, being forced only by $\overline{V}$. But in cases B and C, it has already been seen that $\frac{\partial \overline{v}_i}{\partial t}$ obeys no such rule, and that in fact for the symmetric mode, $\frac{\partial \overline{v}_i}{\partial t}$ and $\frac{\partial \overline{v}_i}{\partial t}$ are similar in both magnitude and sign. Consequently, it should come as no surprise that the GLM accelerations $\frac{\partial \overline{v}_i^L}{\partial t}$ for cases B and C are extremely different from those for case A. In figures 32 and 33, $\frac{\partial \overline{v}_i}{\partial t}$, $\frac{\partial \overline{v}_i}{\partial t}$, and $\frac{\partial \overline{v}_i^L}{\partial t}$ are displayed for the upper and lower layers, respectively, from the symmetric mode of case B. In the upper layer the Eulerian and Stokes accelerations act in concert, producing a very strong net Lagrangian acceleration in the center of the channel; this is completely counter to Uryu's (1979) finding for the Eady mode. Although the Eulerian and Stokes accelerations are of opposite sign in the lower layer, the cancellation is nowhere near complete and the remaining Lagrangian acceleration is still substantial, though nothing like the acceleration in the upper layer. This is also a departure from Uryu's results.

The fields from case C are very similar to those of case B for these quantities, aside from being confined more to the center of the channel. But the antisymmetric mode of case B is worth looking at; this is done in figures 34 and 35. In the upper layer (figure 34), the Eulerian and Stokes corrections neither cancel nor reinforce each other, for they are out of phase. The only exception is at the very center of the channel, where $\frac{\partial \overline{v}_i}{\partial t}$ is nearly zero. Generally, $\frac{\partial}{\partial z}$ is positive where the wave amplitude is strongest, and negative just to the outside of that point. As for the lower layer (figure 35), the picture is essentially the reverse of that for the symmetric mode (figure 33), with the Stokes acceleration still winning over the Eulerian. But here $\frac{\partial \overline{v}_i^L}{\partial t}$ is positive in the center of the channel, whereas with the symmetric mode it is negative.

To calculate $\overline{u}_i^L$, equation (22a) shows it to be made up of two parts: one, the conventional Stokes drift term $\frac{\partial}{\partial y}(\overline{\eta_i u_i})$; and the other, the term $\frac{1}{2}\overline{\eta_i^2}\frac{\partial^2 u(u)}{\partial y^2}$ which is usually neglected. The relative importance of these two terms is shown in figure 36 for the symmetric mode of case B; the situations with the other modes are similar. The second term, while not negligible, is certainly of secondary importance; it has its maximum amplitude at the center of the channel, where both $|U_{yy}|$ and $\overline{\eta_i^2}$ are maximal.

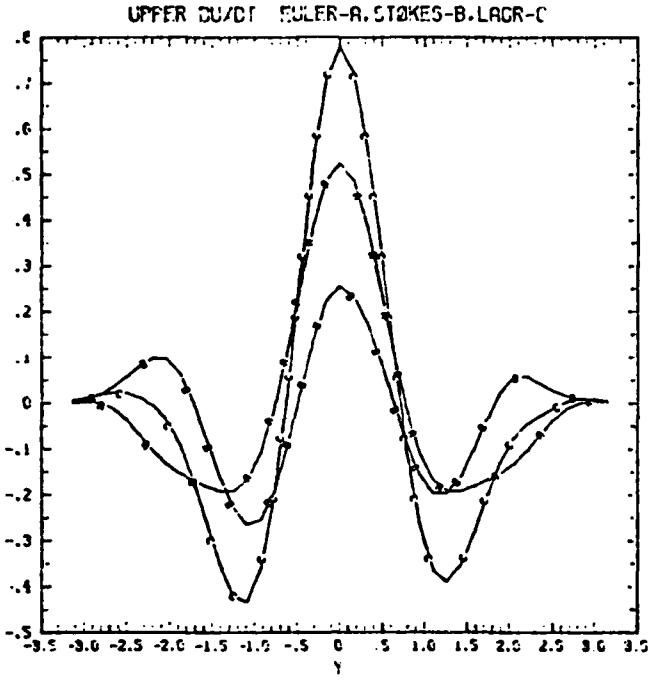

Figure 32: Upper layer zonal wind accelerations for the symmetric mode of case B. A → $\frac{\partial \bar{u}_1^a}{\partial t}$, B → $\frac{\partial \bar{u}_1^s}{\partial t}$, C → $\frac{\partial \bar{u}_1^L}{\partial t}$.

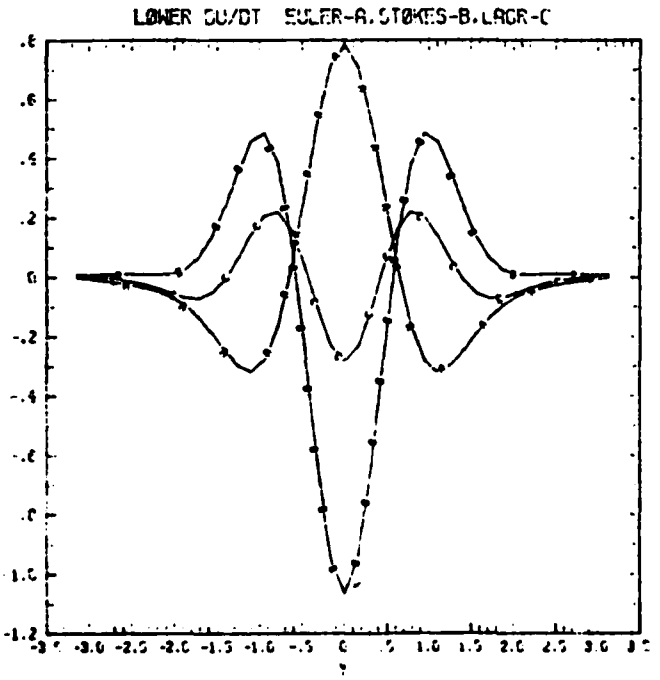

Figure 33: As in figure 32, but for the lower layer.

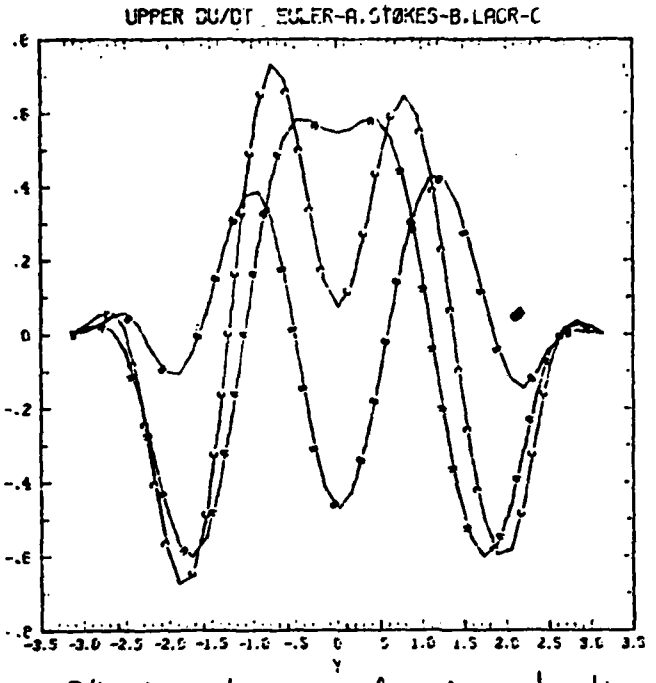

Figure 34: Upper layer zonal wind accelerations for the anti-symmetric mode of case B. A → $\frac{\partial \overline{u}_i}{\partial t}$, B → $\frac{\partial \overline{u}_i^s}{\partial t}$, C → $\frac{\partial \overline{u}_i^L}{\partial t}$.

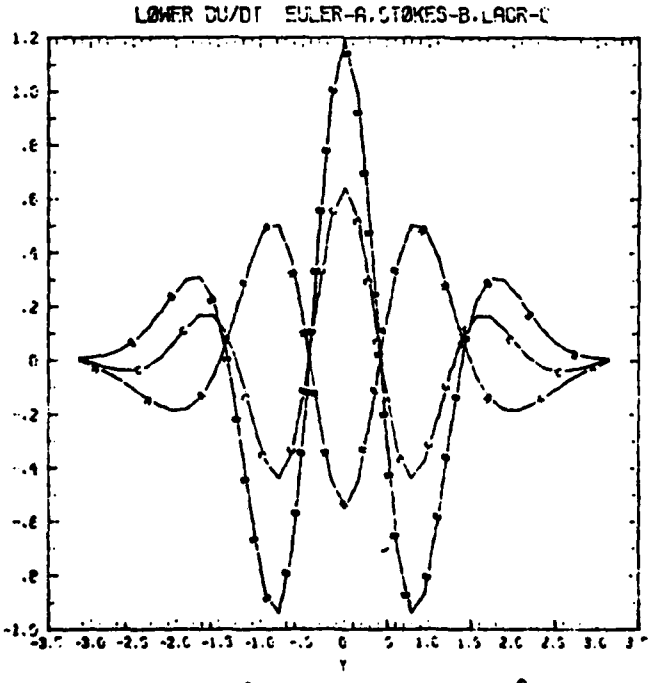

Figure 35: As in figure 34, but for the lower layer.

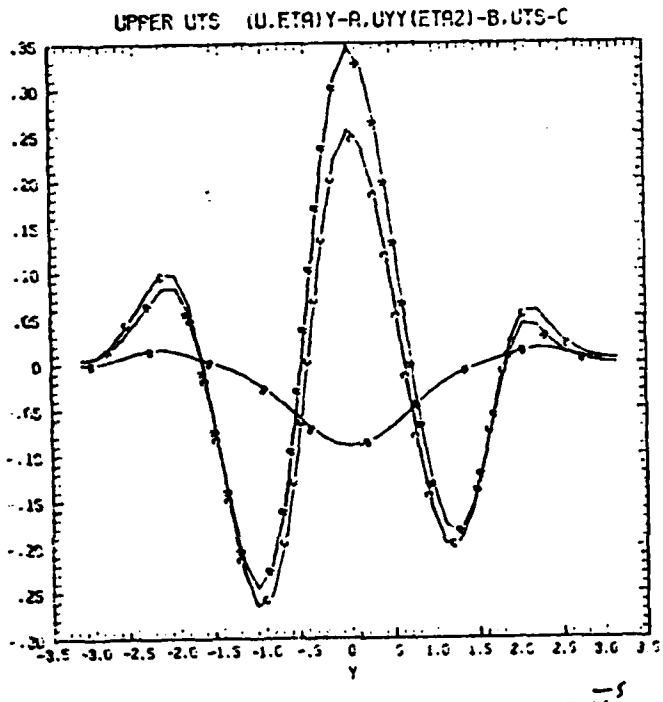

Figure 36: Upper layer Stokes drift $\frac{\partial \bar{u}_1^s}{\partial t}$ for the symmetric mode of case B, decomposed into its two component parts: A → $\frac{\partial}{\partial t}\left[\frac{\partial}{\partial y}(\overline{\eta_1 u_1})\right]$, B → $\frac{\partial}{\partial t}\left[\frac{1}{2}\overline{\eta_1^2}\frac{d^2U(y)}{dy^2}\right]$, C → total $\frac{\partial \bar{u}_1^s}{\partial t}$.

ACKNOWLEDGMENTS

I would like to thank Peter Rhines for helpful discussions, Masaaki Takahashi for pointing out an error in the calculations, and the entire GFD staff for a stimulating environment.

APPENDIX

Substituting the eigenmode forms (4) into (3a,b) with the specific form $u(y,y) = \tilde{u} + \hat{u}\cos(y/2)$, $U(y) \equiv U$, one obtains for the upper layer

$$\underbrace{[(\tilde{u}+\hat{u}-c)}_{(1)} + \hat{u}\cos y]\Big\{\sum_{m=1}^{N}\sin(my)\big[(m^2+k^2+F)A_1^m - FA_2^m\big] + \sum_{m=1}^{N}\cos\big[(m-\tfrac{1}{2})y\big]\big[\big((m-\tfrac{1}{2})^2+k^2+F\big)B_1^m - FB_2^m\big]\Big\}$$

$$-\underbrace{[\beta + F(\tilde{u}+\hat{u})}_{(2)} + (F+1)\hat{u}\cos y]\Big\{\sum_{m=1}^{N}A_1^m\sin(my) + \sum_{m=1}^{N}B_1^m\cos\big[(m-\tfrac{1}{2})y\big]\Big\} = 0 \qquad (A1)$$

The equation for the lower layer is similar, except that the indices 1 and 2 are reversed, (1) is replaced by $[-c]$, and (2) is replaced by $[\beta - F(\tilde{u}+\hat{u}) - F\hat{u}\cos y]$. Then using the identities

$$\cos y \sin(my) = \tfrac{1}{2}\{\sin[(m+1)y] + \sin[(m-1)y]\}$$

$$\cos y \cos\big[(m-\tfrac{1}{2})y\big] = \tfrac{1}{2}\{\cos\big[(m+\tfrac{1}{2})y\big] + \cos\big[(m-\tfrac{3}{2})y\big]\}$$

to compute the interactions between modes, (A1) reduces to the set of N equations

$$(m^2+k^2+F)(\tilde{u}+\hat{u})A_1^m + \tfrac{1}{2}\big((m+1)^2+k^2+F\big)\hat{u}A_1^{m+1} + \tfrac{1}{2}\big((m-1)^2+k^2+F\big)\hat{u}A_1^{m-1}$$

$$-F(\tilde{u}+\hat{u})A_2^m - \tfrac{1}{2}F\hat{u}A_2^{m+1} - \tfrac{1}{2}F\hat{u}A_2^{m-1} - [\beta + F(\hat{u}+\tilde{u})]A_1^m \qquad (A2)$$

$$-\tfrac{1}{2}(F+1)\hat{u}A_1^{m+1} - \tfrac{1}{2}(F+1)\hat{u}A_1^{m-1} = c\big[(m^2+k^2+F)A_1^m - FA_2^m\big]$$

for each $m = 1,\ldots,N$, as well as a corresponding set of N equations for B_i^m with m replaced by $(m - \frac{1}{2})$. There is also a similar set for the lower layer.

As mentioned previously, the problems for the A_i^m's and the B_i^m's are separable. If one transforms coordinates to

$$P_1^m = (m^2+k^2+F)A_1^m - FA_2^m$$

$$P_2^m = (m^2+k^2+F)A_2^m - FA_1^m$$

$$Q_1^m = \big((m-\tfrac{1}{2})^2+k^2+F\big)B_1^m - FB_2^m$$

$$Q_2^m = \big((m-\tfrac{1}{2})^2+k^2+F\big)B_2^m - FB_1^m \qquad [m = 1,\ldots,N]$$

then the eigenvalue problem can be written in matrix form as

$$\mathbf{M}\,\underset{\sim}{v} = c\,\underset{\sim}{v} \qquad (A3)$$

where

$$\underset{\sim}{v} = (P_1^1, \ldots P_1^N\ P_2^1, \ldots P_2^N) \quad \text{or} \quad \underset{\sim}{v} = (Q_1^1 \ldots Q_1^N\ Q_2^1 \ldots Q_2^N)$$

corresponding to the antisymmetric and symmetric problems, respectively, and $\mathbb{M}$ is 'block tridiagonal':

$$\mathbb{M} = \begin{pmatrix} \begin{pmatrix} \times\times & C \\ C & \ddots \end{pmatrix} & \begin{pmatrix} \times\times & C \\ C & \ddots \end{pmatrix} \\ \begin{pmatrix} \times\times & C \\ C & \ddots \end{pmatrix} & \begin{pmatrix} \times\times & C \\ C & \ddots \end{pmatrix} \end{pmatrix}$$

There are many well-established numerical library routines for solving matrix eigenvalue problems of the form (A3). To be satisfied with the numerical solution, one would want the spectral amplitudes $|A_m|$ and $|B_m|$ to decrease rapidly with increasing m, and for the important amplitudes to be independent of the truncation N.

REFERENCES

Andrews, D.G., and M.E. McIntyre, 1976. Planetary waves in horizontal and vertical shear; the generalized Eliassen-Palm relation and the mean zonal acceleration. J. Atmos. Sci., 33, 2031-2048.

Andrews, D.G. and M.E. McIntyre, 1978. An exact theory of nonlinear waves on a Lagrangian-mean flow. J. Fluid Mech., 89, 609-646.

Charney, J.G., 1947. The dynamics of long waves in a baroclinic westerly current. J. Meteor., 4, 135-163.

Charney, J.G. and P.G. Drazin, 1961. Propagation of planetary-scale disturbances from the lower into the upper atmosphere. J. Geophys. Res., 66, 83-109.

Eady, E.T., 1949. Long waves and cyclone waves. Tellus, 1, 33-52.

Edmon, H.J., B.J. Hoskins and M.E. McIntyre, 1980. Eliassen-Palm cross-sections for the troposphere. J. Atmos. Sci., 37, 2600-2616. (See also Corrigendum, J. Atmos. Sci., 38, 1115 (1981) , especially second last item.)

Eliassen, A. and E. Palm, 1961. On the transfer of energy in stationary mountain waves. Geofys. Publ., 22, No. 3, 1-23.

Kim, K., 1978. Instability of baroclinic Rossby waves: energetics in a two-layer ocean. Deep-Sea Res., 25, 795-814.

McIntyre, M.E., 1970. On the non-separable baroclinic parallel flow instability problem. J. Fluid Mech., 40, 273-306.

Pedlosky, J., 1979. Geophysical Fluid Dynamnics. Springer-Verlag.

Phillips, N.A., 1954. Energy transformations and meridional circulations associated with simple baroclinic waves in a two-level, quasi-geostrophic model. Tellus, 6, 273-286.

Rhines, P.E. and W.R. Holland, 1979. A theoretical discussion of eddy-driven mean flows. Dyn. Atmos. Oceans, 3, 289-325.

Simmons, A.J., 1974. The meridional scale of baroclinic waves. J. Atmos. Sci., 31, 1515-1525.

Stone, P.H., 1969. The meridional structure of baroclinic waves. J. Atmos. Sci., 26, 376-389.

Uryu, M., 1979. Lagrangian mean motion induced by a growing baroclinic wave. J. Met. Soc. Japan, 57, 1-20.

Yamagata, T., 1976. Stability of planetary waves in a two-layer system. J. Ocean. Soc. Japan, 32, 116-127.

ISOLATED 2D VORTICES IN THE PRESENCE OF SHEAR

Mark Swenson

INTRODUCTION

There are prominent features of geophysical flows, such as the Red Spot of Jupiter, atmospheric blocking patterns, and oceanic current rings, that are strongly nonlinear, coherent features with planetary scales. In recent years, the quasi-geostrophic equations have been investigated in the search for exact solutions that are steadily propagating, strongly nonlinear and form preserving (Stern 1975; Larichev & Reznik 1976; Flierl et al. 1980), these being the apparent properties of the geophysical coherent features. The applicability of these modons to flows of geophysical interest is still in question. How might they be generated in realistic flows? Are they stable to finite amplitude perturbations? Can they stay coherent in the presence of a non-uniform mean flow?

This report will be concerned only with the latter question. It is known that atmospheric blocking patterns and the Red Spot are found in regions of significant horizontal shear. It is the intention of this report to investigate the robustness of the modon solutions in the presence of horizontal shear. As a first step, we have neglected the influence of the β -effect so that the important balances can be isolated. Accordingly, we focus attention on an ideal, two-dimensional fluid on the f-plane.

FORMULATION

The vorticity equation for this problem is

$$\partial_t \nabla^2\psi + J(\psi, \nabla^2\psi) = 0 \qquad (1)$$

where J is the Jacobian operator and ψ is the stream function. Steady solutions satisfy $J(\psi, \nabla^2\psi) = 0$, which implies that $\nabla^2\psi = F(\psi)$ where F is an arbitrary function.

In regions where the stream lines extend to infinity, the boundary conditions at infinity determine the relationship between vorticity (vorticity $\equiv \omega = \nabla^2\psi$) and the stream function. In closed streamline regions the choice of $\omega = F(\psi)$ is left arbitrary insofar as inviscid fluid theory is concerned. In general, this distribution is determined by the manner in which the steady flow was established, which includes effects such as viscosity. In this report, $F(\psi)$ is chosen arbitrarily in the hope that the nature of these solutions are indicative of the types of balances one will find in more complicated situations.

As a result of this approach, ψ or some derivative of ψ will be discontinuous across a given closed stream line. Let this stream line be given by the curve $r = r(\theta)$. Define

$$\psi = \begin{cases} \psi^{in} , & r < r(\theta) \\ \psi^{out} , & r > r(\theta) \end{cases} \qquad (2)$$

It is required that $\psi^{in} = \psi^{out} = \bar{\psi}$, a constant, on $r = r(\theta)$. Furthermore, $\partial_n \psi^{in} = \partial_n \psi^{out}$ on $r = r(\theta)$, where ∂_n = normal derivative. This ensures continuity of the tangential velocity and, through Bernoulli's equation, pressure.

EXACT SOLUTIONS

Any circularly symmetric vortex is a steady, equilibrium solution to the equations for a two-dimensional, ideal fluid on the f-plane. In the presence of a mean flow the situation is altered:

A. No shear (Batchelor 1967)

If the background flow has no horizontal shear, we may formulate the problem as:

$$\left.\begin{aligned} &\nabla^2 \psi^{out} = 0 \quad ; \quad \psi^{out} \to |\bar{u}| r \sin\theta \quad \text{as} \quad r \to \infty , \\ &\nabla^2 \psi^{in} = -k^2 \psi^{in} , \\ &r(\theta) = 1 , \\ &\psi^{out} = \psi^{in} = 0 \quad \text{on} \quad r = 1 , \\ &\partial_n \psi^{out} = \partial_n \psi^{in} \quad \text{on} \quad r = 1 , \end{aligned}\right\} \qquad (3)$$

where (r, θ) are polar coordinates with the origin at the center of the eddy, $\bar{u}$ is the velocity of the mean flow and k^2 is a constant.

The solution is given by:

$$\left.\begin{aligned} &\psi^{out} = |\bar{u}| (r - \tfrac{1}{r}) \sin\theta , \\ &\psi^{in} = 2 |\bar{u}| [k J_0(k)]^{-1} J_1(kr) \sin\theta , \\ &J_1(k) = 0 , \end{aligned}\right\} \qquad (4)$$

where J_n is the Bessel function of order n. The streamlines are sketched in figure 1, where k has been chosen to be the first zero of J_1. Notice the dipole structure. The mutual advection of these vortices holds the modon steady in the face of the mean flow.

B. Linear shear (Stern & Flierl, private communication)

An exact solution in this case is possible if the center of the modon is at the latitude where the imposed mean flow has zero velocity. The formulation is:

$$\left.\begin{aligned} &\nabla^2 \psi^{out} = -\varepsilon \quad ; \quad \psi^{out} \to -\varepsilon/4 \, r^2 (1 - \cos 2\theta) \quad \text{as} \quad r \to \infty \\ &\nabla^2 \psi^{in} = a - k^2 \psi^{in} , \end{aligned}\right\} \qquad (5)$$

where ε is the shear of the flow at infinity. The rest of the problem is as before.

The solution is given by:

$$\left.\begin{aligned} &\psi^{out} = \varepsilon/4 \, [(r^2 - 1) - (r^2 - r^{-2}) \cos 2\theta] , \\ &\psi^{in} = -\varepsilon [k^2 J_0(k)]^{-1} [J_0(kr) - J_0(k) + 2 J_2(kr) \cos 2\theta] , \\ &r(\theta) = 1, \quad J_2(k) = 0. \end{aligned}\right\} \qquad (6)$$

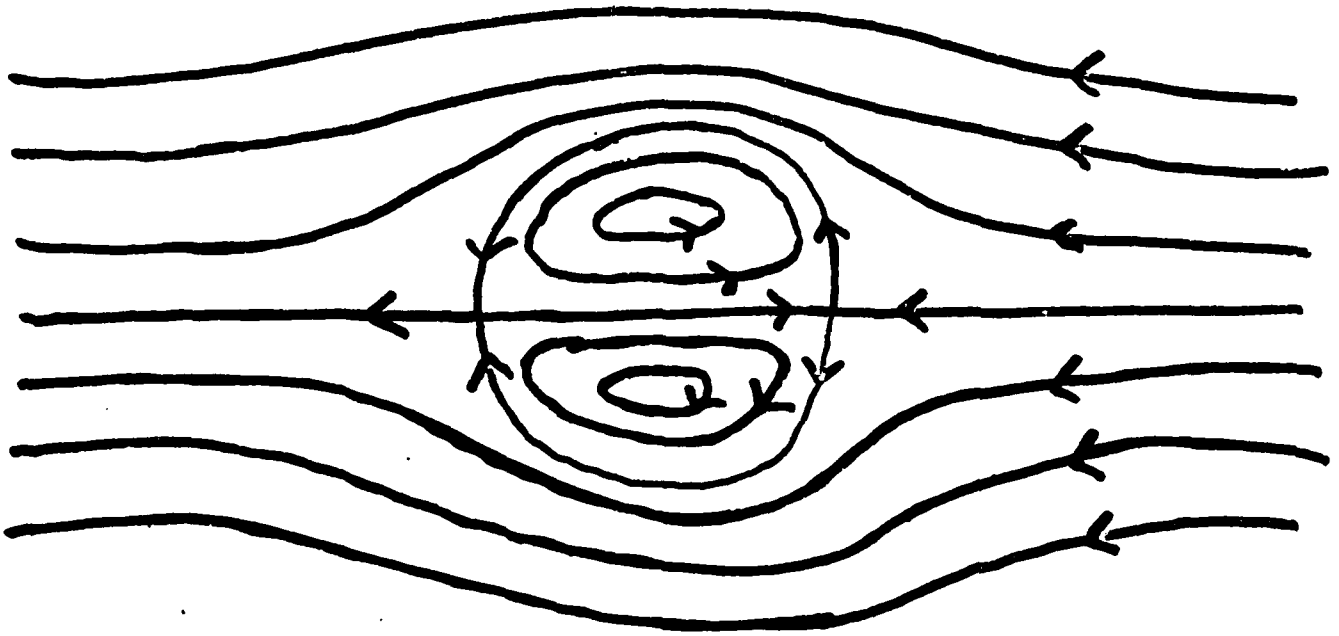

Figure 1. Streamlines for the Batchelor modon.

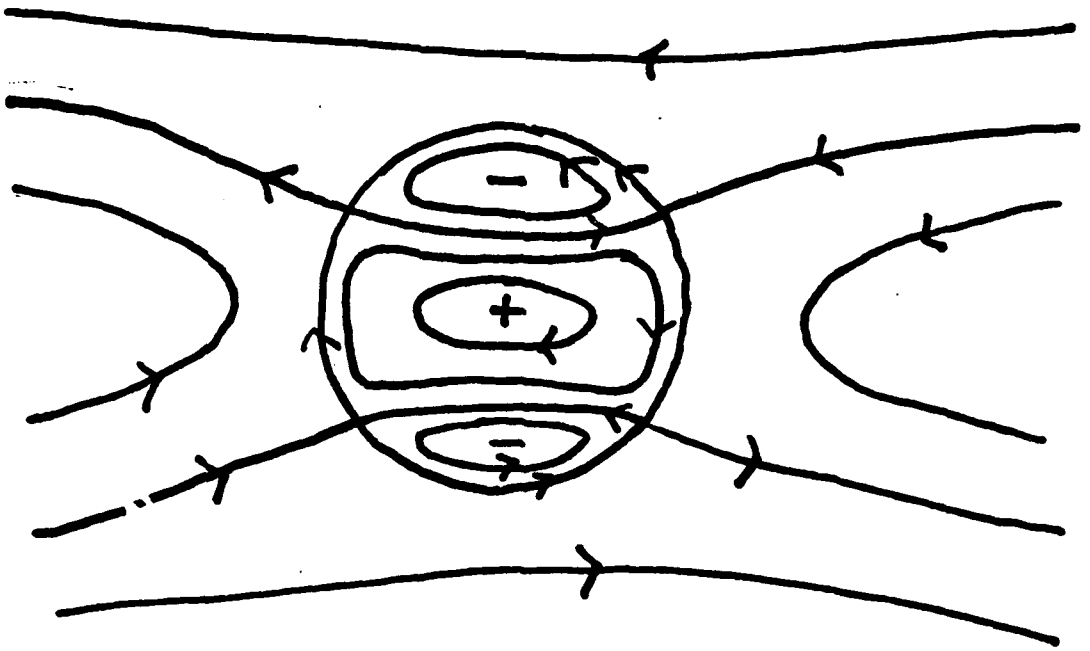

Figure 2. Streamlines for the exact shear solution.

The streamlines are sketched in figure 2, where k has been chosen to be the first zero of J_2.

PERTURBATION APPROACH

A. Simple solutions

When the mean flow at infinity can be considered weak (in a sense to be explained later), a perturbation approach is fruitful. We formulate the problem for the case where there is a linear shear velocity profile at infinity, and where the center of the modon may be on a latitude where the velocity does not equal zero. Special cases will be considered afterwards. Recall that $\nabla^2\psi = F(\psi)$. Write $\psi^{out} = \varphi + \Psi$ where $\varphi \to 0$ as $r \to \infty$ and $\Psi = -u_0 y - \frac{1}{2}\varepsilon y^2$. Introduce the scaling $\varphi \sim u_s L$ & $y \sim L$, where L = size of eddy and u_s = velocity scale inside eddy. This implies that

$$J(\varphi - \mu y - \tfrac{1}{2}\gamma y^2, \nabla^2\varphi) = 0 \qquad (7)$$

where $\mu = u_0/u_s$ & $\gamma = \varepsilon L/u_s$. Then

$$\nabla^2\varphi = F(\varphi - \mu y - \tfrac{1}{2}\gamma y^2) \; . \qquad (8)$$

Assume $\mu \sim \gamma \ll O(1)$. (This is the condition that the mean flow at infinity be weak.) Expanding φ, F and $r(\theta)$ in powers of γ (i.e., $\varphi = \varphi_0 + \gamma\varphi_1 + \ldots$, etc.) we obtain a hierarchy of problems that can be solved in terms of lower order solutions only. F_0^{out} and F_1^{out} are determined from the boundary conditions at infinity, while F_0^{in} and F_1^{in} are arbitrary.

(i) $\mu = 0$.

(a) $F_0^{in} = \omega_0$ and $F_1^{in} = 0$.

The formulation of this problem is:

$$\left.\begin{aligned}
&\nabla^2\psi_0^{out} = 0 \;;\; \psi_0^{out} \to 0 \text{ as } r \to \infty, \\
&\nabla^2\psi_1^{out} = -1 \;;\; \psi_1^{out} \to -\tfrac{1}{4}r^2(1-\cos 2\theta) \text{ as } r \to \infty, \\
&\nabla^2\psi_0^{in} = \omega_0, \qquad (a) \\
&\nabla^2\psi_1^{in} = 0, \qquad (b) \\
&\psi_0^{out} = \psi_0^{in} = 0 \quad \text{on } r = 1, \\
&\partial_r\psi_0^{out} = \partial_r\psi_0^{in} \quad \text{on } r = 1, \\
&\psi_1^{out} + r_1(\theta)\,\partial_r\psi_0^{out} = \psi_1^{in} + r_1(\theta)\,\partial_r\psi_0^{in} = 0 \quad \text{on } r = 1, \\
&\partial_r\psi_1^{out} + r_1(\theta)\,\partial_r^2\psi_0^{out} - [\partial_\theta r_1(\theta)][\partial_\theta\psi_0^{out}] \\
&\quad = \partial_r\psi_1^{in} + r_1(\theta)\,\partial_r^2\psi_0^{in} - [\partial_\theta r_1(\theta)][\partial_\theta\psi_0^{in}] \quad \text{on } r = 1.
\end{aligned}\right\} \qquad (9)$$

The result is:

$$\left.\begin{aligned}
\psi^{out} &= \tfrac{1}{2}\omega_0 \ln r + \gamma\left[\tfrac{1}{2} - \tfrac{1}{4}r^2 + \tfrac{1}{4}(r^2 + r^{-2})\cos 2\theta\right] + O(\gamma^2), \\
\psi^{in} &= \tfrac{1}{2}\omega_0(r^2 - 1) + \gamma\left[\tfrac{1}{4} + \tfrac{1}{2}r^2\cos 2\theta\right] + O(\gamma^2), \\
r(\theta) &= 1 - \gamma\left[\tfrac{1}{2\omega_0} + \tfrac{1}{\omega_0}\cos 2\theta\right] + O(\gamma^2).
\end{aligned}\right\} \qquad (10)$$

The streamlines are sketched in figure 3 for $|\gamma| = .2$. It is interesting to note that no streamlines extend to infinity for $\gamma = -.2$. This indicates that the eddy is not isolated in the sense that it has infinite total energy due to the log term. In the following example, the eddy is required to have finite energy, which dictates a different form for F^{in}.

$$\text{(b)}\quad F^{in}(\psi^{in}) = F_0^{in}(\psi^{in}) + \gamma F_1^{in}(\psi^{in}) + O(\gamma^2) = a - k^2\psi_0^{in} - \gamma k^2 \psi_1^{in} + O(\gamma^2)$$

The formulation is the same as the previous problem, except that equations (9a,b) become:

$$\left.\begin{aligned} &\nabla^2\psi_0^{in} + k^2\psi_0^{in} = a, \\ &\nabla^2\psi_1^{in} + k^2\psi_1^{in} = 0. \end{aligned}\right\} \quad (11)$$

The result is:

$$\left.\begin{aligned} \psi^{out} &= \gamma\left[-\tfrac{1}{4}r^2 + \tfrac{1}{4}(r^2 - r^{-2})\cos 2\theta\right] + O(\gamma^2), \\ \psi^{in} &= -a\left[k^2 J_0(k)\right]^{-1}\left[J_0(kr) - J_0(k)\right] + \gamma\left[\tfrac{-1}{4J_0(k)} J_0(kr)\right] + O(\gamma^2), \\ r(\theta) &= 1 - \gamma\left[a^{-1}\left(\tfrac{1}{2} - \cos 2\theta\right)\right] + O(\gamma^2), \\ J_1(k) &= 0. \end{aligned}\right\} \quad (12)$$

The streamlines are sketched in figure 4. For this solution, the flow outside of the eddy is very weak [$O(\gamma)$]. Inside of the eddy there is O(1) flow with a single extremum in ψ and whose sense of flow depends solely on a. This differs from the exact shear solution since cos2θ terms cannot enter at O(1).

(ii) $\mu \neq 0$.

For this case, we choose a linear vorticity function, as in case (b) above. Writing $a = a_0 + \gamma a_1 + \ldots$ we find that

$$\left.\begin{aligned} &\nabla^2\psi_0^{out} = 0 \;;\; \psi_0^{out} \to 0 \text{ as } r\to\infty, \\ &\nabla^2\psi_1^{out} = -1 \;;\; \psi_1^{out} \to -\mu/\gamma\, r\sin\theta - \tfrac{1}{4}r^2(1-\cos 2\theta) \text{ as } r\to\infty, \\ &\nabla^2\psi_0^{in} + k^2\psi_0^{in} = a_0, \\ &\nabla^2\psi_1^{in} + k^2\psi_1^{in} = a_1, \end{aligned}\right\} \quad (13)$$

with the matching conditions unchanged. The result is:

$$\left.\begin{aligned} \psi^{out} &= \gamma\left[\tfrac{1}{4} - \tfrac{1}{4}r^2 - \mu/\gamma\,(r - \tfrac{1}{r})\sin\theta + \tfrac{1}{4}(r^2 - r^{-2})\cos 2\theta\right] + O(\gamma^2), \\ \psi^{in} &= -a_0\left[k^2 J_0(k)\right]^{-1}\left[J_0(kr) - J_0(k)\right] \\ &\quad + \gamma\left\{-a_1\left[k^2 J_0(k)\right]^{-1}\left[J_0(kr) - J_0(k)\right] - \mu/\gamma\, \tfrac{2}{kJ_0(k)} J_1(kr)\sin\theta\right\} + O(\gamma^2), \\ r(\theta) &= 1 - \gamma\left[\tfrac{1}{2a_0}(1 - 2\cos 2\theta)\right] + O(\gamma^2), \\ J_1(k) &= 0. \end{aligned}\right\} \quad (14)$$

This solution is equivalent to that of the previous problem (weak shear and no ln r term), except that a small amount of the Batchelor modon has been added throughout the field.

BATCHELOR MODON PERTURBED BY WEAK LINEAR SHEAR

This is the natural extension of the previous problem, yet there are difficulties unlike any encountered previously. First, we indicate the nature of the difficulty (solvability) and then we explore a

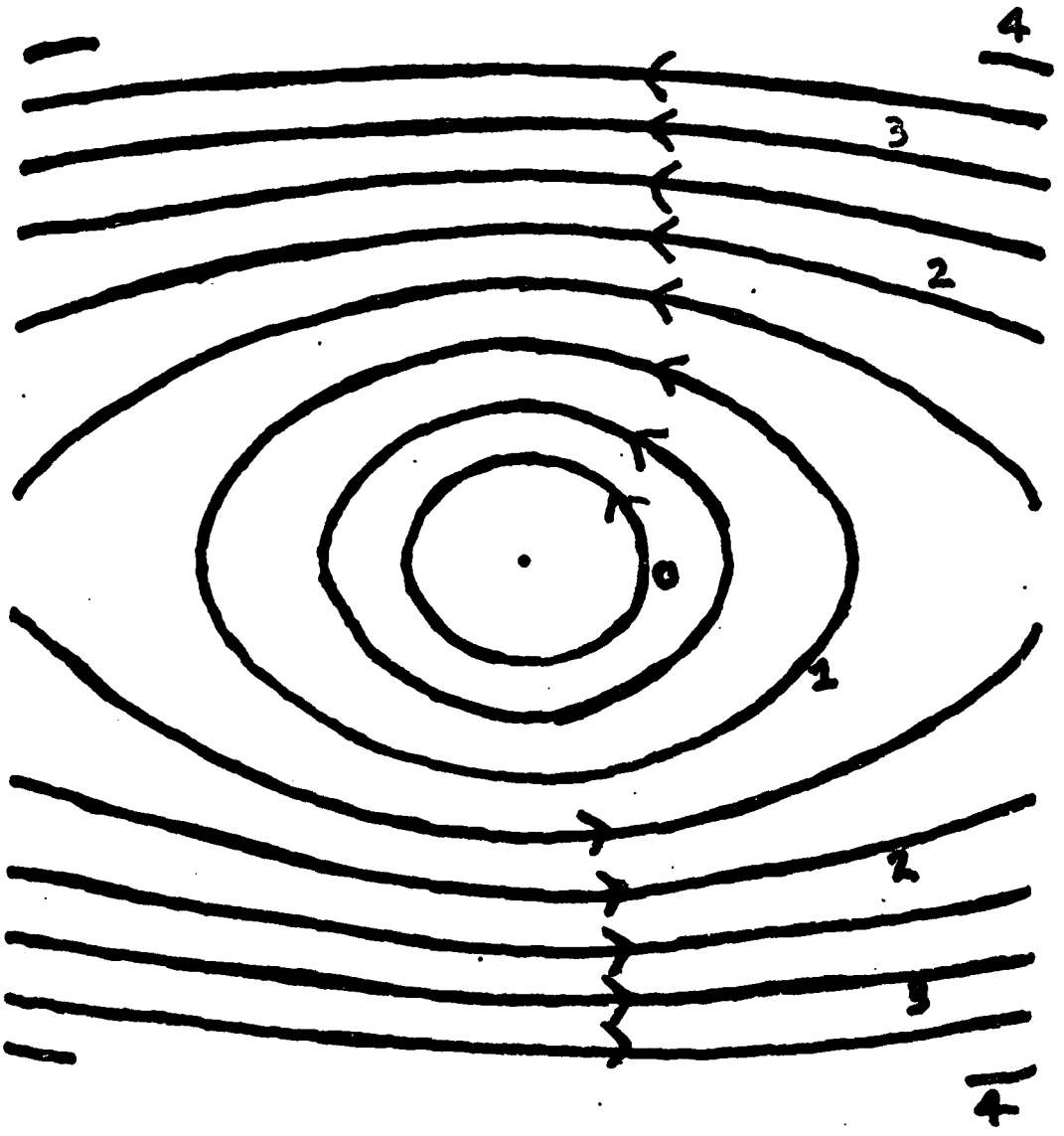

Figure 3. (a) Streamlines for perturbation problem with weak shear and the ln r term, $\gamma = -.2$. The inner streamlines are approximately at r = 1.

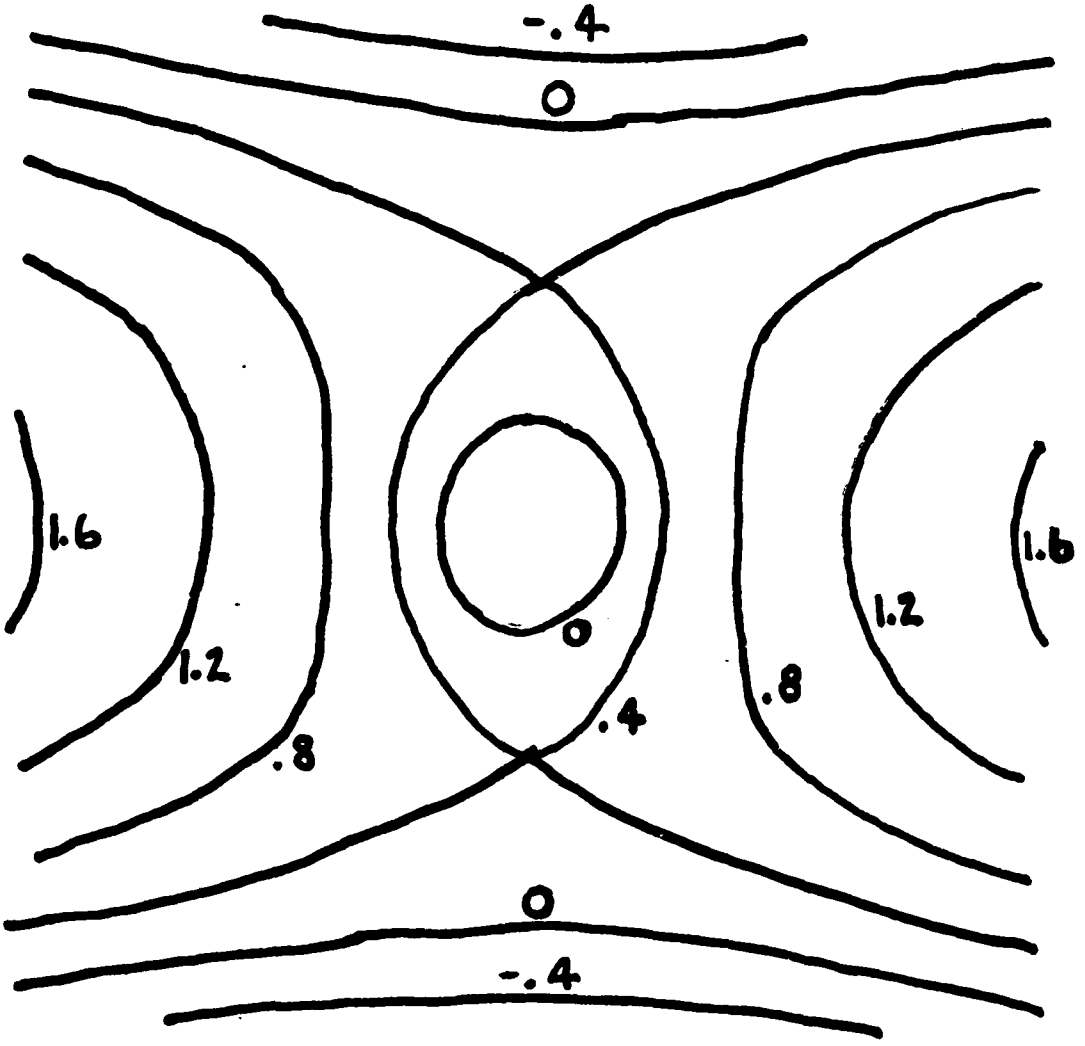

Figure 3. (b) Streamlines for perturbation problem with weak shear and the ln r term. = .2. The inner streamlines are approximately at r = 1.

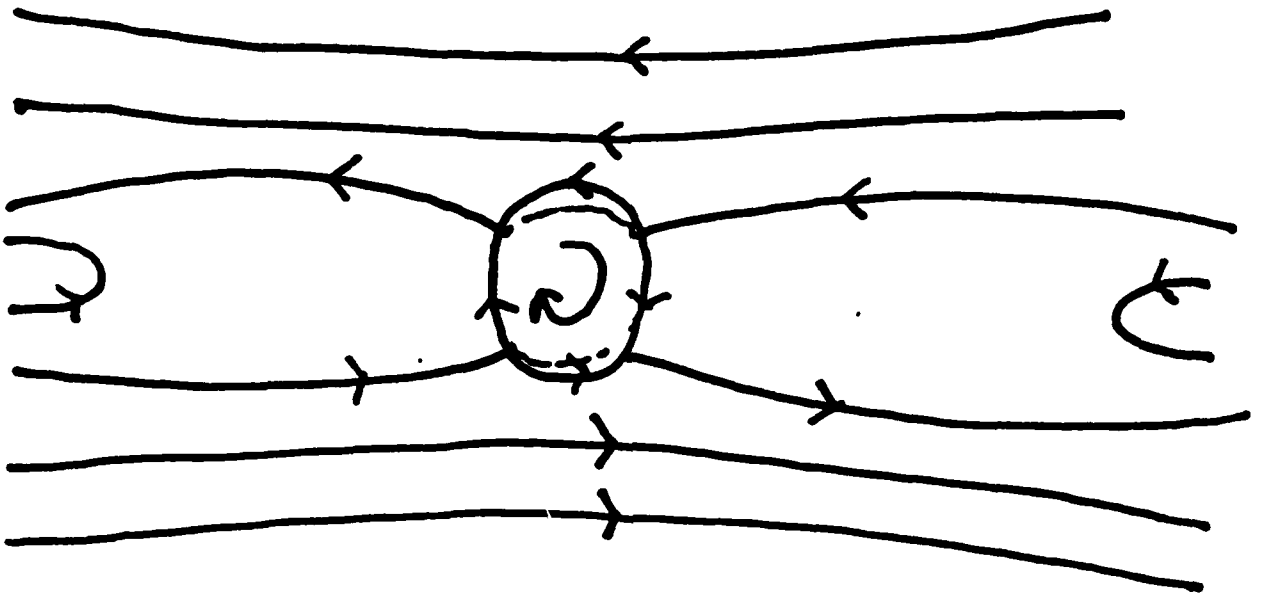

FIGURE 4a.

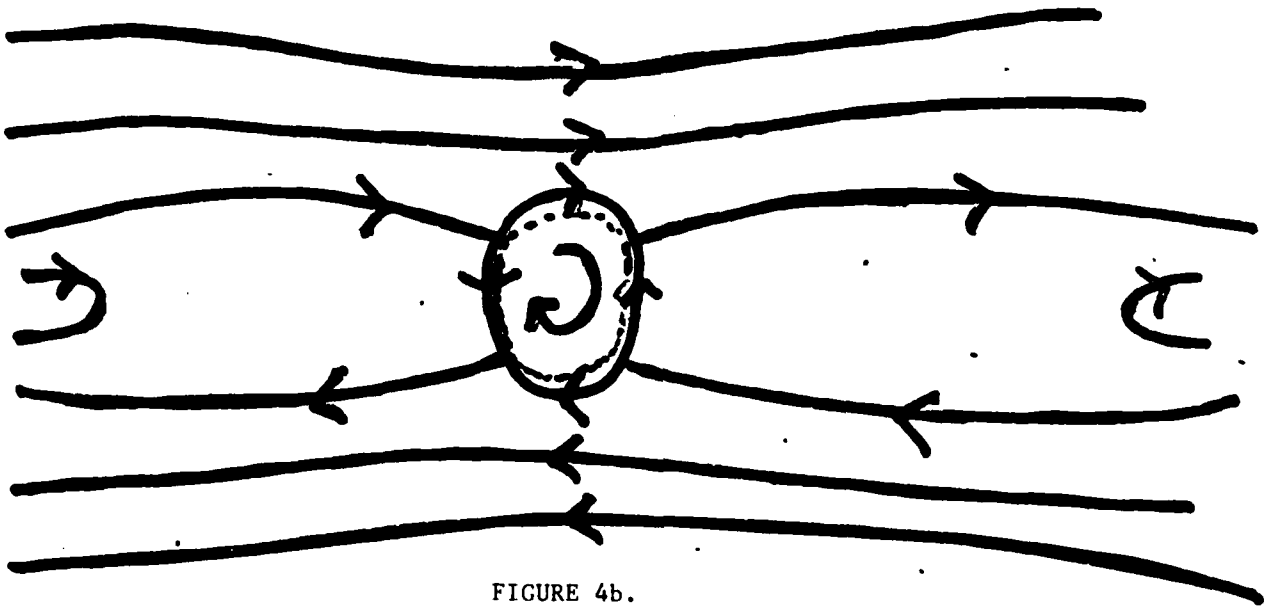

FIGURE 4b.

Figure 4. (a) Streamlines for perturbation problem with weak shear, but no ln r term, $\gamma = .2$. The dotted line indicates $r = 1$. (b) $\gamma = -.2$

remedy (allowing F_1^{in} to be a nonlinear function.)

Since the mean flow at infinity is O(1), it provides a natural scaling for ψ and we are left with $\mu = 1$. The formulation is then the same as in the last problem save the boundary conditions at infinity, which now are:

$$\left.\begin{aligned} \psi_0^{out} &\to -r\sin\theta \quad \text{as} \quad r\to\infty\,, \\ \psi_1^{out} &\to -\tfrac{1}{4}r^2(1-\cos 2\theta) \quad \text{as} \quad r\to\infty\,. \end{aligned}\right\} \quad (15)$$

The lowest order solution is precisely the Batchelor modon. Solutions of the first order problem have the form

$$\left.\begin{aligned} \psi_1^{out} &= A_0 + A_1\ln r - \tfrac{1}{4}r^2 + \tfrac{1}{4}r^2\cos 2\theta + \tfrac{B}{r}\sin\theta + \tfrac{C}{r^2}\cos 2\theta\,, \\ \psi_1^{in} &= D\,J_0(kr) + E\,J_1(kr)\sin\theta + F\,J_2(kr)\cos 2\theta\,, \end{aligned}\right\} \quad (16)$$

where A_0, A_1, B, C, D, E, F are constants to be determined. The matching conditions are

$$\left.\begin{aligned} \psi_1^{out} &= \bar{\psi}_1 + 2r_1(\theta)\sin\theta \quad \text{on} \quad r=1\,, \\ \psi_1^{in} &= \bar{\psi}_1 + 2r_1(\theta)\sin\theta \quad \text{on} \quad r=1\,, \\ \partial_r\psi_1^{in} &= \partial_r\psi_1^{out} \quad \text{on} \quad r=1\,. \end{aligned}\right\} \quad (17)$$

We now investigate the solvability of this problem. Define $\mathcal{J}_n(\psi) = r^2\psi_{rr} + r\psi_r + (k^2r^2 - n^2)\psi = 0$, where $\psi_r = d\psi/dr$. Write $\psi^{in} = \psi_{10} + \psi_{11}\sin\theta + \psi_{12}\cos 2\theta$. Since $(\nabla^2+k^2)\psi_1^{in} = a_1 \Rightarrow$

$$\left.\begin{aligned} \mathcal{J}_0(\psi_{10}) &= a_1\,, \\ \mathcal{J}_1(\psi_{11}) &= 0\,, \\ \mathcal{J}_2(\psi_{12}) &= 0\,. \end{aligned}\right\} \quad (18)$$

Since Bessel's equation is self-adjoint, we consider the integrals:

$$\int_0^1 r\,dr \begin{Bmatrix} J_0(kr) \\ J_1(kr) \\ J_2(kr) \end{Bmatrix} \begin{Bmatrix} \mathcal{J}_0(\psi_{10}) \\ \mathcal{J}_1(\psi_{11}) \\ \mathcal{J}_2(\psi_{12}) \end{Bmatrix} = 0\,, \quad (19)$$

where the brackets are vertically ordered. Integration by parts and application of the boundary conditions implies that

$$\left.\begin{aligned} J_0(k)(A_0 - 1/4) &= 0\,, \\ -kJ_1'(k)\,B &= 0\,, \\ -J_0(k) &= 0\,, \end{aligned}\right\} \quad (20)$$

where the prime denotes differentiation with respect to the argument. Since $J_1(k) = 0$, the third condition cannot be met and the problem cannot be solved as formulated.

One way to reformulate the problem so that it can be solved is as follows. Recall that

$$\left.\begin{aligned} &\Rightarrow \nabla^2\psi_0^{in} + \gamma\nabla^2\psi_1^{in} = F_0(\psi_0^{in}) + \gamma\psi_1^{in}F_0'(\psi_0^{in}) + \gamma F_1(\psi_0^{in}) \\ &\Rightarrow \nabla^2\psi_0^{in} + k^2\psi_0^{in} = 0 \quad \text{and} \\ &\nabla^2\psi_1^{in} + k^2\psi_1^{in} = F_1(\psi_0^{in})\,. \qquad (*) \end{aligned}\right\} \quad (21)$$

Choose $F_1(\psi_0^{in}) = \alpha + \beta(\psi_0^{in})^2 + \Delta(\psi_0^{in})^4$. The lowest order problem is unchanged and its solution is again the Batchelor modon. Thus,

$$\psi_0^{in} = g(r)\sin\theta\,, \quad \text{where} \quad g(r) \equiv -2u_0\left[kJ_0(k)\right]^{-1}J_1(kr)\,. \quad (22)$$

Substitution into equation (21a) yields

$$\nabla^2 \psi_1^{in} + k^2 \psi_1^{in} = \left(a + \tfrac{1}{2}\delta g^2 + \tfrac{3}{8}\Delta g^4\right) - \left(\tfrac{1}{2}\delta g^2 + \tfrac{1}{2}\Delta g^4\right)\cos 2\theta + \tfrac{1}{8}\Delta g^4 \cos 4\theta \quad . \qquad (23)$$

Rewrite equation (16a) as

$$\psi_1^{out} = A_0 + B_0 \ln r - \frac{r^2}{4} + \frac{r^2}{4}\cos 2\theta + \frac{A_2}{r^2}\cos 2\theta + \frac{A_4}{r^4}\cos 4\theta \quad . \qquad (24)$$

We now investigate the solvability of this problem. Write

$$\psi_1^{in} = \psi_{10} + \psi_{12}\cos 2\theta + \psi_{14}\cos 4\theta \quad \& \quad r_1(\theta) = r_{11}\sin\theta + r_{13}\sin 3\theta \quad . \qquad (25)$$

Equation (23) implies

$$\left.\begin{aligned} \mathcal{J}_0(\psi_{10}) &= a + \tfrac{1}{2}\delta g^2 + \tfrac{3}{8}\Delta g^4 , \\ \mathcal{J}_2(\psi_{12}) &= -\tfrac{1}{2}\delta g^2 - \tfrac{1}{2}\Delta g^4 , \\ \mathcal{J}_4(\psi_{14}) &= \tfrac{1}{8}\Delta g^4 \end{aligned}\right\} \qquad (26)$$

The matching conditions can be expanded in a similar way and yield

$$\left.\begin{aligned} &\psi_{10}(1) = \bar{\psi}_1 + r_{11} , && \psi_{12}(1) = r_{13} - r_{11} , && \psi_{14}(1) = -r_{13} , \\ &\psi_{10}(1) = A_0 - 1/4 , && \psi_{12}(1) = \tfrac{1}{4} + A_2 , && \psi_{14}(1) = A_4 , \\ &\partial_r \psi_{10}(1) = B_0 - \tfrac{1}{2} , && \partial_r \psi_{12}(1) = \tfrac{1}{2} - 2A_2 , && \partial_r \psi_{14}(1) = -4A_4 . \end{aligned}\right\} \qquad (27)$$

Applying the solvability criteria implies that

$$\left.\begin{aligned} \tfrac{1}{2}\delta N_{02} + \tfrac{3}{8}\Delta N_{04} &= (B_0 - \tfrac{1}{2})\, J_0(k) , \\ -\tfrac{1}{2}\delta N_{22} - \tfrac{1}{2}\Delta N_{24} &= -J_0(k) , \\ \tfrac{1}{8}\Delta - 4A_4 J_0(k) &= 0 , \end{aligned}\right\} \qquad (28)$$

where $N_{nm} = \int_0^1 r\,dr\, J_n(kr)\, g^m$. Integration $\Rightarrow N_{22} = 2N_{02}$ and $N_{24} = 3/2\, N_{04}$. Thus, the only way that the first two equations are compatible is if $B_0 = 1$.

For $B_0 = 1$, not only can the problem be solved, but there is a great deal of flexibility in choosing the parameters.

The simplest is $\Delta = 0 = r_{11}$. Then

$$\left.\begin{aligned} \psi_1^{out} &= \ln r - \tfrac{1}{4}r^2 + \tfrac{1}{4}(r^2 - r^{-2})\cos 2\theta , \\ (\nabla^2 + k^2)\psi_1^{in} &= a + \tfrac{1}{2}J_0(k)\, N_{02}^{-1}\, g^2 (1 - \cos 2\theta) , \\ r(\theta) &= 1 \end{aligned}\right\} \qquad (29)$$

Numerical integration provides the profiles of $\psi_{10}(r)$ and $\psi_{12}(r)$, which are sketched in figure 5. The streamlines are not obvious and, as part of my continuing research, will be plotted by computer, though not in this report.

Results for $\Delta \neq 0$ are intriguing, but have not been thoroughly explored. A graph of $F^{in}(\psi)$ is presented in figure 6 for $\gamma = .2$ and $\Delta = -50, 0, 50$. It is interesting to note that even for a large value of Δ ($\Delta = -50$), only small effects are felt in A_4 and r_{13} ($A_4 = .01$, $r_{13} = -.01$). This suggests that the Batchelor modon resists deformations of this type.

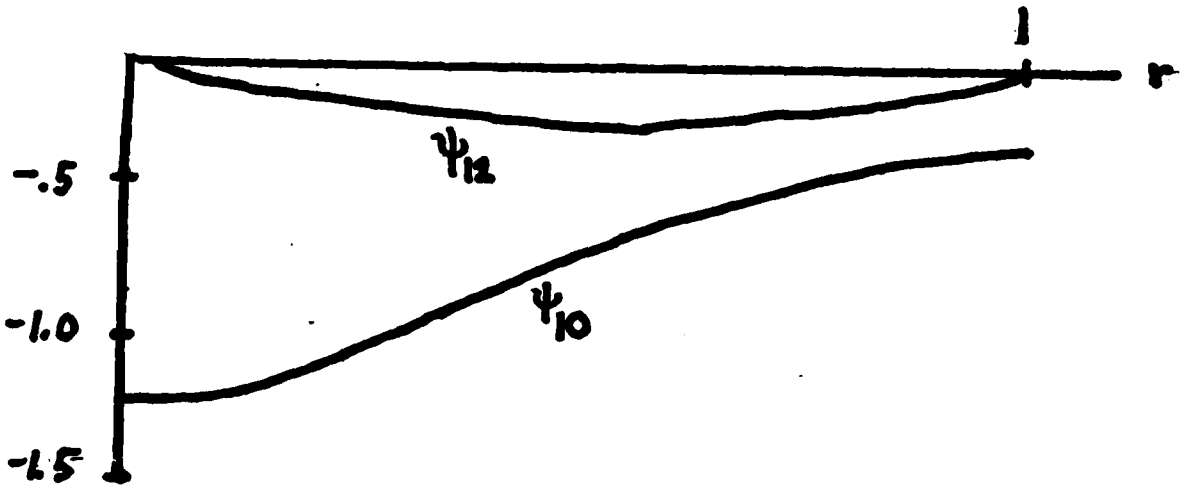

Figure 5. Plots of $\psi_{10}(r)$ and $\psi_{12}(r)$ for the Batchelor modon in a weak shear flow.

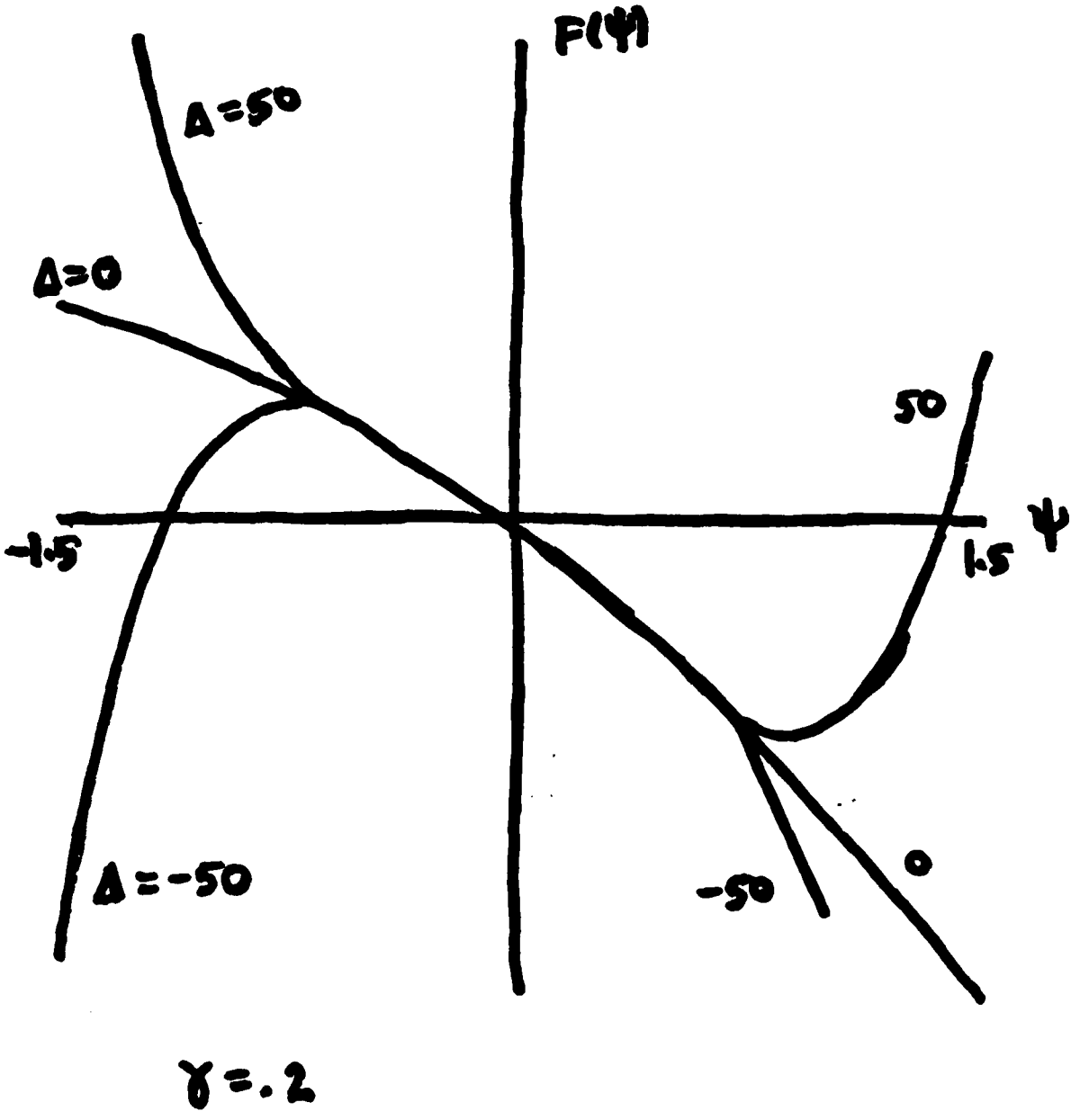

Figure 6. $F(\Psi)$ versus Ψ , Δ = 50, 0, -50.

CONCLUSIONS

Indications are that strong, isolated, two-dimensional vortices can exist in the presence of an O(1) mean flow with weak shear. It is intriguing that a nonlinear vorticity function is required to find an appropriate perturbation to the Batchelor modon. The flexibility encountered in this solution offers hope that perturbation solutions on the β-plane may be obtained via a similar approach.

The implications of the need for a nonlinear functional indicates that a subtle balance is needed for coherent structures to maintain their identity in non-uniform mean flows. It also points to the fact that the processes that might generate such steady flows are complicated.

These questions will be explored in future work.

ACKNOWLEDGEMENTS

I am indebted to the entire GFD staff and Fellows for helpful discussions. In particular, I wish to express my gratitude to Glenn Flierl for his help and encouragement.

REFERENCES

Batchelor, G.K., 1967. An Introduction to Fluid Dynamics. Cambridge Univ. Press, p.534-535.

Flierl, G.R., V.D. Larichev, J.C. McWilliams and G.M. Reznik, 1980. The dynamics of baroclinic and barotropic solitary eddies. Dyn. Atmos. Oceans 5, 1-41.

Larichev, V.D. and G.M. Reznik, 1976. Two-dimensional Rossby soliton: an exact solution. Polymode News 19, p.3.

Stern, M., 1975. Minimal properties of planetary eddies. J. Mar. Res. 33, 1-13.

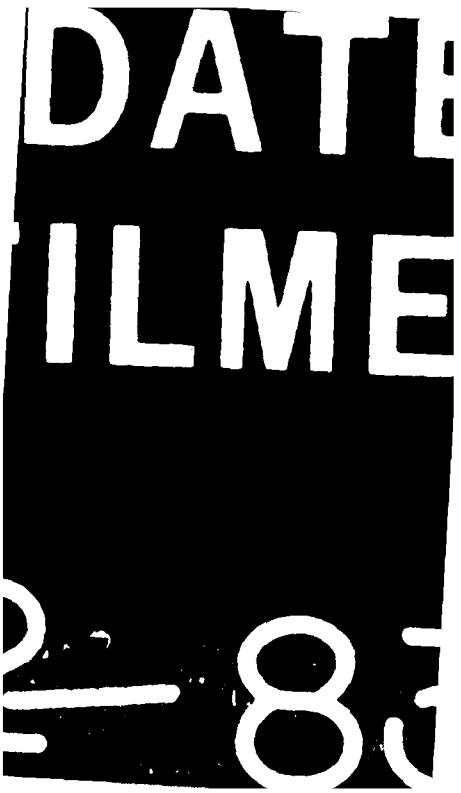
DAT
ILME